SPECTROSCOPIC OBSERVATIONS OF HIGH REDSHIFT QSOs: GALAXIES AND THE INTERGALACTIC MEDIUM AT EARLY EPOCHS

Thesis by

Charles C. Steidel

In Partial Fulfillment of the Requirements

for the Degree of

Doctor of Philosophy

California Institute of Technology

Pasadena, California

1990

(Submitted 22 August 1989)

To Sarah, for always being there...

ACKNOWLEDGEMENTS

It seems like a long time ago that I arrived in Pasadena as a terrified new graduate student, with not a very good idea as to why I was here or what I wanted to do. In retrospect I find it amazing the way things worked out, given that many decisions were made without the benefit of an understanding of what they meant or why they were being made. Anyway, during the 5 years that I've been here in Pasadena, I feel as though I've learned an incredible amount and I've become a little bit less terrified (although I'm still intimidated by people who appear to know what they're talking about) and none of it would have been possible without the help of the people whom I will now proceed to thank. If I have left anyone out, I am sorry.

I would first of all like to thank my advisor, Wal Sargent, from whom I have learned so much, not the least of which being the finer points of the art of "skulking." Seriously, I feel incredibly lucky to have had an advisor so interested in the welfare of his student, in both scientific and non–scientific areas. In addition to providing generous financial support, including travel to many conferences and 4 observing trips to Chile, Wal also donated a great deal of his own observing time to my "toenails of waterfleas" thesis projects. I have benefited so much from the many "preliminary reconnaissances" that we have worked on together; I am proud to have been a (the) member of his "team." I hope that someday Wal will forgive my having spent thousands of dollars on a set of narrow–band interference filters I didn't end up using for my thesis (but which I insist will prove useful to *someone* in the future...probably around the same time the Dodgers are again contenders in the N. L.) The advice and guidance I have received from Wal have been invaluable.

Next I would like to thank all of my fellow graduate students who have passed through Robinson during the years 1984–1989, especially my office (and class) mates Steve Myers and Blaise Canzian, Dave Hough, Jim Mc Carthy, Rick Edelson, Mike Rich, Zuo Lin, Rich Rand, Chris Tinney, Josh Roth, Chris Wilson, Alain Picard, Karl Stapelfeldt, and Debbie Padgett. These people helped make Pasadena not such a bad place after all. I'd also like to thank the postdocs who were always willing to interrupt their own work to provide their help or advice, or to just plain exchange gossip: Jim Schombert, Neill Reid, and Don Hamilton.

Andy Long and Nels Van der Linden are friends without whom I might not have made it through that difficult first year–I will never forget them.

I'd like to thank the staffs of both Palomar and Las Campanas Observatories for their dedicated help in making observations go smooothly: In particular, thanks go to John Henning, Mike Doyle, Dave Tennant, Skip Staples, and Juan Carrasco at Palomar and Angel Guerra and Fernando Perralta at Las Campanas. Palomar Observatory is also acknowledged for financial support during the last couple of years.

I'd like to thank all former and present members of Green Goghs/On Beyond Zebra for joining me in a "hobby" that provided much needed fun and "noise therapy": Gil Rodriguez, Ray Gonzalez, Doug Appleton, Victor B., and Steve Myers.

I'd like to thank all of the professors for sharing their punditry, advice, and comments on various problems and/or manuscripts, especially Jeremy Mould, Sterl Phinney, Roger Blandford, Nick Scoville, Maarten Schmidt, George Djorgovski, and Tony Readhead. Thanks also go to Marilynne Nyberg for continual words of encouragement and for taking care of countless things along the way, and Margaret Katz for going well beyond the call of duty in making innumerable finding charts. Judy Cohen and the rest of the computer pundits are gratefully acknowledged for keeping things going, often against all odds, and for help when it was needed. I would also like to thank Alex Filippenko and Hy Spinrad for their support and enthusiasm in helping me to secure a postdoctoral position at Berkeley, beginning this fall.

Finally, I would like to thank my wife Sarah, without whom, in all honesty, I don't think I could have finished in one piece. Despite frequent attacks of various neuroses on my part, Sarah always provided the love and support which kept me going. Sarah helped to show me by example what things are important and what things are less so, thereby helping me to stay sane. I admire her approach to life tremendously.

ABSTRACT

The thesis consists primarily of 4 parts, which are separate but related insofar as each makes use of spectra of high redshift QSOs in order to investigate the properties of intervening gaseous material. Briefly summarized, the sections are as follows:

I. Wide–slit spectrophotometry of a sample of very high redshift QSOs is used to establish that the cumulative effect of the Lyman α forest of absorption lines is statistically the same in all of the QSOs. By combining these results with high resolution observations of QSO Lyman α forests, a new upper limit on the density of generally distributed intergalactic neutral hydrogen (the Gunn–Peterson limit) is obtained. Implications for the nature of the intergalactic medium and the baryonic mass density of the universe are discussed.

II. Observations of a number of high redshift QSOs close to each other on the plane of the sky are presented; based on the occurrence of heavy element absorption systems over a narrow range of redshifts in each of the spectra, evidence for the presence of a huge, elongated supercluster of galaxies at $z = 2$ is discussed.

III. Results of a survey for heavy element absorption systems at the largest observable redshift ($2.7 < z < 3.8$) are presented; the data are combined with the very large survey for C IV absorption recently completed by Sargent, Boksenberg, and Steidel (1988). The data show very clear evolution of the heavy element absorbers with time over the redshift range $1.5 < z < 3.5$. The changes are interpreted as a gradual evolution of the heavy element abundances in gas associated with sites where galaxies have formed. The implications for galaxy formation and evolution are discussed.

IV. Moderate dispersion spectra of a sample of Lyman limit absorption systems at $z \approx 3$ have been obtained in order to determine the heavy element abundances and other physical parameters of the gas clouds responsible for the high redshift, heavy-element absorption systems in the spectra of QSOs. Photoionization models are used to conclude that the clouds are ionized primarily by the metagalactic UV flux, which has a spectral energy distribution comparable to that of AGNs. The abundances of C, O, and Si are in general between 0.001 and 0.01 of the solar abundances, comparable to the most metal–poor stars in the halo of the Galaxy. The clouds have sizes in the range 1–15 kpc and masses in the

range $10^6 - 10^9\ M_\odot$. The clouds are discussed within the context of the hypothesis that the heavy element absorption systems are associated with the extended halos of high redshift galaxies. Diffuse gas in the form of such clouds may account for a significant fraction of the baryonic material in the universe, and it has probably played an important role in the evolution of galaxies over time.

INTRODUCTORY NOTE

This thesis consists of five self–contained but related chapters, each of that is comprised of an article or articles which have been published, or are intended for publication, in *The Astrophysical Journal.* The "unifying theme" throughout the five chapters is an attempt to use spectroscopic observations of high redshift QSOs to understand the physical properties of intervening material–galaxies and the intergalactic medium– at large redshifts and thus at early epochs. The QSO absorption lines represent perhaps the most sensitive tool available for investigating the nature of "normal" gaseous material at very high redshifts; much of this thesis represents a first–order attempt to extract the physical and statistical information provided by the absorption systems in the context of a universe containing galaxies that are forming and evolving.

Chapter 1 consists of 2 reprinted articles (both written in collaboration with W. L. W. Sargent), from *The Astrophysical Journal* (1987, **313**, 171–184) and *The Astrophysical Journal (Letters)* (1987, **318**, L11–L13), respectively. Chapter 2, also written in collaboration with W. L. W. Sargent, is reprinted from *The Astrophysical Journal* (1987, **322**, 142–163). Chapter 3 has been accepted for publication in the *Astrophysical Journal Supplements*; Chapter 4, written in collaboration with Wal Sargent, will appear in the 15 August 1989 issue of *The Astrophysical Journal (Letters).* Chapter 5 has been submitted to *The Astrophysical Journal Supplements.* The article in Appendix 1, written in collaboration with W. L. W. Sargent and A. Boksenberg, is reprinted from *The Astrophysical Journal (Letters)* (1988, **333**, L5–L8).

TABLE OF CONTENTS

Chapter 1

SPECTROPHOTOMETRY OF HIGH REDSHIFT QSOs AND LIMITS ON THE DENSITY OF GENERALLY DISTRIBUTED INTERGALACTIC NEUTRAL HYDROGEN

Reprinted from *The Astrophysical Journal* (1987, **313**, pp. 171–184)

and

The Astrophysical Journal (Letters) (1987, **318**, pp. L11–L13)

THE ASTROPHYSICAL JOURNAL, 313:171–184, 1987 February 1

THE EFFECT OF THE LYMAN-ALPHA FOREST ON THE ULTRAVIOLET CONTINUA OF VERY HIGH REDSHIFT QUASARS

CHARLES C. STEIDEL AND WALLACE L. W. SARGENT
Palomar Observatory, California Institute of Technology
Received 1986 June 9; accepted 1986 July 30

ABSTRACT

Absolute spectral energy distributions have been obtained for eight very high redshift quasars ($z_{em} \geq 2.7$) with the Hale double spectrograph in the observed wavelength range 3200–10,000 Å (typically 800–2500 Å in the rest frame of the quasar). The spectra represent a significant improvement in resolution and signal-to-noise (S/N) ratio over that achieved previously, allowing more accurate evaluation of the true ultraviolet continuum. It is found that the true continuum in the region of the "Lyα forest" can be represented by the extrapolation of the continuum defined longward of Lyα emission by $f_\nu \propto \nu^{-\alpha}$, where $0.28 \leq \alpha \leq 0.99$. Low-resolution quasar spectra in the ultraviolet (i.e., *IUE* spectra) can yield apparent continuum levels which are significantly *below* the true continuum level which would be observed at very high spectral resolution. Such spectra indicate a steepening in the continuum slope which is not intrinsic to the quasar but which is due to line and continuum absorption by neutral hydrogen along the line of sight to the quasar. Observed ultraviolet spectral energy distributions can therefore yield misleading values of fitted parameters in quasar models. The fractional flux decrement below Lyα emission and above Lyβ due to the cumulative effects of absorption lines, D_A, is statistically the same in all of the quasars (0.24 ± 0.05), supporting the hypothesis that this absorption is due to material distributed cosmologically along the line of sight. The corresponding fractional flux decrement between Lyβ and the emission redshift Lyman limit is $D_B = 0.36 \pm 0.07$.

Subject headings: galaxies: intergalactic medium — quasars — spectrophotometry — ultraviolet: spectra

I. INTRODUCTION

In quasars with an emission-line redshift of ~ 2.7 or greater, the Lyα forest down to the Lyman limit ($\lambda_0 = 912$ Å) is observable at optical wavelengths. Previous work (Oke and Korycansky 1982) obtained spectral energy distributions for 19 high-redshift quasars, but the resolution (~ 80 Å shortward of 5600 Å, ~ 160 Å longward of 5600 Å) was too low to permit an accurate definition of the continuum both in the Lyα forest and to the red of Lyα emission. Osmer (1979) obtained low (~ 40 Å) resolution spectra of eight quasars with $z_{em} \geq 3.0$ to investigate the nature of the absorption shortward of Lyα emission. Two-dimensional spectroscopic detectors have made possible spectrophotometric observations with much higher spectral resolution, thereby removing much of the uncertainty involved in defining the continuum and thus in the magnitude of depressions in the apparent continuum. Ideally, of course, one would like to measure the absolute continuum energy distribution at the highest possible spectral resolution, thus minimizing any "blanketing" of the true continuum by unresolved Lyman series absorption lines; unfortunately, a compromise between resolution and spectrophotometric accuracy is necessitated by finite seeing disks and the effects of atmospheric dispersion. For the observations of eight high-redshift quasars presented in this paper, we have adopted such a compromise and have obtained spectra at moderate resolution with very good absolute spectrophotometric characteristics, allowing a detailed study of the continuum energy distribution.

It has been noted for some time that there is an apparent steepening of the continuum slope toward the short wavelength side of Lyα emission in quasars as compared to the slope defined on the red side of Lyα by $f_\nu \propto \nu^{-\alpha}$. This effect has been observed in *IUE* spectra of low- to moderate-redshift quasars (e.g., Bechtold *et al.* 1984) as well as in optical spectra of high-redshift quasars. It is generally believed that this apparent change in the continuum slope is due to the effects of Lyα, Lyβ, and Ly continuum absorption from H I clouds along the line of sight to the quasar. If indeed this is the case, and if the distribution of H I clouds as a function of distance is the same along all lines of sight (as one would expect according to the "intervening" hypothesis), then one should observe the same characteristic depression of the apparent continuum level shortward of Lyα emission in all quasars of a given redshift observed at a given spectral resolution. However, it has been suggested (Hazard *et al.* 1986) that visual inspection of crude spectra of high-redshift quasars taken for identification purposes indicates a surprising variability in the apparent characteristics of this change in the continuum in the region of the "Lyα forest." This represents a potential problem with the "intervening" hypothesis and could indicate that a substantial component of ejected material (i.e., material associated with the quasar) is contributing to the Lyα forest. The importance of obtaining high-quality spectra of a sample of quasars is clear: to determine whether the apparent change in the slope of the continuum shortward of Lyα emission is inherent to the quasar itself or whether it is due to a cosmological distribution of intervening material.

II. OBSERVATIONS AND REDUCTIONS

The eight quasars observed were selected on the basis of their redshift and apparent magnitude from the catalog of Veron-Cetty and Veron (1985) and from Hazard *et al.* (1986). The criteria for selection were $z_{em} > 2.7$ and $m_V < 19$, although one object (Q1358+1134) was observed which does not quite meet the redshift requirement but is especially bright. All of the spectra were obtained on the Hale 5.08 m telescope during 1986 January 12 and 13 (UT). Details concerning the observa-

TABLE 1

OBSERVATIONS

Object	z_{em}	m_V	Date (1986)	UT(Start)	Exposure (s)
Q0014+8118[a]	3.380	16.5	Jan 13	3:50	1800
Q0308+1902[b]	2.831	18.2	Jan 12	4:53	4000
Q0731+6519[c]	3.029	18.7	Jan 12	8:24	5000
Q0805+0441[d,f]	2.875	18.4	Jan 13	8:04	3000
Q0903+1734[b]	2.775	18.0	Jan 13	9:03	2500
Q0941+2608[e,f]	2.901	18.7	Jan 12	10:30	4000
Q0956+1217[b]	3.299	17.5	Jan 13	10:21	1500
Q1358+1134[b]	2.571	17.4	Jan 12	13:13	1000

[a] Kuhr *et al.* 1983.
[b] Hazard *et al.* 1986.
[c] Arp *et al.* 1979.
[d] Q0805 + 0441 = 4C 05.34; Lynds and Wills 1970; see also, e.g., Lynds 1971 and Chen *et al.* 1981.
[e] Wills and Wills 1976.
[f] Continua studied by Oke and Korycansky 1982.

tions are listed in Table 1. We used the double spectrograph (Oke 1982) at the Cassegrain focus with a dichoric beam splitter in place such that $\lambda < 5500$ Å was diverted to the "blue side" and $\lambda > 5500$ Å to the "red side." On the blue side was attached the "2D-FRUTTI" photon counting detector (Shectman 1982), which we used in the configuration having 3040 pixels in the direction of the dispersion and 128 pixels in the spatial direction. The grating on the blue side had 600 lines mm^{-1} and was blazed at 3780 Å in first order, resulting in a dispersion on the detector of 0.975 Å per pixel. This grating was selected to maximize the S/N ratio in the UV. The detector on the redside was a Texas Instruments 800 × 800 CCD, and the grating used had 158 lines mm^{-1} with the blaze at 7560 Å in first order. This resulted in a scale on the CCD of 6.08 Å per 15 μm pixel. The instrumental set up provided complete wavelength coverage from 3200 to 10,000 Å.

A slit width of 4″ was used for all of the observations so that absolute spectrophotometry might be accomplished while minimizing the degradation of the S/N ratio because of sky contamination. The projected slit width at the detector was ~12 pixels (~11.7 Å) on the blue side and 6.9 pixels (~41.9 Å) on the red side. However, great care was taken in accurately guiding the object at the center of the slit during all integrations, so with a typical seeing disk of 1.″5 and allowing for some guiding errors, we estimate that the actual resolution achieved corresponds more closely to the projection of ~2″ on the detectors, yielding an effective resolution of ~6 Å on the blue side and 20 Å on the red side. It should be noted that seeing fluctuations which might have occurred from integration to integration would have the effect of making the resolution inconstant from spectrum to spectrum, but we estimated that the seeing was fairly consistent for the duration of the two nights on which the data were taken.

The effects of atmospheric dispersion were minimized by observing all objects at the parallactic angle (Filippenko 1982). The faint standard stars GD 248 and G60-54 (Filippenko and Greenstein 1984) were used to flux-calibrate both the blue and red spectra, and the stars BD +26°2606 and HD 19445 (Oke and Gunn 1983) were used to remove atmospheric absorption features in the red and near-infrared regions of the spectra. Continuum fluxes for two of the objects (Q0805+0441 and Q0903+1734) may be slightly low (~0.2 mag) because of some thin cirrus which may have drifted overhead during the integrations. Otherwise, all fluxes are estimated to be within ~0.1 mag of absolute, and uncertainties in the relative flux levels are probably less than 5%, based upon calibration of one standard star using the observation of the other. Integration times were chosen to attain (S/N) ratios in the continuum of ~20 in the UV. Signal-to-noise ratios for the CCD (red) spectra are typically greater than 100.

III. THE DATA

a) Observational Results

Newly determined redshifts and apparent continuum visual magnitudes are listed in Table 1, and the observed spectra are plotted in Figure 1. Figure 2 shows plots of the spectral energy distributions log f_{ν_0} versus log ν_0, where $f_{\nu_0} = f_{\nu_{obs}}/(1 + z_{em})$, $\nu_0 = \nu_{obs}/(1 + z_{em})$, z_{em} is the redshift of the quasar as defined by the emission lines, and ν_0 is the rest frequency. We have estimated the amount of reddening due to interstellar material in the Galaxy for all of the objects based upon Burstein and Heiles (1982). Two of the objects, Q0014+8118 and Q0308+1902, are sufficiently reddened ($E_{B-V} = 0.21$ and 0.12 mag respectively) that a correction has been applied to the spectra. The reddening curves of Seaton (1979) and Nandy *et al.* (1975) have been used. For the other six objects, E_{B-V} is estimated to be less than 0.03 mag, and no correction has been applied. Spectral indices α (defined longward of Lyα emission by $f_\nu \propto \nu^{-\alpha}$) were measured and the adopted continua are shown in Figure 2. The estimated uncertainty in the measured values of α is ± 0.05. The values of α are listed in Table 2. Also listed in Table 2 are the continuum flux density (measured at log $\nu_0 = 15.240$) and the total "luminosity density" (also at log $\nu_0 = 15.240$) assuming a Friedmann universe with $q_0 = 0$, $H_0 = 100h_{100}$, and isotropic radiation.

Emission-line intensities and equivalent widths have been measured and are given in Table 3. No attempt has been made to correct for the presence of absorption in the emission lines, so the values listed, particularly for the O VI+Lyβ and Lyα+N V lines, are probably lower limits. We also did not attempt to separate blended emission lines into individual components; virtually all of the lines measured have probable contributions from more than one ion. Uncertainties in emission-line equivalent widths are probably of order 10% for the stronger lines and are somewhat larger for the weaker lines. Emission lines were not measured for the quasar Q0903+1734 because of the presence of broad absorption troughs.

TABLE 2

CONTINUUM DATA

Object	α[a]	log f_{ν_0}[b]	L_{ν_0}[c]/h_{100}^2	D_A	D_B	D_B/D_A
Q0014+8118[d]	0.77	2.594	35.8	0.21	0.34	1.62
Q0308+1902[d]	0.55	1.853	3.59	0.22	0.33	1.53
Q0731+6519	0.67	1.525	2.08	0.31	0.43	1.37
Q0805+0441	0.80	1.669	2.46	0.20	0.27	1.37
Q0903+1734	0.99	1.882	3.56	0.49	0.83	1.69
Q0941+2608	0.28	1.535	1.87	0.17	0.29	1.68
Q0956+1217	0.45	1.976	7.74	0.26	0.38	1.46
Q1358+1134	0.34	2.060	4.24	0.29	0.47	1.59

[a] The spectral index, defined to the red of Lyα emission by $f_\nu \propto \nu^{-\alpha}$.
[b] In units of 10^{-29} ergs s^{-1} cm^{-2} Hz^{-1}, evaluated at log $\nu_0 = 15.240$.
[c] Total luminosity, in units of 10^{31} ergs s^{-1} Hz^{-1}, assuming a Friedmann universe with $q_0 = 0$ and isotropic radiation, evaluated at log $\nu_0 = 15.240$ (h_{100} is the Hubble constant in units of 100 km s^{-1} Mpc^{-1}).
[d] After correction for galactic reddening.

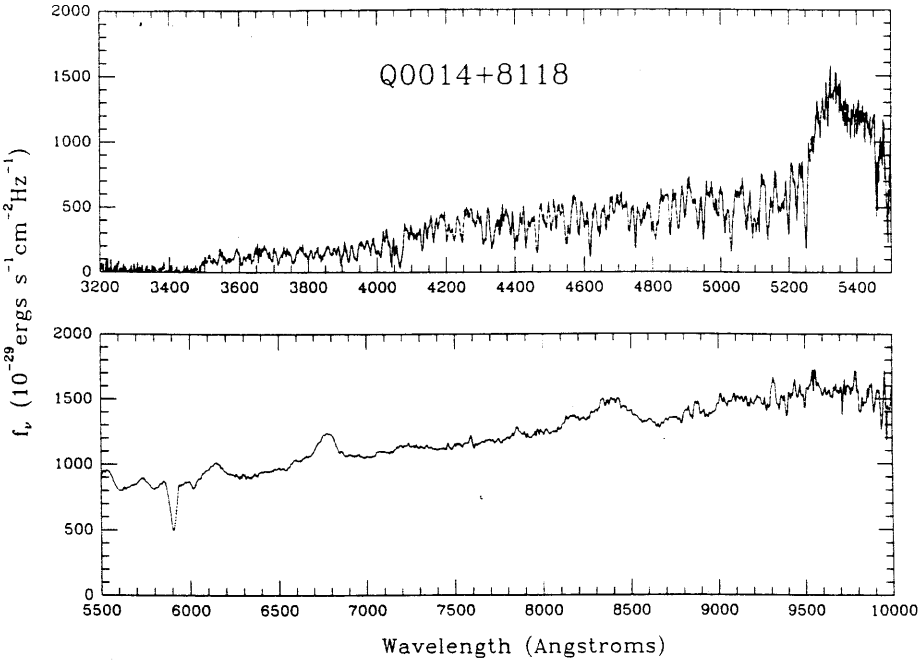

FIG. 1*a*

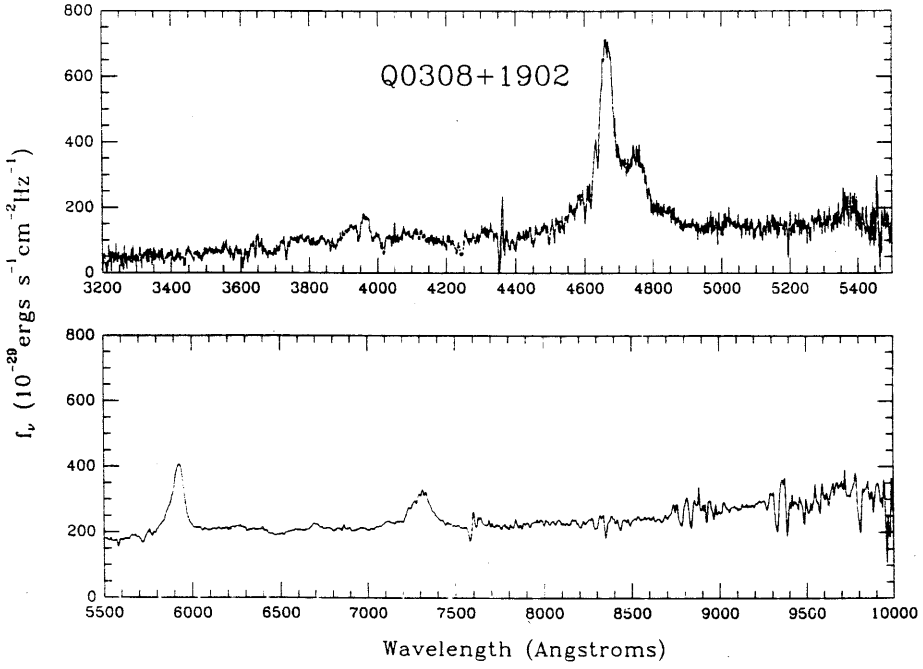

FIG. 1*b*

FIG. 1.—Plots of the observed flux density versus observed wavelength for the eight observed quasars. Top panels are the blue 2D-FRUTTI spectra, with typical resolution of 6 Å and S/N ratio of 20; lower panels are the red CCD spectra, with typical resolution of 20 Å and S/N ratio of greater than 100.

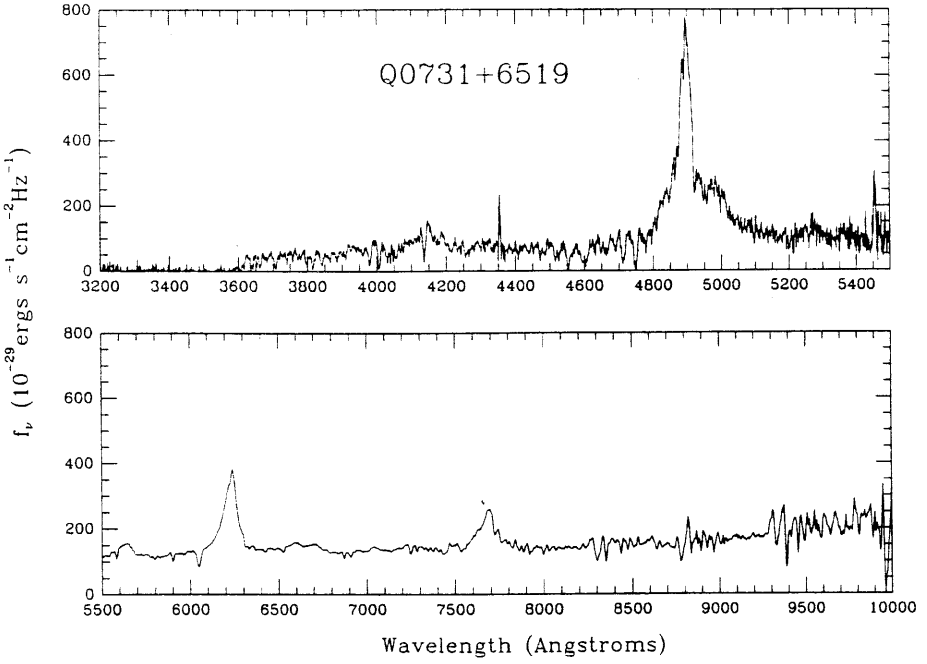
Q0731+6519
f_ν (10^{-29}ergs s^{-1}cm^{-2}Hz^{-1})
Wavelength (Angstroms)

FIG. 1c

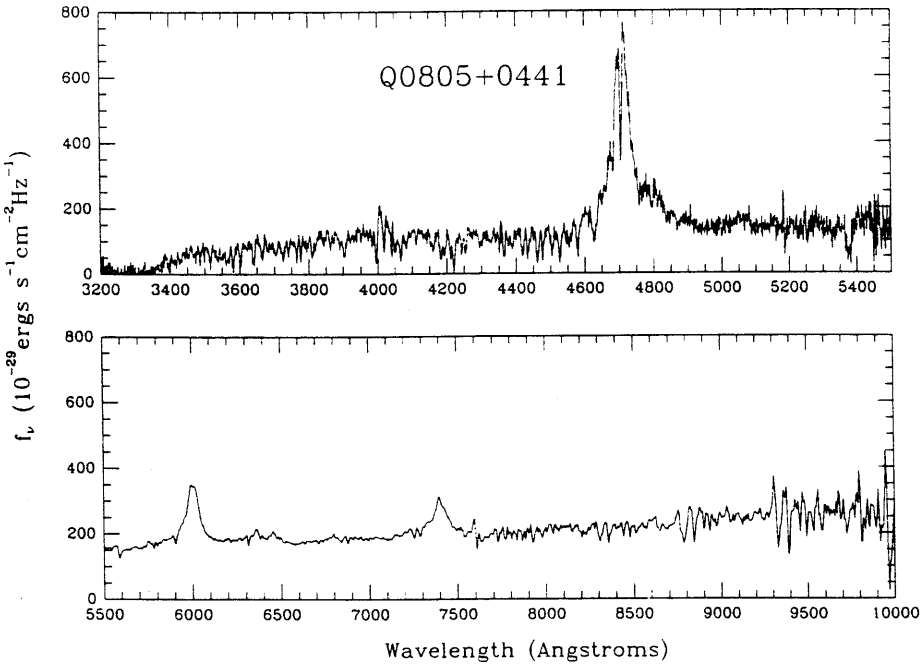
Q0805+0441
f_ν (10^{-29}ergs s^{-1}cm^{-2}Hz^{-1})
Wavelength (Angstroms)

FIG. 1d

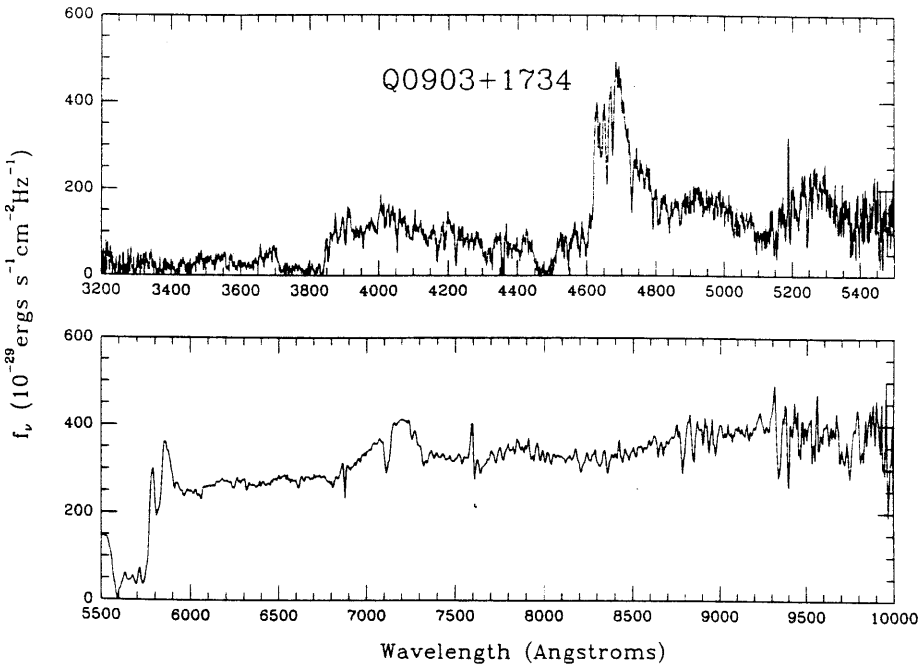
Q0903+1734
f_ν (10^{-29}ergs s^{-1}cm^{-2}Hz^{-1})
Wavelength (Angstroms)

FIG. 1e

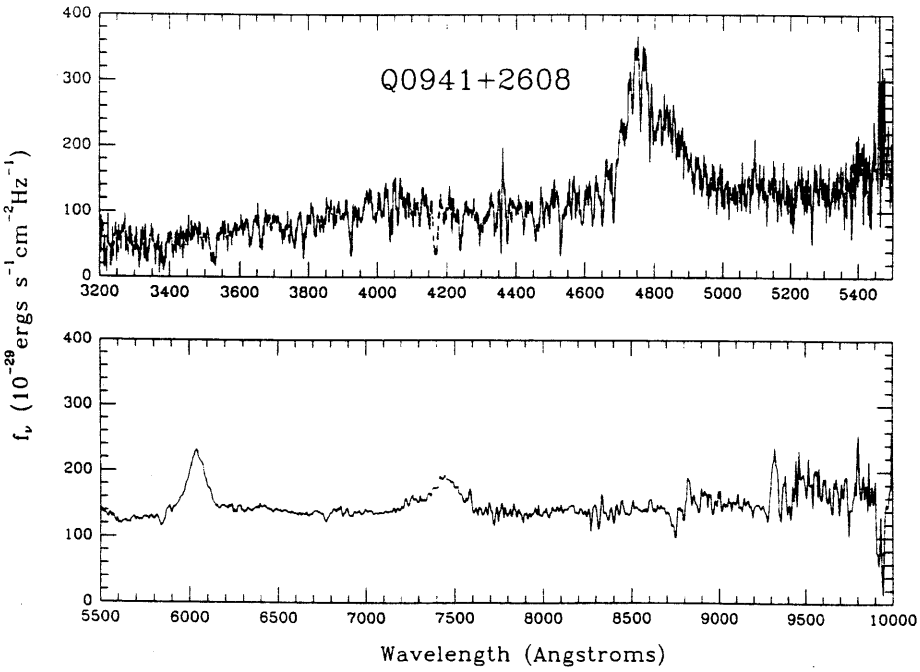
Q0941+2608
f_ν (10^{-29}ergs s^{-1}cm^{-2}Hz^{-1})
Wavelength (Angstroms)

FIG. 1f

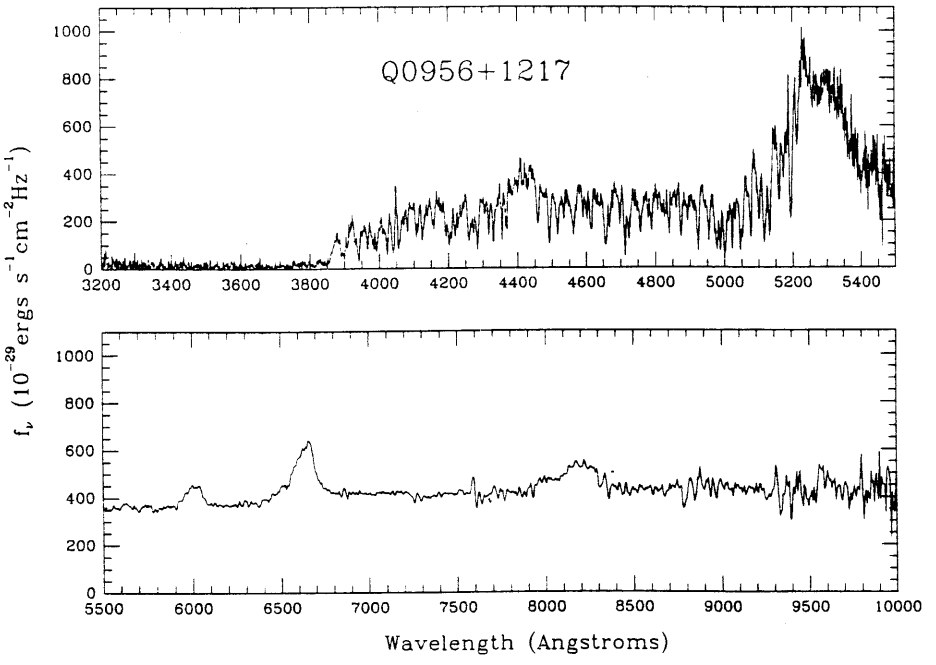
Q0956+1217
f_ν (10^{-29}ergs s^{-1}cm^{-2}Hz^{-1})
Wavelength (Angstroms)

FIG. 1*g*

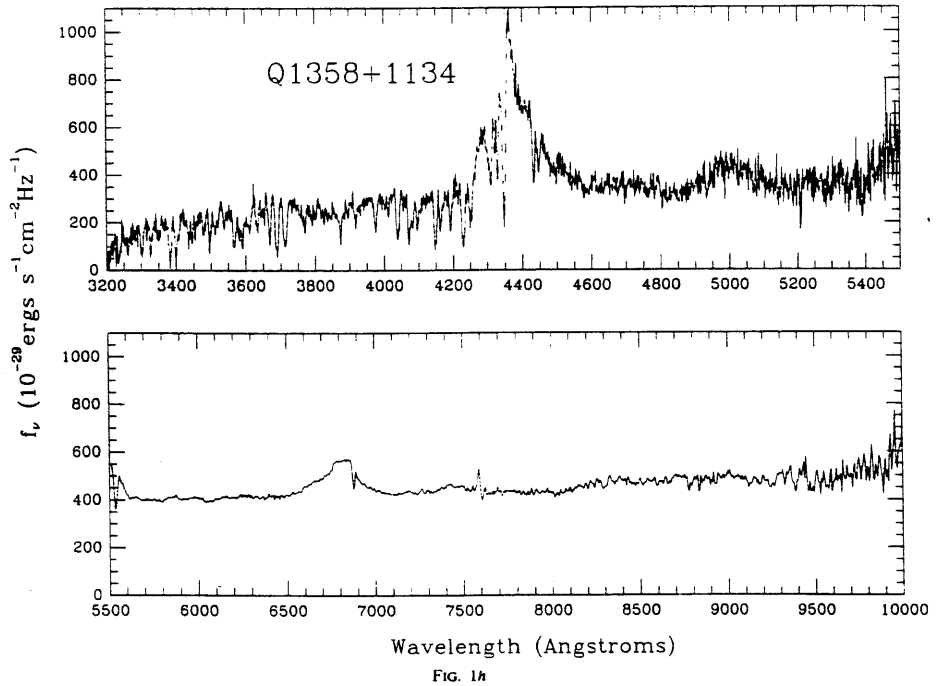
Q1358+1134
f_ν (10^{-29}ergs s^{-1}cm^{-2}Hz^{-1})
Wavelength (Angstroms)

FIG. 1*h*

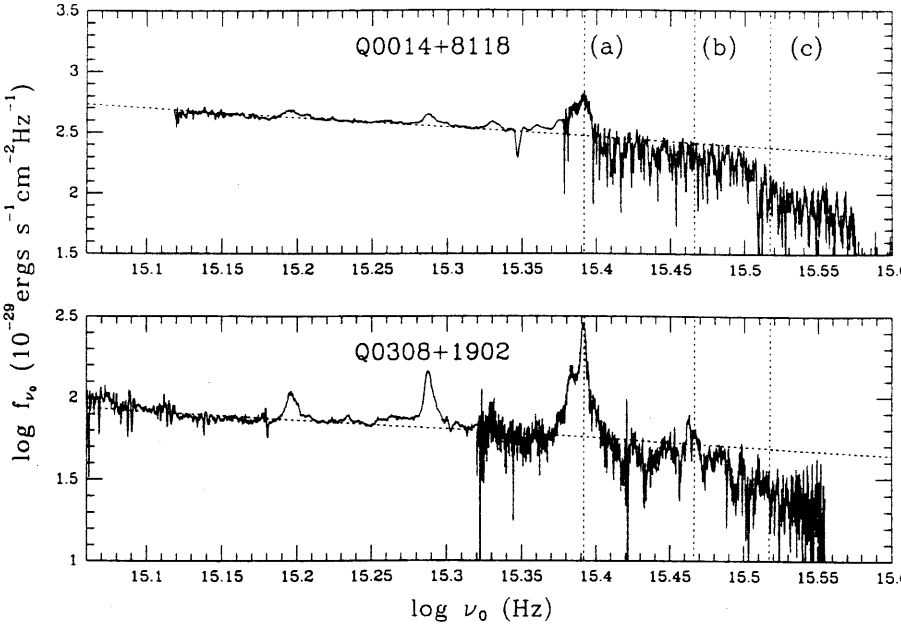

FIG. 2*a*, *b*

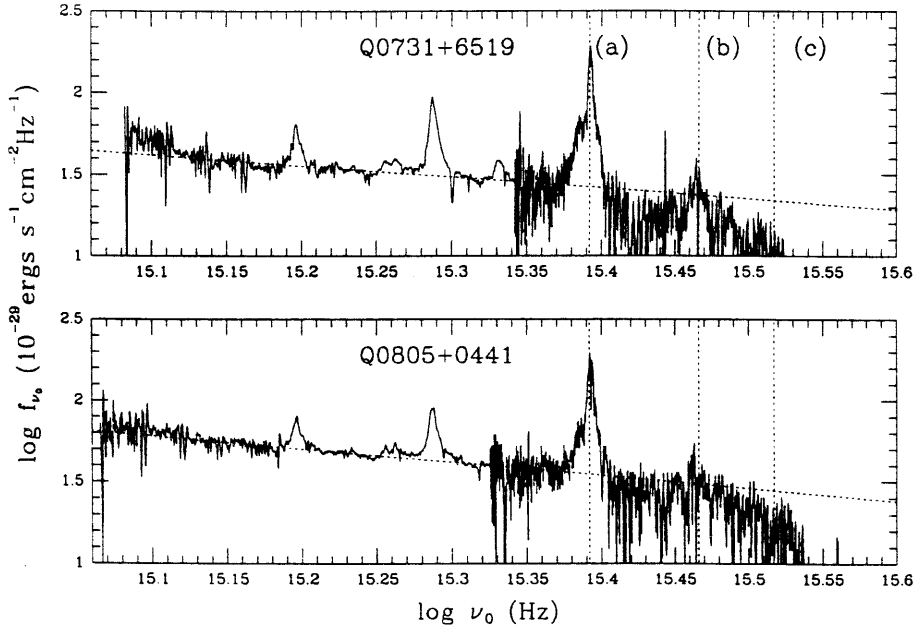

FIG. 2*c*, *d*

FIG. 2.—Plots of the spectral energy distributions for the eight observed quasars. The horizontal dashed line is the adopted continuum. Vertical dashed lines refer to (*a*) Lyα λ1216, (*b*) Lyβ λ1025, (*c*) Lyman limit λ912; f_{ν_0} is the flux per unit rest frequency, with $f_{\nu_0} = f_{\nu_{obs}}/(1 + z_{em})$. The red and blue spectra have been plotted on the same axes without smoothing, hence the noticeable change in the S/N ratio which occurs near log ν_0 = 15.30–15.35.

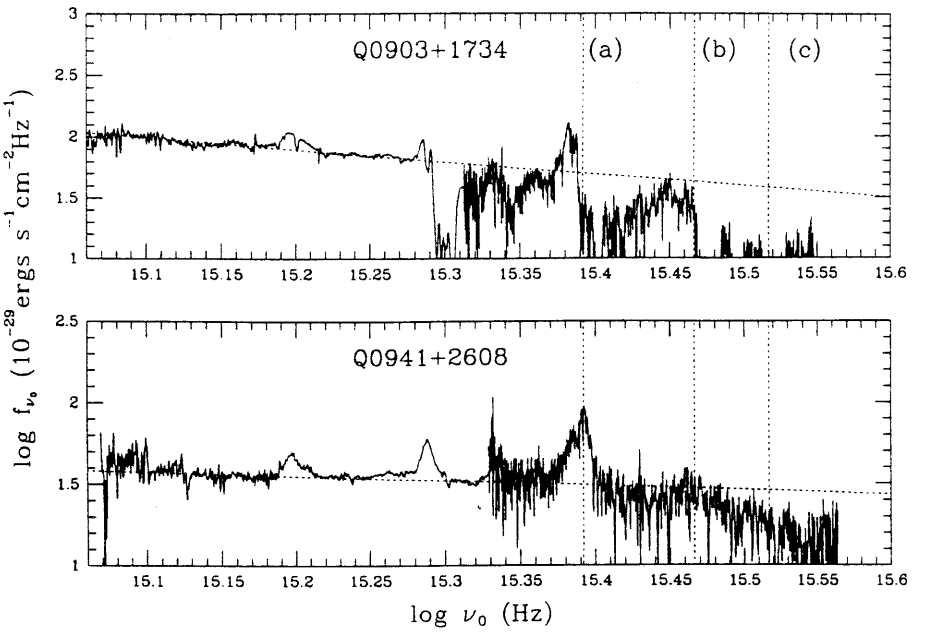

FIG. 2*e*, *f*

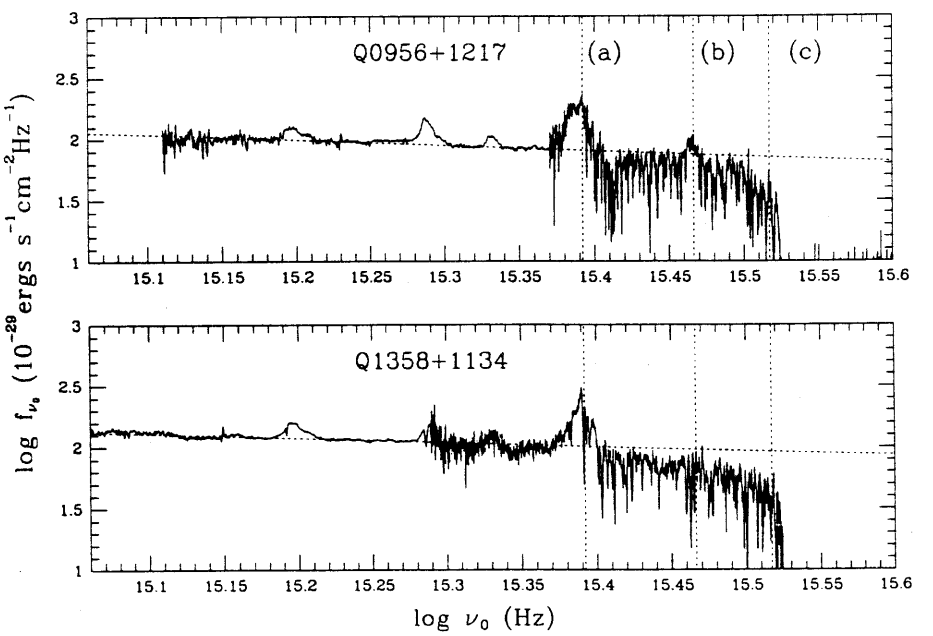

FIG. 2*g*, *h*

TABLE 3

OBSERVED EMISSION-LINE EQUIVALENT WIDTHS AND FLUXES[a]

	O VI + Lyβ[b]		Lyα + N V[c]		Si II + O I[d]		Si IV + [O IV][e]		C IV[f]		He II + O III][g]		N III][h]		C III] + Si III][i]	
OBJECT	W	J	W	J	W	J	W	J	W	J	W	J	W	J	W	J
Q0014+8118.....	...	...	138	3.39	10	0.77	17	1.21	37	2.44	8	0.52	3	0.15	42	2.30
Q0308+1902.....	23	0.45	499	8.43	18	0.28	[15]	[0.24]	103	1.73	15	0.22	5	0.12	88	1.05
Q0731+6519.....	88	0.94	828	7.59	33	0.31	44	0.46	189	1.88	35	0.31	11	0.09	106	0.73
Q0805+0441.....	26	0.51	410	6.57	25	0.37	[18]	[0.28]	144	1.93	42	0.53	13	0.15	87	0.90
Q0941+2608.....	39	0.66	287	4.22	15	0.22	31	0.38	114	1.22	25	0.25	3	0.03	84	0.63
Q0956+1217.....	25	1.03	382	11.34	6	0.19	28	0.85	111	2.89	22	0.53	...	...	67	1.27
Q1358+1134.....	...	...	213	10.19	29	1.24	48	1.88	[35]	[1.38]	5	0.04	...	...	83	2.27

[a] Equivalent widths (W) are measured in Å, and fluxes (J), are in units of 10^{-14} ergs s^{-1} cm^{-2}. Bracketed values are particularly uncertain because of the coincidence of the emission line with the λ5500 Å dichroic.

[b] Lyβ λ1026 + O VI λ1034.

[c] Lyα λ1216 + N V λ1240.

[d] Si II λ1308 + O I λ1304.

[e] Si IV λ1397 + [O IV] λ1406.

[f] C IV λ1549, with possible contribution from N IV] λ1485.

[g] He II λ1640 + O III] λ1663.

[h] N III λ1750.

[i] C III] λ1909 + Si III] λ1892.

b) *Discussion*

Following is a brief discussion of the eight objects observed:

Q0014+8118.—This object (z_{em} = 3.380, m_V = 16.5) is one of the most intrinsically bright quasars known (and is at least 3 times brighter than the next-brightest in our sample). The strengths of the emission lines are unusually small, and the ratio of the intensities of Lyα+N V and C IV is less than half that in any of the other six quasars for which emission lines were measured. The precipitous drop in the continuum level shortward of $\lambda \approx 3480$ Å would seem to indicate a "Lyman limit" system with $z_{abs} \approx 2.82$. Infrared spectrophotometry has been obtained for this object by Kuhr *et al.* (1984).

Q0308+1902.—This object (z_{em} = 2.831, m_V = 18.2) is one from Hazard *et al.* (1986). The Lyα forest appears to be more sparse in this object than in the others observed. This could have been due to a seeing fluctuation during the exposure. If not, this object could present a problem to the intervening hypothesis. It would be useful to obtain high-resolution data for the Lyα forest region of this object.

Q0731+6519.—Photometry and an earlier value for the redshift for this quasar (z_{em} = 3.035, m_V = 18.7) are due to Arp, de Ruiter, and Willis (1979). Some very strong absorption features are evident in the Lyα forest; it is difficult to say with certainty whether this is due to the blending of narrower, weaker features, although the fact that they still approach zero intensity at the center may indicate that they are intrinsically strong. The sharp drop in the continuum level to zero intensity shortward of $\lambda \approx 3600$ Å is evidence for the presence of a "Lyman limit" system with $z_{abs} \approx 2.95$.

Q0805+0441.—This quasar (z_{em} = 2.875, m_V = 18.4) is a 4C radio source (4C 05.34); its absorption spectrum has been studied by Lynds (1971) and by Chen *et al.* (1981), and its continuum and emission-line spectrum have been studied by, e.g., Baldwin (1977), Osmer and Smith (1976), and Oke and Korycansky (1982). Infrared photometry for this object has been obtained by Soifer *et al.* (1983). An earlier value for the redshift was determined by Lynds and Wills (1970). We detect a possible "Lyman limit" system corresponding to the apparent drop in the continuum to zero intensity somewhere between 3300 and 3400 Å, although Tytler (1982) has concluded that, based on the spectrum presented in Chen *et al.* (1981), there is no evidence for such a system.

Q0903+1734.—This broad absorption-line quasar (z_{em} = 2.775, m_V = 18.0) is from Hazard *et al.* (1986) and was included in our sample for comparison purposes. Very broad absorption troughs of C IV, Si IV, N V, and O VI are present in the spectrum. The Lyα emission line is virtually absent because of the strong N V absorption. A detailed study of the absorption spectrum of this object is in preparation.

Q0941+2608.—The continuum energy distribution of this quasar (z_{em} = 2.901, m_V = 18.7) has been studied by Oke and Korycansky (1982), and Soifer *et al.* (1983) have obtained measurements in the infrared. An earlier determination of its redshift was made by Wills and Wills (1976). The N V emission appears to be quite strong relative to Lyα.

Q0956+1217.—This quasar (z_{em} = 3.299, m_V = 17.5) is another from Hazard *et al.* (1986). Like Q0941+2608, it appears to have N V emission which is strong relative to Lyα. The spectrum goes sharply to zero intensity at $\lambda \approx 3850$ Å, indicating a "Lyman limit" system with $z_{obs} \approx 3.22$.

Q1358+1134.—This object (z_{em} = 2.571, m_V = 17.4) was observed despite its failure to meet the redshift criterion because of its brightness and because it was remarked by Hazard *et al.* (1986) that the apparent continuum level in the Lyα forest region of the identification spectrum was especially low. It is also interesting because, in our spectrum, the strength of C III] is greater than that of C IV, whereas the typical ratio C IV/C III] is 2 or greater for five of the other six quasars for which emission lines were measured. The He II emission in this spectrum is also particularly weak as compared to the other quasars in our sample.

IV. CONTINUUM BLANKETING BY NEUTRAL HYDROGEN ABSORPTION

It is clear that the apparent continuum level shortward of Lyα emission in high-redshift quasars will exhibit at least some effects of "blanketing" because of the large number and high density of sharp absorption lines observed in this region, most of which are generally assumed to be Lyα absorption lines due to neutral hydrogen in intervening clouds (e.g., Sargent *et al.*

1980). The magnitude of the blanketing effect will be a function of the instrumental resolution, in the sense that lower resolution will result in a lower apparent continuum level because of unresolved lines. Under the assumption that all of the absorption lines below Lyα emission are due to absorption by neutral hydrogen, there will be three distinct regions, and for each one would expect a different effect on the continuum level:

1. Region I: between Lyα emission and Lyβ (λ_0 = 1025 Å) emission (as defined by the redshift of the other emission lines), we expect only Lyα absorption lines.

2. Region II: between Lyβ emission and the Lyman limit, we expect absorption due to Lyα lines plus Lyβ (and higher order Lyman lines) corresponding to the Lyα lines in Region I.

3. Region III: shortward of the Lyman limit as defined by the emission-line redshift, we expect line absorption from the entire Lyman series (dominated by Lyα and Lyβ), plus Lyman continuum absorption. It is in this region that we see the effects of "Lyman limit" systems—systems with large-enough optical depth in the Lyman lines to cause a sharp discontinuity in the apparent continuum level at the Lyman limit as defined by the redshift of the absorption system.

Strong Lyman limit systems are seen in at least three of the objects studied in this paper, Q0014+8118, Q0731+6519, and Q0956+1217 (see Fig. 1), and possibly in a fourth (Q0805+0441). It is likely that these optically thick clouds which give rise to Lyman limit systems are chiefly responsible for the dramatic change in the observed slope of the continuum in *IUE* spectra of quasars (Bechtold *et al.* 1984). However, such systems cannot affect the apparent continuum level in either region I or region II, but only in region III. The break in the continuum slope in low-resolution spectra of high-redshift quasars is usually seen to correspond to Lyα emission, so something is clearly occurring in regions I and II. We will concentrate our analysis on these two regions of the quasar spectra.

With our moderate resolution ($\sim$6 Å) in the UV, the apparent continuum level in regions I and II, if affected by line blanketing, is likely to be much closer to the true continuum level than, for example, in *IUE* or multichannel spectra. The continua of two of our observed quasars, Q0941+2608 and Q0805+0441, have been studied previously by Oke and Korycansky. It is significant that, while our absolute continuum flux (at log ν_0 = 15.240) agrees very well with Oke and Korycansky for Q0941+2608 and reasonably well (0.2 mag difference) for Q0805+0441, the spectral indices we obtain are quite different. We attribute this to two factors. One is that, in the observed wavelength range (which is the same as in Oke and Korycansky), there is very little continuum that is uncontaminated by emission-line wings, and with low-resolution (160 Å in the red for Oke and Korycansky) it is doubtful whether any of the data points represents true continuum. In addition, for observed wavelengths above 7500 Å, strong atmospheric features are present which can be removed fairly well with data sampled every 6 Å but which cause very large scatter in the data points with very low resolution. Thus, defining a continuum slope on the long wavelength side of Lyα emission becomes very difficult for low-resolution spectra. We tried binning our data into 100 Å bins and remeasuring the apparent continuum slope and obtained values which differed from the higher resolution values by as much as 30% (and this is without the large scatter of the points at long wavelengths such as was present in the Oke and Korycansky data). We conclude that some degree of spectral resolution is necessary even longward of Lyα emission in order to accurately determine the spectral index and the true continuum level, and in this respect our data should represent a significant improvement; furthermore, our data have a much higher S/N ratio, especially at longer wavelengths, making the definition of the continuum considerably less uncertain.

In order to gauge the magnitude of the effect that 6 Å resolution would have on the true continuum level, we have performed some experiments on high-resolution (0.6 Å) observations obtained in 1985 of three high-redshift quasars. The typical rest frame wavelength range covered in these observations is 1050–1200 Å (region I). Using a Gaussian smoothing function, the data were smoothed to $\sim$6 Å resolution, and the relative apparent continuum levels were compared. Figure 3 shows a plot of some of the high-resolution data with the smoothed data plotted on the same set of axes. We found that, for the three high-redshift quasars (z_{em} = 3.33, 3.53, and 3.56), the drop in the apparent continuum level is $\sim$12%–15% for the 6 Å resolution smoothed spectra. This corresponds to $\sim$0.05 in logf_{ν_0}. Looking at Figure 2, with the exception of the broad absorption-line quasar Q0903+1734, the continua of the quasars at frequencies higher than that of Lyα emission, in region I, are consistent with the power-law continua defined to the red of Lyα emission if the above correction for the continuum blanketing factor at 6 Å resolution is applied. This correction is, of course, by no means exact; the resolution for the various spectra is not constant because of fluctuations in the seeing, and the size of the correction is also based upon observations of objects with higher redshifts (on average) than for our sample. However, it is evident by visual inspection of the plots in Figure 2 that for most of the objects, the continuum level in Region I appears to be consistent with the drawn-in power-law continuum even without the application of a blanketing correction. Figure 3 shows that for low-resolution data the apparent continuum level is *significantly* reduced (by as much as 30%–35%) because of the presence of unresolved sharp absorption lines. This would help explain the observed break in the continuum slope in *IUE* spectra which seems to occur just shortward of Lyα emission. The fact that a change in *slope*, rather than a discontinuity, is observed may be ascribed to the smoothing effect of low-resolution spectroscopy and the fact that there are more and more possible contributors to the continuum blanketing as the frequency increases. The decrement in flux relative to the extrapolated continuum might therefore appear to be a smooth, increasing function of frequency that can be fit by a simple power law.

Thus it appears that the true continuum in region I of the Lyα forest can be represented by the extrapolation of the power-law continuum defined longward of Lyα emission and that the apparent change in the slope shortward of Lyα emission which has been observed in low-resolution quasar spectra is due to the blanketing effects of numerous unresolved absorption lines (presumably of neutral hydrogen). We will assume (for the moment) that the extrapolated power-law continuum is the true continuum in region II as well, and that the further deviation of the apparent continuum level in this region relative to the extrapolated continuum is due to the presence of Lyβ (and higher order lines of the Lyman series) in addition to the Lyα absorption lines. This will be discussed further in § V. It should be noted that the effect of low-resolution on the apparent continuum level shortward of Lyα emission is very important when one is studying continua as representing the

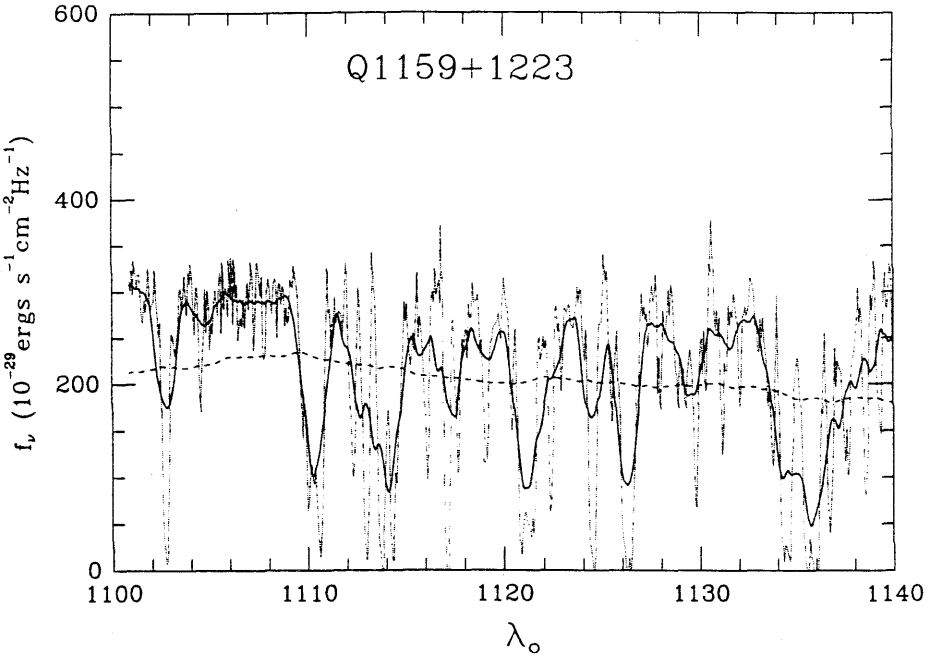

FIG. 3.—The effects of the variation of spectral resolution on the apparent continuum level in the Lyα forest. The dotted curve is a spectrum with 0.6 Å resolution, the solid curve is the same data smoothed (with a Gaussian) to ~6 Å resolution, and the dashed curve is the data smoothed to ~100 Å resolution.

inherent spectral energy distribution for quasars. Although X-ray observations of quasars indicate that the spectral index must steepen somewhere between the ultraviolet and the X-ray, it is not at all clear that this steepening occurs at frequencies which are accessible to either optical or *IUE* observations. The *apparent* observed steepening in the Lyα forest region of high-redshift quasar spectra may be completely unrelated to the energetics of the "central engine" of the quasar. It is therefore dangerous to use *IUE* spectral energy distributions without adequate corrections for Lyman line and continuum absorption in the ultraviolet. The implications of neutral hydrogen continuum blanketing for the modeling of quasars will be discussed in § VI.

V. A TEST OF THE "INTERVENING" HYPOTHESIS

Assuming that the true continuum in the Lyα forest region of the spectra of high-redshift quasars can be represented by the extrapolated power-law continuum as discussed above, we can examine the statistics of the neutral hydrogen absorption lines without necessarily needing to resolve them and count them. The total flux decrement due to the cumulative effects of absorption lines below Lyα emission is preserved regardless of the spectral resolution. For comparison, we will make use of several parameters introduced by Oke and Korycansky: D_A, D_B, and D_B/D_A. The parameter D_A is essentially the fraction of the flux that has been subtracted from the spectrum according to the extrapolated true continuum in region I:

$$D_A \equiv \left\langle 1 - \frac{f_{\rm obs}}{f_{\rm cont}} \right\rangle , \qquad (1)$$

where $f_{\rm obs}$ is the observed flux in each bin and $f_{\rm cont}$ is the true continuum level which would correspond to that bin. Regions of the spectrum which may be affected by Lyα or O VI + Lyβ emission-line wings are excluded from the calculation. The parameter D_B is the analogous quantity measured in region II of the spectra.

Calculated values D_A, D_B, and D_B/D_A are listed in Table 2. For the sample as a whole, we find $D_A = 0.24 \pm 0.05$, $D_B = 0.36 \pm 0.07$, and $D_B/D_A = 1.52 \pm 0.12$, where we have excluded Q0903 + 1734 from the calculations of the mean values because of the presence of broad absorption troughs in its spectrum. These values are consistent with the values found by Oke and Korycansky for their sample of high-redshift quasars, although we point out a possible error in their quotation of standard deviations in the mean. They claim to have obtained $D_A = 0.29 \pm 0.02$, $D_B = 0.39 \pm 0.02$, and $D_B/D_A = 1.40 \pm 0.06$, but in reevaluating the standard deviations based on their tabulated values, we find that their data give $D_A = 0.29 \pm 0.07$, $D_B = 0.39 \pm 0.08$, and $D_B/D_A = 1.40 \pm 0.24$. We attribute the much larger standard deviation in D_B/D_A obtained by Oke and Korycansky to greater uncertainties in defining the continuum slope for data having relatively low resolution and S/N ratio. For the two objects which both this paper and Oke and Korycansky have studied, Q0805 + 0441 and Q0941 + 2508, our values of D_A are significantly smaller, while our values of D_B are consistent with those of Oke and Korycansky. These disagreements are probably due to differences in the adopted continuum levels and in the measured spectral indices α. A systematic tendency with low-resolution data might be to draw the continuum too high because of the effects of emission-line

wings longward of Lyα emission, resulting in larger values of D_A and D_B.

In order to determine whether the values of D_A and D_B we have obtained are consistent with the "intervening" hypothesis, we estimate the expected uncertainty involved in the measurement of an individual value of D_A assuming that the hypothesis is true. If the Lyα forest is due to a population of clouds distributed isotropically throughout space, then not only measurement uncertainties, but also statistical fluctuations in the number of clouds encountered along a line of sight will contribute to the standard deviation in individual values of D_A. We concentrate on the parameter D_A because its value would be most directly linked to the number of intervening clouds (presumably each cloud is responsible for one Lyα absorption line), because *only* Lyα absorption is presumed to be contributing to the value and because many statistical studies of Lyα lines have been made. We estimate that, for a typical quasar in our sample, with $z_{em} \approx 3.0$ and $\alpha \approx 0.7$ (and uncertainties in α of ± 0.05), the expected standard deviation in D_A from measurement uncertainties alone is ± 0.05. Assuming that the "intervening" hypothesis is correct, we adopt the Lyα equivalent width distribution function of Sargent *et al.* (1980, hereafter SYBT):

$$n(W) = \frac{N^*}{W^*} \exp\left(\frac{-W}{W^*}\right), \tag{2}$$

where N^* and W^* are constants. SYBT found that $N^* = 154 \pm 11$ and $W^* = 0.362 \pm 0.02$ for their sample which has $\langle z_{abs} \rangle = 2.44$. This includes Ly$\alpha$ lines identified as part of "heavy element" absorption systems and was derived for $W > 0.32$ Å. We will assume that the distribution can be extrapolated to smaller equivalent widths. A typical quasar from our sample has $\langle z_{abs} \rangle \approx 2.64$ for the region of the spectrum where D_A is measured. It has become the convention to express the line density as a function of redshift; the density of Lyα lines evolves with z according to

$$\frac{dN}{dz} \propto (1+z)^{\gamma}. \tag{3}$$

The value of γ is a matter of dispute; we have adopted the most recent determination, from Murdoch *et al.* 1986, $\gamma = 1.79 \pm 0.35$ (including Lyα lines from known "heavy element" systems). Since the value of W^* obtained when the Lyα lines from heavy element systems are included by Murdoch *et al.* agrees well with the SYBT result, we will use $W^* = 0.36$. Taking SYBT's value of N^* and scaling it by equation (3) to $\langle z_{abs} \rangle = 2.64$, we obtain $N^* \approx 170$. For a typical quasar in our sample with $z_{em} \approx 3.0$, the interval of redshift covered in the region where D_A is measured is $\Delta z_{abs} \approx 0.38$. Equation (2) can then be integrated to obtain an estimate of the total equivalent width of Lyα absorption lines in the redshift range $\Delta z_{abs} = 0.38$ centered on $z_{abs} = 2.64$:

$$W_{tot} \approx \frac{170}{0.36}(0.38)\int_0^{\infty} W e^{-W/0.36} dW \approx 24 \text{ Å}. \tag{4}$$

Several workers have found that this exponential law of SYBT does not hold for equivalent widths smaller than ~ 0.3 Å (e.g., Murdoch *et al.* 1986; Atwood, Baldwin, and Carswell 1985; Carswell *et al.* 1984), in the sense that there are more weak lines than would be predicted by an extrapolation of the exponential distribution with $W^* \approx 0.16$ for $W \geq 0.033$ Å, and use this in the region $0 \leq W \leq 0.32$, where this second exponential distribution has been normalized so that it connects with the SYBT distribution at $W = 0.32$ Å, then the expected total equivalent width would be increased to ~ 25 Å. Clearly the total equivalent width is fairly insensitive to the behavior of the equivalent width distribution for very weak lines.

The rest wavelength interval corresponding to $\Delta z_{abs} = 0.38$ for a quasar with $z_{em} = 3.0$ is ~ 115 Å. Thus the *predicted* value of D_A would be $1 - 90/115 \approx 0.22$. Our result of $D_A = 0.24 \pm 0.05$ is consistent with this estimate. The fact that the mean value of D_A which we find is somewhat larger than that expected according to the empirically derived Lyα equivalent width spectrum might be partially explained by the presence of "metal" lines, e.g., lines of Mg II of Fe II from absorption systems at lower redshifts.

We can also estimate the expected deviation in total equivalent width according to the adopted equivalent width distribution. We find that $\sigma(W_{tot}) \approx 7$ Å, which, when folded in with the measurement uncertainties estimated above, gives $\sigma(D_A) \approx 0.07$. Statistical deviations alone would give $\sigma(D_A) \approx 0.06$. We have performed a χ^2 test on the data assuming a parent Gaussian distribution with $\langle D_A \rangle = 0.24$ and $\sigma(D_A) = 0.07$, and the resulting value of the reduced χ^2 is 0.87, corresponding to a probability of ~ 0.60 that a random sampling of the distribution would result in a reduced χ^2 as large or larger than is found. Thus, our data are consistent with the value of D_A being statistically the same in all of the objects. This supports the idea that the distribution of Lyα clouds is cosmological and the same along all lines of sight and that it is unlikely that the gas responsible for the Lyα forest absorption is associated with the quasar.

If the number density of Lyα lines does not evolve with redshift, then one would clearly expect the value of D_B to be larger than the value of D_A; however, as has already been pointed out, recent work (e.g., Murdoch *et al.* 1986) suggests quite rapid evolution with redshift (this seems to preclude a constant comoving density of absorbing clouds, regardless of the cosmological model), and the number of Lyα absorption lines per unit redshift in region II would be significantly smaller than in region I. For a quasar with $z_{em} = 3.0$, the mean redshift for a Lyα line in the part of region II where D_B is measured is $\langle z_{abs} \rangle \approx 2.18$. Using equation (3) and the Murdoch *et al.* value for γ, the Lyα line densities at the center of the frequency ranges where D_B and D_A are measured should be in the ratio 0.79:1. The ratio of oscillator strengths for Lyβ and Lyα is 0.19:1. Assuming we would find one Lyβ line in the D_B region for every Lyα line in the D_A region and assuming negligible contributions to the total equivalent width from higher order lines of the Lyman series, then if all lines were unsaturated, we might expect $D_B/D_A \leq 1$ because the evolution of the Lyα line density would more than account for the additional 20% contribution in total equivalent width due to Lyβ lines. Oke and Korycansky derived a characteristic value of the Doppler broadening parameter b (Spitzer 1978) based on their measured value of $\langle D_B/D_A \rangle$; however, they assumed that the density of Lyα lines in the D_A and D_B regions of the spectrum was the same. With evolution added, their analysis would imply that $\langle b \rangle$ is significantly less than 20 km s^{-1} in order to produce our observed $\langle D_B/D_A \rangle = 1.52$. Such a low value of $\langle b \rangle$ seems unlikely (e.g., Carswell *et al.* 1984).

The relatively high value of $\langle D_B/D_A \rangle$ which we observe is clearly inconsistent with the lines being unsaturated; i.e., most of the lines are probably well off the linear part of the curve of

growth. This in turn implies that the strengths (relative to Lyα) of the higher order Lyman lines are greater than is implied by their relative oscillator strengths. Thus it may be inappropriate to assume that the contribution of these lines to the total equivalent width in the D_B region is negligible. There is also the rather puzzling problem that, although the number density of Lyα lines is observed to be proportional to $(1 + z)^\gamma$ and $\gamma \approx 2$ when the Lyα forests of objects of different redshifts are studied, the reverse trend is sometimes observed for an individual object. That is, the number density of Lyα lines per unit redshift is seen to *decrease* with increasing z_{abs}. This problem is discussed by Murdoch *et al.* (1986). The favored interpretation of this phenomenon is an enhancement of the ionizing radiation field in the vicinity of intrinsically bright quasars, thereby decreasing the column density of neutral hydrogen in clouds physically closer to the quasar. Such an effect would tend to decrease the observed value of D_A relative to D_B. Thus, because of the uncertainty in the relative contributions of the Lyα, Lyβ, and higher order Lyman lines to the total equivalent width in the D_B region, it does not seem feasible to estimate values of physical parameters (such as $\langle b \rangle$) in the "Lyα clouds" based on the observed ratio $\langle D_B/D_A \rangle$.

An alternative interpretation of the large observed value of $\langle D_B/D_A \rangle$ would be that there *is* some intrinsic steepening in the quasar continua which occurs shortward of Lyβ, in region II. Since the physics of the "Lyα clouds" is not well understood, it is not clear how much of the flux decrement in region II is due to optically thick radiative transfer effects, or even whether one can account for such a large decrement (especially when evolution of the Lyα line density is considered) using plausible physical parameters in the clouds. Therefore, whether or not the continuum slope as defined longward of Lyα emission can be extrapolated as far down as the Lyman limit is not well determined.

It should be noted that there is no observed break in the ultraviolet continuum of low redshift ($z_{em} \approx 0.5$) quasars (Kinney *et al.* 1985) observed with *IUE*. If the empirically derived number density of Lyα absorption lines per unit redshift can be extrapolated to such low redshifts, the expected value of D_A would be ~ 0.035, and the true spectral energy distribution, at least in regions I and II, should be accurately represented in low-resolution data. However, the fact that a significant continuum depression ($D_A = 0.11 \pm 0.05$) is observed even for moderately low redshift ($z_{em} \approx 1.0$) by Bechtold *et al.* (1984) may represent evidence for deviations from the power-law spectrum of Lyα line density at low redshifts in the sense that there may be more lines at low redshift than would be expected. (A simple extrapolation using $\gamma = 1.79$ would predict $D_A \approx 0.06$ for $z_{em} \approx 1.0$.)

VI. IMPLICATIONS FOR QUASAR MODELS

The mean value of the spectral indices we measure for the eight quasars is $\langle \alpha \rangle \approx 0.6$. This is consistent with what has been observed previously for large samples of quasars measured in the optical and infrared (e.g., Richstone and Schmidt 1980; Neugebauer *et al.* 1979; Richstone 1977; Oke *et al.* 1970). The observed values of α range from -0.3 to $+3.0$ (Richstone and Schmidt 1980, hereafter RS). However, it has been suggested (Malkan and Sargent 1982) that measured power laws based solely on a fairly narrow range of frequency (i.e., the optical/UV) can be much flatter than the power law which would be found if observations over a broad range of frequency were made. They connect the infrared region of the spectrum to the X-ray with an underlying, presumably nonthermal, power law of the form $f_\nu \propto \nu^{-1}$, with a departure from the power law in the optical and UV which results in measured continua which are flatter than ν^{-1}. Malkan and Sargent explain this "UV excess," which is a broad component of flux above the ν^{-1} infrared power law which begins below ~ 6000 Å and continues well into the ultraviolet, as a combination of Balmer continuum emission and thermal emission from a hot ($T \approx 20{,}000$–$30{,}000$ K) gas, perhaps in an accretion disk surrounding a massive black hole. This interpretation is supported by the more recent work of Elvis *et al.* (1986), who have combined observations in the infrared, optical, UV, and X-ray for eight PG quasars. Malkan and Sargent also conclude that the steepening in the spectra of quasars above $\nu_0 = 2 \times 10^{15}$ Hz is due to the exponential cutoff of the thermal component (modeled as a single-temperature blackbody). We have shown that much of the apparent steepening beyond this frequency may be due to absorption by intervening material and may be unrelated to the quasar itself. Thus, if one attributes the "UV excess" (in the ultraviolet, where the Balmer continuum contribution is small) to thermal emission from a hot blackbody (e.g., an idealized accretion disk), then the characteristic temperature which is obtained based on fits to the observed spectral energy distribution may be too low. That is, ambiguities as to the true shape of the ultraviolet continuum caused by absorption in intervening material prevent the setting of sound upper limits on the temperature of the gas which is presumably responsible for the "UV excess." If models of optically thick accretion disks are used, as by Malkan (1983), this would affect the deduced values of the black hole mass and the mass infall rate.

If it is assumed that the ultraviolet spectra of all quasars are comprised of an underlying nonthermal ν^{-1} power law with the addition of a thermal component, then the spectral index for the ultraviolet continuum (which we have measured) should provide some information concerning that thermal spectrum and its contribution to the total spectral energy in the ultraviolet. The fairly large range of spectral indices which we and other investigators have found would then seem to imply a significant difference in the shape and in the relative contribution of the thermal components from quasar to quasar, even though (for our sample) the total quasar luminosities are comparable. This is consistent with the fact that no correlation is observed between optical/UV spectral indices and luminosity for quasars (RS). Also, Malkan (1983) found no correlation between quasar luminosity and the ratio of thermal to nonthermal components of the observed flux. The distribution of spectral indices in Figure 3 of RS shows the vast majority of values to be in the range $0 \leq \alpha \leq 1$ (using our definition of α); this may indicate upper and lower limits on the contribution of the thermal component to the spectral energy in the optical/UV region of quasar spectra. That is, quasars with spectral indices near 1 have a weak thermal component (relative to the underlying nonthermal power law), and those with $\alpha \approx 0$ (or even $\alpha < 0$) are dominated by a strong thermal component. Such an interpretation is consistent with the fact that quasars with steep optical/UV continua are more often highly polarized violently variable, or both (Nordsieck 1976; Oke *et al.* 1970), possibly indicating the lack of a large amount of thermal material surrounding the black hole. Those quasars which have relatively flat ultraviolet continua would be those with a large amount of optically thick material whose emission dominates over the nonthermal component in the ultraviolet region

of the spectrum, and therefore little polarization or variability is observed.

VII. SUMMARY

We have studied the spectral energy distributions of eight very high redshift ($z_{em} \geq 2.7$) quasars in the observed wavelength range 3200–10,000 Å with moderate spectral resolution. Our primary conclusions are the following.

1. The true continuum level in the Lyα forest region of quasar spectra can be represented by an extrapolation of the power-law continuum defined longward of Lyα emission. This conclusion becomes less certain below $\lambda_0 = 1040$ Å.

2. The diminution of flux due to the cumulative effects of absorption lines in the spectra of quasars with $z_{em} \approx 3$ between Lyα emission and Lyβ is statistically the same for all objects ($24\% \pm 5\%$), supporting the hypothesis that the absorption is due to cosmologically distributed objects (Sargent *et al.* 1980). The corresponding decrement of flux between Lyβ and the Lyman limit is $36\% \pm 7\%$.

3. The ultraviolet spectral steepening which has been observed in *IUE* spectra of quasars may be largely or completely due to absorption by intervening material, therefore intrinsic ultraviolet spectral energy distributions cannot be well defined.

We would like to thank A. Filippenko for help with the observations, as well as J. Henning, C. Price, S. Staples, and D. Tennant for their assistance at Palomar Observatory. We thank R. Blandford and S. Phinney for useful discussions and suggestions and referee M. Malkan for very helpful comments on the original version of this paper. This work has been supported by NSF grant AST 84-16704.

REFERENCES

Arp, H., de Ruiter, H. R., and Willis, A. G. 1979, *Astr. Ap.*, **77**, 86.
Atwood, B., Baldwin, J. A., Carswell, R. F. 1985, *Ap. J.*, **292**, 58.
Baldwin, J. A. 1977, *Ap. J.*, **214**, 679.
Bechtold, J., Green, R. F., Weymann, R. J., Schmidt, M., Estabrook, F. B., Sherman, R. D., Wahlquist, H. D., and Heckman, T. M. 1984, *Ap. J.*, **281**, 76.
Burstein, D., and Heiles, C. 1982, *A.J.*, **87**, 1133.
Carswell, R. F., Morton, D. C., Smith, M. G., Stockton, A. N., Turnshek, D. A., and Weymann, R. J. 1984, *Ap. J.*, **278**, 486.
Chen, J., Morton, D. C., Peterson, B. A., Wright, A. E., and Jauncey, D. L. 1981, *M.N.R.A.S.*, **196**, 715.
Elvis, M., *et al.* 1986, *Ap. J.*, **310**, 291.
Filippenko, A. V. 1982, *Pub. A.S.P.*, **94**, 715.
Filippenko, A. V., and Greenstein, J. L. 1984, *Pub. A.S.P.*, **96**, 581.
Hazard, C., Morton, D. C., McMahon, R. G., Sargent, W. L. W., and Terlevich, R. 1986, *M.N.R.A.S.*, submitted.
Kinney, A. L., Huggins, P. J., Bregman, J. N., and Glassgold, A. E. 1985, *Ap. J.*, **291**, 128.
Kuhr, H., Liebert, J. W., Strittmatter, P. A., Schmidt, G. D., and Mackay, C. 1983, *Ap. J. (Letters)*, **275**, L33.
Kuhr, H., McAlary, C. W., Rudy, R. J., Strittmatter, P. A., and Riecke, G. H. 1984, *Ap. J. (Letters)*, **284**, L5.
Lynds, C. R. 1971, *Ap. J. (Letters)*, **164**, L73.
Lynds, C. R., and Wills, D. 1970, *Nature*, **226**, 532.
Malkan, M. A. 1983, *Ap. J.*, **268**, 582.
Malkan, M. A., and Sargent, W. L. W. 1982, *Ap. J.*, **254**, 22.
Murdoch, H. S., Hunstead, R. W., Pettini, M., and Blades, J. C. 1986, *Ap. J.*, **309**, 19.
Nandy, K., Thompson, G. I., Jamar, C., Monfils, A., and Wilson, R. 1975, *Astr. Ap.*, **44**, 195.
Neugebauer, G., Oke, J. B., Becklin, E. E., and Matthews, K. 1979, *Ap. J.*, **230**, 79.
Nordsieck, K. H. 1976, *Ap. J.*, **209**, 653.
Oke, J. B. 1982, *Pub. A.S.P.*, **94**, 580.
Oke, J. B., and Gunn, J. E. 1983, *Ap. J.*, **266**, 713.
Oke, J. B., and Korycansky, D. G. 1982, *Ap. J.*, **255**, 11.
Oke, J. B., Neugebauer, G., and Becklin. E. E. 1970, *Ap. J.*, **159**, 341.
Osmer, P. S. 1979, *Ap. J.*, **227**, 18.
Osmer, P. S., and Smith, M. G. 1976, *Ap. J.*, **210**, 267.
Richstone, D. O. 1977, *Ann. N.Y. Acad. Sci.*, **302**, 611.
Richstone, D. O., and Schmidt, M. 1980, *Ap. J.*, **235**, 361 (AS).
Sargent, W. L. W., Young, P. J., Boksenberg, A., and Tytler, D. 1980, *Ap. J. Suppl.*, **42**, 41 (SYBT).
Seaton, M. J. 1979, *M.N.R.A.S.*, **187**, 73P.
Shectman, S. A. 1982, in *Ann. Rept. Dir. Mt. Wilson and Las Campanas Obs.* (Carnegie Institute of Washington), pp. 676–677.
Soifer, B. T., Neugebauer, G., Oke, J. B., Matthews, K., and Lacy, J. H. 1983, *Ap. J.*, **265**, 18.
Spitzer, L., Jr. 1978, *Physical Processes in the Interstellar Medium* (New York: Wiley), p. 51.
Tytler, D. 1982, *Nature*, **298**, 427.
Veron-Cetty, M.-P., and Veron, P. 1985, *A Catalogue of Quasars and Active Nuclei* (2d ed.), ESO Scientific Rept. No. 4.
Wills, D., and Wills, B. J. 1976, *Ap. J. Suppl.*, **31**, 143.

W. L. W. SARGENT and C. C. STEIDEL: Palomar Observatory, 105-24, California Institute of Technology, Pasadena, CA 91125

THE ASTROPHYSICAL JOURNAL, 318:L11–L13, 1987 July 1

A NEW UPPER LIMIT ON THE DENSITY OF GENERALLY DISTRIBUTED INTERGALACTIC NEUTRAL HYDROGEN

CHARLES C. STEIDEL AND WALLACE L. W. SARGENT
Palomar Observatory, California Institute of Technology
Received 1987 March 30; accepted 1987 April 22

ABSTRACT

A new upper limit on the number density of generally distributed intergalactic neutral hydrogen is obtained based upon recent spectrophotometric observations of very high redshift QSOs coupled with high-resolution statistical studies of the Lyα forest in QSOs. The new limit, $n_{\rm H\,I}$ $(z = 0.0) < 9.0 \times 10^{-14} h_{100}$ cm^{-3}, is approximately 15 times smaller than the limit originally proposed by Gunn and Peterson. If the intergalactic medium (at $z = 2.64$) is in ionization equilibrium due to the UV background, then this new limit implies $n_{\rm H}$ $(z = 0.0) < 4.6 \times 10^{-7} h_{100}$ cm^{-3} and $\Omega_{\rm H} < 0.05 h_{100}^{-1}$.

Subject headings: galaxies: intergalactic medium — quasars

I. INTRODUCTION

Shortly after the discovery of the first QSO whose redshift placed Lyα emission in the optical spectrum (Schmidt 1965), Gunn and Peterson (1965) showed that any generally distributed intergalactic neutral hydrogen would produce a depression in the QSO continuum on the short wavelength side of Lyα emission because of Lyα absorption. By examining Schmidt's spectrum of 3C 9 ($z_{\rm em} = 2.016$), they concluded that the integrated optical depth in Lyα, $\tau_{\rm GP}$, was less than or of order 0.5. The optical depth $\tau_{\rm GP}$ can be related to the number density of neutral hydrogen through the relation

$$\tau_{\rm GP}(z) = \frac{n_{\rm H\,I}(z)}{(1+z)(1+2q_0z)^{1/2}}\left(\frac{\pi e^2 f}{m\nu_\alpha H_0}\right)$$

$$= \frac{4.14 \times 10^{10} h_{100}^{-1} n_{\rm H\,I}(z)}{(1+z)(1+2q_0z)^{1/2}}, \qquad (1)$$

where h_{100} is the Hubble constant in units of 100 km s^{-1} Mpc^{-1}. Thus, for $q_0 = 1/2$, they obtained an upper limit on the number density of intergalactic neutral hydrogen of $n_{\rm H\,I}(z = 2) \approx 6 \times 10^{-11} h_{100}$ cm^{-3}.

More recently, Davidson, Hartig, and Fastie (1977) used observations of 3C 273 ($z_{\rm em} = 0.158$) obtained by a rocket-borne telescope for a similar analysis. They found no evidence for a trough in the continuum on the short wavelength side of Lyα emission. They estimated that $\tau_{\rm GP} < 0.2$, which corresponds to a limit on the H I density (at the present epoch) of $n_{\rm H\,I} < 3.9 \times 10^{-12}$ cm^{-3}.

After Lynds (1971) identified the large number of absorption lines seen on the short wavelength side of Lyα emission in the spectra of high redshift QSOs as discrete Lyα absorption lines, the Gunn–Peterson test received little attention in the literature. The new focus was on the origin and evolution of what are now believed to be the intergalactic H I clouds responsible for the narrow Lyα absorption lines (Sargent *et al.* 1980). Also, the Lyα forest presents a problem for the Gunn–Peterson test because the rich absorption-line spectrum shortward of Lyα emission makes the definition of the true continuum in that region very difficult, and it is therefore hard to separate the effects of absorption in discrete "clouds" from absorption due to generally distributed gas. Recently, however, Steidel and Sargent (1987) have obtained spectra of a sample of QSOs with $z \approx 3$ for which very accurate continua on the long wavelength side of Lyα emission can be extrapolated to the short wavelength side and thus, we believe, a new and much smaller limit can be placed on the density of intergalactic neutral hydrogen.

II. THE NEW LIMIT

There are several difficulties encountered in attempting to measure small continuum changes from QSO spectra. One is that there is a compromise between resolution and obtaining an accurate continuum level; with high-resolution data, the apparent local continuum is likely to be more certain because line blanketing and blending will not be as important, but the more global continuum slope cannot be considered accurate because of light losses due to narrow slits and the effects of atmospheric dispersion, and the relatively small spectral coverage. For low-resolution data, the apparent continuum level can be greatly affected by unresolved absorption lines.

Steidel and Sargent (1987) obtained spectra of eight high-redshift QSOs ($\langle z_{\rm em} \rangle = 2.98$) with simultaneous spectral coverage from 3200 to 10000 Å and moderate resolution (one of the QSOs has been excluded for our purposes because it is a broad absorption line QSO). The spectra were taken through a wide slit (set at the parallactic angle) so that the resolution was determined by the seeing disk, which was about 1".5. They were carefully flux-calibrated so that the continua on the long wavelength side of Lyα emission could be very

accurately defined. Steidel and Sargent estimated the degree to which the resolution of ~ 4 Å lowered the continuum in the Lyα forest by smoothing high-resolution data with the appropriate filter. With this correction they showed that the power-law continua defined redward of Lyα also fitted the Lyα forest region at least down to Lyβ λ1025 (in the rest frame of the QSO). Thus, on visual inspection of the spectra, there was no evidence for any Gunn-Peterson discontinuity across the Lyα emission lines. Again by such visual inspection, we estimate that an upper limit on such a discontinuity (for the best data) is $\tau_{GP} < 0.05$. A more quantitative limit may be obtained by the following procedure. For the sample of seven QSOs it was found that the fractional flux decrement (assuming the extrapolated continuum) in the region of the Lyα forest longward of $\lambda_0 = 1025$ Å is $D_A = 0.24 \pm 0.02$. This includes the effects of all the absorption lines plus any residual Gunn-Peterson effect. This value applies to a mean redshift between Lyα and Lyβ emission of $\langle z_{abs} \rangle = 2.64$. They then calculated that the predicted value of the flux decrement due to Lyα lines alone is $D_L = 0.22 \pm .02$ for $\langle z_{abs} \rangle = 2.64$. In making this calculation they took the equivalent width distributions from Carswell *et al.* (1984) and Sargent *et al.* (1980) and used Murdoch *et al.*'s (1986) formula for the Lyα line density evolution with redshift. (The quoted errors on D_A and D_L are standard deviations in the mean for a sample of seven objects. The error in D_L was obtained by considering Poisson statistics for the number of lines in each equivalent width bin in the integral over the equivalent width distribution.)

In such a manner we obtain an upper limit on any Gunn-Peterson discontinuity, $D_{GP} < (D_A - D_L) = 0.02 \pm 0.03$. It should be noted that this would represent a conservative upper limit, since D_L includes *only* Lyα lines and does not account for a possible contribution to the fractional flux decrement from lines of heavy elements occurring in the Lyα forest. Using the fact that $D_{GP} = 1 - e^{-\tau_{GP}} \approx \tau_{GP}$ for small τ_{GP}, we obtain

$$\tau_{GP} < 0.02 \pm 0.03. \quad (2)$$

Thus, the 1 σ upper limit on τ_{GP} is 0.05 and the value is consistent with zero. The corresponding upper limit on the H I density, evaluated at the mean absorption redshift of $\langle z_{abs} \rangle = 2.64$, is

$$N_{H\,I}(z = 2.64) < 4.4 \times 10^{-12} h_{100}\ (\mathrm{cm}^{-3})\ (q_0 = 0)$$
$$< 8.4 \times 10^{-12} h_{100}\ (\mathrm{cm}^{-3})\ (q_0 = 1/2). \quad (3)$$

The maximum sensitivity for obtaining limits on $n_{H\,I}$ at $z = 0$ can be achieved by analyzing the spectra of objects at very high redshift if, as proposed by Sargent *et al.* (1980), the Lyα clouds are confined by the pressure of the intergalactic medium. In this case the recombination time scale t_{rec}^M for the medium is given by

$$t_{rec}^M(z) \approx 2 \times 10^{18} (1 + z)^{-3/2}\ (\mathrm{s}), \quad (4)$$

whereas the Hubble time is given by

$$t_H(z) \approx \frac{3 \times 10^{17}\ (\mathrm{s})}{h_{100}(1 + z)(1 + 2q_0 z)^{1/2}}. \quad (5)$$

Thus the recombination time scale is larger than the expansion time scale for the universe at all relevant ($z < 4$) epochs; the ionization time scale for neutral hydrogen atoms is always significantly less than the Hubble time for reasonable values of the ionizing UV flux (Ikeuchi and Ostriker 1986). Once the medium has been highly ionized at early epochs, it will remain highly ionized even as the universe expands and the ionizing UV flux from QSOs has significantly diminished. We are justified, therefore, in obtaining a present-epoch limit on the H I density by simply dividing the value obtained for large z by $(1 + z)^3$. The resulting value for the upper limit on the intergalactic H I density at the present epoch is

$$n_{H\,I}(z = 0) < 9.1 \times 10^{-14} h_{100}\ (\mathrm{cm}^{-3})\ (q_0 = 0)$$
$$< 1.7 \times 10^{-13} h_{100}\ (\mathrm{cm}^{-3})\ (q_0 = 1/2). \quad (6)$$

This limit is a factor of ~ 23 smaller than the limit obtained based on observations of 3C 273. This value is still an upper limit even if, as Rees (1986) has suggested, the Lyα clouds are not supported by the pressure of an external medium.

III. IMPLICATIONS FOR THE DENSITY PARAMETER

Sargent *et al.* (1980) proposed that the Lyα clouds are in pressure equilibrium with a hotter and less dense intergalactic medium; the resulting possible range of values of n_H^M and n_H^C was quite small.[1] More detailed calculations were carried out by Ostriker and Ikeuchi (1983) and Ikeuchi and Ostriker (1986); their results were consistent with the conclusions of Sargent *et al.* (1980). We have calculated a new curve of constraint in the $\log T_{IGM}$–$\log n_H$ plane which results from the new value of the Gunn–Peterson limit (cf. Fig. 1 of Ostriker and Ikeuchi 1983 and Fig. 11 of Ikeuchi and Ostriker 1986). Assuming that the IGM is in photoionization equilibrium in the UV radiation from QSOs (at $z = 2.64$), this curve of constraint, shown in Figure 1, is obtained from the ionization equilibrium equation

$$\frac{n_{H\,II}^M}{n_{H\,I}^M} = 7.6 \times 10^{-3} T_M^{3/4} n_e^{-1} \left(\frac{I_{\nu c}}{10^{-21}} \right) + 4.1 \times 10^{-1} T_M^{5/4}$$
$$\times \exp\left(-1.58 \times 10^5 / T_M\right). \quad (7)$$

Here $I_{\nu c}$ is the integrated UV flux due to QSOs (at $z = 2.64$), which we have taken to be 10^{-21} ergs s^{-1} cm^{-2} Hz^{-1} sr^{-1} (a

[1] An error was made in Fig. 6 of this paper. The line corresponding to the constraint $\Omega_H > 0.1$ with $H_0 = 60$ km s^{-1} Mpc^{-1} should be drawn at $\log_{10} n_H^M = -4.55$ and not at $\log_{10} n_H^M = -5.00$. This excludes *all* values of n_H^M; clearly the constraint $\Omega_H > 0.1$ is itself questionable.

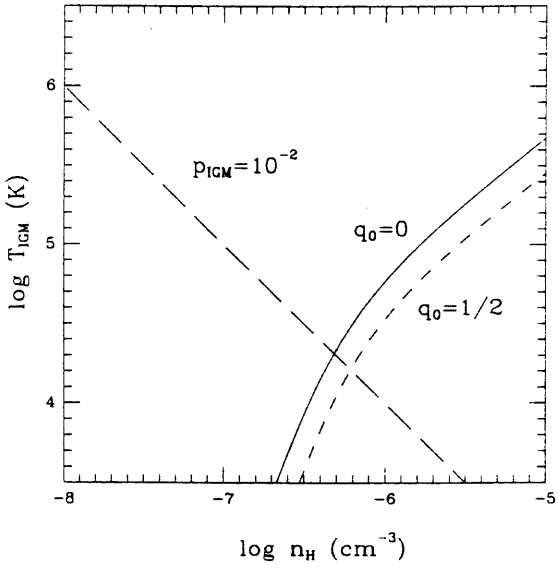

FIG. 1.—The plotted curves represents limits on the density and temperature of the intergalactic medium at the present epoch. In all cases the allowed regions are to the left of the curves. The long-dashed curve represents a limit on the pressure of the IGM obtained from observations of the double QSO 2345+007. The solid and short-dashed curves represent limits obtained based upon the new Gunn-Peterson limit for $q_0 = 0$ and $q_0 = 1/2$, respectively.

fairly conservative upper limit, according to Tytler 1986). In order to obtain limits which pertain to the present epoch, we have assumed that the IGM has expanded adiabatically since the epoch corresponding to $z = 2.64$, i.e., that $n_H(z) \propto (1 + z)^3$ and $T_{IGM}(z) \propto (1 + z)^2$. The lower limit on Ly$\alpha$ cloud sizes obtained by Foltz *et al.* (1984) from their observations of the double QSO 2345+007 (and assuming a cloud temperature of 3×10^4 K), enables a further constraint, also shown in Figure 1, to be placed on the density and temperature of the IGM (see eq. [78] of Ikeuchi and Ostriker 1986). The result is that the new upper limit on the density of hydrogen in the IGM at $z = 0$ is

$$n_H < 4.6 \times 10^{-7} h_{100}\ \mathrm{cm}^{-3}\ (q_0 = 0)$$
$$< 6.0 \times 10^{-7} h_{100}\ \mathrm{cm}^{-3}\ (q_0 = 1/2). \quad (8)$$

We note that the quoted value is still an upper limit even if the Lyα clouds are not confined solely by the pressure of the intergalactic medium. If the clouds are in equilibrium and are at least partially supported by, e.g., gravity or magnetic fields, then the upper limit on the pressure of the IGM can only be smaller than the adopted limit. If the clouds are freely expanding, then clearly the pressure of the IGM must be smaller than the limit obtained assuming equilibrium. It is clear from Figure 1 that decreasing p_{IGM} causes the upper limit on n_H to decrease as well.

In terms of the cosmological density parameter, this upper limit corresponds to

$$\Omega_H < 0.05 h_{100}^{-1}. \quad (9)$$

The upper limit on the contribution of baryonic material to Ω has been calculated based on models of Big Bang nucleosynthesis and is in the range $\Omega_B < 0.034 h_{100}^{-2} - 0.048 h_{100}^{-2}$ (Boesgaard and Steigman 1985). The contribution to Ω from the luminous inner parts of galaxies has been estimated to be in the range $0.01 < \Omega_{GAL} < 0.02$ (Yang *et al.* 1984). Thus, if h_{100} is close to 1, then it is possible that hydrogen in the IGM together with the luminous regions of galaxies may account for all of the baryonic material in the universe; if Ω_H were much larger than the limit we have proposed, it would be difficult to reconcile the nucleosynthesis limit with the large values of H_0 which seem to be currently popular. In any case, the limit on Ω_H resulting from the new value of the Gunn-Peterson limit is consistent with the Big Bang nucleosynthesis limit on Ω_B.

We would like to thank Craig Hogan for suggesting the idea of re-examining the Gunn-Peterson test in light of our new data. We also thank S. Phinney, R. Blandford, and an anonymous referee for their very helpful comments on an earlier draft of the paper. This work has been supported in part by grant AST84-16704 from the National Science Foundation.

REFERENCES

Boesgaard, A. M., and Steigman, G. 1985, *Ann. Rev. Astr. Ap.*, **23**, 319.
Carswell, R. F., Morton, D. C., Smith, M. G., Stockton, A. N., Turnshek, D. A., and Weymann, R. J. 1984, *Ap. J.*, **278**, 486.
Davidson, A., Hartig, G. F., and Fastie, W. G. 1977, *Nature*, **269**, 203.
Foltz, C. B., Weymann, R. J., Roser, H. J., and Chaffee, F. H. 1984, *Ap. J. (Letters)*, **281**, L1.
Gunn, J. E., and Peterson, B. A. 1965, *Ap. J.*, **142**, 1633.
Ikeuchi, S., and Ostriker, J. P. 1986, *Ap. J.*, **301**, 522.
Lynds, C. R. 1971, *Ap. J. (Letters)*, **164**, L73.
Murdoch, H. S., Hunstead, R. W., Pettini, M., and Blades, J. C. 1986, *Ap. J.*, **309**, 19.
Ostriker, J. P., and Ikeuchi, S. 1983, *Ap. J. (Letters)*, **268**, L63.
Rees, M. J. 1986, *M.N.R.A.S.*, **218**, 25P.
Sargent, W. L. W., Young, P. J., Boksenberg, A., and Tytler, D. 1980, *Ap. J. Suppl.*, **42**, 41.
Schmidt, M. 1965, *Ap. J.*, **141**, 1295.
Steidel, C. C., and Sargent, W. L. W. 1987, *Ap. J.*, **313**, 171.
Tytler, D. 1986, private communication.
Yang, J., Turner, M. S., Steigman, G., Schramm, D. N., and Olive, K. A. 1984, *Ap. J.*, **281**, 493.

W. L. W. SARGENT and C. C. STEIDEL: Palomar Observatory, 105-24, California Institute of Technology, Pasadena, CA 91125

Chapter 2

ABSORPTION IN THE WIDE QSO PAIR TOLOLO 1037–2704 AND TOLOLO 1038–2712 EVIDENCE FOR A SPECIALLY ALIGNED SUPERCLUSTER AT z=2?

Reprinted from *The Astrophysical Journal* (1987, **322**, pp. 142–163)

THE ASTROPHYSICAL JOURNAL, 322:142–163, 1987 November 1

ABSORPTION IN THE WIDE QSO PAIR TOLOLO 1037–2704 AND TOLOLO 1038–2712: EVIDENCE FOR A SPECIALLY ALIGNED SUPERCLUSTER AT $z = 2$?[1]

WALLACE L. W. SARGENT AND CHARLES C. STEIDEL
Palomar Observatory, California Institute of Technology
Received 1987 January 19; accepted 1987 April 22

ABSTRACT

Spectra with a resolution of ~2 Å have been obtained of the QSO pair Tol 1037–2704 ($z_{em} = 2.193$, $m_B = 17.4$) and Tol 1038–2712 ($z_{em} = 2.331$, $m_B = 17.8$). These objects are separated by 17'.9 on the sky and were discovered by Jakobsen and his coworkers to have extensive, possibly correlated absorption spectra. We have confirmed the existence of the four absorption systems between $z_{abs} = 1.95$ and $z_{abs} = 2.14$ in both QSOs, and we also found a fifth system in each spectrum, with $z_{abs} \sim 1.90$ in each case. Lower resolution (~6 Å) spectra were obtained of three other QSOs in the field. One of these, Tol 1038–2707 ($z_{em} = 1.937$, $m_B \sim 19.5$), is only ~5' away from Tol 1038–2712 and appears to have a strong absorption system at $z_{abs} \sim 1.89$, corresponding closely to the newly discovered fifth system in Tol 1037–2704 and Tol 1038–2712. While each absorption system in the spectrum of Tol 1037–2704 corresponds (in redshift) to within ~2000 km s^{-1} with a system in the spectrum of Tol 1038–2712, we have shown that the system-by-system correlations may not be significant based on consideration of *a posteriori* statistics. What is significant is that the two QSOs have extremely rich absorption spectra confined to the same redshift range $1.88 < z_{abs} < 2.15$. This is shown to be a very unlikely chance occurrence if the number of absorption systems per QSO spectrum follows a Poisson distribution. We have ruled out the possibility that the absorption is due to material ejected from either of the QSOs (and covering the line of sight to both) on geometrical or energetic grounds or on both. It is unlikely that line locking has produced the observed redshift ratios. Based on energy arguments, it is shown that independent ejection from both of the QSOs is also highly unlikely for at least some of the observed absorption systems. Like Jakobsen *et al.*, we conclude that the absorption is caused by material associated with a large supercluster (~50 Mpc along the line of sight at the epoch corresponding to $z \sim 2$). On our interpretation the orientation of the supercluster with respect to the line of sight must be very unusual—it is possible that the line of sight passes along the axis of a large-scale "filament" or is in the plane of a "sheet" of galaxies. If all QSO absorption systems are associated with such large-scale structures, then the number of absorption systems per QSO should not follow a Poisson distribution; in particular, spectra of richness comparable to Tol 1037–2704 and Tol 1038–2712 would be expected 1%–2% of the time.

Subject headings: galaxies: clustering — galaxies: intergalactic medium — quasars

I. INTRODUCTION

There is now general agreement that the sharp absorption lines observed in QSO spectra are produced by cosmologically distributed, intervening objects—either galaxy halos or intergalactic clouds (for reviews see Weymann, Carswell, and Smith 1981; Sargent and Boksenberg 1983; Boksenberg and Sargent 1983). This being the case, spectra of two or more QSOs very close to one another on the plane of the sky enable one to place limits on the physical extent of the absorbing material by searching for common absorption systems. Observations of this kind have indicated that the characteristic sizes for the gas clouds resulting in narrow metal line absorption systems may be as large as ~400 kpc (Shaver and Robertson 1983; Sargent and Boksenberg 1987; Crotts 1986). The angular separation of the QSO pairs used in such studies has typically been ~1', corresponding to galactic rather than intergalactic dimensions at typical redshifts $z \sim 2$.

It was, therefore, surprising when Jakobsen *et al.* (1986) drew attention recently to the QSO pair Tol 1037–2704 ($z_{em} = 2.193$, $m_B = 17.4$) and Tol 1038–2712 ($z_{em} = 2.331$, $m_B = 17.8$), which are separated by 17'.9 and which exhibit apparent correlations in their unusually rich absorption spectra extending over the redshift range $z_{abs} = 1.95$–2.14. If these correlations are significant, then the distance between the two lines of sight (~4.3 h_{100}^{-1} Mpc for $q_0 = 0.5$ at the time when the light transversed the absorbers) would represent the largest distance over which correlated absorption has been observed. Jakobsen *et al.* (1986) suggest that the near-matches in redshift of four absorption systems would be a very unlikely chance occurrence. Jacobsen *et al.* noted that both spectra appeared to exhibit low-level broad absorption line (BAL) characteristics, and it is generally believed that these troughs are caused by outflowing material associated with the QSO. Furthermore, the consistency in the ratios of $(1 + z_{abs})$ for adjacent absorption systems was interpreted as possible evidence that a line-locking mechanism may be in effect, thereby producing a common pattern in the observed ejection velocities. However, their preferred interpretation of the coincidences between the absorption systems is that they are due to an intervening supercluster whose dimensions would be at least ~33 Mpc (at the epoch corresponding to $z = 2.08$ for $q_0 = 0.5$ and $H_0 = 100$) along the line of sight. This would just be consistent with the sizes of superclusters observed in our vicinity at the present epoch. The hypothetical supercluster must be either a very rare kind of

[1] The observations described in this paper were obtained at the Las Campanas Observatory as part of the agreement between the California Institute of Technology and the Carnegie Institution of Washington.

structure or a more common one seen from a very unusual angle if we are to understand the unusual nature of the absorption spectra of the two QSOs.

In view of the extreme importance of establishing the nature of the absorption in this pair of quasars, we have obtained spectra which represent an improvement in both resolution and signal-to-noise (S/N) ratio over those presented by Jakobsen *et al.* (1986) (the spectra used by Jacobsen *et al.* consisted of their own spectrum of Tol 1038−2712 with an effective resolution of ~6 Å, and spectra of Tol 1037−2704 obtained by Ulrich and Perryman [1986] at ~7 Å and ~3.8 Å resolution). We have also obtained lower resolution spectra of three of the fainter quasar candidates identified by Bohuski and Weedman (1979) in the same field as Tol 1037−2704 and Tol 1038−2712. One of these, Tol 1038−2707 ($z_{em} = 1.937$, $m_B \sim 19.5$), is only 5′ away from Tol 1038−2712 and appears to have a strong absorption system whose redshift corresponds to within ~1500 km s^{-1} with a fifth system which we observe near $z_{abs} \sim 1.9$ in the spectra of both Tol 1037−2704 and Tol 1038−2712. These new spectra confirm the remarkable nature of the absorption spectra of these objects.

The new observations and the reductions of the raw data are described in § II. The analyses of the spectra, including a critical discussion of the absorption and emission redshifts, is given in § III. We also discuss the possible coincidences in absorption redshift and their statistical significance in this section. In § IV we examine the consequences of various hypotheses for the origins of the absorption features—ejection from one or both QSOs or the effects of an intervening supercluster. We show that ejection is highly implausible on energetic grounds, and that the observations point to an elongated intervening supercluster observed along its major axis. The overall state of affairs is summarized in § V.

II. OBSERVATIONS AND REDUCTIONS

Spectra of Tol 1037−2704 and Tol 1038−2712 were obtained during 1986 March 5, 6, and 9 with the "2-D Frutti" photon-counting detector (Shectman 1982) which was attached to the Boller & Chivens spectrograph on the Las Campanas Observatory 2.5 m du Pont telescope. All observations were made through a 1.″5 slit. The exposures were broken into intervals of 2000 s and a He-Ar calibration arc was exposed before and after each interval in order to keep track of wavelength shifts. The slit was aligned at the appropriate parallactic angle for the midpoint of each 2000 s interval in order to reduce the effects of differential atmospheric refraction. For the first two nights a grating having 1200 lines mm^{-1} blazed at 5000 Å was used, with the 2-D Frutti in the format having 3040 pixels in the dispersion direction. The wavelength scale on the detector was 0.7 Å pixel^{-1}, resulting in a spectral resolution of ~2 Å (FWHM). The wavelength range covered was 3800–5300 Å. With this setup, the data consist of integrations totaling 24,000 and 22,000 s for Tol 1037−2704 and Tol 1038−2712, respectively, giving S/N ratios of ~40 in the continuum. On March 9 we used a 600 lines mm^{-1} grating blazed at 3750 Å in second order to maximize the instrumental efficiency in the Lyα forest regions of the spectra of both quasars. A liquid copper sulfate filter was used to eliminate contamination from first order. The resolution was again ~2 Å, and the wavelength range covered was 3300–4800 Å. Integrations totaled 12,000 s for Tol 1037−2704 and 14,000 s for Tol 1038−2712, resulting in S/N ratios of ~20 in the continuum for each object (~10 at the shortest wavelengths). In addition, we observed three other objects from the list of faint QSO candidates in the same field at lower resolution (~4 Å). These were Nos. 6, 21, and 23 from the candidate list of Bohuski and Weedman (1979). A journal of observations is given in Table 1.

The spectra were reduced in the usual way, using flat-field exposures to remove pixel-to-pixel variations in the response of the detector. Observations of spectrophotometric standard stars were used to calibrate the spectra to an approximate absolute flux scale. The resulting spectra of Tol 1037−2704 and Tol 1038−2712 are plotted in Figure 1; data for the two overlapping wavelength regions have been combined to produce a single spectrum of each object. The spectra of the three quasars are shown in Figure 2.

III. ANALYSIS OF THE SPECTRA

a) Overall Properties

It can easily be seen from Figure 1 that the spectra of both Tol 1037−2704 and Tol 1038−2712 are unusually rich in absorption features. The strong absorption complexes near 4750 and 4900 Å in the spectrum of Tol 1037−2704, which appeared to be broad and almost troughlike in the spectra presented by Jakobsen *et al.* (1986), are seen to consist of several overlapping or adjacent narrow components. Tol 1037−2704 is clearly *not* a BAL QSO. For Tol 1038−2712, on the other hand, our observations have not resolved the two C IV absorption complexes near 4750 and 4900 Å into narrower features. These, especially the former, appear to be quite smooth and troughlike. The classification of Tol 1038−2712 as a marginal BAL QSO may still be a possibility. From the peaks of the observed emission lines, we find that the z_{em} =

TABLE 1

OBSERVATIONS

Object	Date 1986	Exposure (s)	λ Range (Å)	FWHM (Å)	Candidate Number[a]
Tol 1032−2740.....	Mar 7	2000	3500–6500	4	6
Tol 1037−2704.....	Mar 5	6000	3800–5300	2	19
	Mar 6	16000	3800–5300	2	...
	Mar 9	12000	3300–4500	2	...
Tol 1037−2742.....	Mar 7	4000	3500–5500	4	21
Tol 1038−2712.....	Mar 5	16000	3800–5300	2	22
	Mar 6	8000	3800–5300	2	...
	Mar 9	14000	3300–4500	2	...
Tol 1038−2707.....	Mar 7	4000	3500–6500	4	23

[a] See Bohuski and Weedman 1979, Table 2.

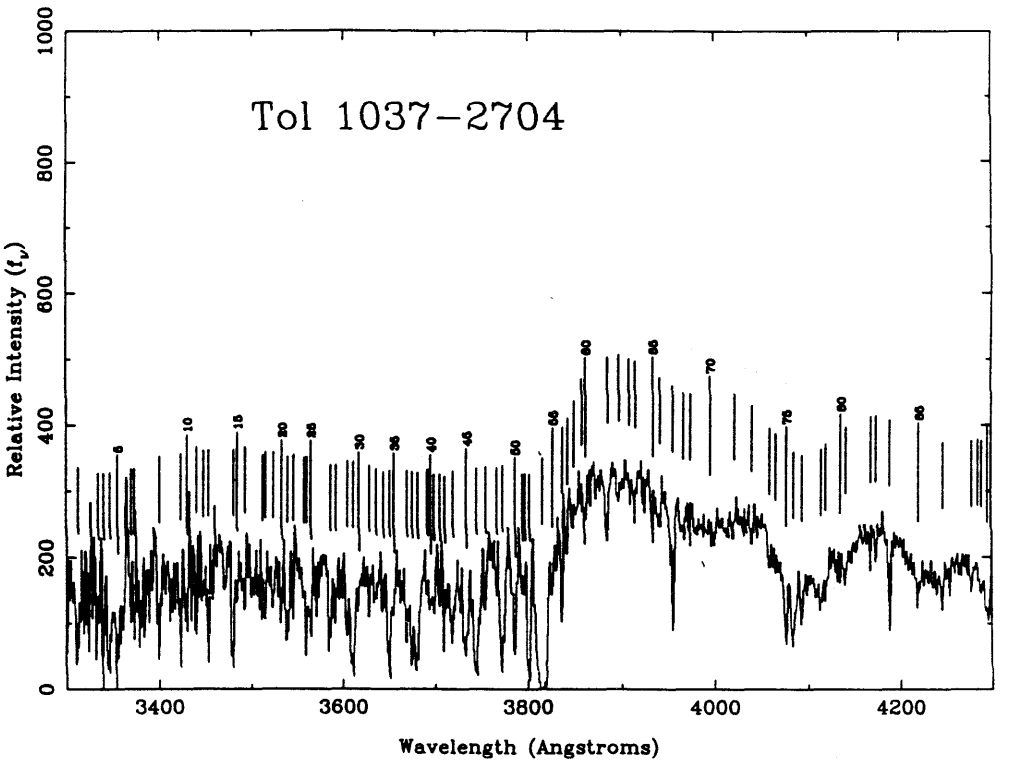

FIG. 1*a*

FIG. 1.—Spectra of (*a*) Tol 1037 − 2704 and (*b*) Tol 1038 − 2712 at ~2 Å resolution. The data are plotted without smoothing. Measured absorption lines listed in Tables 2 and 3 are indicated.

2.193 ± 0.007 and $z_{em} = 2.331 \pm 0.006$ for Tol 1037 − 2704 and Tol 1038 − 2712, respectively, in good agreement with the redshifts measured by Ulrich and Perryman (1986) and Jakobsen *et al.* (1986). (We suspect, however, that the slightly sharper Lyα emission-line profile obtained by those authors for Tol 1037 − 2704 may be due to contamination from a nearby faint galaxy which happens to have [O II] λ3727 coinciding with Lyα from the QSO.)

We see from the lower resolution spectra in Figure 2 that Tol 1032 − 2704 ($m_g \sim 19.5$) appears to have an emission line near 3900 Å, and possibly one near 6000 Å. There is too little information to estimate a redshift for this object. We identify Tol 1037 − 2742 ($m_g \sim 19.4$) as a QSO with $z_{em} = 1.886 \pm 0.006$; no strong absorption system is obvious with the relatively poor S/N ratio and low resolution. We identify Tol 1038 − 2707 ($m_g \sim 19.5$) as a QSO with $z_{em} = 1.937 \pm 0.004$; a very strong absorption system is evident in the spectrum, and from the measured wavelengths of lines identified as H I λ1215, Si IV λ1396, and C IV λ1549, we find $z_{abs} = 1.887 \pm 0.007$. The significance of this discovery will be discussed in § IV. The relative positions of the observed QSOs, plus several other QSOs and QSO candidates from the same field (Bohuski and Weedman 1979), are shown in Figure 3. Redshifts which are only estimates from objective-prism spectra are shown in brackets.

b) Absorption Lines

The absorption lines were measured interactively using a method described in Young *et al.* (1979). Tables 2 and 3 list the absorption lines measured from the spectra of Tol 1037 − 2704 and Tol 1038 − 2712, respectively, along with suggested identifications. The tabulated wavelengths are vacuum, heliocentric values. The spectra covering the different wavelength regions were measured separately in order to provide a check on the wavelength calibration and on the reality of weak features. Line lists obtained from measurements of the separate spectra were then merged, with lines appearing in both lists being weighted by the square of the S/N ratio to arrive at the tabulated values. The criterion for acceptance of a feature as real is that it be greater than 5 $\sigma(W)$ Å in equivalent width, and that the observed equivalent width be greater than 0.3 Å. It should be noted that the tabulated values of $\sigma(W)$ represent the expected error due to statistics, and do not include the uncertainties arising because of the high degree of subjectivity in defining the continuum. These uncertainties are typically at least 10%–20% and possibly larger in regions of the spectra dominated by broad absorption troughs or complexes.

Because of the complexity of the spectra, the assignment of individual lines, especially within troughs or crowded regions, is necessarily quite subjective. We have attempted to indicate

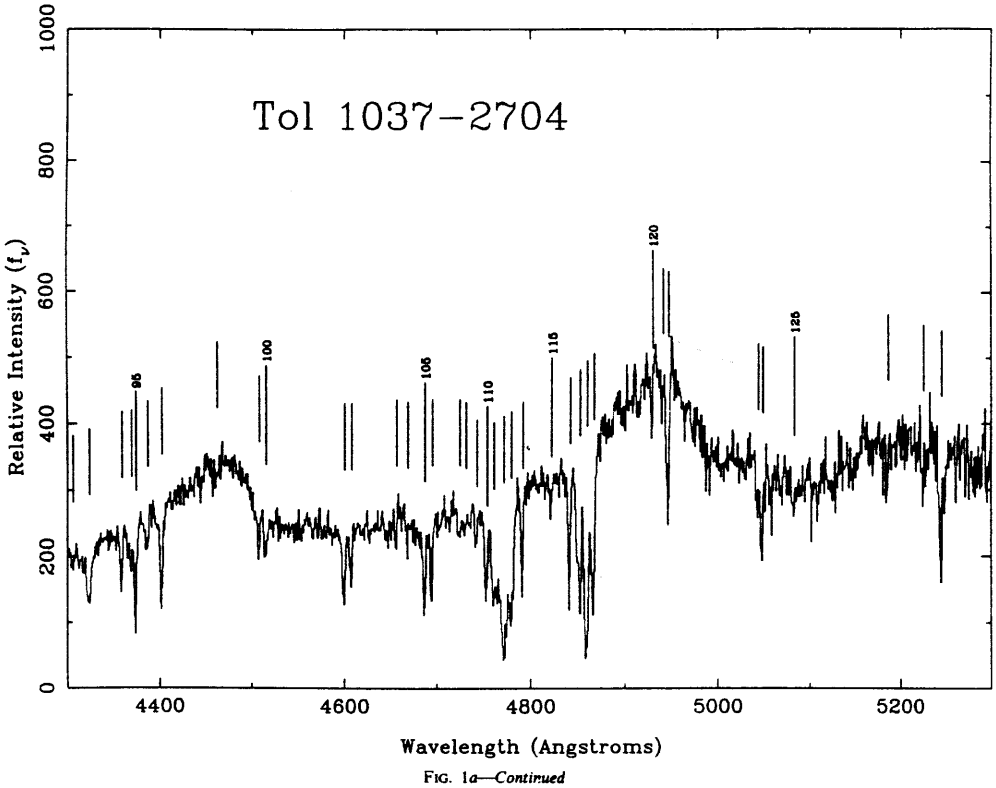

FIG. 1*a*—*Continued*

in Tables 2 and 3 the lines which appear to be components of troughs or complexes so that we might identify structures within absorption systems, and so that we might resolve partially overlapping lines from systems having different absorption redshifts. For such lines, the tabulated equivalent width is not reliable and cannot be used to calculate physical conditions in the absorbing gas. Because of the large number of absorption systems occurring in a relatively small interval of redshift, there is a great deal of ambiguity in the identification of many of the lines, particularly those shortward of Lyα emission. For example, for several of the systems in both spectra the Lyα absorption is confused with N v absorption from another system. For this reason many of the identifications are only suggestions and many of the equivalent width measurements are very approximate. With these caveats in mind, we have grouped all of the identified lines into suggested absorption systems in Tables 4 and 5 for Tol 1037−2704 and Tol 1038−2712, respectively. We now discuss each absorption system individually, and compare our results with those obtained previously by Ulrich and Perryman (1986) and Jakobsen *et al.* (1986).

i) *Tol 1037−2704*

System 1: $\langle z_{abs} \rangle = 1.9122$.—This system is the weakest of the five major absorption systems identified in the spectrum of Tol 1037−2704, but it is almost certainly real, based upon the clear C IV $\lambda\lambda$1548, 1550 doublet and lines of H I, N V, Si II, C II, and Si IV. The identification of the line at 4687.68 Å as Fe II λ1608 may not be correct, since the line is also identified as C IV λ1548 in system 3 and as Si II λ1526 in system 4*a*. The line at 4867 Å has also been identified as C IV λ1550 in system 5*b*. As will be the case for all of the systems discussed below, the identifications of Si II $\lambda\lambda$1190, 1193 and Si III λ1206 in the Lyα forest must be considered very tentative. The ratio of the equivalent widths of the lines identified as Si IV $\lambda\lambda$1393, 1402 is unphysical because these lines are sharp trough components; only the wavelengths can be considered reliable. This system was not identified by Ulrich and Perryman (1986), probably because of the weakness of the features.

System 2: $\langle z_{abs} \rangle = 1.9722$.—This is a certain system based on the close correspondence in absorption redshift between the lines identified as C IV $\lambda\lambda$1548, 1550 and Si IV $\lambda\lambda$1393, 1402. There is a significant discrepancy in redshift between the lines identified as N V λ1238 and N V λ1242, possibly caused by blending with Lyα lines at different redshifts. Si II λ1190 is probably blended with H I λ1215 from system 1, while the contribution of Si II λ1260 at $z_{abs} = 1.9718$ to the strong line at 3745.70 Å is quite uncertain. The line identified as Fe II λ1608 may also be blended with C IV λ1550 in system 4*c*. The line list of Ulrich and Perryman (1986) agrees fairly well for the lines identified as Lyα, Si III λ1206, Si IV, and C IV; they did not identify lines of N V for this system, or any of the weaker lines which we have identified. In general, the equivalent widths of the lines from Ulrich and Perryman are higher, and the wave-

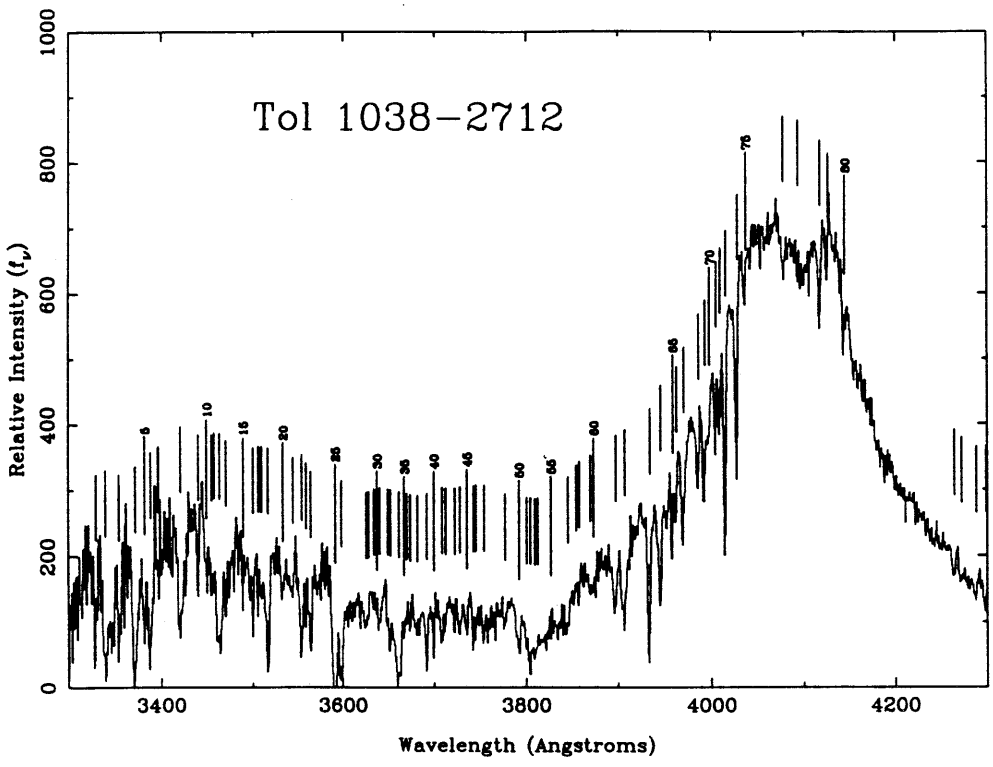

FIG. 1*b*

lengths differ from ours by as much as 2 Å. Both systematic effects are probably due to line blending, which represents a bigger problem in the lower resolution spectra.

System 3: $\langle z_{abs} \rangle = 2.0289$.—This certain system also has good agreement in redshift between the doublets of C IV and Si IV. Lyα may be blended with N V λ1238 from system 2 and possibly with Si II λ1193 from system 4*b*. Si II λ1190 and Si II λ1193 are probably blended with N V λ1238 from system 1 and H I λ1215 from system 2, respectively. The identifications of Si II λ1260 and O I λ1302 are tentative because of probable blending with lines from other systems, while C II λ1334, if real, barely satisfies the equivalent width criterion for inclusion in the line list. The lines identified as Si III λ1206 may be blends or misidentified Lyα lines or both. It is interesting that the N V doublet, which appears to be real because of the close redshift agreement of the two lines and because the equivalent width ratio is reasonable, differs in redshift from the C IV doublet in this system by $\sim$350 km s^{-1}. Our identifications of Lyα, Si II λ1260, Si IV, and C IV agree fairly well with those of Ulrich and Perryman (1986), although again the equivalent widths and wavelengths differ somewhat. Ulrich and Perryman did not detect lines of N V in their data.

The strong, certain, absorption complex at $z_{abs} \sim 2.08$ has been divided into three components based upon the structure in the C IV lines. Other identifications have been grouped (somewhat arbitrarily in some instances) into one of the three components 4*a*, 4*b*, and 4*c*.

System 4a: $\langle z_{abs} \rangle = 2.0708$.—Although this component of the absorption system appears to be real, many of the lines (e.g., Si II λ1190, Si II λ1526, Si III λ1206, N V $\lambda\lambda$1238, 1242, and H I λ1215) have been identified as other lines from other absorption systems as well (compare Tables 2 and 4). Ulrich and Perryman (1986) identified a component using identifications of only Lyα and C IV which agrees closely in redshift with what we have found.

System 4b: $\langle z_{abs} \rangle = 2.0755$.—This component is the least certain of the three—its existence is deduced based upon the strength of the line at 4761.73 Å (it is too strong to be solely due to C IV λ1550 from system 4*a*). The C IV lines in system 4 are sufficiently blended that no individual line corresponding to C IV λ1550 is identified. The suggested identifications of the lines of Si II, Si III, and Si IV clearly represent only weak evidence for this component which was not found by Ulrich and Perryman in their lower resolution data.

System 4c: $\langle z_{abs} \rangle = 2.0825$.—This component is certain, since all of the strong lines usually associated with "heavy-element" absorption systems at this redshift are identified. Again, the suggested identifications of Si II λ1190 and Si II λ1193 are uncertain because of the possible misidentification of a Lyα forest line. N V λ1238 is almost certainly blended with at least H I λ1215 from system 5*b*. The line at 4114.99 Å is regarded as the more likely of the two lines identified as C II λ1334 in the $z = 2.08$ complex. The C IV and Si IV lines are certain, and the redshift agreement is very good. We note that N V $\lambda\lambda$1238,

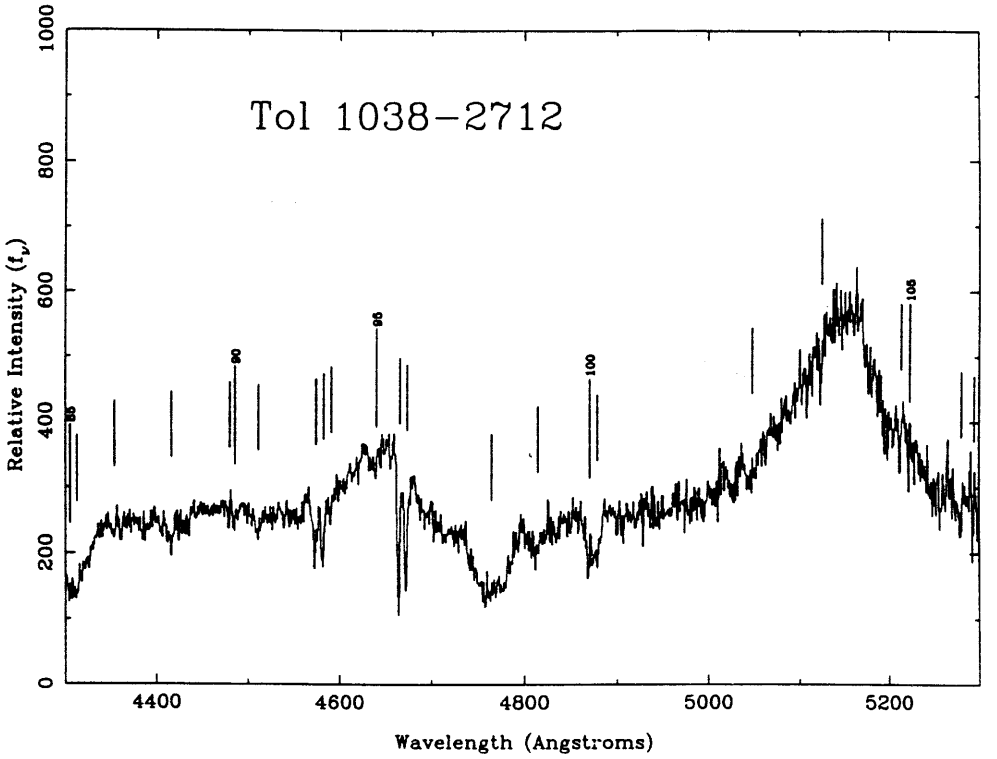

FIG. 1*b*—*Continued*

1242 are separated by ~ 250 km s^{-1} from the mean absorption redshift, $z_{abs} \sim 2.0825$, of the component as a whole, including the C IV lines. Our identifications are in the good agreement with all of those suggested by Ulrich and Perryman for this component.

The strong, certain complex near $z_{abs} \sim 2.14$ is more easily separable, in this case into two strong subsystems, one with $z_{abs} \approx 2.128$ and one with $z_{abs} \approx 2.138$.

System 5a: $\langle z_{abs} \rangle = 2.1283$.—In this component, H I λ1215 is blended with N V λ1238 from system 4*a*. The line identified as Si II λ1193 is also identified as possibly Si II λ1190 from system 5*b* or as H I λ1215 from system 4*a*. The C IV λ1550 line is blended with C IV λ1548 from system 5*b*, hence the large equivalent width and the slight redshift discrepancy of ~ 135 km s^{-1}. This subsystem was identified from the Lyα and C IV lines by Ulrich and Perryman.

System 5b: $\langle z_{abs} \rangle = 2.1378$.—There is some indication from the appearance of the C IV doublet that this subsystem is actually double, with components at $z_{abs} \sim 2.135$ and $z_{abs} \sim 2.139$, the latter being the more prominent. There appears to be the same structure in Fe II λ1608 and Si IV λ1393. Si II λ1190 and Si II λ1193 are blended with lines from other systems, and Si III λ1206 is probably blended with a Lyα forest line. N V absorption occurs at a redshift that is about halfway between the redshifts of the structures in C IV, probably indicating that the N V lines from these structures are blended. Our identifications for this system agree well with those of Ulrich and Perryman, although they did not see the possible additional splitting in the C IV and Si IV lines which we find with higher resolution data.

ii) *Tol 1038−2712*

System 1: $\langle z_{abs} \rangle = 1.8502$.—Despite the number of suggested identifications listed in Table 5 for this system, it must be regarded as marginal. The line which is identified as C IV appears to be blended or somehow affected by a noise spike; we have assigned it a nominal rest wavelength of 1549.0 Å. If the identifications are correct, there appears to be some structure associated with this system. It is just as likely, however, that many of the lines, particularly below 4100 Å, are either lines from one of the other five absorption systems or lines of the Lyα forest. The existence of this system was suspected by Jakobsen *et al.* (1986), but by detection of the Lyα and C IV lines only.

System 2: $\langle z_{abs} \rangle = 1.8936$.—This is another marginal system; the C IV $\lambda\lambda$1548, 1550 doublet is very weak, and no N V absorption is detected. Si IV λ1393 is also a marginal line. Si II λ1190, Si II λ1193, and Si II λ1260 show good redshift agreement at $z_{abs} \approx 1.8976$, but H I λ1215 and C IV $\lambda\lambda$1548, 1550 seem to indicate a different redshift by ~ 500 km s^{-1}. H I λ1215 may be blended with Si II λ1190 from system 3. The line identified as Si II λ1526 is also identified as C IV λ1549 in system 1.

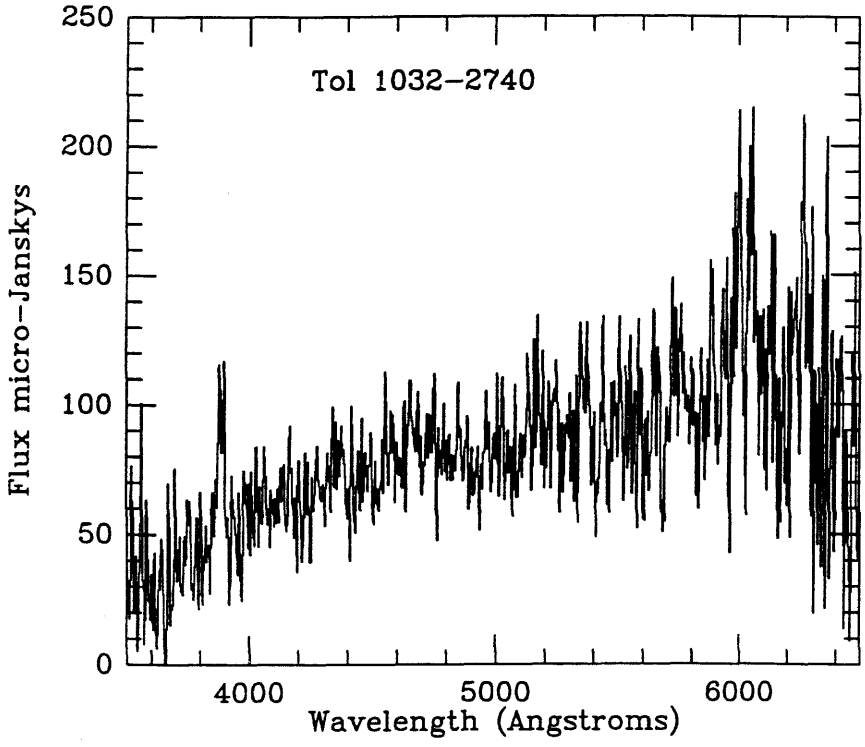

FIG. 2a

FIG. 2.—Spectra of (*a*) Tol 1032 – 2740, (*b*) Tol 1037 – 2742, and (*c*) Tol 1038 – 2707. The data have been smoothed to ~ 10 Å resolution.

This system was not identified by Jakobsen *et al.*, probably because of the weakness of the features and the lower resolution of their data.

System 3: $\langle z_{abs} \rangle = 1.9564$.—This system is fairly certain, and there is some evidence for structure, with one component (the stronger) at $z_{abs} \sim 1.955$ and one at $z_{abs} \sim 1.960$. The presence of the weaker component is suggested by lines identified as H I λ1215, N V λ1238, O I λ1302, and C IV $\lambda\lambda$1548, 1550. If the components are both real, the implied velocity separation is ~ 500 km s^{-1}. The identifications we have suggested agree well with those suggested by Jakobsen *et al.*, although the possible fine splitting of the system and many of the weaker lines were not detected in their lower resolution data.

System 4: $\langle z_{abs} \rangle = 2.0144$.—This system is the strongest (in C IV) of the four identified narrow-line absorption systems. It is interesting that no Si IV lines are detected; however, the Si II lines, if identified correctly, are very strong. It is possible that they are blended with strong lines of the Lyα forest. Some structure may be indicated by lines of Si III λ1206, H I λ1215, and Si II λ1260, although the redshift splittings are not consistent from ion to ion. The dispersion in redshift of the identified lines for this system is large—probably because of blending with other systems. Jakobsen *et al.* identified this system based upon the detection of Lyα and C IV only.

Identifications for the strong system with $z_{abs} \sim 2.08$ are extremely difficult because the system is broad and troughed; many of the lines are attempted identifications of trough components, and the result may be a larger percentage of spurious lines. There is no detectable structure in the strong C IV trough with $z_{abs} \sim 2.076$; however, identifications of lines of Si II–Si IV seem to indicate some structure. Somewhat arbitrarily, we have divided the system into three subsystems based on these Si lines. In addition, the tabulated equivalent widths for this system are especially unreliable, since the majority of the identified lines are trough components. The data of Jacobsen *et al.* did not have adequate resolution to allow detection of structures within this system; it was identified purely on the basis of broad troughs of N V, Si IV, and C IV.

System 5a: $\langle z_{abs} \rangle = 2.0652$.—The lines identified as H I λ1215 and N V $\lambda\lambda$1238, 1242 appear to indicate structure, with one component at $z_{abs} \sim 2.061$ and one at $z_{abs} \sim 2.068$, corresponding to a velocity difference of ~ 700 km s^{-1}. However, the only structure in the Si IV trough which we have been able to identify has $z_{abs} = 2.0646$.

System 5b: $\langle z_{abs} \rangle = 2.0768$.—This component is at the redshift of the center of the broad, strong C IV trough. The consistency in absorption redshift among the identified lines is not particularly good, probably because of the subjectivity involved in identifying structures within broad complexes. Confusion and coincidence are also a problem—e.g., Si II λ1190 is possibly blended with other lines from three different absorption systems (see Table 3).

System 5c: $\langle z_{abs} \rangle = 2.0851$.—The reality of this component is quite uncertain, since all but two of the lines are below Lyα

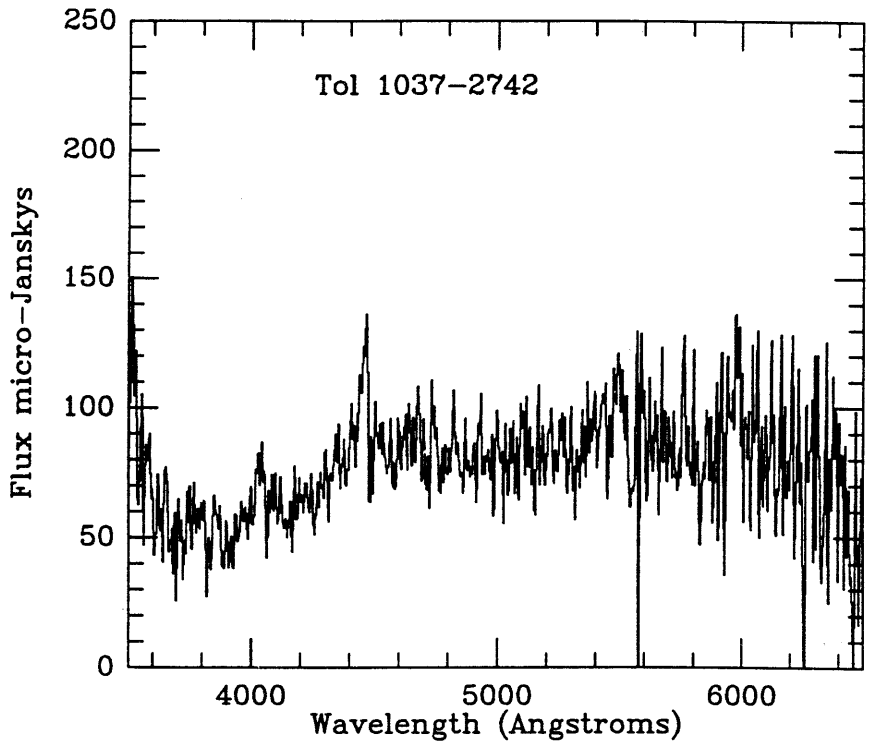

FIG. 2b

emission, and the two that are not have been also identified as lines in other systems. However, the identified lines of Si II, Si III, C II, and Si IV are consistent enough in redshift that the component is listed as a possibility.

System 6: $\langle z_{abs} \rangle = 2.1455$.—This certain system is based upon a fairly broad C IV feature similar in appearance to the system at $z_{abs} \sim 2.08$, although it is not nearly as strong. Two apparent sharp features in the C IV complex have been identified, and the redshift agreement is very good (the ratio of line strengths is off because the identified features are "trough components"). The associated H I λ1215 is very weak and may not be present at all. Si IV is not detected at all. The N V lines do not agree well in redshift, and the ratio of equivalent widths is not correct; this may be due in part to blending with Lyα forest lines. Jacobsen *et al.* do not find associated Lyα for this system either; their identifications of C IV and N V agree reasonably well with ours.

We note that the N V absorption features which frequently occur in the redshift systems described above are always in the Lyα forest and often show poor redshift agreement with the more certain lines in the systems. We are therefore uncertain as to whether the N V lines in these QSOs really have unusual strengths for "intervening" systems.

c) *Statistics of Absorption Systems*

Considered individually, both Tol 1037–2704 and Tol 1038–2712 have unusually complex and rich absorption spectra. Based on the results of Young, Sargent, and Boksenberg (1982), the mean number of C IV $\lambda\lambda$1548, 1550 doublets per quasar (where the region between Lyα and C IV λ1549 emission is observable) for which the rest equivalent width of both components is greater than 0.3 Å is ~ 1. We find five C IV doublets which satisfy this equivalent width criterion in the spectrum of Tol 1037–2704, and four in the spectrum of Tol 1038–2712 (blended systems, e.g., at $z_{abs} \sim 2.08$ and $z_{abs} \sim 2.13$ are counted as only one system). If the number of observed absorption systems obeys a Poisson distribution, the probability of observing five in the spectrum of any *one* quasar is $\sim 3 \times 10^{-3}$, and the probability of observing four is $\sim 1.5 \times 10^{-2}$. Thus the probability of observing a fairly large number of strong absorption systems (at *any* redshift) in the spectra of two neighboring QSOs is quite small if the absorption is uncorrelated. If we restrict ourselves to the absorption redshift range actually seen in one of the spectra, $1.91 < z_{abs} < 2.14$ for Tol 1037–2704, then the Poisson probability of observing four systems *in this range* for Tol 1038–2712 becomes $\sim 4 \times 10^{-4}$ if the absorption is uncorrelated.[2]

The absorption systems for Tol 1037–2704 and Tol 1038–2712 are summarized in Table 6. The tabulated absorption redshifts are based upon identified lines of C IV and

[2] If the fairly broad systems in the two spectra ($z_{abs} \sim 2.08$ and $z_{abs} \sim 2.13$) are not included because of the possibility that they are ejected, then the redshift interval of interest becomes $1.91 < z_{abs} < 2.03$, and the Poisson probability that Tol 1038–2712 would have two strong systems in this range becomes $\sim 1.5 \times 10^{-2}$.

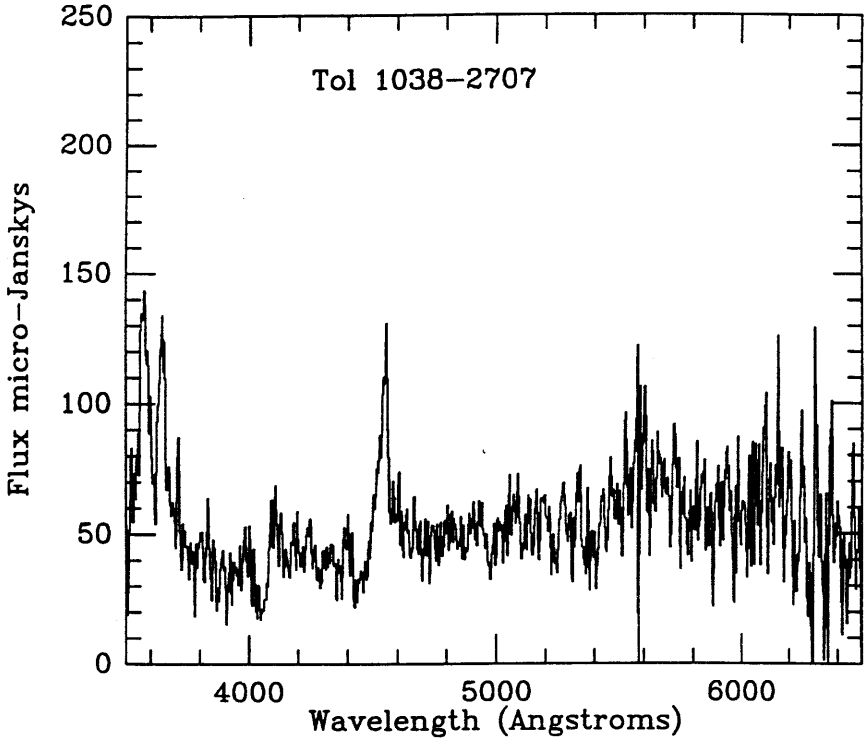

FIG. 2c

include structures within each absorption system. We have organized the table so as to compare corresponding systems in each spectrum, and the parameter Δv is the implied velocity difference for the absorption in one QSO as compared with the absorption in the other.

Jacobsen *et al.* (1986) emphasized that four absorption systems in each spectrum matched a corresponding system in the other within ~ 2000 km s^{-1}. We have confirmed that this is the case, and have found a fifth system in each spectrum, with $z_{abs} = 1.9125$ for Tol 1037–2704 and $z_{abs} = 1.8933$ for Tol 1038–2712. Jakobsen *et al.* pointed out that the probability of a random correspondence of the degree observed for four systems cast in the available redshift window ($\Delta z \approx 0.58$), assuming uniform distribution in velocity, is $\sim 8 \times 10^{-5}$. However, we believe that this is a significant *underestimate* of the true probability, as the reader can confirm by visually comparing the spectra in Figures 1*a* and 1*b*. It is difficult to assess post hoc the significance of the "matches" in absorption redshift numerically; we can first take a simpleminded approach and distribute five discrete systems in the redshift window of $\Delta z_{abs} = 0.58$ (the redshift range over which systems could be observed in *both* spectra, i.e., the region where C IV absorption would fall between the wavelengths of Lyα emission in Tol 1038–2712 and C IV emission in Tol 1037–2704) and require that each of five systems from the other spectrum correspond to one (and only one) of the fiducial systems so that $\Delta z_{abs} < 0.02$. The corresponding probability would then be $\sim 5!$ $[(0.02 \times 2)/0.58]^5 \sim 2 \times 10^{-4}$. Alternatively, we can take note of the fact that *both* QSOs show a very high density of absorption systems in the same redshift range $1.88 < z_{abs} < 2.15$. A possible explanation for this is that there happens to be a very high density of absorbing clouds in that particular redshift range along both lines of sight. In this case, testing for correlations in the actual pattern of the absorption systems is equivalent to testing for whether there is any strong evidence for the material along the two lines of sight being somehow associated. We wish to evaluate the probability that, given the relatively small range of redshifts and the large number of systems, the patterns which the absorption systems exhibit will be as similar as observed. This is not at all straightforward; one complication is that we have grouped the systems somewhat arbitrarily. A glance at Table 6 shows that there are really more than five systems to distribute for each object if we go down to smaller scales in Δv. In some cases we have grouped as many as three systems in one spectrum with only one in the other. If we require only that each system from one spectrum match (to within $\Delta z_{abs} = 0.02$) any system from the other spectrum, then the probability would be at least $\sim [(5 \times 0.02 \times 2)/0.27]^6 \sim 0.2$ (taking Tol 1037–2704 to be the fiducial object). It is clear from the two cases considered that the actual significance of the possible correlations seen in these spectra is difficult to evaluate numerically. It is possible, as we have seen with the latter case, that any system-by-system correlations between the two spectra may not be significant at all. Because of this

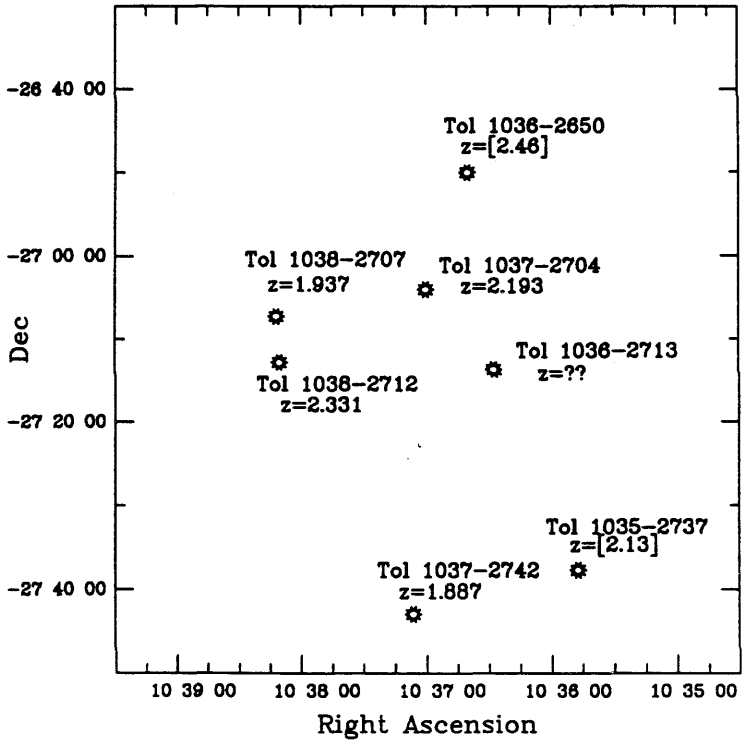

FIG. 3.—The field containing Tol 1037−2704, Tol 1038−2712, and several other QSOs and QSO candidates. Redshifts indicated in brackets are estimates from objective-prism spectra only. At the epoch corresponding to $z \sim 2$, 1′ is equivalent to a distance of $\sim 0.25\ h_{100}^{-1}$ Mpc for a $q_0 = 0.5$ cosmology.

ambiguity, we choose not to emphasize the absorption redshift "matches," but instead to concentrate on the indisputable fact that such a high density of absorption systems is observed in the same relatively narrow redshift range in two objects close to one another on the plane of the sky. The spectrum of Tol 1038−2707 is another very suggestive piece of evidence for some sort of very large scale concentration of material between $z_{abs} = 1.88$ and $z_{abs} = 2.15$ in this field. It will be an important next step to obtain spectra of several of the other QSOs in the same field (see Fig. 3). We will discuss in detail the possibilities for the nature of the absorption in § IV.

IV. INTERPRETATIONS OF THE ABSORPTION

a) Ejection

One interpretation for the observed absorption in Tol 1037−2704 and Tol 1038−2712 is that it is due to material ejected from one or both of the QSOs. The fact that at least one of the QSOs, Tol 1038−2712, appears to have BAL-like characteristics even at 2 Å resolution may support such an interpretation, as the conventional view at the present time is that broad absorption troughs are due to ejected material. A first possibility is that the absorption may be due to material ejected from one of the QSOs which happens to intersect *both* lines of sight. This would then explain the possible correlations, since corresponding absorption systems in the two spectra would arise from physically coherent material. Under this hypothesis, the physical extent of the ejected material must be large enough so that it covers an angle of at least ~17'.9 on the sky (the angular distance between the lines of sight to the QSOs). We shall discuss several possible ejection scenarios. Throughout it will be assumed that peculiar velocities are negligible, so that the emission redshifts of the QSOs are indicative of distances. Using a Friedmann cosmological model with $q_0 = 0.5$, the distance corresponding to the 17'.9 separation of the lines of sight is $\sim 4.4\ h_{100}^{-1}$ Mpc at the epoch corresponding to $z \approx 2.0$. The scale (at this epoch) on the plot in Figure 3 is then $\sim 0.25\ h_{100}^{-1}$ Mpc per minute of arc. The distance along the line of sight between Tol 1037−2704 and Tol 1038−2712 is $\sim 24\ h_{100}^{-1}$ Mpc at the same epoch.

1. Suppose that material has been ejected from the nearer of the two quasars, Tol 1037−2704 ($z_{em} = 2.193$). If each observed absorption system corresponded to an ejected shell of material spherically symmetric about Tol 1037−2704, we would expect to see two absorption systems in the spectrum of Tol 1038−2712 for every one in Tol 1037−2704, the additional system arising because of the receding side of the shell. (One set of absorptions would only be seen if the shells have radii larger than the distance between the two quasars, ~ 24 h_{100}^{-1} Mpc). Because the Hubble expansion at the epoch $z \sim 2$ is $\sim 520\ h_{100}$ km s^{-1} Mpc^{-1}, the *minimum* velocity separation between the emission redshift of Tol 1037−2704 and the absorption systems would be ~12,600 km s^{-1} in such a case. There are at least two very strong absorption system ($z_{abs} \sim$

TABLE 2

ABSORPTION-LINE LIST FOR TOL 1037 – 2704

Line No.	λ_{obs}	$\sigma(\lambda)$	W_{obs}	$\sigma(W)$	S/N	ID	z_{abs}	Notes
1	3312.95	0.19	3.81	0.25	8.7			c
2	3334.53	0.18	2.24	0.20	8.8			c
3	3340.77	0.16	2.51	0.19	8.7			c
4	3347.26	0.16	4.17	0.23	8.9			b,c
5	3355.78	0.14	3.57	0.19	9.4			c
6	3370.18	0.21	0.91	0.15	9.6			c
7	3374.01	0.15	1.30	0.14	9.6			c
8	3401.27	0.17	2.51	0.18	10.2			
9	3423.99	0.17	1.93	0.16	10.6			c
10	3430.57	0.21	1.54	0.17	10.5			c
11	3441.25	0.14	1.38	0.12	11.4			c
12	3448.78	0.25	0.79	0.14	11.5			c
13	3454.35	0.15	2.00	0.14	11.8			
14	3480.90	0.14	2.86	0.15	11.8			b
15	3485.12	0.22	0.74	0.13	11.6			b,d
16	3493.77	0.16	0.64	0.10	12.2			d
17	3512.95	0.18	0.73	0.10	13.1	SiIII(1206)	1.9117	d
18	3515.80	0.17	1.05	0.11	13.1	SiIII(1206)	1.9140	d
19	3524.32	0.17	0.93	0.11	14.0			d
20	3533.48	0.16	1.09	0.11	14.0			
21	3540.05	0.15	2.57	0.14	14.0	HI(1215)	1.9120	b
						SiII(1190)	1.9738	
22	3546.45	0.17	0.75	0.10	14.5	SiII(1193)	1.9720	
23	3557.95	0.19	0.78	0.10	14.7			a,d
24	3561.10	0.13	1.71	0.09	15.0			a
25	3565.42	0.15	2.06	0.12	15.1			a
26	3587.10	0.14	2.31	0.11	16.1	SiIII(1206)	1.9731	a,b
27	3592.97	0.18	1.24	0.11	15.7			a
28	3605.39	0.14	1.78	0.11	15.3	NV(1238)	1.9103	a
						SiII(1190)	2.0287	
29	3611.68	0.14	4.96	0.15	15.5	HI(1215)	1.9709	a,b
						SiII(1193)	2.0267	
30	3617.80	0.17	0.88	0.10	15.8	NV(1242)	1.9110	a
31	3629.54	0.18	0.82	0.10	15.9			
32	3636.90	0.22	1.18	0.12	16.7			b
33	3644.49	0.16	0.98	0.09	17.4			
34	3651.36	0.13	3.71	0.12	17.1	SiIII(1206)	2.0264	a
35	3656.12	0.16	1.27	0.10	17.3	SiIII(1206)	2.0303	a
						SiII(1190)	2.0713	
36	3670.62	0.13	1.97	0.09	18.4	SiII(1260)	1.9122	a
						SiII(1193)	2.0761	
						SiII(1190)	2.0835	
37	3676.22	0.13	3.12	0.10	17.7	SiII(1193)	2.0808	a
38	3682.13	0.14	4.72	0.13	17.7	NV(1238)	1.9723	a
						HI(1215)	2.0289	
						SiII(1193)	2.0850	
39	3692.11	0.16	0.49	0.07	17.6	NV(1242)	1.9708	a
40	3695.53	0.15	1.11	0.09	17.7	NV(1242)	1.9735	a
41	3699.35	0.16	1.23	0.10	17.7			a
42	3705.55	0.15	0.81	0.08	17.1	SiIII(1206)	2.0713	
43	3710.67	0.13	1.25	0.08	18.3	SiIII(1206)	2.0755	a
44	3719.93	0.15	3.68	0.14	17.8	SiIII(1206)	2.0832	b
45	3734.44	0.14	4.83	0.13	18.8	HI(1215)	2.0719	b
						SiII(1193)	2.1295	
						SiII(1190)	2.1371	
46	3745.70	0.14	7.27	0.15	20.1	SiII(1260)	1.9718	b
						HI(1215)	2.0812	
						SiII(1193)	2.1390	
47	3755.62	0.16	1.30	0.09	20.0	NV(1238)	2.0316	

TABLE 2—*Continued*

Line No.	λ_{obs}	$\sigma(\lambda)$	W_{obs}	$\sigma(W)$	S/N	ID	z_{abs}	Notes
48	3767.44	0.17	0.73	0.08	20.6	NV(1242)	2.0314	a,d
49	3774.11	0.14	5.06	0.12	20.6	SiIII(1206)	2.1281	b
50	3786.81	0.15	3.89	0.12	22.3	SiIII(1206)	2.1386	b
51	3794.65	0.15	0.92	0.07	22.5	OI(1302)	1.9141	a
52	3797.51	0.13	0.75	0.06	23.7	SiII(1304)	1.9114	a
53	3802.43	0.13	4.30	0.09	24.2	NV(1238)	2.0694	a
						HI(1215)	2.1278	
54	3816.10	0.09	13.54	0.09	35.3	SiII(1260)	2.0276	b
						NV(1242)	2.0706	
						NV(1238)	2.0804	
						HI(1215)	2.1391	
55	3827.02	0.10	1.09	0.04	36.2	NV(1242)	2.0793	a,d
56	3837.41	0.09	1.50	0.04	39.5			a
57	3842.99	0.11	0.77	0.04	40.2			a
58	3849.65	0.11	0.48	0.03	41.4			a
59	3858.40	0.14	0.43	0.04	31.1			a
60	3862.63	0.10	0.76	0.03	43.8			d
61	3886.04	0.12	1.30	0.05	46.5	CII(1334)	1.9119	b
						SiII(1260)	2.0831	
						NV(1238)	2.1369	
62	3897.77	0.17	0.41	0.05	32.8	NV(1242)	2.1363	a,d
63	3908.68	0.21	0.40	0.05	36.2			a,d
64	3915.61	0.13	0.32	0.03	50.6			a,d
65	3934.43	0.13	0.68	0.04	39.0			
66	3941.87	0.11	0.84	0.04	51.6	OI(1302)	2.0272	b
						SiII(1260)	2.1274	
67	3955.97	0.14	3.11	0.07	40.0	SiII(1260)	2.1386	
68	3967.11	0.19	0.94	0.06	37.0	CII(1334)	1.9727	b
69	3974.66	0.14	0.30	0.03	36.6			d
70	3995.85	0.15	0.72	0.06	29.5	OI(1302)	2.0686	
71	4021.70	0.16	0.39	0.05	27.3	SiII(1304)	2.0833	a,d
72	4040.33	0.15	0.39	0.04	38.1	CII(1334)	2.0275	d
73	4059.33	0.10	0.61	0.04	44.7	SiIV(1393)	1.9125	a
74	4065.80	0.14	0.33	0.04	35.4			a,d
75	4077.17	0.10	2.36	0.05	42.0			a
76	4084.91	0.13	2.59	0.06	33.6	SiIV(1402)	1.9120	a,b
						OI(1302)	2.1370	
77	4094.44	0.10	1.46	0.05	42.8	SiII(1304)	2.1390	
78	4114.99	0.13	1.17	0.05	33.1	CII(1334)	2.0835	a
79	4119.97	0.14	0.63	0.04	32.1	CII(1334)	2.0872	a
80	4136.03	0.17	0.37	0.05	31.6			a
81	4141.71	0.13	0.93	0.05	39.7	SiIV(1393)	1.9716	a
82	4168.69	0.15	0.32	0.04	31.2	SiIV(1402)	1.9718	
83	4174.24	0.12	0.46	0.04	40.3	CII(1334)	2.1279	
84	4189.27	0.09	1.92	0.05	39.9	CII(1334)	2.1391	
85	4220.75	0.11	1.34	0.05	40.3	SiIV(1393)	2.0283	
86	4247.50	0.11	1.17	0.05	40.1	SiIV(1402)	2.0279	
87	4279.08	0.11	0.75	0.04	42.1	SiIV(1393)	2.0702	
88	4285.58	0.13	0.70	0.06	22.2	SiIV(1393)	2.0748	a,b
89	4289.78	0.10	0.99	0.04	42.5			a,b
90	4296.22	0.10	2.67	0.05	42.4	SiIV(1393)	2.0825	a,b
91	4306.38	0.14	0.42	0.04	42.3	SiIV(1402)	2.0699	a
92	4324.25	0.11	2.20	0.05	42.3	SiIV(1402)	2.0827	a,b
93	4359.66	0.10	1.24	0.04	46.3	SiIV(1393)	2.1280	
94	4370.12	0.13	0.67	0.03	41.0	SiIV(1393)	2.1355	a
95	4374.93	0.09	2.35	0.04	47.8	SiIV(1393)	2.1389	a
96	4387.73	0.11	0.80	0.04	46.3	SiIV(1402)	2.1279	b
97	4403.14	0.13	1.96	0.05	41.3	SiIV(1402)	2.1389	

TABLE 2—*Continued*

Line No.	λ_{obs}	$\sigma(\lambda)$	W_{obs}	$\sigma(W)$	S/N	ID	z_{abs}	Notes
98	4463.20	0.19	0.32	0.04	41.7			b,d
99	4509.11	0.14	0.89	0.05	36.9	CIV(1548)	1.9125	
100	4516.63	0.14	0.96	0.05	35.8	CIV(1550)	1.9125	b
101	4600.86	0.14	1.91	0.06	33.2	CIV(1548)	1.9717	
102	4608.64	0.13	1.13	0.05	33.7	CIV(1550)	1.9718	
103	4657.42	0.16	0.37	0.05	30.0			d
104	4669.33	0.16	0.38	0.05	31.4			d
105	4687.68	0.13	2.03	0.06	32.2	FeII(1608)	1.9144	
						CIV(1548)	2.0278	
						SiII(1526)	2.0704	
106	4695.74	0.13	1.54	0.06	31.3	CIV(1550)	2.0280	
						SiII(1526)	2.0757	
107	4725.42	0.19	0.43	0.06	27.6			a,b,d
108	4731.89	0.23	0.33	0.06	27.7			a
109	4743.66	0.20	0.63	0.07	28.5			a
110	4754.32	0.14	2.01	0.07	30.0	CIV(1548)	2.0709	a
111	4761.73	0.13	2.23	0.07	29.8	CIV(1550)	2.0706	a
						CIV(1548)	2.0757	
112	4772.04	0.12	4.69	0.07	30.5	CIV(1548)	2.0823	a,b
113	4780.36	0.12	3.42	0.07	30.5	FeII(1608)	1.9720	a,b
						CIV(1550)	2.0826	
114	4792.57	0.14	1.31	0.07	29.6	SiII(1526)	2.1391	
115	4823.40	0.25	0.48	0.07	28.4			d
116	4843.24	0.16	1.97	0.08	29.5	CIV(1548)	2.1283	
117	4853.41	0.13	3.41	0.08	29.2	CIV(1550)	2.1297	a,b
						CIV(1548)	2.1349	
118	4860.95	0.12	4.63	0.07	30.6	CIV(1550)	2.1345	a,b
						CIV(1548)	2.1397	
119	4867.93	0.13	2.96	0.07	31.1	AlII(1670)	1.9135	a,b
						CIV(1550)	2.1390	
120	4930.36	0.16	0.44	0.05	29.9	FeII(2373)	1.0771	e
121	4941.37	0.23	0.31	0.06	30.3	FeII(1608)	2.0721	
122	4947.29	0.14	1.59	0.07	30.8	FeII(1608)	2.0758	e
						FeII(2382)	1.0763	
123	5043.92	0.18	0.58	0.07	25.3	FeII(1608)	2.1359	a
124	5048.86	0.16	1.44	0.09	24.8	FeII(1608)	2.1389	a
125	5083.26	0.19	0.56	0.07	23.9			d
126	5186.17	0.18	0.56	0.08	19.8			
127	5225.51	0.23	0.59	0.10	18.8	AlII(1670)	2.1275	
128	5245.44	0.16	1.83	0.12	18.1	AlII(1670)	2.1395	

[a] Apparent component in complex or trough.
[b] Probable blend.
[c] Very uncertain equivalent width.
[d] Possibly spurious line.

2.08 and $z_{abs} \sim 2.13$) with implied ejection velocities which are less than this value. This rules out such large shells. No absorption systems are observed with redshifts between that of Tol 1037−2704 and that of Tol 1038−2712 in the spectrum of the latter, therefore shells (of any size) ejected from Tol 1037−2704 appear to be ruled out. In addition, we would expect a velocity shift due to differing line-of-sight components of shell motion in the sense that the absorption in Tol 1038 would be expected at a somewhat higher redshift. The opposite is observed in all but one of the apparent correlations in absorption redshift (see Table 6).

2. The possibility that the absorption is due to shells of material ejected from Tol 1038−2712 seems even more unlikely; the ejecta must be at least as distant from Tol 1038−2712 as is Tol 1037−2704 in order to appear in absorption in both spectra, and at epoch $z \sim 2$ this distance is ~ 24 h_{100}^{-1} Mpc. If the velocity differences between the corresponding systems were attributed to differing line-of-sight components of shell velocity, assuming spherically symmetric ejection from Tol 1038−2712, then the implied distance of the absorbing material from Tol 1038−2712 would be less than or of the order of 9 h_{100}^{-1} Mpc. Clearly this is a contradiction. Also, it would be difficult to explain why some of the values of Δv are negative; one would expect that all of the systems in the spectrum of Tol 1038−2712 would be at a slightly lower redshift under the present assumption because the component of shell velocity along the line of sight would be larger because of the angle effect. Spherically symmetric ejection from either one of the quasars appears to be ruled out from geometrical considerations alone.

3. A third possibility is that each absorption system corresponds to an asymmetrical cloud of gas (i.e., a "blob") ejected from Tol 1037−2704. This requires that our line of sight be a relatively special one. Each cloud would have to be at least ~ 4.4 h_{100}^{-1} Mpc across in order to intersect both lines of sight. The clouds' distances from Tol 1037 are uncertain, but it seems reasonable to expect that they would be at least as far away from Tol 1037 as the physical separation between the two lines of sight.

By far the strongest argument against the absorption's being

TABLE 3

ABSORPTION-LINE LIST FOR TOL 1038 – 2712

Line No.	λ_{obs}	$\sigma(\lambda)$	W_{obs}	$\sigma(W)$	S/N	ID	z_{abs}	Notes
1	3329.97	0.15	2.39	0.15	11.3			c
2	3340.26	0.14	4.69	0.18	10.8			b,c
3	3354.76	0.13	1.70	0.12	11.3			c
4	3372.50	0.15	5.87	0.19	11.8			c
5	3382.45	0.14	2.65	0.14	12.9			c
6	3388.95	0.14	4.46	0.15	13.4	SiII(1190)	1.8469	c
7	3397.09	0.15	1.18	0.10	14.7	SiII(1193)	1.8468	d
8	3421.00	0.14	4.28	0.14	16.3			b
9	3440.28	0.17	1.19	0.10	17.1	SiIII(1206)	1.8514	c
10	3449.45	0.16	1.44	0.10	18.1			a
						SiII(1190)	1.8977	
11	3455.02	0.13	0.98	0.06	18.6			a
12	3457.71	0.13	1.06	0.07	18.8	SiII(1193)	1.8976	a
13	3463.48	0.13	5.49	0.12	19.4	HI(1215)	1.8490	a,b
14	3470.49	0.13	1.71	0.08	20.5	HI(1215)	1.8548	c
15	3489.66	0.14	0.90	0.07	22.7	SiIII(1206)	1.8924	a,c
16	3500.60	0.13	1.56	0.07	22.3			c
17	3506.42	0.13	0.93	0.06	21.8			c,d
18	3509.87	0.14	1.15	0.07	21.2			a,c,d
19	3516.76	0.13	4.69	0.11	21.0	HI(1215)	1.8929	
						SiII(1190)	1.9542	
20	3533.97	0.19	1.40	0.10	20.0	NV(1238)	1.8527	b,c
21	3545.03	0.16	0.58	0.07	20.1	NV(1242)	1.8525	b,c
22	3554.57	0.13	2.73	0.09	20.6			a,c
23	3559.43	0.14	0.98	0.07	20.8			a,c
24	3564.71	0.13	2.36	0.09	20.9	SiIII(1206)	1.9546	a,c
25	3591.49	0.13	6.49	0.11	20.1	HI(1215)	1.9543	b,c
						SiII(1190)	2.0170	
26	3598.39	0.13	5.01	0.10	20.4	HI(1215)	1.9600	b
						SiII(1193)	2.0155	
27	3625.52	0.14	1.57	0.08	20.8			b
28	3628.26	0.14	0.71	0.06	21.0			
29	3633.89	0.17	0.49	0.07	21.5	SiIII(1206)	2.0119	a
30	3637.21	0.15	0.48	0.06	20.6	SiIII(1206)	2.0147	a
31	3640.10	0.13	1.15	0.07	20.4	SiIII(1206)	2.0170	a
32	3649.06	0.13	0.63	0.05	21.2	SiII(1260)	1.8951	a,d
						SiII(1190)	2.0654	
33	3652.19	0.13	2.23	0.08	21.4	SiII(1260)	1.8976	a
						SiII(1190)	2.0680	
34	3661.49	0.13	6.14	0.11	21.1	NV(1238)	1.9556	a
						HI(1215)	2.0119	
						SiII(1193)	2.0684	
						SiII(1190)	2.0758	
35	3667.27	0.13	1.44	0.07	21.6	NV(1238)	1.9603	a,d
						HI(1215)	2.0167	
36	3670.13	0.13	0.53	0.05	21.7	SiII(1193)	2.0757	a,d
37	3673.74	0.16	1.16	0.08	21.7	NV(1242)	1.9560	a,d
						SiII(1190)	2.0861	
38	3681.62	0.16	2.78	0.12	20.5	SiII(1193)	2.0853	b
39	3691.64	0.13	2.66	0.09	20.5			
40	3699.38	0.14	1.51	0.09	20.1	SiIII(1206)	2.0662	
41	3708.41	0.15	1.86	0.10	19.4	OI(1302)	1.8479	b
						SiIII(1206)	2.0737	
42	3712.58	0.16	0.63	0.08	19.2	OI(1302)	1.8511	a,d
						SiIII(1206)	2.0771	
43	3722.28	0.17	0.57	0.07	20.2	SiII(1260)	1.9532	a,d
						HI(1215)	2.0619	
						SiIII(1206)	2.0852	
44	3728.05	0.17	1.17	0.09	19.8	HI(1215)	2.0667	a
45	3735.24	0.18	1.04	0.09	19.8	NV(1238)	2.0152	a

TABLE 3—*Continued*

Line No.	λ_{obs}	$\sigma(\lambda)$	W_{obs}	$\sigma(W)$	S/N	ID	z_{abs}	Notes
46	3742.65	0.14	1.04	0.07	20.2	HI(1215)	2.0787	a
47	3745.28	0.15	0.84	0.07	20.0	NV(1242)	2.0136	a
						HI(1215)	2.0808	
						SiII(1190)	2.1462	
48	3753.98	0.15	1.25	0.09	19.8	HI(1215)	2.0880	a,d
						SiII(1193)	2.1459	
49	3776.96	0.17	0.77	0.09	19.0			b
50	3792.07	0.16	2.68	0.12	19.7	NV(1238)	2.0610	b
						SiIII(1206)	2.1430	
51	3800.65	0.14	1.48	0.08	19.5	CII(1334)	1.8479	a
						SiII(1260)	2.0154	
						NV(1238)	2.0680	
52	3804.47	0.13	2.68	0.08	19.8	CII(1334)	1.8508	a
						SiII(1260)	2.0184	
						NV(1242)	2.0612	
53	3809.45	0.13	2.50	0.09	18.8	CII(1334)	1.8545	a
						NV(1238)	2.0751	
54	3812.55	0.14	0.65	0.08	15.5	NV(1238)	2.0776	a
						NV(1242)	2.0677	
55	3826.45	0.17	0.59	0.09	15.6	NV(1242)	2.0789	a
						HI(1215)	2.1476	
56	3845.15	0.11	2.02	0.07	28.7	OI(1302)	1.9529	
57	3854.35	0.19	0.86	0.08	22.6	SiII(1304)	1.9550	a
						OI(1302)	1.9599	
58	3857.74	0.15	0.35	0.05	22.8			a
59	3869.59	0.16	0.61	0.06	23.4			a
60	3873.26	0.12	0.95	0.05	31.8	SiII(1260)	2.0730	a
61	3897.67	0.10	1.88	0.05	38.4	NV(1238)	2.1463	b
62	3907.26	0.13	3.14	0.07	31.3	NV(1242)	2.1439	b
63	3934.23	0.10	3.02	0.05	46.2			
64	3945.74	0.13	2.62	0.06	36.1	CII(1334)	1.9566	
65	3958.77	0.10	0.85	0.03	50.2			
66	3962.92	0.10	0.83	0.03	50.4	SiII(1260)	2.1441	
67	3970.48	0.10	1.63	0.05	51.3	SiIV(1393)	1.8488	
68	3986.40	0.11	0.99	0.03	57.8			
69	3993.45	0.09	1.13	0.03	60.3	SiIV(1402)	1.8468	b
						OI(1302)	2.0668	
70	3998.13	0.10	0.59	0.02	62.3	SiIV(1402)	1.8502	b
						SiII(1304)	2.0652	
71	4005.63	0.10	0.60	0.02	64.3	OI(1302)	2.0761	
72	4009.70	0.10	0.57	0.02	65.3			
73	4015.63	0.09	1.70	0.03	67.9	OI(1302)	2.0838	
74	4027.87	0.09	1.51	0.03	75.7			
75	4036.77	0.11	0.40	0.02	77.3	SiIV(1393)	1.8963	
76	4077.39	0.19	0.62	0.04	56.3			a
77	4093.58	0.15	0.44	0.03	56.5	CII(1334)	2.0674	a,d
78	4117.78	0.10	0.82	0.02	83.4	SiIV(1393)	1.9544	a
						CII(1334)	2.0856	
79	4126.03	0.12	0.44	0.02	80.0	SiIV(1393)	1.9604	a
80	4144.65	0.10	0.63	0.03	73.2	SiIV(1402)	1.9546	c
81	4263.30	0.13	0.61	0.04	45.2			a
82	4271.32	0.15	0.62	0.04	39.3	SiIV(1393)	2.0646	a
83	4287.85	0.14	0.44	0.04	40.5	SiIV(1393)	2.0765	a
84	4298.97	0.14	1.09	0.05	41.3	SiIV(1402)	2.0646	a
						SiIV(1393)	2.0845	
85	4305.12	0.16	0.48	0.04	39.4			a,d
86	4312.53	0.15	0.95	0.05	39.6	SiIV(1402)	2.0743	a
87	4353.66	0.22	0.36	0.05	37.2			

TABLE 3—*Continued*

Line No.	λ_{obs}	$\sigma(\lambda)$	W_{obs}	$\sigma(W)$	S/N	ID	z_{abs}	Notes
88	4416.16	0.18	1.12	0.06	41.2	CIV(1548)	1.8524	b
						SiII(1526)	1.8926	
89	4479.99	0.17	0.34	0.04	40.5	CIV(1548)	1.8937	
90	4485.74	0.17	0.41	0.04	40.2	CIV(1550)	1.8926	
91	4511.56	0.18	0.48	0.05	40.8	SiII(1526)	1.9551	
92	4574.43	0.16	1.55	0.06	40.7	CIV(1548)	1.9547	b,c
93	4582.82	0.15	1.68	0.06	41.8	CIV(1550)	1.9552	b
						CIV(1548)	1.9601	
94	4590.96	0.16	0.47	0.04	42.2	FeII(1608)	1.8543	
						CIV(1550)	1.9604	
95	4640.13	0.19	0.39	0.05	37.5			a
96	4665.99	0.13	2.55	0.06	38.9	CIV(1548)	2.0138	
97	4673.87	0.14	2.69	0.07	37.6	CIV(1550)	2.0139	b
98	4765.19	0.27	19.35	0.22	29.0	AlII(1670)	1.8519	
						CIV(1549)	2.0760	
99	4811.66	0.43	4.05	0.16	27.4			
100	4870.16	0.16	1.37	0.08	26.3	CIV(1548)	2.1457	a,b
101	4878.54	0.21	2.42	0.12	24.9	CIV(1550)	2.1459	a,b
102	5047.21	0.37	1.11	0.11	28.8			d
103	5125.09	0.22	0.45	0.06	32.1	AlII(1670)	2.0674	d
104	5213.13	0.23	0.45	0.08	23.4	MgI(1827)	1.8519	d
105	5222.77	0.20	0.43	0.07	22.5			d
106	5280.45	0.21	0.64	0.09	19.7	AlIII(1854)	1.8470	d
107	5294.47	0.20	0.52	0.09	18.9	AlIII(1854)	1.8546	d
						MgI(1827)	1.8964	

[a] Apparent component in complex or trough.
[b] Probable blend.
[c] Very uncertain equivalent width.
[d] Possibly spurious line.

due to ejected material from one of the quasars (whether it be in clouds or shells) is an energy argument. If we consider the strong absorption systems at $z_{abs} \approx 2.08$, the implied ejection velocity of the cloud with respect to the quasar is of order 10,500 km s^{-1}. Assuming that the cloud is moving at the implied ejection velocity, that it is at least of order 5 Mpc wide, and that the column density of hydrogen for the cloud is $\sim 10^{19}$ cm^{-2} (for the troughlike system observed in the spectrum of Tol 1038–2712, assuming solar abundances, linear curve of growth, and that all of the C is in C IV, then a *lower* limit on the hydrogen column density is $\sim 4 \times 10^{18}$ cm^{-2}), then a lower limit for the kinetic energy of the cloud is $\sim 10^{62}$ ergs. Following the arguments of Goldreich and Sargent (1976), in a single scattering event, a photon can contribute at most a fraction v/c (where v is the velocity of the scatterer) of its energy to the kinetic energy of the scatterer. Continuum photons from the source are converted rapidly into line photons, and the line photons are made isotropic after one scattering. Thus, for the cloud in question, the maximum energy transfer efficiency for converting radiative energy into kinetic energy is $v/c \sim 10^{-2}$. In order for the cloud to have been accelerated by radiation pressure, the minimum total radiative output of the continuum source (beyond the Lyman limit) is of order 10^{65} ergs, approximately equivalent to a luminosity of 10^{47}–10^{48} ergs s^{-1} for the age of the universe. This is a lower limit for one cloud in the most energetically reasonable case. Furthermore, the implied cloud is much less thick than it is wide (i.e., it is sheetlike), and it would be difficult for such a structure, if ejected, to remain intact because it would be subject to Rayleigh-Taylor instability. We can reject as even more implausible the possibility that the material is ejected from Tol 1038–2712 because of the greater distances over which the material would have to be accelerated. We conclude that, if the absorption systems are indeed correlated, it is unlikely that they can be caused by material ejected from one of the two quasars intersecting both lines of sight.

b) Independent Ejection

The possibility remains that what we are seeing is simply two independent cases of ejected material which just happen to have similar complex ejection patterns. If the absorption redshift coincidence were due purely to chance, there is a very small probability that the ejection patterns would be so similar in two presumably unrelated objects, especially since BAL QSOs and other QSOs with absorption systems thought to be due to ejected material are fairly rare. If, on the other hand, as Jakobsen *et al.* (1986) pointed out, some sort of line-locking mechanism favored a particular ejection pattern, then we would require only one chance match in velocity to explain the observations. However, the curious coincidence in the ratios of $(1 + z_{abs})$ between consecutive systems as found by Jakobsen *et al.* does not appear to be so strong in our data. If absorption-absorption line locking were in effect, the ejection patterns in the two spectra should be such that the systems in one spectrum would be offset from those in the other by an essentially constant velocity (the velocity should vary by no more than the typical velocity width of sharp absorption lines, ~ 150 km s^{-1}); it can be seen from Table 6 that Δv varies from ~ -1700 km s^{-1} to $\sim +2000$ km s^{-1}, i.e., the absorption patterns do not match closely enough. We therefore consider the line-locking possibility to be very unlikely.[3]

[3] It has been pointed out by an anonymous referee that there exists the possibility of line locking of the two components of the C IV $\lambda\lambda$1548, 1550 doublet in the two complex systems ($z_{abs} \sim 2.08$ and $z_{abs} \sim 2.13$) in the spectrum of Tol 1037–2704. Higher resolution data are required to determine whether or not this is the case.

TABLE 4

LINE IDENTIFICATIONS AND ABSORPTION SYSTEMS FOR TOL 1037 – 2704*

ID	λ_0	λ_{obs}	z_{abs}	W_{obs}
SiIII	1206.51	3512.95	1.9117	0.73
SiIII	1206.51	3515.80	1.9140	1.05
HI	1215.67	3540.05	1.9120	2.57
NV	1238.82	3605.39	1.9103	1.78
NV	1242.80	3617.80	1.9110	0.88
SiII	1260.42	3670.62	1.9122	1.97
OI	1302.17	3794.65	1.9141	0.92
SiII	1304.37	3797.51	1.9114	0.75
CII	1334.53	3886.04	1.9119	1.30
SiIV	1393.76	4059.33	1.9125	0.61
SiIV	1402.77	4084.91	1.9120	2.59
CIV	1548.20	4509.11	1.9125	0.89
CIV	1550.77	4516.63	1.9125	0.96
FeII	1608.46	4687.68	[1.9144]	2.03
AlII	1670.81	4867.93	[1.9135]	2.96
			$\langle z_{abs} \rangle$ = 1.9122	
SiII	1190.42	3540.05	1.9738	2.57
SiII	1193.28	3546.45	1.9720	0.75
SiIII	1206.51	3587.10	1.9731	2.31
HI	1215.67	3611.68	1.9709	4.96
NV	1238.82	3682.13	[1.9723]	4.72
NV	1242.80	3692.11	[1.9708]	0.49
NV	1242.80	3695.53	[1.9735]	1.11
SiII	1260.42	3745.70	[1.9718]	7.27
CII	1334.53	3967.11	1.9727	0.94
SiIV	1393.76	4141.71	1.9716	0.93
SiIV	1402.77	4168.69	1.9718	0.32
CIV	1548.20	4600.86	1.9717	1.91
CIV	1550.77	4608.64	1.9718	1.13
FeII	1608.46	4780.36	[1.9720]	3.42
			$\langle z_{abs} \rangle$ = 1.9722	
SiII	1190.42	3605.39	2.0287	1.78
SiII	1193.28	3611.68	[2.0267]	4.96
SiIII	1206.51	3651.36	[2.0264]	3.71
SiIII	1206.51	3656.12	[2.0303]	1.27
HI	1215.67	3682.13	2.0289	4.72
NV	1238.82	3755.62	2.0316	1.30
NV	1242.80	3767.44	2.0314	0.73
SiII	1260.42	3816.10	[2.0276]	13.54
OI	1302.17	3941.87	[2.0272]	0.84
CII	1334.53	4040.33	2.0275	0.39
SiIV	1393.76	4220.75	2.0283	1.34
SiIV	1402.77	4247.50	2.0279	1.17
CIV	1548.20	4687.68	2.0278	2.03
CIV	1550.77	4695.74	2.0280	1.54
			$\langle z_{abs} \rangle$ = 2.0289	
SiII	1190.42	3656.12	2.0713	1.27
SiIII	1206.51	3705.55	2.0713	0.81
HI	1215.67	3734.44	2.0719	4.83
NV	1238.82	3802.43	[2.0694]	4.30
NV	1242.80	3816.10	[2.0706]	13.54
OI	1302.17	3995.85	[2.0686]	0.72
SiIV	1393.76	4279.08	2.0702	0.75
SiIV	1402.77	4306.38	2.0699	0.42
SiII	1526.72	4687.68	2.0704	2.03
CIV	1548.20	4754.32	2.0709	2.01
CIV	1550.77	4761.73	2.0706	2.23
FeII	1608.46	4941.37	[2.0721]	0.31
			$\langle z_{abs} \rangle$ = 2.0708	
SiI	1193.28	3670.62	2.0761	1.97
SiIII	1206.51	3710.67	2.0755	1.25
SiIV	1393.76	4285.58	2.0748	0.70
SiII	1526.72	4695.74	[2.0757]	1.54
CIV	1548.20	4761.73	2.0757	2.23
FeII	1608.46	4947.29	[2.0758]	1.59
			$\langle z_{abs} \rangle$ = 2.0755	
SiII	1190.42	3670.62	[2.0835]	1.97
SiII	1193.28	3676.22	2.0808	3.12
SiII	1193.28	3682.13	[2.0850]	4.72
SiIII	1206.51	3719.93	2.0832	3.68
HI	1215.67	3745.70	[2.0812]	7.27
NV	1238.82	3816.10	[2.0804]	13.54
NV	1242.80	3827.02	[2.0793]	1.09
SiII	1260.42	3886.04	2.0831	1.30
SiII	1304.37	4021.70	2.0833	0.39
CII	1334.53	4114.99	2.0835	1.17
SiIV	1393.76	4296.22	2.0825	2.67
SiIV	1402.77	4324.25	2.0827	2.20
CIV	1548.20	4772.04	2.0823	4.69
CIV	1550.77	4780.36	2.0826	3.42
			$\langle z_{abs} \rangle$ = 2.0825	
SiII	1193.28	3734.44	2.1295	4.83
SiIII	1206.51	3774.11	2.1281	5.06
HI	1215.67	3802.43	2.1278	4.30
SiII	1260.42	3941.87	2.1274	0.84
CII	1334.53	4174.24	2.1279	0.46
SiIV	1393.76	4359.66	2.1280	1.24
SiIV	1402.77	4387.73	2.1279	0.80
CIV	1548.20	4843.24	2.1283	1.97
CIV	1550.77	4853.41	2.1297	3.41
AlII	1670.81	5225.51	2.1275	0.59
			$\langle z_{abs} \rangle$ = 2.1283	
SiII	1190.42	3734.44	2.1371	4.83
SiII	1193.28	3745.70	[2.1390]	7.27
SiIII	1206.51	3786.81	2.1386	3.89
HI	1215.67	3816.10	[2.1391]	13.54
NV	1238.82	3886.04	2.1369	1.30
NV	1242.80	3897.77	2.1363	0.41
SiII	1260.42	3955.97	2.1386	3.11
SiII	1304.37	4094.44	[2.1390]	1.46
CII	1334.53	4189.27	2.1391	1.92
SiIV	1393.76	4370.12	2.1355	0.67
SiIV	1393.76	4374.93	2.1389	2.35
SiIV	1402.77	4403.14	2.1389	1.96
SiII	1526.72	4792.57	2.1391	1.31
CIV	1548.20	4853.41	2.1349	3.41
CIV	1550.77	4860.95	2.1345	4.63
CIV	1548.20	4860.95	2.1397	4.63
CIV	1550.77	4867.93	2.1390	2.96
FeII	1608.46	5043.92	[2.1359]	0.58
FeII	1608.46	5048.86	2.1389	1.44
AlII	1670.81	5245.44	2.1395	1.83
			$\langle z_{abs} \rangle$ = 2.1378	

* Identifications whose implied z_{abs} appears in brackets are particularly uncertain because the line has been multiply identified, because of obvious blending, or because the feature is very weak. They have not been included in the calculation of $\langle z_{abs} \rangle$ for each absorption system.

TABLE 5

LINE IDENTIFICATIONS AND ABSORPTION SYSTEMS FOR TOL 1038 – 2712[a]

ID	λ_0	λ_{obs}	z_{abs}	W_{obs}
SiII	1190.42	3388.95	1.8469	4.46
SiII	1193.28	3397.09	1.8468	1.18
SiIII	1206.51	3440.28	1.8514	1.19
HI	1215.67	3463.48	[1.8490]	5.49
HI	1215.67	3470.49	1.8548	1.71
NV	1238.82	3533.97	1.8527	1.40
NV	1242.80	3545.03	1.8525	0.58
OI	1302.17	3708.41	[1.8479]	1.86
OI	1302.17	3712.58	[1.8511]	0.63
CII	1334.53	3800.65	[1.8479]	1.48
CII	1334.53	3804.47	[1.8508]	2.68
CII	1334.53	3809.45	[1.8545]	2.50
SiIV	1393.76	3970.48	1.8488	1.63
SiIV	1402.77	3993.45	1.8468	1.13
SiIV	1402.77	3998.13	1.8502	0.59
CIV	1549.0	4416.16	1.8509	1.12
FeII	1608.46	4590.96	[1.8543]	0.47
AlII	1670.81	4765.19	[1.8520]	19.35
MgI	1827.94	5213.13	[1.8519]	0.45
AlIII	1854.72	5280.45	[1.8470]	0.64
AlIII	1854.72	5294.47	[1.8546]	0.52
			$\langle z_{abs} \rangle$ = 1.8502	
SiII	1190.42	3449.45	[1.8977]	1.44
SiII	1193.28	3457.71	[1.8976]	1.06
SiIII	1206.51	3489.66	1.8924	0.90
HI	1215.67	3516.76	1.8929	4.69
SiII	1260.42	3649.06	[1.8951]	0.63
SiII	1260.42	3652.19	[1.8976]	2.23
SiIV	1393.76	4036.77	1.8963	0.40
SiII	1526.72	4416.16	[1.8926]	1.12
CIV	1548.20	4479.99	1.8937	0.34
CIV	1550.77	4485.74	1.8926	0.41
MgI	1827.94	5294.47	[1.8964]	0.52
			$\langle z_{abs} \rangle$ = 1.8936	
SiII	1190.42	3516.76	[1.9542]	4.69
SiIII	1206.51	3564.71	1.9546	2.36
HI	1215.67	3591.49	1.9543	6.49
HI	1215.67	3598.39	1.9600	5.01
NV	1238.82	3661.49	1.9556	6.14
NV	1238.82	3667.27	1.9603	1.44
NV	1242.80	3673.74	1.9560	1.16
SiII	1260.42	3722.28	1.9532	0.57
OI	1302.17	3845.15	[1.9529]	2.02
SiII	1304.37	3854.35	[1.9550]	0.86
OI	1302.17	3854.35	[1.9599]	0.86
CII	1334.53	3945.74	1.9566	2.62
SiIV	1393.76	4117.78	1.9544	0.82
SiIV	1393.76	4126.03	1.9604	0.44
SiIV	1402.77	4144.65	1.9546	0.63
SiII	1526.72	4511.56	1.9551	0.48
CIV	1548.20	4574.43	1.9547	1.55
CIV	1550.77	4582.82	1.9552	1.68
CIV	1548.20	4582.82	1.9601	1.68
CIV	1550.77	4590.96	1.9604	0.47
			$\langle z_{abs} \rangle$ = 1.9564	
SiII	1190.42	3591.49	[2.0170]	6.49
SiII	1193.28	3598.39	[2.0155]	5.01
SiIII	1206.51	3633.89	[2.0119]	0.49
SiIII	1206.51	3637.21	[2.0147]	0.48
SiIII	1206.51	3640.10	[2.0170]	1.15
HI	1215.67	3661.49	[2.0119]	6.14
HI	1215.67	3667.27	[2.0167]	1.44
NV	1238.82	3735.24	2.0152	1.04
NV	1242.80	3745.28	2.0136	0.84
SiII	1260.42	3800.65	2.0154	1.48
SiII	1260.42	3804.47	[2.0184]	2.68
CIV	1548.20	4665.99	2.0138	2.55
CIV	1550.77	4673.87	2.0139	2.69
			$\langle z_{abs} \rangle$ = 2.0144	
SiII	1190.42	3649.06	[2.0654]	0.63
SiII	1190.42	3652.19	2.0680	2.23
SiII	1193.28	3661.49	[2.0684]	6.14
SiIII	1206.51	3699.38	2.0662	1.51
HI	1215.67	3722.28	2.0619	0.57
HI	1215.67	3728.05	2.0667	1.17
NV	1238.82	3792.07	2.0610	2.68
NV	1238.82	3800.65	2.0680	1.48
NV	1242.80	3804.47	2.0612	2.68
NV	1242.80	3812.55	2.0677	0.65
OI	1302.17	3993.45	[2.0668]	1.13
SiII	1304.37	3998.13	[2.0652]	0.59
CII	1334.53	4093.58	2.0674	0.44
SiIV	1393.76	4271.32	2.0646	0.62
SiIV	1402.77	4298.97	2.0646	1.09
AlIII	1670.81	5125.09	[2.0674]	0.45
			$\langle z_{abs} \rangle$ = 2.0652	
SiII	1190.42	3661.49	[2.0758]	6.14
SiII	1193.28	3670.13	[2.0757]	0.53
SiIII	1206.51	3708.41	[2.0737]	1.86
SiIII	1206.51	3712.58	[2.0771]	0.63
HI	1215.67	3742.65	2.0787	1.04
NV	1238.82	3809.45	[2.0751]	2.50
NV	1238.82	3812.55	2.0776	0.65
NV	1242.80	3826.45	2.0789	0.59
SiII	1260.42	3873.26	2.0730	0.95
OI	1302.17	4005.63	[2.0761]	0.60
SiIV	1393.76	4287.85	2.0765	0.44
SiIV	1402.77	4312.53	[2.0743]	0.95
CIV	1549	4765.19	2.076	19.35
			$\langle z_{abs} \rangle$ = 2.0768	
SiII	1190.42	3673.74	[2.0861]	1.16
SiII	1193.28	3681.62	2.0853	2.78
SiIII	1206.51	3722.28	2.0852	0.57
HI	1215.67	3745.28	[2.0808]	0.84
HI	1215.67	3753.98	[2.0880]	1.25
OI	1302.17	4015.63	[2.0838]	1.70
CII	1334.53	4117.78	2.0856	0.82
SiIV	1393.76	4298.97	2.0845	1.09
			$\langle z_{abs} \rangle$ = 2.0851	
SiII	1190.42	3745.28	[2.1462]	0.84
SiII	1193.28	3753.98	[2.1459]	1.25
SiIII	1206.51	3792.07	[2.1430]	2.68
HI	1215.67	3826.45	[2.1476]	0.59
NV	1238.82	3897.67	2.1463	1.88
NV	1242.80	3907.26	[2.1439]	3.14
SiII	1260.42	3962.92	2.1441	0.83
CIV	1548.20	4870.16	2.1457	1.37
CIV	1550.77	4878.54	2.1459	2.42
			$\langle z_{abs} \rangle$ = 2.1455	

[a] Identifications whose z_{abs} appears in brackets are particularly uncertain because the line has been multiply identified, because of obvious blending, or because the feature is very weak. They have not been included in the calculation of $\langle z_{abs} \rangle$ for each system.

TABLE 6

ABSORPTION SYSTEMS AND VELOCITY DIFFERENCES[a]

z_{abs}		Δv[b]
Tol 1037−2704	Tol 1038−2712	(km s^{-1})
...	1.8509	...
1.9125	1.8933	1980
1.9717	1.9549	1700
...	1.9602	1160
2.0279	2.0138	1400
2.0708	...	−510
2.0757	2.076	−30
2.0825	...	620
2.1283	...	−1670
2.1348	2.1458	−1050
2.1390	...	−600

[a] Based on observed lines of C IV λλ1548, 1550.

[b] The velocity separation between corresponding absorption systems in the two spectra, where $\Delta v \sim c\Delta z_{abs}/(1 + z_{abs})$.

Even if we ignore the statistical improbability of independent ejection, the existence (or nonexistence) of lines of excited fine-structure states of, e.g., C II and Si II can be used to place limits on the density of the absorbing gas and the distance of the gas from the QSO (Bahcall and Wolf 1968). The line resulting from the excited fine-structure state of C II (C II λ1335) is separated from the ground-state line (C II λ1334) by 1.2 Å in the rest frame, so at the observed redshifts the separation should be ~3.5–4.0 Å and the lines should be easily resolved if both are present. However, because of the complexity of the spectra of Tol 1037−2704 and Tol 1038−2712, the positive identification of excited fine-structure lines is difficult, especially if the ground-state line (e.g., C II λ1334) lies in a trough or a region of the spectrum when many lines of other species at different redshifts happen to occur. The strongest C II λ1334 line from the spectrum of Tol 1037−2704 is a member of the system with $z_{abs} = 2.1390$ and has an observed equivalent width of 1.92 Å. We find that the strength of C II λ1335 from this system (if present) is at least 10 times weaker. Using this fact, we can place a lower limit on the distance of the absorbing material from the QSO by assuming that the gas is in photoionization equilibrium (and that the QSO provides the ionizing photons). From the results of McKee, Tarter, and Weisheit (1973), the relative line strengths of C II and C IV we observe are fairly well satisfied when the ionization parameter $\Gamma = n(\mathrm{H})/n_\gamma \approx 10^3$, where n_γ is the number density of ionizing photons. The critical density for the C II fine-structure state to be collisionally populated is $n_C \approx 100$ for $T \approx 2 \times 10^4$ K (Bahcall and Wolf 1968). That C II λ1335 is not observed implies that $n_H \ll n_C$; thus the approximation can be made that $n_{ex}/n_{gr} \approx n_e/n_C$, where n_{ex}, n_{gr}, and n_e are the number densities in the excited fine-structure state and the ground state and the number density of electrons. If the absorption is on the linear part of the curve of growth, then $n_{ex}/n_{gr} = W(\mathrm{C\ II}\ \lambda1335)/W(\mathrm{C\ II}\ \lambda1334)$ and $n_H \approx n_e \leq 0.1 n_C \approx 10$ cm^{-3}. If the lines are off the linear part of the curve of growth, then a more stringent limit is placed on n_H. From Sargent *et al.* (1979), the photon density at a distance d from a QSO is given by

$$n_\gamma \approx 9 \times 10^{-5} \left(\frac{1\ \mathrm{Mpc}}{d}\right)^2 \left(\frac{L_{\nu_0}}{3 \times 10^{30}}\right) \mathrm{cm}^{-3},$$

where L_{ν_0} is the QSO luminosity in ergs s^{-1} Hz^{-1} evaluated at the ionization limit for hydrogen. Combining this with the above value for Γ, and using $L_{\nu_0} = 1.24 \times 10^{30} h_{100}^{-2}$ ($q_0 = 0.5$) for Tol 1037−2704, we find $d \geq 110\ h_{100}^{-1}$ kpc. The implied ejection velocity for the system with $z_{abs} = 2.1390$ is ~2600 km s^{-1}; if it is assumed that the column density of hydrogen for the gas is $\sim 10^{19}$ cm^{-2} and that the gas is in the form of an ejected shell, the kinetic energy of the shell is $> 10^{61}$ ergs. The maximum radiative to kinetic energy conversion efficiency discussed above requires a minimum radiative output of $\sim 10^{63}$ ergs if the shell has been accelerated by radiation pressure. This number is still so large that even the possibility of independent ejection seems unlikely on the basis of energy arguments.

Despite the above argument, the broad system near $z_{abs} \sim 2.08$ in the spectrum of Tol 1038−2712 is similar enough to systems usually associated with ejected material that it warrants closer scrutiny. The ions for which troughs are observed (C IV, N V, and Si IV) are the ones most typically observed in the spectra of BAL QSOs. We also note that the N V emission in Tol 1038−2712 is strong relative to Lyα, also typical of BAL QSOs (Turnshek 1984). We have measured approximate equivalent widths for the C IV, Si IV, and N V absorption troughs, and they are 24, 21, and 24 Å, respectively. For the C IV trough we have included not only the central component (line 98 in Table 3), but we have also included the more diffuse feature just redward of that component (identified as line 99). The equivalent width of C IV, ~8 Å, in the rest frame is somewhat smaller than the minimum in the range given by Turnshek (1984) of 12–69 Å for a sample of 14 BAL QSOs. The implied ratio of the Si IV to C IV column density (assuming a linear curve of growth) is ~0.6, about twice as large as the *upper* value in the range found by Turnshek. The ratio of N V to C IV column densities is typical of the values found by Turnshek. The total velocity widths of the troughs are ~5000 km s^{-1} for C IV, ~4300 km s^{-1} for Si IV, and ~5000 km s^{-1} for N V. If ejected, the implied ejection velocity of the material responsible for this absorption system is ~24,000 km s^{-1}, within the range of velocities observed in the spectra of BAL QSOs. It is certainly possible, then, that the $z_{abs} \sim 2.08$ system in the spectrum of Tol 1038−2712 (and possibly also the $z_{abs} \sim 2.14$ system) is due to ejected material, while the other absorption systems in the two spectra would be due to intervening material. We also note that the two corresponding systems in the spectrum of Tol 1037−2704 are not unlike systems in the spectrum of GC 1556+335, which Morris *et al.* (1986) have concluded may be consistent with either intervening *or* ejected material. This question will be discussed further in the next section.

c) *Intervening Material: The Case for a Supercluster*

A completely different interpretation of the absorption systems in Tol 1037−2704 and Tol 1038−2712 would be that they arise because the lines of sight intersect intervening material, possibly gas clouds in the halos of galaxies. In this picture, the different redshift systems correspond not to different ejection velocities but to different distances along the lines of sight. If the absorption redshift coincidence we observe is not simply due to chance, then the material responsible for the

absorption has a huge physical extent. The redshifts at which a concentration of absorption systems is seen in both spectra span the range $z_{abs} \approx 1.895$ to $z_{abs} \approx 2.146$; this corresponds to a size of $\sim 50\ h_{100}^{-1}$ Mpc along the line of sight at the epoch $z \sim 2.0$. Such a size is just consistent with the sizes of observed superclusters (e.g., Oort 1983) and would correspond to $\sim 3°$ on the plane of the sky at $z \sim 2$. Redshifts for several of the other QSOs in the field of Tol 1037–2704 and Tol 2712 (see Fig. 3) fall in the same redshift range as the supposed supercluster; Tol 1035–2737 with $z_{em} \sim 2.13$, and Tol 1037–2742 with $z_{em} \sim 1.887$ are $\sim 40'$ and $\sim 35'$ away from the Tol 1037–2704/Tol 1038–2712 pair, respectively. If these QSOs are members of the supercluster, a lower limit of $\sim 10\ h_{100}^{-1}$ Mpc can be placed on the size of the supercluster in the plane transverse to the line of sight. Phillipps (1986) has concluded that QSOs at redshifts above $z = 1$ must be associated with rich clusters. This conclusion is based upon the two observed cases of "associated" absorption (close line-of-sight pairs where absorption is seen in the spectrum of the more distant QSO at the redshift of the nearer QSO) (Robertson and Shaver 1983; Robertson, Shaver, and Swings 1986) and a calculation of the very small probability of such an occurrence if the quasar-galaxy correlation function were the same as the observed galaxy-galaxy correlation function. The presence of many QSOs of comparable redshift in this field may then indicate a large-scale conglomeration of rich clusters of galaxies.

The existence of small velocity splittings observed within some of the absorption systems represents evidence in favor of the presence of galaxy clusters in the field. The 2 Å resolution of the spectra corresponds to ~ 130 km s^{-1} resolution in velocity at the wavelengths at which the C IV lines of the absorption systems are seen. The splittings we observe, however, are of the order of 500–1000 km s^{-1}, e.g., in the systems near $z_{abs} \sim 2.08$ and $z_{abs} \sim 2.13$ in the spectrum of Tol 1037–2704. Velocity splittings of this size are consistent with the hypothesis that each component arises as a result of an individual galaxy in a cluster. The more complex systems would then correspond to lines of sight passing through denser regions of a cluster, and the single-component systems would correspond to lines of sight passing through the less dense outer regions of a cluster. Pettini *et al.* (1983) observed two complex C IV absorption systems in the spectrum of the BL Lac object 0215+015, and suggested that the absorption may be due to two rich clusters of galaxies oriented along the line of sight. Assuming clusters of the same richness as Coma, they concluded that the line of sight must be within ~ 0.2 Mpc of the cluster center (for both clusters) in order to account for the number of observed components in absorption. The probability of intersecting two clusters in this way is very small on the basis of observations at the present epoch; however, the impact parameter and hence the probability involved is highly dependent on the cross section for C IV absorption for a typical cluster galaxy at high redshift, and on the lower luminosity limit for galaxies producing C IV halos. It is still not clear at what epoch cluster galaxies are stripped of much of their interstellar media and gaseous halos; that we observe two absorption complexes in the spectrum of Tol 1037–2704 which are similar to those in 0215+015 may indicate that cluster galaxies at high redshift are significantly more gas-rich than their counterparts at the present epoch. Perhaps the line of sight need not be so close to the cluster center in order to intersect several galaxy halos per cluster.

Clearly the separation of the two lines of sight is much too large for possibly corresponding systems to have arisen from clouds in the halo of a single galaxy; however, ~ 5 Mpc is a reasonable size for a rich cluster of galaxies (although the core radii of clusters are typically much less than 1 Mpc). The observed velocity differences between corresponding absorption systems (Δv in Table 6), typically of order 1500 km s^{-1}, are consistent with the typical velocity dispersions in rich clusters of ~ 1000 km s^{-1}. (If clusters of galaxies are responsible for the correlated absorption systems, then velocity differences would be expected to be less than or of the order of 2000 km s^{-1} [$\sim 2\ \sigma_v$], and this is what is observed.) However, an explanation of possible system-by-system correlations between the two spectra which requires the two lines of sight to intersect the opposite edges of the same five rich clusters is very implausible, expecially since we have seen that the system-by-system correlations may not even be significant.

One of the remaining difficulties with the intervening supercluster hypothesis is that, qualitatively, the absorption spectra of Tol 1037–2704 and Tol 1038–2712 are very similar in richness; each one has at least five absorption systems which are strong enough to be easily detected. One might expect that two random lines of sight (i.e., lines of sight which are far enough apart to exclude the possibility of their passing through the same galaxies or clusters) through a supercluster might yield very different absorption spectra. The fact that two lines of sight separated by ~ 5 Mpc at $z \sim 2$ yield such rich absorption spectra leads us to conclude that we are seeing the supercluster from a special direction such that there is an unusually high line-of-sight density of absorbing material. If this is the case, it seems possible that our line of sight happens to be oriented along a large-scale "filament" or in the plane of a large-scale "sheet" of galaxies; both observational and theoretical studies have indicated that such structure exist on large scales (e.g., de Lapparent, Geller, and Huchra 1986; Davis *et al.* 1985; Dekel, West, and Aarseth 1984). Limits on the physical extent of the supercluster may be better determined by obtaining spectra of all the QSOs in the field with emission redshifts greater than the low-redshift "edge" implied by the spectra of Tol 1037–2704 and Tol 1038–2712 (i.e., with $z_{em} > 1.88$). In this respect, the spectrum we have obtained of Tol 1038–2707 is extremely important. Given the separation ($\sim 17'.9$) of Tol 1037–2704 and Tol 1038–2712, if the unusually rich absorption does result from a special orientation of the supercluster, then from geometry alone one might hope to see evidence for this high line-of-sight concentration of material in the spectrum of a QSO only 5′ away from one of the pair. Unfortunately, the emission redshift of Tol 1038–2707 ($z_{em} = 1.937$) would place it close to the nearer edge of the supercluster; it is, however, encouraging for this hypothesis that we *do* see absorption at $z_{abs} \sim 1.9$, corresponding closely to the supercluster edge implied by the other spectra. It is clearly very important to obtain high-quality spectra of the other nearby QSOs, Tol 1036–2713, Tol 1036–2650, and Tol 1035–2737.[4]

If we are indeed seeing the result of a special line of sight that

[4] [Added in manuscript.] We have obtained slit spectra (~ 4 Å resolution) of Tol 1036–2713 and Tol 1035–2737 at Las Campanas Observatory in 1987 April. We identify Tol 1036–2713 as a QSO with $z_{em} = 3.084$. Tol 1035–2737 is a QSO with $z_{em} = 2.168$. In its spectrum we find a definite absorption system with $z_{abs} = 2.125$, and possible systems with $z_{abs} = 2.040$ and $z_{abs} = 1.905$. If real, all three systems would fall in the redshift range of interest. It is extremely important to obtain a higher resolution spectrum of this object.

happens to lie in an elongated large-scale filament, then it immediately raises the question: Do *all* absorption-line systems arise from material associated with structures like this? If they do, then the number of absorption systems seen in the spectrum of a QSO would be dependent upon the *orientation* of one of these filaments with respect to the line of sight. This would mean that the number of absorption systems per QSO spectrum would *not* be expected to follow a Poisson distribution, but instead would be a function of the distribution of path lengths through the filamentary or sheetlike structure as determined by their orientation with respect to the line of sight. If we suppose that a typical filament is ~ 50 Mpc long and ~ 5–10 Mpc across, then the fraction of time a line of sight would see the filament end-on is ~ 0.01–0.04. Thus, based on this hypothesis, the probability of observing five absorption-line systems in the redshift interval $\Delta z_{abs} \sim 0.3$ would be of the order of 100 times greater than would be predicted assuming a Poisson distribution.

As discussed in § III, there is some question as to the nature of the absorption systems near $z_{abs} \sim 2.08$ and $z_{abs} \sim 2.14$ in the spectra of both Tol 1037−2704 and Tol 1038−2712. The C IV absorption in these systems in the spectrum of Tol 1037−2704 appears to consist of several adjacent narrow doublets, with fine splittings of ~ 500–1000 km s^{-1} as discussed above. A natural explanation for this would be that the line of sight passes through gas clouds in the halos of several galaxies in a cluster. On the other hand, absorption systems of this kind have been shown to be consistent with ejection as well (Morris *et al.* 1986). The strongest arguments in favor of the ejection origin for the absorbing material has been that the probability of intersecting two clusters along a line of sight is very small, and so this could be ruled out if such systems were not extremely rare (Pettini *et al.* 1983; Morris *et al.* 1986). However, under the filament-orientation hypothesis for the statistics of absorption systems outlined above, the probability of such an occurrence is significantly increased.

The relatively smooth, broad absorption in the systems in Tol 1038−2712 present somewhat more of a problem. These systems are, as we have pointed out, marginally consistent with the absorption seen in BAL QSOs. The FWHM of the C IV λ1549 absorption at $z_{abs} = 2.076$ is ~ 60 Å. If the width of the line were due to thermal broadening, the implied velocity in the gas would be ~ 2000 km s^{-1}, corresponding to a temperature of $\sim 5 \times 10^8$ K. This is clearly much too high to be consistent with the observed ionic species. Thus it appears that the breadth of the absorption trough must be due to gas motion or result from the Hubble flow over a large extent along the line of sight. However, the implied velocity dispersion of ~ 2000 km s^{-1} is too large for any gas associated with a single galaxy or cluster, and there is no obvious mechanism for producing such absorption features from intervening material associated with a supercluster. Even so, the absence of any broad absorption systems outside the range of redshifts observed in the spectrum of Tol 1037−2704, along with the physical arguments against ejection, persuades us that the absorption is due to intervening material associated with a supercluster.

V. CONCLUSIONS

Our higher resolution spectra have confirmed the discovery by Jakobsen *et al.* (1986) that Tol 1037−2704 and Tol 1038−2712 have an unusual concentration of absorption systems in the same redshift range. While we agree for the most part with the findings of Jakobsen *et al.*, this work represents a modification or improvement over the previous results in the following ways:

1. We have identified five absorption redshift systems in each QSO (we have confirmed the four systems found by Jakobsen *et al.* 1986 and have identified a new one), many of them having substructure. Our higher resolution data have shown that many of the absorption systems which appeared to be smooth or troughlike in the spectra used by Jakobsen *et al.* actually consist of several narrow components. Qualitatively, this makes the possibility that the absorption is due to ejection less likely (although we cannot completely rule out an ejected origin for some of the systems). The systems extend in redshift from $z_{abs} = 1.88$ to 2.15.

2. We have found that the QSO Tol 1038−2707, only 5′ away from Tol 1038−2712 on the plane of the sky, has a strong absorption system at $z_{abs} \sim 1.9$. This is in the same redshift range ($1.88 < z_{abs} < 2.15$) as the five systems in both Tol 1037−2704 and Tol 1038−2712.

3. We were able to show that ejection from either Tol 1037−2704 or Tol 1038−2712 which covers the line of sight to the other can be dismissed on energetic or on geometrical grounds or on both. Similarly, independent ejection from both QSOs can be eliminated on energetic grounds for at least some of the systems. Line locking does not seem likely to play a role in determining the observed redshift ratios.

4. The most likely possibility is that Tol 1037−2704, Tol 1038−2712, and a third nearby QSO, Tol 1038−2707, are in a large supercluster. The material responsible for the absorption in all three QSOs would then be intervening gas associated with galaxies in the supercluster. While this is in general agreement with the favored interpretation of Jakobsen *et al.* (1986), we differ in our interpretation of the details of the situation. Jakobsen *et al.* emphasized the fact that each system in the spectrum of Tol 1037−2704 matches (in redshift) a system in the spectrum of Tol 1038−2712 to within ~ 2000 km s^{-1}. While we agree that this is true, we argue that the significance of these correlations is difficult to gauge; in fact, it would be extremely difficult to explain these correlations if they were significant. We consider most important the fact that both Tol 1037−2704 and Tol 1038−2712 have unusually rich absorption spectra, and in both cases the high density of strong absorption systems is confined to the redshift range $1.88 < z_{abs} < 2.15$. For this reason we suggest that our line of sight may be intersecting the supercluster in such a way as to make the line-of-sight density of absorption systems extraordinarily high, i.e., the line of sight is along the axis of a filament or in the plane of a sheet of galaxies. If the supercluster is in the form of a filament, then its implied dimensions are $\sim 50\ h_{100}^{-1}$ Mpc along the line of sight and of order $10\ h_{100}^{-1}$ Mpc on the plane of the sky (at the epoch corresponding to $z = 2$). Such a size (~ 150 Mpc at the present epoch, if superclusters expand with the general Hubble flow) is near the upper limit of plausibility based on our local knowledge. Possibly the most important next step is to investigate the spectra of the several QSOs already discovered by Bohuski and Weedman (1979) in the surrounding field.

5. If *all* QSO absorption systems arise from material associated with such large-scale structures, then one would predict that the number of absorption systems per QSO spectrum would *not* follow a Poisson distribution. This will be tested

when better statistics of CIV absorption systems become available.

It is clear that the existence of absorption phenomena like those observed in the spectra of Tol 1037−2704 and Tol 1038−2712 offers the fascinating possibility of leading to detailed insights into the large-scale distribution of galaxies at large redshift—information which cannot be obtained by other means.

We thank P. Jakobsen and his colleagues for sending a preprint of their paper. We also would like to thank S. Phinney and an anonymous referee for very helpful comments on an earlier draft of this paper. Angel Guerra is thanked for his dedicated help at the telescope. The work was supported in part by grant AST84-16704 from the National Science Foundation.

REFERENCES

Bahcall, J. N., and Wolf, R. A. 1968, *Ap. J.*, **152**, 701.
Bohuski, T. J., and Weedman, D. W. 1979, *Ap. J.*, **231**, 653.
Boksenberg, A., and Sargent, W. L. W. 1983, in *Proc. 24th Liège Symposium, Quasars and Gravitational Lenses* (Liège: Institut d'Astrophysique), p. 589.
Crotts, A. P. 1986, *Ap. J.*, **298**, 732.
Davis, M., Efstathiou, G., Frenk, C. S., and White, S. D. M. 1985, *Ap. J.*, **292**, 371.
Dekel, A., West, M. J., and Aarseth, S. J. 1984, *Ap. J.*, **279**, 1.
de Lapparent, V., Geller, M. J., and Huchra, J. P. 1986, *Ap. J. (Letters)*, **302**, L1.
Goldrich, P., and Sargent, W. L. W. 1976, *Comm. Astr. Ap.*, **6**, 133.
Jakobsen, P., Perryman, M. A. C., Ulrich, M. H., Machetto, F., and Di Serego Alighieri, S. 1986, *Ap. J. (Letters)*, **303**, L27.
McKee, C. F., Tarter, C. B., and Weisheit, J. C. 1973, *Ap. Letters*, **13**, 13.
Morris, S. L., Weymann, R. J., Foltz, C. B., Turnshek, D. A., Shectman, S., Price, C., and Boroson, T. A. 1986, *Ap. J.*, **310**, 40.
Oort, J. H. 1983, *Ann. Rev. Astr. Ap.*, **21**, 373.
Pettini, M., Hunstead, R. W., Murdoch, H. S., and Blades, J. C. 1983, *Ap. J.*, **273**, 436.
Phillipps, S. 1986, *M.N.R.A.S.*, **223**, 173.
Robertson, J. G., and Shaver, P. A. 1983, *M.N.R.A.S.*, **204**, 69P.
Robertson, J. G., Shaver, P. A., and Swings, J. P. 1986, *M.N.R.A.S.*, **219**, 403.
Sargent, W. L. W., and Boksenberg, A. 1983, in *Proc. 24th Liège Symposium, Quasars and Gravitational Lenses* (Liège: Institut d'Astrophysique), p. 518.
———. 1987, *Ap. J.*, in preparation.
Sargent, W. L. W., Young, P. J., Boksenberg, A., Carswell, R. F., and Whelan, J. A. J. 1979, *Ap. J.*, **230**, 49.
Shaver, P. A., and Robertson, J. G. 1983, *Ap. J. (Letters)*, **268**, L57.
Shectman, S. A. 1982, in *Annual Report of the Director, Mount Wilson and Las Campanas Observatories* (Washington, DC: Carnegie Institution of Washington), pp. 676–677.
Turnshek, D. A. 1984, *Ap. J.*, **280**, 51.
Ulrich, M. H., and Perryman, M. A. C. 1986, *M.N.R.A.S.*, **220**, 429.
Weymann, R. J., Carswell, R. F., and Smith, M. G. 1981, *Ann. Rev. Astr. Ap.*, **19**, 41.
Young, P., Sargent, W. L. W., and Boksenberg, A. 1982, *Ap. J. Suppl.*, **48**, 455.
Young, P. J., Sargent, W. L. W., Boksenberg, A., Carswell, R. F., and Whelan, J. A. J. 1979, *Ap. J.*, **229**, 891.

W. L. W. SARGENT and C. C. STEIDEL: Palomar Observatory, 105-24, California Institute of Technology, Pasadena, CA 91125

Chapter 3

A HIGH-REDSHIFT EXTENSION OF THE SURVEY FOR C IV ABSORPTION IN THE SPECTRA OF QSOs: THE REDSHIFT EVOLUTION OF THE HEAVY ELEMENT ABSORBERS [1]

CHARLES C. STEIDEL

Palomar Observatory, California Institute of Technology

To appear in *The Astrophysical Journal Supplement Series*

[1] The observations described in this paper were obtained primarily at the Las Campanas Observatory as part of the agreement between the California Institute of Technology and the Carnegie Institute of Washington.

ABSTRACT

We have obtained spectra with a resolution of 60 km $s^{-1}$of 11 QSOs with $3.045 \leq z_{em} \leq 4.104$. In general, the spectra cover the wavelength range between the C IV λ1549 and Lyman α emission lines. The QSOs were chosen to supplement the large survey for C IV absorption in the spectra of high redshift QSOs recently published by Sargent, Boksenberg, and Steidel (1988). The combined sample of C IV $\lambda\lambda$1548, 1550 doublets now contains 275 redshifts, spanning the redshift range $1.3 \leq z_{abs} \leq 4.0$. The new data considerably improve the statistics of the C IV absorbers for $z_{abs} > 2.5$. Unbiased subsamples of C IV redshifts have been isolated in order to investigate the evolution of the properties and distribution of the absorbers with redshift, with the following principal results:

The number of C IV absorption systems per unit redshift range $N(z)$ *decreases* with increasing redshift in the range $1.3 \leq z_{abs} \leq 3.7$ in a manner inconsistent with a constant comoving density of absorbers. This inconsistency is at the 3.1σ level for $q_0 = 1/2$ and at the 4.0σ level for $q_0 = 0$. Thus, the properties of the absorbers are almost certainly evolving with time. The $N(z)$ curve exhibits a gradual decline for $z > 2$, as opposed to the rapid fall–off suggested by earlier results.

The peak in the C IV 2–point correlation function on velocity scales $200 \leq \Delta v \leq 600$ km s^{-1}appears to have the same power in high–redshift ($z_{abs} > 2.2$) and low–redshift ($z_{abs} < 2.2$) subsamples. There is marginal evidence that the width of the correlation peak on these small velocity scales is smaller in the high redshift subsample. A 2σ excess of power on velocity scales $1000 \leq \Delta v \leq 10{,}000$ km s^{-1}exists in the low redshift subsample, but not in the high redshift subsample.

Arguments are presented that appear to rule out a significant evolution of the gas velocity dispersion parameter b with redshift in the clouds which give rise to the C IV absorption, and therefore the evolution of the number of observed C IV systems is interpreted as a systematic change in the mean C IV column density of the clouds. A changing abundance of C, and not a systematically changing ionization state in the gas, is probably dominating the observed evolution. The evolution of the mean C IV doublet ratio and a changing distribution of equivalent width with redshift indicate that the typical C IV

column density, and by extension the typical abundance of C, is increasing by a factor of ~ 3 over the redshift range $3 \geq z \geq 1.5$, corresponding to lookback times of $12.4h_{50}^{-1}$ to $9.8h_{50}^{-1}$ Gigayears ($q_0 = 1/2$) and an e–folding time for chemical enrichment of between 1 and 2 Gigayears. An attempt is made to relate the chemical evolution of the absorbers to early enrichment in galactic halos.

Subject headings: cosmology–galaxies–quasars

I. INTRODUCTION

It has been recognized for some time now that the QSO heavy element absorption systems in principle offer a means of studying the properties and distribution of baryonic material at redshifts that are largely inaccessible to other observational means. The first step toward using the heavy element systems for such study was necessarily to show that they indeed arise from an intervening population of absorbers, as opposed to material that may be somehow associated with the QSO itself. Young, Sargent, and Boksenberg (1982) undertook a statistical study of the distribution in redshift and in apparent "ejection" velocity relative to the QSO of the C IV absorption systems in the spectra of 33 QSOs. They found that the distribution in velocity space was indeed consistent with uniformly distributed absorbers, and that the velocities of the absorbers relative to the QSO rest frame are for the most part cosmological in origin, i.e., resulting from the general Hubble flow and not due to ejection of material from the QSO itself. More recently, Sargent, Boksenberg, and Steidel (1988) (hereinafter SBS) completed a larger and more sensitive survey for C IV absorption, this time in the spectra of 55 QSOs. The general findings of Young, Sargent, and Boksenberg (1982) were confirmed; in addition, the improved statistics allowed an investigation of the evolution in redshift of the number density of C IV absorbers, as well as a determination of the two–point correlation function (in velocity space) of the absorbers. It was found that the number of C IV absorbers actually decreases with increasing redshift over the range $1.25 \leq z_{abs} \leq 3.3$, very much contrary to the evolution of the Lyman α forest absorption lines (e.g., Murdoch *et al.* 1986) and the Lyman Limit absorption systems (e.g., Sargent, Steidel, and Boksenberg 1989 (hereinafter SSB), Lanzetta 1988, Tytler 1982). This observed evolution of the C IV absorbers could be naturally explained by a systematic evolution in the heavy element enrichment in the gaseous material as a function of time, or a systematic change in the level of ionization in the clouds as a function of redshift, or both. The decline in the number of C IV absorption systems (subject to a minimum rest equivalent width criterion) with increasing redshift actually appeared as if there might be a rather precipitous "drop–off" for redshifts larger than ~ 2.8, although this could not be substantiated statistically given the existing data. Although the survey of SBS was sensitive

to absorption in the redshift range $1.25 \leq z_{abs} \leq 3.5$, the data were sparse for $z_{abs} > 2.7$. There were two primary reasons for this: One was that there just were not many bright, high–redshift QSOs known during the time that the observations were being made for the survey, and secondly, the observations were made with the photon–counting IPCS detector, whose efficiency was quite low for wavelengths above ~ 6000 Å. In view of the importance of improving the statistics of the C IV absorption systems at the highest redshifts (where it appeared that the evolution may be occurring quite rapidly), a high redshift "extension" of the SBS survey was undertaken, this time with a sample of QSOs with $z_{em} \geq 3.0$, using red–sensitive CCD detectors. The new survey is intended to be completely complementary to the SBS survey, and was deliberately carried out with comparable spectral resolution and sensitivity for the detection of weak C IV doublets. In combination with the previously completed survey, the new data allow the properties of the heavy element absorption systems to be investigated over the whole redshift range $1.25 \leq z_{abs} \leq 3.7$.

We present the new observations in §II, and the new sample of C IV absorption systems in §III. We rediscuss the evolution of the C IV absorption systems in light of the new data (and combined with the previous survey results) in §IV, and discuss the implications of the chemical evolution of the absorbers at early epochs in §V. The conclusions are summarized in §VI.

II. OBSERVATIONS AND REDUCTIONS

As in SBS, the QSOs observed as part of this survey were selected solely on the basis of their brightness and emission redshift. Since it was important to improve the statistics of the absorption systems with $z_{abs} > 2.7$, the sample was restricted to QSOs with $z_{em} > 3.0$. In fact, the mean emission redshift of the 11 objects observed is $\langle z_{abs} \rangle = 3.473$. In order to produce a large enough sample of objects with very high redshift, it was necessary to relax the apparent magnitude criterion from $m_V \leq 18.0$ in SBS to $m_V \leq 18.5$ for the current sample.

Spectra of all but one of the 11 objects observed were obtained at the Las Campanas 2.5 m DuPont Telescope in 1988 September; the spectrum of Q1208+101 was obtained in 1988 February at the Palomar Hale Telescope. The complete journal of observations is

presented in Table 1.

The new Modular Spectrograph at Las Campanas Observatory turned out to be ideally suited to the type of observations necessary for this project. The detector used was a Texas Instruments 800 X 800 CCD, which is extremely efficient for wavelengths above 4500 Å. The Modular Spectrograph was used in "echellette" mode, where a special echelle "immersion grating" (e.g., Dekker 1988) with 150 lines/mm was used as the primary disperser, and a "grism" ruled with 300 lines/mm (with an effective blaze of 5000 Å) was used as a cross–disperser. With this setup, it was possible to record orders 15 through 25 on the CCD simultaneously, giving a total wavelength coverage of 5000–8400 Å. The pixel size in the dispersion direction is 25 km s^{-1}, and the resolution obtained over the entire chip (using a slit width of 1.5 $''$) was less than 2.3 pixels FWHM, giving a spectral resolution of $\leq$ 60 km s^{-1}in each order. The size of the pixels in the spatial direction projected to 0.85 $''$. Because the objects observed are all high redshift QSOs with $m > 17$ (and more typically with $m > 18$), it is very necessary to have good sky subtraction even under dark observing conditions. Thus, a slit length of $\sim$ 35 $''$was used; this slit length allowed for a sufficient amount of sky in each order without the orders overlapping on the CCD. Because of the rather large wavelength range observed simultaneously, the spectrograph slit was maintained at the parallactic angle during all of the observations in order to minimize light losses caused by atmospheric dispersion.

Individual exposures were usually 5400 seconds (in order to minimize the effects of read-out noise, which for the CCD used was 11 electrons per pixel), bracketed by exposures of Fe–Ar Hollow Cathode + Ne comparison lamps to calibrate the wavelength scale. The spectrograph flexure was minimal from exposure to exposure, with the positions of arc lines changing by less than 0.15 pixels over several hours with the telescope pointed to a given position. The spectrophotometric standard star EG 274 was observed each night in order to correct the spectra for broad variations in response across the CCD that were due to the echelle blaze function and the variation in sensitivity of the CCD to different wavelengths.

While the accumulation of data was extremely efficient using the above setup, the data reduction presented special problems because of the long–slit echelle format. The best procedure finally arrived upon after significant experimentation is as follows. The

two–dimensional echelle format CCD frames were first cleaned of cosmic rays, and then polynomials were fit to each order of a spectrum of the standard star. The frames were then rectified so that each order fell parallel to the rows of the frame (a great deal of care was taken in aligning the slit with the columns of the CCD at the time the observations were made, so that no rectification in this direction was unnecessary in the reduction stage). The same corrections were applied to the flat field frame. The data were next flat–fielded, extracted, and sky–subtracted; for each order, the frame was median–filtered along the dispersion direction, producing a one–dimensional cross–cut, which was then used to determine which rows to extract for the object and for sky. The rows extracted as object were weighted according to the median number of counts above the sky level, in a manner similar to the algorithm suggested by Robertson (1986). The sky was calculated for each dispersion column by taking the median of the pixel values for the rows selected as sky. A variance array was also calculated for each order by assuming a Poisson counting model in which the CCD read–out noise and gain were accounted for. The extraction procedure produced an 800 CCD column by 10 order data structure, along with the corresponding error values. Arc spectra were extracted from the same CCD rows as the object spectra, and then each order was fit with a third–order polynomial wavelength solution. The average residual in the wavelength solution was $\sim$ 0.08 Å. The wavelength solutions were then applied to all of the QSO spectra, which were rebinned to the same wavelength scale, with the same dispersion (25 km s^{-1} per pixel) at which the data were obtained. Individual exposures of the same object were then added together, weighting by the variance at each pixel value in each order. The same steps were applied to the spectra of the standard star, and then the star spectrum was smoothed and features were removed. This spectrum was then divided into the "echellogram" for each object, thereby removing the echelle blaze function from each order and leaving only the stellar energy distribution, which happens to be extremely flat over the observed wavelength range. The echellograms were then merged into continuous, one–dimensional spectra; in spectral regions where adjacent orders "overlapped" in wavelength coverage, the orders were combined by again weighting according to the variances. The new error spectrum was maintained for each object for subsequent use in the measurement of the absorption lines and estimation of signal–to–noise ratios (S/N). The resulting spectra have a resolution of

60 km s^{-1}over the wavelength range 5000–8400. The unsmoothed spectra are plotted in Figure 1.

The spectrum of Q1208+101 was obtained in 1988 February at the Palomar 5.0 m Hale telescope, using the Double Spectrograph Red Camera with a 1200 line/mm grating in first order. Observations were made through a 1″ slit, which again was aligned at the parallactic angle. Three separate grating settings were necessary in order to cover the appropriate wavelength range at $\sim$ 80 km s^{-1}resolution. The separate observations were merged using a method similar to that described above; the final spectrum is presented in Figure 1.

Unfortunately, the very bright and complicated night–sky spectrum longward of $\sim$ 7300 Å degraded the quality of the spectra in that wavelength region for all but the brightest objects. Consequently, in the interest of conserving space, only the spectral regions for which the data were deemed "useful" were included in the plots in Figure 1.

III. THE ABSORPTION SYSTEMS

a) Absorption Line Measurement

The absorption lines in each of the 11 spectra shown in Figure 1 were measured interactively using methods similar to those used by SBS, except that the actual calculated variance arrays were used for error and S/N calculation rather than estimates made from the fluctuations in the data in the neighborhood of each measured line. Each absorption line that satisfies the criterion $W_{obs} \geq 5.0\sigma(W)$ has been included in Table 2. The wavelengths are all heliocentric in vacuum. The positions of the tabulated lines are indicated on the spectra in Figure 1. Where lines are involved in complexes or blends, an attempt has been made to separate the features into individual components; this is to a certain extent a subjective process, and in such cases the tabulated equivalent widths and wavelengths are somewhat more uncertain than the formal errors suggest.

Column 6 of Table 2 lists the S/N calculated over the range of pixel values included in each absorption line; thus, for the weakest lines, the value in column 6 represents the actual continuum S/N, whereas for strong lines the tabulated value is likely to be considerably less than the actual continuum S/N. In general, as was the case for SBS, the spectra have

continuum S/N $\geq$ 20.

The absorption line lists were examined and lines were identified using methods identical to those employed by SBS. Below we discuss each spectrum and the identified absorption systems. Reference has been made to previous work only when it involved analysis of absorption spectra. Again, complete references for the published QSOs in the sample can be found in Hewitt and Burbidge (1987) or Veron–Cetty and Veron (1987).

b) Discussion of Individual Spectra

i) Q0000−263 (z_{em} = 4.104)

This QSO, discovered by Hazard and McMahon (1988), is the brightest QSO known with a redshift larger than 4.0. It was observed as part of a survey for Lyman limit absorption by SSB, although the spectrum was of low resolution. There is an unambiguous damped Lyman α line at $\sim$ 5350 Å, which is associated with the Lyman limit found at z_{abs} = 3.39 by SSB. We have attempted to fit a damped profile to the line in our new, higher–resolution spectrum in order to determine the HI column density. The definition of the continuum in this region is slightly complicated by the fact that the absorption line falls very near the expected position of the OVI/Ly β emission line. Nevertheless, we find that $\log N(HI) = 21.3 \pm 0.1$ cm^{-2}. The narrow lines identified in the wings of the line were measured by using the calculated damped profile as the continuum level. A glance at Figure 1 shows that the spectrum longward of 7300 Å is badly affected by the strong night sky lines, as well as the effects of a blocked column crossing the spectrum on the CCD chip (between 7500 and 7600 Å); however, the spectrum is shown all the way out to the C IV emission line because of the very interesting strong C IV feature just longward of the emission line. This redshift system will be discussed below.

z_{abs} = 3.3898: This is the redshift system with the associated damped Lyman α line discussed above. Very strong C IV and Si IV doublets are identified, along with Si II λ1526, Si II λ1260, C II λ1334, O I λ1302, and Si II λ1304. The C IV doublet shows evidence for being made up of a number of components, as is usual for heavy element lines associated with damped Lyman α systems.

z_{abs} = 3.5363: A weak C IV doublet defines this system. There is a moderately strong Lyman α line also identified.

z_{abs} = 4.1324: This system consists of a very strong C IV doublet at a redshift roughly 1700 km s^{-1}higher than the emission line redshift of the QSO. Aside from its very high redshift, this system is unusual (for a system with $z_{abs} \approx z_{em}$) in that it appears to be of mixed ionization state–a strong Si II λ1526 line is identified, and there is a strong Lyman α line near 6240 Å. The absorption redshift of this system may be the highest for any known heavy–element absorption system.

ii) Q0041−266 (z_{em} = 3.045)

This object is another that was discovered in an objective prism search for QSOs in several SGP fields by Hazard and McMahon (1988). The emission redshift, which is not particularly well–determined from the spectrum because of the broad, weak emission lines, is the lowest of the 11 newly observed QSOs. The following absorption redshifts have been identified in its spectrum:

z_{abs} = 0.8626: A rather weak Mg II doublet defines this low redshift system.

z_{abs} = 2.2659 : This redshift is identified only by a weak C IV doublet.

z_{abs} = 2.3392: There is some evidence for a multiple–component structure in this weak C IV doublet.

z_{abs} = 2.7413: Along with the C IV doublet, there is a very weak Si II λ1526 line identified with this redshift. There is some evidence for a second, weaker component at z_{abs} = 2.7432.

z_{abs} = 2.7576: Another very weak C IV doublet.

iii) Q0042−264 (z_{em} = 3.298)

This object is another discovered by Hazard and McMahon (1988). It is only 15.6 ′ away from Q0041−266 on the plane of the sky. The following absorption redshifts were identified in its spectrum:

z_{abs} = 2.0298: Although this lower redshift systems is identified by only the Al III $\lambda\lambda$1854, 1862 doublet, the redshift agreement between the two components is sufficiently

good that the identification is likely to be correct.

$z_{abs} = 2.4758$: An unambiguous C IV doublet defines this redshift.

$z_{abs} = 3.1466$: This system is identified by a weak C IV doublet.

$z_{abs} = 3.2374$: Another system defined by a weak C IV doublet.

$z_{abs} = 3.2921$: While the redshift agreement between the two components of the C IV doublet is not particularly good, the identification of a moderately strong associated Lyman α line lends credence to the identification.

iv) Q0055−269 ($z_{em} = 3.653$)

The absorption spectrum of this QSO has been studied previously at low resolution by SSB. No strong Lyman limit system was found by these authors. The following absorption redshifts were found in the new spectrum:

$z_{abs} = 1.5335$: A Mg II doublet and two Fe II lines make this a certain low redshift system.

$z_{abs} = 2.9494, 2.9513$: It is possible to identify two closely spaced C IV doublets in this system. This system was identified in the spectrum analyzed by SSB, although the two components were not resolved.

$z_{abs} = 3.1910, 3.1943$: Although C IV doublets have been identified for two components in this complex, it is likely that more components would be found with higher spectral resolution. A very weak Si IV doublet is also found at this redshift. The redshift system was also detected by SSB, although again the multiple components were not resolved. Surprisingly, there is no evidence even *a posteriori* for the presence of a Lyman discontinuity at this redshift in the low–resolution spectrum of SBS.

$z_{abs} = 3.6013$: This system has a relatively strong C IV doublet along with the Lyman α line.

$z_{abs} = 3.6764$: Although the redshift agreement between the components of the putative C IV doublet is good, there is a high probability that this system is not real; the C IV doublet falls in a region of the spectrum where the data become very noisy because of poor sky subtraction.

v) Q0256−000 (z_{em} = 3.370)

The spectrum of this QSO has also been studied previously (at low resolution) by SSB. While no C IV systems were identified on the basis of the low–resolution spectra, two low redshift Mg II systems were found. Our new higher resolution spectrum confirms the reality of the system at z_{abs} = 1.198, but if the system at z_{abs} = 1.025 is real, then the equivalent widths of the lines must be somewhat smaller than the SSB measurement suggested. There is a line at λ5663 in our new spectrum with an observed equivalent width of 0.5 Å for which the wavelength agreement with the Mg II λ2796 line (with measured equivalent width of 0.94 Å) identified by SSB is very good. The following systems are identified on the basis of the new spectrum:

z_{abs} = 1.1983 : A certain low redshift system, with 3 Fe II lines identified in addition to the Mg II doublet.

z_{abs} = 3.0919, 3.0945: The reality of these two C IV doublets is far from being certain because of their weakness and the relatively poor redshift agreement between the two lines of the doublet for each component; however, if real, it is quite possible that these lines are associated with the Lyman limit system found at z_{LLS} = 3.090 by SSB.

vi) Q0347−383 (z_{em} = 3.222)

The following absorption systems have been identified in the spectrum of this QSO:

z_{abs} = 1.4565, 1.4581: The two–component nature of this system is evident only in some of the Fe II lines, not in the strong Mg II doublet.

z_{abs} = 1.5263: Despite the fact that the doublet ratio of the moderately strong Mg II doublet is unphysical, the system is certainly real, as several Fe II lines are also identified. It is likely that one of the Mg lines has been affected by a noise spike, possibly because of imperfect sky subtraction.

z_{abs} = 2.3852 : A clear C IV doublet defines this redshift.

z_{abs} = 2.5706 : This system is identified by only a weak C IV doublet.

z_{abs} = 2.6508, 2.6524: This C IV complex was rather arbitrarily separated into individual lines; there are two likely redshifts suggested, but again there may be many subcomponents, which would appear in higher resolution spectra. The lines identified as

the Si IV doublet from this system are certainly blended with other lines in the Lyman α forest, if they are indeed present.

$z_{abs} = 2.8103$: This is an unambiguous C IV doublet in which the λ1548 line has been affected by poor sky subtraction, resulting in an unphysical doublet ratio. A strong Si IV doublet is also found for this redshift.

$z_{abs} = 2.8487$: This system consists of a relatively weak C IV doublet, along with a very weak Al II λ1670 and possibly Al III $\lambda\lambda$1854, 1862.

$z_{abs} = 3.0252$: Along with the relatively strong C IV doublet (which appears to be affected somewhat by poor sky subtraction), Fe II λ1608, Si II λ1526, Si IV $\lambda\lambda$1393, 1402, C II λ1334, and Si II λ1260 are found for this redshift.

vii) Q0428−136 ($z_{em} = 3.244$)

This QSO is another discovered by Hazard and McMahon (1988). The following absorption redshifts are identified in its spectrum:

$z_{abs} = 1.5189, 1.5201$: The double nature of this very strong absorption system is easily seen in the Fe II lines; only noise prevents the same structure from being seen in the Mg II doublet.

$z_{abs} = 2.3639, 2.3663$: Only two of probably many components in this complex of C IV absorption redshifts have been identified. It is unlikely that this complex is indicative of marginal BAL behavior, since the velocity separation from the emission redshift is very large and there are no other such complexes at smaller relative velocities.

$z_{abs} = 2.5496$: An unambiguous C IV doublet defines this redshift.

viii) Q1208+101 ($z_{em} = 3.811$)

The spectrum of this object was the only one of the 11 new observations to be obtained at Palomar Observatory. The resolution of the spectrum is slightly lower than for the Las Campanas observations, but is the same as the resolution for the 55 QSOs in SBS. The following absorption redshifts have been identified:

$z_{abs} = 2.8573, 2.8606, 2.8640$: This complex of C IV doublets would undoubtedly reveal more complex structure at higher spectral resolution.

z_{abs} = 2.9147, 2.9158: In addition to the two identified C IV doublets, Si II λ1526 and the Si IV doublet are found for this redshift system. The structure is not resolved in the Si lines.

ix) Q2000−330 (z_{em} = 3.777)

The absorption spectrum of this QSO has been fairly extensively discussed in the literature. The Lyman α forest region has been discussed by Hunstead *et al.* (1986a), while the spectral region longward of the Lyman α emission line has been studied by Hunstead *et al.* (1986a,b, 1987), and Meyer and York (1987). The last three papers have dealt primarily with relatively small spectral regions. The spectrum obtained by Meyer and York (1987) covered the wavelength range 6220–6620 at $\sim$ 2 Å resolution and S/N $\sim$ 100, while Hunstead *et al.* (1986b) concentrated their discussion on lines occurring in the range 6300–6550 Å, and Hunstead *et al.* (1987) briefly discussed the heavy element abundance in the z_{abs} = 3.1723 absorption system. Detailed comparisons will be made wherever possible below, where we outline the systems identified in the new spectrum:

z_{abs} = 1.4542: This low redshift system is identified based on a weak Mg II doublet and several weak Fe II lines.

z_{abs} = 2.0330: The lines of FeII λ2344, λ2374, and λ2382 define this redshift.

z_{abs} = 2.9780: In addition to a relatively strong C IV doublet, Fe II λ1608, Si II λ1526, and several other lines that are less certain (because they fall in the Lyman α forest) are found for this absorption system.

z_{abs} = 3.1726: This system was discussed by Hunstead *et al.* (1987) as an example of a low–ionization component of the absorption "complex" that spans the redshift range 3.172–3.192. No C IV or Si IV was found in their spectra; the system was identified primarily on the basis of several lines usually associated with mostly neutral absorbers. However, we do find both C IV and Si IV doublets in our new spectrum, which has comparable resolution but higher signal–to–noise ratio than that of Hunstead *et al.* . In their lower resolution, higher S/N spectrum, Meyer and York (1987) also found the C IV doublet for this system. We are unable to comment on the relative strengths of Si II and Si III, since Si III λ1206 is expected at a wavelength where our spectrum is not of very good quality. However,

we have attempted to measure the column densities of Si II and Si IV based upon the λ1526 and Si IV $\lambda\lambda$1393, 1402 lines. For the Si IV doublet, the λ1393 line is blended with a line from another system, so that the fit is dictated primarily by the λ1402 line. We find that $\log N(Si\ II) = 13.1 \pm 0.1$, and $\log N(Si\ IV) = 13.1 \pm 0.1$. The column density measured from profile fits to the C IV doublet is $\log N(C\ IV) = 13.4 \pm 0.1$. Assuming that the HI column density for this system is as measured by Hunstead *et al.* (1987), $\log N(H\,I) = 19.78$, and adopting the C II column density limit placed by Hunstead *et al.* , we find that photoionization models suggest abundances which are just slightly smaller than those suggested by Hunstead *et al.* , i.e., $[C/H] \approx -2.5$ and $[Si/H] \approx -2.4$ (the disagreement arises because the models suggest that the cloud is $\sim$ 50% neutral, rather than $\sim$ 100% as was assumed by Hunstead *et al.*). However, since the absorption system appears to be a complex, the estimation of abundances is rather uncertain.

z_{abs} = 3.1875: As was also found by Hunstead *et al.* (1986b), this system appears to have no C IV or Si IV lines strong enough to be identified, although it does have reasonably strong lines of Fe II, Al II, Si II, and C II (although the C II feature falls in the Lyman α forest and therefore its strength must be regarded as an upper limit).

z_{abs} = 3.1914: There is evidence for some unresolved structure in the C IV lines at this redshift. We find a weak Si IV doublet, Al II λ1670, C II λ1334, Si III λ1206, and several Si II lines also associated with this system. This redshift was also identified by Hunstead *et al.* (1986a,b) and by Meyer and York (1987).

z_{abs} = 3.3334, 3.3375: The stronger component of this double system was identified by Hunstead *et al.* (1986b) on the basis of lines in the Lyman α forest; in our spectrum, we find the C IV and Si IV doublets, as well as the Al II λ1670 line, in addition to many of the lines found by Hunstead *et al.* . For the weaker, higher redshift component, we find only the C IV doublet in the spectral region longward of Lyman α emission. Meyer and York (1987) have found a possible Si II λ1526 line associated with the lower redshift.

z_{abs} = 3.5479, 3.5503, 3.5523, 3.5552, 3.5575: The multiple component nature of this complex can easily be seen in the C IV absorption near 7050 Å in the plot in Figure 1. We have somewhat arbitrarily divided the complex into 5 redshift systems, although again more may be present. A heavy–element redshift with z_{abs} = 3.5519 was identified by Hunstead

et al. (1986a) on the basis of the Lyman series lines and several low–ionization lines, most of which fall in the Lyman α forest. Hunstead *et al.* suggested the presence of an aggregate of clouds with a total velocity span of $\sim$ 900 km s^{-1}; the identified components of the C IV complex on the basis of our new spectrum have a total velocity span of $\sim$ 640 km s^{-1}. Very similar velocity structure is seen in the Si IV doublet and the C II λ1334 line. It is this complex of absorption redshifts that is responsible for the Lyman limit absorption edge near λ4150, which was noted by Hunstead *et al.* (1986a).

x) Q2204−408 (z_{em} = 3.169)

The following absorption redshifts have been found:

z_{abs} = 1.8145 : This redshift, based on the Al III $\lambda\lambda$1854, 1862 doublet, is likely to be real, given the strength of the lines.

z_{abs} = 2.6280: This redshift is based on an unambiguous C IV doublet. There is some indication of a weaker C IV doublet at z_{abs} = 2.6296.

z_{abs} = 2.8375: A certain C IV doublet defines this system.

z_{abs} = 2.8500, 2.8545: While the division into components of this complex of systems is uncertain, the lines are definitely those of C IV. Corresponding Al II λ1670 and Si IV $\lambda\lambda$1393, 1402 are also found.

z_{abs} = 3.1580, 3.1596: This double C IV doublet is found near the peak of the C IV emission line.

xi) Q2239−386 (z_{em} = 3.511)

This QSO is by far the faintest in the newly observed sample. It is another object that was discovered by Hazard and McMahon (1988). The emission lines are unusually broad and weak; hence the determination of the emission redshift is more uncertain than for most of the other QSOs in the sample. The following absorption redshifts have been identified:

z_{abs} = 1.0328: A rather weak Mg II doublet defines this redshift.

z_{abs} = 2.3765, 2.3786: The double nature of this moderate redshift system is exhibited by the strong Fe II λ1608 and Al II λ1670 lines; the Al III $\lambda\lambda$1854, 1862 doublet is also found.

$z_{abs} = 2.6006$: An unambiguous C IV doublet defines this redshift.

c) Statistical Samples of Absorption Systems

An *unbiased* survey for a particular class of absorption system must have a rest equivalent width threshold above which an absorption system could have been found at any redshift where the survey is sensitive, in any of the spectra. The intent of the present work was to extend the C IV survey of SBS to higher redshifts using spectra of similar resolution and signal–to–noise ratio. However, the new spectra were obtained in an echelle format, using a CCD detector (as opposed to the photon–counting detector, which was used for most of the observations comprising the SBS survey), and consequently it was somewhat more difficult to monitor the quality of the spectra as the observations were being made. In addition, the multi–order format makes it more difficult to obtain a completely uniform signal–to–noise ratio over the entire observed spectral range. It is therefore necessary to re–examine the reduced spectra in order to gauge the sensitivity to detection of C IV doublets as a function of redshift. This was accomplished by using the variance arrays that were maintained during the reduction process. These "error spectra" account for CCD read–out noise, Poisson noise, sky, and sky subtraction; together with the actual reduced data, these then provide a pixel–by–pixel estimate of the signal–to–noise ratio for each spectrum. The spectra were then run through a program in which the rest equivalent width of the weakest 5σ C IV line was calculated for every pixel of each spectrum. It was assumed for the purposes of the calculation that the full width of a weak line is $\sim$ 5 pixels. It turned out that for all of the spectra, a C IV line with $W_0 = 0.15$ could have been detected over most of the spectral region longward of Lyman α emission and shortward of C IV emission. However, for some of the highest redshift objects in the new sample, and for the very faint Q2239–386, there are small spectral regions in the red where the sensitivity to the detection of weak C IV doublets was only marginally acceptable. In columns 3 and 4 of Table 3, we have listed the minimum and maximum absorption redshifts at which C IV doublets with each line having $W_0 \geq 0.15$ Å could have been detected (this is exactly the same criterion used by SBS). Wherever column 4 contains only three dots, the maximum absorption redshift is equal to the measured emission redshift, which is listed in column 2.

These emission redshifts were measured primarily on the basis of the peaks of the Lyα and C IV emission lines for each object.

Also listed in Table 3 are the detected C IV doublets for each spectrum, and the corresponding measured equivalent widths for the λ1548 and λ1550 absorption lines. Because the spectral resolution of the new observations slightly exceeds that of most of the spectra used in the SBS survey, any detected C IV doublets that were separated by $\leq$ 150 km s^{-1}have been listed as a single system and the tabulated equivalent width is the sum of the equivalent widths for the two components. This was done so that weak systems that were resolved into two components in the new spectra (and that would not have been resolved in the spectra of SBS) would not be excluded from the "complete sample" of systems with $W_0 \geq 0.15$ Å.

In all of the following discussion, the sample summarized in Table 3 has been combined with the C IV sample of SBS to form a new sample of 275 redshifts found in the spectra of 66 QSOs. Figure 2 is a histogram illustrating the "redshift coverage", or the number of lines of sight observed in which a C IV doublet satisfying the criterion $W_0 > 0.15$ Å with a given redshift could have been found. The solid histogram represents the redshift coverage of the SBS survey, while the dashed histogram represents the redshift coverage of the survey with the new observations added. Clearly, the new observations have added significantly to the survey's sensitivity for redshifts above $z_{abs} \sim 2.5$.

Following SBS, it is useful to define a number of different subsamples of C IV absorption systems for the purposes of various statistical tests. These samples are summarized in Table 4, and will be discussed in subsequent sections.

IV. THE EVOLUTION OF THE C IV ABSORPTION SYSTEMS

a) Evolution in the Number of Systems With Redshift

The observed number of absorption systems that are due to cosmologically distributed, intervening absorbers is expected to have the form

$$N(z) = N_0(1+z)(1+2q_0z)^{-1/2} \qquad (1)$$

where $N(z) \equiv dN/dz$, the number of absorption systems per unit redshift evaluated at

redshift z. This equation holds in a standard Friedmann Universe if the properties of the absorbers do not vary with redshift; however, if the properties of the absorbers do in fact change systematically with redshift, then $N_0 = \pi r_0^2 \phi_0 c/H_0 = N_0(z)$. Here ϕ_0 is the comoving space density of absorbers, and r_0 is the mean effective cross–sectional radius within which a line of sight will exhibit detectable heavy element absorption. In principle, these two quantities can be influenced by a number of factors, including the ionization state of the gas in the clouds (dictated primarily by the mean gas density and the intensity of the ionizing radiation), and by actual changes in the sizes or numbers of absorbing objects as a function of redshift.

As usual, it is convenient to compare the actual observations with a power law of the form $N(z) = C(1+z)^\gamma$, where C is a constant. A glance at Equation (1) then shows that in the case of non–evolving absorbers, $\gamma = 1$ for $q_0 = 0$ and $\gamma = 1/2$ for $q_0 = 1/2$. Only recently have samples of heavy element absorption systems become large enough to justify any significant statement concerning evidence for evolution of the absorbers with redshift. The usual way of proceeding is to calculate the maximum likelihood estimate of γ for a sample of absorption systems and compare it with the "no–evolution" values above. For sample S2 of SBS, which was regarded as their primary sample for the investigation of the evolution of the number density of absorbers with redshift, a maximum likelihood estimation gave $\gamma = -1.20 \pm 0.71$; qualitatively similar results were found for various other subsamples extracted from their data and from Young, Sargent, and Boksenberg (1982; hereinafter YSB) and Foltz *et al.* (1986) using somewhat different selection criteria. The results allowed the certain exclusion of "no–evolution" if $q_0 = 0$, and exclusion at the 2.3σ significance level if $q_0 = 1/2$. However, there was some indication from the data that the actual $N(z)$ curve was not well–represented by a power law, and that in fact there may be a rather sharp drop in $N(z)$ for redshifts above $z_{abs} \sim 2.5$ (see Figure 6 of SBS). The present work was largely motivated by the need to establish more firmly the real trend of the $N(z)$ curve at these redshifts.

Following SBS, for the purposes of evaluating the redshift dependence of the number density of absorbers, we have formed unbiased subsamples of C IV redshifts by applying the constraint that "clumps" of C IV redshifts on scales less than 1000 km $s^{-1}$are counted

as only one system. The properties of these samples (called the "Poisson samples" by SBS) are summarized in Table 4. Sample ES2, which is identical to sample S2 of SBS, with the addition of the new data presented in this paper, will again be regarded as the "primary" sample; sample ES5 is identical to sample S5 of SBS (again, with the addition of the new data), and includes data from YSB and from Foltz *et al.* (1986). As is discussed in detail in SBS, the absorption systems within 5000 km $s^{-1}$of the QSO emission redshift have been excluded in order to prevent possible contamination of the unbiased sample by "associated" absorption. Several authors (e.g., Foltz *et al.* 1986) have found that there is an excess number (over the number expected from a uniform, intervening population of absorbers) of absorption systems with $z_{abs} \approx z_{em}$ for certain classes of radio–loud QSOs. In addition, it is likely that the ionizing radiation of the QSO itself influences the state of ionization of the clouds for $z_{abs} \approx z_{em}$. In all samples the distribution of absorption systems in terms of the apparent ejection velocity

$$\beta = \frac{(1+z_{em})^2 - (1+z_{abs})^2}{(1+z_{em})^2 + (1+z_{abs})^2} \tag{2}$$

is seen to be uniform for $\beta c > 5000$ km s^{-1}. Although no significant excess of absorption systems with $z_{abs} \approx z_{em}$ was found in the SBS sample, we have again chosen to be conservative and exclude the systems with $\beta c < 5000$ km $s^{-1}$from the primary sample.

A maximum likelihood fit to the unbinned data in sample ES2 gives $\gamma = -1.26 \pm 0.56$ (see Table 4), in very good agreement with that found by SBS, but with substantially smaller uncertainty. The real improvements introduced by the extended sample are most evident, however, from a plot of the binned data, as shown in Figure 3. The last two bins are much better determined than for the original SBS plot, and in fact the present data really extend the spanned redshift range up to ~ 3.7 from the original ~ 3.4. A gradual declining trend with increasing redshift is evident beginning at $z_{abs} \sim 2$ until $N(z)$ has decreased by a factor of $\sim$3 by $z \sim 3.5$. Although the possibility of a steep "discontinuity" at $z \sim 3$ appears to be ruled out by the new data, one gets a clear impression that a power–law representation of the curve is also not appropriate; the curvature appears to be in the opposite sense. In fact, there is the impression that the $N(z)$ curve is essentially flat until $z \sim 2$, and not increasing steeply to lower redshifts as required by the power law form. This qualitative behavior in the redshift range $1.2 \leq z_{abs} \leq 2.2$ is completely consistent with the $N(z)$ curve observed

for Mg II absorption systems in this range (SSB;Sargent, Steidel, and Boksenberg 1988). Taking the maximum likelihood fit for the power–law form at face value, "no evolution" of the absorbers can now be excluded at the 4.0 σ level if $q_0 = 0$ and the 3.1σ level if $q_0 = 1/2$. Therefore, it can be said with certainty that the absorbers evolve with redshift for any reasonable value of q_0.

As in SBS, the value of γ found for the sample in which both doublet components must exceed 0.30 Å (sample S5 in SBS and sample ES5 in the present paper) in rest equivalent width is somewhat steeper than for the samples containing weaker doublets (samples S2 and ES2). This suggests the possibility that the $N(z)$ curve may be different for weak and strong C IV doublets. In Figure 4 we have plotted the binned $N(z)$ distribution for two subsets of sample ES2, one containing the 44 doublets with $0.15 \leq W_0(1548) < 0.40$ Å and the other containing the 60 with $W_0(1548) > 0.40$ Å. The trend for the weaker sample appears to be in the *opposite* sense to that of the stronger; this impression is supported by the results of maximum likelihood estimates of γ, which are $\gamma = -2.35 \pm 0.77$ for the strong sample and $\gamma = 0.14 \pm 0.85$ for the weaker sample. A Kolmogorov–Smirnov (KS) test has been performed on the two unbinned distributions of absorption redshifts, with the result that one may reject the null hypothesis that the two samples were drawn from the same parent distribution with $\sim 93\%$ confidence; thus, formally, the two subsamples are marginally different from one another. It should be noted that the division of sample ES2 at $W_0(1548) = 0.40$ Å was arbitrary, with the value chosen to approximately divide the sample into equal subsamples. It is quite possible that if an adequate sample of very weak C IV doublets could be assembled, the difference in redshift evolution would be much more striking. Unfortunately, even now the weak line subsample is very incomplete at the low equivalent width end, since doublets with $W_0(1548) \approx 0.15$ Å are on the optically thin part of the curve of growth for reasonable ($b > 5$ km s^{-1}) values of the gas velocity dispersion and would have doublet ratios near 2. It would therefore be necessary to be able to detect $W_0(1550) = 0.075$ in order to be "complete." In an effort to do this, the 21 QSOs in which lines of that strength could have been detected at the 5σ level over the whole relevant redshift range were selected; however, there are only 29 systems with $0.15 \leq W_0(1548) \leq 0.40$ Å in the whole sample, and the redshift path "coverage" is not particularly uniform, making

the $N(z)$ curve rather poorly determined; the maximum likelihood fit to the power–law form gives $\gamma = 1.64 \pm 1.03$, which is consistent with "no evolution," although there is the suggestion of an *increasing* comoving density of weak C IV systems. We will return to a discussion of the possible implications of this result in §V. In the future, an important project would be to assemble a list of bright QSOs spanning a large range of emission redshift and obtain very high signal–to–noise ratio spectra in order to create a new sample of weak C IV doublets. This could be accomplished relatively efficiently, since the number of weak doublets is probably much higher than the number of strong ones; thus the same statistical accuracy could be achieved with a significantly smaller number of QSO spectra.

b) Evolution of the Clustering Properties With Redshift

A primary motivation for the large survey for C IV absorption conducted by SBS was to investigate the clustering properties of the C IV absorption redshifts on scales $\Delta v > 200$ km s^{-1}. Prior to this, it had been well–established that velocity splittings of $\Delta v \sim 150$ km $s^{-1}$are common in the heavy–element absorption systems, and such splittings have been interpreted as being due to absorption arising in discrete clouds within the halo of a single galaxy (Bahcall and Spitzer 1969). SBS argued that velocity splittings $\Delta v > 200$ km $s^{-1}$are unlikely to be due to the relative motions of clouds within galaxies, and therefore that any excess number of splittings on scales $\Delta v > 200$ km s^{-1}in the absorption system velocity two–point correlation function (see SBS for a thorough discussion) may be ascribed to actual clustering of the absorbers. While it is not intended to repeat all of the details of the two–point correlation function analysis presented by SBS, the new data justify a re–examination of the clustering properties of the absorbers, particularly investigating the possibility that these properties may change as a function of redshift.

The construction of the absorption system 2–point correlation function is described in detail in §VIIa-c of SBS. We have plotted the two–point correlation function for sample EA2 (see Table 4; EA2 should be compared with sample A2 of SBS) in Figure 5a. As in SBS, the abscissa is $\Delta v = c\Delta z/(1+z)$, where $z = (z_1 + z_2)/2$ for each pair of absorption redshifts (z_1, z_2) which are found along a single line of sight (i.e., pairs that appear in the same QSO spectrum). The ordinate is the number of pairs observed, where corrections have

been made for the fact that large splittings are less likely to be observed than smaller ones because of the finite "redshift window" spanned by a given QSO spectrum. The dotted line represents the adopted background level $\langle N_p \rangle$, which has been estimated by taking the mean number of pairs per bin for velocity splittings in excess of 1000 km s^{-1}. Thus, in the usual expression for the covariance function,

$$dP = \Phi_0 dV[1 + \xi(r)], \tag{3}$$

the correlation amplitude is given by $\xi = (Np/\langle N_p \rangle) - 1$. Following SBS again, in calculating the 2–point correlation function, all splittings on scales less than 200 km s^{-1}have been excluded in order not to give too much weight to QSOs which were observed at somewhat higher resolution, and also because the number of splittings on such small velocity scales is incomplete given the typical resolution of the spectra. The individual 2–point correlation functions for each observed QSO are then added together, resulting in a correlation function that is essentially averaged over all of the lines of sight. This is necessary because, clearly, any individual QSO spectrum will have only a few identified absorption systems and therefore only a handful of velocity splittings. Sample EA2 contains all of the identified absorption redshifts that have $\beta c > 5000$ km s^{-1}; in order to increase the size of the available sample, no particular minimum W_0 is required. Thus, Figure 5a is just a composite histogram of all the velocity splittings between members of sample EA2 that occur in the same spectrum.

Not surprisingly (since only 11 QSOs have been added), the qualitative aspects of the 2–point correlation function in Figure 5a are very similar to that of Figure 11b of SBS. However, the new extended sample is much more complete at high ($z_{abs} > 2.2$) redshifts; therefore, we have divided sample EA2 arbitrarily at $z = 2.2$ (this roughly divides the sample in half) and have constructed separate two–point correlation functions for systems with $z_{abs} \leq 2.2$ and those with $z_{abs} > 2.2$. The results are shown in Figure 5b and 5c, respectively. We recall that SBS found a significant peak in the absorption system two–point correlation function on velocity scales $200 \leq \Delta v \leq 600$ km s^{-1}; for sample A2, the mean amplitude ξ was found to be 5.7 ± 0.6. For sample EA2, we find $\xi = 6.1 \pm 1.2$, in very good agreement with the previous result (it should be noted that the error on the

determination of ξ of 0.6 given by SBS is underestimated by a factor of two, and should have been 1.2). The corresponding amplitudes have been calculated for the two subsets of sample EA2, and they are $\xi = 5.8 \pm 1.4$ for $z \leq 2.2$ and $\xi = 6.0 \pm 2.0$ for $z > 2.2$; thus, there is no significant difference in the power in the correlation function on small velocity scales for the low– and high–redshift samples of absorption systems. While the general appearance of the two–point correlation function for $\Delta v > 1000$ km s^{-1}is flat, it was found by SBS that there appears to be a marginally significant (2.0 σ) excess of splittings on velocity scales between 1000 and 10,000 km s^{-1}, and a corresponding deficiency of systems (relative to $\xi = 0$) for scales between 10,000 and 20,000 km s^{-1}. We find the same sort of effect in the present work; however, when the two subsamples are examined individually, it is found that for the $z_{abs} \leq 2.2$ sample, there is a 2.2 σ excess of splittings with $1000 \leq \Delta v \leq 10,000$ km s^{-1}over the adopted mean background level, but for the $z_{abs} > 2.2$ subsample, the number of splittings in the same velocity range is within $\sim 0.6\sigma$ of the expected number. That is, at a marginally significant level, there is more power on scales $1000 \leq \Delta v \leq 10,000$ km s^{-1}for low redshift absorption systems than for higher redshift systems. [2]

It is of interest to note (see Figures 5b and 5c) that the greater part of the power in the 2–point correlation function on small scales occurs in the velocity range $200 \leq \Delta v \leq 300$ km s^{-1}; while this would be expected if the absorption line 2–point correlation function is analogous to the local galaxy–galaxy 2–point correlation function (see SBS), it is worthwhile comparing the amplitude of the "tail" of the peak on small scales for the low– and high– redshift subsamples discussed above. If the bin covering the velocity

[2] Very recently, however, the results of a more complete analysis of the clustering in the SBS sample by Heisler, Hogan, and White (1989) has shown that virtually all of the excess power on large velocity scales is produced by the absorption in one object, PKS 0237–233. All of the absorption systems in this object have $z_{abs} < 2.2$; if PKS 0237–233 is removed from the sample, then there is no significant power in the 2–point correlation function on scales $1000 \leq \Delta v \leq 10,000$ km s^{-1}in either the low–redshift or high–redshift subsamples. Clearly, while it is not correct to "remove" anomalous objects from the samples, there is not yet enough data to support a claim that the type of structure seen in the spectrum of PKS 0237–233 does not exist at high redshift as well.

range $200 \leq \Delta v \leq 300$ km s^{-1}is excluded, then the new amplitudes are $\xi = 4.0 \pm 1.4$ for $z_{abs} \leq 2.2$ and $\xi = 1.9 \pm 1.4$ for $z_{abs} > 2.2$, corresponding to significance levels of 2.9 and 1.4 σ, respectively. Thus, for the high–redshift sample, the peak near the origin would not be considered significant if systems with $\Delta v < 300$ km s^{-1}were excluded. While the difference between the two subsamples is certainly not overwhelmingly significant, it is suggestive. A strong prediction of any gravitational instability model for the formation of large–scale structure (including "Cold Dark Matter" scenarios) is that the correlation power near the origin in the two–point correlation function should decrease substantially with increasing redshift (or, alternatively, increase substantially with time)(see, e.g., Salmon and Hogan 1986). In addition, such a picture also predicts that the systematic velocities associated with gravitationally bound systems (i.e., groups and clusters) would also increase with time as they reach virial equilibrium. This would then be consistent with the fact that the peak in the 2–point correlation function extends only to ~ 300 km s^{-1}for $z > 2.2$, but to ~ 600 km s^{-1}for $z \leq 2.2$.

V. DISCUSSION

a) Interpretation of the N(z) Relation

We have seen in §IVa that it is the changing distribution of C IV equivalent widths with redshift that results in the observed decreasing trend of $N(z)$ with increasing redshift. There are a number of systematic effects that may be operating to produce this observed evolution; in this section we will attempt to weigh the various possibilities in an effort to isolate the dominant factor or factors.

Another useful way of illustrating the changing distribution of C IV equivalent widths is to compare the actual histograms of $W_0(1548)$ for high– and low–redshift samples. In Figure 6, 2 such histograms have been plotted. Sample ES2 was arbitrarily divided at $z_{abs} = 2.2$ into two roughly equal samples. The high– and low–redshift samples are shown with the dotted and solid histograms, respectively. A K–S test on the unbinned distributions shows that the samples are different at the 94% confidence level. Of course, since the change in the distribution of equivalent widths with redshift is gradual, it is not surprising that an

arbitrary division of the data does not produce an overwhelmingly significant difference. From Figure 6 it is clear that an exponential distribution of the form (usually used to describe the distribution of Lyman α forest line strengths)

$$n(W_0)dW = \left(\frac{N^*}{W^*}\right) \exp(-W_0/W^*)dW \tag{4}$$

is probably not appropriate for either of the two distributions. In fact, the maximum likelihood estimates of N^* and W^* for the two distributions lead to fits which are quite poor in terms of the K–S test, even taking into account the fact that the distributions are incomplete for $W_0(1548) < 0.30$ Å. It is also interesting to note the broad "peak" in the distribution for $0.5 \leq W_0(1548) \leq 0.7$ Å, which is most evident in the low redshift sample. Toward understanding this effect, we now turn to a discussion of the C IV curve of growth.

It has now been rather firmly established that, when observed at very high spectral resolution, the C IV doublets almost always break up into several discrete velocity components, and that the Doppler parameter b for the individual components is in the range $5 \leq b \leq 20$ km s^{-1}, with the most typical values being 7–10 km s^{-1}(e.g., Blades 1987; York *et al.* 1984; Pettini *et al.* 1983). Such b values are consistent with thermal line broadening with temperatures in the range expected for gas in photoionization equilibrium at $T \sim 3-7\times10^4$ K. Thus, for spectra with 60–100 km s^{-1}resolution such as those discussed in the present paper, the components will be unresolved and the measured equivalent widths of the lines represent the ensemble equivalent widths. However, Jenkins (1986) has shown through extensive simulations involving ensembles of clouds having a distribution of column densities and b values that the total column densities inferred on the basis of moderate resolution spectra agree remarkably well with those determined on the basis of spectra in which the individual velocity components are resolved. This has been seen to be the case in practice as well; e.g., for two very strong, unusually complex C IV systems in the spectrum of the BL Lac object 0215+015, Pettini *et al.* found that the total C IV column densities were underestimated by only about 25% in spectra with $\sim$ 115 km s^{-1}as compared with spectra in which a very large number of components was resolved. It is likely that for a typical C IV system found in the present survey, which is much weaker and much less complex than those discussed by Pettini *et al.* , the errors are likely to be comparable or smaller.

Unfortunately, most of the high dispersion work on heavy–element QSO absorption systems has been confined to very complex absorption systems, such as those discussed by Pettini *et al.* , and such as the $z_{abs} = 1.79$ complex in the spectrum of Q1225+317 (York *et al.* 1984; Bechtold, Green, and York 1987). Such complexes represent only a very small percentage of the systems included in the present sample, and it is certainly possible that they have different origins from the more "typical" absorption systems.

The most important result found by Jenkins (1986) for the present work is that despite the fact that we know that each C IV doublet is likely to consist of several discrete components, a single–component curve–of–growth analysis can be used to infer *total* column densities for each system (although, in this case, the inferred b values have no physical meaning in terms of temperatures). There is always the *possibility* that there are very highly saturated velocity components that have very large column densities but contribute only a small amount to the equivalent width; however, we argue that this is unlikely to be the case for light elements like C if the clouds are in photoionization equilibrium; with $7 \leq b \leq 10$ km s^{-1}, components with appreciable column density will also have appreciable equivalent width. For all of the high–resolution observations of C IV we are aware of in the literature, components that dominate the total column density also make significant contributions to the total equivalent width of a complex. In the analysis of Pettini *et al.* (1983), it is the case that the components with the *smallest* inferred b values also have the *smallest* inferred C IV column densities. Thus, in the discussion which follows, since only moderate resolution spectra are available, ***it will be assumed that the conclusions of Jenkins (1986) apply.***

To aid in the discussion, Figures 7 and 8 show plots of parameters related to the theoretical C IV curve of growth. It can be seen from a glance at Figure 7 that C IV doublets with $0.5 \leq W_0(1548) \leq 0.7$ Å (i.e., $-0.3 \leq \log W_0 \leq -0.15$) are just beginning to become saturated for "effective" velocity dispersions $b = 25 - 50$ km s^{-1}. Thus, the "peak" in the W_0 histogram near $W_0 \sim 0.6$ suggests that a large proportion of the absorbers in sample ES2 have "effective" b values in that range, suggesting typical C IV column densities in the range $\log N(C\ IV) = 13.8 - 14.3$ cm^{-2}. It thus turns out that $W_0(1548) \sim 0.40$ Å is a fairly natural place to divide the sample, since it is the equivalent width at which most of

the systems are beginning to leave the linear part of the curve of growth, as seen in Figure 7.

With the aid of Figures 7 and 8, it can be argued that a significant evolution with redshift of the velocity dispersion parameter b (i.e., the "effective" b value of the ensemble, and by extension the b value of the individual components) is not likely. In Figure 7, at a fixed column density $N(C\ IV)$, a systematic *decrease* in mean line strength with increasing redshift (i.e., what is observed) requires that b become systematically *smaller*. However, referring now to Figure 8, again at a fixed column density, a systematic decrease in b results in a general *decrease* of the C IV doublet ratio $DR = W_0(1548)/W_0(1550)$. This is contrary to the actual observations, which show that the mean DR is significantly increasing with redshift (SBS). It is worth re–examining the evolution of DR with redshift, given the improvements to the sample afforded by the additional data. A plot of the mean doublet ratio (as in SBS, this is taken from a reduced sample in which $W_0(1548)$ must exceed 0.30 Å and in which doublets that are obviously involved in blends are excluded) is shown in Figure 9; DR changes from a value of $\sim$ 1.35 at $z_{abs} \approx 1.5$ to $\sim$ 1.65 at $z_{abs} \approx 3$. If it is assumed that there is no general change of the velocity dispersion parameter b with increasing redshift, then Figure 8 shows that the evolution of DR corresponds to a factor of $\sim$3 decrease in the *mean* C IV column density over the redshift range $1.5 \leq z_{abs} \leq 3$. (It should be pointed out that the trend of decreasing line strength together with increasing (toward the optically thin limit) DR suggests that there are *fewer* saturated components in each absorption system with increasing redshift; the trends cannot be explained by invoking changes in only the optically thin components, and they cannot be adequately explained by changes in only the *number* [and not the column density] of components with redshift.)

It is worth discussing the possible implications of Figure 4, which shows the $N(z)$ curves for the weak–line and strong–line subsamples of sample ES2. It should be emphasized that the behavior of the weak–line subsample, which is consistent with no evolution in comoving number density, is to be expected under the hypothesis that all of the absorbers are undergoing a gradual change in C IV column density (the number of systems that evolve out of the range $0.15 \leq W_0(1548) \leq 0.40$ is roughly the same as the number of systems that originally had $W_0 < 0.15$ Å, but that, over time, evolved *into* the observed range

of rest equivalent widths). Recalling that the weak–line subsample is incomplete at the small equivalent width end because systems with doublet ratios close to 2 would remain undetected (this probably explains the dearth of systems in the highest redshift bin, where the weak lines dominate), it is conceivable that if the surveys for C IV absorption were complete to a smaller rest equivalent width, we should eventually find that the population of detected C IV systems should be consistent with no evolution in *number*, especially if they are indeed associated with the apparently non–evolving high column density HI systems (SSB). Figure 10 shows a plot similar to Figure 4, except that the weak–line subsample has been taken from the 21 QSOs in which all doublets with $W_0(1548) = 0.15$ Å could have been detected, even for $DR \approx 2$ (see §IVa). It is striking how the curve (despite the rather large error bars because of the relatively small sample size) appears to exhibit a behavior opposite that of the strong–line sample. The implication is that if our entire survey were complete to $W_0(1548) = 0.15$ Å, then the overall $N(z)$ curve would be very close to being consistent with no evolution in comoving number density; however, the extreme change in the distribution of equivalent widths with redshift is clear. *The most natural interpretation of the data is that weak systems simply become strong ones over time.*

That we are able to observe (with a detection threshold of $W_0(1548) = 0.15$ Å) nearly the same comoving number of absorbers at $z \sim 3$ that are eventually observable at $z \sim 1.5$ allows us to speculate further. Suppose that all of the systems at $z \sim 3$ with equivalent widths in the range $0.15 \leq W_0(1548) \leq 0.40$ become systems with $W_0(1548) > 0.4$ Å by the epoch corresponding to $z \sim 1.5$. Taking $N_{weak}(z) \sim 3$ at $z \sim 3$, then to preserve the comoving number density of absorbers we expect to see $3(2.5/4)^\gamma$ at a redshift of 1.5, or $N(z) \approx 1.9$ and $N(z) \approx 2.3$ for $q_0 = 0$ and $q_0 = 1/2$, respectively. This agrees well with the actual number of *strong* systems at $z \sim 1.5$. For all of the systems in the weak subsample to evolve into the strong sample requires that the typical value of $N(C\ IV)$ change by at least a factor $0.4/0.15 \approx 2.7$; the value would have to be larger if a significant fraction of the systems are not on the linear part of the C IV curve of growth, which, however, we have argued is unlikely to be the case. *Thus, again, a factor of* ≈ 3 *change in mean C IV column density over the redshift range* $3 \geq z \geq 1.5$ *is indicated.* Under the assumption that all of the absorbers undergo a gradual increase in C IV column density with time, the weak

systems observed at $z \sim 1.5$ are then likely to be systems whose $N(C\ IV)$ was too small to be detected at the epoch corresponding to $z \sim 3$.

b) The Chemical Evolution of the Absorbers

Having established that the evolution in $N(z)$ can best be interpreted as a systematic change in the mean C IV column density with redshift, it remains to be discussed whether this change is attributable to a change in actual *chemical abundance* of carbon in the gas clouds, or to a gradually changing *ionization level.* The latter effect could result from either a systematically changing gas density or from a change in the nature of the ionizing continuum as a function of redshift (or both). There are several lines of evidence that suggest that the ionization level in the gas clouds is not changing significantly with time. First, as mentioned in SBS, there does not appear to be any correlation in the ratio of the equivalent widths of the C IV λ1548 and the Si IV λ1393 absorption lines with redshift; this ratio is expected to increase as the ionization level in the gas decreases. Spearman and Kendall rank correlation tests have been performed on the absorption systems (from Sample ES2) which have unambiguously detected Si IV, with the result that any correlation between $W_0(C\ IV)/W_0(Si\ IV)$ and redshift that might exist has a significance of $< 0.5\sigma$. It should also be noted that this test would be fairly inconclusive even if a correlation were found, since the relative column densities of Si and C can be affected by, e.g., depletion onto dust grains. The best test for evaluating whether or not the ionization level changes systematically is the relative strengths of C IV and C II λ1334. Unfortunately, more often than not the C II line corresponding to an observed C IV doublet falls in the Lyman α forest so that equivalent widths are extremely difficult to interpret, and in general it is only for the strongest C IV doublets that C II λ1334 is observable without very high S/N spectra. A somewhat more indirect piece of evidence in favor of an ionizing continuum that does not vary significantly with redshift is provided by limits placed on the intensity of the metagalactic ionizing flux $J_\nu(z)$ from the so–called "proximity effect" in QSOs (Bajtlik, Duncan, and Ostriker 1988; Bechtold 1988). Although subject to many uncertainties, this method estimates the intensity of the general UV background relative to the ionizing flux produced by a QSO by measuring the deficit of Lyman α forest absorption lines with

$z_{abs} \approx z_{QSO}$. By examining data for QSOs with a range of emission redshifts, Bajtlik, Duncan, and Ostriker (1987) found that $J_\nu(z)$ appears to be independent of z in the range $1.8 \leq z \leq 3.8$. However, it must be pointed out that the effects of "local" sources (i.e., over and above the metagalactic UV radiation) of ionizing flux, for example, regions where massive star formation is occurring, make an unknown contribution to the total radiation field impinging on the gas clouds. The possibility would remain that this contribution is significant and evolves with redshift.

Additional evidence favoring a non–evolving ionization state in the clouds giving rise to the heavy element absorption systems is provided by the observed evolution of the Lyman limit absorption systems. These systems, which are found on the basis of the clear Lyman edge produced when $N(HI) > 10^{17}$ cm^{-2}, exhibit an $N(z)$ curve that is consistent with *no evolution* over the redshift range $0.2 \leq z \leq 4$ (SSB; Lanzetta 1988; Bechtold *et al.* 1984; Tytler 1982). The Lyman limit systems are largely the same population of absorbers that give rise to C IV absorption, particularly at high redshift. In their low–resolution survey for LLSs, SSB found that $N_{LLS}(z) \approx 2$ at $z_{abs} \approx 3$, to be compared with $N_{C\ IV}(z) \approx 1.5 - 2$ at $z_{abs} \sim 3$ for the C IV systems as defined by sample ES2. In the same low–resolution survey, SSB found detectable C IV doublets associated with about 70% of the observed LLSs in the redshift range $2.5 \leq z_{LLS} \leq 3.5$ (it was estimated that lines of strength $W_0(1548) \sim 0.40$Å could have been found in a typical spectrum). Preliminary results at higher dispersion have shown that C IV doublets are present in the great majority of cases where no C IV was originally detectable (Steidel 1989). Thus, one can argue that the LLSs trace the hydrogen component of the same population of absorbers that gives rise to a large fraction of the C IV redshifts; therefore, that the LLS distribution in redshift is consistent with no evolution (i.e., constant comoving density of absorbers) is very important to the interpretation of the evolution of the C IV systems. (Also, recall that the density of C IV systems appears to be consistent with no evolution if one can detect very weak lines; §IVa, §Va). The important question to ask is, if the change in the mean C IV column density with redshift is an ionization effect, then how would the HI component (i.e., the LLSs) be expected to change? In an effort to answer this question, it is necessary to make use of a model "cloud." Figure 11 shows the model predictions for a cloud with a total

hydrogen column density of 1×10^{20} cm^{-2} which is being photoionized by a continuum that has the shape of the "Medium" integrated QSO spectrum calculated by Bechtold *et al.* (1987). The models are constructed using Ferland's CLOUDY photoionization program (Ferland 1988), and are calculated in terms of the ionization parameter $\Gamma = n_\gamma/n_H$, where n_γ is the number density of photons capable of ionizing hydrogen and n_H is the number density of hydrogen. The other parameters used in the grid of models (namely, the total H column density and the assumed heavy–element abundance) are those that have been determined to be "reasonable" for typical LLSs in a detailed study which is in preparation (Steidel 1989). The relative column densities of several important ions are shown, along with the predicted HI column density (the *relative* column densities of the heavy element ions are fairly insensitive to the assumed abundances). It can be seen that a significant decrease in the C IV column density could occur only with a substantial decrease in Γ. If, for example, $\log\Gamma$ changed from ~ -2.1 to ~ -2.8, the C IV column density would change by a factor of $\sim$3; however, the associated HI column density would change from $\log N(HI) \approx 16.5$ to $\log N(HI) \approx 17.5$, or a factor of 10. In the LLS survey conducted by SSB, the limiting column density that would have resulted in a detection of a Lyman limit was $\log N(HI) \geq 17.38$. If the ionization parameter evolved systematically by a factor of ~ 5 between a redshift of 1.5 and 3, then the above arguments show that clouds with $\log N(HI) \sim 16.4$ and greater at low redshift would have detectable Lyman limits at $z = 3$. Given that the spectrum of HI column densities appears to conform approximately to a power law $n[N(HI)] \propto N(HI)^{-1.5}$ (SSB; Tytler 1987), this would mean that the *comoving* number of detectable LLSs would be expected to *triple* between $z = 1.5$ and $z = 3$. Clearly, this is inconsistent with the observations. Thus, we conclude that it is unlikely that the evolution of the C IV absorbers is caused by a significant systematic change in the ionization state of the gas. *It is therefore suggested that the bulk of the observed evolution of the C IV systems results from a change in the average abundance of C with redshift.*

Steidel, Sargent, and Boksenberg (1988; hereinafter Paper I) summarized the method by which the timescale for the chemical evolution in galactic halos could be determined based on the assumption that the C IV evolution in number with redshift is the result of a gradually changing carbon abundance. The method also assumes that the LLSs represent

the (non–evolving) HI component of the same population of absorbers that gives rise to the C IV absorption redshifts. The arguments presented above show that both of these assumptions are reasonable. It is interesting to point out that there is rather good agreement between the estimate of the "typical" change in $N(C\ IV)$ with redshift in the range $1.5 \leq z_{abs} \leq 3.0$ deduced from the change in the $\langle DR \rangle$, and the consideration of the relative numbers of weak and strong C IV systems as a function of redshift, and that which would be predicted by the arguments given in Paper I. Paper I uses the ratio of the number of detected C IV absorption systems to the number of LLSs as a function of redshift to describe the rate of change of the cross section for C IV absorption, which is assumed to be proportional to changes in the mean C abundance. However, the problem with this type of analysis is that it depends to a large extent on the (unknown) abundance distribution of those systems that are initially (i.e., at $z > 3$) beyond the detection limit of the survey. That is, it is not sufficient to consider only the *number* of C IV systems satisfying a given rest equivalent width criterion; we have seen above that the observed $N(z)$ relation is largely a function of the equivalent width threshold of the sample used. Thus, although the timescale for changes in the C abundance deduced in Paper I agrees remarkably well with that found in the present work, the agreement is fortuitous.

Many of the above arguments are tentative; as discussed by SSB1 and in Paper I, the situation can be completely resolved only through detailed chemical composition (and ionization state) studies of the heavy–element absorption systems over a wide range in redshift. The best way to proceed is probably to select systems on the basis of their HI content (particularly the LLSs, since they can be detected in an unbiased manner and they are closely related to the systems detected on the basis of C IV) and then to study the associated heavy element lines to determine chemical abundances. Such a study has been initiated, the results of which will be presented elsewhere (Steidel 1989). In addition to detailed studies, it would also be extremely useful, as mentioned in §IVa, to undertake a survey for C IV absorption which is more sensitive to the weakest C IV doublets.

c) Implications for the Heavy Element Enrichment in Galaxies

As discussed in Paper I and in SBS, the majority of absorbers that give rise to C IV

systems are thought to be associated with the halos of intervening galaxies; however, at present virtually all of the evidence that associates the absorbers with galaxies is indirect (a comprehensive review of the evidence, including comparisons of the high redshift C IV systems to halo gas in the Galaxy, is given by Boksenberg and Sargent (1983); more recently, several interpretations of the origins of the absorbers are discussed by York (1987), and references therein). The clustering properties of the C IV absorbers on both small and moderate velocity scales are certainly consistent with what would be expected if the clouds were associated with galactic halos (and they are quite different from the clustering properties of the Lyman α forest lines, which are thought to be intergalactic) (SBS; Webb 1987; Sargent *et al.* 1980). The very presence of heavy elements in the gas indicates that star formation has occurred, and the chemical evolution indicated by the above discussion suggests that star formation is ongoing over the epoch we are able to observe. While we naturally associate sites where star formation is occurring with galaxies, it is certainly possible that a significant fraction of the observed "heavy–element" absorption systems arise in small (but numerous) clumps of intergalactic material, which might not be considered "galaxies" at all if we could actually detect them. Since the *typical* HI column densities of the systems are of the order of 10^{17} cm^{-2} (although they can be as small as $\sim 10^{16.5}$ or as large as $\sim 10^{21.5}$ in the relatively rare instance of absorbers that would give rise to damped Lyman α absorption), the local population of such objects could have easily escaped detection in even the most sensitive HI surveys completed up to the present time. On the other hand, there are several arguments in favor of the absorbers being very large (up to several hundred kpc), which are reviewed by SBS. There is also now a substantial body of direct evidence associating the Mg II absorption systems with bright galaxies (Bergeron 1988); however, Mg II requires a significantly higher HI column density than does C IV in order to be strong enough for detection, and these systems are relatively nearby ($z_{abs} \leq 0.7$) so that a direct comparison for C IV will not be possible until Space Telescope data are available. In any case, the C IV absorbers are tracing baryonic material where the conditions have been such that stars have been able to form; in the remaining discussion we will refer to these sites as "galaxies," and because at least 95 % of the C IV absorbers have corresponding HI column densities which are too small to be associated with the galactic HI disks discussed by Wolfe

et al. (1986) (i.e., the damped Lyman α systems), it seems natural to refer to the absorbers as "halo systems."

Because of the statistical nature of the preceding arguments, it is difficult to comment on the bearing the results may have on the chemical enrichment history of an *individual* galaxy. For example, the type of observational results from which the "global" increase in C abundance over time is deduced cannot readily distinguish between a scenario in which the absorbers all undergo a gradual evolution in heavy–element abundance and one in which an increasing (with time) fraction of absorbers have undergone rapid bursts of star formation which transform weak–line systems into strong ones. However, in the latter case one might expect to observe a "bimodal" distribution of equivalent widths at a given time, and this does not appear to be the case (although the curve of growth effects that set in near $W_0 = 0.5$ Å certainly complicate the matter). Further, the fact that we still see a substantial number of weak systems at relatively low redshift (even though all of the weak systems seen at high z are required to account for the number of strong systems at low z) seems to indicate that there is a population of absorbers at high redshift which is somewhat below our threshold for detection, but which becomes observable with time. Thus, while alternative models cannot be ruled out, the currently available data appear to be most consistent with a gradual heavy–element enrichment in the absorbers over time.

Taking $q_0 = 1/2$, the corresponding time over which the typical carbon abundance in the C IV absorbers changed by a factor of ~ 3 is $\sim 1.7 h_{50}^{-1}$ billion years, where h_{50} is the Hubble constant in units of 50 km s^{-1}Mpc^{-1}. Thus, the e–folding time for heavy–element enrichment in the "halo" gas is between 1 and 2 billion years. The age of the universe as a function of redshift z (for $q_0 = 1/2$) is given by

$$t = t_0(1+z)^{-1.5} \quad ,$$

where $t_0 = 13.7 h_{50}^{-1}$ billion years, so that the time "window" over which we can observe the C IV absorbers is between $t = 1.3 h_{50}^{-1}$ and $t = 3.9 h_{50}^{-1}$ billion years, corresponding to look–back times of $12.4 h_{50}^{-1}$ to $9.8 h_{50}^{-1}$ Gigayears. For the purposes of discussion, suppose that a value of H_0 is chosen so that the age of the universe (as given by the formula $t_0 = 2/3H_0$) approximately matches the ages of globular clusters as determined by main

sequence turnoffs in color–magnitude diagrams, $H_0 \sim 40$. Thus, $t_0 \approx 17$ Gigayears and the lookback times corresponding to the epoch over which the C IV absorbers have been observed are $\sim 12 - 16$ Gigayears. Taken at face value, this span of time is of considerable interest in terms of the time over which the halo of our Galaxy is thought to have formed. Whether or not there is a significant age spread (thought to be indicative of a relatively slow formation of the halo compared to that envisaged by Eggen, Lynden–Bell, and Sandage (1962)) in the globular cluster systems of our Galaxy is still unclear. However, there have been some recent indications that there may exist halo globular clusters that have ages roughly 30% smaller than the bulk of the other well–studied clusters (e.g., Gratton and Ortolani 1988), possibly suggesting that the halo may have been forming over as much as 4 Gigayears. We are able to observe significant chemical evolution in the halo gas of intervening galaxies over a time which is (coincidentally?) very similar to the time corresponding to the collapse of our Galaxy. It would admittedly be difficult to interpret the absorption line data in terms of galactic halo formation and evolution if indeed all halo systems evolved to completion over very short timescales (i.e.,$\leq$ 1Gyr).

On the other hand, what is observed *would* be consistent with the halo formation scenario of Searle and Zinn (1978), who proposed that the properties of the *outer* halo globular clusters could be explained if they originated in proto–galactic fragments which have the character of gas–rich irregular galaxies (cf., York *et al.* 1986) and which continued to evolve both chemically and dynamically for timescales much longer than that for the collapse of the more central regions of the galaxy. The number of C IV absorption systems observed, if the absorbers are to be associated with galaxies, requires that the typical galaxy cross section for absorption have dimensions of at least several Holmberg radii (see, e.g., SBS), indicating that, on average, a line of sight through a galaxy will be intersecting it at a very large galactocentric radius. Thus, under the hypothesis that the absorbers are associated with galaxies as we understand them, the absorption lines must be probing primarily *outer* halo gas, and absorption systems arising in disk gas must be very rare in comparison. Hence, the suggestion of the QSO absorption line data is that there may indeed be significant outer halo evolution over timescales that are longer than the collapse times of galaxies in the process of formation. If the hypothesis of the gradual chemical

evolution of the absorbers is correct, and if the Lyman limit absorption systems really do not evolve significantly with redshift (recall that such systems are tracing the HI component of essentially the same absorbers giving rise to the C IV redshifts), then it is possible that the absorption line data are probing material that is associated with sites where galaxies have formed or are in the process of forming, but that does not participate in the rapid collapse. That is, the gas may be the "left–over" outer remnants of large proto–galactic clouds which were the precursors of galaxies. Such a picture would also be consistent with that of Rees (1987), who has suggested that the formation of the outer parts of disk galaxies must be ongoing until a redshift of at least $z \sim 2$.

Clearly, there is not yet enough information to make more than a passing remark about the above coincidences in timescales, especially considering the very controversial nature of the subject of the formation of the Galactic halo. The interpretation is also complicated by the fact that the absorption lines provide information about the *ensemble* of galactic halos as a function of time (and they may be tracing material with a variety of origins), and at present it is impossible to deconvolve the history of individual galactic halos (in order to compare to what is known about the history of the halo of our Galaxy) from that ensemble. However, in the future, the QSO absorption lines' connection to the formation and evolution of galactic halos may be strengthened if it is found that 1) the heavy–element abundances of the absorption systems are consistent with halo metallicities seen in the Galaxy, and 2) there is some redshift $z < 1.5$ at which the chemical evolution of the heavy–element absorbers appears to reach a "saturation value," as mentioned by SSB. The latter condition would be expected if there is some epoch by which star formation in galactic halos comes to a halt, as it presumably did in our Galaxy.

VI. CONCLUSIONS

New spectroscopic observations of 11 very high redshift QSOs ($\langle z_{em} \rangle = 3.4$) have been combined with the previously published data of 55 QSOs to enhance the redshift coverage of a large survey for C IV absorption. The new extended sample contains 275 C IV redshifts spanning the range $1.3 \leq z_{abs} \leq 4.1$. The sample has been used to discuss the evolution of the properties and distribution of the gas clouds giving rise to heavy–element absorption in

the spectra of QSOs, with the following principal results:

1. As in SBS, unbiased subsamples of C IV redshifts were created. Sample ES2, which contains all of the C IV doublets satisfying the criterion $W_0 > 0.15$ Å (lines of this strength could have been detected in any of the 66 QSOs) and apparent ejection velocities (relative to the QSO emission redshift) $\beta c > 5000$ km s^{-1}, is regarded as the primary unbiased sample for evaluation of the evolution of the absorption systems with redshift. As in SBS, this sample was constructed by counting pairs and clumps of absorption redshifts separated by less than 1000 km s^{-1}as one system. Sample ES5 was constructed by requiring that $W_0 > 0.30$ Å and was supplemented with uniform data from other sources. A third sample, EA2, was constructed for the purposes of determining the absorption system 2–point correlation function. Redshifts in this sample need only satisfy the criteria $\beta c > 5000$ km s^{-1}.

2. The number of C IV absorbers per unit redshift range, $N(z)$, is found to be inconsistent with a constant comoving density of absorbers at the 3.1σ level for $q_0 = 1/2$ and at the 4.0σ level for $q_0 = 0$. Thus, the absorbers must be evolving with time. A maximum likelihood fit to a power–law form for the $N(z)$ distribution gives $N(z) \propto (1+z)^{-1.26\pm0.56}$ for sample ES2. The distribution is significantly steeper for subsamples containing only strong (in terms of W_0) C IV doublets. The trend of the $N(z)$ curve is seen to be a gradual decline for $z_{abs} > 2$; the precipitous fall–off possibly indicated by the data in the original SBS survey is ruled out.

3. We have re–examined the C IV redshift 2–point correlation function in light of the new data. As found by SBS, there is significant power ($\xi = 6.1 \pm 1.2$) in the correlation function for velocity scales $200 \leq \Delta v \leq 600$ km s^{-1}. If the data are divided into 2 subsamples, one with $z_{abs} < 2.2$ and the other with $z_{abs} > 2.2$, it is found that the power on these velocity scales is statistically the same for the two. However, there is marginal evidence suggesting that the power extends only to $\Delta v \sim 300$ km s^{-1}in the high–redshift subsample. The low–redshift subsample shows a $\sim 2\sigma$ excess of power on velocity scales $1000 \leq \Delta v \leq 10{,}000$ km s^{-1}; there is no corresponding excess in the higher–redshift subsample. However, most of this power has been shown to be due to absorption in the spectrum of a single object, and thus the lack of such structure in the high–redshift

subsample may not be significant.

4. The C IV equivalent width distributions for $z_{abs} \leq 2.2$ and $z_{abs} > 2.2$ have been compared; they are different at the 94% confidence level. A broad peak in the equivalent width distribution for $0.5 \leq W_0(1548) \leq 0.7$ Å is interpreted as a curve of growth effect. Consideration of the theoretical C IV curve of growth appears to rule out a significant evolution of b with redshift; thus the evolution in $N(z)$ is interpreted as a systematic change in the mean C IV column density with redshift.

5. The evolution of the C IV doublet ratio $DR = W_0(1548)/W_0(1550)$ (as originally found by SBS) is re–examined. The change in $\langle DR \rangle$ between $z = 3$ and $z = 1.5$ is consistent with a factor of ~ 3 decrease in the mean C IV column density over that redshift range.

6. Various arguments lead to the conclusion that the evolution in $N(z)$ for the C IV absorbers is dominated by a systematic change in the abundance of carbon in the gas, not by a significant change in the ionization state of the gas with redshift.

7. The behavior of the $N(z)$ curves for weak and strong C IV doublets is consistent with the hypothesis that the weak systems observed at high redshift evolve into the strong systems observed at lower redshift, and that when the numbers are considered, the typical increase in the C IV column density would have to be somewhat greater than a factor of ~ 3 between $z \sim 3$ and $z \sim 1.5$. This factor is in agreement with that determined from the consideration of the change in the mean C IV doublet ratio. It is thus suggested that the typical gas cloud giving rise to a C IV absorption system has an abundance of C which increases by a factor of ~ 3 over this redshift range.

8. The implications of this chemical evolution are discussed in the context of early heavy–element enrichment in galactic halos. The implied e–folding time for chemical enrichment is between 1 and 2 billion years for lookback times between $9.8h_{50}^{-1}$ and $12.4h_{50}^{-1}$ billion years ($q_0 = 1/2$). The implications are that there may be significant evolution of galactic halos over timescales much longer than the galaxy collapse timescales. If the absorbers are associated with the high–redshift analogues of galaxies observed at the present epoch, then the vast majority of the absorption systems must arise in outer halo gas. It is suggested that the absorbers may in fact represent the outer parts of large proto–galactic clouds which do not participate in the actual collapse.

I would like to thank C. Hazard and R. Mc Mahon for providing the positions for several unpublished high–redshift QSOs. B. Kunkel and A. Guerra at Las Campanas Observatory, and S. Staples, D. Tennant, M. Doyle, and J. Henning at Palomar Observatory are thanked for their help with the observations. I would also like to thank P. Schechter for explaining the workings of the Modular Spectrograph at Las Campanas, and J. McCarthy for computer programs upon which the reduction software used to reduce the Modular Spectrograph data was based. G. Ferland is thanked for providing a copy of his photoionization program CLOUDY. J. Mould and W. Sargent are acknowledged for extremely useful discussions and comments.

TABLE 1

OBSERVATIONS

Object	Telescope	Date (UT)	Exposure (s)	λ Range (Å)	FWHM (km s^{-1})
Q0000−263	LCO	1988 Sep 16	14400	5000–8450	60
Q0041−286	LCO	1988 Sep 19	15300	5000–8450	60
Q0042−264	LCO	1988 Sep 17	10800	5000–8450	60
	LCO	1988 Sep 18	5400	5000–8450	60
Q0055−269	LCO	1988 Sep 14	10800	5000–8450	60
	LCO	1988 Sep 15	5400	5000–8450	60
Q0256−000	LCO	1988 Sep 15	5000	5000–8450	60
	LCO	1988 Sep 16	9000	5000–8450	60
Q0347−383	LCO	1988 Sep 18	12600	5000–8450	60
Q0428−136	LCO	1988 Sep 19	12600	5000–8450	60
Q1208+101	PAL	1988 Feb 20	7200	5350–6000	80
	PAL	1988 Feb 21	3600	5905–6535	80
	PAL	1988 Feb 21	3600	6485–7115	80
	PAL	1988 Feb 21	3600	7065–7695	80
Q2000−330	LCO	1988 Sep 15	10800	5000–8450	60
	LCO	1988 Sep 16	3600	5000–8450	60
	LCO	1988 Sep 19	5400	5000–8450	60
Q2204−408	LCO	1988 Sep 14	10800	5000–8400	60
	LCO	1988 Sep 15	5400	5000–8400	60
Q2239−386	LCO	1988 Sep 14	3600	5000–8400	60
	LCO	1988 Sep 16	5400	5000–8400	60
	LCO	1988 Sep 18	13500	5000–8400	60

TABLE 2
Absorption Lines

No.	λ_{obs}	$\sigma(\lambda)$	W_{obs}	$\sigma(W)$	S/N	ID	z_{abs}
				Q0000–263			
1	5031.98	0.14	0.99	0.19	4.9		
2	5040.25	0.16	0.75	0.14	7.3		
3	5042.24	0.13	1.13	0.19	4.9		
4	5044.77	0.14	1.21	0.19	5.4		
5	5051.97	0.13	1.45	0.18	6.1		
6	5059.75	0.23	9.64	0.56	4.1		
7	5070.01	0.14	1.40	0.14	8.8		
8	5081.24	0.13	1.59	0.13	10.3		
9	5084.99	0.12	1.31	0.12	10.4		
10	5092.08	0.12	1.12	0.11	10.4		
11	5095.87	0.12	2.42	0.16	9.0		
12	5100.17	0.12	1.87	0.13	10.3		
13	5104.88	0.13	1.70	0.12	12.3		
14	5112.36	0.13	3.74	0.17	10.5		
15	5119.34	0.12	1.90	0.13	10.6		
16	5123.39	0.10	1.08	0.09	11.2		
17	5129.11	0.13	4.92	0.22	8.4		
18	5137.38	0.11	2.43	0.16	7.9		
19	5140.79	0.10	1.77	0.16	6.7		
20	5145.74	0.12	4.09	0.19	8.9		
21	5154.42	0.11	0.91	0.08	14.3		
22	5158.33	0.11	2.26	0.14	9.3		
23	5162.38	0.11	2.90	0.18	7.4		
24	5184.31	0.13	0.96	0.09	14.8		
25	5190.22	0.13	3.10	0.16	11.4		
26	5198.50	0.13	1.18	0.10	12.7		
27	5202.29	0.12	0.92	0.09	13.0		
28	5209.10	0.12	1.21	0.10	11.9		
29	5213.90	0.13	2.38	0.15	9.8		
30	5219.31	0.12	1.78	0.16	7.8		
31	5223.92	0.12	1.91	0.16	7.5		
32	5226.39	0.10	1.04	0.13	6.8		
33	5228.60	0.12	1.69	0.20	5.3		
34	5231.88	0.11	1.13	0.10	11.1		
35	5238.27	0.14	1.22	0.11	13.7	SiII(1193)	3.3898
36	5247.10	0.12	1.88	0.13	10.6		
37	5252.06	0.11	2.08	0.13	10.4		
38	5262.50	0.18	9.91	0.43	5.6	HI(1025)	4.1305
39	5271.13	0.14	2.00	0.20	6.7		
40	5274.30	0.11	1.13	0.12	7.9		
41	5286.21	0.14	0.87	0.13	8.5		
42	5289.06	0.15	1.34	0.21	5.0		
43	5381.29	0.16	1.25	0.19	6.3		
44	5385.77	0.15	3.04	0.31	4.6		
45	5403.34	0.13	1.23	0.11	11.1		
46	5410.88	0.15	1.56	0.12	12.6		
47	5417.15	0.12	0.95	0.09	12.9		
48	5428.00	0.12	1.76	0.14	9.0		
49	5433.65	0.11	0.78	0.08	12.4		
50	5439.76	0.15	5.60	0.29	6.7		

TABLE 2 –*Continued*

No.	λ_{obs}	$\sigma(\lambda)$	W_{obs}	$\sigma(W)$	S/N	ID	z_{abs}
51	5445.97	0.12	1.95	0.16	8.1		
52	5449.26	0.12	0.83	0.08	14.3		
53	5457.70	0.12	1.70	0.13	10.6		
54	5461.49	0.11	0.97	0.09	12.6		
55	5465.12	0.11	1.55	0.12	11.1		
56	5470.00	0.12	0.94	0.09	13.1		
57	5479.78	0.12	0.38	0.06	15.0		
58	5485.38	0.12	1.73	0.12	12.5		
59	5489.30	0.11	1.60	0.12	10.7		
60	5495.37	0.14	0.78	0.08	15.4		
61	5501.09	0.11	2.95	0.18	8.1		
62	5504.89	0.11	2.02	0.13	10.4		
63	5513.33	0.13	4.90	0.24	7.6		
64	5519.35	0.11	2.27	0.14	10.2		
65	5523.87	0.11	1.96	0.11	12.3		
66	5531.36	0.08	7.62	0.09	20.8	SiII(1260)	3.3885
67	5539.21	0.09	6.18	0.12	16.4		
68	5546.67	0.10	1.31	0.08	17.4		
69	5552.29	0.09	3.30	0.10	15.4		
70	5557.38	0.09	2.72	0.10	15.0		
71	5567.27	0.10	12.49	0.18	14.9		
72	5585.35	0.09	10.83	0.15	16.9		
73	5594.43	0.09	2.34	0.09	15.2		
74	5598.60	0.14	1.29	0.11	13.8		
75	5608.07	0.09	1.12	0.05	24.9		
76	5611.39	0.09	1.45	0.05	25.8		
77	5621.06	0.09	9.33	0.08	33.1		
78	5645.20	0.10	1.79	0.08	20.7		
79	5650.08	0.11	0.58	0.05	21.9		
80	5655.26	0.09	1.23	0.06	20.1		
81	5658.62	0.09	2.45	0.08	19.1		
82	5665.29	0.09	1.30	0.06	18.0		
83	5668.78	0.09	1.88	0.07	16.9		
84	5671.42	0.09	1.33	0.06	16.6		
85	5674.12	0.09	1.62	0.08	16.1		
86	5677.50	0.10	1.11	0.07	16.6		
87	5679.65	0.08	1.43	0.06	16.7		
88	5681.80	0.08	1.80	0.06	16.4		
89	5684.81	0.10	2.12	0.09	16.1		
90	5691.11	0.11	1.20	0.08	17.3		
91	5708.88	0.10	3.02	0.08	23.6		
92	5717.44	0.10	1.96	0.07	24.2	OI(1302)	3.3907
						+SiII(1260)	3.5355
93	5727.25	0.10	1.77	0.07	24.0	SiII(1304)	3.3908
94	5732.19	0.11	0.74	0.05	24.0		
95	5734.64	0.09	0.92	0.04	26.2		
96	5736.55	0.09	0.87	0.04	27.0		
97	5741.96	0.11	1.90	0.08	20.5		
98	5747.95	0.10	3.56	0.10	16.9		
99	5754.73	0.13	0.69	0.09	13.1		

TABLE 2 –*Continued*

No.	λ_{obs}	$\sigma(\lambda)$	W_{obs}	$\sigma(W)$	S/N	ID	z_{abs}
100	5758.29	0.12	2.32	0.13	12.5		
101	5772.57	0.09	17.44	0.13	23.7		
102	5784.84	0.11	2.37	0.12	12.6		
103	5788.96	0.11	1.65	0.11	12.2		
104	5794.37	0.11	1.78	0.10	14.9		
105	5799.99	0.09	3.31	0.10	16.6		
106	5803.41	0.09	0.86	0.05	22.4		
107	5808.74	0.09	4.75	0.07	26.1		
108	5825.18	0.08	4.35	0.06	30.0		
109	5828.83	0.08	1.32	0.03	30.7		
110	5832.11	0.08	3.37	0.05	30.1		
111	5839.57	0.09	4.87	0.07	27.6		
112	5845.34	0.08	3.66	0.06	27.1		
113	5853.60	0.09	3.76	0.07	25.2		
114	5858.29	0.08	3.55	0.06	25.9	CII(1334)	3.3898
115	5863.95	0.09	3.29	0.07	26.0		
116	5870.56	0.11	0.44	0.05	23.0		
117	5873.30	0.09	0.76	0.05	21.6		
118	5875.64	0.10	0.90	0.06	21.6		
119	5879.17	0.09	1.66	0.06	21.2		
120	5885.68	0.10	1.52	0.07	19.7		
121	5888.69	0.09	1.70	0.06	22.0		
122	5896.80	0.10	2.78	0.08	22.4		
123	5904.15	0.09	2.52	0.07	22.4		
124	5909.81	0.09	6.19	0.09	22.4		
125	5915.95	0.09	3.00	0.06	24.4		
126	5921.81	0.08	2.38	0.05	24.5		
127	5925.36	0.08	2.75	0.06	25.1		
128	5930.37	0.09	0.95	0.05	25.9		
129	5933.22	0.09	1.00	0.05	25.8		
130	5940.96	0.10	0.92	0.05	24.1		
131	5943.13	0.08	0.84	0.04	24.3		
132	5945.31	0.09	0.88	0.04	25.9		
133	5948.13	0.09	1.54	0.05	26.7		
134	5952.48	0.10	0.57	0.04	25.0		
135	5954.52	0.09	0.50	0.04	25.7		
136	5960.84	0.09	2.07	0.06	25.5		
137	5968.71	0.10	3.17	0.09	22.6		
138	5976.95	0.10	3.75	0.09	21.4		
139	5983.49	0.09	2.31	0.07	21.3		
140	5987.25	0.09	2.47	0.07	21.2		
141	5990.71	0.10	0.88	0.06	21.1		
142	5999.59	0.09	6.35	0.08	25.0		
143	6006.58	0.10	1.77	0.10	13.4		
144	6009.39	0.10	2.06	0.12	11.0		
145	6013.83	0.10	1.52	0.09	14.7		
146	6016.55	0.10	1.03	0.07	15.1		
147	6021.24	0.11	2.62	0.12	14.0		
148	6025.77	0.10	1.60	0.09	14.4		
149	6029.76	0.11	1.61	0.09	17.0		

TABLE 2 –*Continued*

No.	λ_{obs}	$\sigma(\lambda)$	W_{obs}	$\sigma(W)$	S/N	ID	z_{abs}
150	6034.22	0.11	1.53	0.08	17.8		
151	6039.75	0.10	3.00	0.13	12.2		
152	6044.51	0.11	2.96	0.12	14.4		
153	6051.93	0.21	0.52	0.07	23.4		
154	6060.37	0.10	4.05	0.14	13.3		
155	6065.04	0.09	2.00	0.09	14.5		
156	6068.11	0.09	1.76	0.08	15.0		
157	6072.70	0.09	2.04	0.09	15.5		
158	6076.13	0.09	2.54	0.12	11.6		
159	6081.08	0.10	4.28	0.13	13.5		
160	6088.48	0.09	3.62	0.10	17.6		
161	6093.99	0.10	1.24	0.06	28.0		
162	6101.65	0.09	1.94	0.06	23.8		
163	6108.62	0.10	4.71	0.10	22.4		
164	6118.61	0.09	3.48	0.08	23.7	SiIV(1393)	3.3900
165	6123.85	0.11	0.41	0.03	37.2		
166	6127.68	0.09	2.04	0.05	27.9		
167	6131.09	0.11	0.58	0.04	35.2		
168	6139.07	0.12	0.31	0.03	40.3		
169	6142.64	0.11	0.34	0.03	41.2		
170	6147.83	0.09	1.32	0.04	34.9		
171	6152.67	0.09	3.60	0.09	17.2		
172	6156.15	0.08	1.39	0.04	27.3		
173	6158.82	0.08	1.59	0.05	24.4	SiIV(1402)	3.3905
174	6161.96	0.08	2.16	0.05	26.4		
175	6168.44	0.09	1.33	0.04	41.9		
176	6175.50	0.09	0.76	0.03	44.5		
177	6179.23	0.09	0.56	0.03	45.3		
178	6181.82	0.09	0.61	0.03	44.1		
179	6186.51	0.08	2.95	0.05	31.5		
180	6190.46	0.08	1.50	0.04	38.4		
181	6196.05	0.09	1.10	0.03	43.4		
182	6200.99	0.08	2.11	0.04	40.3		
183	6210.30	0.11	0.82	0.03	52.1		
184	6218.49	0.08	1.44	0.03	42.6		
185	6221.10	0.09	0.48	0.03	48.1		
186	6231.54	0.09	1.38	0.04	39.9		
187	6238.76	0.09	7.21	0.11	20.8	HI(1215)	4.1305
188	6442.98	0.16	0.73	0.06	31.2		
189	6702.62	0.15	1.51	0.10	19.9	SiII(1526)	3.3902
190	6732.12	0.25	0.50	0.07	24.5		
191	6796.25	0.12	4.26	0.13	18.1	CIV(1548)	3.3898
192	6807.24	0.12	3.61	0.12	19.0	CIV(1550)	3.3896
193	6823.62	0.21	0.81	0.08	25.0		
194	7022.88	0.20	0.71	0.10	17.2	CIV(1548)	3.5362
195	7034.97	0.25	0.61	0.10	18.3	CIV(1550)	3.5264
196	7061.03	0.18	0.81	0.10	17.3	FeII(1608)	3.3899
197	7155.13	0.21	0.50	0.07	23.5	SiIV(1393)?	4.1337
198	7176.81	0.17	0.45	0.07	22.4		
199	7835.66	0.25	2.02	0.22	10.5	SiII(1526)	4.1324
200	7945.98	0.21	5.32	0.41	5.8	CIV(1548)	4.1324
201	7959.14	0.24	4.59	0.35	7.7	CIV(1550)	4.1324

TABLE 2 –*Continued*

No.	λ_{obs}	$\sigma(\lambda)$	W_{obs}	$\sigma(W)$	S/N	ID	z_{abs}
				Q0041−266			
1	5056.54	0.15	0.51	0.08	14.1	CIV(1548)	2.2661
2	5064.17	0.15	0.41	0.07	14.8	CIV(1550)	2.2656
3	5077.05	0.11	0.37	0.06	14.0		
4	5169.94	0.15	0.78	0.08	15.4	CIV(1548)	2.3393
5	5178.25	0.15	0.52	0.08	14.9	CIV(1550)	2.3391
6	5209.16	0.14	1.24	0.12	10.7	MgII(2796)	0.8628
7	5221.38	0.14	0.71	0.11	10.0	MgII(2803)	0.8624
8	5456.48	0.12	0.37	0.06	15.2	AlII(1670)	2.2658
9	5525.74	0.12	0.43	0.06	17.0	CIV(1548)?	2.5691
10	5527.58	0.13	0.42	0.06	16.8	CIV(1548)?	2.5703
11	5711.18	0.15	0.28	0.05	21.3	SiII(1526)	2.7408
12	5792.28	0.12	0.99	0.07	18.4	CIV(1548)	2.7413
13	5795.19	0.12	0.42	0.05	20.0	CIV(1548)	2.7432
14	5801.85	0.12	0.53	0.06	20.1	CIV(1550)	2.7413
15	5817.57	0.17	0.57	0.07	20.9	CIV(1548)	2.7576
16	5827.18	0.14	0.32	0.05	21.1	CIV(1550)	2.7576
17	6553.12	0.15	0.45	0.08	16.2		
				Q0042−264			
1	5120.06	0.12	1.89	0.14	9.0		
2	5123.20	0.12	1.95	0.17	7.3		
3	5134.14	0.12	3.26	0.16	10.6		
4	5151.12	0.12	5.14	0.18	10.8	HI(1215)	3.2373
5	5159.80	0.15	0.60	0.07	19.6		
6	5169.95	0.12	1.41	0.08	18.3		
7	5175.19	0.09	0.79	0.06	16.1		
8	5177.77	0.10	1.61	0.08	15.9	SiIII(1206)	3.2915
9	5217.60	0.10	2.91	0.09	17.7	HI(1215)	3.2920
10	5239.30	0.15	0.58	0.05	27.6		
11	5326.65	0.14	0.40	0.05	22.5		
12	5381.07	0.12	0.84	0.07	18.0	CIV(1548)	2.4757
13	5390.47	0.12	0.56	0.06	18.1	CIV(1550)	2.4760
14	5619.23	0.17	0.68	0.08	17.3	AlIII(1854)	2.0297
15	5644.03	0.17	0.47	0.08	16.5	ALIII(1862)	2.0299
16	5774.85	0.15	1.08	0.11	13.6		
17	5793.10	0.23	0.40	0.08	17.8		
18	6353.19	0.18	1.05	0.13	12.7		
19	6419.54	0.18	0.52	0.08	18.3	CIV(1548)	3.1464
20	6430.92	0.26	0.48	0.09	18.7	CIV(1550)	3.1469
21	6493.50	0.17	0.44	0.07	18.5		
22	6560.02	0.14	0.54	0.08	15.4	CIV(1548)	3.2372
23	6571.72	0.16	0.43	0.08	15.8	CIV(1550)	3.2377
24	6645.48	0.15	0.24	0.05	22.7	CIV(1548)	3.2924
25	6655.35	0.11	0.26	0.04	21.8	CIV(1550)	3.2916
26	6729.63	0.15	0.29	0.06	19.3		
27	6732.34	0.16	0.55	0.08	18.0		
28	6735.57	0.17	0.35	0.07	18.8		
29	6840.90	0.20	1.07	0.12	14.9		
30	6863.59	0.21	0.49	0.09	14.9		

TABLE 2 -*Continued*

No.	λ_{obs}	$\sigma(\lambda)$	W_{obs}	$\sigma(W)$	S/N	ID	z_{abs}
				Q0055−269			
1	5289.64	0.12	7.04	0.25	7.9		
2	5298.34	0.10	1.33	0.09	14.6		
3	5313.69	0.12	0.85	0.08	14.7		
4	5317.90	0.11	2.27	0.14	9.4		
5	5323.67	0.12	3.02	0.21	6.8		
6	5327.04	0.10	1.30	0.10	10.8		
7	5344.71	0.10	0.94	0.08	12.3		
8	5348.22	0.10	1.33	0.10	12.2		
9	5358.22	0.10	1.53	0.10	12.9		
10	5363.25	0.11	1.98	0.11	12.4		
11	5368.61	0.12	3.82	0.20	8.2		
12	5376.45	0.11	4.31	0.18	9.8		
13	5382.28	0.11	1.56	0.10	13.9		
14	5393.62	0.12	4.99	0.20	9.4		
15	5400.70	0.10	2.94	0.10	15.0		
16	5418.29	0.11	1.20	0.10	12.5		
17	5434.97	0.11	1.07	0.09	13.5		
18	5446.01	0.13	7.08	0.21	11.5		
19	5456.73	0.12	0.76	0.07	16.4	OI(1302)?	3.1905
20	5462.78	0.12	2.30	0.12	14.3	OI(1302)?	3.1951
21	5471.19	0.12	2.57	0.13	12.7	SiII(1304)?	3.1945
22	5475.42	0.11	1.13	0.08	14.4		
23	5482.81	0.11	2.33	0.12	12.4		
24	5486.72	0.10	1.17	0.09	12.3		
25	5491.44	0.11	1.50	0.10	14.1		
26	5504.39	0.13	5.87	0.19	11.1		
27	5515.56	0.11	2.19	0.10	17.8		
28	5524.96	0.11	1.04	0.07	21.2		
29	5528.32	0.12	0.56	0.05	23.7		
30	5533.71	0.10	2.15	0.08	18.5		
31	5537.23	0.10	2.34	0.18	6.2		
32	5540.36	0.09	2.89	0.12	11.6		
33	5549.95	0.09	1.97	0.07	18.9	SiIII(1206)	3.6000
34	5557.73	0.09	2.27	0.08	17.6		
35	5563.66	0.09	4.91	0.11	16.1		
36	5569.43	0.09	2.82	0.08	17.5		
37	5574.62	0.10	1.69	0.06	25.4		
38	5581.97	0.09	2.51	0.07	23.4		
39	5594.85	0.09	5.41	0.11	17.7	CII(1334)	3.1924
						+HI(1215)	3.6023
40	5600.79	0.09	1.08	0.04	31.3		
41	5605.35	0.09	3.63	0.07	25.4		
42	5615.58	0.11	0.28	0.03	44.3		
43	5627.44	0.10	0.36	0.02	46.6		
44	5631.64	0.11	0.27	0.02	48.8		
45	5636.64	0.10	0.34	0.02	48.6		
46	5639.43	0.09	0.86	0.03	44.1		
47	5646.47	0.12	0.25	0.02	51.8		
48	5652.60	0.11	0.24	0.02	53.2		
49	5657.88	0.09	1.82	0.04	43.4		
50	5842.06	0.13	0.42	0.05	24.9	SiIV(1393)	3.1916

TABLE 2 –*Continued*

No.	λ_{obs}	$\sigma(\lambda)$	W_{obs}	$\sigma(W)$	S/N	ID	z_{abs}
51	5879.15	0.21	0.29	0.06	23.2	SiIV(1402)	3.1911
52	6037.44	0.16	0.36	0.07	16.2	FeII(2382)	1.5338
53	6114.41	0.14	0.39	0.06	18.8	CIV(1548)	2.9494
54	6117.51	0.13	0.95	0.08	17.7	CIV(1548)	2.9514
55	6124.81	0.15	0.26	0.05	19.4	CIV(1550)	2.9495
56	6127.18	0.15	0.56	0.07	19.0	CIV(1550)	2.9511
57	6484.76	0.12	0.86	0.07	20.7	CIV(1548)?	3.1886
58	6488.60	0.10	2.35	0.11	15.4	CIV(1548)	3.1911
59	6493.51	0.13	0.83	0.07	21.3	CIV(1548)	3.1942
60	6498.78	0.12	1.47	0.09	18.1	CIV(1550)	3.1907
61	6502.03	0.11	0.63	0.06	20.2	CIV(1550)?	3.1928
62	6504.67	0.12	0.49	0.06	21.4	CIV(1550)	3.1945
63	6553.17	0.16	0.60	0.09	15.5	FeII(2586)	1.5335
64	6587.65	0.15	0.43	0.09	12.9	FeII(2600)	1.5335
65	6869.66	0.18	0.84	0.11	15.4		
66	6943.67	0.14	0.72	0.09	13.6		
67	6947.21	0.18	0.68	0.11	12.5		
68	7084.48	0.16	0.82	0.11	13.0	MgII(2796)	1.5335
69	7103.25	0.15	0.79	0.10	14.2	MgII(2803)	1.5337
70	7123.68	0.15	1.56	0.12	15.7	CIV(1548)	3.6013
71	7135.73	0.16	0.81	0.08	20.5	CIV(1550)	3.6014
72	7140.32	0.15	0.54	0.07	21.4	SiII(1526)?	3.6769
73	7240.17	0.17	0.58	0.09	17.2	CIV(1548)?	3.6765
74	7251.92	0.22	0.61	0.09	19.4	CIV(1550)?	3.6763
				Q0256+000			
1	5201.28	0.12	2.46	0.20	6.0		
2	5204.78	0.16	3.27	0.39	3.4	FeII(2367)	1.1983
3	5211.46	0.12	1.68	0.11	12.7		
4	5217.45	0.10	1.06	0.09	11.4		
5	5219.99	0.11	1.30	0.10	11.8	FeII(2374)	1.1984
6	5227.68	0.12	1.14	0.10	12.9		
7	5236.63	0.10	2.13	0.12	11.1	FeII(2382)	1.1977
8	5243.51	0.11	1.11	0.07	19.4		
9	5256.97	0.11	3.25	0.09	21.3		
10	5264.54	0.12	0.28	0.03	31.5		
11	5268.85	0.11	0.57	0.04	32.8		
12	5282.94	0.09	1.80	0.05	34.0		
13	5287.98	0.10	1.50	0.05	36.6		
14	5521.18	0.20	0.48	0.07	19.3		
15	5662.98	0.16	0.50	0.07	17.1		
16	6147.11	0.11	2.18	0.10	17.6	MgII(2796)	1.1983
17	6163.00	0.13	1.78	0.10	19.1	MgII(2803)	1.1983
18	6334.70	0.19	0.55	0.09	15.7	CIV(1548)?	3.0916
19	6339.90	0.19	0.54	0.09	15.9	CIV(1548)?	3.0950
20	6346.18	0.18	0.50	0.09	14.7	CIV(1550)?	3.0923
21	6348.87	0.14	0.54	0.08	14.2	CIV(1550)?	3.0940
22	6498.88	0.16	0.46	0.07	19.7		
23	6552.30	0.18	0.58	0.09	16.7		
24	6978.24	0.23	0.80	0.13	12.5		
25	7093.42	0.14	1.22	0.12	13.0		

TABLE 2 –*Continued*

No.	λ_{obs}	$\sigma(\lambda)$	W_{obs}	$\sigma(W)$	S/N	ID	z_{abs}
				Q0347−383			
1	5047.19	0.11	2.00	0.13	10.2		
2	5067.04	0.10	2.69	0.11	13.3		
3	5072.63	0.10	2.89	0.11	13.5	SiII(1260)	3.0248
4	5090.93	0.11	0.59	0.05	23.4	SiIV(1393)	2.6524
5	5096.20	0.11	0.37	0.04	26.9		
6	5098.11	0.10	0.35	0.04	27.0		
7	5102.91	0.10	2.20	0.07	23.1		
8	5108.97	0.13	0.31	0.04	30.6		
9	5114.70	0.10	1.19	0.05	28.0		
10	5122.18	0.09	1.43	0.05	26.8	SiIV(1402)	2.6515
11	5129.50	0.10	0.59	0.04	32.5		
12	5174.88	0.15	0.19	0.03	31.3		
13	5240.93	0.11	1.40	0.07	19.4	CIV(1548)	2.3852
14	5249.87	0.11	0.91	0.06	20.5	CIV(1550)	2.3853
15	5310.48	0.11	1.10	0.07	19.6	SiIV(1393)	2.8102
16	5345.23	0.14	0.77	0.07	21.1	SiIV(1402)	2.8105
17	5370.72	0.12	3.24	0.11	17.1	CII(1334)	3.0244
18	5376.86	0.15	0.48	0.06	21.7		
19	5456.15	0.14	0.45	0.07	16.7		
20	5527.72	0.13	0.66	0.07	19.9	CIV(1548)	2.5704
21	5537.70	0.18	0.46	0.06	22.1	CIV(1550)	2.5709
22	5609.95	0.12	1.33	0.08	20.5	SiIV(1393)	3.0251
23	5646.97	0.12	0.99	0.07	19.7	SiIV(1402)	3.0256
24	5651.31	0.10	1.26	0.08	17.3	CIV(1548)	2.6504
25	5654.61	0.11	0.92	0.07	18.4	CIV(1548)	2.6524
26	5662.41	0.12	0.89	0.07	18.2	CIV(1550)	2.6513
27	5758.39	0.14	0.42	0.06	19.3	FeII(2344)	1.4564
28	5760.49	0.10	0.55	0.06	16.6	FeII(2344)	1.4573
29	5762.53	0.10	0.70	0.07	16.3	FeII(2344)	1.4582
30	5836.76	0.10	0.42	0.04	24.5	FeII(2374)	1.4581
31	5853.68	0.10	1.63	0.07	22.8	FeII(2382)	1.4567
32	5856.98	0.10	1.21	0.06	23.6	FeII(2382)	1.4581
33	5899.16	0.10	0.77	0.06	19.7	CIV(1548)	2.8103
34	5908.73	0.11	0.95	0.06	22.9	CIV(1550)	2.8102
35	5959.25	0.16	0.81	0.08	20.2	CIV(1548)	2.8491
36	5967.66	0.19	0.45	0.07	21.2	CIV(1550)	2.8482
37	6019.27	0.18	0.59	0.07	20.2	FeII(2382)	1.5262
38	6144.70	0.10	1.68	0.09	16.9	SiII(1526)	3.0248
39	6231.70	0.18	1.28	0.11	17.8	CIV(1548)	3.0251
40	6242.46	0.24	0.67	0.09	18.8	CIV(1550)	3.0254
41	6317.39	0.19	0.74	0.09	16.9		
42	6354.16	0.15	0.81	0.08	18.4	FeII(2586)	1.4565
43	6357.69	0.15	0.61	0.07	18.9	FeII(2586)	1.4579
44	6387.83	0.10	1.41	0.08	19.4	FeII(2600)	1.4567
45	6391.42	0.10	1.11	0.07	20.7	FeII(2600)	1.4581
46	6430.46	0.18	0.26	0.05	28.4	AlII(1670)	2.8488
47	6473.84	0.12	0.81	0.05	29.5	FeII(1608)	3.0249
48	6504.66	0.15	0.32	0.04	31.9		
49	6568.28	0.20	0.45	0.07	23.5	FeII(2600)	1.5261
50	6725.30	0.14	2.00	0.11	18.5	AlII(1670)	3.0252
51	6871.46	0.12	4.46	0.16	14.4	MgII(2796)	1.4573

TABLE 2 -*Continued*

No.	λ_{obs}	$\sigma(\lambda)$	W_{obs}	$\sigma(W)$	S/N	ID	z_{abs}
52	6888.22	0.14	3.12	0.17	11.5	MgII(2803)	1.4570
53	7064.31	0.14	1.33	0.13	12.1	MgII(2796)	1.5263
54	7082.63	0.15	1.51	0.13	12.4	MgII(2803)	1.5263
55	7140.14	0.18	0.51	0.08	18.4	AlIII(1854)	2.8497
56	7171.59	0.21	0.98	0.11	16.7	AlIII(1862)	2.8499
				Q0428−136			
1	5064.25	0.16	3.37	0.21	8.4		
2	5077.13	0.11	1.13	0.10	10.9		
3	5086.83	0.14	4.72	0.20	10.1		
4	5104.79	0.11	3.59	0.13	13.5	MgI(2026)	1.5190
5	5115.42	0.15	0.63	0.06	20.9		
6	5126.43	0.10	2.64	0.09	17.5		
7	5131.34	0.11	0.40	0.04	24.6		
8	5133.83	0.15	0.29	0.04	26.4		
9	5208.33	0.11	1.25	0.08	17.3	CIV(1548)	2.3641
10	5211.92	0.10	1.82	0.10	14.1	CIV(1548)	2.3664
11	5216.29	0.11	1.83	0.10	13.1	CIV(1550)	2.3637
12	5220.16	0.12	1.06	0.08	16.1	CIV(1550)	2.3662
13	5495.43	0.15	1.04	0.12	11.8	CIV(1548)	2.5496
14	5504.71	0.18	0.66	0.10	13.0	CIV(1550)	2.5497
15	5904.95	0.11	2.01	0.12	11.2	FeII(2344)	1.5189
16	5907.74	0.11	1.38	0.10	13.7	FeII(2344)	1.5201
17	5980.98	0.13	0.42	0.08	12.6	FeII(2374)	1.5189
18	5983.68	0.14	0.71	0.09	13.2	FeII(2374)	1.5200
19	6001.53	0.12	1.82	0.19	6.6	FeII(2382)	1.5187
20	6004.72	0.13	1.67	0.14	10.1	FeII(2382)	1.5201
21	6515.40	0.10	1.77	0.09	16.7	FeII(2586)	1.5189
22	6518.58	0.10	1.75	0.09	15.6	FeII(2586)	1.5201
23	6549.16	0.10	2.77	0.15	9.4	FeII(2600)	1.5187
24	6552.57	0.10	2.75	0.14	11.3	FeII(2600)	1.5201
25	7023.63	0.23	0.94	0.17	9.0	MgII(2796)	1.5192
26	7044.59	0.20	5.69	0.42	5.4	MgII(2803)	1.5194
27	7063.22	0.21	5.18	0.34	7.0		
28	7110.23	0.32	1.10	0.17	12.2		
29	7173.11	0.19	1.51	0.17	10.7		
30	7188.59	0.18	1.22	0.16	9.8	MgI(2852)	1.5197
				Q1208+101			
1	5350.31	0.11	0.83	0.06	27.6		
2	5357.79	0.08	3.85	0.12	19.6		
3	5362.93	0.07	3.44	0.11	18.2		
4	5368.51	0.10	1.36	0.07	28.7		
5	5374.76	0.23	0.45	0.06	33.1		
6	5383.23	0.09	3.59	0.10	24.1		
7	5391.75	0.08	4.96	0.14	16.0		
8	5397.62	0.08	2.64	0.09	24.7		
9	5405.42	0.07	2.65	0.09	23.4		
10	5408.87	0.07	1.26	0.06	26.4		
11	5415.54	0.08	1.31	0.06	27.7		
12	5423.31	0.09	7.61	0.16	17.7		

TABLE 2 -*Continued*

No.	λ_{obs}	$\sigma(\lambda)$	W_{obs}	$\sigma(W)$	S/N	ID	z_{abs}
13	5434.79	0.07	2.74	0.09	21.0		
14	5440.19	0.09	5.54	0.18	12.5		
15	5448.13	0.07	4.01	0.12	18.5		
16	5453.23	0.07	1.81	0.07	21.8		
17	5457.54	0.07	2.44	0.09	22.1		
18	5464.42	0.09	2.45	0.13	15.1		
19	5469.94	0.08	5.72	0.16	15.4		
20	5477.50	0.07	2.33	0.08	23.0		
21	5481.87	0.07	2.08	0.08	22.6		
22	5487.15	0.08	2.67	0.09	23.1		
23	5492.52	0.07	2.18	0.08	22.0		
24	5496.43	0.07	2.79	0.09	21.9		
25	5504.74	0.08	1.92	0.07	27.8		
26	5510.48	0.07	3.30	0.11	17.7		
27	5516.87	0.10	6.70	0.26	9.5		
28	5525.56	0.10	7.66	0.24	10.9		
29	5533.55	0.08	2.29	0.08	26.9		
30	5540.02	0.09	1.32	0.06	31.0		
31	5546.52	0.08	5.89	0.16	15.7		
32	5552.73	0.07	2.14	0.07	27.1		
33	5560.91	0.10	1.39	0.07	33.7		
34	5570.97	0.08	6.21	0.14	20.4		
35	5578.97	0.12	3.42	0.21	10.2		
36	5587.88	0.07	1.47	0.06	30.0		
37	5592.40	0.08	1.90	0.07	31.8		
38	5608.03	0.08	4.39	0.10	28.7		
39	5630.41	0.09	11.61	0.16	23.7		
40	5647.39	0.08	1.52	0.06	36.0		
41	5656.33	0.07	4.77	0.10	26.6		
42	5665.34	0.07	2.13	0.06	31.2		
43	5671.63	0.07	4.00	0.09	25.4		
44	5679.44	0.07	4.36	0.10	25.7		
45	5689.67	0.09	4.67	0.11	24.2		
46	5698.81	0.08	2.29	0.07	33.6		
47	5709.61	0.13	0.59	0.05	43.2		
48	5716.60	0.08	2.79	0.07	37.7		
49	5726.61	0.08	2.51	0.06	37.4		
50	5741.18	0.07	5.15	0.09	29.4		
51	5748.05	0.07	0.91	0.04	43.2		
52	5755.01	0.07	1.91	0.05	40.3		
53	5763.12	0.07	2.94	0.06	36.0		
54	5769.27	0.08	0.94	0.05	41.4		
55	5778.51	0.10	0.56	0.04	48.8		
56	5787.19	0.07	5.92	0.09	29.4		
57	5803.03	0.09	2.50	0.05	43.0		
58	5809.99	0.09	1.11	0.04	49.8		
59	5816.96	0.09	1.26	0.04	49.4		
60	5823.15	0.09	1.51	0.04	47.6		
61	5828.58	0.09	1.34	0.04	46.8		
62	5833.23	0.08	1.48	0.04	46.2		
63	5837.09	0.08	1.47	0.04	42.6		
64	5840.96	0.08	2.97	0.05	39.8		
65	5846.40	0.09	0.87	0.03	54.3		

TABLE 2 -*Continued*

No.	λ_{obs}	$\sigma(\lambda)$	W_{obs}	$\sigma(W)$	S/N	ID	z_{abs}
66	5850.30	0.09	0.63	0.03	61.7		
67	5856.53	0.08	1.77	0.04	52.9		
68	5861.20	0.09	1.49	0.03	58.2		
69	5912.25	0.23	0.15	0.03	59.6		
70	5971.69	0.09	1.77	0.04	49.6	CIV(1548)	2.8572
71	5977.26	0.10	0.56	0.03	57.6	CIV(1548)	2.8608
						+SiII(1526)	2.9151
72	5982.03	0.09	1.84	0.04	44.9	CIV(1550)	2.8574
						+CIV(1548)	2.8639
73	5986.81	0.09	1.41	0.04	51.3	CIV(1550)	2.8605
						+CIV(1548)?	2.8669
74	5992.39	0.09	1.29	0.04	47.1	CIV(1550)	2.8641
75	6059.10	0.11	0.85	0.08	21.5	CIV(1548)	2.9136
76	6062.32	0.12	2.14	0.11	21.1	CIV(1548)	2.9157
77	6069.60	0.13	0.65	0.07	22.8	CIV(1550)	2.9139
78	6072.83	0.15	1.19	0.09	23.5	CIV(1550)	2.9160
79	6179.88	0.26	0.53	0.09	22.4		
80	6186.47	0.29	0.47	0.09	22.5		
81	6489.12	0.23	0.54	0.08	27.3	CIV(1548)?	3.1914
82	6501.25	0.20	0.43	0.06	29.9	CIV(1550)?	3.1923
				Q2000−330			
1	5001.71	0.18	1.16	0.22	5.1	SiII(1193)	3.1916
2	5010.04	0.17	1.94	0.29	4.0		
3	5015.44	0.17	2.35	0.32	3.9		
4	5023.93	0.16	2.10	0.21	6.5		
5	5028.11	0.16	2.22	0.25	5.4		
6	5036.16	0.13	1.71	0.17	7.0		
7	5040.57	0.15	3.84	0.28	5.7		
8	5056.59	0.12	2.20	0.18	7.2	SiIII(1206)	3.1911
9	5084.19	0.24	37.02	0.63	6.9		
10	5111.75	0.11	3.82	0.14	11.9		
11	5121.96	0.10	2.67	0.12	12.8		
12	5131.16	0.11	0.54	0.05	20.5		
13	5133.55	0.10	1.23	0.07	18.0		
14	5142.59	0.12	7.47	0.17	13.4		
15	5150.89	0.10	1.74	0.08	17.7		
16	5157.01	0.10	1.55	0.08	18.9		
17	5160.54	0.10	1.36	0.07	17.2		
18	5166.65	0.11	3.73	0.12	16.1		
19	5173.38	0.10	0.73	0.05	21.1		
20	5179.09	0.10	2.59	0.10	15.3		
21	5182.63	0.09	0.61	0.05	18.1		
22	5184.96	0.09	1.23	0.07	16.6		
23	5187.44	0.10	0.56	0.05	19.3		
24	5211.33	0.12	3.90	0.12	16.9		
25	5228.31	0.10	1.71	0.10	12.1	SiIII(1206)	3.3334
26	5232.35	0.10	1.36	0.08	14.6	SiIII(1206)	3.3368
27	5236.20	0.10	2.70	0.12	11.6		
28	5240.72	0.10	1.62	0.09	14.1		
29	5247.72	0.09	0.81	0.06	17.1		
30	5249.98	0.09	1.16	0.07	15.6		

TABLE 2 -*Continued*

No.	λ_{obs}	$\sigma(\lambda)$	W_{obs}	$\sigma(W)$	S/N	ID	z_{abs}
31	5254.50	0.10	3.29	0.14	10.7		
32	5259.90	0.10	2.92	0.13	11.4	SiII(1260)	3.1731
33	5267.54	0.12	4.94	0.26	6.2	HI(1215)	3.3330
34	5271.52	0.09	1.20	0.10	9.1	HI(1215)	3.3363
35	5273.64	0.09	1.57	0.09	11.7	HI(1215)	3.3381
36	5277.91	0.10	3.35	0.15	9.5	SiII(1260)	3.1874
37	5283.49	0.10	3.82	0.15	10.6	SiII(1260)	3.1919
38	5289.53	0.10	2.48	0.09	16.7		
39	5296.57	0.09	1.98	0.08	17.6		
40	5305.91	0.09	0.64	0.04	21.2		
41	5307.66	0.09	0.67	0.04	21.0		
42	5310.73	0.10	2.72	0.09	19.3		
43	5329.76	0.12	0.69	0.05	25.5		
44	5338.09	0.10	5.25	0.12	16.2		
45	5345.14	0.10	2.70	0.08	20.4		
46	5357.27	0.09	2.13	0.07	20.6		
47	5362.92	0.10	1.90	0.07	24.5		
48	5371.42	0.10	1.18	0.06	25.5		
49	5381.26	0.12	1.09	0.06	27.6		
50	5389.55	0.10	5.45	0.13	14.7		
51	5395.76	0.09	2.40	0.08	17.6		
52	5405.82	0.10	7.29	0.16	13.4		
53	5411.74	0.10	0.76	0.05	23.6		
54	5418.44	0.11	3.26	0.10	19.6	SiII(1190)	3.5517
55	5426.33	0.10	3.13	0.11	15.2		
56	5431.28	0.10	2.60	0.10	15.5	SiII(1193)	3.5515
57	5462.12	0.11	0.69	0.06	21.5	SiII(1260)	3.3336
						+SiII(1304)	3.1876
58	5466.98	0.13	0.78	0.06	12.6	SiII(1304)	3.1913
						+SiII(1260)	3.3374
59	5472.50	0.11	0.72	0.06	21.4		
60	5476.63	0.10	2.99	0.16	8.5		
61	5479.35	0.11	1.47	0.22	4.1		
62	5482.69	0.10	3.06	0.15	9.7		
63	5490.15	0.10	1.98	0.12	10.5	SiIII(1206)	3.5504
64	5493.05	0.09	1.52	0.08	15.6	SiIII(1206)	3.5528
65	5498.78	0.10	0.97	0.06	20.0	SiIII(1206)	3.5576
66	5502.04	0.11	0.90	0.06	21.5		
67	5506.37	0.10	1.34	0.07	17.9		
68	5511.27	0.10	3.14	0.11	15.6		
69	5517.38	0.10	1.46	0.07	20.4		
70	5524.56	0.10	2.11	0.10	12.5		
71	5533.91	0.17	8.53	0.49	4.1	HI(1215)	3.5521
72	5540.47	0.10	3.00	0.13	10.3	HI(1215)	3.5575
73	5545.93	0.10	3.78	0.15	10.4	MgI(1827)?	2.0340
74	5550.54	0.09	2.52	0.09	16.9		
75	5555.34	0.10	0.33	0.04	26.2		
76	5559.18	0.10	2.36	0.08	20.3		
77	5565.00	0.12	0.62	0.05	27.0		
78	5569.24	0.10	0.83	0.05	26.0	CII(1334)	3.1732

TABLE 2 -*Continued*

No.	λ_{obs}	$\sigma(\lambda)$	W_{obs}	$\sigma(W)$	S/N	ID	z_{abs}
79	5572.33	0.09	1.56	0.07	16.8		
80	5575.70	0.09	1.69	0.08	13.7		
81	5584.99	0.09	2.55	0.08	17.5		
82	5588.87	0.09	1.71	0.07	17.9	CII(1334)	3.1879
83	5593.74	0.09	2.07	0.07	17.6	CII(1334)	3.1915
84	5596.99	0.09	0.76	0.04	26.1		
85	5600.66	0.09	2.29	0.07	20.2		
86	5605.28	0.09	0.95	0.05	25.1		
87	5608.62	0.09	3.27	0.13	10.6		
88	5612.97	0.09	3.77	0.09	19.6		
89	5625.31	0.09	1.68	0.06	25.4	AlIII(1854)	2.0330
90	5629.05	0.09	1.63	0.06	20.9		
91	5632.27	0.09	1.13	0.05	25.8		
92	5637.09	0.09	3.09	0.08	18.5		
93	5640.52	0.09	0.64	0.04	25.6		
94	5661.59	0.09	0.84	0.04	26.1		
95	5667.82	0.10	3.57	0.10	18.4		
96	5681.94	0.09	2.52	0.08	21.4		
97	5686.27	0.09	1.90	0.08	16.3		
98	5690.47	0.10	4.14	0.14	11.4		
99	5697.46	0.10	0.95	0.05	28.5		
100	5701.24	0.09	0.93	0.04	26.5		
101	5703.83	0.09	1.10	0.05	24.0		
102	5707.94	0.09	1.36	0.05	26.7		
103	5714.14	0.09	0.47	0.03	30.5		
104	5719.23	0.09	2.22	0.07	20.7		
105	5724.35	0.10	1.72	0.06	27.9		
106	5729.53	0.09	1.75	0.06	24.4		
107	5733.93	0.09	2.04	0.06	24.6	SiII(1260)	3.5492
108	5738.71	0.09	2.45	0.07	24.1	SiII(1260)	3.5530
109	5743.71	0.11	0.51	0.04	35.0	SiII(1260)	3.5570
110	5750.21	0.10	0.53	0.03	35.8		
111	5753.45	0.09	0.61	0.03	34.7	FeII(2344)	1.4543
112	5756.64	0.09	2.04	0.05	30.2		
113	5760.77	0.09	0.59	0.03	40.0		
114	5767.59	0.10	0.85	0.03	46.1		
115	5775.71	0.14	0.30	0.03	52.7		
116	5783.26	0.09	1.43	0.03	47.6	CII(1334)	3.3335
117	5786.44	0.08	1.37	0.03	46.9	CII(1334)	3.3359
118	5792.55	0.11	0.55	0.03	63.6		
119	5802.31	0.12	0.40	0.02	76.0		
120	5808.39	0.14	0.13	0.02	80.5	FeII(2367)	1.4533
121	5814.74	0.09	0.64	0.02	75.1	SiIV(1393)	3.1720
122	5842.46	0.10	0.57	0.03	55.9	SiIV(1393)	3.1919
123	5853.50	0.17	0.19	0.03	54.9	SiIV(1402)	3.1728
124	5879.97	0.12	0.28	0.03	48.1	SiIV(1402)	3.1917
125	5925.00	0.16	0.16	0.03	45.6	OI(1302)	3.5501
126	5952.28	0.19	0.25	0.04	38.4		
127	6039.62	0.11	0.94	0.05	31.1	SiIV(1393)	3.3333
128	6072.30	0.12	0.50	0.04	32.1	SiII(1526)	2.9774
						+CII(1334)	3.5501

TABLE 2 –*Continued*

No.	λ_{obs}	$\sigma(\lambda)$	W_{obs}	$\sigma(W)$	S/N	ID	z_{abs}
129	6075.54	0.10	0.55	0.04	31.7	CII(1334)	3.5526
130	6078.74	0.10	0.52	0.04	32.3	SiIV(1402)	3.3334
						+CII(1334)	3.5550
131	6085.98	0.12	0.48	0.04	34.1		
132	6088.40	0.14	0.15	0.03	35.8		
133	6102.04	0.17	0.21	0.03	36.0		
134	6158.95	0.12	1.16	0.06	31.7	CIV(1548)	2.9781
135	6168.85	0.12	0.84	0.05	33.6	CIV(1550)	2.9779
136	6334.65	0.18	0.38	0.05	30.7		
137	6338.92	0.11	0.88	0.05	27.6	SiIV(1393)	3.5481
138	6342.40	0.10	0.89	0.05	25.1	SiIV(1393)	3.5506
139	6345.23	0.09	0.81	0.05	23.3	SiIV(1393)	3.5526
140	6348.38	0.12	0.71	0.06	25.1	SiIV(1393)	3.5549
141	6351.75	0.10	0.56	0.05	25.8	SiIV(1393)	3.5577
142	6354.22	0.11	0.46	0.04	27.4		
143	6356.52	0.13	0.24	0.04	27.9		
144	6370.22	0.15	0.39	0.04	31.3	SiII(1526)	3.1725
145	6379.66	0.11	0.27	0.03	31.8	FeII(2600)	1.4536
						+SiIV(1402)	3.5479
146	6382.78	0.12	0.40	0.04	32.4	SiIV(1402)	3.5501
147	6385.87	0.10	0.66	0.04	30.1	SiIV(1402)	3.5523
148	6393.43	0.12	0.64	0.05	32.5	SiII(1526)	3.1877
						+SiIV(1402)	3.5577
149	6399.49	0.11	0.92	0.05	32.0	FeII(1608)	2.9787
						+SiII(1526)	3.1917
150	6460.38	0.12	0.32	0.04	34.0	CIV(1548)	3.1728
151	6470.56	0.18	0.29	0.04	34.1	CIV(1550)	3.1725
152	6489.25	0.15	1.27	0.07	31.6	CIV(1548)	3.1915
153	6499.69	0.20	0.66	0.06	31.7	CIV(1550)	3.1913
154	6709.01	0.12	0.99	0.06	27.2	CIV(1548)	3.3334
155	6715.27	0.16	0.41	0.05	30.1	CIV(1548)	3.3375
156	6720.22	0.17	0.36	0.05	31.3	CIV(1550)	3.3335
157	6726.30	0.15	0.18	0.04	31.8	CIV(1550)	3.3374
158	6735.46	0.23	0.30	0.05	32.6	FeII(1608)	3.1875
159	6862.45	0.16	0.46	0.05	28.5	MgII(2796)	1.4541
160	6880.84	0.19	0.28	0.05	29.4	MgII(2803)	1.4543
161	6974.55	0.16	0.34	0.06	23.5	FeII(1608)	3.3362
162	6996.44	0.17	0.53	0.07	23.3	AlII(1670)	3.1875
163	7002.86	0.13	0.85	0.08	20.4	MgI(2852)	1.4546
						+AlII(1670)	3.1914
164	7041.08	0.13	0.81	0.07	21.5	CIV(1548)	3.5479
165	7044.71	0.11	1.16	0.09	16.3	CIV(1548)	3.5503
166	7047.82	0.11	0.81	0.08	16.7	CIV(1548)	3.5523
167	7052.73	0.13	0.98	0.08	18.6	CIV(1550)	3.5479
						+CIV(1548)	3.5554
168	7056.09	0.11	0.79	0.07	18.8	CIV(1550)	3.5550
						+CIV(1548)	3.5576
169	7059.40	0.15	0.56	0.07	21.5	CIV(1550)	3.5522
170	7067.47	0.22	0.33	0.07	21.9	CIV(1550)	3.5574

TABLE 2 -*Continued*

No.	λ_{obs}	$\sigma(\lambda)$	W_{obs}	$\sigma(W)$	S/N	ID	z_{abs}
171	7110.00	0.16	1.33	0.09	23.0	FeII(2344)	2.0330
172	7201.51	0.15	0.35	0.05	25.9	FeII(2374)	2.0329
173	7226.57	0.12	1.33	0.08	23.2	FeII(2382)	2.0329
174	7238.76	0.24	0.35	0.07	24.2	AlII(1670)	3.3325
				Q2204−408			
1	5025.77	0.10	1.21	0.11	8.2		
2	5027.72	0.10	1.17	0.11	9.7		
3	5045.31	0.16	0.27	0.05	20.6		
4	5055.59	0.10	3.13	0.10	16.1	HI(1215)	3.1587
5	5059.71	0.09	1.22	0.05	24.2		
6	5070.63	0.09	1.77	0.05	27.5		
7	5075.85	0.09	2.45	0.06	26.4		
8	5220.19	0.12	1.57	0.10	14.4	AlIII(1854)	1.8145
9	5242.90	0.12	0.75	0.08	14.4	AlIII(1862)	1.8145
						+SiII(1260)	3.1597
10	5367.64	0.19	0.49	0.08	15.4	SiIV(1393)	2.8512
11	5402.44	0.15	0.43	0.07	15.8	SiIV(1402)	2.8513
12	5616.94	0.11	0.93	0.08	14.3	CIV(1548)	2.6280
13	5619.29	0.14	0.51	0.07	16.9	CIV(1548)	2.6296
14	5626.42	0.14	0.77	0.08	15.8	CIV(1550)	2.6281
15	5887.69	0.13	0.29	0.05	18.1		
16	5941.54	0.13	0.93	0.10	13.0	CIV(1548)	2.8377
17	5950.98	0.19	0.56	0.09	13.9	CIV(1550)	2.8374
18	5960.13	0.14	0.73	0.10	12.1	CIV(1548)	2.8497
19	5962.19	0.13	0.43	0.07	13.4	CIV(1548)	2.8510
20	5967.58	0.17	0.50	0.09	13.9	CIV(1548)	2.8545
21	5970.45	0.12	0.34	0.07	12.7	CIV(1550)	2.8500
22	6257.73	0.15	0.49	0.08	14.1	AlII(1670)	2.8546
23	6437.65	0.12	0.49	0.04	29.5	CIV(1548)	3.1581
24	6440.26	0.12	0.46	0.04	30.2	CIV(1548)	3.1598
25	6447.97	0.16	0.22	0.04	32.0	CIV(1550)	3.1579
26	6450.33	0.13	0.19	0.03	31.9	CIV(1550)	3.1594
27	6633.80	0.20	0.48	0.09	14.9		
				Q2239−386			
1	5414.82	0.13	3.07	0.16	10.7		
2	5430.82	0.10	2.31	0.17	7.1	FeII(1608)	2.3764
3	5434.25	0.11	2.56	0.22	5.4	FeII(1608)	2.3786
4	5437.60	0.11	3.83	0.22	6.1		
5	5444.81	0.11	1.10	0.10	10.7		
6	5448.86	0.13	1.91	0.15	9.7		
7	5456.68	0.16	2.28	0.17	9.8		
8	5461.37	0.20	0.48	0.08	15.7		
9	5475.05	0.12	0.92	0.08	14.4		
10	5481.13	0.14	3.53	0.21	8.5		
11	5487.50	0.12	1.44	0.10	14.8		
12	5491.22	0.14	0.66	0.07	18.4		
13	5517.83	0.13	0.52	0.06	21.1		

TABLE 2 -*Continued*

No.	λ_{obs}	$\sigma(\lambda)$	W_{obs}	$\sigma(W)$	S/N	ID	z_{abs}
14	5574.23	0.12	1.38	0.09	16.3	CIV(1548)	2.6005
15	5584.02	0.16	0.70	0.07	20.0	CIV(1550)	2.6008
16	5641.53	0.11	3.57	0.18	9.3	AlII(1670)	2.3766
17	5645.12	0.12	1.86	0.15	8.6	AlII(1670)	2.3787
18	5684.10	0.19	0.92	0.13	11.1	MgII(2796)	1.0327
19	5699.52	0.15	0.63	0.10	11.8	MgII(2803)	1.0330
20	5711.89	0.13	1.93	0.18	7.4		
21	6105.31	0.18	0.70	0.11	12.3	SiII(1808)?	2.3768
22	6156.56	0.22	0.52	0.10	13.4		
23	6263.66	0.15	1.09	0.13	10.3	AlIII(1854)	2.3771
24	6290.99	0.17	0.74	0.12	10.8	AlIII(1862)	2.3772
25	6386.05	0.18	0.69	0.11	13.3		
26	6398.79	0.19	0.47	0.09	14.6		
27	6944.32	0.14	0.94	0.13	9.7		
28	7040.18	0.17	0.73	0.13	10.4		
29	7087.22	0.31	1.28	0.22	8.4		
30	7101.46	0.24	1.00	0.19	8.3		

TABLE 3

CIV λλ1548, 1550 ABSORPTION LINES

QSO	z_{em}	z_{min}	z_{max}	z_{abs}	$W_0(1548)$	$W_0(1550)$	Note
Q0000−263	4.104	3.03	3.68	3.3897	0.97	0.82	
				3.5363	0.16	0.13	
				4.1324	1.04	0.89	a
Q0041−266	3.045	2.23	...	2.2659	0.16	0.13	
				2.3392	0.23	0.16	
				2.7413	0.26	0.14	
				2.7576	0.15	0.09	
Q0042−264	3.298	2.38	...	2.4758	0.24	0.16	
				3.1466	0.13	0.12	
				3.2374	0.13	0.10	
				3.2921	0.06	0.06	b
Q0055−269	3.653	2.66	...	2.9500	0.31	0.21	c
				3.1910	0.56	0.35	d
				3.1943	0.20	0.10	d
				3.6013	0.34	0.18	
Q0256−000	3.370	2.44	...	3.0919	0.13	0.12	b, d
				3.0945	0.13	0.13	b, d
Q0347−383	3.222	2.32	...	2.3852	0.41	0.27	
				2.5706	0.18	0.13	
				2.6512	0.60	0.24	c, d
				2.8103	0.25	0.25	d
				2.8487	0.21	0.12	
				3.0252	0.32	0.17	
Q0428−136	3.244	2.33	...	2.3639	0.37	0.37	d
				2.3663	0.54	0.31	d
				2.5496	0.30	0.19	
Q1208+101	3.811	2.79	3.72	2.8573	0.46	0.46	d
				2.8606	0.15	0.15	d
				2.8640	0.48	0.33	d
				2.9137	0.22	0.17	d
				2.9158	0.55	0.30	d
Q2000−330	3.777	2.75	3.69	2.9780	0.29	0.21	
				3.1726	0.08	0.07	
				3.1914	0.30	0.16	
				3.3334	0.23	0.09	d
				3.3375	0.09	0.04	d
				3.5479	0.18	0.18	d
				3.5503	0.25	0.25	d
				3.5523	0.18	0.12	d
				3.5552	0.22	0.17	d
				3.5575	0.14	0.07	d
Q2204−408	3.169	2.28	...	2.6280	0.26	0.21	
				2.8375	0.24	0.14	
				2.8500	0.30	0.15	c,d
				2.8545	0.13	0.11	d
				3.1588	0.23	0.10	c
Q2239−386	3.511	2.55	3.39	2.6006	0.38	0.19	

a) Doublet detected in a spectral region in which the S/N is not adequate to detect lines with $W_0 = 0.15$ Å.

b) The reality of the features is somewhat doubtful as there is relatively poor redshift agreement between the two lines of the doublet.

c) The separation of two redshift systems was less than 150 km s^{-1}, so the tabulated equivalent widths represent the sum of the two systems.

d) The equivalent widths are uncertain because the lines are part of a complex or blend.

TABLE 4

THE C IV ABSORPTION SYSTEM SAMPLES

Criteria	Sample	Number	$\langle z_{abs} \rangle$	N^a	$\sigma(N)$	γ^b	$\sigma(\gamma)$
$W_0 > 0.15$, $\beta c > 5000$	ES2	104	2.134	2.44	0.29	−1.26	0.56
$W_0 > 0.30$, $\beta c > 5000$[c]	ES5	79	1.998	1.31	0.16	−1.84	0.68
$\beta c > 5000$[d]	EA2	209	2.167	...	...	...	...

a) Mean number density of absorption systems per unit redshift interval.
b) Maximum likelihood estimation assuming the form $N(z) \propto (1+z)^\gamma$.
c) Includes data from YSB and Foltz *et al.* (1986).
d) Sample used for discussion of the 2-point correlation function. (See text).

REFERENCES

Bahcall, J. N., and Spitzer, L. 1969, *Ap. J. (Letters)*, **156**, L63.

Bajtlik, S., Duncan, R. C., and Ostriker, J. P. 1988, *Ap. J.*, **327**, 570.

Bechtold, J. 1988, in *High Redshift and Primeval Galaxies,* eds. D. Kunth, J. Bergeron, B. Rocca–Volmerange, and J. Tran Thanh Van (Paris: Editions Frontieres), p. 397.

Bechtold, J., Green, R., and York, D. G. 1987, *Ap. J.*, **312**, 50.

Bechtold, J., Weymann, R. J., Lin, Z., and Malkan, M. A. 1987, *Ap. J.*, **315**, 180.

Bechtold, J., Green, R. F., Weymann, R. J., Schmidt, M., Estabrook, F. B., Sherman, R. D., Wahlquist, H. D., and Heckman, T. M. 1984, *Ap. J.*, **281**, 76.

Bergeron, J, 1988, in *Large Scale Structure of the Universe*, eds. J. Audouze and A. S. Szalay (Dordrecht: Reidel), p. 454 .

Blades, J. C. 1987, in *QSO Absorption Lines: Probing the Universe*, proc. Space Telescope Science Institute Syposium No. 2, eds. J. C. Blades, D. Turnshek, and C. A. Norman, p. 147.

Boksenberg, A., and Sargent, W. L. W. 1983, in *Proc. 24th Liege Symposium: Quasars and Gravitational Lenses* (Liege: Institut d'Astrophysique), p. 589.

Dekker, H. 1988, in *Instrumentation for Ground–Based Optical Astronomy*, ed. L. B. Robinson (New York: Springer–Verlag), p. 183.

Eggen, O., Lynden–Bell, D., and Sandage, A. 1962, *Ap. J.*, **136**, 748.

Ferland, G. J. 1988, OSU Astronomy Department Internal Report, 87-001 .

Foltz, C. B., Weymann, R. J., Peterson, B. M., Sun, L., Malkan, M. H., and Chaffee, F. H. 1986, *Ap. J.*, **307**, 504.

Gratton, R. G., and Ortolani, S. 1988, *Astr. Ap. Suppl.*, **73**, 137.

Hazard, C., and McMahon, R. G. 1988, private communication.

Heisler, J., Hogan, C. J., and White, S. D. M. 1989, preprint.

Hewitt, A., and Burbidge, G. 1987, *Ap. J. Suppl.*, **63**, 1.

Hunstead, R. W., Murdoch, H. S., Peterson, B. A., Blades, J. C., Jauncey, D. L., Wright, A. E., Pettini, M., and Savage, A. 1986a, *Ap. J.*, **305**, 496.

Hunstead, R. W., Murdoch, H. S., Pettini, M., and Blades, J. C. 1986b, *Astr. and Space*

Sc.; **118**, 505.

Hunstead, R. W., Pettini, M., Blades, J. C., and Murdoch, H. S. 1987, in *Observational Cosmology*, eds. A. Hewitt *et al.* (Dordrecht: Reidel), p. 799.

Jenkins, E. B. 1986, *Ap. J.*, **304**, 739.

Lanzetta, K. M. 1988, *Ap. J.*, **332**, 96.

Meyer, D. M., and York, D. G. 1987, *Ap. J.(Letters)*, **315**, L5.

Murdoch, H. S., Hunstead, R. W., Pettini, M., and Blades, J. C. 1986, *Ap. J.*, **309**, 19.

Pettini, M., Hunstead, R. W., Murdoch, H. S., and Blades, J. C. 1983, *Ap. J.*, **273**, 463.

Rees, M. J. 1987, in *QSO Absorption Lines: Probing the Universe*, proc. Space Telescope Science Institute Syposium No.2, p. 107.

Robertson, J. G. 1986, *P.A.S.P.*, **98**, 1220.

Salmon, J., and Hogan, C. 1986, *M.N.R.A.S.*, **221**, 93.

Sargent, W. L. W., Young, P. J., Boksenberg, A., and Tytler, D. 1980, *Ap. J. Suppl.*, **42**, 41.

Sargent, W. L. W., Boksenberg, A., and Steidel, C. C. 1988, *Ap. J. Suppl.*, **68**, 539 (SBS).

Sargent, W. L. W., Steidel, C. C., and Boksenberg, A. 1989, *Ap. J. Suppl.*, in press (SSB).

Sargent, W. L. W., Steidel, C. C., and Boksenberg, A. 1988, *Ap. J.*, **334**, 22.

Searle, L., and Zinn, R. 1978, *Ap. J.*, **225**, 357.

Steidel, C. C., Sargent, W. L. W., and Boksenberg, A. 1988, *Ap. J. (Letters)*, **333**, L5 (Paper I).

Steidel, C. C. 1989, in preparation.

Tytler, D. 1982, *Nature*, **298**, 427.

Tytler, D. 1987, *Ap. J.*, **321**, 49.

Veron–Cetty, M.–P., and Veron, P. 1987, in *ESO Scientific Rept.*, No. 5, *A Catalogue of Quasars and Active Nuclei* (3d ed; Munich: ESO).

Webb, J. 1987, in *IAU Symposium 124, Observational Cosmology*, eds. A. Hewitt, G. Burbidge, and L. Z. Fang (Dordrecht: Reidel), p. 803.

Wolfe, A. M., Turnshek, D. A., Smith, H. E., and Cohen, R. D. 1986, *Ap. J. Suppl.*, **61**, 249.

York, D. G. 1987, in *QSO Absorption Lines: Probing the Universe*, proc. Space Telescope Science Institute Syposium No. 2, eds. J. C. Blades, D. Turnshek, and C. A. Norman, p. 227.

York, D. G., Green, R., Bechtold, J., and Chaffee. F. H. 1984, *Ap. J. (Letters)*, **280**, L1.

York, D. G., Dopita, M., Green, R., and Bechtold, J. 1986, *Ap. J.*, **311**, 610.

Young, P. J., Sargent, W. L. W., and Boksenberg, A. 1982, *Ap. J. Suppl.*, **48**, 455.

FIGURE CAPTIONS

FIG 1.—The spectra of the 11 newly observed QSOs. The spectra have 60 km s^{-1} resolution, and are plotted without smoothing. All of the absorption lines that exceed 5σ in equivalent width have been indicated; they are listed in Table 2.

FIG 2.—The histogram showing the number of lines of sight sampled versus C IV absorption redshift. The solid histogram represents the coverage of the original SBS survey, and the dotted histogram represents the improvements in the coverage at high redshift afforded by the new data.

FIG 3.—Plot showing the arbitrarily binned number of C IV absorption systems (in sample ES2) per unit redshift range versus absorption redshift. The error bars are $\pm 1\sigma$. The dotted curve represents the result of a maximum likelihood fit to the unbinned data assuming the form $N(z) \propto (1+z)^{\gamma}$. Here, $\gamma = -1.26 \pm 0.56$.

FIG 4.—Same as Figure 3, except that here sample ES2 has been divided into two subsamples. The heavy crosses represent the binned data for those absorption redshifts in sample ES2 which have $W_0(1548) > 0.40$ Å, and the lighter crosses represent those systems with $0.15 \leq W_0(1548) < 0.40$ Å.

FIG 5.—(a) The two–point correlation function for C IV redshifts in sample EA2. As discussed in the text, velocity scales less than 200 km s^{-1} have been excluded in the determination. The dotted line represents the adopted background level or the mean number of pairs per bin $\langle N_p \rangle$ (excluding velocity scales less than 1000 km s^{-1}). The correlation amplitude for each bin is then $\xi = (N_p/\langle N_p \rangle) - 1$.

(b) Same as for (a), except that only those absorption redshifts in sample EA2 with $z_{abs} < 2.2$ have been used.

(c) Same as for (b), but for $z_{abs} > 2.2$.

FIG 6.—Comparison of the distributions of rest equivalent widths $W_0(1548)$ in sample ES2. The solid histogram represents all those systems with $z_{abs} < 2.2$, and the dotted histogram represents those with $z_{abs} > 2.2$. The distributions are different at the 93% confidence level (see text).

FIG 7.—Theoretical C IV curve of growth for various values of the gas velocity disper-

sion parameter b (in km s^{-1}).

FIG 8.—Curves showing the expected value of the C IV doublet ratio as a function of C IV column density and gas velocity dispersion parameter b.

FIG 9.—Plot showing the mean C IV doublet ratio, $W_0(1548)/W_0(1550)$, versus absorption redshift.

FIG 10.—Plot similar to Figure 4, except that here the light crosses represent those systems with $0.15 \leq W_0(1548) < 0.40$ found in the spectra of the 21 QSOs in the sample for which C IV λ1550 lines with $W_0(1550) = 0.075$ Å could have been detected at the 5σ level. This sample is thus complete, regardless of the C IV doublet ratio. The heavy crosses are the same as in Figure 4.

FIG 11.—Curves showing the predicted column densities of various ions for a model gas cloud versus ionization parameter Γ. The total hydrogen column density is 10^{20} cm^{-2}. The models were calculated by assuming that the chemical abundances are 1/100 solar, and that the cloud is being photoionized by the integrated UV spectra of QSOs (see text for discussion).

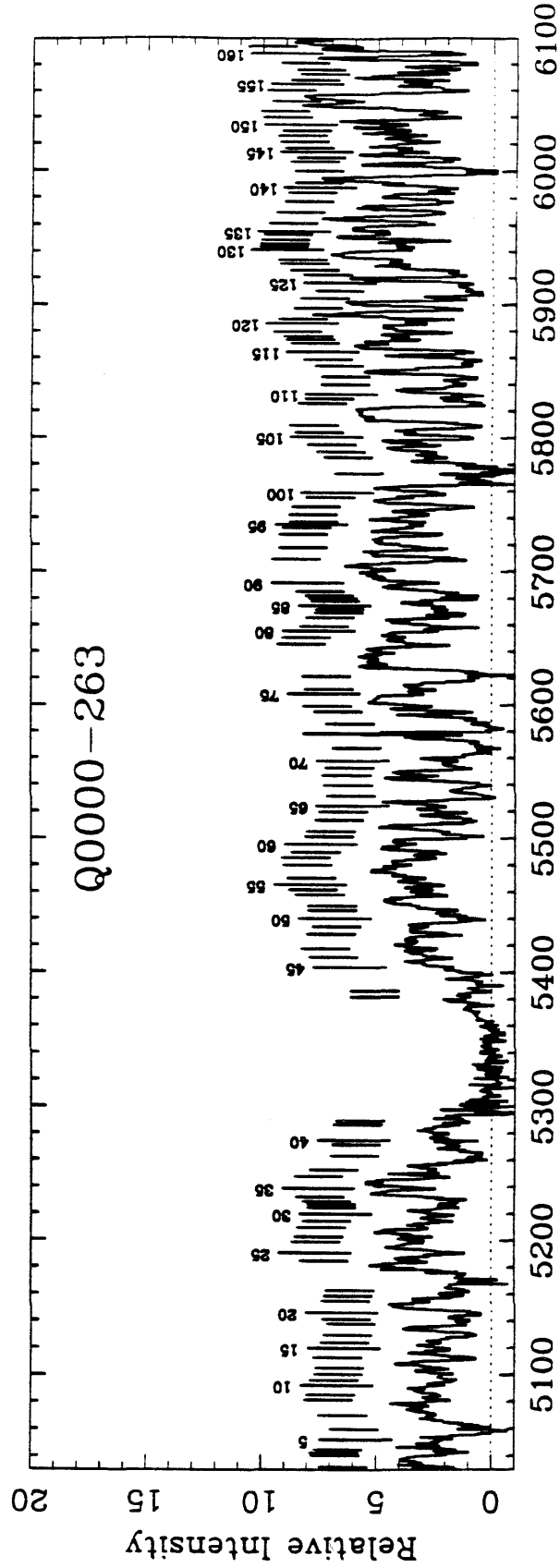
Q0000−263
Relative Intensity
Wavelength (Angstroms)
0
5
10
15
20
5100
5200
5300
5400
5500
5600
5700
5800
5900
6000
6100

Figure 1 *a.*

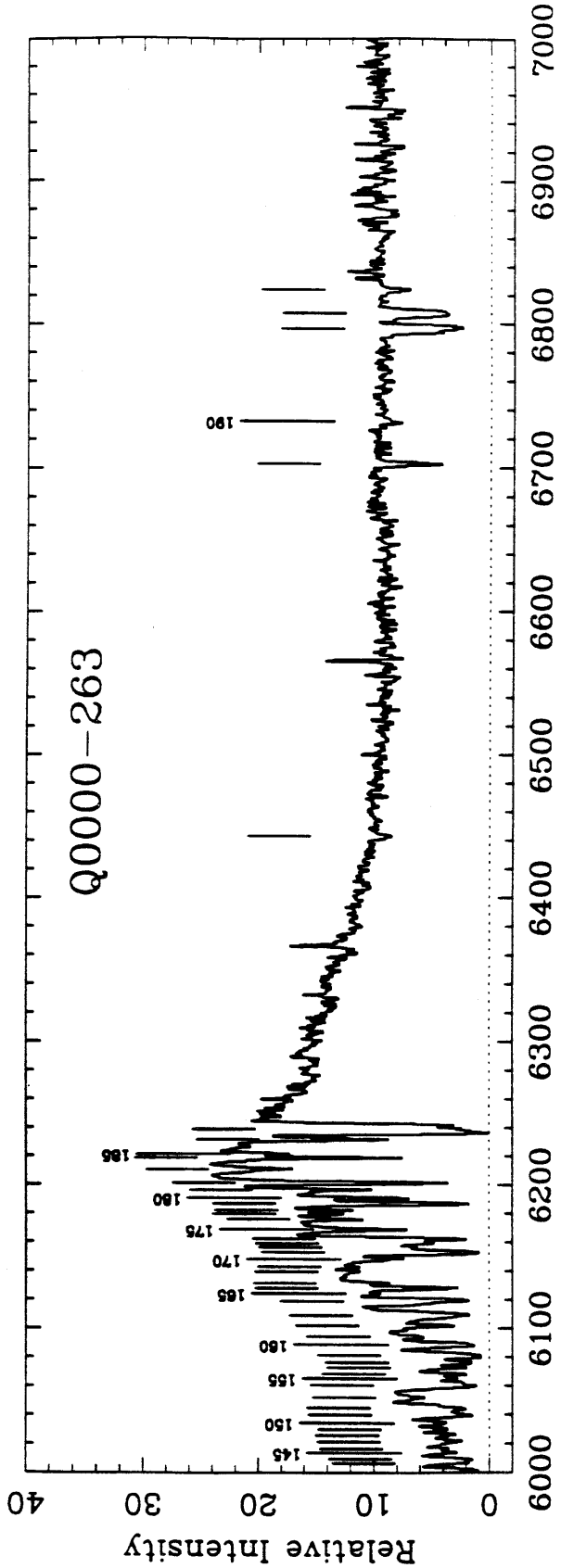

Figure 1 *a. (cont.)*

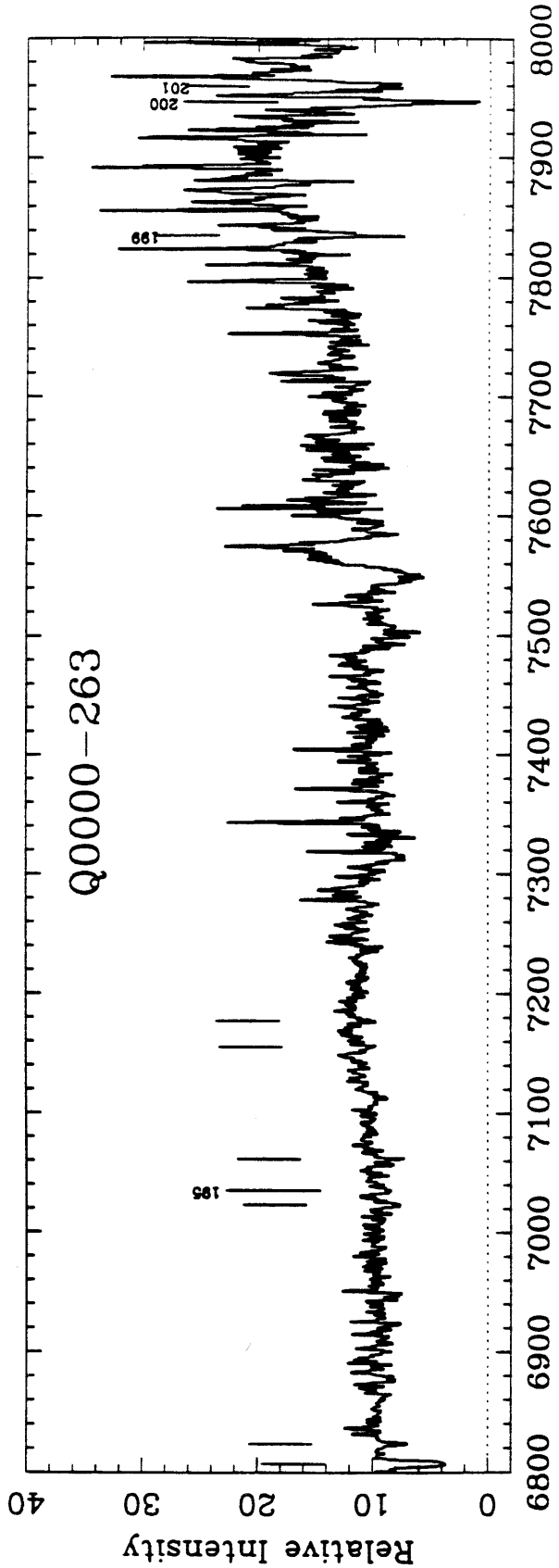

Figure 1 *a. (cont.)*

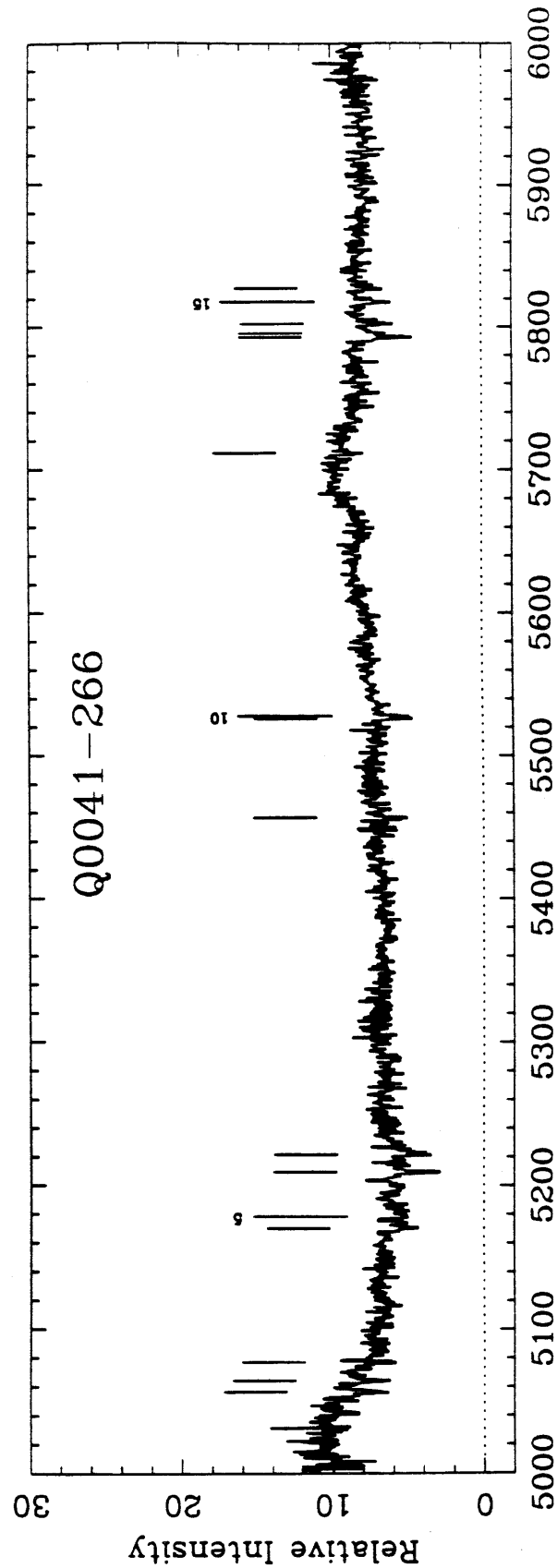
Q0041−266
δ
10
15
Relative Intensity
0
10
20
30
Wavelength (Angstroms)
5000
5100
5200
5300
5400
5500
5600
5700
5800
5900
6000

Figure 1 *b*.

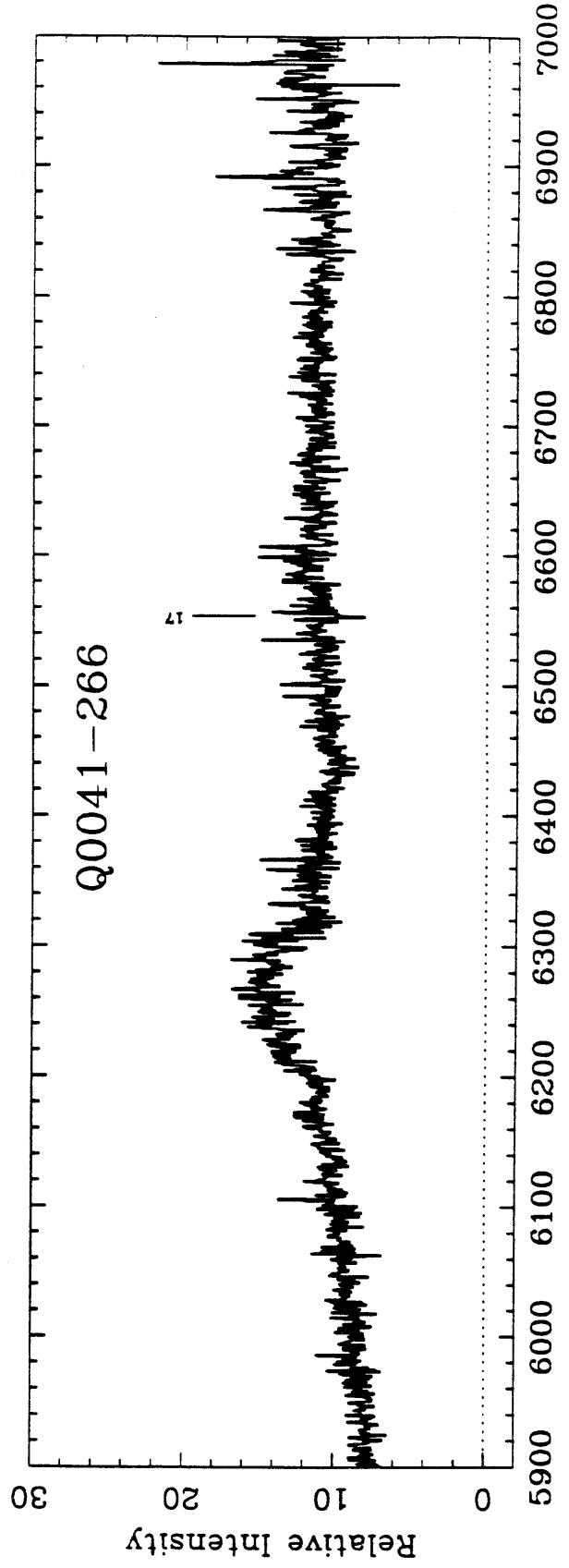

Figure 1 *b. (cont.)*

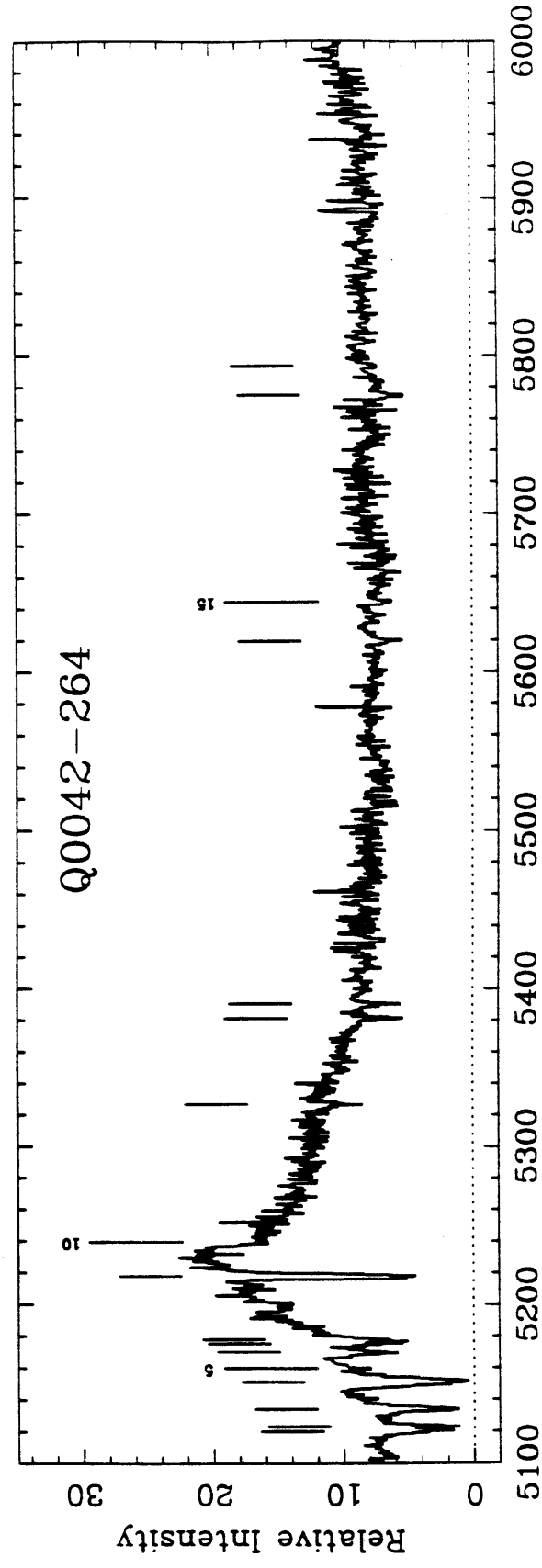
Q0042−264
Relative Intensity
Wavelength (Angstroms)
0
10
20
30
5100
5200
5300
5400
5500
5600
5700
5800
5900
6000
5
10
15

Figure 1 *c.*

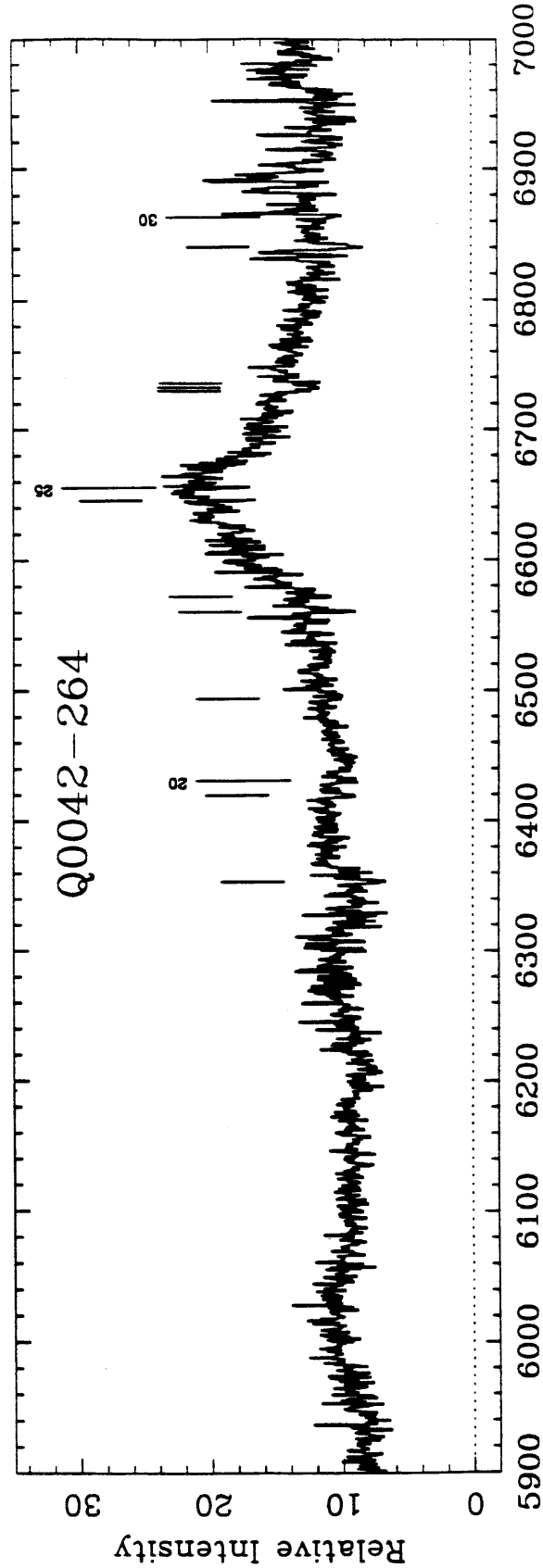

Figure 1 *c. (cont.)*

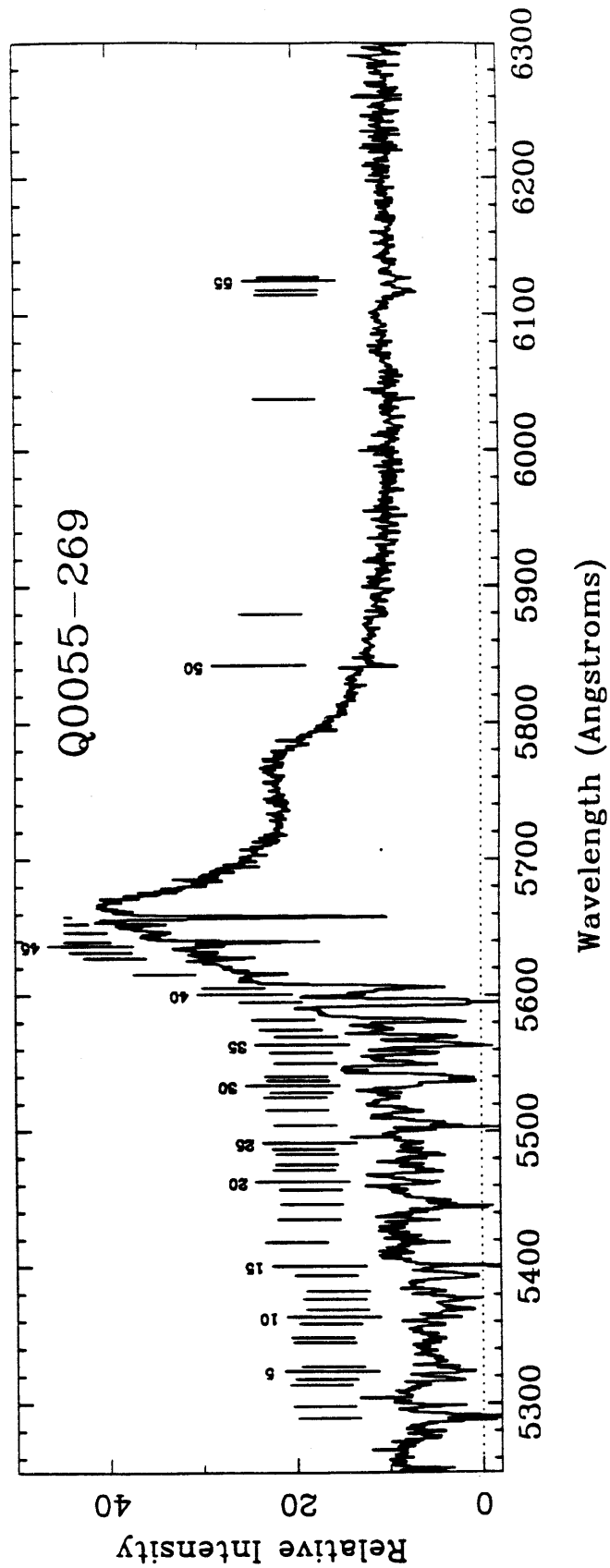
Q0055−269
Relative Intensity
Wavelength (Angstroms)
0
20
40
5300
5400
5500
5600
5700
5800
5900
6000
6100
6200
6300
5
10
15
20
25
30
35
40
45
50
55

Figure 1 *d.*

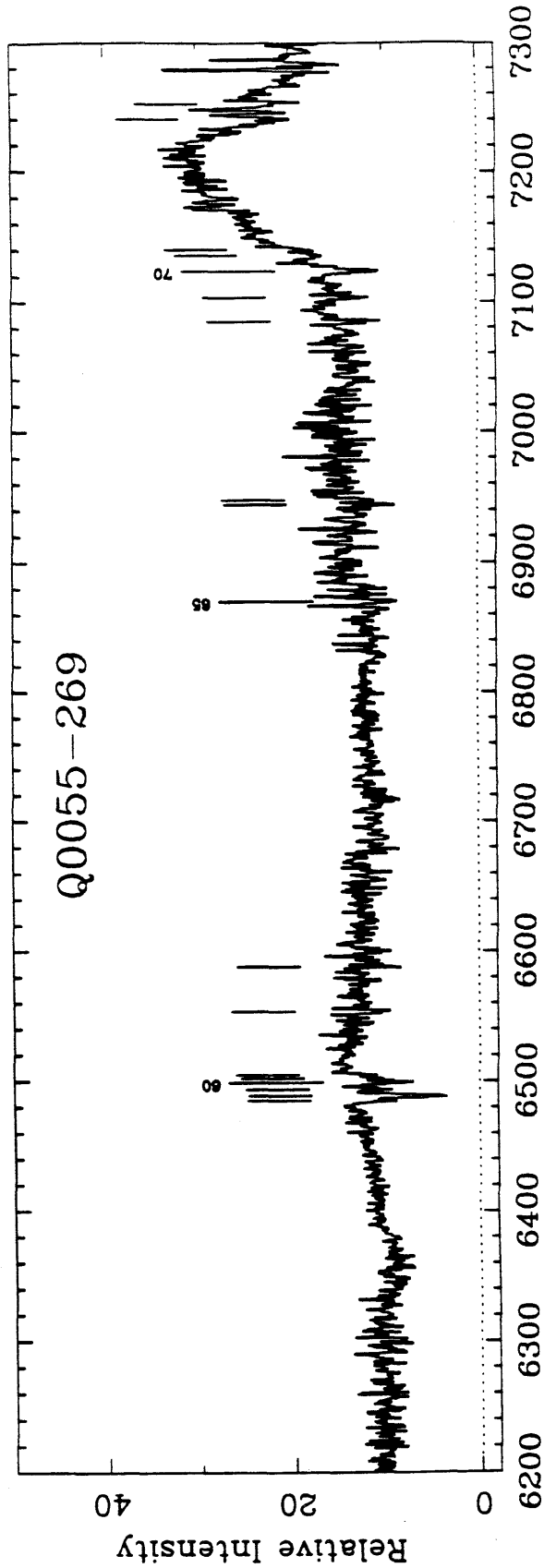

Figure 1 *d. (cont.)*

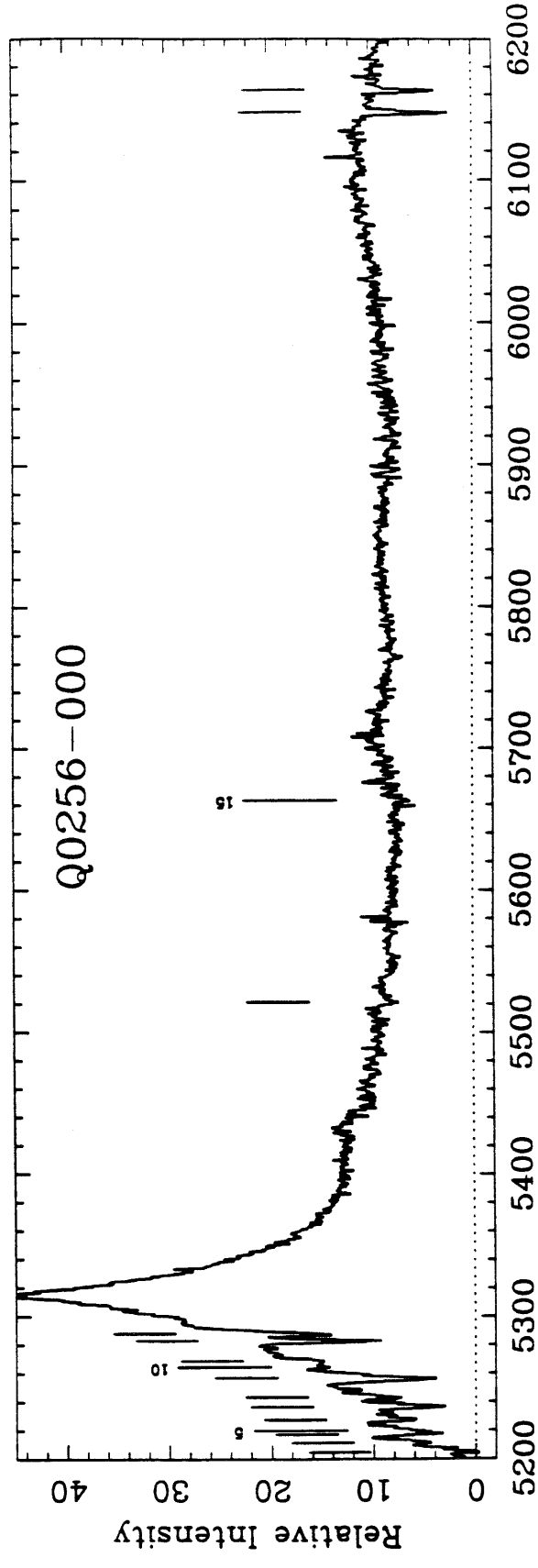
Q0256−000
15
10
5
Relative Intensity
0
10
20
30
40
5200
5300
5400
5500
5600
5700
5800
5900
6000
6100
6200
Wavelength (Angstroms)

Figure 1 *e.*

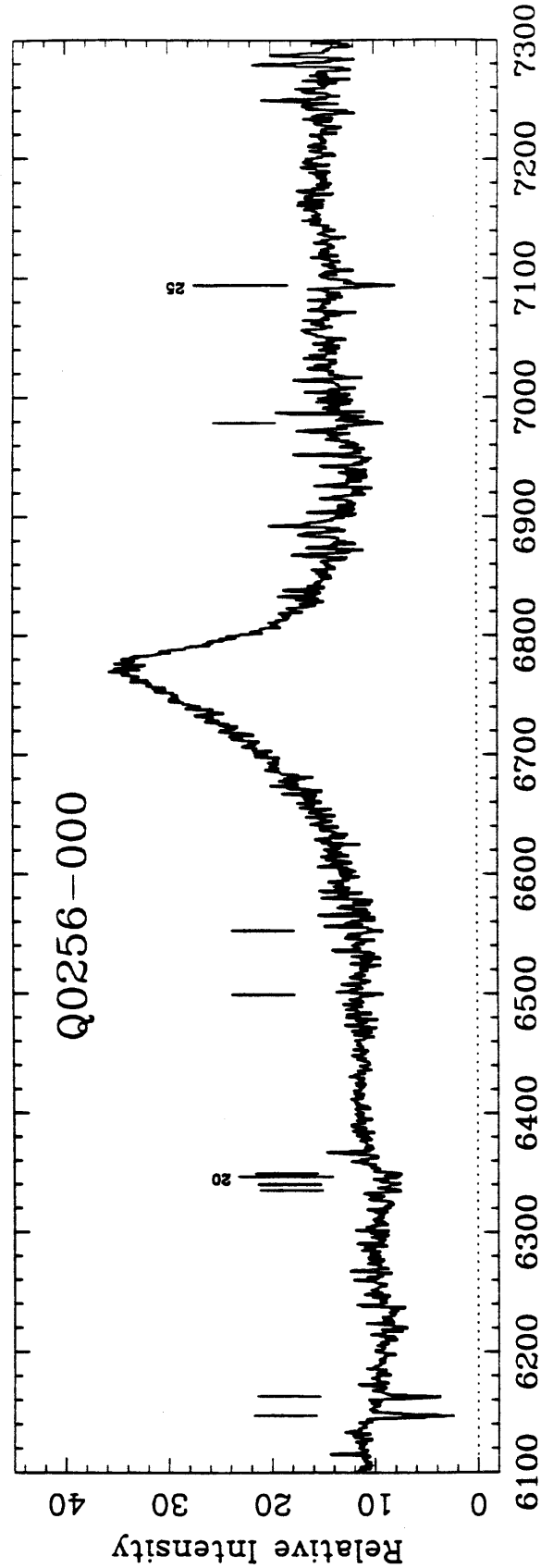

Figure 1 *e. (cont.)*

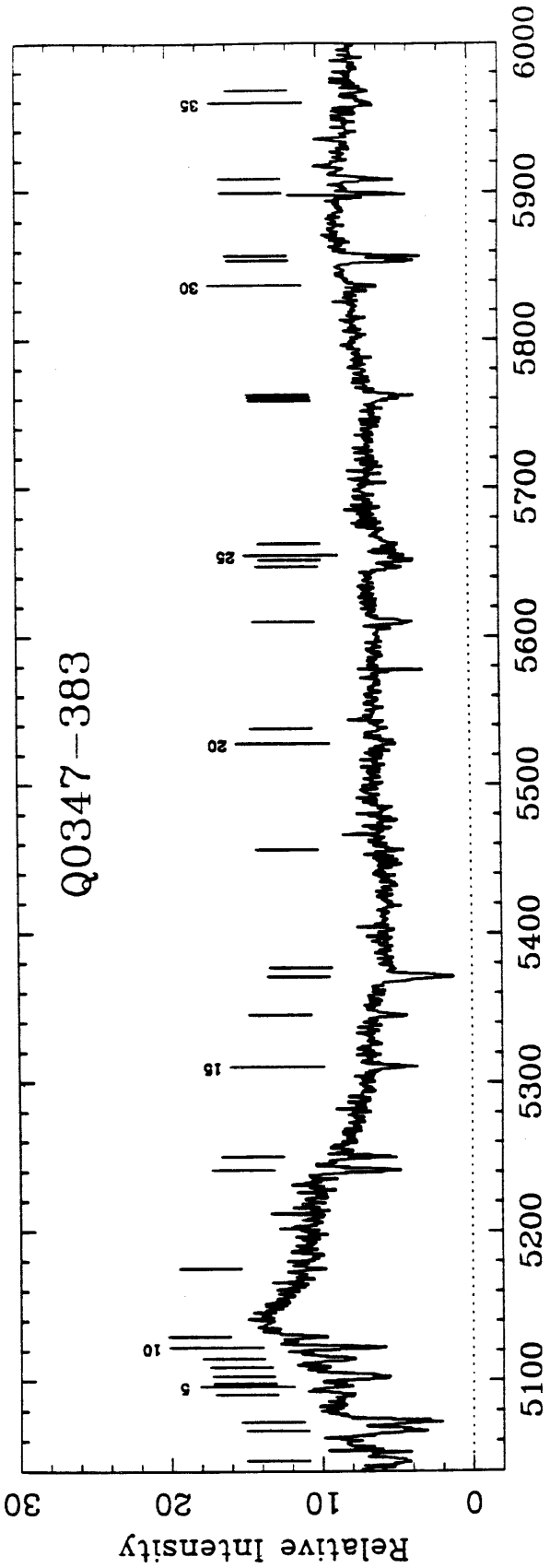
Q0347−383
Relative Intensity
Wavelength (Angstroms)
0
10
20
30
5100
5200
5300
5400
5500
5600
5700
5800
5900
6000
5
10
15
20
25
30
35

Figure 1 *f*.

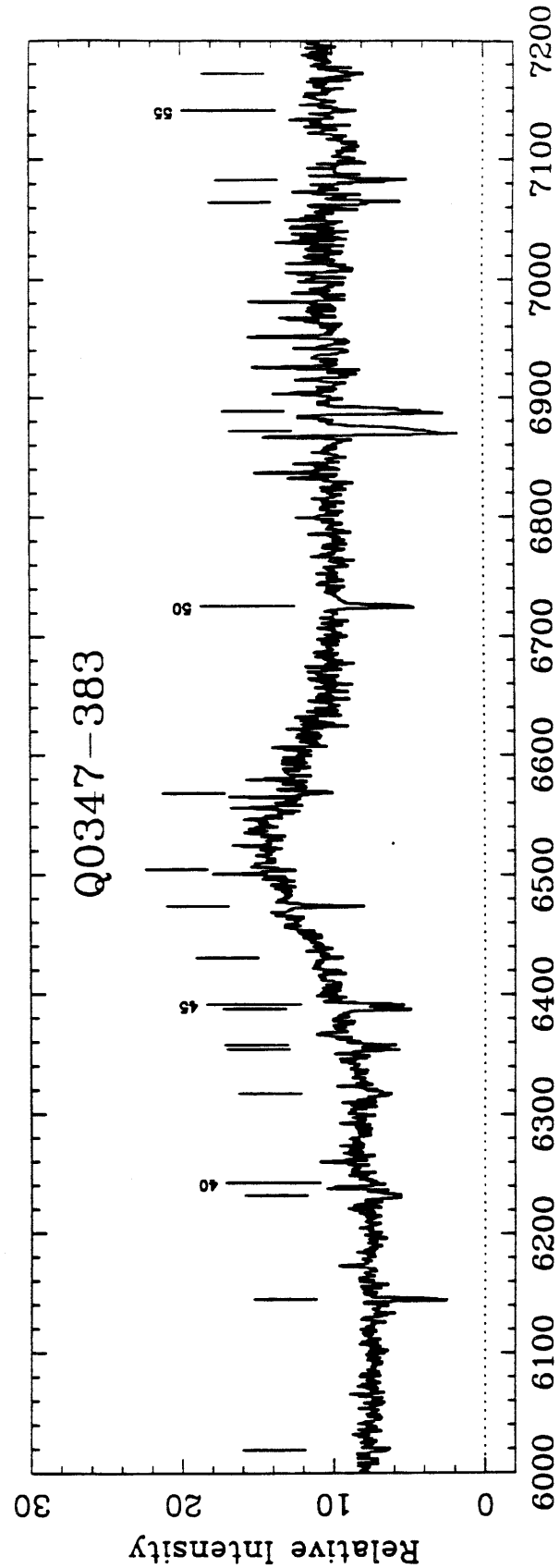

Figure 1 *f. (cont.)*

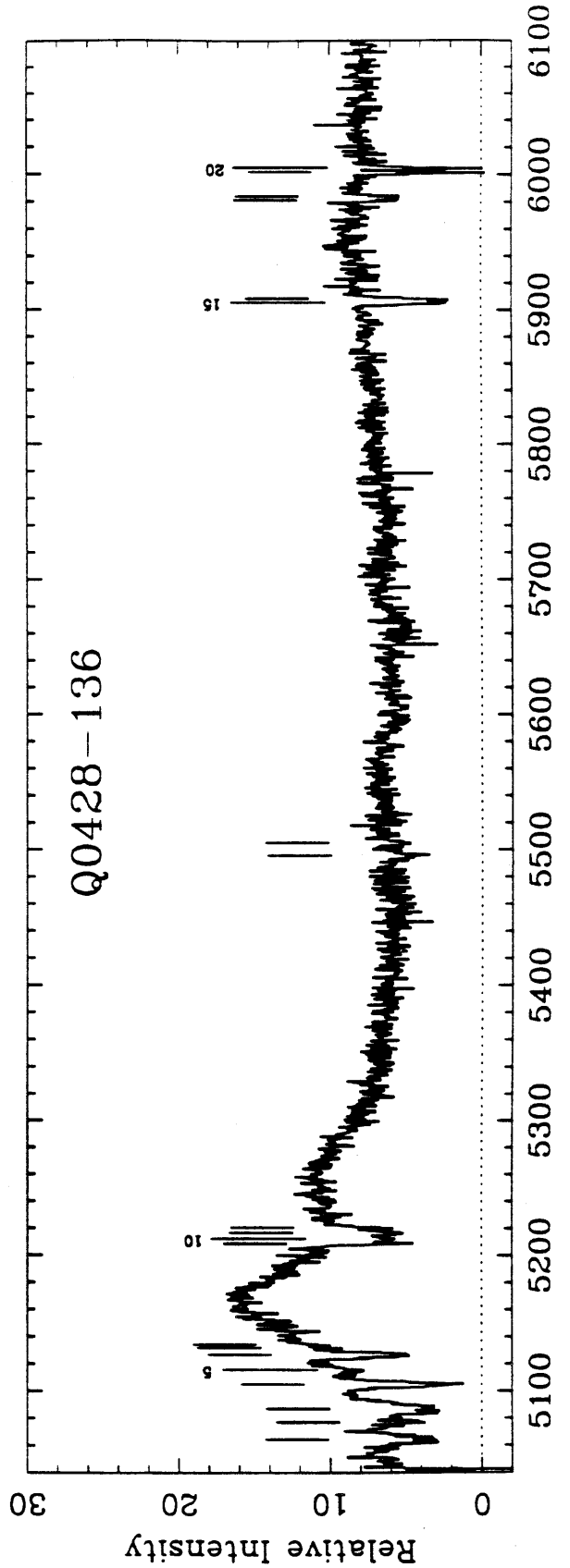
Q0428−136
Relative Intensity
Wavelength (Angstroms)
0
10
20
30
5100
5200
5300
5400
5500
5600
5700
5800
5900
6000
6100
5
10
15
20

Figure 1 *g*.

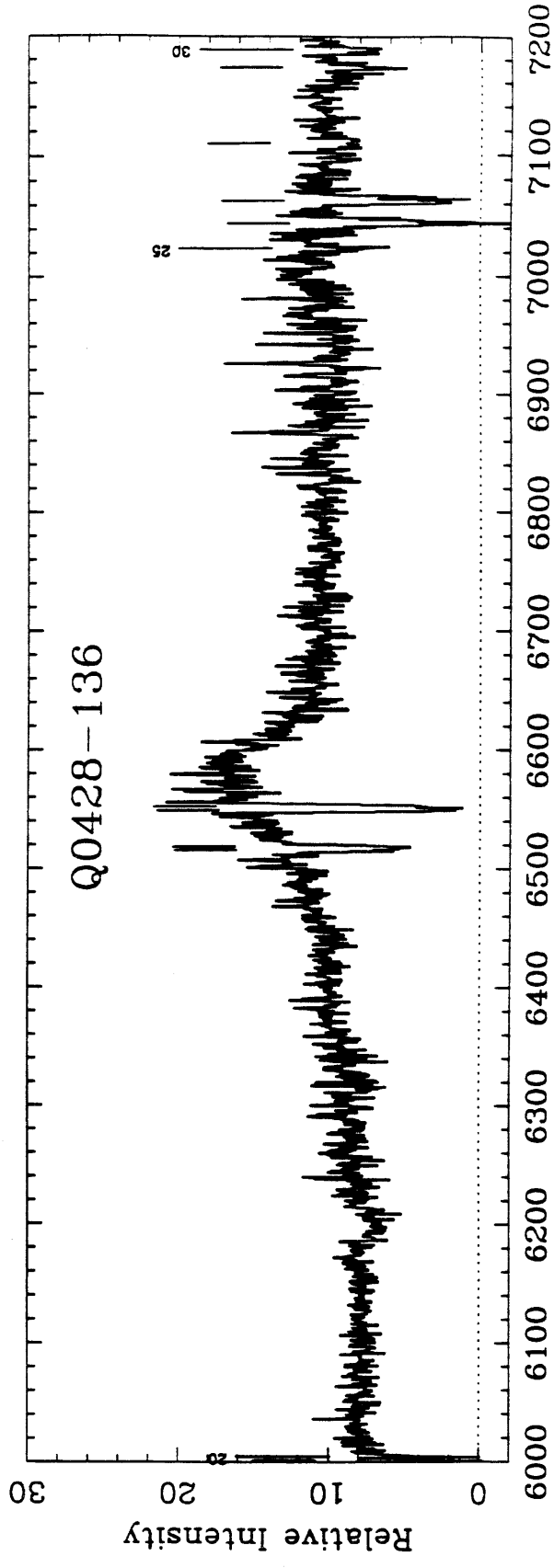

Figure 1 *g. (cont.)*

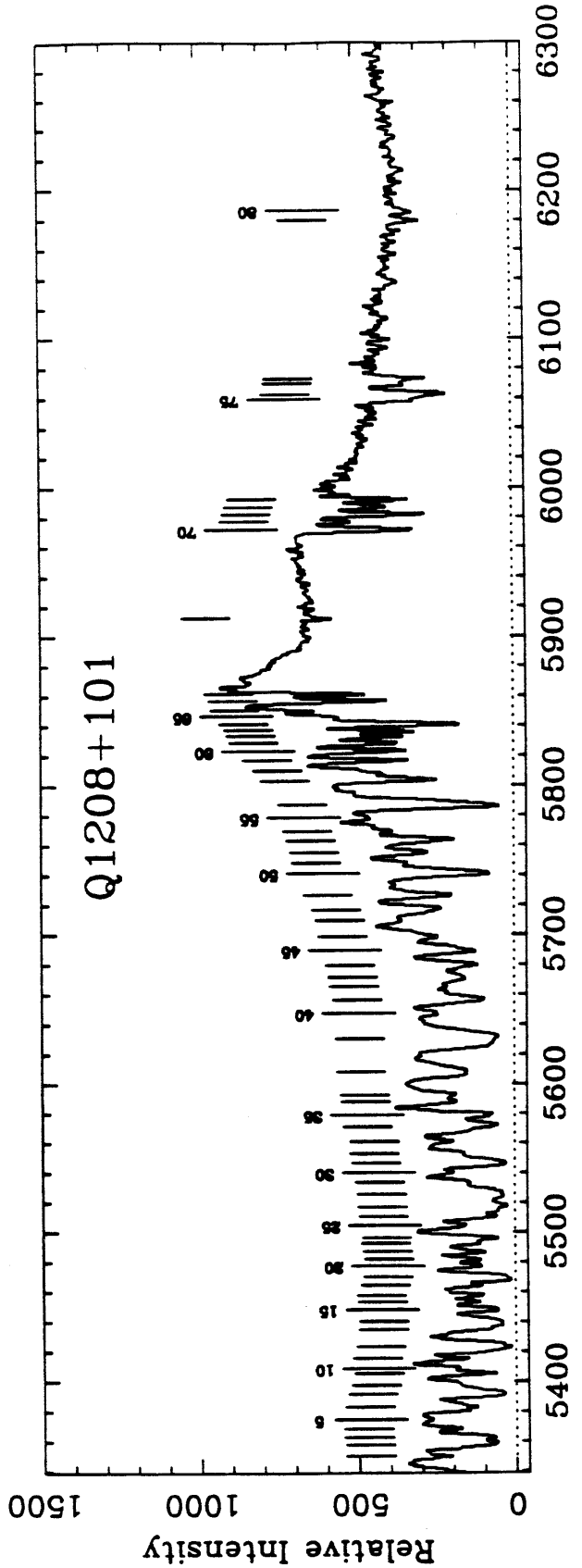
Q1208+101
Relative Intensity
0
500
1000
1500
Wavelength (Angstroms)
5400
5500
5600
5700
5800
5900
6000
6100
6200
6300

Figure 1 *h*.

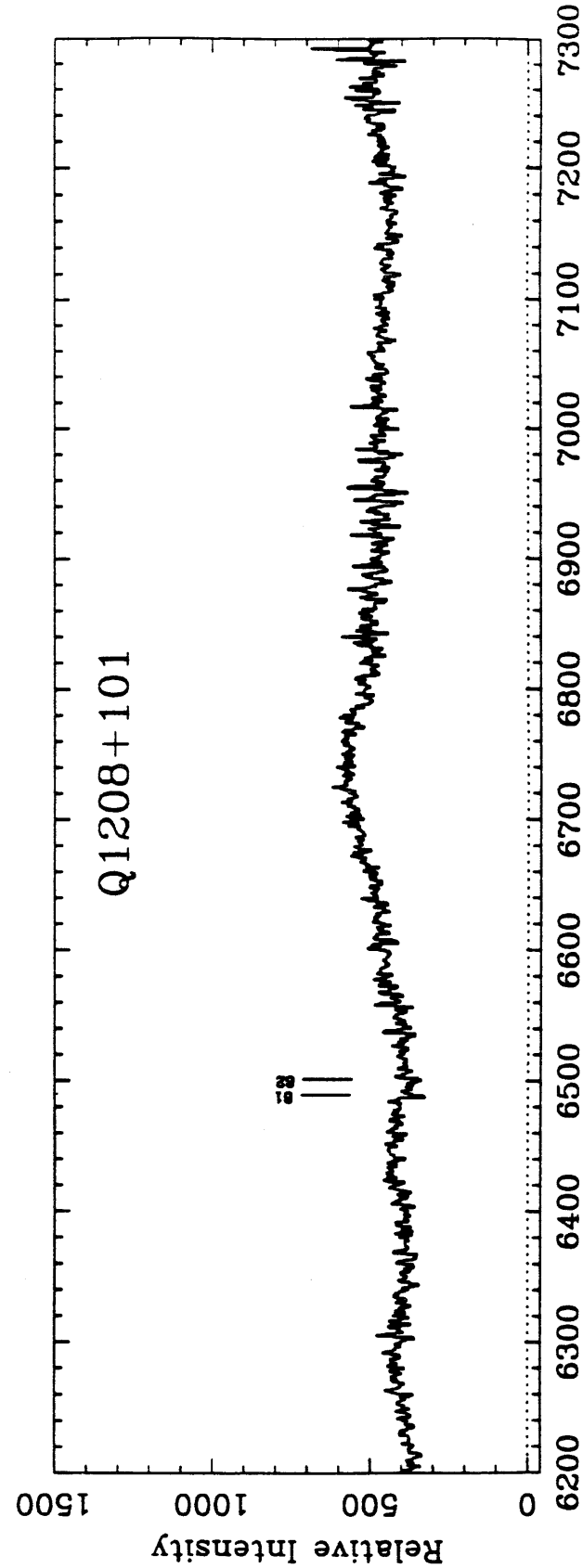

Figure 1 *h. (cont.)*

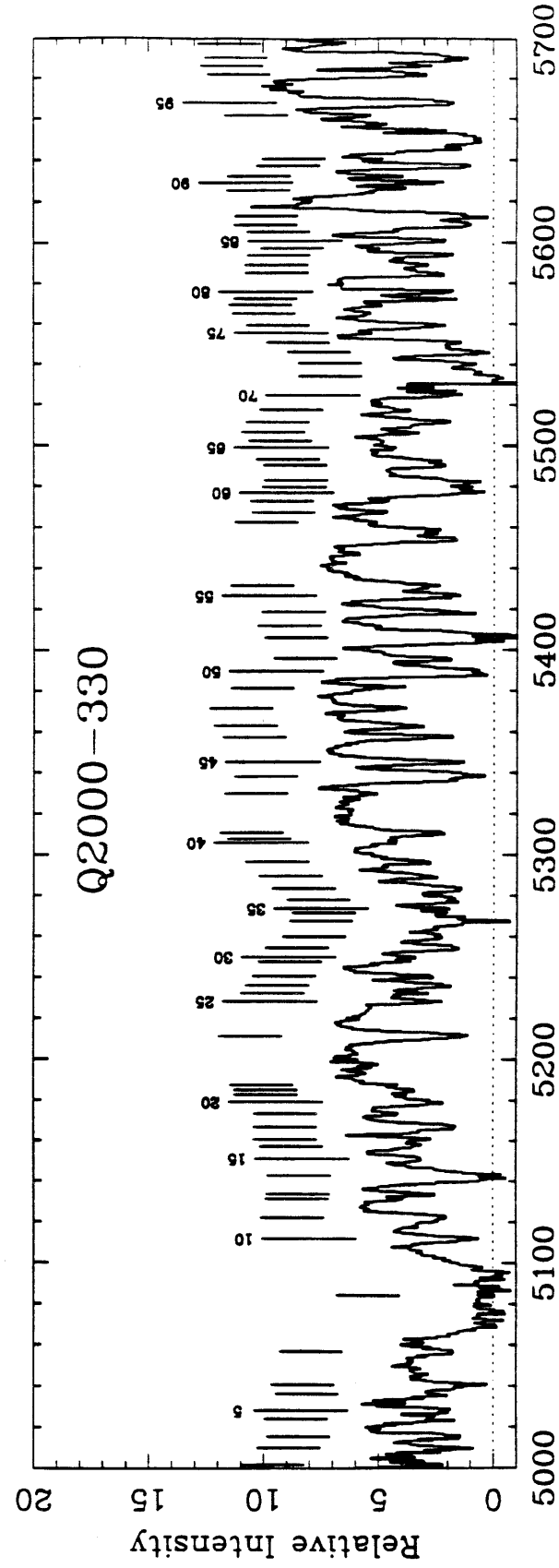
Q2000−330
Relative Intensity
Wavelength (Angstroms)
0
5
10
15
20
5000
5100
5200
5300
5400
5500
5600
5700

Figure 1 *i.*

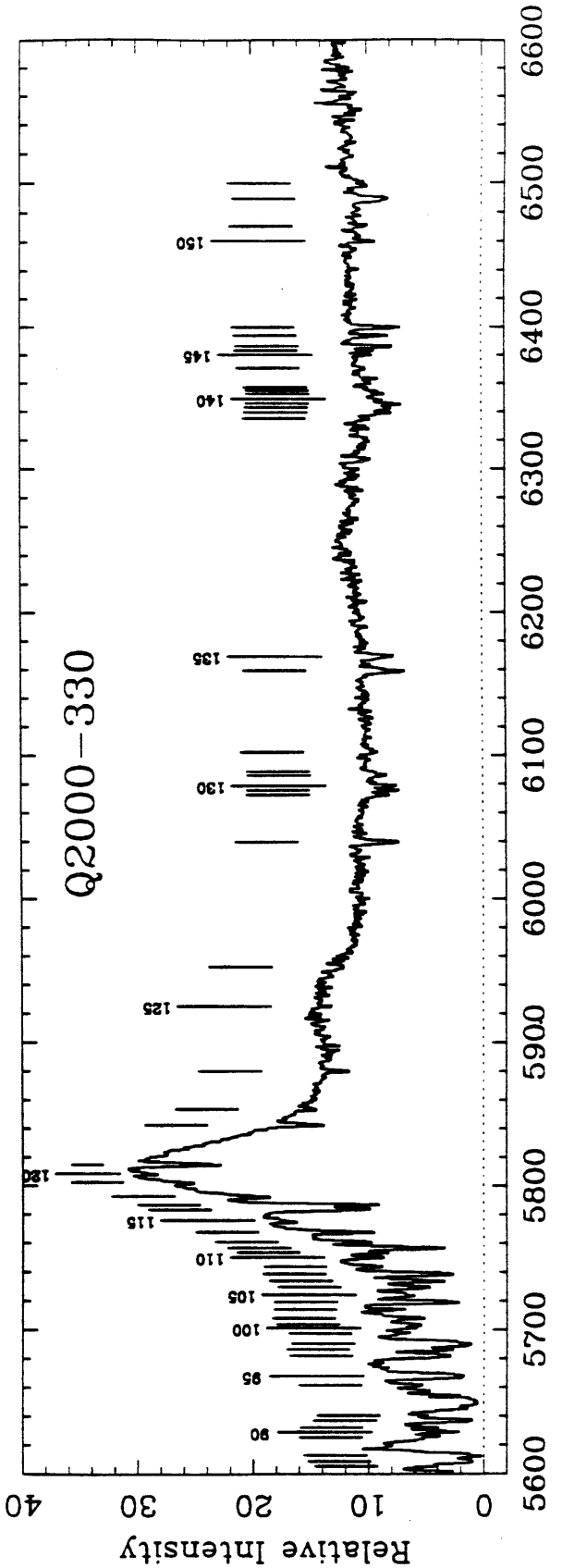

Figure 1 *i. (cont.)*

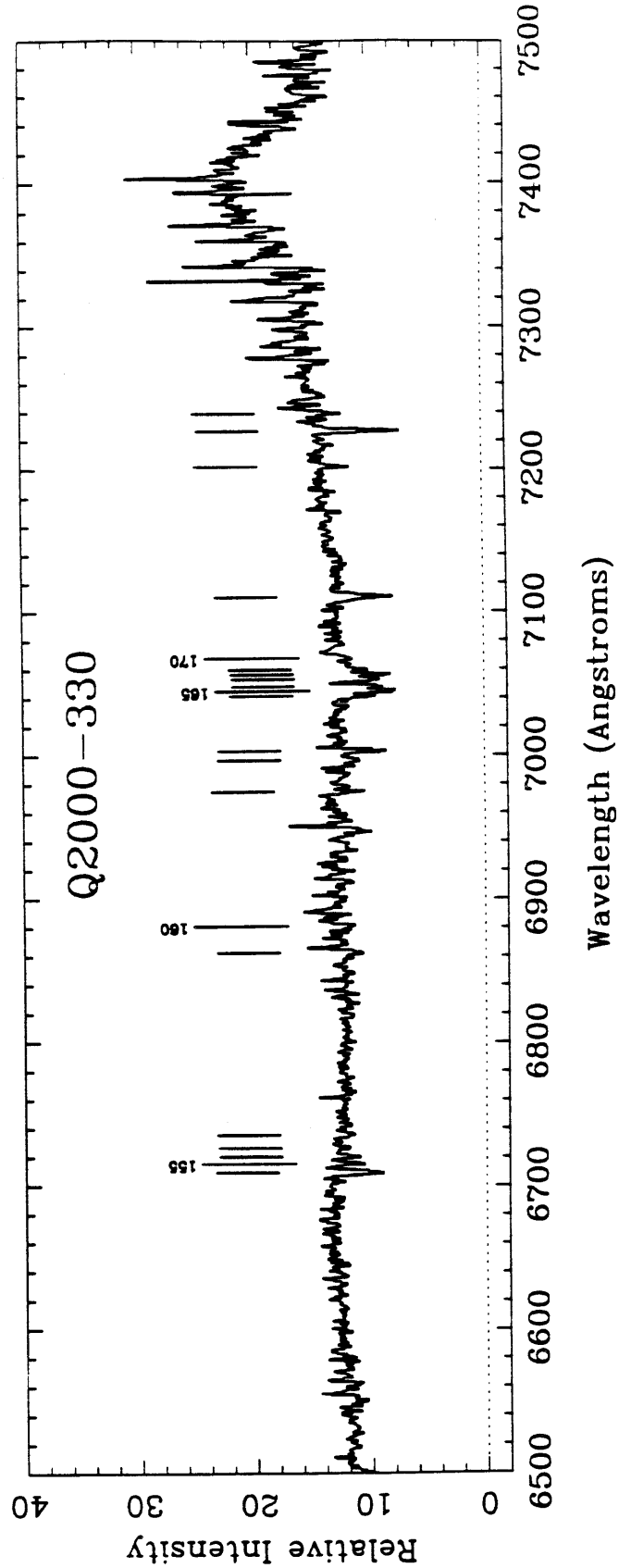

Figure 1 *i. (cont.)*

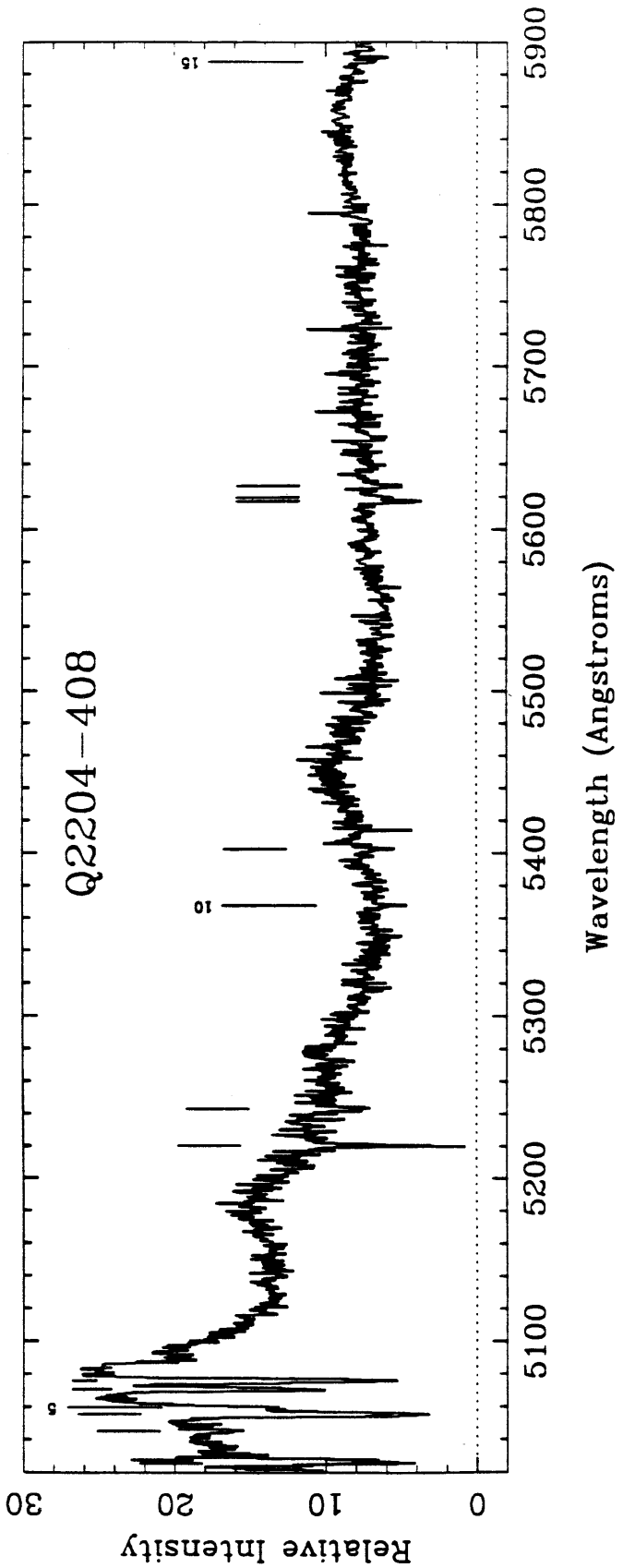
Q2204−408
Relative Intensity
Wavelength (Angstroms)
0
10
20
30
5100
5200
5300
5400
5500
5600
5700
5800
5900

Figure 1 *j*.

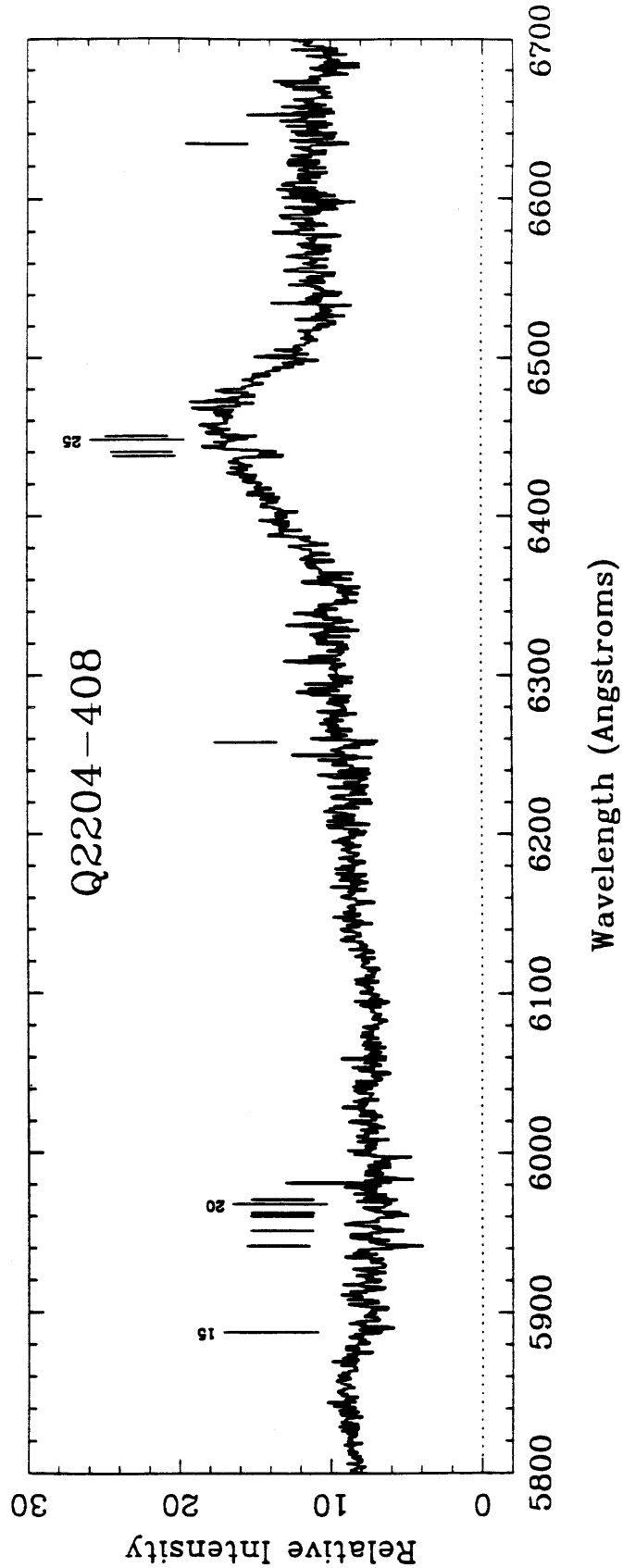

Figure 1 *j. (cont.)*

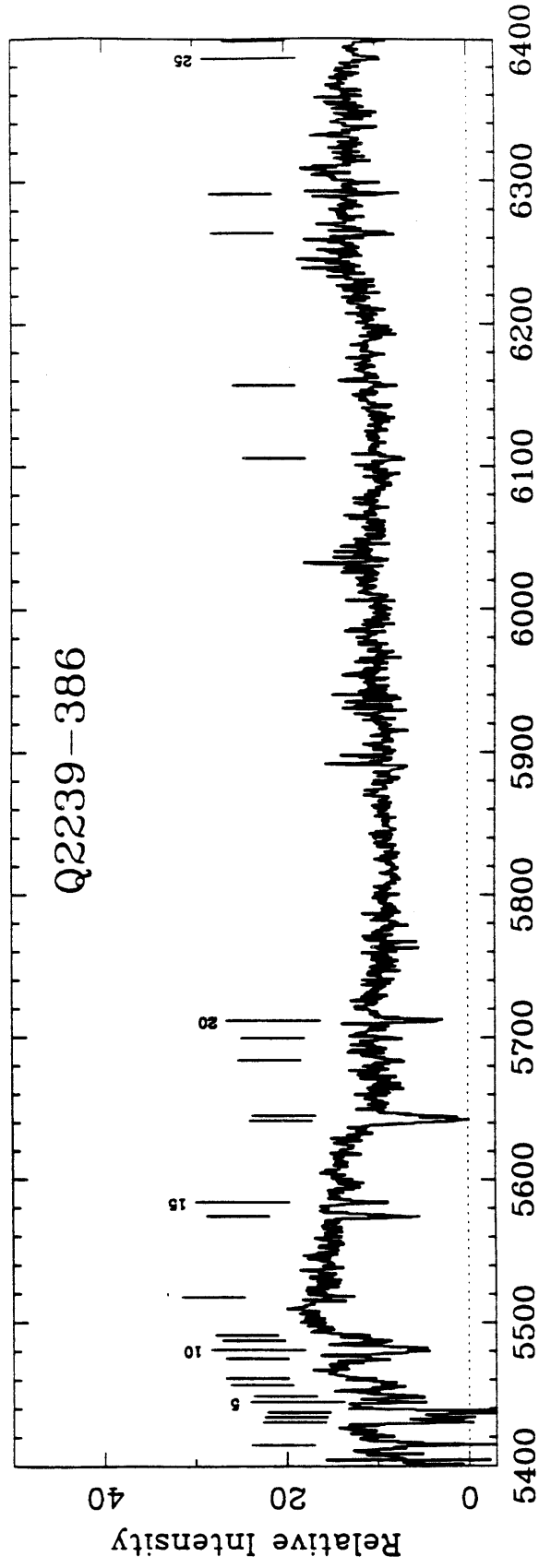
Q2239−386
Relative Intensity
Wavelength (Angstroms)
0
20
40
5400
5500
5600
5700
5800
5900
6000
6100
6200
6300
6400
5
10
15
20
25

Figure 1 *k*.

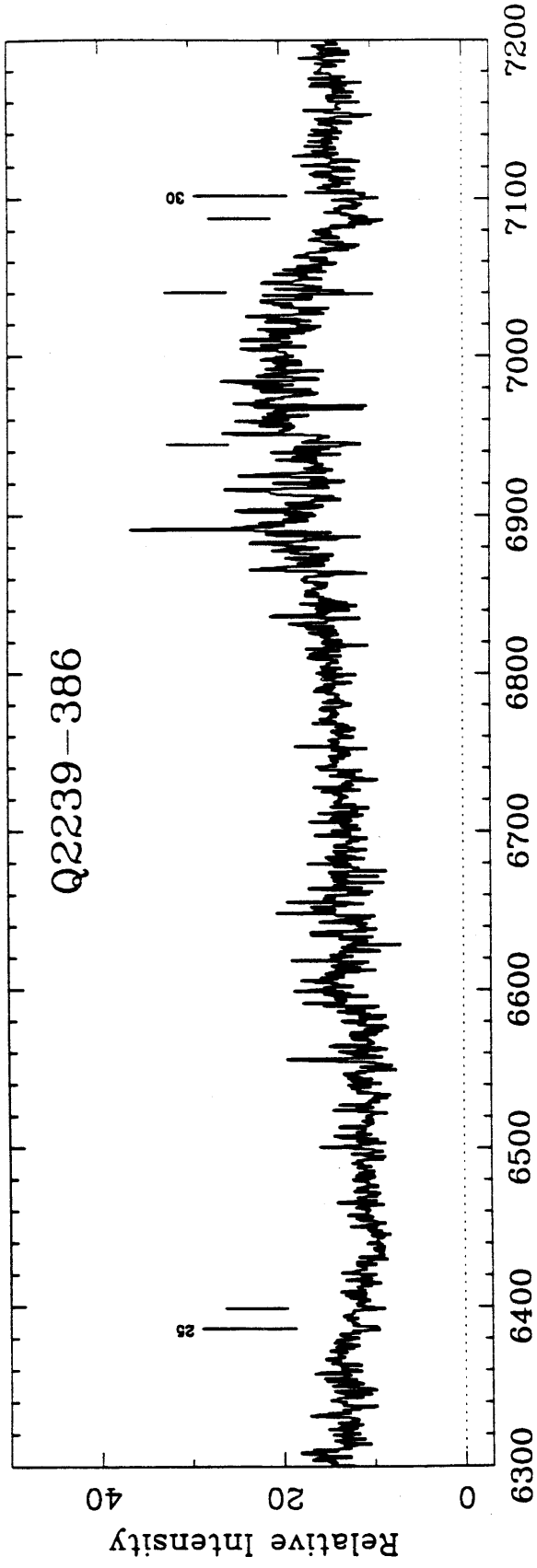

Figure 1 *k. (cont.)*

Figure 2

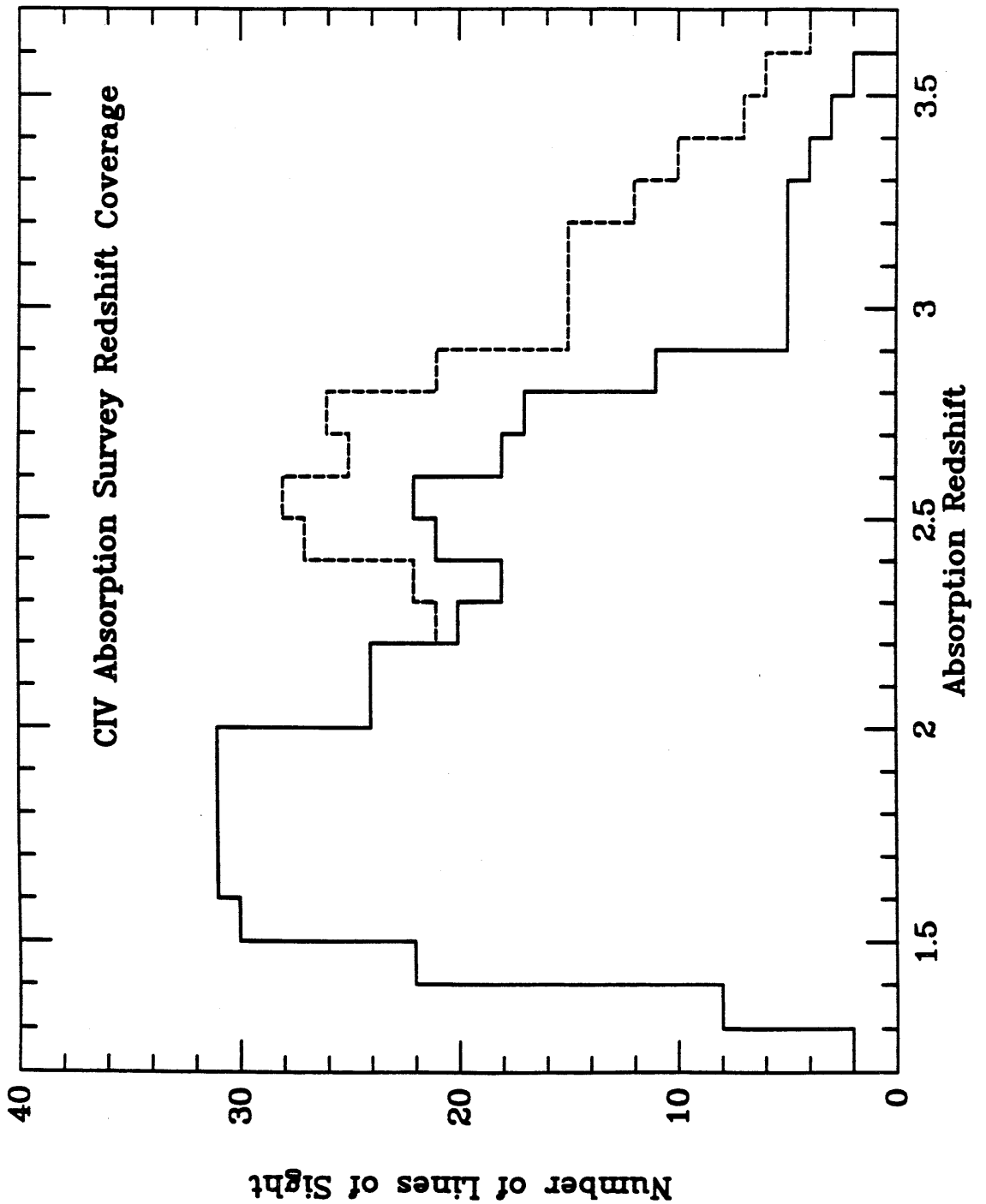
CIV Absorption Survey Redshift Coverage
Number of Lines of Sight
Absorption Redshift
0
10
20
30
40
1.5
2
2.5
3
3.5

Figure 3

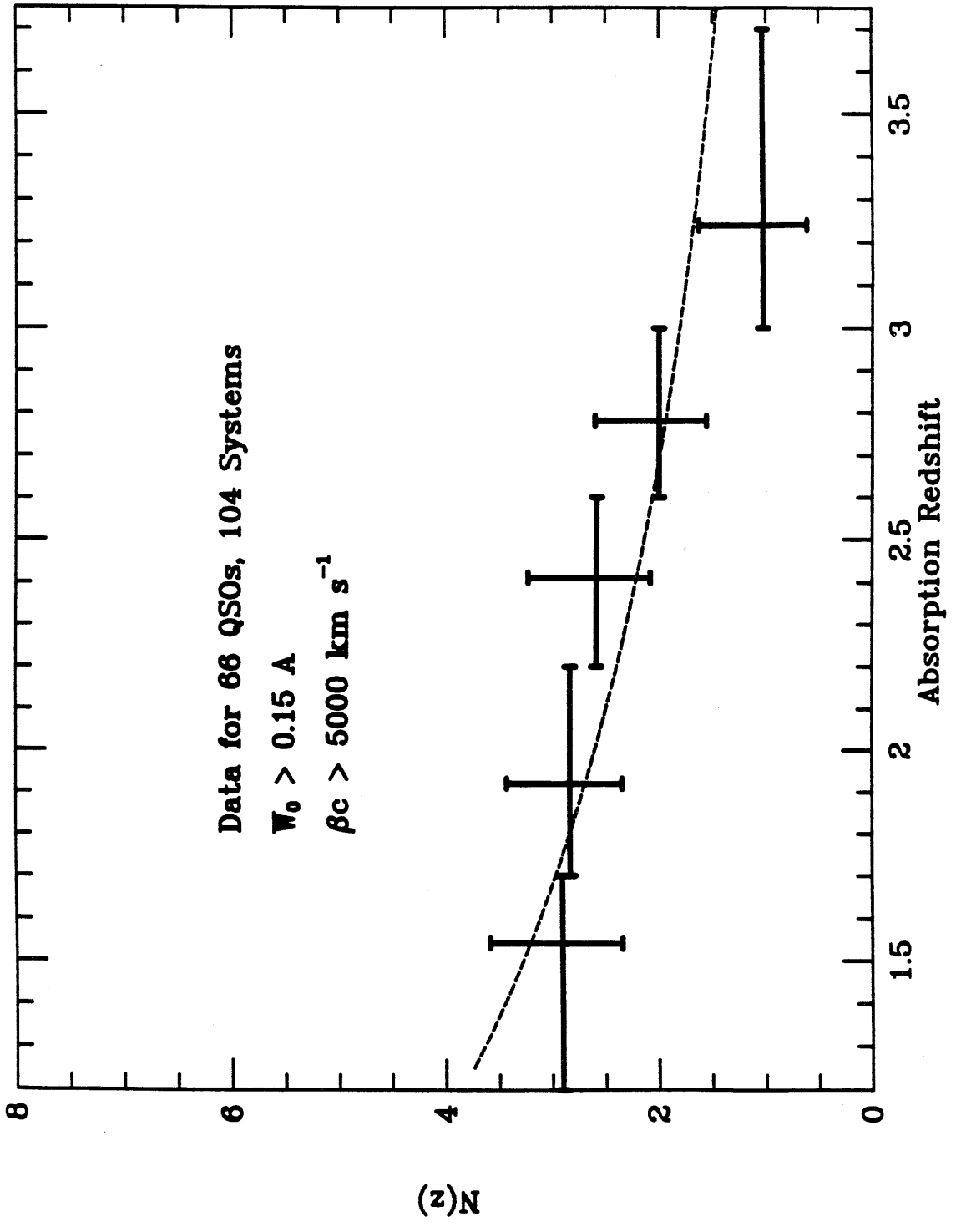
Data for 66 QSOs, 104 Systems
$W_0 > 0.15$ A
$\beta c > 5000$ km s^{-1}
N(z)
Absorption Redshift
0
2
4
6
8
1.5
2
2.5
3
3.5

Figure 4

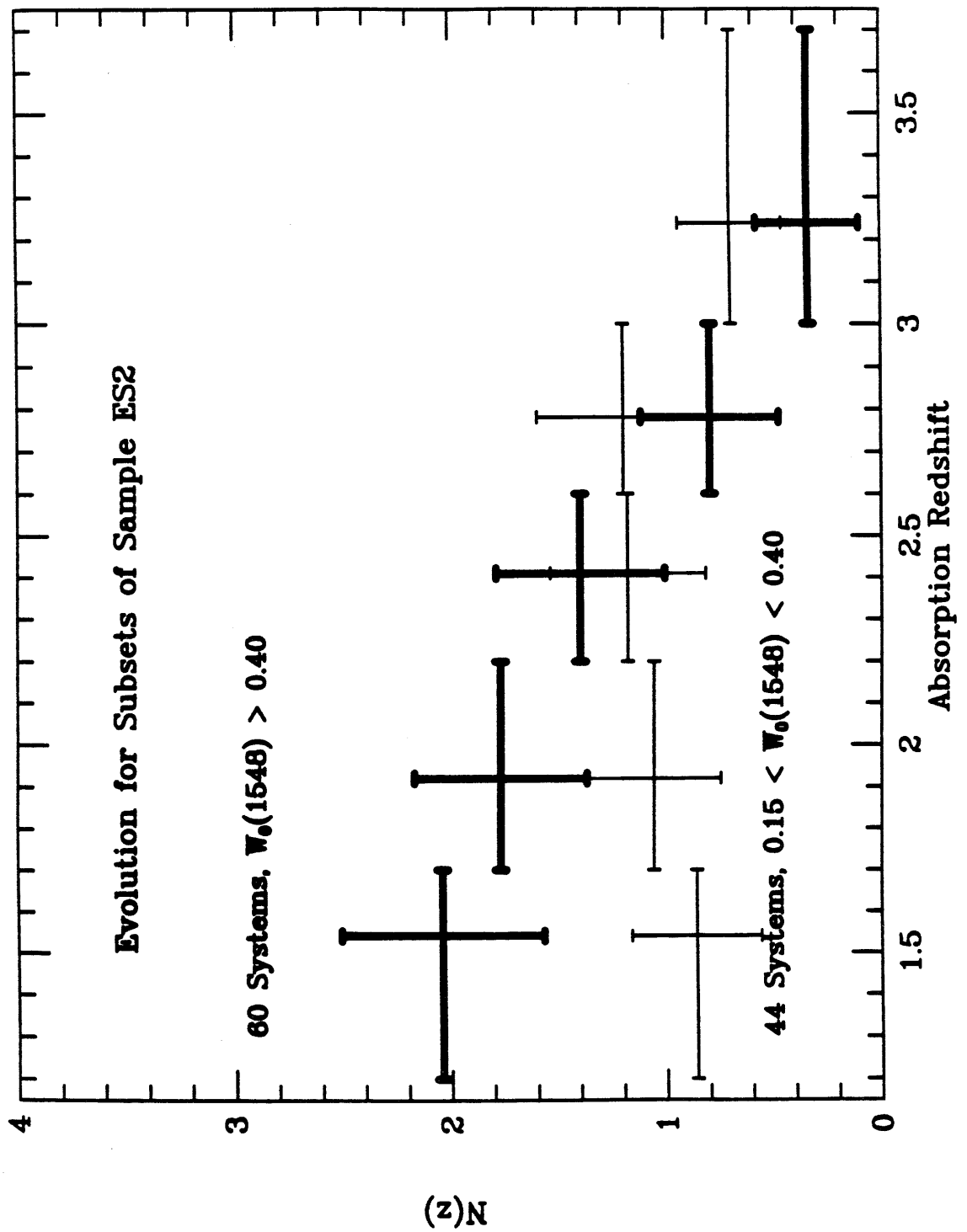
Evolution for Subsets of Sample ES2
60 Systems, W₀(1548) > 0.40
44 Systems, 0.15 < W₀(1548) < 0.40
N(z)
Absorption Redshift
0
1
2
3
4
1.5
2
2.5
3
3.5

Figure 5 *a*.

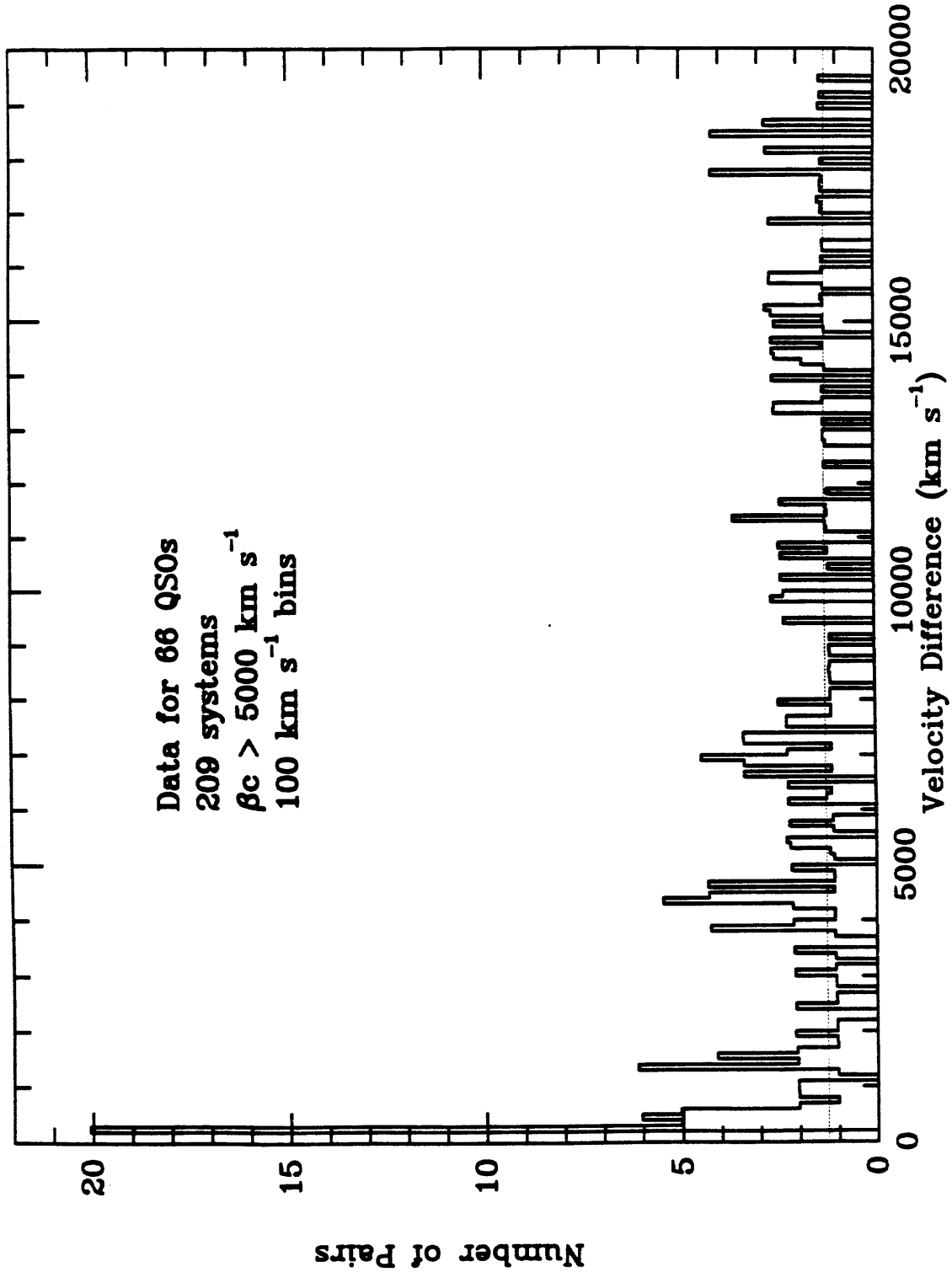
Data for 66 QSOs
209 systems
βc > 5000 km s⁻¹
100 km s⁻¹ bins
Number of Pairs
Velocity Difference (km s⁻¹)
0
5
10
15
20
5000
10000
15000
20000

Figure 5 *b*.

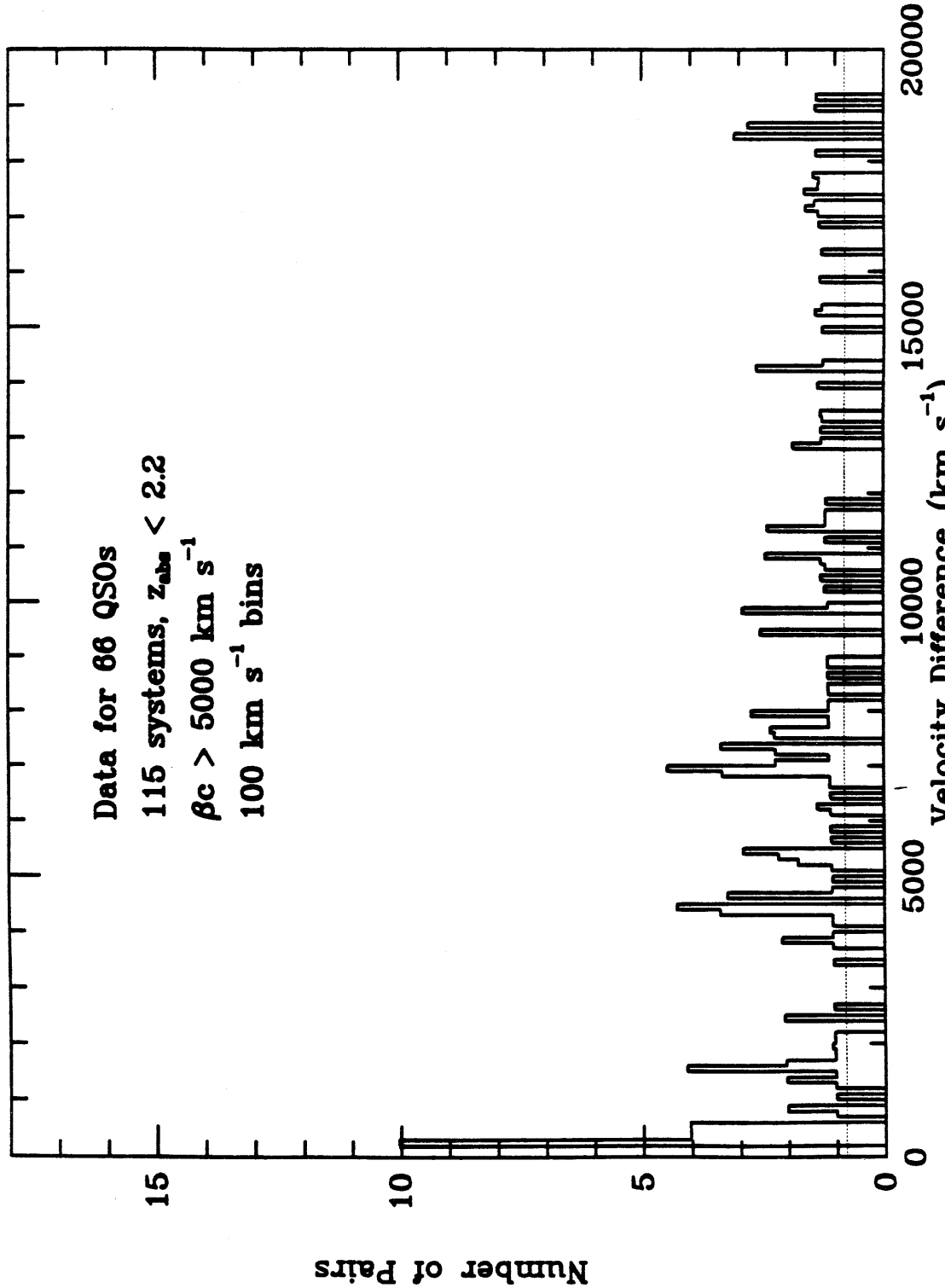
Data for 66 QSOs
115 systems, $z_{abs} < 2.2$
$\beta c > 5000$ km s^{-1}
100 km s^{-1} bins
Number of Pairs
Velocity Difference (km s^{-1})
0
5
10
15
0
5000
10000
15000
20000

Figure 5 *c*.

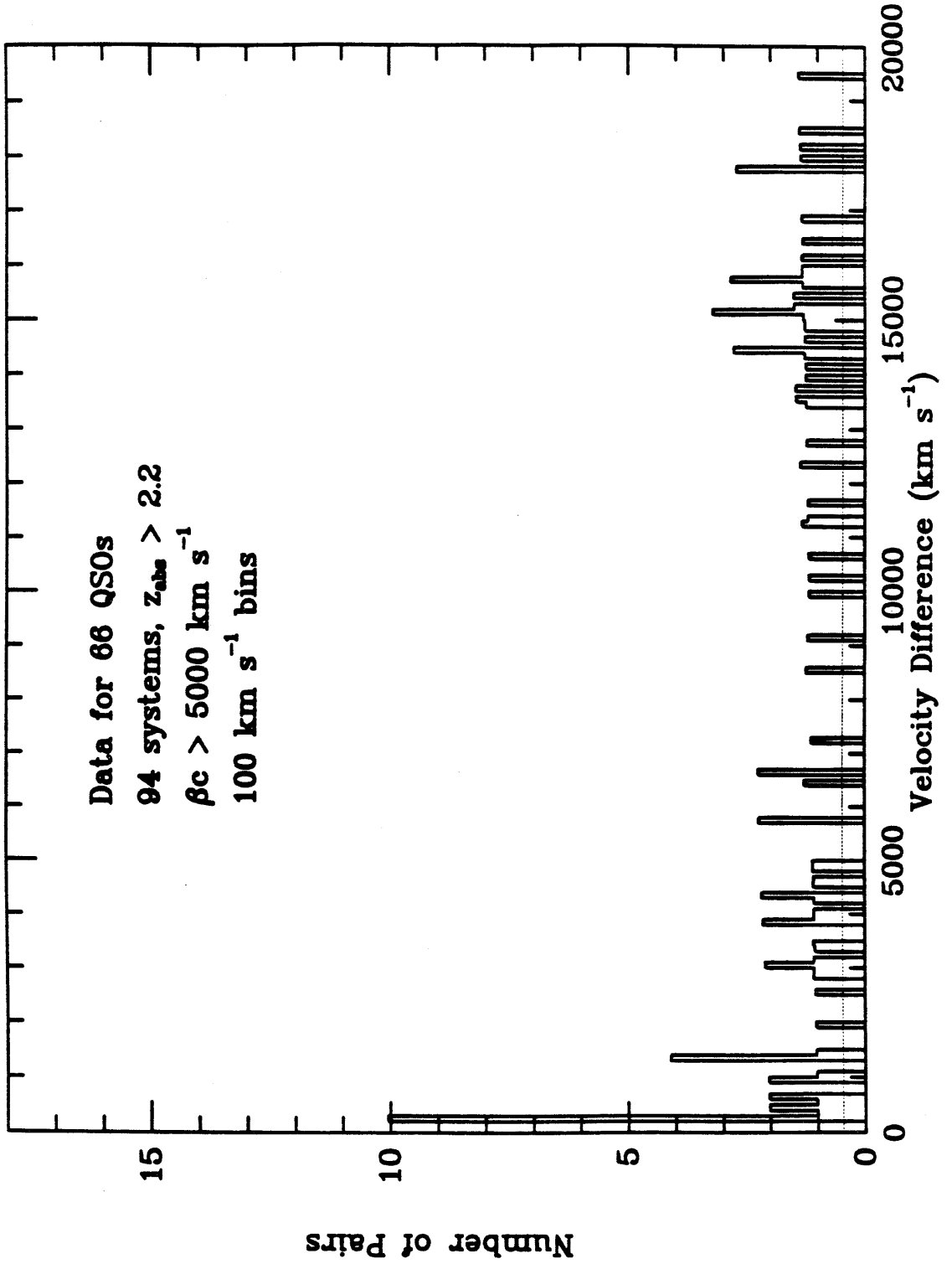
Data for 66 QSOs
94 systems, $z_{abs} > 2.2$
$\beta c > 5000$ km s^{-1}
100 km s^{-1} bins
Number of Pairs
Velocity Difference (km s^{-1})
0
5
10
15
0
5000
10000
15000
20000

Figure 6

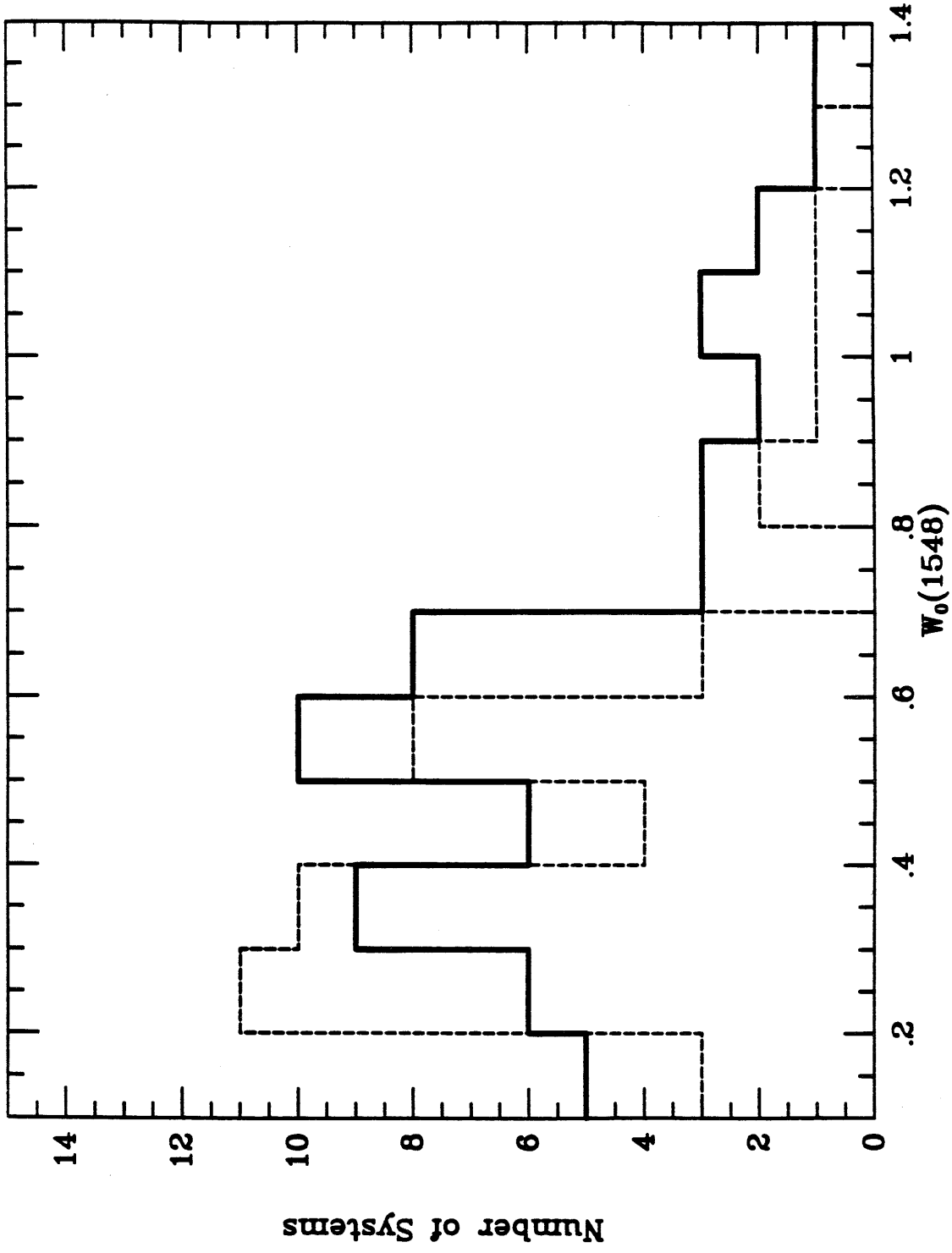

Figure 7

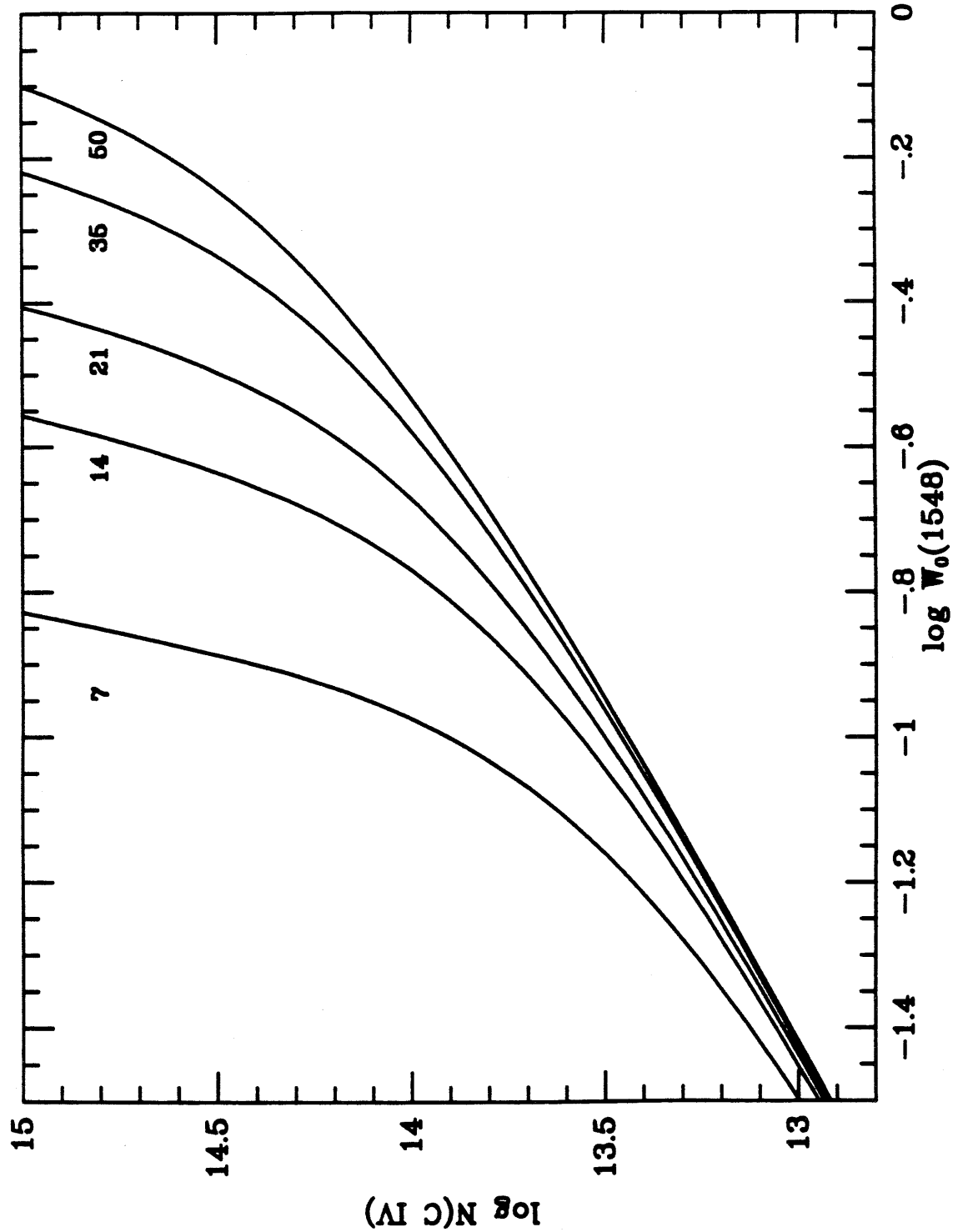

Figure 8

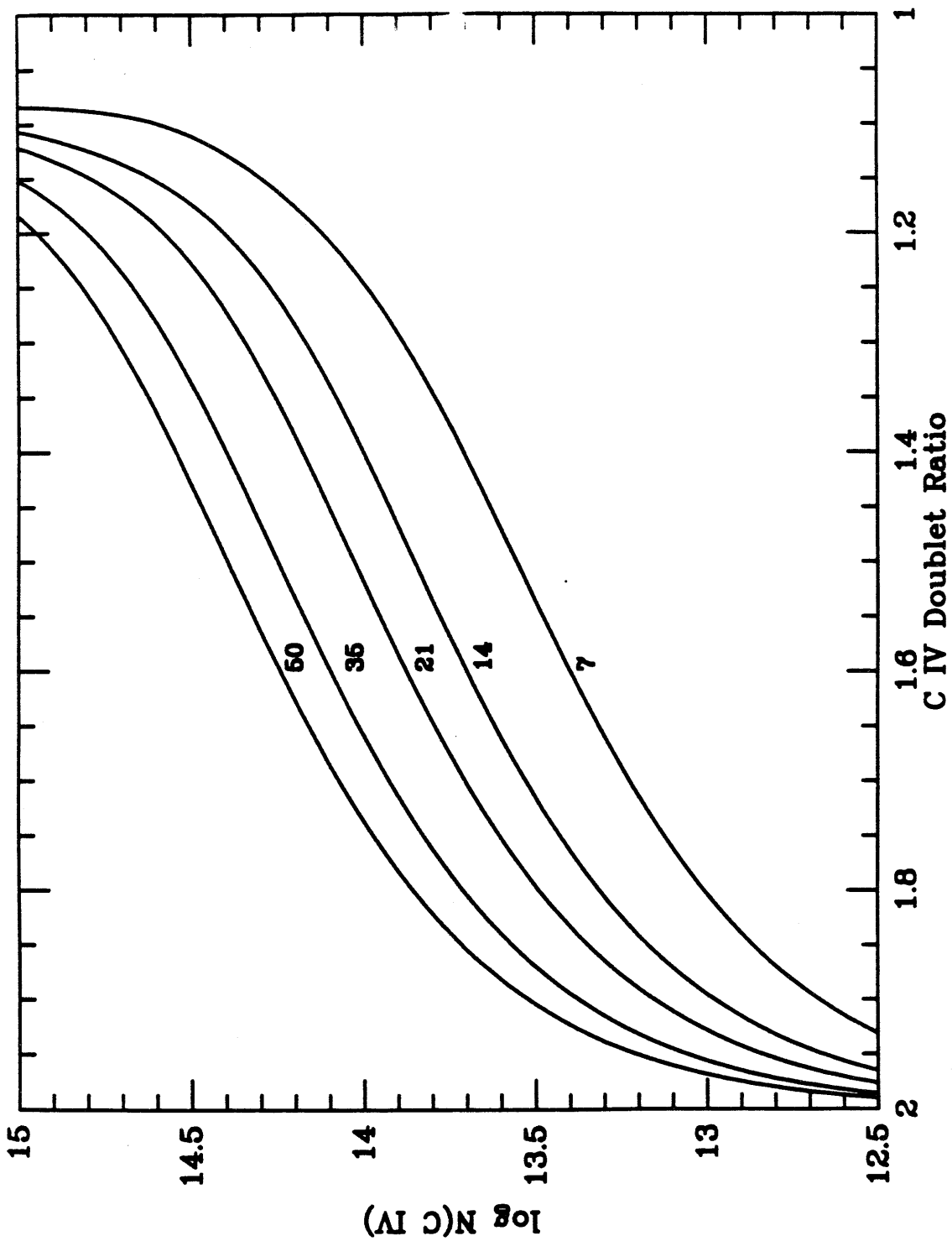
log N(C IV)
15
14.5
14
13.5
13
12.5
C IV Doublet Ratio
1
1.2
1.4
1.6
1.8
2
60
35
21
14
7

Figure 9

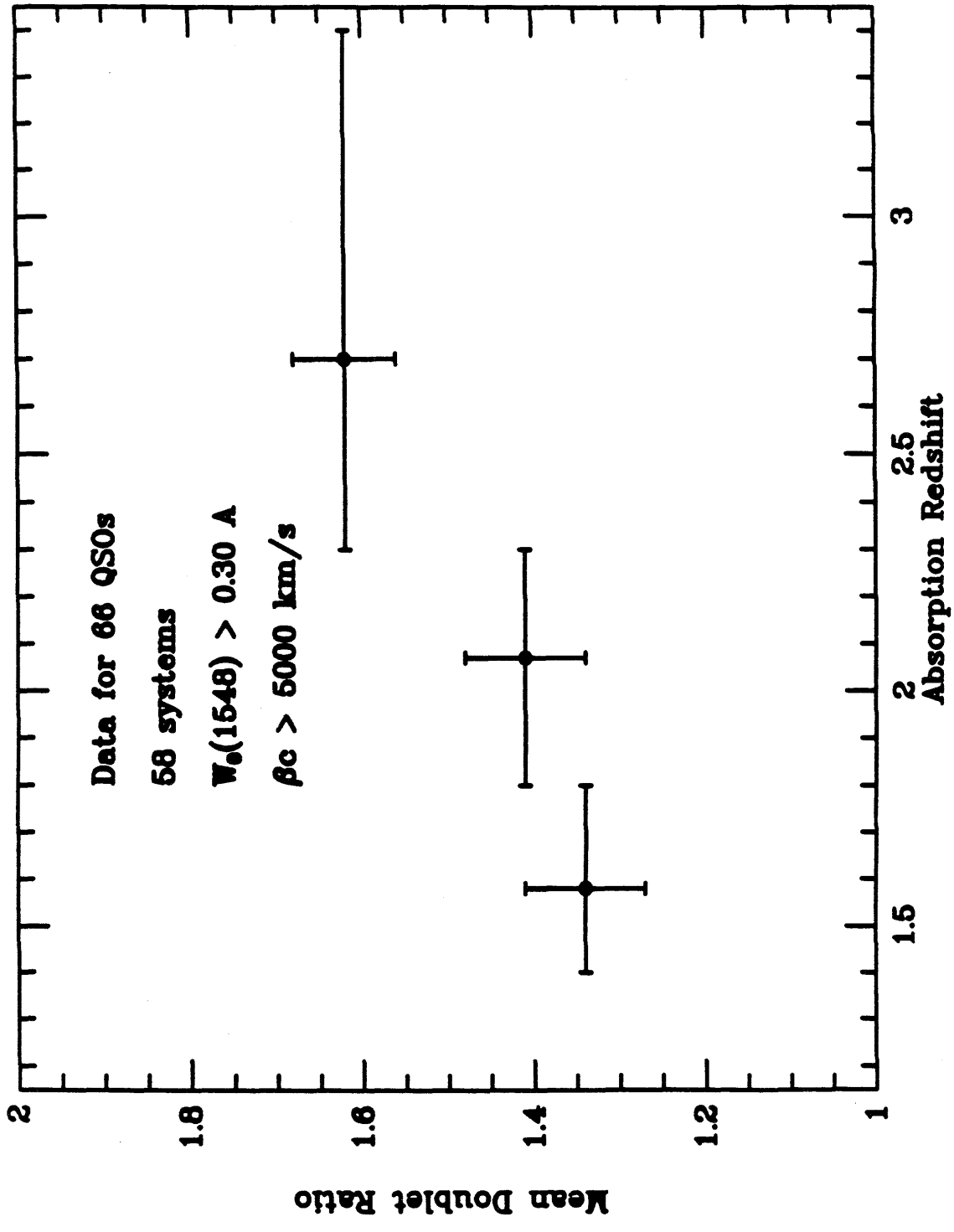
Data for 66 QSOs
58 systems
W_o(1548) > 0.30 A
βc > 5000 km/s
Mean Doublet Ratio
Absorption Redshift
2
1.8
1.6
1.4
1.2
1
1.5
2
2.5
3

Figure 10

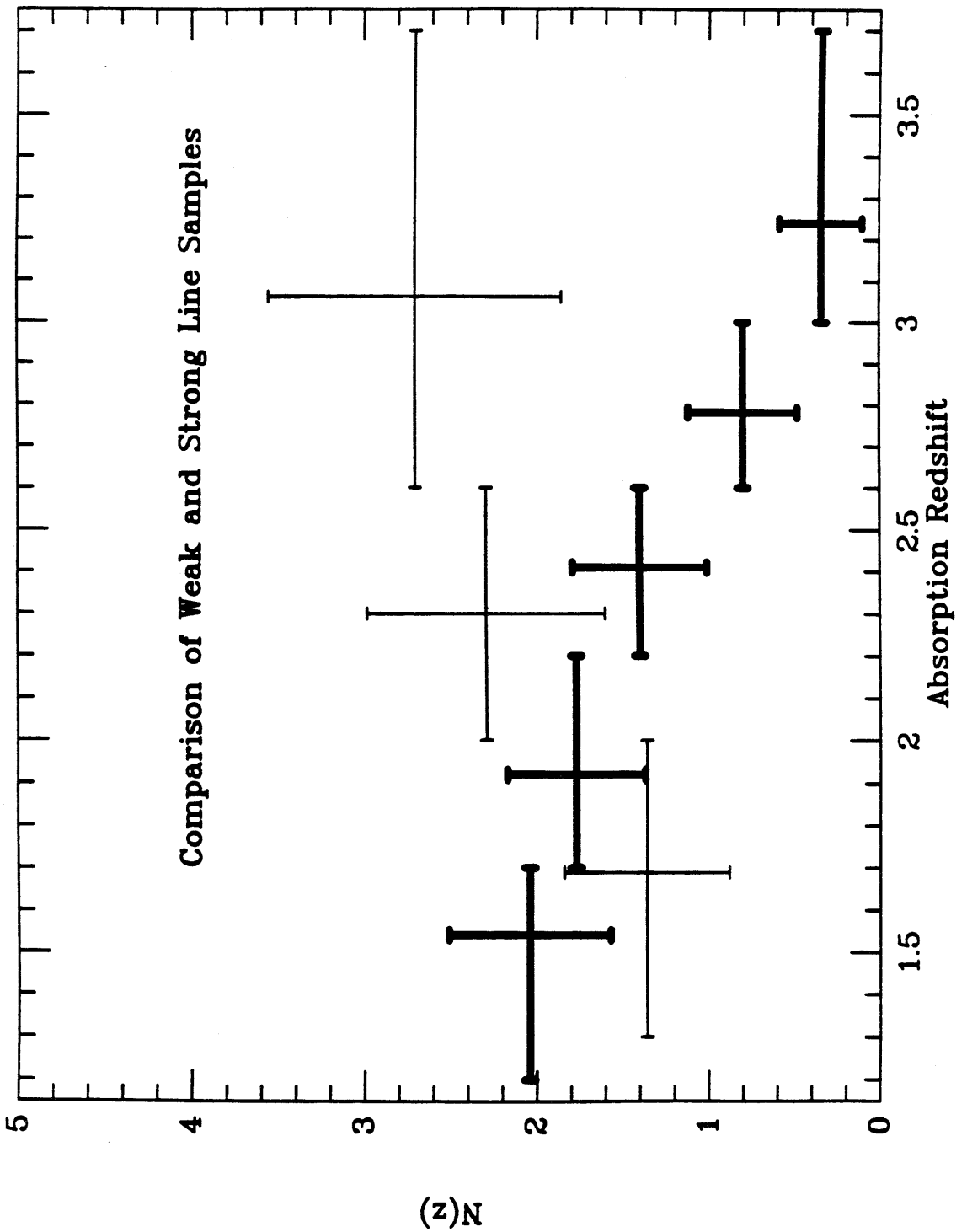
Comparison of Weak and Strong Line Samples
N(z)
Absorption Redshift
0
1
2
3
4
5
1.5
2
2.5
3
3.5

Figure 11

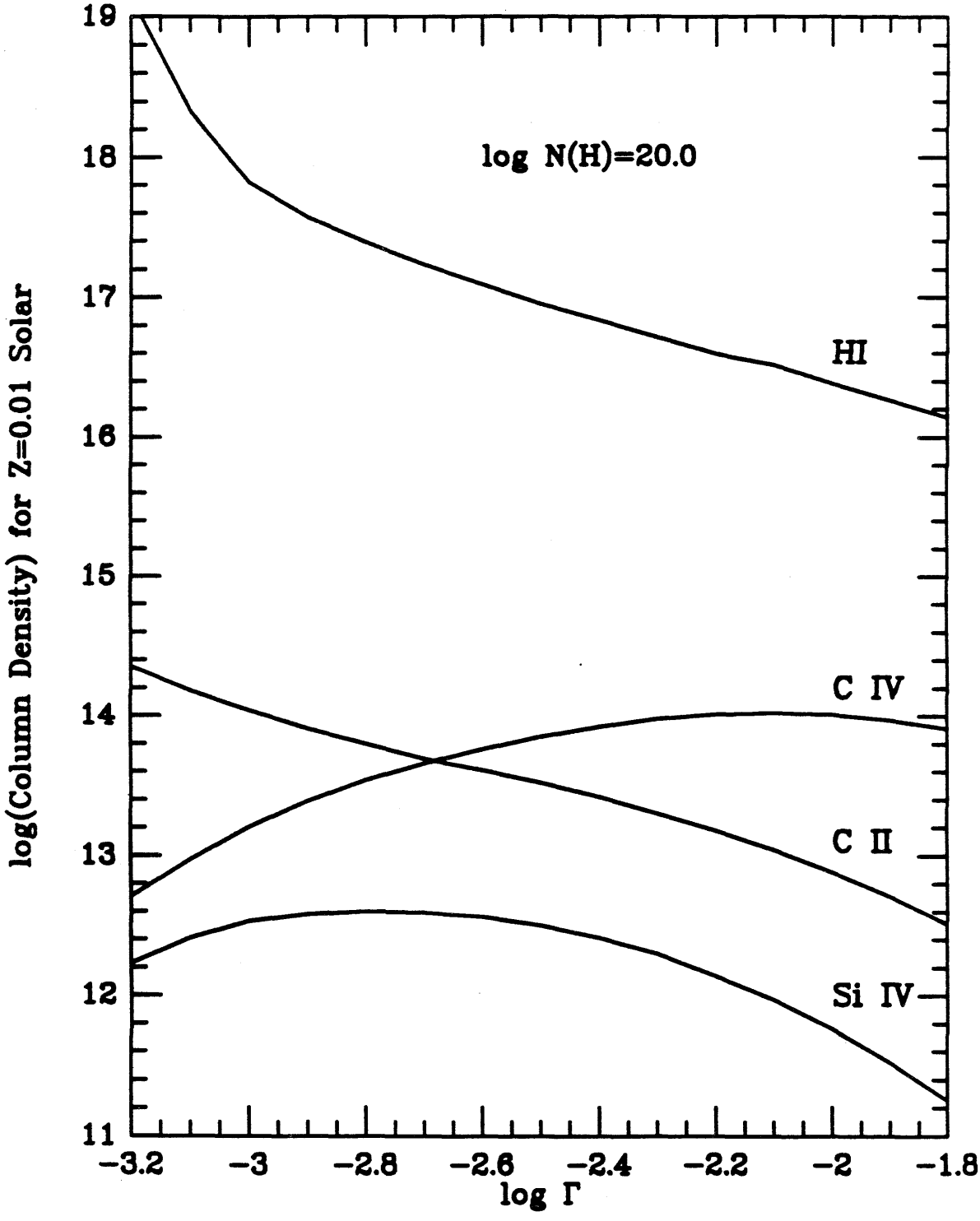
log N(H)=20.0
HI
C IV
C II
Si IV
log(Column Density) for Z=0.01 Solar
log Γ
19
18
17
16
15
14
13
12
11
-3.2
-3
-2.8
-2.6
-2.4
-2.2
-2
-1.8

Chapter 4

QSO HEAVY-ELEMENT ABSORPTION SYSTEMS AND THE NATURE OF THE METAGALACTIC IONIZING FLUX AT HIGH REDSHIFT

CHARLES C. STEIDEL and WALLACE L. W. SARGENT

Palomar Observatory, California Institute of Technology

To appear in *The Astrophysical Journal (Letters)*, **v. 343**

ABSTRACT

Given that the observed QSOs cannot account for the intensity of the metagalactic ultraviolet flux at high redshift, the possible contribution from early–type stars in young or forming galaxies is examined. Given the observed ionization state of heavy element absorption systems in the spectra of QSOs, and using photoionization models, arguments are presented that appear to rule out the possibility that early–type stars in young or forming galaxies are dominating the metagalactic ultraviolet flux up to a redshift of at least $z \sim 4$. Specifically, the stellar contribution cannot be more than comparable to the AGN contribution, and thus it appears that unaccounted–for sources of ionizing radiation that have spectral energy distributions similar to those of AGNs must be present at high redshifts.

Subject headings: cosmology–intergalactic medium–galaxies–quasars

I. INTRODUCTION

The discovery of the absence of a significant decrement across the Lyman α emission line in QSO spectra (Gunn and Peterson 1965) represented the first, and to this day one of the strongest, pieces of evidence supporting the idea that the universe was somehow highly ionized at early epochs. Recent discussions on the ionization of the intergalactic medium and the strength of the metagalactic ionizing flux at high redshifts have raised several important new questions (e.g., Shapiro and Giroux 1987, 1989; Bajtlik, Duncan, and Ostriker 1988; Donahue and Shull 1987; Steidel and Sargent 1987; Bechtold *et al.* 1987; Lin and Phinney 1989; Miralda-Escude and Ostriker 1989). A general conclusion of many of the investigations is that the observed QSOs cannot possibly have produced enough hydrogen-ionizing flux early enough to have ionized the intergalactic medium such that no appreciable Gunn-Peterson discontinuity has been observed to the highest well-observed redshifts. In particular, the very abrupt turnover in the QSO luminosity function at $z \sim 3$ (e.g., Osmer 1982; Koo, Kron, and Cudworth 1986; Schmidt, Schneider, and Gunn 1986) would suggest that rather abrupt changes in the ionization state of the intergalactic gas ought to be observable if indeed the QSOs are responsible for providing the bulk of the ionizing flux. There is no evidence for such changes, based not only on Gunn-Peterson limits, but also on observations of the Lyman α forest of absorption lines (e.g., Murdoch *et al.* 1986) and the Lyman limit and heavy element absorption systems (Sargent, Steidel, and Boksenberg 1989; Sargent, Boksenberg, and Steidel 1988; Steidel 1989a). In fact, there are several pieces of evidence that suggest that the intensity of the metagalactic flux at the hydrogen Lyman limit, $J_{\nu_0} \equiv J_0/10^{-21}$ ergs s^{-1} cm^{-2} Hz^{-1} sr^{-1}, does not change significantly with redshift over the range $1.5 \leq z \leq 3.5$.

The most direct arguments to date are provided by observations of the QSO "proximity effect" (Bajtlik, Duncan, and Ostriker 1988), from which (in principle) a direct determination of J_0 may be obtained by measuring the extent to which the radiation field of a QSO alters the state of ionization of intergalactic clouds in its vicinity. This would be reflected in the number of observed Lyman α forest lines with z_{abs} near the QSO emission redshift; the statistics would be expected to be altered only when the QSO

makes a contribution to the radiation field which is comparable to or greater than that of the general metagalactic ionizing background. Using this method, Bajtlik, Duncan, and Ostriker obtained a value $J_0 \approx 1$, which does not appear to change significantly with redshift over the range $1.8 < z < 3.8$. Formally, this value is really a lower limit on J_0, as pointed out by Miralda–Escude and Ostriker (1989). By the latest estimate, the observed QSOs can account for only about 5% of this *lower limit* (Lin and Phinney 1989). Thus the question arises: What can possibly account for the bulk of the ionizing flux at high redshift? One obvious possibility that has been considered as a source of ionizing photons at high redshift is young star–forming galaxies where the spectra are dominated by early–type stars (e.g., Bechtold *et al.* 1987); another possibility is that many QSOs exist at high redshift, but we cannot observe them for one reason or another (e.g., because they are extinguished by dust (Heisler and Ostriker 1988)). Both of these possibilities are explored in a comprehensive paper by Miralda–Escude and Ostriker (1989); however, we believe that we have a very simple and powerful argument that can be used to rule out galaxies as dominant contributors to the metagalactic ionizing background at high redshift.

II. THE IONIZATION OF THE HEAVY ELEMENT ABSORBERS

Sargent *et al.* (1979) first suggested that the heavy element QSO absorption systems, which are believed to be associated with the halos of intervening galaxies (see, e.g., Sargent, Boksenberg, and Steidel 1988 and references therein), are probably in photoionization equilibrium and are ionized by the integrated UV flux from QSOs. It was argued that early type stars in the disk of the galaxy could not provide enough high–energy photons to produce the observed ionization state in the diffuse halo gas that is seen in absorption. Subsequent studies have also concluded that the QSO absorption line systems are most probably photoionized by the metagalactic UV flux (e.g., Bergeron and Stasinska 1986; Chaffee *et al.* 1986). Consideration of the evolution in number density with redshift of the C IV absorption systems and of the Lyman limit systems (which to a large extent represent the same population of absorbers) has also led to the conclusion that the value of J_0 is probably not changing significantly over the redshift range $1.5 \leq z \leq 3.5$ (Steidel 1989a), in agreement with the "proximity effect" results described above.

During the course of a project designed to determine the chemical abundances and ionization states of the gas in a sample of Lyman limit systems at $z \approx 3$, we have constructed photoionization models using the CLOUDY program (Ferland 1988). Spectroscopic observations of a number of spectral regions in each QSO have been made in order to determine the column densities of HI and of several ionization stages of various heavy elements (C and Si in particular) in each Lyman limit absorption system. Details of the observations and on the construction of the models will be given elsewhere (Steidel 1989b); briefly, the models take as input the observed HI column density and the *shape* of the ionizing continuum, and the output is a grid of models which predicts the relative column densities of the heavy–element ionic species as a function of the ionization parameter $\Gamma \equiv \frac{n_\gamma}{n_H}$, where n_γ is the number density of photons capable of ionizing H incident on the cloud, and n_H is the density of H atoms in the cloud. Thus, for a given value of J_0, the run of Γ represents a varying gas density. The models that we will discuss assume that $\log N(HI) = 17.5$ cm^{-2}, a value which is typical for the sample of Lyman limit systems. We have found that the relative column densities of the observed ions can best be reproduced when the UV spectrum has approximately the shape of a power law with spectral index $\alpha \approx 1.5$, where $f_\nu \propto \nu^{-\alpha}$. This is in good agreement with the results of similar models described by Bergeron and Stasinska (1986), and it corresponds to the typical value of α_{ox} measured for AGNs between optical and soft x–ray wavelengths (e.g., Zamorani *et al.* 1981). The $\alpha = 1.5$ power law models are indistinguishable from those constructed using the "Medium" hardness integrated QSO spectrum calculated by Bechtold *et al.* (1987), and they do not differ significantly from models using a number of other plausible AGN spectral energy distributions (Steidel 1989b). An example of a grid of photoionization models with a power–law ionizing spectrum is given in Figure 1a. The relative column densities, particularly of C II, C III, and C IV, usually require that the ionization parameter be in the range $-2.6 \leq \log\Gamma \leq -2.2$ for systems which are just optically thick in the Lyman continuum. For a value of $J_0 = 1$, this suggests particle densities in the gas of $\sim 10^{-2}$ cm^{-3} and sizes of 1–10 kpc for the gas clouds.

Consider, on the other hand, the possibility that the clouds are ionized by a metagalactic UV spectrum which is dominated by hot stars in young or forming galaxies. We will first examine the limiting case where all of the ionizing photons come from early–type stars

in galaxies. We have adopted a star–forming galaxy spectral energy distribution calculated by Bruzual (1983) based on the model stellar atmospheres of Kurucz (1979) and assuming a Salpeter type initial mass function. Figure 1b shows the grid of photoionization models for a cloud with $\log N(HI) = 17.5$ and the Bruzual young galaxy UV spectral energy distribution. We would emphasize that no initial assumption is made about the *intensity* of the ionizing spectrum – only its shape is assumed. (It should also be pointed out that the assumption that the metagalactic flux has the same spectral shape as the intrinsic spectrum of a single contributing source is not too bad; Lin and Phinney (1989) have shown that because of the effective opacity of the universe to ionizing photons which is due to intervening material, the ionizing photons reaching $z \approx 3$ must for the most part have originated in the range $3.0 < z < 3.17$, and so it is not necessary to make large corrections for the superposition of spectral energy distributions emitted at very different redshifts.) The difference between the grid in Figure 1b and that shown in Figure 1a is striking. For LLSs with $\log N(HI) \approx 17.5$, it is always the case that $N(C\ IV) \geq N(C\ II)$; given this model, this would require that $\log \Gamma > -1.1$, implying a neutral fraction $n(HI)/n(H) < 4 \times 10^{-5}$ and thus a total hydrogen column density $N(H) > 8 \times 10^{21}$ cm^{-2}. In addition, it would predict that $N(C\ III) > 100N(C\ IV)$ and $N(Si\ IV) > 10N(C\ IV)$ (for abundances scaled with solar), in clear contradiction with the observations.

It is no doubt more reasonable to assume that the actual metagalactic flux has contributions from both power–law AGN spectral energy distributions and early–type stars in forming galaxies. In this case, let us assume that the QSOs account for as much as ~15% of the value of J_0, which is the absolute maximum that the *observed* QSOs can contribute at $z \sim 3$ if $J_0 = 1$. [This neglects absorption by high column density, intervening absorption systems, which are likely to decrease the contribution by another factor of ~ 5. (Bechtold *et al.* 1987; Lin and Phinney 1989)] Thus, in this composite model, 85% of the photons with $\lambda = 912$ Å come from young galaxies, while virtually all of the photons beyond ~ 300 Å would come from power–law AGN spectra. The resulting grid of models is shown in Figure 1c. Here the results are much closer to being consistent with the observations; however, there remain some problems. In order to satisfy the criterion $N(C\ IV) \geq N(C\ II)$, we must have $\log \Gamma \geq -2$. Moreover, although C III λ977 falls in the Lyman α forest and is therefore

difficult to observe, the observations suggest that, in general, $N(C\ III) \leq 10N(C\ IV)$, requiring $\log \Gamma \approx -1.5$. The composite model also requires the column densities of Si III and Si IV to be stronger relative to $N(C\ IV)$ than is observed. It is interesting to note that if $\Gamma \sim -1.5$, the derived carbon abundance for the halo clouds at $z \sim 3$ would be $\sim 10^{-3}$ of the solar abundance. Furthermore, if $J_0 = 1$, then the implied size of the clouds is ~ 1 Mpc, which seems highly unlikely.

Given that we have seen that the UV radiation from hot stars in young galaxies is probably not *dominating* J_0, it is of interest to find the ratio J_0(galaxies)/J_0(AGNs) at which the photoionization models would be consistent with the observations. Figure 1d shows the photoionization results for a final model for which it is assumed that the AGNs and the early–type stars make equal contributions to J_0. In terms of the ionization of C, which is better constrained by the observations than that of Si, this model is virtually indistinguishable from the power–law–only model shown in Figure 1a. The only significant difference that would be observable at $z \sim 3$ is a slightly enhanced population of Si III relative to C IV. This would be difficult to sort out observationally because the Si III λ1206 absorption line invariably falls in the Lyman α forest and thus precise column density measurements are not usually possible. Thus we deduce on the basis of the above considerations that early–type stars in young galaxies can contribute at most roughly the same number of photons at the Lyman limit as AGNs with power–law spectra. Whether such a large stellar contribution is feasible on other grounds is beyond the scope of this *Letter.*

III. CONCLUSIONS

Clearly, if the estimates of the integrated contribution to J_0 by the observed QSOs are correct (i.e., roughly 5% of 10^{-21} or $\sim 5 \times 10^{-23}$), and the contribution from early–type stars in young galaxies is at most comparable to the AGN contribution, then in order to achieve agreement with the proximity effect results, one needs to find *at least a factor of 10 more UV radiation at high redshift from some other source, and it appears that this source must have a spectral energy distribution that resembles a power–law, AGN–like spectrum.* One possibility is that the luminosity function for QSOs and AGNs at the faint end has a

considerably steeper slope at high redshift than is observed locally.

Assuming that unaccounted–for AGNs are providing the remainder of the metagalactic UV flux that is inferred to be present at high redshift, a strong prediction resulting from the above arguments would be that if there *is* an observable redshift at which the AGNs have not yet turned on, or where their contribution is diminished significantly, the ionization state of the heavy–element systems will be very different from what has been seen to the highest currently–observed redshifts. Specifically, heavy–element absorbers ionized by a predominantly stellar energy distribution will be dominated by low–ionization species [e.g., $N(C\ II) > N(C\ IV)$, $N(Si\ IV) > N(C\ IV)$], even when they are optically thin in HI. Such a change in the general character of the heavy–element redshifts has not been observed so far up to a redshift of at least $z \sim 4$.

We are grateful to Z. Lin, S. Phinney, J. Miralda–Escude, and J. Ostriker for early copies of their preprints and for stimulating discussions. We also thank G. Ferland for providing a copy of his CLOUDY program, and for comments on an earlier draft of this paper.

REFERENCES

Bajtlik, S., Duncan, R. C., and Ostriker, J. P. 1988, *Ap. J.*, **327**, 570.

Bechtold, J., Weymann, R. J., Lin, Z., and Malkan, M. A. 1987, *Ap. J.*, **315**, 180.

Bergeron, J., and Stasinska, G. 1986, *Astr. Ap.*, **169**, 1.

Bruzual, G. 1983, *Ap. J. Suppl.*, **53**, 497.

Chaffee, F. H., Foltz, C. B., Bechtold, J., and Weymann, R. J. 1986, *Ap. J.*, **301**, 116.

Donahue, M. J., and Shull, J. M. 1987, *Ap. J. (Letters)*, **313**, L13.

Ferland, G. J. 1988, OSU Astronomy Department Internal Report, 87-001.

Gunn, J. E., and Peterson, B. A. 1965, *Ap. J.*, **142**, 1633.

Heisler, J., and Ostriker, J. P. 1988, *Ap. J.*, **332**, 543.

Koo, D. C., Kron, R. G., and Cudworth, K. M. 1986, *Pub. A.S.P.*, **98**, 285.

Kurucz, R. L. 1979, *Ap. J. Suppl.*, **40**, 1.

Lin, Z., and Phinney, E. S. 1989, preprint.

Miralda–Escude, J., and Ostriker, J. P. 1989, preprint.

Murdoch, H. S., Hunstead, R. W., Pettini, M., and Blades, J. C. 1986, *Ap. J.*, **309**, 19.

Osmer, P. 1982, *Ap. J.*, **253**, 28.

Sargent, W. L. W., Boksenberg, A., and Steidel, C. C. 1988, *Ap. J. Suppl.*, **68**, 539.

Sargent, W. L. W., Steidel, C. C., and Boksenberg, A. 1989, *Ap. J. Suppl.*, **69**, 703.

Sargent, W. L. W., Young, P. J., Boksenberg, A., Carswell, R. F., and Whelan, J. A. J. 1979, *Ap. J.*, **230**, 49.

Schmidt, M., Schneider, D. P., and Gunn, J. E. 1986, *Ap. J.*, **310**, 518 .

Shapiro, P. R., and Giroux, M. L. 1987, *Ap. J. (Letters)*, **321**, L107.

Shapiro, P. R., and Giroux, M. L. 1989, in *The Epoch of Galaxy Formation*, ed. C. S. Frenk (Dordrecht:Reidel), in press.

Steidel, C. C., and Sargent, W. L. W. 1987, *Ap. J. (Letters)*, **313**, L11.

Steidel, C. C. 1989a, *Ap. J. Suppl.*, submitted.

Steidel, C. C. 1989b, in preparation.

Zamorani, G., Henry, J. P., Maccacaro, T., Tananbaum, H., Soltan, A., and Avni, Y. 1981, *Ap. J.*, **245**, 357.

FIGURE CAPTIONS

FIG 1.—Photoionization model grids for a cloud having $\log N(HI) = 17.5$. The ordinate is the relative column density of the various ions for abundances scaled with the solar values, and the abscissa is the ionization parameter. The assumed forms for the ionizing continuum are: a) Power-law, with $f_\nu \propto \nu^{-1.5}$, b) Bruzual "young galaxy" spectrum, c) Power-law (AGN) spectrum plus young galaxy spectrum, where $f_\nu^{gal}/f_\nu^{AGN} = 5$ at 912 Å, d) Power-law (AGN) spectrum plus young galaxy spectrum, where $f_\nu^{gal}/f_\nu^{AGN} = 1$ at 912 Å.

Figure 1

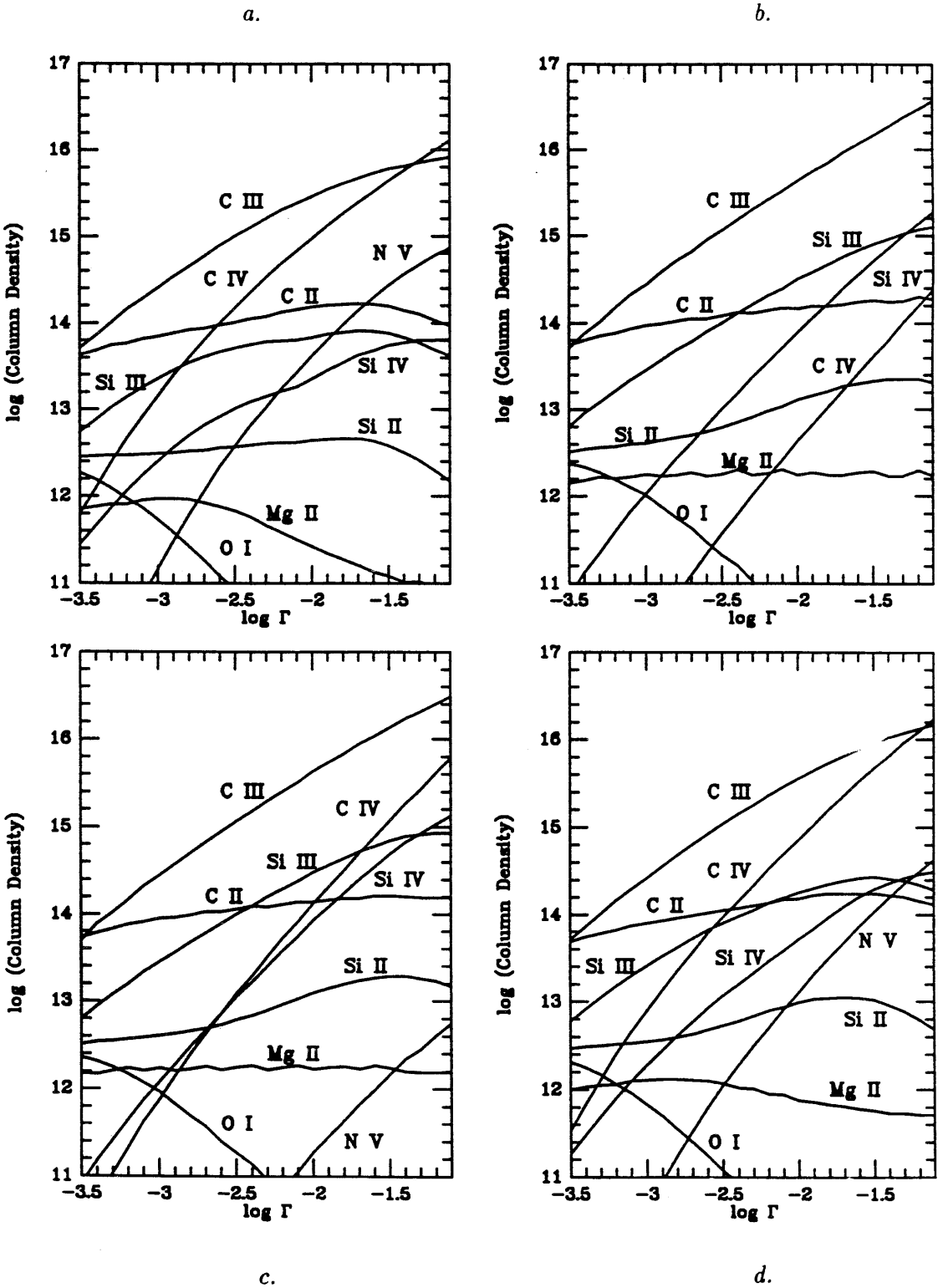
a.
b.
c.
d.
log (Column Density)
log Γ
C III
C IV
C II
N V
Si III
Si IV
Si II
Mg II
O I

Chapter 5

THE PROPERTIES OF LYMAN LIMIT ABSORBING CLOUDS AT $z = 3$: PHYSICAL CONDITIONS IN THE EXTENDED GASEOUS HALOS OF HIGH REDSHIFT GALAXIES

CHARLES C. STEIDEL

Palomar Observatory, California Institute of Technology

Submitted to *The Astrophysical Journal Supplement Series*

ABSTRACT

A detailed study of 8 known Lyman limit absorption systems with $2.90 \leq z_{abs} \leq 3.23$ has been undertaken in order to provide an unbiased preliminary survey of the properties of heavy–element absorption systems at very high redshift. Selected spectral regions for each QSO have been observed at 35–80 km s^{-1}resolution and high S/N so that the column densities of H I and associated ions of heavy elements might be determined. The H I column densities are in the range $17.0 \leq \log N(H\ I) \leq 19.3$. The column density measurements have been used in conjunction with photoionization models in order to estimate the physical parameters of the clouds or cloud ensembles responsible for the Lyman discontinuities. The heavy element abundances are in the range $-3.0 \leq [M/H] \leq -1.5$, and the relative abundances of C, O, and Si, although uncertain, appear to be consistent with a uniform depletion relative to the solar values. The particle density in the clouds is in the range $0.01 \lesssim n_H \lesssim 0.1$, and the corresponding cloud sizes and masses are inferred to be in the range $1 \leq D_c \leq 15$ kpc and $10^6 \leq M_c \leq 10^9\ M_\odot$, respectively. Such parameters would be expected on theoretical grounds for clouds that condensed in extended ($\gtrsim$ 100 kpc) gaseous halos during the early evolution of normal galaxies. A considerable fraction of the inferred visible mass of present–day galaxies was probably in the form of these diffuse clouds at the epoch corresponding to $z \approx 3$; thus, they have probably played an important role in the evolution of galaxies with time. The possibility that the heavy–element absorbing clouds and the "Lyman α forest" clouds have a common origin (but evolve differently because of their environment) is discussed.

Subject headings: cosmology–galaxies–quasars

I. INTRODUCTION

Narrow line absorbers that have a sufficiently large column density of neutral hydrogen ($N(HI) > 10^{17}$ cm^{-2}) to be optically thick to Lyman continuum photons are referred to as Lyman limit systems (LLSs). The signature of an LLS in the spectrum of a QSO is a marked discontinuity in the QSO continuum shortward of 912 Å in the rest frame of the absorber, often reducing the amount of observed flux to zero. Thus, LLSs may be discovered fairly easily in relatively low–dispersion, low–S/N spectra over a very wide range of redshifts; with IUE, LLSs with $0.4 \leq z_{abs} \leq 2.2$ can be discovered, and those with $2.5 \leq z_{abs} \leq 4.7$ are observable with ground–based telescopes. The incidence of LLSs has been studied recently by Tytler (1982), Bechtold *et al.* (1984), Lanzetta (1988), and Sargent, Steidel, and Boksenberg (1989a; hereinafter SSB), and the LLSs have been shown to be consistent with a population of cosmologically distributed, intervening absorbers. In addition, the comoving number of LLSs per unit redshift is found to be consistent with non–evolving absorbers over the entire redshift range $0.4 \leq z \leq 4.1$.

There is a growing body of evidence that the LLSs are associated with the halos of intervening galaxies (at most a small percentage of LLSs can be associated with the Lyman α forest of absorbers (SSB)); that is, the LLSs represent essentially the same population of absorbers as the systems detected by means of absorption lines of heavy–element species, in particular the Mg II $\lambda\lambda$2796, 2803 and C IV $\lambda\lambda$1548, 1550 doublets. However, recent large surveys for the heavy–element systems (Tytler 1987; Lanzetta, Turnshek, and Wolfe 1987; Sargent, Boksenberg, and Steidel 1988; SSB; Steidel 1989) have indicated that the number of systems detected on the basis of heavy–element lines satisfying a given threshold in rest equivalent width is *not* consistent with no evolution in the properties of the absorbers. The most significant results are for the C IV absorption systems, where the comoving number of detected systems decreases (with increasing redshift) by roughly a factor of $\sim 6 - 10$ (depending on the value of q_0) over the redshift range $1.5 \leq z \leq 3.5$ (Steidel 1989). This change is interpreted as evolution in the typical C IV column density of the clouds, suggesting either significant changes in the ionization state of the gas with redshift, or actual chemical enrichment in the gas over time, or both.

In any case, now that statistical results are available describing the evolution in number of the various types of QSO absorption line systems, and because the heavy element absorption systems are probably associated with sites where galaxies have formed or are in the process of forming, it is a crucial next step to try to understand the physical properties of the gas, and the processes that are controlling the observed evolution of the gas over time. The hope is that with sufficient understanding of what factors are influencing the evolution, the QSO absorption lines may be used to study directly the evolution of galaxies at redshifts inaccessible to any other means of observation.

Thus, the work described in this paper has been undertaken as a preliminary effort to determine the chemical abundances and other physical parameters of the gas clouds giving rise to the high–redshift heavy–element absorption systems. By selecting absorption systems for more detailed study solely on the basis of their HI column density, there is no bias involved in undertaking an abundance study. Also, by choosing systems on the basis of their Lyman continuum opacity, one avoids any bias involving the velocity dispersion in the absorbing gas. The LLSs turn out to be ideal systems for detailed study because there tend to be observable lines of several different ionization stages (necessary for an accurate determination of the ionization state of the absorber), and many of the heavy element lines of abundant ions are not badly saturated, as they invariably are in damped Lyman α systems. Moreover, it is quite likely that the LLSs are providing information on quite a different component of the gas associated with high–redshift galaxies than that of the much–rarer damped Lyman α systems.

In addition, it is extremely important to study the nature of the LLSs in their own right; if LLSs can be found that have very low heavy–element abundance (in which case they may be part of the high HI column density tail of the Lyman α forest population), then placing sensitive upper limits on the abundance would be invaluable to an understanding of the nature of the Lyman α clouds. Also, detailed study of a sample of LLSs at a particular redshift (in this case, $z_{LLS} \approx 3$) can be used to place constraints on the nature of the metagalactic ionizing UV radiation field at high redshift, which is very important to theories of galaxy formation and the evolution of AGNs.

The observations and data reductions will be described in §II; short summaries of the

identified absorption redshifts in the new spectra follow in §III. A description of the methods used for measuring the HI and heavy element column densities associated with the LLSs will be given in §IV. §V and §VI contain a detailed discussion of the use of photoionization models in the determination of chemical abundances and ionization states for the LLSs. A discussion of the results and their implications follow in §VII, and the principal conclusions are summarized in §VIII.

II. OBSERVATIONS AND DATA REDUCTION

a) Selection of Objects

Using the sample of high–redshift ($z_{abs} > 2.5$) Lyman limit absorption systems found in the recently completed survey of SSB, QSOs were selected for observation based on the following criteria:

1. The LLSs are in the redshift range $2.9 \leq z_{abs} \leq 3.2$, both for the convenience of the observations and so that the properties of the clouds at similar redshift may be compared.

2. The red continuum magnitude of the QSO is brighter than 18.5, so that spectra of high S/N may be obtained in a reasonable amount of time.

3. The emission redshift of the QSO is not so high relative to the z_{LLS} that the C II λ1334 line falls in the Lyman α forest of absorption lines. It is important for the purposes of constraining the ionization state of the gas that this line can be measured in an uncrowded region of the spectrum.

4. The absorption redshift of the LLS is well separated from the emission redshift of the QSO ($c\Delta z/(1+z) > 5000$ km s^{-1}), in order to exclude material that is possibly associated with the QSO or that may be influenced by the ionizing radiation from the QSO.

5. The sample is selected without regard to the apparent strength of heavy–element lines which have been detected in the low–resolution spectra obtained as part of the LLS survey. Once criteria 1–4 were satisfied, only the position of the QSO in the sky at the times of the observing runs influenced whether or not a given object was actually observed. There were 14 objects that satisfied criteria 1–4; complete data were obtained for 7 of these; some data were obtained for another (PKS 2126-158) in order to complement already existing

spectra (the data and analysis for this QSO will be published elsewhere (Sargent, Steidel, and Boksenberg 1989b)), and incomplete data were obtained for Q0642+6654. Only the complete data for the total of 8 objects will be discussed in the present paper.

The criteria outlined above result in what we believe to be an unbiased sample of absorption systems with $N(HI) \geq 2.4 \times 10^{17}$ cm^{-2}.

b) Observations

All of the spectra described in this paper were obtained using the Palomar 5-meter Hale telescope and the Double Spectrograph. The data were obtained during the course of three observing runs, in 1988 February, 1988 October, and 1989 January. A complete journal of observations is presented in Table 1.

In general, 4 spectral regions were observed per object, and the exact wavelength range of each of the intervals varied from QSO to QSO, depending on the absorption redshift of the Lyman limit system of interest. The objective was to obtain spectra that would include the regions containing the expected positions of the following absorption lines at the redshift of the cloud giving rise to a Lyman discontinuity:

Region I: The Lyman continuum, the lower Lyman series absorption lines (usually Ly γ and below), and C III λ977.

Region II: Lyman α, Si III λ1206, N V $\lambda\lambda$1238, 1242, and in some cases Si II λ1260.

Region III: C II λ1334, Si IV $\lambda\lambda$1393, 1402, and in some cases O I λ1302, Si II λ1304.

Region IV: Si II λ1526, C IV $\lambda\lambda$1548, 1550, and in some cases Fe II λ1608.

Using the Double Spectrograph, it was possible to obtain spectra of two of these regions simultaneously; i.e., Region I or II could be recorded on the blue side of the spectrograph, while Region III or Region IV was recorded on the red side of the spectrograph. Thus, for a given object, the required observations could be accomplished using two different observational setups. Both sides of the Double Spectrograph use Texas Instruments 800 X 800 CCDs. Most of the observations were made using 1200 line/mm gratings in first order, blazed at λ5000 and λ7100 for the blue and red sides, respectively. A dichroic filter was used to divert light with $\lambda < 5200$ Å into the blue camera and $\lambda > 5200$ Å into the red camera. In combination with the 1″ slit, which was used for all of the observations, the

spectral resolution was $\approx$ 1.1 Å for the blue camera and $\approx$ 1.6 Å for the red camera. [An additional blue spectrum was obtained of the spectral region centered on the wavelength of the Lyman α absorption line at the redshift of the LLS for two of the brighter objects in the sample (Q0956+1217 and Q0636+6801). For these spectra, a 1200 line/mm grating blazed at λ9400 was used in second order, giving a spectral resolution of $\sim$ 0.6 Å FWHM.]

Individual exposure times were usually 3600 seconds, and the slit was always rotated to the parallactic angle appropriate to the midpoint of the exposure in order to reduce light losses caused by atmospheric dispersion. A spectrophotometric standard star was observed at the beginning and end of each instrumental setup (usually a given set of grating angles was used for 2 to 4 hours before being changed) so that the response function of the detectors could be determined for each observed wavelength range. Individual exposures were also bracketed by Fe–Ar hollow cathode + Ne comparison lamp exposures for the purposes of wavelength calibration.

The data were reduced using a method similar to that described by Steidel (1989). After each separate exposure was reduced and the wavelength solution was applied (typical residuals in the wavelength solutions were $\sim$ 0.05 Å on the blue side and $\sim$ 0.07 Å on the red side), observations of the same spectral region in a given QSO were rebinned to a common wavelength scale and merged, weighting by the variance spectrum which was maintained during the reduction process. The quality of the individual exposures varied considerably because of seeing fluctuations during the course of the observations. The resulting spectra, along with the 1σ noise spectra, are plotted on the same axes in Figures 1–7.

c) Absorption Lines

Absorption lines were measured using a method identical to that used by SBS, except that the actual noise spectra calculated during the reduction process were used in estimating the significance of features, rather than estimates of the noise based on the nearby spectral regions. For each spectrum in Figures 1–7, line lists were produced containing all lines exceeding 5σ in equivalent width. These lists are presented in Tables 2–8. Also tabulated are the uncertainties in the wavelengths and equivalent widths for each line, as well as the signal–to–noise ratio per channel over the range of spectrum spanned by each measured

line. Thus, for weak lines, S/N represents the true continuum S/N per channel. All of the wavelengths are vacuum heliocentric values.

As usual, apparently blended lines were separated wherever possible into individual components. The usual warnings about the uncertainties in measuring the equivalent widths and positions of lines in the Lyman α forest apply. Although we are particularly interested in the absorption system which gives rise to the observed Lyman discontinuity in the spectrum of each object, in the interest of completeness we will discuss each identified absorption system individually in §III.

III. DISCUSSION OF INDIVIDUAL OBJECTS

Short descriptions of the overall spectra for all 7 of the QSOs are found in SSB, as are absorption line identifications based on the low–resolution spectra. In this section, we discuss the redshifts identified in the new spectra, making comparisons (where applicable) to what was found by SSB.

a) Q0029+0722

As noted by SSB, the spectrum of this object has broad features that are reminiscent of BAL objects; however, neither of the very strong C IV complexes results in a corresponding Lyman discontinuity (see Figure 1), indicating very highly ionized gas, as would be expected for ejected material. The following absorption redshifts have been identified; all but the last two we regard as being due to intervening material:

z_{abs} = 1.8282: While only 3 lines from this system fall longward of the Lyman α emission line (Fe II λ2344, Fe II λ2374, and Al III λ1862), the identification is undoubtedly correct. This system was not identified in the low–resolution spectrum of SSB.

z_{abs} = 2.4063: As will be discussed in §IV, this redshift is based solely on a relatively weak C IV doublet which happens to coincide closely with the expected positions of O I λ1302 and Si II λ1304 associated with the Lyman limit system. Thus, the identification must be regarded as tentative.

z_{abs} = 2.4375: There is some evidence for structure in the C IV doublet identified with this redshift. In addition to C IV, identifications of lines of Si IV and Si II have been made,

although all of these lie in the Lyman α forest. Unfortunately, none of the observed spectral regions cover the expected wavelength of any of the H Lyman series lines for this redshift. The C IV doublet was identified by SSB.

$z_{abs} = 2.6500$: Doublets of C IV and Si IV are identified, although the latter is in the Lyman α forest; in addition, possible lines of C II λ1334 and Si II λ1304 are found.

$z_{abs} = 3.0488$: This absorption system is the one responsible for the Lyman limit system found by SSB (they suggested that $z_{LLS} \approx 3.059$ on the basis of the low–resolution spectrum). No associated C IV doublet was found by SSB; in the new spectrum, we find a possible identification of the doublet, although the spectral region is rather badly affected by confusion because of poor night sky subtraction. This could explain the unphysical doublet ratio. Several low–ionization lines are identified (C II λ1334, Si II λ1526, O I λ1302, and Si II λ1304), as well as C III λ977, Si III λ1206, and several Lyman series lines, including a very strong Lyman α line. A detailed discussion of the system will be made in §IV. The presence of the low–ionization species indicates that this system cannot be associated with the QSO, and is thus a normal "intervening" system.

$z_{abs} \approx 3.12$: As noted by SSB, this broad complex probably has its origin in ejected material; this hypothesis is supported by probable N V and O VI complexes in the low–resolution SSB spectrum. Identification of individual components would be quite arbitrary; thus, it has not been attempted. There is no evidence for strong Lyman α absorption from this redshift.

$z_{abs} = 3.1943$, 3.1977: A strong C IV complex defines this redshift. The lack of identified Lyman α lines and the presence of the N V doublets suggests a very high ionization state for the system; for this reason, we consider it likely that the system arises in material ejected from the QSO.

b) Q0256+0000

In addition to the low–resolution spectrum in SSB, this object has been studied as part of a high–redshift survey for C IV absorption by Steidel (1989). While the spectrum presented by Steidel (1989) is of somewhat higher resolution than the new observations, the signal–to–noise ratio was considerably lower. It should be noted that this object was

incorrectly called Q0256−000 by both SSB and Steidel (1989). The following absorption redshifts were found on the basis of the spectra shown in Figure 2:

z_{abs} = 1.1984: Along with the very strong Mg II doublet, 5 lines of Fe II are also observed at this redshift. The system was previously identified by both SBS and Steidel (1989).

z_{abs} = 3.0175: Although the C IV λ1550 line from this system did not qualify for the linelist, the identification of 4 Lyman series lines as well as C III λ977 strengthens the case for its being real.

z_{abs} = 3.0843: Although this system is certainly real on the basis of the Lyman series absorption lines and the Lyman discontinuity (it was estimated to have $z_{abs} \approx 3.090$ by SSB), the only identified feature longward of Lyman α emission is the C IV doublet, which is probably affected by the complicated night sky features in the same spectral region. As we shall see in §IV, this redshift may actually have structure over quite a large range of velocities.

z_{abs} = 3.1976: The case for this redshift relies on a rather ambiguous looking weak C IV doublet. The line identified at C IV λ1548 was found by Steidel (1989), although the λ1550 line was not (it is too weak to have exceeded the 5σ criterion in that spectrum). There is a moderately strong Lyman α line that may be associated with this redshift.

c) Q0301−0035

The following absorption redshifts have been identified based on the new spectra:

z_{abs} = −0.0002: This is a clear case of galactic Na I absorption; the interstellar cloud has a heliocentric velocity of $\sim$ 60 km s^{-1}. In the low-resolution spectrum of SSB, these features were blended and the line remained unidentified.

z_{abs} = 2.4292: There is evidence for some structure in the rather weak C IV doublet. The features were identified in the SSB spectrum, but the equivalent widths were substantially overestimated because of uncertainties in the continuum level of the low resolution spectrum. In addition to C IV, Fe II λ1608, C II λ1334, and a possible Si IV doublet are identified.

z_{abs} = 2.7235: Although the expected wavelength of the C IV doublet for this redshift

is not covered by any of the new spectra, the SSB spectrum shows a very strong doublet. Strong lines of Si IV, C II λ1334, Si II λ1304, Si II λ1260, and Lyman β are found in the new spectra, along with a rather weak Al II λ1670.

z_{abs} = 2.9400: SSB suggested that this redshift is giving rise to the observed Lyman discontinuity, which they measured to be at $z_{abs} \approx 2.947$. In the new spectra, we find several lines of the Lyman series, including a strong Lyman α, along with C IV and Si IV doublets (the λ1402 line is probably blended with a line from another redshift, as it is markedly broader than the λ1393 line), C II λ1334, Si III λ1206, and C III λ977. This redshift will be discussed in more detail in §IV.

z_{abs} = 2.9572: The redshift agreement between the two lines identified as the C IV doublet is not particularly good; however, there is a strong Lyman α line at $z_{abs} = 2.9571$, and possibly some lower Lyman series lines as well. Several other identifications are suggested for this redshift, but again the wavelength agreement is not particularly good.

d) Q0636+6801

As noted by SSB, this QSO is much brighter [m($\lambda_0$1450)=16.4] than its published magnitude of $m_V \approx 19$. It was therefore possible to obtain spectra of very high S/N. The following redshifts are found on the basis of the new spectra:

z_{abs} = 0.0000: This is another case of galactic Na I absorption. From the measured wavelengths, the gas cloud has a heliocentric velocity of < 10 km s^{-1}. These lines were erroneously identified as a C IV doublet in SSB; at 6 Å resolution, the lines were not resolved adequately and thus the true separation was impossible to judge.

z_{abs} = 2.3112: Only a C IV doublet and Al II λ1670 define this redshift; none of the expected Lyman series lines fall in any of the observed regions. This redshift was not found by SSB.

z_{abs} = 2.4749: An unambiguous C IV doublet defines this system; again, no expected lines of H I fall in the observed regions. This redshift was identified by SSB, although the equivalent widths were overestimated (the C IV doublets are not well resolved in the spectra with $\sim$ 6 Å resolution.)

z_{abs} = 2.8683 : Although both lines of the C IV doublet did not qualify for the line list

(only the λ1548 line is stronger than 5σ), several Lyman series lines strengthen the case for this redshift.

$z_{abs} = 2.8920$: A weak C IV doublet, several Lyman series lines (including a strong Lyman α), and C III λ977 are found for this redshift. The C IV λ1548 line was detected by SSB, but remained unidentified. This redshift is separated from the system giving rise to the Lyman discontinuity by only ~ 900 km s^{-1}.

$z_{abs} = 2.9040$: This system, which is associated with the Lyman limit (SSB suggested $z_{LLS} \approx 2.909$), has obvious structure in C IV and Si IV even at ~ 80 km s^{-1}resolution. Many other lines are also identified; the redshift will be discussed in detail in §IV

$z_{abs} = 3.0174$: A relatively weak C IV doublet and C III λ977 are identified for this redshift. Although Lyman α falls just out of the range of our spectra, we find a probable Lyman δ line. The C IV doublet was found by SSB, with rather good agreement in measured equivalent widths.

e) Q0956+1217

On the basis of the low–resolution data obtained by SSB, the Lyman limit system in the spectrum of this QSO was estimated to be at $z_{LLS} \approx 3.10$. However, the new spectrum at ~ 1.1 Å resolution (see Figure 5) shows that the system resulting in the obvious Lyman discontinuity is in fact at $z_{LLS} \approx 3.22$. There is clearly residual flux in the Lyman continuum until another system with $z_{LLS} \approx 3.11$ reduces the flux to zero at ~ 3750 Å. The following absorption redshifts have been identified in the new spectra:

$z_{abs} = 0.0456$: If the identification is correct, the Na I doublet has a heliocentric velocity of $\sim 13,700$ km s^{-1}, suggesting that the absorption may arise in a relatively nearby galaxy along the line of sight to the QSO. The lines are too weak for the identification to be certain, but they do not correspond to the expected positions of any line from another known redshift in the spectrum. A search of the Palomar Sky Survey print in the vicinity of Q0956+1217 shows no obvious bright galaxy within 1′.

$z_{abs} = 2.3104$: The expected position of the C IV doublet for this redshift is within the Lyman α forest; however, there is a weak Al II λ1670 line longward of Lyman α emission, and a strong Lyman α line with a measured redshift of $z_{abs} = 2.3099$. The redshift cannot

be regarded as certain.

z_{abs} = 2.7169: A weak C IV doublet, Al II λ1670, and possible C II λ1334 define this redshift. All of the expected Lyman series lines fall outside of the observed wavelength range (Lyman β would be expected near 3810 Å, which is shortward of the Lyman edge at z_{abs} = 3.223); thus, we regard the system as probable, but not certain.

z_{abs} = 2.7261: The reality of this system is somewhat doubtful, as the redshift agreement between the two putative C IV lines is not particularly good, and the lines are very weak.

z_{abs} = 2.8320: This redshift is defined by another very weak C IV doublet, but the redshift agreement between the two C IV lines is good, and a line has been identified as Lyman β (Lyman α is outside of the observed wavelength ranges). In addition, there are possible identifications of Si II λ1260 and C II λ1334, although both lines are in the Lyman α forest and so may not be correct identifications.

z_{abs} = 3.1045: The λ1550 line of the C IV doublet identified with this system is probably affected by poor night sky subtraction , resulting in somewhat poor redshift agreement between the two lines of the doublet. The strong Lyman α line (and possibly Lyman γ and Lyman δ) and C III λ977 make the reality of this redshift secure.

z_{abs} = 3.1142: This redshift is probably responsible for the second Lyman discontinuity mentioned above; in addition to the C IV doublet, we identify three Lyman series lines (including strong Lyman α), Si III λ1206, C III λ977, and Si II λ1260. As for the system at z_{abs} = 3.1045, the C IV doublet for this system falls in a region where the night sky is particularly messy, so the relative strength of the two lines may be affected.

z_{abs} = 3.1530: The appearance of the weak C IV doublet identified with this system suggests possible multiple structure; the same type of structure may also be present in Si IV (the λ1402 line may have been barely resolved into two – see Figure 5). In addition to C IV and Si IV, we find several Lyman series lines, and probable identifications of C III and Si III lines.

z_{abs} = 3.2228: As discussed above, it is this certain redshift that is responsible for the obvious Lyman discontinuity near 3860 Å (see Figure 1e). C IV and Si IV doublets are identified, as well as Lyman series lines and several other lines which fall in the Lyman α

forest. The redshift will be discussed in detail in §IV.

f) Q1017+1055

As for Q0029+0722, the spectrum of this QSO has some features that are likely to be due to ejected material, based on the broad, complex appearance of the absorption and also on the implied ionization state of the gas (e.g., strong C IV and N V absorption and weak or absent lines of HI). However, the absorption system that gives rise to the Lyman discontinuity ($z_{abs} \sim 3.05$) is of a very different nature (e.g., the C IV is weak and the Lyman series lines are strong), and so it is unlikely that the gas is in any way associated with the QSO itself. The following absorption redshifts have been identified on the basis of the new spectra:

$z_{abs} = 0.9979$: The possible Mg II doublet for this system is weak; an additional identification of Fe II λ2382 is suggested, but the system must be regarded as tentative.

$z_{abs} = 1.2400$: A strong Mg II doublet, several lines of Fe II, and Al II λ1670 define this redshift. It was identified by SSB on the basis of a low–resolution spectrum.

$z_{abs} = 2.5651$: Although the identified C IV doublet is strong, the reality of this system is not absolutely certain because the lines fall in a region of the spectrum that is complicated by the presence of complex, broad Si IV features from one of the BAL–like systems. Unfortunately, none of the expected Lyman series lines fall in any of the observed spectral regions.

$z_{abs} = 2.9400$: In addition to a weak C IV doublet and several Lyman series lines of HI, lines of C III, Si II, and Si III are identified.

$z_{abs} \approx 2.972$: This system has a broad, unresolved C IV complex and a diffuse Si IV doublet (the λ1402 feature is affected by residuals from the λ5577 night sky emission line). As noted by SSB, there is no strong H I absorption evident for this redshift. The low–resolution spectrum also shows broad features at the expected position of the O VI $\lambda\lambda$1031, 1037 doublet. The expected N V features, if present, are not obvious in the low–resolution spectrum of SSB. In the new higher–resolution spectra, there is some evidence for a depression in the continuum near $\sim$ 4925 Å, which may be a diffuse N V feature. This corresponds closely in wavelength to the Lyman α line from the absorption

system giving rise to the Lyman discontinuity. This diffuse, high ionization system is probably due to material associated with the QSO.

$z_{abs} = 2.9970$: The C IV doublet identified with this redshift, if correct, shows evidence for being diffuse, and possibly of similar origin to the diffuse system at $z_{abs} \sim 2.972$. A line at $\lambda 4859$ may be the associated Lyman α line. The system must be regarded as tentative, particularly since the redshift agreement between the C IV doublet lines is not good.

$z_{abs} = 3.0098$: The narrow C IV doublet and several Lyman series lines, including a strong Lyman α, suggest that this redshift has an intervening origin.

$z_{abs} = 3.0542$: This redshift is unusual in the sense that it is has a high H I column density which results in the observed Lyman discontinuity (the system was estimated to have $z_{LLS} \approx 3.048$ by SSB), yet there are no certain identifications of associated heavy element lines. Although a pair of lines is identified as a N V doublet, this is not likely to be correct, given the absence of a detectable C IV doublet and the strength of the H I lines. This system will be analyzed in detail in §IV.

$z_{abs} = 3.0765, 3.0793$: The reality of this pair of systems is suspect because of the very complicated nature of the spectrum near the positions of the identified C IV doublets. It is difficult to judge which features are real and which are due to poor night sky subtraction. Neither system has a strong Lyman α line identified with it.

$z_{abs} = 3.1109$: Although this system is not particularly broad or diffuse, the strong C IV and N V doublets and absence of strong H I lines indicate that it is likely to be associated with ejecta from the QSO. Si III $\lambda 1206$ and C III $\lambda 977$ are also identified, although the former is weak, and the absence of the Si IV doublet casts some doubt on the Si III identification.

g) Q2233+1341

With $m(\lambda_0 1450) = 18.64$, this QSO is the faintest of the 8 observed. No heavy element lines were identified longward of Lyman α emission which could be associated with the observed Lyman limit (estimated to have $z_{LLS} \approx 3.035$ by SSB) on the basis of the low–resolution spectrum obtained by SSB. However, given the new higher–resolution data, the system giving rise to the Lyman discontinuity appears to have $z_{LLS} = 3.0618$. It can be

seen in Figure 7c and 7d that there are considerable problems with subtraction of the night sky, particularly near λ5577 and λ6300. Also, the spectrum covering the wavelength range $\lambda\lambda 5200 - 5830$ (Figure 7c) does not have a signal–to–noise ratio as high as would have been desirable. The following redshifts have been identified:

$z_{abs} = 0.0101$: This redshift is based on the identification of two $\sim 5\sigma$ lines as the Na I doublet; if it is correct, then the heliocentric velocity of the system is $\sim$ 3040 km s^{-1}. A casual inspection of the Palomar Sky Survey field does not show any obvious galaxy near the line of sight to Q2233+1341.

$z_{abs} = 2.1668$: This redshift is identified on the basis of very strong Lyman α and Al II λ1670 lines. We also find Si III λ1206, Si II λ1526, C IV λ1548 (the λ1550 line is probably blended with another strong line, and thus remains unidentified), Fe II λ1608, and Mg I λ2026.

$z_{abs} = 2.8886$: There appears to be some structure in the C IV doublet identified with this redshift; also found are Si IV λ1393 (the λ1402 component of the doublet may be present, but it would not satisfy the 5σ criterion for acceptance in the line list), Lyman α, Lyman β, Si II λ1260, and C III λ977. This redshift was found in the low–resolution spectrum of SSB.

$z_{abs} = 2.9420$: Although only the λ1548 line of the C IV doublet is found (the λ1550 line is just beyond the 5σ threshold), several Lyman series lines make the redshift beyond doubt.

$z_{abs} = 2.9990$: A very weak C IV doublet is found to be associated with this redshift, as well as Lyman α, γ, δ, and ϵ (Lyman β does not fall within the observed wavelength ranges), and C III λ977.

$z_{abs} = 3.0618$: Although the new high dispersion spectra show that it is this system that causes the pronounced Lyman discontinuity, the identification is based solely on the Lyman series lines and the Lyman limit; there are no convincing identifications of heavy–element lines associated with the system (as will be seen, an *a posteriori* search will yield the C II λ1334 line), although the expected position of the C IV doublet corresponds to the spectral region near 6300 Å, which is badly confused by poor night sky subtraction. A detailed discussion of this redshift will be given in §IV.

IV. THE LYMAN LIMIT SYSTEMS

a) H I Column Density Measurements

The survey for Lyman limit absorption conducted by SSB was considered to be sensitive to the detection of systems having $\log N(H\ I) \geq 17.32$, or $\tau_{LL} \geq 1.5$. However, it was only for the relatively rare case in which $1.5 \leq \tau_{LL} \leq 3$ that an accurate estimate of N(H I) could be made on the basis of the low–resolution spectra. In general, high–resolution spectra of the Lyman α line alone are not sufficient to determine uniquely the H I column density and b parameter for a high column density system, and such measurements result in a rather large range of possible combinations of parameters. In order to reduce the uncertainties involved, it is really necessary to observe many lines of the Lyman series, particularly the lower lines, which are much less saturated than Lyman α. In the present work, the QSOs are in general too faint to allow echelle–resolution spectra of the appropriate wavelength ranges required to resolve the Lyman lines, which typically have b values in the range 10–45 km s^{-1}(Atwood, Baldwin, and Carswell 1985; Carswell *et al.* 1984). Thus, some compromise was necessary in order to study a statistical sample of LLSs.

The method of obtaining an accurate measurement of the H I column density for each Lyman limit system involves the $\sim$ 1 Å resolution spectra of the regions containing the Lyman α absorption line (Region II as described in §IIb) and convergence of the Lyman series to the Lyman limit (Region I). Because the velocity resolution of the spectra is generally $\sim$ 60 – 80 km s^{-1}(with the exception of Region II for Q0636+6801 and Q0956+1217, which have $\sim$ 35 km s^{-1}resolution), profile fitting to any single member of the Lyman series is not adequate for anything but placing limits on the H I column density of the system; however, the observed spectral regions encompass many of the Lyman series lines, along with the Lyman limit. Because the observed Lyman lines span a very large range in optical depth for a given set of parameters b and N(H I), they allow (in principle) a standard curve of growth analysis to be performed in order to substantially reduce the uncertainties substantially. However, in practice, the analysis cannot be accomplished by simply measuring equivalent widths because the Lyman series lines are invariably blended with lines from other redshifts. A more productive approach involves simultaneous profile

fitting of the Lyman series lines until a consistent result is obtained. In addition, as first pointed out by Tytler (1982), the observed shape of the convergence of the Lyman series toward the Lyman limit is fairly sensitive to the gas velocity dispersion parameter, b. That is, the overlapping lower Lyman series lines produce significantly different observed Lyman edges depending on the b parameter. In order to make best use of the data toward accurate H I column density measurements, an interactive computer program was devised which calculates Voigt profiles for the first 20 Lyman series lines and includes the Lyman limit and Lyman continuum. Since the lines are unresolved at $\sim$ 60 km s^{-1}resolution, the instrumental profile plays an important role in the observed shape of the line profiles. Thus, the instrumental resolution was carefully determined for each spectrum by combining comparison–lamp spectra taken during the course of the observations in the same way in which the actual data were combined; the instrumental FWHM was then measured as a function of wavelength for each spectrum. The computer model spectra are convolved with the instrumental profile so that a direct comparison with the data is possible. The two parameters $N(H\ I)$ and b are then varied until the line profiles *and* the shape of the Lyman edge and Lyman continuum are consistent with the observations. As will be seen, it is sometimes the case that more than one strong H I component is contributing to the observed Lyman limit; in such cases, the situation clearly becomes more complicated. However, the computer program allows the superposition of as many as 8 systems at different redshifts to be calculated. The results of the H I column density determinations for each LLS are given in Table 9. The uncertainties in the H I column densities listed in Table 9 have been estimated based on repeated trials; they are not formal χ^2 uncertainties. Figure 8 shows the data and model spectra for the two most complicated Lyman limits, along with the corresponding Lyman α line profiles. It is worth noting that considerable uncertainties in the continuum arise near the convergence of the Lyman series; the presence of any moderately strong line from another redshift system can have a very large effect on the apparent level of the data. In general, the "true" continuum has been assumed to be a monotonic extrapolation from higher wavelengths. This is reasonable unless there is a system with a significant Lyman continuum optical depth that has a higher redshift than the LLS of interest. When this appears to be the case, the continuum has been adjusted accordingly.

There is no indication from the observed Lyman series absorption (recall that there is no bias in terms of the gas velocity dispersion expected if the systems are chosen solely on the basis of an observed Lyman discontinuity) of velocity components with substantial column densities but very small b values. In fact, the inferred Lyman series b values (typically $\sim$ 25 km s^{-1}) are consistent with the range found in general for the Lyman α forest lines (Atwood, Baldwin, and Carswell 1985; Carswell *et al.* 1984). This is not surprising, since both types of clouds are thought to be photoionized, and the b values are generally interpreted as thermal line widths.

b) The Heavy Element Ionic Column Densities

The measurement of the column densities of the heavy–element ions in QSO absorption systems is subject to many possible difficulties which have been widely discussed in the literature. One of the most commonly cited problems is that since the presence of fine velocity structure appears to be the rule rather than the exception in QSO heavy element absorption systems (e.g., Blades 1988 and references therein), there always remains the possibility that there exist components in the absorption systems that have high column densities but low b values and therefore are not accounted for whenever the individual velocity components are unresolved. If this is often the case, then it may be that the inferred column densities are substantially underestimated. High–resolution observations of C IV have shown that typical b values for individual velocity components are 7–15 km s^{-1}(York *et al.* 1984; Pettini *et al.* 1983; Blades 1988), whereas the inferred "effective" b value found from the classical doublet ratio method may be as high as $\sim$ 50 km s^{-1}for moderate resolution data and strong lines. Thus there is little doubt that higher–resolution observations of strong lines would invariably reveal finer velocity structure than is obvious in the present spectra. However, Jenkins (1986) has shown that as long as the velocity components comprising a heavy element absorption system are not very strongly saturated, the value of the *total* column density derived on the basis of relatively low–resolution spectra and a standard single–component curve of growth analysis will only underestimate the true total column density by a small amount (usually less than 10%). While this is somewhat counter–intuitive, it has been seen to be true in practice as well when moderate and high

resolution column density measurements for the same absorption systems are compared (e.g., Pettini *et al.* 1983; Carswell *et al.* 1984; Boksenberg, Carswell, and Sargent 1979). In the present situation, the results of Jenkins are really applicable only to doublets, since it is usually the case that only one transition is observed for each ion. Thus, the most accurate column density measurements are possible for doublets such as C IV $\lambda\lambda$1548, 1550 and Si IV $\lambda\lambda$1393, 1402, since the total column density and "effective" b values (which now bear no relation to actual gas temperatures) can be uniquely determined from the line strength and doublet ratio. For transitions that are not doublets, many of the lines being measured turn out to be on the linear part of the curve of growth, in which case (when the spectral resolution $\sigma_{obs} > b$) the precise b value does not affect the observed line profile and is not important in determining the column density (as long as b is not smaller than the thermal width for a gas at $\sim 10^4$ K). However, ambiguity arises when the lines being measured are strong; for lines that are *not* on the linear part of the curve of growth, or for lines that are undetected, the column density limits are obtained by taking b to be the thermal width implied by the H I b values obtained above from fits to the Lyman series lines. This leads to a typical b value for C of 7–10 km s^{-1}, in agreement with existing high-resolution observations. If indeed there is fine velocity structure, then this procedure may in fact lead to *overestimates* of the column densities for some moderately strong lines (e.g., C II) because it requires that all of the line equivalent width be contributed by a single velocity component on the flat part of the curve of growth, when in fact the line profile may be the superposition of several lower column density, less saturated components. This is certainly true in some instances, where no reasonable value of the column density will produce a strong enough line if it is assumed to be due to a single component; in such a case, the column density is determined by assuming that the b value is the same as the "effective" b value determined for a doublet transition of the same element (when it is available).

Another difficulty arises for lines that are expected to fall within the Lyman α forest region, e.g., C III λ977 and Si III λ1206. In such cases, any measurement is really only an upper limit on the column density, because the probability is very high that any given spectral feature is blended with a line (usually Lyman α) from another redshift system. It is often the case that the expected position of one of these lines coincides with a very strong

line in the Lyman α forest, so that no useful column density limits can be set.

With the above *caveats* in mind, all of the column density measurements and limits have been determined by assuming that the velocity structure is no more complicated than appears obvious in the spectra of (in most cases) 60 – 80 km s^{-1}resolution. We have made use of an interactive computer program that fits Voigt profiles (convolved with the appropriate instrumental profile, which has been carefully measured as described in §IVa) to observed spectral features. The line profiles used in determining the column densities have been calculated using the rest wavelengths and oscillator strengths which have recently been compiled by Morton, York, and Jenkins (1989). Table 9 contains the column densities and column density limits for all of the observable ions for each Lyman limit system. The parameters for the LLS in the spectrum of PKS 2126–158, determined using identical methods, have been included in Table 9 as well; a more in–depth discussion of this system can be found in Sargent, Steidel, and Boksenberg (1989b). A brief discussion of the 7 other LLSs follows:

Q0029+0722 (z_{LLS} = 3.0488): This system, with log N(H I)= 19.3, has the highest H I column density of the 8 LLSs presented in Table 9. As expected, the system is dominated by lower ionization species. As mentioned in §III, the Si II λ1304 and O I λ1302 lines are partially blended with a possible C IV system; however, the measurement of the Si II λ1526 line provides a check, and the two measurement of N(Si II) agree well. As is the case for several of the LLSs in Table 9, the limits on the C IV column density are not quite as low as they might be because of a very complicated night sky spectrum in the vicinity of 6300 Å. The non–detection of the excited fine structure line C II*λ1335.68 can be used to place limits on the gas density in the cloud, as originally proposed by Bahcall and Wolf (1968). The critical electron density at which the excited and ground states of C II are populated equally (for $T \sim 10^4$ K) is $n_e \approx 100$ cm^{-3}; thus, for sufficiently high electron densities, one would expect to observe the fine structure line if the ground state line is strong. Using the expression given by Morris *et al.* (1986),

$$\frac{N(C\ II^*)}{N(C\ II)} = 3.9 \times 10^{-2} n_e[1 + (0.22 n_p/n_e)]$$

where n_e and n_p are the electron and proton number densities, respectively, then for $n_e \approx n_p$

and $n_p \approx n_H$,

$$\frac{N(C\ II^*)}{N(C\ II)} = 4.8 \times 10^{-2} n_H.$$

Therefore, given the measurements shown in Table 9, one finds that $n_H \leq 0.7$ cm^{-3} for this system.

Q0256+0000 ($z_{LLS} = 3.0823$): The procedure outlined in §IVa for measuring the H I column densities indicates that there are several components making significant contributions to this Lyman limit discontinuity (the fits based on the adopted parameters are shown in Figure 8). Table 9 shows the limits placed on the various ionic column densities for each of the three components. The only certain detections are for C IV and Si IV in the highest redshift component. There is evidence for the presence of C IV associated with the other two components, but again the spectra are unfortunately not pristine near the expected positions of the lines because of poor night sky subtraction. Because of the extremely strong Lyman α emission line and the very steep line profile, column density limits from the O I λ1302 and Si II λ1304 lines were not possible to assess. Since there are no strong C II lines detected, no useful limits can be placed on the gas density for any of the three components.

Q0301−0035 ($z_{LLS} = 2.9400$): The upper bound for the H I column density in this system is well determined because the Lyman α absorption line shows no evidence for the onset of damping wings, which occurs for $\log N(H\ I) \gtrsim 18.8$; the lower bound is considerably more uncertain. Although there are unambiguous detections of C II, C IV, and Si IV for this LLS, there appear to be small redshift disagreements between the high–ionization (C IV and Si IV) and lower–ionization (H I and C II) species of roughly 15 km s^{-1}. It is not completely clear whether this difference is real or is simply due to uncertainty in the line positions. Using the arguments discussed above, the limit for N(C II*) along with the measurement of N(C II) implies that $n_H < 2$ cm^{-3} for this system.

Q0636+6801 ($z_{LLS} = 2.9038$): Just as for Q0256+0000 above, the analysis of the H I column density from the Lyman series lines required more than one high column density component to produce an adequate fit (the fit is shown in Figure 8). This LLS is by far the richest in terms of the number of detectable lines in the spectrum, and is due in part to higher column densities and in part to higher–quality spectra. The relatively low

b value determined from the H I Lyman series lines for the higher–redshift component combined with the rather strong observed line made the measurement of the C II column density ambiguous; if the b value is taken to be the thermal width suggested by the Lyman series lines, then no value of N(C II) will produce a line strong enough to be in agreement with the observations. The lower column density value (see Table 9) has therefore been obtained by assuming that $b \sim 25$ km s^{-1}, the "effective" b value measured from the C IV doublet. A similar assumption has been made in order to measure the Si II lines. Given the non–detection of the excited fine structure line C II*λ1335.68, the resulting limit on the particle density in the gas is $n_H < 0.7$ if log N(C II)= 14.5; if N(C II) is as high as log N(C II)= 15.5, then the density limit is $n_H < 0.07$. We shall see in §VI that the density is unlikely to be smaller than this limiting value, and thus we have given log N(C II) = 15.5 as an upper limit in Table 9.

Q0956+1217 (z_{LLS} = 3.2228): The H I column density for this system is quite well determined because τ_{LL} is sufficiently small that there is still residual flux shortward of the Lyman edge (see Figure 5a). Since no C II line is detected, no useful upper limits on n_H can be set for this cloud.

Q1017+1055 (z_{LLS} = 3.0540): While the H I column density is again well–determined because of the residual flux in the Lyman continuum (see Figure 6a), only upper limits can be set on the observable heavy–element ionic species even in *a posteriori* searches.

Q2233+1341 (z_{LLS} = 3.0618): Other than the H I Lyman series with log N(H I) = 18.5, only C II λ1334 is a certain detection. The gas number density limit from the non–detection of the C II* line is $n_H < 1.3$ cm^{-3}.

V. THE PHOTOIONIZATION MODELS

a) Description of the Models

The physical properties of the heavy–element QSO absorption systems were first discussed in detail by Sargent *et al.* (1979), who suggested that the observed ionic species were consistent with what would be expected in a highly photo–ionized gas, and inconsistent with what would be expected for a gas that was collisionally ionized. Subsequent workers

(e.g., Pettini *et al.* 1983; Chaffee *et al.* 1986) have reached the same conclusions, arguing that the observed velocity dispersions are too small to admit the very high temperatures required in a collisionally ionized diffuse gas, and that a gas heated by shocks could not maintain a high temperature for significant lengths of time because it is thermally unstable and would require constant energy input. Thus, it is appropriate to attempt to model the gas clouds using the very comprehensive photoionization computer codes which have become available. Several authors have recently applied such photoionization models to the QSO absorption systems (e.g., Chaffee *et al.* 1986; Bechtold, Green, and York 1987; Morris *et al.* 1986; Bergeron and Stasinska 1986); in this paper, we have made observations specifically designed to constrain such models so that the physical properties of the Lyman limit absorption systems (and by extension the heavy element systems) might be inferred.

The photoionization models which will be used have been calculated using Ferland's CLOUDY program (Ferland 1988); except for some recent adjustments, the program is identical to that used by Bechtold, Green, and York (1987), Chaffee *et al.* (1986), and by Morris *et al.* (1986). As usual, the clouds are modeled as plane–parallel slabs, illuminated on one side by the ionizing radiation field. The clouds are assumed to have a constant density; in the regime of interest for the LLSs, such models are indistinguishable from models in which a constant pressure is assumed instead. Grids of models have been generated which take as input the *observed* H I column density, the heavy–element abundances for He, C, N, O, Ne, Mg, Al, Si, S, Ar, Ca, and Fe, and the spectral shape of the ionizing radiation field. Instead of assuming a value for the intensity of the ionizing radiation field and varying the particle density in the gas, as was done by Chaffee *et al.* (1986), we will instead calculate the models in terms of the ionization parameter

$$\Gamma \equiv \frac{n_\gamma}{n_H},$$

where n_γ is the number density of photons capable of ionizing H incident on the face of the cloud, and n_H is the number density of hydrogen atoms in the gas. Thus, the models are similar to those calculated by Bergeron and Stasinska (1986); varying Γ is equivalent to varying the particle density at a fixed value of the incident intensity of ionizing radiation, or to varying the intensity at a fixed particle density. The models output the predicted

relative column densities in the various ionization stages for each element considered, as a function of Γ.

Most of the model grids that will be described have been run for $-4 \leq \log\Gamma \leq -1$ (Bergeron and Stasinska (1986) have found that the allowed domain for the ionization parameter based on the general properties of the various classes of heavy element absorption systems is (roughly) $-3.5 \leq \log\Gamma \leq -1.5$). Of the input parameters required by the models, the only ones that significantly affect the resulting model grids are the spectral shape of the ionizing continuum and the H I column density. As pointed out by Chaffee *et al.* and by Bergeron and Stasinska, the adopted chemical abundances have only a very small influence on the thermodynamic properties of the cloud, and thus the *relative* column densities of the various ionic species of a given element depend very weakly on the assumed metallicity. Thus, a scaling relation with chemical abundance exists for the predicted column densities; for the purposes of the calculations, we have assumed that the metallicities are equal to 0.01 of the solar values ($[M/H] = -2$). Since the models are calculated in terms of Γ, the grids are also unchanged by the assumed particle density, as long as n_H is small enough that collisional excitation and cooling is not important. As discussed in §IV above, the absence of the C II excited fine–structure line implies (in the most stringent cases) that $n_H < 1$ cm^{-3}, and therefore, if $T \sim 10^4$K, collisional processes are negligible. Thus, the homology relationship will be preserved between models with different photon and gas densities but the same ionization parameter.

b) The Ionizing Radiation Field

Since N(H I) has been determined from the observations, the most uncertain parameter in the models is the nature of the radiation field that is ionizing the clouds. Sargent *et al.* (1979) suggested that the heavy–element absorption systems are ionized by the integrated ultraviolet radiation field from QSOs; recently, Bechtold *et al.* (1987) have discussed the spectrum of such a radiation field by integrating over the empirical QSO luminosity function and accounting for the strong redshift evolution of the QSO number counts. This is the radiation field that has been used by both Chaffee *et al.* (1986) and Morris *et al.* (1986) as input to their photoionization model grids. Bergeron and Stasinska (1986), on the other

hand, have used pure power–law ionizing spectra of the form $f_\nu \propto \nu^{-\alpha}$; most of the grids which they discuss use $\alpha = 1.5$. This is a reasonable value to use for an AGN–like spectrum, since the mean spectral index for AGNs between optical and x–ray wavelengths is $\alpha_{ox} \approx 1.5$. However, as pointed out by Bechtold *et al.* (1987), the EUV spectrum of AGNs is still very uncertain, since the spectrum of all high–redshift objects is altered to some extent by intervening absorption, and no observations have been possible for more nearby (lower–redshift) objects in the energy range of interest (.2 KeV– 10 eV).

The nature of the metagalactic ionizing flux is a subject of considerable controversy; however, recently, a basic conclusion of many workers is that the generally accepted empirical QSO luminosity functions cannot account for nearly enough ionizing photons at high redshift to explain the absence of a Gunn–Peterson (1965) effect due to neutral material in the intergalactic medium (e.g., Shapiro and Giroux 1987, 1989; Donahue and Shull 1987; Bechtold *et al.* 1987; Lin and Phinney 1989; Miralda–Escude and Ostriker 1989). Bajtlik, Duncan, and Ostriker (1988) have used the QSO "proximity effect" to directly determine the intensity of the metagalactic flux at the Lyman limit, J_{ν_0}, at high redshift. They found that $J_{\nu_0} \approx 10^{-21}$ ergs s^{-1} cm^{-2} Hz^{-1} sr^{-1}, and that the value stays roughly constant over the redshift range $1.8 < z < 3.8$. The quoted value is still rather uncertain, but, as pointed out by Miralda–Escude and Ostriker (1989), it represents a formal lower limit. The observed QSOs can account for only about 5% of this value when the effects of intervening absorption are completely taken into account (Lin and Phinney 1989). Because it is important to determine the most likely ionizing radiation field in order to trust the model results, we now turn to a discussion and comparison of the various possibilities.

Very recently, Miralda–Escude and Ostriker have discussed two possible sources of the bulk of the ionizing radiation in detail – hot stars in young and forming galaxies and "obscured" QSOs. For the present purposes, the important question is the *shape* of the spectral energy distribution (and, for the moment, not necessarily its intensity); thus, we must determine the most likely form for the intrinsic spectral energy distribution of the dominant sources; i.e., are most of the ionizing photons provided by stars in galaxies, or by AGNs? Steidel and Sargent (1989) argue (using data presented in this paper) that the spectral shape of the EUV spectrum of hot stars cannot account for the observed

ionization state in the heavy–element absorption systems, and thus radiation from young galaxies cannot represent the *dominant* component of the metagalactic flux at high redshift ($z \approx 3$). This conclusion has been reached by comparing photoionization models constructed as described above. In Figure 9 we have plotted the spectral energy distributions for 6 different ionizing radiation fields: a simple power law with $\alpha = 1.5$ (as used by Bergeron and Stasinska), a power law with $\alpha = 1.0$, the Bechtold *et al.* (1987) "Medium" integrated QSO spectrum, the Bechtold *et al.* "Hard" integrated QSO spectrum, and a young galaxy spectral energy distribution calculated by Bruzual (1983). The shape of the ionizing radiation field at both lower and higher energies than those shown in Figure 9 makes very little difference to the ionization structure of the cloud. All of the curves shown in Figure 9 are normalized to the same intensity at the Lyman limit (1 Rydberg); thus the ionization parameter Γ would be the same for each. Figure 10 shows the results of the photoionization model calculations for a cloud with log N(H I)= 17.5 (this figure is similar to Figure 1 of Steidel and Sargent 1989) for four assumed radiation fields. It is immediately clear that the model cloud ionized by starlight (Figure 10d) is very different from the ones ionized by AGN–like spectra (Figures 10a,b,c). As discussed by Steidel and Sargent, the model ionized by starlight is completely at odds with the observations, particularly in the sense that not nearly enough C IV is produced relative to C II and Si IV. The $\alpha = 1.5$ and the Bechtold *et al.* "Medium" model grids are virtually indistinguishable, and the Bechtold *et al.* "Hard" model grid is essentially the same in terms of the ionization of C as the $\alpha = 1.5$ model; the only differences are a slight suppression of the Si species and a slight enhancement of N V. The range of intrinsic EUV AGN spectra discussed by Bechtold *et al.* (1987) is likely to produce an integrated spectrum with a spectral shape somewhere in between the "Medium" and "Hard" radiation fields. We will assume, as concluded by Steidel and Sargent (1989), that the bulk of the ionizing radiation field is produced by AGN–like spectra and that, if additional radiation is present because of unaccounted–for AGNs, the spectral shape will be similar to that calculated based on the AGNs which are known to be present at high redshift. Thus, in our subsequent analysis of the LLSs, we will discuss results using both the "Medium" and "Hard" integrated QSO ionizing continua, assuming only the *shape* of the spectral energy distribution and not the intensity.

c) Uncertainties in the Models

Clearly, modeling the clouds as constant density, plane–parallel slabs of gas illuminated on one side by the ionizing radiation field is an idealization of what is no doubt a much more complicated situation. For example, as discussed above, it is well known that the QSO heavy–element absorption systems often exhibit velocity structure on scales of $\sim$ 150 km s^{-1}, indicative of a fairly "clumpy" medium. When substantial velocity substructure is present, it is also often the case that separate velocity components exhibit different line–strength ratios, e.g. C II/C IV. This is possibly due to a varying particle density among the clouds which may be in the halo of a single galaxy and which happen to lie along the line of sight to the QSO, resulting in a varying value of Γ among the components. By using spectra with a resolution of $\sim$ 80 km s^{-1}, we are effectively averaging the properties of the gas over this velocity scale; the uncertainties introduced are probably most important for the systems with strong heavy element lines, such as the $z_{abs} = 2.9046$ system in the spectrum of Q0636+6801. However, if local sources of ionization are not dominating, all of the gas clouds considered are being ionized by roughly the same radiation field (since they are all at approximately the same redshift), and we shall see that the inferred range of particle densities in the gas is not large among the clouds. Therefore, although clearly it is desirable eventually to obtain very high dispersion spectra for all of the absorption systems, it is unlikely that large *systematic* errors are being introduced by the assumptions and methods used.

VI. APPLICATIONS OF THE MODELS

a) Estimates of the Heavy–Element Abundances

In order to estimate the heavy–element abundances in each Lyman limit system, photoionization model grids as described above have been generated; since each measurement of N(H I) has a significant uncertainty, several models were usually made for each LLS, spanning the possible range of N(H I) and using both the "Medium" and "Hard" ionizing radiation fields discussed in §V. Several examples of models using various values of N(H I) are shown in Figure 11.

Once a model grid has been produced, we use the values of the column densities and column density limits for C II, C III, and C IV to locate the allowed range of Γ which predicts the appropriate column density ratios. Carbon is the best element to use in constraining Γ for several reasons; first, for the whole range of Γ being considered, at least 90% of the C is expected to be in the form of C II, C III, and C IV, and lines of all 3 ions are observable. The ratio N(C IV)/N(C II) is a particularly sensitive discriminant since it changes rapidly with Γ (see Figure 11), and lines of both ions are observable longward of the Lyman α emission line (and therefore free of the confusion present in the Lyman α forest). In principle, the relative column densities of the silicon ions (Si II, Si III, and Si IV) would also be quite useful in constraining Γ, but in practice there are several reasons why Si is not nearly so useful as C. First, the cosmic abundance of Si is roughly a factor of 10 lower than for C, and it is relatively rare to find systems with measurable Si II, Si III, and Si IV lines. Secondly, the balance between Si III and Si IV is greatly affected by one of the largest uncertainties remaining in the photoionization models – the correct treatment of the He II Lyman α transport within the clouds (see, e.g., Netzer and Ferland 1984). The He II line has an energy of 40.8 eV, which is midway between the ionization potentials of Si III and Si IV; in any model where there is a significant He III zone (this will be most important for models with log N(H I) < 18.5), the predicted Si III/Si IV ratio is very model–dependent. For this reason, we will not use the observed Si column densities to estimate Γ; however, as we shall see, it will prove useful to use the *sum* of N(Si III) and N(Si IV) [versus N(Si II)] in evaluating the heavy–element abundances.

In view of the above discussion, we have chosen to use only the ionic species of C to constrain Γ. Since the observed C III column density is always an upper limit, it is only in the case where both C II and C IV are detected that a fairly accurate single value of Γ can be inferred (the limits on N(C III) are useful as a consistency check). In several cases, only one of these ions has been observed (see Table 9) so that only upper or lower limits can be set on Γ from the C ionization arguments. Once Γ has been constrained, the heavy element abundances follow immediately by examining the photoionization grid and applying the scaling relation with metallicity. The inferred values of Γ and the abundances of C, Si, and O for each of the LLSs are summarized in Table 10; the quoted errors reflect the range

of possible values, given the uncertainties in the H I column density determinations and in the determination of Γ. Because each LLS presents somewhat different problems to an evaluation these quantities, we discuss each one as an individual case.

i) Q0029+0072

A comparison of the measured value of N(C II) with the upper limit on N(C IV) implies that $\log\Gamma \leq -2.9$ for this high H I column density system. Despite the fact that only an upper limit on Γ results from the photoionization grid, the abundances are fairly well-determined from the measurements of N(C II), N(Si II), and N(O I); these column densities do not change appreciably for a given value of N(H I) for the allowed range of Γ. The errors on the abundances therefore result mainly from the uncertainty in the H I column density measurement. As can be seen from Table 10, the abundances of C, O, and Si are consistent with a uniform depletion relative to the solar abundances.

ii) Q0256+0000

i. $z_{abs} = 3.0843$: The lower limit on the the ratio N(C IV)/N(C II) suggests that $\log\Gamma \geq -2.5$ for this system, leading to an upper limit on the abundance of C. The sum $N_{3+4}(Si) \equiv$ N(Si III)+N(Si IV) is predicted to remain essentially constant for the allowed range of Γ, and the observations provide the constraint $13.0 \leq \log N_{3+4} \leq 13.4$, leading to well-defined limits on [Si/H]. These limits are listed in Table 10; the quoted errors on the limiting values reflect the possible range of N(H I) for the cloud. The fact that the upper limit on [C/H] agrees well with the allowed range for [Si/H] suggests that $\log\Gamma$ probably has a value very near the lower limit of -2.5 (assuming that the elements have roughly the same depletion relative to solar values).

ii. $z_{abs} = 3.0823$: Because there are no detections for any of the ionization stages of C, the ionization parameter cannot be constrained for this system. However, upper limits on [C/H] result from the upper limit on N(C II), and upper limits on [Si/H] follow from the upper limit on N_{3+4} (assuming that $\log\Gamma$ is somewhere in the range $[-3.7, -1.5]$).

iii) Q0301−0035

Because measurements are available for both N(C II) and N(C IV), the value of Γ is

well determined for this system. The quoted errors in the value of [C/H] result from the uncertainties in N(H I); only upper limits on [O/H] can be set because O I λ1302 is not detected. The upper limit on N(Si II) provides the most sensitive upper limit on [Si/H], and the lower limit on N_{3+4} provides a lower limit for [Si/H]. The resulting allowed range for [Si/H] is in tolerable agreement with the value of [C/H], although a slight enhancement of Si relative to C over their solar abundance ratio is suggested.

iv) Q0636+6801

i. $z_{abs} = 2.9046$: As discussed in §IVb, there is considerable uncertainty in the value of N(C II) for this system. The possible range for N(C II), along with the rather well determined value for N(C IV), suggest a range of possible values for $\log\Gamma$, as shown in Table 10. Unfortunately, this leads to abundance limits which are not particularly tight, since the allowed range for Γ corresponds to a region on the model grids where the expected column densities are changing rapidly. The sense of the change is that as $\log\Gamma$ becomes smaller, the inferred abundances become larger. It is interesting to note that the abundances that would be inferred if Γ were near the upper limit of the allowed range agree very well in terms of an implied uniform depletion of C, O, and Si relative to the solar values (and they would be only a few hundredths of the solar abundances), whereas, if $\log\Gamma \approx -3.1$, Si and O are significantly depleted relative to C. In either case, the abundances in this system are significantly higher than in any of the other LLS studied, and they may be as high as $[M/H] \approx -1$.

ii. $z_{abs} = 2.9030$: The lower limit on N(C IV)/N(C II) suggests that $\log\Gamma \geq -2.3$ for this system. The limit on N(C II) is likely to be a detection, since there appears to be some asymmetry to the blue in the strong C II λ1334 profile from the $z = 2.9046$ redshift component. It is therefore likely that the true value of $\log\Gamma$ lies near the lower limit of -2.3. The photoionization grids for this system show that N_{3+4} is increasing with increasing Γ for $\log\Gamma \geq -2.3$, whereas N(Si II) is decreasing; thus, the upper limits on these two quantities constrain the value of [Si/H], as shown in Table 10. That $\log\Gamma \approx -2.3$ is also suggested by the limits on [C/H] and [Si/H], if one insists that the depletions relative to solar values for C and Si be in rough agreement.

v) Q0956+1217

The N(C IV)/N(C II) limit for this system implies that $\log\Gamma \geq -2.2$, providing an upper limit on [C/H]. Here again, as Γ increases, N_{3+4} increases while N(Si II) decreases, thereby suggesting upper and lower bounds on [Si/H]. This is yet another case where, if the depletions of C and Si are to be in rough agreement, then Γ must be close to its lower limit, i.e., $\log\Gamma \approx -2.2$.

vi) Q1017+1055

As for the $z = 3.0823$ system in the spectrum of Q0256+0000, the absence of any detectable heavy-element lines associated with this system prevents one from determining Γ; however, since the values of N(C II) and N(Si II) change very little with Γ for models with N(H I)$\approx$ 17.5 (see Figure 9), upper limits on [C/H] and [Si/H] can be set using the non-detections of C II and Si II in the spectra.

vii) Q2126-158

The value of the ionization parameter for this system is well determined because of the detections of both C II and C IV in the spectra; a detailed discussion of this system is found in Sargent, Steidel, and Boksenberg (1989b).

viii) Q2233+1341

Since C II, but not C IV, is detected for this system, an upper limit on Γ results. The photoionization grids show that N(C II) changes little for $\log\Gamma \leq -2.8$, so that a reasonably accurate determination of [C/H] follows. N(Si II) decreases very slowly with Γ over the allowed range; thus, given the observational limit log N(Si II)$\leq$ 13.0, [Si/H] is listed as an upper limit, where the error reflects the uncertainty in the H I column density.

b) Additional Physical Properties of the Gas

Because the photoionization models we have discussed are uniquely determined (except for the assumed spectral shape of the ionizing radiation field, which is discussed in §Vb) by the ionization parameter Γ, and because Γ is essentially just the ratio of the incident intensity of radiation at the Lyman limit J_{ν_0} to the particle density n_H in the cloud, then

n_H can be determined if the value of J_{ν_0} is known. As mentioned in §Vb, a recent direct estimate of J_{ν_0} at high redshift has been made by Bajtlik, Duncan, and Ostriker (1988); they suggest that $\log J_{\nu_0} = -21.0 \pm 0.5$ ergs s^{-1} cm^{-2} Hz^{-1} sr^{-1} over the redshift range $1.8 \leq z \leq 3.8$. It has been pointed out that if the QSO "proximity effect" upon which the analysis was based was not really detected, then the value of J_{ν_0} becomes a *lower limit.* In any case, in order to discuss further the physical conditions in the gas clouds, we define a variable $J_0 \equiv J_{\nu_0}/10^{-21}$ ergs s^{-1} cm^{-2} Hz^{-1} sr^{-1}. The particle density n_H can then be expressed as a function of Γ and J_0,

$$n_H = 6.3 \times 10^{-5} J_0/\Gamma \quad \mathrm{cm}^{-3},$$

or

$$\log n_H = -4.2 + \log J_0 - \log \Gamma \quad \mathrm{cm}^{-3}.$$

It can be seen immediately that, for the range of values of Γ which are inferred to be appropriate for the LLSs, i.e., $-3.5 \leq \log \Gamma \leq -2$, the gas density is in the range $0.006 \leq n_H \leq 0.2$ cm^{-3} for $J_0 \approx 1$. Thus, most of the limits on n_H inferred from the absence of the C II excited fine–structure line (typically $n_H \leq 1$ cm^{-3}; see §IVb) do not correspond to very strong constraints, although they are consistent with the limits from the photoionization models. In the case of the $z_{abs} = 2.9046$ system in the spectrum Q0636+6801, however, limits as small as $n_H \leq 0.07$ cm^{-3} were obtained in the case that log N(C II) is as large as 15.5 cm^{-3}. Using the above expression, this means that $\log \Gamma \geq -3.1 + \log J_0$; if N(C II) were any larger, then a larger value of Γ would be suggested and the photoionization models would be inconsistent with the observations. Thus, log N(C II)=15.5 was adopted as the upper limit for this system, assuming that $J_0 \gtrsim 1$ (see §IVb).

Once n_H has been inferred, the linear extent of the clouds, D_c, follows directly from the total hydrogen column density N_H (see Table 10); i.e., $D_c = N_H/n_H$ cm. In terms of the quantities derived from the models,

$$D_c = 5.2 \frac{N_{20}\Gamma_{-2}}{J_0} \quad \mathrm{kpc},$$

where N_{20} is the total hydrogen column density in units of 10^{20} cm^{-2}, and Γ_{-2} is the ionization parameter in units of $\Gamma/10^{-2}$. If the clouds are then assumed to be spherically

symmetric with radius $D_c/2$, the cloud mass is

$$M_c = 4.4 \times 10^7 N_{20}^3 \Gamma_{-2}^2 J_0^{-2} \quad M_\odot .$$

Clearly, the sizes and especially the masses are highly dependent on the parameters N_H and Γ, which are derived from the photoionization models. However, for the purposes of discussion it is interesting to calculate these quantities for the absorption systems that have been studied. Thus, n_H, D_c, and M_c are listed in Table 11.

c) Summary and Discussion

While we will postpone until §VII a discussion of the implications of the derived physical properties of the gas clouds outlined in Tables 10 and 11, it is worth making a few general comments at this point. First, it is clear from Table 10 that the typical heavy element abundances for the Lyman limit absorbing clouds lie in the range $-3.0 < [M/H] < -1.5$, which is at odds with the somewhat vague notion commonly cited, that the heavy–element absorption systems have abundances of order a few tenths of the solar values. The principal result found above is that, by and large, *the abundances of the heavy–element absorption systems which are optically thick in the Lyman continuum are quite low*, at least at $z \approx 3$.

It is of interest to review briefly some of the previous abundance determinations for QSO absorption systems from the literature (there have not been many). Sargent *et al.* (1979) suggested that a typical heavy–element system, with log N(H I) = 18.3, is probably about 3% neutral, with abundances of roughly [M/H] = −1. However, if we apply the methods used above to the column density measurements given by Sargent *et al.* al for the $z = 2.2765$ system in the spectrum of Q0453−423, we find that $\log \Gamma \geq -2.2$, $-2.2 \leq [Si/H] \leq -1.5$, and $[C/H] \leq -2.0$, suggesting that $[M/H] \approx -2$, in good agreement with the high end of the abundance distribution which we find at $z \approx 3$. Chaffee *et al.* al (1986) have briefly discussed the $z = 2.12$ system in Q1225+317 (chosen to represent a "typical" heavy element absorption system), finding that $[M/H] \approx -1.5$, based on consideration of photoionization models that are very similar to the ones used in the present work; with their adopted column densities, we find that $[C/H] \lesssim -1.6 \pm 0.1$ (depending on the ionizing radiation field used), in good agreement, although a firm lower bound cannot be quoted until lines in addition to

C IV are detected. Hunstead *et al.* (1987) discussed the $z = 3.1723$ system in the spectrum of PKS 2000−330, which has log N(HI) = 19.8 and detections for low–ionization species only. They found a fairly uniform depletion of $[M/H] \approx -2.2$; this is in good agreement with the present results for the LLSs with similarly high H I column densities (and similar redshifts; see Table 10). Bechtold, Green, and York (1987) have used photoionization models to discuss the very complex system with $z_{abs} = 1.79$ in the spectrum of Q1225+317, concluding that the abundances are consistent with the ISM values in the Galaxy. Very recently, Pettini and Boksenberg (1988) have presented evidence for a depletion of $[M/H] \approx -1.5$ in a $z = 2.3$ damped Lyman α system by using absorption lines that are likely to be unsaturated even in the very high H I column density clouds. It should be emphasized that this result may not be directly comparable to results for the LLSs, which have much smaller H I column densities and probably have different origins; this will be discussed further in §VII.

Thus, in general, the results of previous abundance estimates indicate somewhat higher abundances than we find for the Lyman limit systems, although the redshifts are typically lower than for the present study (and we shall see in §VII that there exists evidence for chemical evolution of the absorbers with redshift). Also, it is a fundamentally different approach to select absorption systems on the basis of detected heavy–element lines; this may preferentially select systems having higher abundances than would be found in an unbiased sample of absorbing clouds. In particular, the detailed studies of the very strong, complex systems such as in the spectra of Q1225+317 and the BL Lac object 0215+015, while extremely important, do not necessarily provide information on the properties of the absorbing clouds giving rise to the bulk of the QSO heavy element absorption systems.

VII. DISCUSSION

a) The Heavy Element Abundances

Since the original suggestion of Bahcall and Spitzer (1969), a great deal of evidence has accumulated in favor of the hypothesis that QSO heavy–element absorption systems are associated with gas in the halos of intervening galaxies (see, e.g., Boksenberg and Sargent 1983, Sargent, Boksenberg, and Steidel 1988, and references therein). Under this hypothesis,

taking what is known about the halo stellar populations in our Galaxy, it would naively be expected that the gas in galaxy halos at early epochs would have about the same heavy element enrichment, namely, $-3.5 \leq [M/H] \leq -1.5$, where the lower limit corresponds to the most metal–poor field halo stars, and the upper limit is typical for the metal–rich globular cluster population. Therefore, it would be somewhat surprising if the QSO heavy–element absorption systems really did turn out to have depletions of only a factor of a few from the solar abundances, unless one invokes a mechanism for getting enriched material from the disk out to large galactocentric radii. It is well known that if one requires that the observed heavy element absorption systems at high redshift are associated with galaxies analogous to the local population, then the numbers require very large galaxy cross sections for absorption, possibly exceeding 100 Kpc for a galaxy with luminosity L_* (see, e.g., Sargent, Boksenberg, and Steidel 1988). Thus, the *typical* heavy–element absorption system must be arising at very large distances from the center of a galaxy, and would certainly qualify as "extreme halo" material.

In view of these arguments, that we find heavy–element abundances $-3.0 \leq [M/H] \leq -1.5$ for the sample of Lyman limit systems is perfectly consistent with the "galaxy halo" picture, and in fact represents an additional piece of evidence in favor of this interpretation, since such abundances would be one of the strongest predictions of the hypothesis.

Recently, it has become clear that the heavy–element absorption systems are actually evolving with redshift, in the sense that there are increasingly fewer systems found on the basis of C IV absorption with increasing redshift (Sargent, Boksenberg, and Steidel 1988; Steidel 1989) over the redshift range $1.5 \leq z_{abs} \leq 3.5$. Steidel, Sargent, and Boksenberg (1988) and Steidel (1989) have presented arguments that favor the interpretation that the observed evolution is caused by an actual change in the average chemical abundance of the absorbers over time, rather than by significant changes in the UV radiation field or other physical properties of the absorbers. This typical change in the abundances was estimated by Steidel (1989) to be a factor of $\gtrsim 3$, or $\Delta[M/H] \gtrsim 0.5$ over the redshift range $3.0 \geq z_{abs} \geq 1.5$. If this interpretation is correct, and if the typical heavy element abundances of the LLSs at $z \approx 3$ is taken to be $[M/H] = -2.5$, then it would be predicted that if an unbiased sample of absorbers at $z \approx 1.5$ could be compiled, their typical abundances would

be $[M/H] \gtrsim -2$. Unfortunately, it is much more difficult to determine the abundances for low–redshift Lyman limit systems than for the $z \approx 3$ systems because an accurate measurement of the H I column density is not possible, since the Lyman series lines and the Lyman limit are not redshifted to optical wavelengths (and IUE not does not have a large enough collecting area to obtain high–dispersion spectra of high redshift QSOs).

It would be interesting to be able to say something about the relative abundances of the elements in the gas clouds, since they would provide some insight into the types of stars and nucleosynthetic processes that were important in the early enrichment history of the gas. For example, metal–poor stars in the halo of the Galaxy appear to have enhanced [O/Fe] and, to a lesser extent, [C/Fe] relative to the solar values. The trend is for these enhancements to increase with decreasing overall metallicity, possibly indicating a changing distribution of stellar masses (and therefore the type of supernovae responsible for enrichment of the gas) with time. Unfortunately, at present, the uncertainties in the gas abundance determinations for the QSO absorption systems are so large that little can be said about relative abundances. For the absorption systems with the best–determined abundance estimates (Table 10), the relative abundances appear to be consistent with the solar values. It appears that Si is not depleted relative to C as it is in the interstellar medium of our Galaxy (see, e.g., Jenkins 1987); this could be explained by the absence of dust in the gas clouds, so that depletion onto grains would be unimportant. Even in the higher H I column density damped Lyman α systems, dust grain depletion has been shown to be well below that in the ISM (Meyer and York 1987; Pettini and Boksenberg 1988); (Fall, Pei, and McMahon 1989 have claimed a detection of dust in the damped Lyman α systems, at the level of $\sim 1/10$ that in the Milky Way); it would not be surprising if little or no dust were present in the typical LLSs, since they are not very optically thick to UV radiation and the grains are not likely to survive.

b) The Cloud Sizes and Masses

Whatever uncertainties exist in the photoionization models strongly affect the derived masses and sizes for the absorbing clouds, as discussed in §VI; however, the numbers turn out to be very important to further discussion of the galactic halo hypothesis for the origin

of the QSO heavy–element absorption systems. It is again appropriate to caution (see also §Vc) that what we are calling "clouds" are likely to be ensembles of clouds, and the sizes and masses are likely to be describing the ensembles, particularly in cases where the heavy–element lines are strong and several unresolved velocity components are probably contributing to the observed lines. Taking $J_0 = 1$ and adopting the suggestions given in §VIa for "probable" values of Γ for the cases in which only an upper or lower limit was obtained (in most cases this means adopting the upper or lower limit as the actual value), then the cloud sizes span the range $1 \lesssim D_c \lesssim 15$ kpc, and the cloud masses are in the range $10^6 \lesssim M_c \lesssim 10^9\ M_\odot$. This size range is consistent with the limits suggested by observations of heavy–element absorption in the spectra of gravitationally lensed QSOs (Weymann *et al.* 1979; Young *et al.* 1981; Foltz *et al.* 1984), and with the range suggested by Bergeron and Stasinska (1986) and by Chaffee *et al.* (1986) on the basis of photoionization models. In addition, Brown *et al.* (1988) have derived properties of an intervening cloud with $z = 0.47$ along the line of sight to 3C 196 using VLBI techniques. The inferred size (> 2.25 kpc) and estimated mass ($\sim 7 \times 10^7\ M_\odot$) agree remarkably well with the properties we have estimated for the Lyman limit clouds at $z \sim 3$.

It is worth mentioning that clouds at the high end of the size range are just stable gravitationally, since the Jeans length is given by

$$D_J \approx 15 \left(\frac{T_4}{n_{-2}} \right)^{1/2} \quad \text{kpc},$$

where n_{-2} is the particle number density in units of 10^{-2} cm^{-3}, so that typically $D_J \approx 15$ kpc and the corresponding Jeans mass is $\sim 10^9\ M_\odot$. It has been argued on theoretical grounds by many workers that even if galaxies formed out of gas clouds with total masses of order $\sim 10^{12} M_\odot$, substructure must have formed quickly because of both thermal and gravitational instabilities (e.g., Saslaw 1968; Larson 1969; Tinsley 1978; Fall and Rees 1985; Rees 1988; Lake 1988). The masses of these "proto–fragments" have in fact been estimated to be in the range 10^7 to $10^9\ M_\odot$ because this is the expected range for the Jeans mass in the proto–galactic material. Many theories of galactic halo formation involve clouds in this range of masses, which over time fall into the general galactic potential from an initial radius of ~ 100 kpc. The only currently observable remnants of this primordial substructure would

then be the halo globular clusters (Tinsley 1978) and an occasional satellite dwarf galaxy. Searle and Zinn (1978) have discussed evidence for the previous existence of such gas clouds in the outer halo of the Galaxy based on the nature of outer halo globular clusters; they envision a scenario in which the proto–fragments at large galactocentric distances continued to evolve on timescales much longer than the timescale for the initial collapse of the central regions of the galaxy. These clouds eventually collapsed because of dissipation and formed the globular clusters, and the unprocessed gas is assumed to have been swept into the galactic disk. The preferred mass scale of $\sim 10^6\ M_\odot$ emerges because larger gas clouds would be broken down by tidal disruption as they fall into the galactic potential, and smaller mass clouds have evaporation timescales significantly smaller than a Hubble time (Fall and Rees 1985; Silk and Norman 1979). *An obvious possible interpretation is that the clouds we observe in absorption are the subgalactic fragments which are thought to have existed during the early evolution of the extended halos of galaxies.* [This interpretation is in agreement with that of Lake (1988), who has suggested that gas clouds with properties similar to those inferred for the absorbers would be a natural consequence under any standard galaxy formation theory.] Under the hypothesis that the absorbing clouds are such subgalactic fragments, it is interesting to note that the tidal radius for a satellite object in a general galactic potential as given by the Jacobi limit is

$$r_t \approx \left(\frac{M_c}{3M_g}\right)^{1/3} R_g,$$

where M_g is the total mass of the galaxy and R_g is the galactocentric radius of the cloud's orbit. For a cloud with mass $\sim 10^9\ M_\odot$ and $M_g \sim 10^{12}\ M_\odot$, and for a radius comparable to the typical inferred galaxy cross section of ~ 100 kpc, then $r_t \sim 10$ kpc (the corresponding tidal radius for a cloud with a mass of a few times 10^6 would be ~ 1 kpc). These simple arguments suggest that despite the uncertainties involved, the derived cloud properties are not physically implausible.

Thus, it may be reasonable to expect that if the high mass clouds are falling in to the gravitational potential of a galaxy, then over time they may be tidally disrupted to produce somewhat smaller clouds, possibly those at the lower range of the inferred masses and sizes. Speculation of this kind is particularly interesting, given that the lower mass range, of order

10^6 to 10^7 $M_\odot$, is remarkably similar to the masses of globular clusters (this coincidence has been remarked by Chaffee *et al.* 1986). The implications are that the QSO heavy–element absorption systems are providing information about galaxy formation and early galactic halo evolution – they may be probing both clouds that are proto–globular clusters, and clouds that have properties similar to gas–rich dwarf galaxies like the Magellanic clouds (as has been suggested by York *et al.* 1986).

c) The Total Baryonic Content of the Heavy Element Absorbers

It can be seen from Table 10 that the typical total hydrogen column density inferred for the Lyman limit absorbing clouds is a few times 10^{20} cm^{-2}. These values are remarkably consistent despite the rather large range of H I column density represented in the sample, and in fact turn out to be roughly the same as the total H column density of the damped Lyman α systems (Wolfe *et al.* 1986). Together with the statistics of the heavy–element and Lyman limit absorption systems compiled from recent large surveys (Sargent, Boksenberg, and Steidel 1988; Sargent, Steidel, and Boksenberg 1989; Steidel 1989), it is possible to estimate the total contribution of the absorbing clouds to the mass density of the universe.

The number of LLSs per unit redshift range along a line of sight to a high redshift QSO is $N(z) \approx 2$ at $z \sim 3$ (SSB); if *all* detected heavy–element systems, including the ones with log N(H I)< 17, are considered, then $N(z) \approx 6$ (Steidel 1989). Assuming that, on average, log N(H)=20.3 for all heavy–element absorption systems, then the total hydrogen column in a unit redshift interval between, say, $z = 2.5$ and $z = 3.5$, is $\sim 1.2 \times 10^{21}$ cm^{-2}. For $q_0 = 0.5$, the corresponding total coordinate distance spanned by the redshift range is $\sim 210h^{-1}$ Mpc. The contribution to Ω by the clouds, Ω_c, is then given approximately by

$$\Omega_c = \frac{1.2 \times 10^{21}}{6h^{-1} \times 10^{26}} \frac{1.3m_p}{1.9h^2 \times 10^{-29}} \left(\frac{1}{1+\langle z \rangle} \right)^3,$$

where $h = H_0/100$ km s^{-1}Mpc^{-1} and m_p is the mass of a hydrogen atom. Evaluating this at $\langle z \rangle \approx 3$,

$$\Omega_c \approx 4h^{-1} \times 10^{-3},$$

which is a substantial fraction of the baryonic mass density of the universe under the standard Big Bang nucleosynthesis scenario ($\Omega_B < 0.034h^{-2} - 0.048h^{-2}$; Boesgaard and

Steigman 1985) and is comparable to the mass density that is due to optically visible galaxies ($0.01 < \Omega_{GAL} < 0.02$; Yang *et al.* 1984) and somewhat greater than the mass density contributed by gas involved in the damped Lyman α systems ($\Omega_{DLA} \approx 2.5 \times 10^{-3}$; Wolfe 1988). The implication is that at early epochs, a substantial fraction of the gas associated with galaxies was in the form of diffuse clouds in an extended halo.

d) Comparison With the Lyman α Forest Clouds

It is interesting to compare the inferred properties of the heavy–element absorption systems with those of the Lyman α forest clouds, which are believed to be intergalactic, and not associated with galaxies. Sargent *et al.* (1980) first suggested that the clouds are pressure–confined by a hot intergalactic medium, and that they have masses in the range $10^7 - 10^8\ M_\odot$, remarkably similar to the range of masses implied by the results of the present work for the Lyman limit absorbing clouds. Limits on the sizes of the Lyman α forest clouds have been set by observations of close QSO pairs and gravitationally lensed objects; the lower limit on the size is $\sim$ 8 kpc (Foltz *et al.* 1984) based on observations of the gravitational lens Q2345+007A,B, and the upper limit is $\sim$ 400 kpc, based on the observation of the QSO pair UM 680, UM 681 (Shaver and Robertson 1983). This suggests that the forest clouds are in general larger and more diffuse than the range inferred for the heavy element absorbing clouds. However, the coincidence in the inferred masses of the two types of clouds that are believed to be distinct suggests the possibility that they actually have similar origins (cf. Tytler 1987), and the principal difference is just the gas density, and hence the ionization level. In fact, using identical photoionization models to those described above, a typical Lyman α forest cloud with N(H I) $\sim 10^{14}$ cm^{-2} would have a density of $\sim 10^{-4}$ cm^{-3} and a size of $\sim$ 50 kpc with an identical gas mass to the inferred mass of the larger heavy–element clouds.

Possibly the strongest demarkation between the Lyman α forest clouds and the heavy element systems is the difference in their clustering properties; as yet, no significant power in the velocity 2–point correlation function has been found on scales $\gtrsim$ 100 km s^{-1}, whereas there is significant clustering of the heavy element systems on scales out to $\sim$ 600 km s^{-1}(Sargent, Boksenberg, and Steidel 1989). However, one might argue that the extended,

diffuse clouds could not exist in the vicinity of a galactic–sized potential, because, for one, they would be tidally disrupted (see §VIIb). Thus, one might expect that the small H I column density clouds would be to some extent *anti–correlated* with galaxies. A similar anti–correlation is expected if the clouds are gravitationally confined by "dark mini–halos" (Rees 1986), or if the pressure of the ambient medium is too high in the vicinity of galaxies to allow the survival of the diffuse clouds (see Sargent 1987) if they are indeed pressure–confined.

One might further suppose that the distribution of heavy element abundance in the clouds would depend on galactocentric distance both because of changing particle densities (and thus H I columns) within the clouds and because of increased probabilities of cloud–cloud collisions which may induce star formation. Chaffee *et al.* (1986) have set an upper limit on the chemical abundance for a possible Lyman α forest cloud of $[M/H] \leq -3.5$, and have concluded that if the clouds really differ from the heavy–element absorbing clouds only in density, then a very wide range of metallicity must exist at high redshift. The low end of the metallicity distribution which we find for the higher H I column density Lyman limit clouds is not far from this upper limit. Thus, the possibility exists that a continuum of heavy element abundances exists, from the very diffuse "forest" clouds (which may have true primordial abundances) to the most metal–rich absorbing clouds with abundances comparable to the solar values.

The differing redshift evolution of the low and high H I column density systems could also be explained by proximity to galactic–sized potentials; the diffuse Lyman α forest clouds may in fact be pressure confined by the intergalactic medium as has been surmised, so that as the universe expands they quickly evaporate, whereas the more dense clouds are presumably falling into the galactic potentials and becoming progressively more dense and more enriched in heavy elements. Thus, at lower redshift, one might expect that most of the observed Lyman lines would be associated with galaxies and therefore would begin to exhibit significant clustering on velocity scales of a few hundred km s^{-1}; in addition, low H I column density clouds would be expected to be extremely rare.

e) The Fate of the Halo Gas

An obvious question to ask, if one accepts the idea of a large number of gas clouds in early galactic halos, is "Where are they now?" As discussed by York (1988, and references therein), there is little evidence that most nearby galaxies have extended gaseous halos. However, as evidenced by the high success rate of finding galaxies associated with moderate redshift ($0.2 \leq z \leq 0.7$) Mg II absorption systems (Bergeron 1988), gaseous halos seem to have been there in the past. It is significant that a very large percentage of the galaxies found by Bergeron and other workers appear to be bright and actively forming stars; it is not a random sampling of field galaxies. A possible interpretation of this fact is that the galaxies are active *because* they have gaseous halos, continuously supplying new gas to the disk. Thus, wherever there are absorbing clouds, there are gaseous halos and therefore star–forming activity. One would then preferentially select young systems that are still evolving by selecting on the basis of the presence of absorption. Under this hypothesis, it would be surprising to find a low–redshift absorption system associated with an elliptical galaxy. By the present epoch, it may be that there is little halo gas left, explaining the many searches for absorption in nearby galaxies which have negative results (e.g., Morton, York, and Jenkins 1986).

VIII. CONCLUSIONS

Observations have been presented for 8 high–redshift QSOs with known Lyman limit absorption systems in the redshift range $2.90 \leq z_{abs} \leq 3.23$. The LLSs have H I column densities in the range $17.0 \leq \log N(\text{H I}) \leq 19.3$. Selected spectral regions were observed with moderate (35–80 km s^{-1}) resolution and high S/N in order to determine both H I and heavy–element column densities in the gas that gives rise to the observed Lyman limit. The column density measurements have been used to constrain photoionization models so that physical properties of the absorbing gas might be inferred. The following principle conclusions resulted:

1. The heavy–element abundances of the clouds at $z \approx 3$ are in the range $-3.0 \lesssim [M/H] \lesssim -1.5$, with a value of $[M/H] \sim -2.5$ being typical. The relative abundances of C, O, and Si are uncertain, but appear to be consistent with uniform depletions relative to the solar

values.

2. For a reasonable assumed intensity of the metagalactic ionizing flux at $z \approx 3$, the densities of the gas cloud ensembles appear to be in the range $0.01 \lesssim n_H \lesssim 0.1$ cm^{-3}, the sizes are in the range $1 \lesssim D_c \lesssim 15$ kpc, and the masses are in the range $10^6 \lesssim M_c \lesssim 10^9$ $M_\odot$. All of the quantities are dependent on the validity of the application of the photoionization models. However, the inferred chemical abundances, sizes, and masses of the clouds responsible for the Lyman limit absorption in the spectra of high redshift QSOs are all consistent with what would be expected for clouds that condensed in extended primordial galactic halos. It is suggested that some of the clouds may be the progenitors of halo globular clusters and satellite dwarf irregular galaxies.

3. The heavy–element absorbing clouds probably represent a significant fraction of the total baryonic mass density observed to be associated with optically visible galaxies at the present epoch, suggesting that a considerable fraction of the gas associated with galaxies was in the form of diffuse clouds in extended halos at early epochs.

4. It is conceivable that the heavy–element absorption systems and the so–called "Lyman α forest" systems have similar origins, but that their differing evolutionary properties are dictated by their association or non–association with galactic gravitational potentials. A continuum of heavy–element abundances may exist among the absorbing clouds, from primordial to near solar abundances.

5. The presence of a gaseous halo is probably indicative of a galaxy that is still actively in the process of forming or evolving. This may explain why galaxies associated with low–redshift QSO heavy–element absorption systems appear to be unusually bright and in the process of forming stars, and why gaseous halos appear to be relatively rare at the present epoch.

Although the results presented are very suggestive, they are far from secure, given the many uncertainties involved. If the association of the heavy–element absorbing clouds with the extended gaseous halos of intervening high redshift galaxies is correct, we may be observing a very important evolutionary era for normal galaxies in the redshift range now accessible ($0.3 \lesssim z_{abs} \lesssim 4$), and the observations of the absorption line systems will provide crucial tests of theories of galaxy formation and evolution. Along these lines, it is clearly of

interest to undertake new *unbiased* surveys of the heavy–element absorption systems over a large range of redshifts, preferably with very high dispersion spectra. In order to obtain an adequate unbiased sample, this will probably have to wait until 10–meter class telescopes are operational.

I would like to thank W. Sargent for the generous donation of observing time which allowed this project to be completed, and for invaluable discussions. J. Carrasco, M. Doyle, J. Henning, S. Staples, and D. Tennant are thanked for their help at Palomar Observatory. Dr. G. Ferland is thanked for providing a copy of his CLOUDY photoionization software.

TABLE 1

OBSERVATIONS

Object	Date (UT)	Exposure (s)	λ Range (Å)	FWHM (Å)
Q0029+0722	1988 Oct 14	7200	4704–5151	1.1
	1988 Oct 14	7200	6085–6739	1.6
	1988 Oct 16	7200	3658–4104	1.1
	1988 Oct 16	7200	6085–6739	1.6
	1988 Oct 17	7200	3658–4101	1.1
	1988 Oct 17	7200	5162–5819	1.6
Q0256+0000	1988 Feb 18	7200	5908–6563	1.6
	1988 Feb 20	7200	5187–5845	1.6
	1989 Jan 8	3600	4728–5175	1.1
	1989 Jan 8	3600	6004–6658	1.6
	1989 Jan 9	7200	3622–4067	1.1
	1989 Jan 9	7200	4728–5175	1.1
	1989 Jan 9	7200	5207–5864	1.6
	1989 Jan 9	7200	6004–6658	1.6
	1989 Jan 10	7200	3622–4067	1.1
	1989 Jan 10	7200	6004–6658	1.6
Q0301−0035	1988 Oct 14	10800	4570–5017	1.1
	1988 Oct 14	10800	5797–6453	1.6
	1988 Oct 16	10800	3550–3995	1.1
	1988 Oct 16	10800	5040–5701	1.6
	1988 Oct 17	7200	3550–3995	1.1
	1988 Oct 17	7200	5040–5701	1.6
Q0636+6801	1988 Feb 18	9000	4664–4876	0.5
	1988 Feb 18	5400	5048–5705	1.6
	1988 Feb 18	3600	5723–6380	1.6
	1988 Oct 17	3600	3550–3995	1.1
	1988 Oct 17	3600	5040–5701	1.6
Q0956+1217	1988 Feb 20	14400	4949–5158	0.5
	1988 Feb 20	14400	6077–6731	1.6
	1988 Feb 21	7200	4949–5158	0.5
	1988 Feb 21	7200	5358–6014	1.6
	1989 Jan 8	7200	3686–4131	1.1
	1989 Jan 8	7200	5322–5980	1.6
	1989 Jan 8	5600	4819–5265	1.1
	1989 Jan 8	5600	6087–6741	1.6
Q1017+1055	1989 Jan 8	7200	3622–4067	1.1
	1989 Jan 8	7200	5959–6614	1.6
	1989 Jan 9	10800	4686–5132	1.1
	1989 Jan 9	10800	5207–5864	1.6
	1989 Jan 9	7200	3622–4067	1.1
	1989 Jan 9	7200	5959–6614	1.6
	1989 Jan 10	10800	3622–4067	1.1
	1989 Jan 10	10800	5959–6614	1.6
Q2233+1341	1988 Oct 14	7200	4704–5151	1.1
	1988 Oct 14	7200	5889–6544	1.6
	1988 Oct 16	14400	3658–4104	1.1
	1988 Oct 16	14400	5889–6544	1.6
	1988 Oct 17	7200	3658–4104	1.1
	1988 Oct 17	7200	5162–5819	1.6

TABLE 2
Absorption Lines in the Spectrum of Q0029+0722

No.	λ_{obs}	$\sigma(\lambda)$	W_{obs}	$\sigma(W)$	S/N	ID	z_{abs}
			3658 – 4104 Å				
1	3708.84	0.17	2.71	0.46	2.4		
2	3712.11	0.20	2.75	0.54	2.1		
3	3714.78	0.12	0.87	0.15	5.9		
4	3717.80	0.12	1.83	0.22	5.2		
5	3720.60	0.12	1.61	0.26	3.5		
6	3722.79	0.13	1.95	0.27	4.0		
7	3725.34	0.20	0.30	0.11	7.9		
8	3729.60	0.16	3.20	0.32	4.3		
9	3733.40	0.17	0.68	0.15	6.6		
10	3736.66	0.14	1.97	0.26	4.4		
11	3738.98	0.12	1.62	0.29	3.2		
12	3743.80	0.14	3.33	0.30	4.7	HI(1025)	2.6499
13	3750.01	0.13	2.62	0.22	6.3		
14	3756.10	0.13	1.26	0.14	8.7		
15	3761.10	0.13	4.45	0.30	5.2		
16	3766.32	0.12	3.18	0.30	3.9		
17	3769.32	0.09	2.04	0.18	6.1		
18	3773.86	0.11	1.64	0.13	10.1	CII(1334)	1.8279
19	3778.17	0.12	0.58	0.08	11.9		
20	3780.37	0.09	0.64	0.08	10.5		
21	3782.98	0.10	2.16	0.18	6.2	CII(1036)	2.6503
22	3785.91	0.08	1.45	0.15	6.2		
23	3787.69	0.08	1.13	0.16	4.6		
24	3789.43	0.08	1.15	0.11	8.4		
25	3794.30	0.08	1.36	0.11	10.2		
26	3796.98	0.09	2.65	0.15	8.3	HI(937)	3.0488
27	3800.60	0.13	0.32	0.06	16.2		
28	3804.28	0.09	0.60	0.06	16.2		
29	3808.19	0.08	2.12	0.10	13.8		
30	3813.34	0.08	2.26	0.10	13.6	CIII(977)	2.9030
31	3820.13	0.07	1.71	0.08	14.9		
32	3822.69	0.07	1.20	0.07	14.7		
33	3828.08	0.09	3.48	0.12	13.7		
34	3837.34	0.07	0.80	0.06	16.4		
35	3841.28	0.08	2.84	0.11	12.1		
36	3845.25	0.10	3.09	0.26	4.4	HI(949)	3.0487
37	3849.56	0.08	4.23	0.14	11.0		
38	3856.07	0.08	0.83	0.06	18.3		
39	3860.28	0.07	1.97	0.09	14.7		
40	3864.12	0.08	0.94	0.06	18.2		
41	3867.88	0.08	1.14	0.07	17.1		
42	3870.37	0.07	0.87	0.06	16.1		
43	3872.74	0.08	0.59	0.05	18.2		
44	3877.84	0.08	1.68	0.09	15.7		
45	3882.40	0.08	3.18	0.15	9.6		
46	3885.94	0.07	1.64	0.12	7.6		
47	3890.21	0.07	1.93	0.12	9.3		
48	3893.70	0.08	2.26	0.12	10.0		
49	3896.62	0.07	0.75	0.06	14.3		
50	3898.97	0.08	0.84	0.07	15.7		

TABLE 2 -*Continued*

No.	λ_{obs}	$\sigma(\lambda)$	W_{obs}	$\sigma(W)$	S/N	ID	z_{abs}
51	3904.38	0.08	2.70	0.12	12.6		
52	3907.94	0.07	1.58	0.10	10.7		
53	3910.09	0.07	0.41	0.04	17.9		
54	3912.27	0.07	0.68	0.05	17.7		
55	3914.93	0.06	1.03	0.06	15.3		
56	3917.70	0.07	1.68	0.08	15.1		
57	3920.97	0.07	0.84	0.05	19.2		
58	3925.44	0.07	1.14	0.06	18.6		
59	3928.82	0.07	1.37	0.06	19.0		
60	3932.24	0.06	1.33	0.06	19.6		
61	3937.72	0.08	5.62	0.15	11.1	HI(972)	3.0489
62	3942.14	0.06	1.21	0.05	18.3	SiIV(1393)	1.8284
63	3944.95	0.07	0.74	0.04	24.9		
64	3947.37	0.09	0.39	0.04	28.4		
65	3951.35	0.11	0.30	0.04	29.6		
66	3956.47	0.07	2.67	0.07	23.2	CIII(977)	3.0495
67	3961.82	0.08	0.46	0.04	29.5		
68	3966.03	0.06	2.71	0.07	21.3	SiIV(1402)	1.8273
69	3971.67	0.07	4.20	0.09	18.9		
70	3979.21	0.09	1.02	0.05	29.3		
71	3983.86	0.11	0.16	0.03	32.5	HI(949)	3.1947
72	3987.93	0.07	1.79	0.06	24.5	HI(949)	3.1990
73	3995.08	0.07	1.53	0.06	26.0		
74	3998.17	0.06	1.24	0.05	21.9		
75	4003.35	0.07	4.37	0.11	14.1	HI(1025)	2.9030
76	4007.75	0.06	1.01	0.04	27.1		
77	4014.12	0.07	0.77	0.04	30.3		
78	4019.60	0.06	3.61	0.07	22.3		
79	4027.52	0.06	3.51	0.08	19.4		
80	4031.18	0.05	1.06	0.04	22.5		
81	4033.92	0.06	2.55	0.06	21.9		
82	4039.89	0.06	1.32	0.04	28.2		
83	4042.67	0.06	0.76	0.03	28.7		
84	4046.72	0.06	1.47	0.06	19.5		
85	4051.88	0.07	4.47	0.10	17.3		
86	4056.52	0.06	1.04	0.04	25.7		
87	4058.61	0.06	0.82	0.03	26.8		
88	4061.80	0.06	1.42	0.05	26.7		
89	4065.66	0.06	1.09	0.04	26.2		
90	4067.77	0.06	0.53	0.03	28.6		
91	4071.07	0.06	0.90	0.04	27.4		
92	4074.82	0.06	1.24	0.04	27.0		
93	4077.63	0.06	0.81	0.04	26.4		
94	4080.60	0.06	1.68	0.06	19.0	HI(972)	3.1958
95	4085.57	0.06	2.51	0.06	22.6		
96	4091.10	0.06	0.99	0.04	28.8		
97	4094.48	0.06	0.85	0.04	29.0		
98	4099.52	0.06	2.09	0.06	20.0	CIII(977)	3.1959

TABLE 2 -*Continued*

No.	λ_{obs}	$\sigma(\lambda)$	W_{obs}	$\sigma(W)$	S/N	ID	z_{abs}
			4704 – 5151 Å				
1	4715.65	0.07	3.07	0.09	18.7		
2	4719.56	0.06	1.65	0.06	19.9		
3	4725.08	0.06	1.65	0.06	21.8	AlII(1670)	1.8281
4	4727.94	0.06	1.52	0.06	21.4		
5	4735.30	0.07	3.62	0.10	15.0		
6	4738.61	0.06	1.50	0.07	15.6		
7	4744.75	0.08	6.16	0.15	12.7	HI(1215)	2.9030
8	4750.29	0.07	0.83	0.05	27.4		
9	4761.66	0.07	1.21	0.05	26.8		
10	4765.72	0.06	1.85	0.06	21.3		
11	4769.07	0.07	1.27	0.05	25.3		
12	4777.69	0.07	1.31	0.06	25.9		
13	4788.12	0.07	1.48	0.06	24.8		
14	4792.05	0.07	1.80	0.06	22.5	SiIV(1393)	2.4382
15	4797.45	0.07	2.99	0.08	21.0		
16	4804.40	0.09	0.90	0.05	27.9		
17	4808.25	0.07	1.20	0.05	25.3		
18	4812.67	0.07	1.04	0.05	26.5		
19	4816.14	0.08	0.74	0.05	27.4		
20	4820.48	0.07	1.68	0.06	23.7	SiIV(1402)	2.4364
						+SiII(1190)	3.0494
21	4824.05	0.07	1.02	0.05	24.8		
22	4832.34	0.08	1.32	0.06	24.5	SiII(1193)	3.0496
23	4835.95	0.07	2.14	0.07	22.0		
24	4841.55	0.10	0.22	0.03	28.6		
25	4843.96	0.09	0.48	0.04	27.3		
26	4847.51	0.07	1.13	0.06	24.3		
27	4852.50	0.09	1.84	0.07	23.9		
28	4861.67	0.08	1.59	0.07	22.7		
29	4867.29	0.07	3.21	0.10	15.4		
30	4872.55	0.08	4.00	0.14	12.4		
31	4876.72	0.07	0.61	0.05	23.2		
32	4883.12	0.07	1.85	0.08	17.3		
33	4886.41	0.07	1.66	0.08	18.3	SiIII(1206)	3.0500
34	4891.73	0.08	1.08	0.06	20.7		
35	4893.99	0.06	0.78	0.05	18.5		
36	4896.29	0.09	0.44	0.05	23.1		
37	4900.07	0.09	0.58	0.05	22.5		
38	4903.63	0.08	1.03	0.06	20.0		
39	4907.19	0.10	0.69	0.06	22.0		
40	4910.84	0.08	1.10	0.07	19.5		
41	4914.92	0.08	3.68	0.14	12.4		
42	4924.21	0.12	11.97	0.30	9.2	HI(1215)	3.0506
43	4939.93	0.09	1.38	0.08	18.9		
44	4942.59	0.09	0.23	0.04	21.9		
45	4945.10	0.12	0.44	0.05	22.5		
46	4947.63	0.08	0.91	0.06	19.6		
47	4953.68	0.08	2.08	0.09	17.5		
48	4957.21	0.07	1.40	0.07	16.4		
49	4960.38	0.07	1.72	0.09	14.0		

TABLE 2 -*Continued*

No.	λ_{obs}	$\sigma(\lambda)$	W_{obs}	$\sigma(W)$	S/N	ID	z_{abs}
50	4963.26	0.07	2.51	0.13	10.2		
51	4967.02	0.07	1.76	0.08	17.4		
52	4972.74	0.12	0.39	0.05	24.2		
53	4979.68	0.08	2.51	0.09	18.3		
54	4983.23	0.10	0.37	0.05	24.0		
55	4986.28	0.12	0.40	0.05	24.6		
56	4988.79	0.11	0.34	0.05	24.8		
57	4991.05	0.08	0.44	0.04	23.2		
58	4996.14	0.09	0.32	0.04	24.9		
59	4998.33	0.07	0.84	0.05	21.0		
60	5002.76	0.08	3.05	0.10	16.8		
61	5008.24	0.07	2.92	0.10	16.3		
62	5015.09	0.06	0.68	0.05	21.5		
63	5017.06	0.06	0.97	0.06	17.6		
64	5019.05	0.06	0.87	0.05	19.1		
65	5021.29	0.06	1.26	0.06	17.6		
66	5027.33	0.09	3.51	0.10	20.6		
67	5034.08	0.08	1.65	0.07	20.9		
68	5038.88	0.07	1.89	0.08	16.9		
69	5042.28	0.08	3.45	0.15	10.2		
70	5048.62	0.06	1.56	0.07	17.1		
71	5051.47	0.07	2.16	0.09	16.6		
72	5061.99	0.08	1.55	0.07	21.2	SiIII(1206)	3.1956
73	5067.29	0.07	3.15	0.11	16.0		
74	5070.84	0.06	1.64	0.09	12.5		
75	5072.97	0.06	0.89	0.06	18.2		
76	5076.65	0.07	2.17	0.09	17.4		
77	5082.76	0.07	2.36	0.10	16.0		
78	5086.64	0.06	1.56	0.09	13.2	SiIV(1393)	2.6496
79	5089.05	0.07	1.76	0.11	10.7		
80	5092.74	0.08	3.46	0.17	9.1		
81	5100.58	0.10	7.89	0.24	9.9	HI(1215)?	3.1957
82	5107.14	0.07	1.97	0.10	12.9		
83	5110.39	0.07	1.83	0.09	14.4		
84	5113.31	0.07	2.21	0.11	11.0		
85	5117.62	0.09	4.28	0.20	7.9		
86	5121.56	0.10	2.78	0.28	4.5	SiIV(1402)	2.6510
87	5124.50	0.07	2.24	0.11	11.8		
88	5128.46	0.06	1.14	0.06	20.5		
89	5133.05	0.07	0.77	0.05	24.6		
90	5137.50	0.07	1.11	0.05	23.6		
91	5141.07	0.06	1.99	0.07	18.5		
92	5143.89	0.06	1.54	0.06	22.7		
			5162 – 5819 Å				
1	5180.89	0.13	0.66	0.07	21.5		
2	5183.67	0.11	0.45	0.06	21.9		
3	5186.06	0.12	0.36	0.05	23.1		
4	5197.03	0.10	2.66	0.11	17.6	NV(1238)	3.1951
5	5201.50	0.10	2.25	0.10	18.7	NV(1238)	3.1988

TABLE 2 -*Continued*

No.	λ_{obs}	$\sigma(\lambda)$	W_{obs}	$\sigma(W)$	S/N	ID	z_{abs}
6	5207.14	0.15	0.34	0.05	26.6		
7	5209.80	0.12	0.35	0.05	26.0	CII(1334)	2.9038
8	5215.97	0.11	4.62	0.13	19.3	NV(1242)	3.1969
9	5224.09	0.18	0.24	0.05	29.6		
10	5236.64	0.09	2.88	0.09	21.9		
11	5244.21	0.10	4.51	0.11	20.7	AlIII(1854)?	1.8275
12	5252.01	0.10	2.00	0.08	26.9		
13	5268.98	0.12	0.63	0.05	32.3	AlIII(1862)	1.8285
14	5273.57	0.12	0.81	0.05	31.8	CIV(1548)	2.4063
						+OI(1302)	3.0498
15	5282.44	0.15	0.55	0.05	33.0	CIV(1550)	2.4063
						+SiII(1304)	3.0498
16	5321.89	0.12	1.39	0.08	24.9	CIV(1548)	2.4375
17	5328.91	0.17	0.40	0.06	27.3	CIV(1550)	2.4363
18	5331.63	0.14	0.40	0.05	26.4	CIV(1550)	2.4380
19	5404.44	0.14	1.31	0.08	23.9	CII(1334)	3.0497
20	5439.85	0.17	0.58	0.07	25.0	SiIV(1393)	2.9030
21	5458.30	0.21	0.36	0.06	24.2	SiIV(1402)	2.9032
22	5475.29	0.18	0.31	0.06	24.8		
23	5645.44	0.18	0.42	0.06	27.1	SiIV(1393)	3.0505
24	5650.93	0.10	2.20	0.09	19.9	CIV(1548)	2.6500
25	5654.28	0.10	0.33	0.04	25.7		
26	5660.44	0.13	1.87	0.09	23.6	CIV(1550)	2.6501
27	5781.88	0.17	1.02	0.09	21.7		
28	5788.62	0.28	0.40	0.08	22.7		
			6085 – 6739 Å				
1	6181.56	0.11	0.51	0.05	31.2	SiII(1526)	3.0489
2	6186.58	0.18	0.21	0.04	33.3		
3	6233.13	0.23	0.29	0.05	35.0		
4	6257.28	0.14	0.26	0.04	34.1		
5	6269.25	0.21	0.23	0.05	36.0	CIV(1548)	3.0494
6	6279.96	0.13	0.54	0.05	34.6	CIV(1550)	3.0496
7	6297.67	0.18	0.38	0.05	33.8		
8	6385.02	0.16	29.70	0.28	22.1	CIV COMPLEX	
9	6486.49	0.11	0.90	0.05	42.3		
10	6493.47	0.06	2.80	0.07	32.6	CIV(1548)	3.1942
11	6498.75	0.06	3.49	0.09	24.0	CIV(1548)	3.1976
12	6504.53	0.06	1.90	0.06	31.8	CIV(1550)	3.1944
13	6509.79	0.07	2.95	0.07	34.6	CIV(1550)	3.1978
14	6529.55	0.14	0.21	0.03	49.0		
15	6532.33	0.13	0.24	0.03	47.1		
16	6630.12	0.08	0.84	0.04	45.1	FeII(2344)	1.8283
17	6715.23	0.17	0.40	0.05	38.9	FeII(2374)	1.8281

TABLE 3
Absorption Lines in the Spectrum of Q0256+0000

No.	λ_{obs}	$\sigma(\lambda)$	W_{obs}	$\sigma(W)$	S/N	ID	z_{abs}
			3622 – 4067 Å				
1	3759.51	0.10	1.83	0.19	5.6		
2	3762.01	0.09	1.27	0.15	6.3		
3	3766.74	0.10	1.77	0.18	5.9		
4	3768.70	0.07	0.78	0.15	4.5	HI(937)?	3.0186
5	3769.97	0.07	0.87	0.13	6.0		
6	3771.62	0.10	0.69	0.10	9.3		
7	3774.60	0.12	0.56	0.09	9.8		
8	3777.26	0.11	1.13	0.13	8.4		
9	3782.08	0.14	3.72	0.24	6.6		
10	3789.38	0.10	1.02	0.12	8.5		
11	3792.42	0.10	0.74	0.10	9.4		
12	3795.03	0.09	0.84	0.10	9.0		
13	3800.32	0.12	4.38	0.26	6.1		
14	3805.11	0.09	1.03	0.11	9.1		
15	3807.26	0.10	0.61	0.09	10.9		
16	3812.30	0.11	0.52	0.08	11.0		
17	3815.17	0.11	0.86	0.10	10.3	HI(949)	3.0171
18	3824.90	0.25	11.57	0.34	9.7		
19	3836.32	0.10	0.51	0.08	10.3		
20	3841.56	0.12	0.52	0.09	10.7		
21	3849.26	0.11	1.01	0.12	9.1		
22	3851.75	0.10	0.54	0.09	9.6		
23	3857.87	0.09	0.86	0.11	8.7		
24	3860.06	0.09	1.06	0.12	7.7		
25	3863.45	0.11	2.86	0.24	5.2		
26	3866.61	0.09	1.24	0.12	8.3		
27	3869.48	0.11	0.58	0.09	11.0		
28	3871.32	0.08	0.45	0.07	10.4		
29	3872.84	0.08	0.54	0.08	9.7		
30	3878.00	0.13	6.42	0.31	6.2	HI(949)	3.0832
31	3884.40	0.12	0.37	0.07	12.0		
32	3886.72	0.09	0.98	0.10	9.9		
33	3888.90	0.09	0.57	0.08	10.7		
34	3891.81	0.15	0.72	0.09	13.1		
35	3898.18	0.09	1.45	0.11	11.4		
36	3902.66	0.10	1.89	0.12	11.4		
37	3907.16	0.09	1.69	0.12	10.3	HI(972)	3.0175
38	3912.09	0.09	0.49	0.07	12.8		
39	3914.56	0.08	1.66	0.11	10.3		
40	3921.19	0.09	2.97	0.14	10.5		
41	3925.24	0.08	1.86	0.11	11.4	CIII(977)	3.0175
42	3934.50	0.11	6.06	0.19	10.7		
43	3941.94	0.13	0.52	0.07	16.4		
44	3946.10	0.13	0.72	0.08	15.8		
45	3954.83	0.11	0.91	0.08	15.0		
46	3959.68	0.09	2.70	0.14	11.4		
47	3970.70	0.11	7.84	0.21	10.7	HI(972)	3.0828
48	3978.12	0.08	0.55	0.06	17.3		
49	3984.62	0.07	0.71	0.06	16.5		
50	3987.40	0.06	1.95	0.11	10.4	HI(949)	3.1984

TABLE 3 -*Continued*

No.	λ_{obs}	$\sigma(\lambda)$	W_{obs}	$\sigma(W)$	S/N	ID	z_{abs}
51	3990.37	0.07	1.55	0.08	14.2	CIII(977)	3.0842
52	4001.07	0.11	0.59	0.06	19.6		
53	4004.83	0.07	2.82	0.13	9.5		
54	4008.23	0.07	2.86	0.15	8.6		
55	4012.55	0.07	2.04	0.10	12.6		
56	4017.98	0.09	5.18	0.16	11.9		
57	4026.23	0.08	1.53	0.08	15.9		
58	4030.50	0.10	0.59	0.06	19.2		
59	4035.61	0.09	0.36	0.05	19.3		
60	4039.10	0.08	1.47	0.08	16.2		
61	4049.64	0.07	1.49	0.09	11.3		
62	4063.44	0.08	1.43	0.08	16.0		
			4728 – 5175 Å				
1	4731.66	0.09	0.27	0.04	24.6		
2	4733.98	0.07	0.93	0.06	20.1		
3	4736.94	0.07	1.26	0.07	18.7		
4	4741.36	0.08	1.81	0.08	19.4		
5	4747.78	0.14	0.71	0.06	24.7		
6	4753.94	0.12	0.47	0.05	24.3		
7	4756.97	0.10	0.62	0.05	23.9		
8	4761.15	0.11	0.21	0.04	25.9		
9	4762.89	0.07	0.42	0.04	23.4		
10	4766.42	0.08	1.10	0.06	22.0		
11	4772.14	0.08	2.57	0.09	19.7		
12	4782.98	0.10	0.23	0.04	25.8		
13	4785.15	0.07	0.69	0.05	21.9		
14	4787.80	0.07	1.22	0.06	18.2		
15	4790.94	0.07	1.25	0.06	19.5		
16	4797.36	0.08	2.51	0.09	19.0		
17	4807.21	0.08	1.29	0.07	20.3		
18	4810.31	0.08	1.07	0.06	20.6		
19	4817.34	0.09	1.07	0.07	21.7		
20	4826.08	0.11	1.00	0.07	22.5		
21	4829.43	0.08	0.50	0.05	22.4		
22	4834.10	0.08	3.41	0.12	15.4		
23	4841.27	0.07	1.43	0.07	17.2		
24	4844.01	0.07	0.98	0.06	19.2		
25	4854.05	0.08	1.79	0.08	18.2		
26	4858.49	0.07	2.17	0.10	15.3		
27	4865.30	0.09	3.69	0.13	13.7		
28	4871.76	0.09	2.55	0.11	16.5		
29	4875.89	0.08	0.47	0.05	19.5	SiII(1193)	3.0861
30	4878.08	0.07	1.24	0.08	15.3		
31	4884.87	0.10	4.09	0.14	14.0	HI(1215)	3.0183
32	4891.18	0.11	0.41	0.06	19.8		
33	4894.66	0.11	0.70	0.07	18.8		
34	4899.23	0.10	1.81	0.10	16.2		
35	4907.00	0.10	1.94	0.10	16.2		
36	4911.71	0.08	0.57	0.06	16.6		
37	4913.60	0.09	0.62	0.06	17.1		
38	4927.68	0.10	1.73	0.10	16.0	SiIII(1206)	3.0842

TABLE 3 -*Continued*

No.	λ_{obs}	$\sigma(\lambda)$	W_{obs}	$\sigma(W)$	S/N	ID	z_{abs}
39	4933.67	0.14	0.22	0.05	20.0		
40	4938.31	0.12	0.67	0.07	18.5		
41	4951.04	0.09	2.98	0.14	11.8		
42	4954.65	0.08	0.91	0.07	15.0		
43	4962.52	0.13	9.80	0.35	6.9	HI(1215)	3.0821
44	4969.46	0.08	2.27	0.18	6.7		
45	4972.37	0.08	2.45	0.16	8.4		
46	4975.34	0.08	0.73	0.07	16.2		
47	4981.20	0.09	1.41	0.10	13.3		
48	4983.84	0.07	0.86	0.08	12.5		
49	4985.92	0.08	1.06	0.08	13.2		
50	5005.19	0.13	0.46	0.06	19.7		
51	5011.46	0.10	3.37	0.14	13.6		
52	5017.13	0.08	2.51	0.13	11.9		
53	5023.05	0.10	1.54	0.10	15.6		
54	5026.22	0.08	1.18	0.09	14.4		
55	5033.87	0.09	2.13	0.12	13.8		
56	5040.03	0.10	1.24	0.09	15.8	MgI(1827)?	1.1981
57	5044.37	0.10	1.97	0.11	13.9		
58	5061.88	0.11	2.82	0.14	13.3		
59	5066.27	0.13	0.61	0.08	15.4		
60	5076.24	0.10	2.18	0.14	10.9		
61	5080.85	0.11	2.09	0.13	12.0		
62	5096.02	0.11	1.47	0.11	14.0		
63	5099.59	0.08	0.39	0.06	15.2		
64	5101.08	0.07	0.62	0.07	12.8		
65	5103.87	0.09	2.33	0.13	11.7	HI(1215)	3.1984
66	5114.75	0.14	0.74	0.08	17.9		
67	5123.92	0.19	0.31	0.06	20.2		
68	5129.32	0.08	2.19	0.11	13.8		
69	5133.50	0.10	3.64	0.24	6.5		
70	5136.91	0.08	1.91	0.15	7.4		
71	5139.81	0.07	1.89	0.12	10.8		
72	5144.97	0.10	5.71	0.19	11.4		
73	5153.24	0.14	0.56	0.07	20.3		
74	5164.59	0.11	0.59	0.06	20.6		
75	5168.40	0.12	0.89	0.07	20.7		
			5187 – 5864 Å				
1	5196.52	0.18	1.20	0.22	6.1		
2	5205.90	0.10	10.21	0.15	19.7	FeII(2367)?	1.1988
3	5219.16	0.14	1.85	0.12	16.4	FeII(2374)	1.1980
4	5228.61	0.16	1.31	0.09	21.6		
5	5236.55	0.12	3.11	0.11	19.4		
6	5243.25	0.15	0.97	0.07	27.9		
7	5256.07	0.10	2.69	0.08	26.1		
8	5259.90	0.10	0.72	0.04	35.7		
9	5264.84	0.13	0.40	0.04	41.0		
10	5268.34	0.14	0.33	0.03	43.5		
11	5282.87	0.09	1.56	0.04	41.7		
12	5287.46	0.09	1.45	0.04	47.5		
13	5298.42	0.16	0.10	0.02	65.6		

TABLE 3 -*Continued*

No.	λ_{obs}	$\sigma(\lambda)$	W_{obs}	$\sigma(W)$	S/N	ID	z_{abs}
14	5424.92	0.22	0.20	0.04	41.0		
15	5521.31	0.24	0.60	0.07	28.1		
16	5716.03	0.19	0.30	0.05	28.9	FeII(2600)	1.1983
				6004 – 6658 Å			
1	6147.46	0.12	2.42	0.11	22.6	MgII(2796)	1.1984
2	6162.90	0.12	1.70	0.10	21.2	MgII(2803)	1.1983
3	6220.41	0.21	0.44	0.07	24.7	CIV(1548)	3.0178
4	6324.09	0.13	0.63	0.08	21.7	CIV(1548)	3.0848
5	6333.72	0.13	0.47	0.07	22.1	CIV(1550)	3.0842
6	6498.36	0.21	0.48	0.08	24.1	CIV(1548)	3.1974
7	6509.79	0.20	0.36	0.06	27.0	CIV(1550)	3.1978

TABLE 4
Absorption Lines in the Spectrum of Q0301−0035

No.	λ_{obs}	$\sigma(\lambda)$	W_{obs}	$\sigma(W)$	S/N	ID	z_{abs}
			3550 – 3995 Å				
1	3648.58	0.14	3.47	0.30	4.5		
2	3651.70	0.11	1.23	0.22	3.7		
3	3653.50	0.12	1.46	0.31	2.6		
4	3656.39	0.11	3.51	0.23	5.9		
5	3665.50	0.12	4.28	0.23	7.1		
6	3672.30	0.12	0.32	0.06	12.9		
7	3676.61	0.10	0.65	0.08	12.2		
8	3682.03	0.09	1.02	0.09	11.3		
9	3685.67	0.09	1.58	0.12	9.4		
10	3689.22	0.10	2.88	0.19	6.6		
11	3694.51	0.11	3.71	0.20	7.3	HI(937)	2.9395
12	3698.83	0.08	0.99	0.09	10.7		
13	3702.67	0.10	3.02	0.16	9.3		
14	3707.06	0.09	0.56	0.07	13.2		
15	3710.22	0.10	1.32	0.10	12.7	HI(937)	2.9563
16	3716.24	0.10	0.47	0.06	14.9		
17	3718.15	0.08	0.74	0.07	13.0		
18	3720.85	0.09	0.48	0.06	15.3		
19	3724.16	0.11	1.02	0.08	15.0		
20	3734.77	0.12	4.62	0.33	4.4		
21	3738.94	0.07	1.23	0.12	6.8		
22	3741.83	0.10	3.19	0.24	5.2	HI(949)	2.9560
23	3746.04	0.08	1.53	0.10	10.7		
24	3751.80	0.08	0.70	0.07	13.1		
25	3757.15	0.09	1.41	0.10	12.1		
26	3768.54	0.09	1.70	0.12	10.0		
27	3771.40	0.09	0.73	0.08	11.5		
28	3775.59	0.10	2.13	0.14	9.2		
29	3788.80	0.11	0.47	0.07	12.7		
30	3794.71	0.14	6.59	0.36	4.8		
31	3799.36	0.08	1.54	0.14	6.8		
32	3805.31	0.07	1.02	0.09	10.8		
33	3807.37	0.07	1.25	0.10	9.3		
34	3811.81	0.08	1.65	0.11	10.1		
35	3817.89	0.11	6.97	0.26	7.3	HI(1025)	2.7221
36	3826.50	0.08	0.56	0.06	16.8		
37	3828.72	0.07	1.81	0.12	8.2		
38	3832.59	0.09	4.63	0.19	7.9	HI(972)	2.9408
39	3838.44	0.09	0.66	0.06	16.8		
40	3842.04	0.08	2.60	0.12	10.9	OVI(1031)?	2.7231
41	3848.92	0.09	5.15	0.17	9.8	HI(972)	2.9576
42	3855.45	0.11	0.28	0.04	21.5		
43	3858.35	0.07	1.44	0.07	15.2	CII(1036)?	2.7231
44	3861.19	0.07	2.11	0.11	10.1		
45	3864.65	0.07	2.51	0.08	17.6	OVI(1037)?	2.7245
						+CIII(977)	2.9555
46	3871.49	0.10	0.55	0.05	25.1		
47	3876.77	0.13	0.46	0.05	25.1		
48	3883.64	0.08	3.18	0.09	17.9		
49	3887.78	0.07	0.55	0.04	20.4		

TABLE 4 -*Continued*

No.	λ_{obs}	$\sigma(\lambda)$	W_{obs}	$\sigma(W)$	S/N	ID	z_{abs}
50	3889.98	0.07	0.91	0.05	20.0		
51	3893.35	0.07	0.83	0.05	21.2		
52	3897.38	0.07	3.41	0.11	12.9		
53	3902.02	0.07	2.99	0.09	15.6		
54	3908.56	0.11	0.38	0.04	25.9		
55	3919.33	0.08	0.89	0.05	25.5		
56	3922.85	0.06	1.07	0.05	23.0		
57	3925.39	0.07	0.78	0.04	25.0		
58	3934.15	0.08	0.74	0.04	27.6		
59	3938.71	0.13	0.35	0.04	29.6		
60	3942.93	0.08	1.06	0.05	24.9		
61	3947.99	0.07	1.54	0.06	22.9		
62	3951.08	0.09	0.41	0.04	28.6		
63	3955.81	0.06	1.99	0.06	19.5		
64	3958.27	0.06	0.90	0.04	20.6		
65	3961.51	0.06	2.36	0.07	18.4		
66	3966.71	0.07	0.68	0.04	28.1		
67	3975.77	0.07	1.61	0.06	23.9		
68	3980.58	0.07	1.53	0.06	23.5		
69	3984.53	0.09	0.31	0.03	29.8		
70	3986.62	0.08	0.27	0.03	30.3		
71	3988.38	0.07	0.28	0.03	29.3		
72	3991.03	0.07	1.02	0.04	26.7		
			4570 – 5017 Å				
1	4575.75	0.12	1.01	0.08	17.5	CII(1334)	2.4287
2	4593.76	0.09	1.57	0.09	15.6		
3	4602.40	0.12	0.89	0.08	18.4		
4	4608.03	0.07	0.88	0.07	15.1		
5	4610.35	0.07	2.01	0.12	10.3		
6	4621.79	0.10	0.87	0.07	18.1		
7	4628.00	0.13	0.29	0.05	20.1		
8	4631.37	0.15	0.50	0.07	20.0		
9	4636.96	0.10	0.86	0.07	18.1		
10	4640.85	0.11	0.74	0.07	18.8		
11	4657.07	0.09	1.10	0.08	16.9		
12	4659.57	0.08	0.79	0.07	15.4		
13	4662.38	0.08	1.17	0.08	15.2		
14	4667.84	0.11	0.83	0.07	18.0		
15	4672.25	0.11	1.00	0.08	17.5		
16	4680.35	0.10	2.31	0.11	15.9		
17	4688.60	0.11	0.67	0.07	18.7		
18	4691.96	0.10	1.46	0.09	17.5		
19	4700.85	0.09	2.68	0.11	15.0		
20	4705.14	0.12	0.55	0.06	19.6		
21	4708.21	0.18	0.33	0.06	20.8		
22	4713.49	0.16	0.31	0.06	20.5		
23	4721.62	0.09	0.82	0.07	18.0	SiII(1193)	2.9568
24	4725.79	0.10	1.25	0.08	17.8		
25	4740.48	0.09	3.21	0.13	13.4		
26	4744.23	0.08	2.00	0.10	12.9		
27	4750.05	0.08	1.37	0.08	16.2		

TABLE 4 -*Continued*

No.	λ_{obs}	$\sigma(\lambda)$	W_{obs}	$\sigma(W)$	S/N	ID	z_{abs}
28	4754.48	0.09	3.53	0.14	12.3	SiIII(1206)	2.9407
29	4766.45	0.10	4.16	0.14	14.3		
30	4771.48	0.09	1.67	0.09	16.4		
31	4778.80	0.13	0.41	0.06	20.2	SiIV(1393)	2.4287
32	4785.59	0.08	3.04	0.13	11.3		
33	4790.27	0.12	5.02	0.34	4.9	HI(1215)	2.9404
34	4794.24	0.07	1.03	0.08	11.8		
35	4796.34	0.07	0.94	0.07	14.8		
36	4799.45	0.16	0.32	0.06	19.9		
37	4810.47	0.11	4.79	0.16	13.4	SiIV(1402)?	2.4293
						+HI(1215)	2.9571
38	4817.20	0.11	0.58	0.06	18.3		
39	4820.47	0.10	0.46	0.06	18.4		
40	4827.15	0.12	0.79	0.08	18.0		
41	4830.32	0.13	0.44	0.06	18.9		
42	4833.09	0.14	0.31	0.06	19.2		
43	4838.90	0.12	2.85	0.13	15.3		
44	4846.27	0.15	1.83	0.11	17.9		
45	4856.11	0.09	3.50	0.16	10.2		
46	4859.80	0.07	1.71	0.11	10.7		
47	4862.59	0.08	0.75	0.07	15.6		
48	4865.00	0.07	1.00	0.08	13.8		
49	4868.89	0.09	1.99	0.11	13.7		
50	4875.10	0.11	2.62	0.13	14.0		
51	4879.40	0.08	1.04	0.08	14.2		
52	4881.80	0.08	0.64	0.07	14.6		
53	4885.57	0.12	2.85	0.14	13.6		
54	4893.15	0.11	1.86	0.12	14.1		
55	4893.15	0.11	1.86	0.12	14.1		
56	4897.56	0.09	1.96	0.12	12.1		
57	4901.42	0.09	0.73	0.08	14.5		
58	4903.36	0.08	0.77	0.08	12.7		
59	4910.85	0.18	0.36	0.07	16.9		
60	4914.62	0.11	1.69	0.11	13.7		
61	4919.27	0.16	0.61	0.08	17.2		
62	4923.96	0.14	0.58	0.08	17.2		
63	4930.59	0.09	1.77	0.11	13.8		
64	4934.67	0.09	2.66	0.15	10.2		
65	4939.10	0.09	0.27	0.05	18.3		
66	4942.03	0.08	1.83	0.11	13.2		
67	4946.10	0.09	3.13	0.13	13.1		
68	4955.72	0.09	1.61	0.09	16.4		
69	4959.44	0.08	0.77	0.06	17.7		
70	4961.79	0.09	0.53	0.06	19.5		
71	4969.45	0.10	5.88	0.16	14.0	CII(1334)	2.7237
72	4984.32	0.08	2.68	0.11	14.6		
73	4988.95	0.08	3.28	0.16	9.4		
74	4992.26	0.07	1.41	0.09	12.8		
75	4995.05	0.07	1.76	0.10	12.5		
76	4997.60	0.08	0.56	0.05	20.9		
77	5002.61	0.10	2.58	0.10	18.9		
78	5012.00	0.08	1.80	0.08	18.8		

TABLE 4 -*Continued*

No.	λ_{obs}	$\sigma(\lambda)$	W_{obs}	$\sigma(W)$	S/N	ID	z_{abs}
			5040 – 5701 Å				
1	5053.87	0.15	1.59	0.13	13.2		
2	5057.51	0.12	0.56	0.08	15.6		
3	5059.89	0.13	0.46	0.07	17.2		
4	5062.88	0.16	0.56	0.08	19.1		
5	5072.15	0.15	0.95	0.08	21.7		
6	5080.19	0.13	2.64	0.11	21.2		
7	5088.51	0.11	3.70	0.11	20.9		
8	5098.57	0.12	3.95	0.10	25.8		
9	5108.58	0.19	0.29	0.04	37.9		
10	5114.26	0.19	0.40	0.04	40.3		
11	5120.23	0.12	0.30	0.03	41.7		
12	5123.42	0.15	0.27	0.03	43.7		
13	5136.13	0.13	0.33	0.03	44.8		
14	5143.60	0.25	0.17	0.03	47.1		
15	5189.87	0.12	2.91	0.08	31.4	SiIV(1393)	2.7237
16	5209.41	0.13	0.30	0.04	37.6		
17	5224.18	0.12	1.55	0.06	34.6	SiIV(1402)	2.7242
18	5258.54	0.16	0.69	0.05	36.0	CII(1334)	2.9404
19	5289.49	0.21	0.32	0.05	32.4		
20	5308.91	0.12	0.78	0.06	28.3	CIV(1548)	2.4291
21	5315.89	0.18	0.26	0.05	30.4		
22	5318.10	0.12	0.21	0.04	29.7	CIV(1550)	2.4293
23	5330.43	0.24	0.44	0.06	30.0		
24	5339.65	0.23	0.32	0.06	29.7		
25	5491.99	0.14	1.58	0.09	24.7	SiIV(1393)	2.9404
26	5515.97	0.17	0.90	0.07	28.7	FeII(1608)	2.4294
						+SiIV(1393)?	2.9576
27	5527.23	0.14	1.59	0.08	26.7	SiIV(1402)	2.9402
28	5631.99	0.18	0.29	0.05	29.6		
29	5635.13	0.17	0.22	0.04	30.0		
			5797 – 6453 Å				
1	5889.89	0.17	0.71	0.12	12.9	NaI(5891)	-0.0003
2	5896.52	0.30	0.65	0.14	13.1	NaI(5897)	-0.0002
3	6100.81	0.12	1.65	0.13	14.1	CIV(1548)	2.9406
4	6111.01	0.18	0.93	0.11	16.7	CIV(1550)	2.9406
5	6125.42	0.16	0.63	0.09	17.1	CIV(1548)?	2.9563
6	6137.62	0.29	0.40	0.09	19.0	CIV(1550)?	2.9578
7	6184.79	0.25	0.71	0.11	19.4		
8	6221.22	0.20	0.45	0.08	19.5	AlII(1670)	2.7235
9	6233.98	0.35	0.72	0.12	19.2		

TABLE 5
Absorption Lines in the Spectrum of Q0636+6801

No.	λ_{obs}	$\sigma(\lambda)$	W_{obs}	$\sigma(W)$	S/N	ID	z_{abs}
			3550 – 3995 Å				
1	3595.12	0.07	3.67	0.14	10.5		
2	3600.81	0.06	2.34	0.12	8.7		
3	3604.59	0.07	3.62	0.12	11.9		
4	3615.88	0.08	4.33	0.14	11.9		
5	3623.13	0.10	0.59	0.06	16.9		
6	3627.90	0.07	1.01	0.07	14.7	HI(937)	2.8685
7	3633.25	0.08	3.36	0.14	9.9		
8	3637.99	0.10	0.36	0.05	16.9		
9	3643.86	0.08	4.53	0.16	10.4		
10	3649.47	0.07	2.57	0.11	11.9	HI(937)	2.9031
11	3655.04	0.10	0.48	0.05	19.3		
12	3660.37	0.07	4.17	0.12	13.6		
13	3673.91	0.06	1.24	0.06	17.6	HI(949)	2.8683
14	3677.85	0.10	0.19	0.03	23.7		
15	3681.22	0.10	0.28	0.04	23.7		
16	3685.21	0.07	0.89	0.05	21.0		
17	3689.08	0.08	0.93	0.06	21.8		
18	3696.64	0.07	1.46	0.06	19.1	HI(949)	2.8923
19	3700.24	0.06	1.05	0.06	17.6		
20	3702.40	0.05	1.41	0.07	14.6		
21	3707.76	0.07	5.19	0.13	12.9	HI(949)	2.9040
22	3714.40	0.06	1.80	0.07	18.0		
23	3717.29	0.06	0.83	0.05	20.4		
24	3721.22	0.14	0.22	0.04	25.4		
25	3725.32	0.08	1.31	0.06	22.3		
26	3731.03	0.06	1.72	0.07	19.4		
27	3735.77	0.07	0.90	0.05	21.5		
28	3738.97	0.07	0.81	0.05	21.0		
29	3743.06	0.10	0.64	0.05	22.9		
30	3746.38	0.07	0.68	0.05	22.1		
31	3749.50	0.10	0.34	0.04	24.0		
32	3754.68	0.07	0.80	0.05	22.0		
33	3762.59	0.06	2.89	0.09	15.8	HI(972)	2.8688
34	3770.56	0.07	3.61	0.11	14.3		
35	3776.17	0.07	3.42	0.12	12.6		
36	3781.41	0.06	0.96	0.06	17.1	CIII(977)?	2.8703
37	3785.21	0.07	3.23	0.11	13.2	HI(972)	2.8921
38	3791.55	0.06	0.62	0.05	19.6		
39	3796.55	0.07	4.19	0.12	13.9	HI(972)	2.9038
40	3802.02	0.07	1.05	0.06	21.4	CIII(977)	2.8914
41	3808.27	0.06	3.45	0.09	16.3	HI(949)	3.0098
42	3813.68	0.07	4.79	0.13	11.8	CIII(977)	2.9035
43	3818.00	0.06	0.45	0.04	24.0		
44	3820.03	0.09	0.23	0.03	26.5		
45	3821.80	0.06	0.25	0.03	27.4		
46	3823.21	0.08	0.25	0.03	28.7		
47	3827.20	0.12	0.29	0.04	30.1		
48	3831.57	0.07	1.29	0.05	25.2		
49	3838.08	0.07	1.71	0.06	25.3		
50	3842.93	0.07	0.45	0.03	29.2		

TABLE 5 –*Continued*

No.	λ_{obs}	$\sigma(\lambda)$	W_{obs}	$\sigma(W)$	S/N	ID	z_{abs}
51	3845.03	0.06	0.70	0.04	26.6		
52	3851.40	0.06	1.50	0.05	26.0		
53	3856.02	0.05	3.91	0.09	17.2		
54	3860.93	0.05	1.55	0.05	24.6		
55	3864.19	0.05	1.13	0.04	27.4		
56	3867.34	0.09	0.17	0.02	34.6		
57	3872.49	0.07	0.85	0.04	31.0		
58	3879.00	0.05	0.97	0.04	28.0		
59	3881.93	0.05	1.90	0.05	22.9		
60	3885.23	0.06	0.55	0.03	28.6		
61	3889.76	0.05	2.12	0.06	19.4		
62	3893.09	0.05	2.46	0.06	21.4		
63	3897.31	0.05	1.78	0.05	24.3		
64	3899.92	0.06	0.48	0.03	32.9	HI(972)	3.0098
65	3903.60	0.05	1.81	0.05	26.1		
66	3907.45	0.05	1.04	0.04	30.9	HI(972)	3.0178
67	3910.25	0.06	0.37	0.03	34.7		
68	3915.72	0.06	0.67	0.03	34.0		
69	3921.34	0.05	0.64	0.03	34.9		
70	3924.69	0.05	0.78	0.03	34.9	CIII(977)	3.1070
71	3928.19	0.05	2.47	0.05	25.4		
72	3931.87	0.05	0.87	0.03	34.7		
73	3934.47	0.06	0.37	0.03	38.3		
74	3938.99	0.07	0.32	0.02	38.7		
75	3940.84	0.07	0.18	0.02	38.7		
76	3943.03	0.06	0.43	0.03	37.0		
77	3945.40	0.05	0.88	0.03	34.4		
78	3950.82	0.06	0.47	0.03	37.9		
79	3953.13	0.05	0.68	0.03	34.6		
80	3956.35	0.05	1.13	0.03	34.0		
81	3965.12	0.06	0.43	0.03	38.1		
82	3968.23	0.05	2.40	0.05	28.6	HI(1025)	2.8687
83	3973.13	0.06	1.06	0.04	36.3		
84	3978.30	0.05	2.27	0.05	29.3		
85	3982.28	0.07	0.34	0.03	39.8		
86	3986.85	0.05	2.87	0.05	27.2		
			4664 – 4876 Å				
1	4668.83	0.04	1.29	0.03	27.4	SiIII(1206)	2.8697
2	4671.10	0.04	0.20	0.02	32.9		
3	4673.36	0.04	1.54	0.04	25.8		
4	4677.89	0.05	0.78	0.03	31.7		
5	4680.38	0.04	0.26	0.02	34.3		
6	4682.28	0.04	0.91	0.03	29.5		
7	4690.46	0.04	0.38	0.02	33.4		
8	4699.05	0.04	1.40	0.03	26.7		
9	4702.84	0.04	3.49	0.05	21.4	HI(1215)	2.8685
10	4709.13	0.03	0.92	0.03	26.4		
11	4711.38	0.04	2.31	0.05	19.6	SiIII(1206)	2.9050
12	4719.56	0.05	0.20	0.02	36.3		
13	4725.54	0.05	0.31	0.02	35.1		
14	4731.55	0.04	6.45	0.08	20.0	HI(1215)	2.8921

TABLE 5–*Continued*

No.	λ_{obs}	$\sigma(\lambda)$	W_{obs}	$\sigma(W)$	S/N	ID	z_{abs}
15	4737.81	0.04	0.50	0.02	31.3		
16	4745.79	0.04	6.09	0.08	17.0	HI(1215)	2.9038
17	4750.62	0.03	0.89	0.03	23.2		
18	4752.21	0.03	1.26	0.04	18.6		
19	4753.85	0.03	0.44	0.02	31.1		
20	4758.30	0.04	2.73	0.04	26.0		
21	4763.18	0.05	0.20	0.02	35.5		
22	4765.67	0.04	1.30	0.03	28.9		
23	4768.81	0.05	0.12	0.01	35.9		
24	4789.25	0.04	1.84	0.04	28.4		
25	4792.49	0.05	0.23	0.02	35.4		
26	4798.79	0.04	1.21	0.03	26.5		
27	4800.52	0.03	0.67	0.02	25.9		
28	4802.36	0.03	1.26	0.03	24.1		
29	4805.19	0.04	1.32	0.03	27.6		
30	4809.45	0.04	0.38	0.02	32.2		
31	4810.77	0.04	0.26	0.02	33.6		
32	4812.72	0.04	0.36	0.02	33.6		
33	4814.51	0.04	0.32	0.02	34.9		
34	4817.58	0.05	0.17	0.02	35.8		
35	4819.83	0.05	0.27	0.02	34.5		
36	4827.58	0.04	0.93	0.03	25.6		
37	4829.20	0.04	0.41	0.02	29.5		
38	4830.81	0.04	0.82	0.03	25.5		
39	4832.63	0.05	0.09	0.01	34.1		
40	4836.89	0.04	0.53	0.02	30.8	SiIII(1206)	3.0090
41	4840.16	0.04	1.23	0.04	20.0		
42	4842.10	0.04	1.58	0.05	14.2		
43	4843.78	0.03	0.39	0.02	27.1		
44	4848.28	0.05	0.24	0.02	30.9	SiIII(1206)	3.0184
45	4850.07	0.04	0.71	0.03	24.6		
46	4851.88	0.04	0.59	0.03	23.2		
47	4853.24	0.04	1.02	0.03	20.0		
48	4856.06	0.05	0.40	0.02	27.7		
49	4857.87	0.04	0.81	0.03	23.3		
50	4860.25	0.04	0.81	0.03	23.7		
51	4863.65	0.04	1.55	0.05	18.6		
52	4867.59	0.04	2.53	0.06	15.4		
53	4875.52	0.04	2.07	0.08	11.1	SiII(1260)	2.8682
						+HI(1215)?	3.0106

5040 – 5705 Å

1	5075.14	0.08	2.14	0.04	56.6		
2	5084.46	0.13	0.24	0.02	66.2	OI(1302)	2.9046
3	5092.68	0.12	0.48	0.03	65.9	SiII(1304)	2.9043
4	5109.44	0.14	0.14	0.02	66.8		
5	5126.49	0.09	0.83	0.03	63.0	CIV(1548)	2.3113
6	5134.95	0.11	0.49	0.03	64.7	CIV(1550)	2.3112
7	5148.47	0.13	0.19	0.02	67.3		
8	5210.98	0.07	1.31	0.03	64.1	CII(1334)	2.9047
9	5366.22	0.19	0.12	0.02	77.0		
10	5379.68	0.08	1.34	0.03	69.6	CIV(1548)	2.4748

TABLE 5 -*Continued*

No.	λ_{obs}	$\sigma(\lambda)$	W_{obs}	$\sigma(W)$	S/N	ID	z_{abs}
11	5388.92	0.10	0.76	0.03	75.2	CIV(1550)	2.4750
12	5441.70	0.07	1.95	0.03	71.8	SiIV(1393)	2.9043
13	5459.85	0.17	0.28	0.02	82.8		
14	5476.87	0.07	1.43	0.02	81.0	SiIV(1402)	2.9043
15	5531.85	0.12	0.39	0.02	91.4	AlII(1670)	2.3109
				5723 – 6380 Å			
1	5891.81	0.07	0.45	0.03	40.7	NaI(5891)	0.0000
2	5897.61	0.07	0.33	0.03	40.3	NaI(5897)	0.0000
3	5961.10	0.06	0.66	0.03	48.9	SiII(1526)	2.9045
4	5988.98	0.16	0.31	0.03	54.0	CIV(1548)	2.8683
5	6025.70	0.09	0.51	0.03	52.0	CIV(1548)	2.8921
6	6035.61	0.14	0.22	0.03	54.4	CIV(1550)	2.8920
7	6044.22	0.06	2.80	0.06	44.2	CIV(1548)	2.9040
8	6054.13	0.07	1.86	0.05	48.0	CIV(1550)	2.9039
9	6207.99	0.21	0.14	0.03	60.1	CIV(1548)?	3.0098
10	6214.06	0.10	0.21	0.02	58.7	CIV(1548)	3.0174
11	6219.81	0.08	0.55	0.03	57.0		
12	6224.62	0.22	0.17	0.03	60.2	CIV(1550)	3.0174
13	6230.07	0.11	0.36	0.03	59.0		
14	6280.42	0.16	0.53	0.04	59.3	FeII(1608)?	2.9046
15	6286.75	0.17	0.18	0.03	59.3		

TABLE 6
Absorption Lines in the Spectrum of Q0956+1217

No.	λ_{obs}	$\sigma(\lambda)$	W_{obs}	$\sigma(W)$	S/N	ID	z_{abs}
				3685 – 4131 Å			
1	3869.78	0.05	1.11	0.06	14.3		
2	3873.09	0.06	1.59	0.07	16.2		
3	3876.60	0.06	1.93	0.07	18.5		
4	3881.97	0.06	2.29	0.09	14.4		
5	3884.66	0.05	1.43	0.07	15.8		
6	3889.97	0.07	4.16	0.13	11.4		
7	3894.80	0.07	3.66	0.17	8.1	HI(937)	3.1531
8	3898.95	0.08	2.99	0.21	5.7	HI(949)	3.1053
9	3902.55	0.06	2.80	0.11	11.6		
10	3907.09	0.05	1.26	0.07	13.8	HI(949)	3.1138
11	3910.37	0.07	3.49	0.13	10.6		
12	3914.30	0.07	0.65	0.05	18.9		
13	3916.84	0.06	1.18	0.07	14.0		
14	3918.78	0.06	0.96	0.06	16.6		
15	3925.09	0.10	0.74	0.06	21.5		
16	3929.85	0.06	2.05	0.08	15.9	HI(1025)	2.8313
17	3932.96	0.06	1.29	0.06	16.1		
18	3938.30	0.07	3.96	0.14	10.7		
19	3943.10	0.07	4.06	0.17	8.5	HI(949)	3.1518
20	3948.35	0.06	0.67	0.05	20.8		
21	3950.35	0.06	0.48	0.04	21.9		
22	3953.62	0.06	2.31	0.08	18.4		
23	3960.19	0.07	1.61	0.06	22.7	HI(937)	3.2228
24	3965.03	0.06	1.78	0.06	20.8		
25	3968.67	0.06	3.18	0.08	17.9		
26	3977.12	0.05	1.72	0.06	19.5		
27	3980.12	0.05	1.43	0.06	18.4		
28	3983.59	0.06	2.56	0.08	14.9		
29	3987.42	0.05	1.61	0.06	19.3		
30	3992.77	0.06	4.40	0.11	14.4	HI(972)	3.1055
31	3997.27	0.06	0.87	0.04	25.0		
32	4001.71	0.06	2.42	0.07	22.0	HI(972)	3.1170
33	4010.15	0.06	3.01	0.08	21.8	CIII(977)	3.1044
						+HI(949)	3.2224
34	4015.77	0.06	1.79	0.06	21.0		
35	4019.16	0.05	1.53	0.06	19.4	CIII(977)	3.1137
36	4023.70	0.06	4.71	0.10	17.0	HI(1215)?	2.3099
37	4033.05	0.07	1.61	0.06	25.8		
38	4038.54	0.06	3.68	0.10	15.1	HI(972)	3.1526
39	4043.73	0.06	3.85	0.10	15.7		
40	4055.14	0.05	3.04	0.08	16.2		
41	4059.00	0.05	2.56	0.07	17.3		
42	4063.38	0.05	2.30	0.06	21.8		
43	4070.40	0.06	0.75	0.04	29.5		
44	4073.59	0.05	0.96	0.04	27.8		
45	4075.90	0.06	0.29	0.03	31.9		
46	4077.55	0.06	0.41	0.03	30.2		
47	4082.65	0.06	2.81	0.06	25.5		
48	4093.37	0.07	0.27	0.03	34.6		
49	4095.36	0.07	0.36	0.03	34.1		

TABLE 6 -*Continued*

No.	λ_{obs}	$\sigma(\lambda)$	W_{obs}	$\sigma(W)$	S/N	ID	z_{abs}
50	4097.66	0.09	0.20	0.03	35.6		
51	4102.13	0.07	0.26	0.03	35.0		
52	4107.40	0.06	2.90	0.06	26.6	HI(972)	3.2234
53	4113.52	0.06	2.10	0.05	27.5		
54	4118.06	0.08	0.31	0.03	35.2		
55	4124.87	0.05	3.22	0.07	22.3	CIII(977)	3.2219
				4949 – 5158 Å			
1	4953.52	0.05	1.14	0.07	10.6	SiII(1193)	3.1531
2	4955.77	0.05	1.27	0.08	10.0		
3	4958.46	0.04	0.57	0.05	12.2		
4	4959.91	0.05	0.63	0.05	12.7	CII(1334)	2.7166
5	4961.90	0.07	0.41	0.05	15.2		
6	4968.83	0.07	0.26	0.04	16.4		
7	4970.48	0.07	0.26	0.04	16.2		
8	4973.02	0.05	1.59	0.08	11.1		
9	4977.41	0.06	3.20	0.13	8.7		
10	4981.47	0.06	3.24	0.15	7.1		
11	4984.65	0.05	0.47	0.04	14.7		
12	4989.62	0.07	5.11	0.17	7.9	HI(1215)	3.1044
13	4994.06	0.09	0.23	0.04	17.2		
14	5000.62	0.07	5.58	0.17	8.6	HI(1215)	3.1135
15	5004.97	0.05	1.61	0.10	7.4		
16	5006.90	0.04	0.52	0.04	13.7		
17	5009.54	0.05	0.60	0.05	14.6	SiIII(1206)	3.1521
18	5011.27	0.03	0.42	0.04	12.5		
19	5012.14	0.03	0.35	0.04	11.7		
20	5013.01	0.04	0.32	0.04	14.2		
21	5014.64	0.04	1.01	0.06	12.1		
22	5017.16	0.06	0.60	0.05	14.9		
23	5020.74	0.05	1.30	0.07	10.9		
24	5022.17	0.03	0.53	0.06	6.9		
25	5023.63	0.06	1.79	0.14	5.3		
26	5025.94	0.05	1.43	0.08	9.8		
27	5028.12	0.06	0.40	0.04	15.7		
28	5032.15	0.06	1.70	0.08	12.9		
29	5035.12	0.05	0.46	0.04	14.4		
30	5036.49	0.06	0.31	0.04	15.9		
31	5041.38	0.06	1.79	0.08	12.1		
32	5047.74	0.08	5.51	0.17	8.6	HI(1215)	3.1522
33	5053.41	0.05	1.86	0.10	8.2		
34	5055.04	0.04	0.72	0.08	6.4		
35	5056.65	0.05	1.50	0.09	8.9		
36	5058.74	0.07	0.25	0.04	15.3		
37	5064.55	0.06	0.38	0.05	13.6		
38	5068.11	0.07	0.93	0.07	12.7		
39	5070.44	0.07	0.28	0.04	14.4		
40	5071.91	0.05	0.14	0.03	14.4		
41	5073.21	0.05	0.68	0.06	11.4		
42	5076.44	0.05	1.30	0.08	9.8		
43	5079.35	0.07	3.62	0.16	6.8		
44	5094.74	0.07	0.67	0.06	13.2	SiIII(1206)	3.2227

TABLE 6 -*Continued*

No.	λ_{obs}	$\sigma(\lambda)$	W_{obs}	$\sigma(W)$	S/N	ID	z_{abs}
45	5096.77	0.07	0.30	0.04	14.3		
46	5098.04	0.06	0.26	0.04	14.3		
47	5101.63	0.05	1.59	0.09	9.0		
48	5103.86	0.05	1.30	0.09	8.9		
49	5106.26	0.05	0.86	0.06	12.2		
50	5110.79	0.09	0.32	0.05	15.5		
51	5114.66	0.05	1.15	0.07	10.5		
52	5116.36	0.06	2.14	0.15	5.8		
53	5118.88	0.06	2.02	0.15	5.4		
54	5121.91	0.05	1.91	0.10	9.1		
55	5125.08	0.04	0.64	0.05	13.9	CIV(1548)?	2.3103
56	5126.55	0.04	0.65	0.05	13.0		
57	5133.80	0.07	5.30	0.16	8.8	HI(1215)	3.2230
58	5139.50	0.05	1.23	0.06	15.5		
			4819 – 5265 Å				
1	4824.39	0.07	1.70	0.05	31.6		
2	4830.01	0.06	0.75	0.04	32.4	SiII(1260)	2.8321
3	4832.61	0.07	1.02	0.04	32.1		
4	4840.50	0.07	2.92	0.07	27.5		
5	4845.28	0.09	0.21	0.03	36.0		
6	4848.90	0.12	0.19	0.03	36.8		
7	4852.45	0.08	0.38	0.03	34.5		
8	4854.66	0.07	0.46	0.03	33.6		
9	4856.83	0.13	0.18	0.03	37.0		
10	4862.05	0.09	1.21	0.05	33.1		
11	4876.01	0.08	4.28	0.09	25.2		
12	4884.16	0.11	0.39	0.04	32.9		
13	4895.33	0.07	1.92	0.06	24.5		
14	4900.57	0.11	0.27	0.04	30.4		
15	4905.83	0.12	0.40	0.04	30.6		
16	4913.55	0.09	1.27	0.06	27.2		
17	4921.96	0.07	3.06	0.08	21.0		
18	4926.64	0.07	2.91	0.08	19.5		
19	4943.96	0.12	1.06	0.06	29.5	SiII(1190)	3.1531
20	4949.41	0.08	0.53	0.04	29.1		
21	4954.60	0.07	3.48	0.09	21.5	SiII(1193)	3.1521
22	4960.19	0.07	1.66	0.06	25.4		
23	4967.56	0.07	0.36	0.03	29.5		
24	4969.45	0.07	0.40	0.03	28.9		
25	4973.39	0.07	2.09	0.07	21.4		
26	4976.47	0.06	1.04	0.05	19.2		
27	4981.05	0.08	5.80	0.14	15.0		
28	4990.03	0.07	5.26	0.12	16.9	HI(1215)	3.1048
29	5002.02	0.08	8.02	0.14	18.2	HI(1215)	3.1146
30	5009.73	0.06	0.74	0.04	26.9	SiIII(1206)	3.1522
31	5012.07	0.06	0.91	0.04	25.0		
32	5014.86	0.06	1.36	0.05	22.5		
33	5017.60	0.07	0.57	0.04	28.7		
34	5020.77	0.06	1.42	0.06	21.8		
35	5023.69	0.07	2.60	0.11	12.4		
36	5026.53	0.06	1.86	0.06	22.4		

TABLE 6 -*Continued*

No.	λ_{obs}	$\sigma(\lambda)$	W_{obs}	$\sigma(W)$	S/N	ID	z_{abs}
37	5032.39	0.07	2.00	0.07	25.0		
38	5036.25	0.07	0.58	0.04	28.2		
39	5041.84	0.07	1.99	0.07	23.9		
40	5048.21	0.07	5.62	0.13	15.1	HI(1215)	3.1526
41	5055.31	0.07	4.29	0.11	16.6		
42	5064.98	0.09	0.53	0.05	27.2		
43	5068.89	0.08	1.08	0.06	24.6		
44	5073.26	0.07	1.16	0.06	22.7		
45	5078.80	0.08	5.05	0.13	16.4		
46	5095.06	0.11	0.79	0.06	25.8	SiIII(1206)	3.2230
47	5098.14	0.12	0.29	0.04	27.4		
48	5102.63	0.07	3.10	0.10	17.0		
49	5106.26	0.07	1.04	0.06	22.7		
50	5110.78	0.09	0.61	0.05	26.3		
51	5117.04	0.08	5.19	0.13	15.8		
52	5122.08	0.06	2.18	0.08	16.6		
53	5125.78	0.06	1.52	0.06	22.4		
54	5133.48	0.08	6.09	0.12	18.2	HI(1215)	3.2228
55	5139.58	0.06	1.39	0.05	25.7		
56	5144.12	0.11	0.44	0.04	33.2		
57	5149.45	0.18	0.24	0.04	35.2		
58	5156.71	0.08	0.66	0.04	32.7		
59	5161.84	0.06	3.12	0.07	22.9		
60	5165.50	0.06	1.38	0.05	28.8		
61	5172.30	0.06	1.11	0.04	31.4	SiII(1260)	3.1036
62	5175.94	0.06	2.00	0.06	25.9		
63	5181.87	0.09	0.32	0.03	36.7		
64	5186.17	0.07	1.00	0.04	32.1	SiII(1260)	3.1146
65	5189.41	0.06	1.11	0.04	28.9		
66	5194.97	0.07	2.92	0.07	25.0		
67	5200.09	0.06	2.95	0.09	18.2		
68	5205.08	0.07	0.68	0.04	31.2		
69	5208.10	0.09	0.51	0.04	32.3		
70	5214.27	0.08	1.47	0.06	28.2		
71	5217.50	0.06	1.52	0.06	23.6		
72	5222.95	0.07	0.85	0.05	25.9		
			5322 – 6014 Å				
1	5530.96	0.12	0.38	0.03	62.1	AlII(1670)	2.3104
2	5661.78	0.15	0.32	0.03	65.6		
3	5754.48	0.15	0.28	0.03	66.7	CIV(1548)	2.7169
4	5764.07	0.13	0.20	0.02	66.1	CIV(1550)	2.7169
5	5768.81	0.18	0.30	0.03	60.7	CIV(1548)?	2.7261
6	5777.24	0.16	0.11	0.02	67.5	CIV(1550)?	2.7254
7	5780.44	0.12	0.10	0.02	67.4		
8	5788.26	0.12	0.83	0.04	60.5	SiIV(1393)	3.1530
9	5824.14	0.13	0.16	0.02	65.7	SiIV(1402)	3.1519
10	5826.80	0.16	0.11	0.02	66.6		
11	5862.90	0.16	0.21	0.03	66.5		
12	5886.18	0.09	0.51	0.03	63.4	SiIV(1393)	3.2233
13	5891.09	0.13	0.20	0.03	48.3		
14	5923.91	0.12	0.31	0.03	66.5	SiIV(1402)	3.2230

TABLE 6 -*Continued*

No.	λ_{obs}	$\sigma(\lambda)$	W_{obs}	$\sigma(W)$	S/N	ID	z_{abs}
15	5932.71	0.11	0.28	0.02	65.2	CIV(1548)	2.8320
16	5936.81	0.15	0.18	0.02	67.6		
17	5942.53	0.14	0.19	0.02	68.4	CIV(1550)	2.8320
			6077 – 6741 Å				
1	6160.33	0.14	0.18	0.03	49.4	NaI(5891)?	0.0456
2	6165.70	0.21	0.07	0.02	51.8	NaI(5897)?	0.0455
3	6209.02	0.16	0.21	0.03	53.2	AlII(1670)	2.7162
4	6274.90	0.14	0.17	0.03	53.6		
5	6354.91	0.16	0.46	0.04	51.9	CIV(1548)	3.1047
6	6363.11	0.17	0.29	0.04	50.3	CIV(1550)?	3.1032
7	6369.62	0.09	0.45	0.03	50.8	CIV(1548)	3.1142
8	6380.16	0.11	0.38	0.03	51.3	CIV(1550)	3.1142
9	6400.23	0.20	0.17	0.03	54.3		
10	6429.27	0.16	0.46	0.04	54.3	CIV(1548)	3.1527
11	6440.71	0.31	0.26	0.04	56.8	CIV(1550)	3.1532
12	6497.50	0.17	0.34	0.03	57.4		
13	6538.02	0.07	0.95	0.03	55.7	CIV(1548)	3.2230
14	6548.95	0.09	0.55	0.03	60.9	CIV(1550)	3.2230

TABLE 7
Absorption Lines in the Spectrum of Q1017+1055

No.	λ_{obs}	$\sigma(\lambda)$	W_{obs}	$\sigma(W)$	S/N	ID	z_{abs}
				3622 – 4067 Å			
1	3713.86	0.11	2.82	0.28	3.9		
2	3718.25	0.08	2.75	0.16	7.8		
3	3721.71	0.07	1.51	0.10	10.1		
4	3726.54	0.08	2.01	0.11	11.5		
5	3732.67	0.10	4.29	0.15	11.1		
6	3742.52	0.09	2.58	0.11	12.9	AlII(1670)	1.2400
						+HI(949)	2.9406
7	3746.44	0.07	1.62	0.10	9.6		
8	3749.32	0.08	2.34	0.14	8.1		
9	3753.68	0.09	3.74	0.20	6.7		
10	3756.84	0.07	1.38	0.12	7.1		
11	3759.53	0.08	1.97	0.15	6.7	HI(937)	3.0089
12	3763.45	0.09	4.23	0.20	7.2		
13	3768.38	0.07	1.50	0.08	12.6		
14	3770.83	0.06	0.89	0.06	13.0		
15	3773.47	0.07	2.19	0.11	10.8		
16	3777.80	0.08	1.09	0.07	15.2		
17	3780.45	0.07	1.03	0.07	13.4		
18	3782.87	0.07	0.88	0.06	16.1		
19	3786.21	0.08	0.77	0.06	17.9		
20	3790.27	0.08	1.11	0.07	16.7		
21	3793.05	0.07	0.94	0.06	16.1		
22	3795.82	0.09	0.33	0.04	20.0		
23	3797.52	0.07	0.33	0.04	19.6		
24	3799.76	0.07	1.43	0.08	12.8		
25	3802.23	0.08	2.12	0.16	6.4	HI(972)	3.0544
26	3806.99	0.09	5.31	0.19	8.8	HI(949)	3.0084
27	3812.31	0.10	0.43	0.05	21.6		
28	3820.82	0.10	0.90	0.06	20.6		
29	3824.26	0.15	0.18	0.04	23.3		
30	3827.40	0.11	0.27	0.04	22.7		
31	3831.51	0.10	1.53	0.08	19.6	HI(972)	2.9397
32	3840.50	0.09	2.07	0.09	18.4		
33	3847.51	0.10	0.25	0.04	21.5		
34	3850.48	0.07	2.37	0.10	12.7	CIII(977)	2.9410
						+HI(949)	3.0542
35	3853.62	0.08	0.54	0.05	19.1		
36	3856.46	0.08	0.43	0.05	19.1	HI(937)	3.1122
37	3858.08	0.07	0.51	0.05	18.4		
38	3861.26	0.10	0.27	0.04	20.9		
39	3864.28	0.10	0.58	0.05	20.1		
40	3871.22	0.14	0.21	0.04	23.0		
41	3874.63	0.09	1.05	0.06	20.0		
42	3877.62	0.07	0.54	0.04	19.5		
43	3880.05	0.06	1.34	0.07	14.7		
44	3883.71	0.08	3.71	0.13	11.9		
45	3891.92	0.07	0.78	0.05	20.1		
46	3895.11	0.10	0.39	0.04	23.5		
47	3899.06	0.07	2.22	0.08	17.1	HI(972)	3.0092
48	3904.15	0.07	2.15	0.08	19.3	HI(949)	3.1107

TABLE 7 -*Continued*

No.	λ_{obs}	$\sigma(\lambda)$	W_{obs}	$\sigma(W)$	S/N	ID	z_{abs}
49	3907.69	0.08	0.22	0.03	25.0		
50	3911.19	0.07	1.16	0.06	20.7		
51	3915.22	0.07	0.76	0.05	21.8		
52	3917.35	0.07	0.48	0.04	24.5	CIII(977)	3.0095
53	3919.75	0.08	0.37	0.04	27.1		
54	3924.67	0.07	2.94	0.08	20.3		
55	3932.26	0.07	2.93	0.08	20.4		
56	3936.85	0.07	1.78	0.06	21.7		
57	3942.68	0.06	2.34	0.07	19.3	HI(972)	3.0540
58	3948.65	0.08	0.43	0.04	26.7		
59	3951.21	0.08	0.55	0.04	26.4		
60	3958.31	0.06	1.57	0.06	19.7		
61	3961.11	0.06	1.33	0.06	19.7	CIII(977)	3.0543
62	3968.73	0.08	2.17	0.07	23.7		
63	3976.14	0.07	1.12	0.05	24.9		
64	3979.13	0.06	0.70	0.04	24.9		
65	3982.12	0.06	1.02	0.05	21.4		
66	3984.45	0.06	1.80	0.07	14.9	CIII(977)	3.0781
67	3987.21	0.06	0.88	0.04	25.7		
68	3993.56	0.06	0.61	0.04	27.9		
69	3996.47	0.06	0.73	0.04	26.6	HI(972)?	3.1093
70	4000.28	0.07	3.95	0.11	14.0		
71	4004.46	0.06	1.41	0.05	20.9		
72	4007.33	0.06	0.77	0.04	24.9		
73	4009.29	0.06	0.60	0.03	27.2		
74	4014.18	0.06	0.70	0.03	26.4		
75	4017.00	0.06	1.50	0.05	24.9	CIII(977)	3.1115
76	4021.22	0.07	0.38	0.03	32.9		
77	4026.13	0.06	1.60	0.05	24.7		
78	4029.06	0.06	1.65	0.05	22.9		
79	4033.58	0.07	0.61	0.03	34.6		
80	4041.18	0.06	2.16	0.05	27.9	HI(1025)	2.9398
81	4054.21	0.08	0.39	0.03	39.2		
82	4056.95	0.08	0.22	0.02	41.1		
			4686 – 5132 Å				
1	4690.83	0.07	0.51	0.04	29.6		
2	4693.40	0.07	0.89	0.04	28.4		
3	4697.48	0.12	0.43	0.04	32.8		
4	4704.81	0.12	0.39	0.04	33.2		
5	4712.84	0.06	2.17	0.07	21.6		
6	4716.12	0.06	1.87	0.06	19.4		
7	4721.24	0.07	4.18	0.09	21.0		
8	4733.70	0.07	1.88	0.06	27.5		
9	4748.51	0.09	0.20	0.03	33.5		
10	4752.04	0.08	0.57	0.04	31.6	SiIII(1206)	2.9387
11	4755.46	0.08	0.35	0.03	32.3		
12	4759.07	0.07	0.93	0.05	29.7		
13	4762.46	0.07	0.67	0.04	30.2		
14	4766.92	0.07	3.03	0.08	23.7		
15	4772.42	0.06	0.61	0.03	27.7		
16	4775.70	0.07	2.51	0.07	23.0		

TABLE 7 –*Continued*

No.	λ_{obs}	$\sigma(\lambda)$	W_{obs}	$\sigma(W)$	S/N	ID	z_{abs}
17	4780.90	0.07	0.97	0.05	29.9		
18	4789.54	0.07	4.04	0.08	24.2	HI(1215)	2.9398
19	4800.35	0.07	1.52	0.05	27.7		
20	4804.66	0.06	1.55	0.05	26.0		
21	4808.27	0.07	1.37	0.05	28.9		
22	4813.03	0.09	0.52	0.04	33.6		
23	4829.55	0.06	0.90	0.04	23.1		
24	4838.68	0.07	1.61	0.06	27.2	SiIII(1206)	3.0105
						+SiII(1193)	3.0549
25	4842.79	0.10	0.55	0.04	32.6		
26	4853.56	0.07	1.33	0.05	27.5		
27	4859.08	0.07	2.16	0.07	25.7	HI(1215)?	2.9970
28	4873.17	0.07	5.44	0.11	19.3	HI(1215)	3.0086
29	4880.42	0.07	3.31	0.09	21.4		
30	4885.55	0.11	0.42	0.04	30.7		
31	4891.78	0.07	1.16	0.05	25.2	SiIII(1206)	3.0761
32	4894.82	0.06	1.39	0.06	21.2		
33	4898.27	0.06	2.13	0.07	21.4		
34	4908.19	0.06	1.35	0.05	24.2		
35	4912.33	0.06	1.27	0.05	24.9		
36	4917.82	0.07	5.18	0.11	17.8		
37	4929.20	0.07	6.37	0.12	18.3	HI(1215)	3.0547
38	4941.01	0.06	1.79	0.06	24.9		
39	4946.29	0.07	2.35	0.06	28.4		
40	4951.60	0.06	1.87	0.05	27.3		
41	4955.69	0.06	1.25	0.04	29.6	HI(1215)	3.0765
42	4958.91	0.09	0.21	0.03	38.0	HI(1215)	3.0792
						+SiIII(1206)	3.1101
43	4964.69	0.06	2.23	0.06	29.1	SiII(1260)	2.9390
44	4968.70	0.08	0.65	0.04	36.3		
45	4972.49	0.07	0.55	0.03	36.4		
46	4977.12	0.06	1.84	0.05	27.4		
47	4980.72	0.06	1.50	0.05	30.0		
48	4987.41	0.06	1.02	0.04	32.8		
49	4990.16	0.06	1.03	0.04	31.6		
50	4993.24	0.06	0.95	0.04	33.2		
51	4999.15	0.06	4.34	0.08	23.1		
52	5004.57	0.06	2.63	0.06	27.4		
53	5010.34	0.06	1.55	0.04	32.3		
54	5014.39	0.06	1.64	0.05	33.3		
55	5020.46	0.07	0.56	0.03	39.0		
56	5023.15	0.06	1.42	0.04	31.7	NV(1238)	3.0548
57	5027.44	0.07	0.43	0.03	39.3		
58	5032.51	0.06	3.80	0.07	25.5		
59	5038.45	0.06	0.90	0.03	35.9	NV(1242)	3.0541
60	5041.63	0.06	2.24	0.06	22.9		
61	5044.92	0.06	1.30	0.04	31.2		
62	5049.28	0.06	1.66	0.04	29.8		
63	5054.81	0.06	1.56	0.04	30.8	SiII(1260)?	3.0104
						+NV(1238)	3.0803

TABLE 7 -*Continued*

No.	λ_{obs}	$\sigma(\lambda)$	W_{obs}	$\sigma(W)$	S/N	ID	z_{abs}
64	5058.00	0.06	1.06	0.04	34.1		
65	5069.52	0.09	0.70	0.04	40.6	NV(1242)	3.0791
66	5078.09	0.06	0.93	0.04	37.5		
67	5092.20	0.06	3.50	0.06	31.0	NV(1238)	3.1105
68	5102.30	0.06	0.97	0.03	36.5		
69	5107.89	0.08	3.01	0.06	37.3	NV(1242)	3.1100
				5207 – 5864 Å			
1	5302.96	0.23	0.56	0.08	20.7	FeII(2367)	1.2398
						+CII(1334)	2.9736
						+OI(1302)	3.0769
2	5308.77	0.22	0.37	0.07	21.0		
3	5337.75	0.27	0.36	0.08	21.9	FeII(2382)	1.2402
4	5342.08	0.16	0.30	0.06	21.0		
5	5481.88	0.15	0.96	0.08	25.0	CIV(1548)	2.5408
6	5490.98	0.23	0.46	0.07	27.2	CIV(1550)	2.5408
						+SiIV(1393)	2.9397
7	5513.19	0.15	0.27	0.05	27.2		
8	5519.33	0.11	1.12	0.07	23.8	CIV(1548)	2.5650
9	5528.94	0.13	1.17	0.08	25.1	CIV(1550)	2.5653
10	5537.74	0.18	2.37	0.11	25.6	SiIV(1393)	2.9733
11	5563.05	0.23	0.53	0.07	28.6		
12	5571.70	0.14	1.68	0.09	25.3	SiIV(1402)	2.9719
13	5584.69	0.10	0.35	0.04	27.1		
14	5587.03	0.10	0.69	0.06	26.3	MgII(2796)	0.9980
15	5600.91	0.19	0.27	0.05	29.4	MgII(2803)	0.9978
16	5681.59	0.23	0.47	0.07	27.2	SiIV(1393)	3.0765
17	5688.56	0.21	0.38	0.07	24.7		
18	5731.84	0.15	0.38	0.05	29.2		
19	5788.07	0.27	0.62	0.08	29.9		
20	5824.37	0.14	0.41	0.05	30.0	FeII(2600)	1.2400
				5959 – 6614 Å			
1	5976.60	0.15	0.17	0.04	30.1		
2	6013.81	0.13	0.16	0.03	37.4	SiII(1526)	2.9390
3	6099.71	0.14	0.34	0.04	45.6	CIV(1548)	2.9399
4	6110.53	0.19	0.24	0.04	47.4	CIV(1550)	2.9403
5	6152.03	0.15	13.26	0.15	39.0	CIV(1549)	2.9720
6	6188.01	0.13	1.17	0.05	48.7	CIV(1548)	2.9969
7	6199.47	0.13	1.02	0.05	49.8	CIV(1550)	2.9978
8	6207.86	0.07	0.60	0.03	49.0	CIV(1548)	3.0097
9	6218.42	0.09	0.38	0.03	52.8	CIV(1550)	3.0099
10	6263.98	0.06	1.69	0.05	43.5	MgII(2796)	1.2401
11	6279.73	0.07	1.19	0.04	48.6	MgII(2803)	1.2399
12	6312.30	0.08	0.45	0.03	54.1	CIV(1548)	3.0772
13	6315.62	0.08	0.50	0.03	54.2	CIV(1548)	3.0793
14	6321.80	0.12	0.29	0.03	55.5	CIV(1550)	3.0765

TABLE 7 -*Continued*

No.	λ_{obs}	$\sigma(\lambda)$	W_{obs}	$\sigma(W)$	S/N	ID	z_{abs}
15	6326.17	0.09	0.41	0.03	55.9	CIV(1550)	3.0794
16	6345.73	0.09	0.25	0.02	59.8		
17	6348.84	0.10	0.22	0.02	59.7		
18	6355.45	0.10	0.85	0.04	57.8		
19	6364.32	0.06	3.32	0.06	45.6	CIV(1548)	3.1108
20	6375.29	0.07	2.34	0.05	56.0	CIV(1550)	3.1110
21	6495.27	0.11	0.78	0.04	57.6		
22	6597.14	0.17	0.36	0.04	53.1		
23	6602.38	0.07	1.38	0.05	42.9		
24	6606.38	0.10	0.23	0.03	41.7		

TABLE 8
Absorption Lines in the Spectrum of Q2233+1341

No.	λ_{obs}	$\sigma(\lambda)$	W_{obs}	$\sigma(W)$	S/N	ID	z_{abs}
			3658 – 4104 Å				
1	3729.61	0.06	1.89	0.10	10.5		
2	3734.51	0.07	2.27	0.11	10.7		
3	3741.36	0.08	5.30	0.17	9.9		
4	3749.70	0.07	3.14	0.13	10.5	HI(937)	2.9984
5	3754.02	0.06	1.66	0.08	12.7		
6	3756.83	0.05	0.93	0.06	14.4		
7	3758.50	0.05	0.69	0.05	15.4		
8	3762.22	0.07	3.07	0.12	11.7		
9	3769.13	0.07	4.04	0.13	11.8	SiII(1190)?	2.1662
10	3779.76	0.09	6.83	0.17	11.9	SiII(1193)	2.1675
11	3787.87	0.06	1.87	0.08	14.0		
12	3791.14	0.06	1.98	0.08	14.8		
13	3798.48	0.08	4.93	0.13	13.5	CIII(977)	2.8878
						+HI(949)	2.9995
14	3810.22	0.07	4.65	0.16	10.0	HI(937)	3.0629
15	3816.28	0.06	2.36	0.10	12.3		
16	3820.50	0.12	4.48	0.36	3.8	SiIII(1206)	2.1666
17	3825.32	0.06	2.94	0.11	12.4		
18	3830.70	0.06	1.39	0.07	15.4		
19	3833.55	0.06	1.45	0.07	13.7	HI(972)	2.9418
20	3836.67	0.06	2.24	0.10	11.4		
21	3840.28	0.06	1.76	0.08	13.8		
22	3848.09	0.15	10.73	0.47	4.5		
23	3857.05	0.11	5.14	0.31	4.8	HI(949)	3.0612
24	3862.14	0.08	3.22	0.19	6.5		
25	3866.22	0.06	2.65	0.09	16.2		
26	3872.87	0.06	1.46	0.06	18.7		
27	3876.85	0.06	0.93	0.05	19.9		
28	3879.32	0.06	0.97	0.05	19.1		
29	3883.48	0.06	2.13	0.08	14.6		
30	3886.24	0.06	1.66	0.10	9.1		
31	3889.40	0.07	2.48	0.10	12.5	HI(972)	2.9992
32	3898.71	0.07	0.56	0.05	20.2		
33	3904.54	0.06	1.14	0.06	16.5		
34	3907.35	0.06	1.70	0.08	16.1	CIII(977)	2.9992
35	3915.53	0.08	4.21	0.11	16.9		
36	3922.40	0.07	1.49	0.06	21.8		
37	3928.25	0.06	1.08	0.05	21.6		
38	3931.14	0.05	0.88	0.04	21.9		
39	3935.04	0.05	1.92	0.07	17.8		
40	3937.50	0.05	0.78	0.04	19.8		
41	3939.51	0.05	0.97	0.04	23.8		
42	3946.80	0.05	2.76	0.08	16.1		
43	3950.61	0.06	3.30	0.10	14.1	HI(972)	3.0622
44	3955.61	0.05	1.07	0.04	23.7		
45	3958.67	0.05	1.91	0.06	21.0		
46	3963.55	0.06	0.50	0.03	29.9		
47	3968.67	0.07	1.74	0.06	28.6	CIII(977)	3.0620
48	3972.58	0.06	0.44	0.03	30.8		
49	3982.36	0.06	1.24	0.05	26.7		

TABLE 8 –*Continued*

No.	λ_{obs}	$\sigma(\lambda)$	W_{obs}	$\sigma(W)$	S/N	ID	z_{abs}
50	3989.05	0.07	6.12	0.13	14.7	HI(1025)	2.8890
51	3995.06	0.05	1.32	0.05	18.4		
52	3997.59	0.05	1.14	0.05	23.2		
53	4000.80	0.05	0.93	0.04	26.0		
54	4005.36	0.05	0.68	0.03	26.7		
55	4009.51	0.06	4.10	0.10	15.6		
56	4017.52	0.06	4.95	0.10	17.3		
57	4022.25	0.05	0.81	0.03	28.7		
58	4027.31	0.05	1.00	0.04	30.2		
59	4030.20	0.05	1.18	0.04	26.6	CII(1036)	2.8889
60	4034.59	0.05	3.80	0.10	14.1		
61	4038.14	0.05	1.49	0.05	22.7		
62	4044.58	0.06	3.80	0.10	15.1		
63	4053.02	0.05	1.22	0.04	27.8		
64	4058.74	0.05	2.01	0.05	24.3		
65	4065.09	0.05	1.75	0.05	23.4		
66	4069.04	0.05	1.30	0.04	28.1		
67	4072.97	0.05	0.64	0.03	31.8		
68	4075.59	0.06	0.43	0.03	32.4		
69	4077.55	0.06	0.37	0.03	31.4		
70	4080.55	0.06	0.44	0.03	32.0		
71	4082.97	0.05	0.85	0.04	29.6		
72	4086.90	0.05	1.93	0.05	24.1		
73	4091.52	0.05	0.65	0.03	29.0		
74	4094.01	0.05	0.83	0.04	28.5		
			4704 – 5151 Å				
1	4720.65	0.09	1.19	0.08	17.6		
2	4727.51	0.08	4.50	0.17	10.4	HI(1215)	2.8888
3	4734.29	0.09	3.69	0.13	14.1		
4	4746.35	0.08	0.68	0.06	18.8		
5	4756.14	0.13	0.36	0.06	21.1	SiIII(1206)	2.9421
6	4761.36	0.08	1.08	0.07	17.4	SiII(1190)?	2.9997
7	4767.01	0.09	0.81	0.07	18.9		
8	4775.10	0.11	0.37	0.05	20.5		
9	4782.84	0.07	1.56	0.09	15.8		
10	4792.51	0.09	3.81	0.13	14.3	HI(1215)	2.9423
11	4797.55	0.08	0.44	0.05	18.8		
12	4799.88	0.06	0.68	0.06	16.4		
13	4802.34	0.08	1.14	0.08	16.7		
14	4807.32	0.10	0.44	0.06	19.5		
15	4816.21	0.08	1.56	0.09	15.1		
16	4820.44	0.09	0.35	0.05	19.0		
17	4828.06	0.08	0.56	0.06	17.9		
18	4833.96	0.08	2.18	0.11	13.9	SiII(1526)	2.1662
19	4842.83	0.19	0.35	0.07	19.6		
20	4846.47	0.11	0.38	0.06	18.6		
21	4849.19	0.08	1.40	0.09	14.0		
22	4856.15	0.10	0.80	0.08	16.9		
23	4862.48	0.10	5.08	0.18	11.7	HI(1215)	2.9998
24	4870.15	0.12	1.27	0.10	15.6		
25	4874.88	0.10	0.71	0.08	15.5		

TABLE 8 -*Continued*

No.	λ_{obs}	$\sigma(\lambda)$	W_{obs}	$\sigma(W)$	S/N	ID	z_{abs}
26	4880.64	0.10	2.56	0.14	11.2		
27	4884.71	0.08	1.32	0.11	11.3		
28	4887.07	0.07	0.98	0.10	10.3		
29	4889.82	0.09	1.84	0.13	10.9		
30	4896.49	0.11	2.20	0.14	12.4		
31	4900.74	0.07	1.20	0.11	10.3	SiII(1260)	2.8882
						+SiIII(1206)	3.0619
32	4903.00	0.11	2.01	0.28	4.0	CIV(1548)?	2.1669
33	4905.38	0.08	1.53	0.12	9.8		
34	4909.16	0.09	2.39	0.18	7.2		
35	4912.11	0.09	2.47	0.15	9.7		
36	4920.60	0.15	0.63	0.09	14.1		
37	4930.37	0.12	0.36	0.07	13.9		
38	4932.54	0.09	0.94	0.10	11.1		
39	4936.95	0.12	4.06	0.31	5.0	HI(1215)	3.0611
40	4940.60	0.10	2.36	0.26	4.6		
41	4944.71	0.11	2.44	0.29	4.2		
42	4947.54	0.09	2.19	0.14	10.8		
43	4960.27	0.18	0.28	0.07	16.0		
44	4963.02	0.11	0.40	0.07	14.8		
45	4964.51	0.11	0.24	0.06	15.5		
46	4971.06	0.10	0.59	0.08	14.5		
47	4976.93	0.10	2.01	0.13	12.5		
48	4983.00	0.08	2.12	0.14	10.4		
49	4986.15	0.09	0.68	0.08	14.7		
50	4988.98	0.08	1.20	0.09	12.9		
51	4992.39	0.09	1.12	0.09	14.5		
52	4997.65	0.11	1.03	0.09	15.9		
53	5001.80	0.08	1.50	0.10	13.2		
54	5005.39	0.08	1.15	0.09	14.2		
55	5012.07	0.10	6.63	0.24	8.9		
56	5020.44	0.09	2.58	0.12	14.9		
57	5037.33	0.09	2.35	0.11	14.7		
58	5044.14	0.13	0.46	0.07	18.7		
59	5049.79	0.07	1.19	0.08	14.7		
60	5056.20	0.08	3.75	0.15	12.5		
61	5065.94	0.07	2.49	0.12	13.0		
62	5069.15	0.06	1.44	0.09	12.0		
63	5071.82	0.07	1.64	0.09	14.7		
64	5076.66	0.09	0.35	0.05	20.3		
65	5078.60	0.12	0.34	0.05	21.3		
66	5083.81	0.16	0.41	0.06	22.3		
67	5092.85	0.06	1.29	0.07	18.5	FeII(1608)	2.1663
68	5096.52	0.06	1.41	0.07	20.0		
69	5100.64	0.07	0.91	0.06	24.4		
70	5113.42	0.06	1.05	0.05	26.5		
71	5117.17	0.06	3.02	0.08	20.6		
72	5121.91	0.07	0.31	0.03	33.8		
73	5125.59	0.07	0.32	0.03	32.4		
74	5127.39	0.07	0.37	0.03	30.9		

TABLE 8 -*Continued*

No.	λ_{obs}	$\sigma(\lambda)$	W_{obs}	$\sigma(W)$	S/N	ID	z_{abs}
				5162 – 5819 Å			
1	5291.05	0.13	2.68	0.16	12.0	AlII(1670)	2.1668
2	5420.86	0.22	0.56	0.11	14.4	CII(1334)	3.0620
3	5515.38	0.20	0.40	0.08	17.9		
				5889 – 6544 Å			
1	5951.11	0.28	0.47	0.09	19.7	NaI(5891)	0.0101
2	5957.51	0.29	0.46	0.09	19.7	NaI(5897)	0.0102
3	6020.24	0.12	0.54	0.07	20.2	CIV(1548)	2.8885
4	6023.56	0.19	0.27	0.06	22.4		
5	6030.48	0.30	0.69	0.10	22.3	CIV(1550)	2.8887
6	6103.05	0.16	0.31	0.06	24.6	CIV(1548)	2.9430
7	6191.76	0.19	0.45	0.07	26.8	CIV(1548)	2.9993
8	6201.11	0.22	0.28	0.06	27.8	CIV(1550)	2.9987
						+SiII(1526)	3.0617
9	6417.99	0.23	0.26	0.05	31.0	MgI(2026)	2.1671
10	6470.07	0.19	0.30	0.05	32.9	NaI(5891)?	0.0982
11	6476.56	0.19	0.37	0.05	35.9	NaI(5897)?	0.0982

TABLE 9

COLUMN DENSITIES MEASURED FOR THE LYMAN LIMIT ABSORPTION SYSTEMS

Ion	λ_0 (Å)	log N (cm^{-2})	b (km s^{-1})	z_{abs}	Comments
		Q0029+0722			
H I	Ly Series	$19.3^{+0.1}_{-0.3}$	28 ± 4	3.0488	
C II	1334.53	14.5 ± 0.1	(9)	3.0488	a,e
C II*	1335.68	≤ 13.0	(9)	(3.0488)	b
C III	977.03	...	(9)	(3.0488)	d
C IV	1548.20	≤ 13.2	(9)	(3.0488)	b,c
N V	1238.82	≤ 14.0	(8)	(3.0488)	b,c
O I	1302.17	14.0 ± 0.1	(6)	3.0488	a,e
Si II	1304.37	13.7 ± 0.1	(6)	3.0488	a,e
Si II	1526.72	13.7 ± 0.1	(6)	3.0488	a
Si III	1206.50	...	(6)	(3.0488)	d
Si IV	1393.72	≤ 13.0	(6)	(3.0488)	b,c
Fe II	1608.45	...	...	(3.0488)	d
		Q0256+0000			
H I	Ly Series	17.0 ± 0.3	25 ± 4	3.0843	
		18.0 ± 0.3	21 ± 4	3.0823	
		16.5 ± 0.2	25 ± 4	3.0801	
C II	1334.53	≤ 13.2	(8)	(3.0843)	b
		≤ 13.1	(8)	(3.0823)	b
		≤ 13.0	(8)	(3.0801)	b
C III	977.03	≤ 15.0	(8)	(3.0843)	b,d
		≤ 15.0	(8)	(3.0823)	b,d
		≤ 15.0	(8)	(3.0801)	b,d
C IV	1548.20	13.6 ± 0.1	(8)	3.0843	a,c
		≤ 13.2	(8)	(3.0823)	b,c
		≤ 13.0	(8)	(3.0801)	b,c
N V	1238.82	≤ 14.1	(7)	(3.0843)	b,c
		≤ 13.1	(7)	(3.0823)	b,c
		≤ 13.1	(7)	(3.0801)	b,c
O I	1302.17	...	...	(3.0823)	d
Si II	1526.72	≤ 13.0	(6)	(3.0843)	b
		≤ 13.0	(6)	(3.0823)	b
		≤ 12.8	(6)	(3.0801)	b
Si III	1206.50	≤ 14.5	(6)	(3.0843)	b,d
		≤ 12.7	(6)	(3.0823)	b
		≤ 12.3	(6)	(3.0801)	b
Si IV	1393.72	13.0 ± 0.1	(6)	3.0845	a,c
		≤ 12.8	(6)	(3.0823)	b,c
		≤ 12.8	(6)	(3.0801)	b,c

TABLE 9

(Continued)

Ion	λ_0 (Å)	log N (cm^{-2})	b ($km\ s^{-1}$)	z_{abs}	Comments
		Q0301−0035			
H I	Ly Series	$18.8^{+0.1}_{-0.5}$	25 ± 3	2.9400	
C II	1334.53	13.9 ± 0.1	(7)	(2.9400)	a,e
C II*	1335.68	≤ 12.9	(7)	(2.9400)	b
C III	977.03	...	(7)	(2.9400)	d
C IV	1548.20	14.2 ± 0.1	30	2.9402	a,c
N V	1238.82	≤ 14.2	(6)	(2.9402)	b,c
O I	1302.17	≤ 13.5	(6)	(2.9400)	b
Si II	1304.37	≤ 13.2	(6)	(2.9400)	b
Si II	1526.72	≤ 13.3	(6)	(2.9400)	b
Si III	1206.50	...	(6)	(2.9402)	d
Si IV	1393.72	13.9 ± 0.1	25	2.9403	a,e
Fe II	1608.45	≤ 13.5	(3)	(2.9400)	b
		Q0636+6801			
H I	Ly Series	18.5 ± 0.2	17 ± 2	2.9046	
		$18.0^{+0.3}_{-0.5}$	24 ± 3	2.9030	
C II	1334.53	15.5 ± 0.1	(10)	2.9046	a
		14.5 ± 0.1	(25)	2.9046	a
		≤ 13.4	(7)	(2.9030)	b
C II*	1335.68	≤ 13.0	(5)	(2.9046)	b
C III	977.03	...	...	(2.9046)	d
		...	...	(2.9030)	d
C IV	1548.20	14.3 ± 0.1	25	2.9046	a,c
		14.0 ± 0.1	30	2.9030	a,c
N V	1238.82	≤ 13.9	(5)	(2.9046)	b,c
		≤ 13.1	(7)	(2.9030)	b,c
O I	1302.17	14.1 ± 0.1	(4)	2.9046	a
		≤ 13.5	(6)	(2.9030)	b
Si II	1304.37	≤ 13.9	(15)	(2.9044)	b,e
		≤ 13.2	(4)	(2.9030)	b
Si II	1526.72	13.8 ± 0.1	(15)	2.9045	a
		≤ 12.7	(4)	(2.9030)	b
Si III	1206.50	≤ 14.5	(15)	(2.9046)	b
		≤ 13.1	(4)	(2.9030)	b
Si IV	1393.72	14.1 ± 0.1	15	2.9046	a,c
		13.5 ± 0.1	20	2.9030	a,c
		Q0956+1217			
H I	Ly Series	17.50 ± 0.1	21 ± 3	3.2228	
C II	1334.53	≤ 13.0	(6)	3.2228	b
C III	977.03	...	(6)	(3.2228)	d
C IV	1548.20	13.85 ± 0.1	20	3.2228	a,c
N V	1238.82	≤ 13.3	(5)	(3.2228)	b,c
O I	1302.17	≤ 13.5	(5)	(3.2228)	b
Si II	1304.37	≤ 12.9	(5)	(3.2228)	b
Si II	1526.72	≤ 12.8	(5)	(3.2228)	b
Si III	1206.50	≤ 13.2	(5)	(3.2228)	b
Si IV	1393.72	13.20 ± 0.1	20	3.2229	a,c

TABLE 9

(Continued)

Ion	λ_0 (Å)	log N (cm^{-2})	b (km s^{-1})	z_{abs}	Comments
		Q1017+1055			
H I	Ly Series	17.5 ± 0.1	21 ± 4	3.0540	
C II	1334.53	≤ 13.1	(6)	(3.0540)	b
C III	977.03	...	(6)	(3.0540)	b
C IV	1548.20	≤ 13.0	(6)	(3.0540)	b,c
N V	1238.82	≤ 15.0	(5)	(3.0540)	b,d
O I	1302.17	≤ 13.8	(5)	(3.0540)	b
Si II	1304.37	≤ 13.1	(5)	(3.0540)	b
Si II	1526.72	≤ 13.4	(5)	(3.0540)	b
Si III	1206.50	≤ 13.4	(5)	(3.0540)	b
Si IV	1393.72	≤ 13.0	(5)	3.0540	b,c
		Q2126−1551			
H I	Ly Series	17.35 ± 0.1	42 ± 7	2.9676	
C II	1334.53	13.40 ± 0.1	(12)	2.9676	a
C III	977.03	≤ 15.3	(12)	(2.9676)	b,d
C IV	1548.20	13.40 ± 0.1	35	2.9676	a,c
N V	1238.82	≤ 14.0	(30)	(2.9676)	b
O VI	1031.93	≤ 14.3	(30)	(2.9676)	b,c
Si II	1526.72	≤ 13.0	(9)	(2.9676)	b
Si III	1206.50	≤ 13.3	(9)	(2.9676)	b
Si IV	1393.72	≤ 12.8	(9)	(2.9676)	b,c
		Q2233+1341			
H I	Ly Series	18.5 ± 0.2	21 ± 4	3.0618	
C II	1334.53	14.2 ± 0.1	(6)	3.0618	a
C II*	1335.68	≤ 13.0	(6)	(3.0618)	b
C III	977.03	...	(6)	(3.0618)	d
C IV	1548.20	≤ 13.5	(6)	(3.0618)	b,c
N V	1238.82	≤ 13.1	(5)	(3.0618)	b,c
O I	1302.17	...	(5)	(3.0618)	d
Si II	1260.42	≤ 13.6	(5)	(3.0618)	b
Si II	1526.72	≤ 13.4	(5)	(3.0618)	b
Si III	1206.50	≤ 14.0	(5)	(3.0618)	b
Si IV	1393.72	≤ 12.8	(5)	(3.0618)	b,c

a) Probable or certain detection.

b) Column density is an upper limit for the given velocity dispersion parameter b.

c) Line is a doublet, and therefore measurements or limits are somewhat more significant.

d) Although the line falls within one of the observed wavelength ranges, no useful limits can be set because of blending or coincidence with a very strong line from another system.

e) Line appears to be involved in a blend, so that the measurement is slightly more uncertain.

TABLE 10

QUANTITIES DERIVED FROM THE PHOTOIONIZATION MODELS

QSO	z_{abs}	log N(H I) (cm^{-2})	Spectrum[a]	log Γ	log N_H (cm^{-2})	[C/H]	[O/H]	[Si/H]
Q0029+0722	3.0488	$19.3^{+0.1}_{-0.3}$	Medium	≤ -2.9	[19.6,20.3]	-1.8 ± 0.2	-1.8 ± 0.2	-1.7 ± 0.2
			Hard	≤ -2.9	[19.6, 20.3]	-1.8 ± 0.2	-1.9 ± 0.2	-1.7 ± 0.2
Q0256+0000	3.0843	17.0 ± 0.3	Medium	≥ -2.5	≥ 20.1	$\leq -2.4 \pm 0.3$	...	$[-2.6 \pm 0.3, -2.2 \pm 0.3]$
			Hard	≥ -2.6	≥ 20.0	$\leq -2.4 \pm 0.3$	...	$[-2.4 \pm 0.3, -2.0 \pm 0.3]$
	3.0823	18.0 ± 0.3	Medium	...	...	$\leq -3.0 \pm 0.3$	...	$\leq -2.0 \pm 0.3$
			Hard	...	...	$\leq -3.0 \pm 0.3$	...	$\leq -2.0 \pm 0.3$
Q0301−0035	2.9400	$18.8^{+0.1}_{-0.5}$	Medium	-2.3 ± 0.1	20.8 ± 0.1	-2.6 ± 0.2	$\leq -1.9 \pm 0.1$	$[-2.5 \pm 0.1, -2.0 \pm 0.1]$
			Hard	-2.4 ± 0.1	20.7 ± 0.1	-2.4 ± 0.2	$\leq -1.2 \pm 0.6$	$[-2.4 \pm 0.1, -2.0 \pm 0.1]$
Q0636+6801	2.9046	18.5 ± 0.2	Medium	[−3.1, −2.6]	[20.0, 20.6]	[−1.8, −0.7]	[−1.8, −1.1]	[−1.7, −1.3]
			Hard	[−3.1, −2.6]	[20.0, 20.6]	[−2.0, −0.8]	[−1.8, −0.7]	[−1.8, −1.3]
	2.9030	$18.0^{+0.3}_{-0.5}$	Medium	≥ -2.3	≥ 20.5	$\leq -2.7 \pm 0.2$	...	$[-2.7 \pm 0.2, -2.4 \pm 0.2]$
			Hard	≥ -2.3	≥ 20.5	$\leq -2.6 \pm 0.1$	...	$[-2.6 \pm 0.2, -2.3 \pm 0.2]$
Q0956+1217	3.2228	17.5 ± 0.1	Medium	≥ -2.2	≥ 20.6	$\leq -2.8 \pm 0.1$	...	[−2.7, −2.0]
			Hard	≥ -2.3	≥ 20.5	≤ -2.7	...	[−2.6, −1.8]
Q1017+1055	3.0540	17.5 ± 0.1	Medium	...	...	$\leq -2.8 \pm 0.3$	...	$\leq -1.7 \pm 0.3$
			Hard	...	...	$\leq -2.8 \pm 0.3$	...	$\leq -1.5 \pm 0.2$
Q2126−158	2.9676	17.35 ± 0.1	Medium	-2.7 ± 0.1	20.1 ± 0.1	-2.3 ± 0.2	...	$\leq -2.3 \pm 0.1$
			Hard	-2.8 ± 0.1	20.0 ± 0.1	-2.2 ± 0.2	...	$\leq -2.2 \pm 0.1$
Q2233+1341	3.0618	18.5 ± 0.2	Medium	≤ -2.8	[19.4, 20.4]	-2.0 ± 0.2	...	$\leq -2.1 \pm 0.2$
			Hard	≤ -2.9	[19.4, 20.3]	-2.0 ± 0.2	...	$\leq -2.2 \pm 0.2$

a) Spectral shape of the ionizing radiation field used in the photoionization models. "Medium" and "Hard" refer to the medium and hard integrated QSO radiation fields of Bechtold *et al.* (1987).

TABLE 11

INFERRED CLOUD SIZES AND MASSES

QSO	z_{abs}	n_H (J_0 cm^{-3})	D_c (J_0^{-1} kpc)	M_c (J_0^{-2} $M_\odot$)
Q0029+0722	3.0488	$[0.04, 0.20]$	$[0.07, 1.1]$	$[3 \times 10^3, 6 \times 10^6]$
Q0256+0000	3.0843	$\lesssim 0.025$	$\gtrsim 2.0$	$\gtrsim 9 \times 10^6$
Q0301−0035	2.9400	~ 0.014	~ 13	$\sim 2 \times 10^9$
Q0636+6801	2.9046	$[0.025, 0.080]$	$[0.04, 5.0]$	$[3 \times 10^5, 2 \times 10^8]$
	2.9030	$\lesssim 0.010$	$\gtrsim 8$	$\gtrsim 3 \times 10^8$
Q0956+1217	3.2228	$\lesssim 0.013$	$\gtrsim 13$	$\gtrsim 1 \times 10^9$
Q2126−158	2.9676	~ 0.035	~ 1.3	$\sim 4 \times 10^6$
Q2233+1341	3.0618	$[0.04, 0.20]$	$[0.04, 2.6]$	$[3 \times 10^4, 3 \times 10^7]$

REFERENCES

Atwood, B., Baldwin, J. A., and Carswell, R. F. 1985, *Ap. J.*, **292**, 58.

Bahcall, J. N., and Wolf, R. A. 1968, *Ap. J.*, **152**, 701.

Bahcall, J. N., and Spitzer, L. 1969, *Ap. J. (Letters)*, **156**, L63.

Bajtlik, S., Duncan, R. C., and Ostriker, J. P. 1988, *Ap. J.*, **327**, 570.

Bechtold, J., Green, R., and York, D. G. 1987, *Ap. J.*, **312**, 50.

Bechtold, J., Weymann, R. J., Lin, Z., and Malkan, M. A. 1987, *Ap. J.*, **315**, 180.

Bechtold, J., Green, R. F., Weymann, R. J., Schmidt, M., Estabrook, F. B., Sherman, R. D., Wahlquist, H. D., and Heckman, T. M. 1984, *Ap. J.*, **281**, 76.

Bergeron, J, 1988, in *Large Scale Structure of the Universe*, eds. J. Audouze and A. S. Szalay (Dordrecht: Reidel), p.454 .

Bergeron, J., and Stasinska, G. 1986, *Astr. Ap.*, **169**, 1.

Blades, J. C. 1988, in *QSO Absorption Lines: Probing the Universe*, proc. Space Telescope Science Institute Symposium No. 2, eds. J. C. Blades, D. Turnshek, and C. A. Norman, p. 147.

Boesgaard, A. M., and Steigman, G. 1985, *Ann. Rev. Astr. Ap.*, **23**, 319.

Boksenberg, A., and Sargent, W. L. W. 1983, in *Proc. 24th Liege Symposium, Quasars and Gravitational Lenses* (Liege: Institut d'Astrophysique), p. 589.

Boksenberg, A., Carswell, R. F., and Sargent, W. L. W. 1979, *Ap. J.*, **227**, 370.

Brown, R. L., Broderick, J. J., Johnston, K. J., Benson, J. M., Mitchell, K. J., and Waltman, W. B. 1988, *Ap. J.*, **329**, 138.

Bruzual, G. 1983, *Ap. J. Suppl.*, **53**, 497.

Carswell, R. F., Morton, D. C., Smith, M. G., Stockton, A. N., Turnshek, D. A., and Weymann, R. J. 1984, *Ap. J.*, **278**, 486.

Chaffee, F. H., Foltz, C. B., Bechtold, J., and Weymann, R. J. 1986, *Ap. J.*, **301**, 116.

Donahue, M. J., and Shull, J. M. 1987, *Ap. J. (Letters)*, **313**, L13.

Fall, S. M., and Rees, M. J. 1985, *Ap. J.*, **298**, 18.

Fall, S. M., Pei, Y., and McMahon, R. G. 1989, *Ap. J. (Letters)*, **341**, L5.

Ferland, G. J. 1988, OSU Astronomy Department Internal Report, 87-001 .

Foltz, C. B., Weymann, R. J., Roser, H. J., Chaffee, F. H., Jr. 1984, *Ap. J (Letters)*, **281**, L1.

Gunn, J. E., and Peterson, B. A. 1965, *Ap. J.*, **142**, 1633.

Heisler, J., Hogan, C. J., and White, S. D. M. 1989, preprint.

Hunstead, R. W., Pettini, M., Blades, J. C., and Murdoch, H. S. 1987, in *Observational Cosmology*, ed. A. Hewitt, p. 799.

Jenkins, E. B. 1986, *Ap. J.*, **304**, 739.

Jenkins, E. B. 1987, in *Interstellar Processes*, eds. D. J. Hollenbach and H. A. Thronson (Boston: Reidel).

Lake, G. 1988, *Ap. J.*, **327**, 99.

Lanzetta, K. M. 1988, *Ap. J.*, **332**, 96.

Lanzetta, Turnshek, and Wolfe 1987, *Ap. J.*, **322**, 739.

Larson, R. B. 1969, *M.N.R.A.S.*, **145**, 405.

Lin, Z., and Phinney, E. S. 1989, *M.N.R.A.S.*, submitted.

Meyer, D. M., and York, D. G. 1987, *Ap. J.(Letters)*, **319**, L45.

Miralda–Escude, J., and Ostriker, J. P. 1989, *Ap. J.*, submitted.

Morris, S. L., Weymann, R. J., Foltz, C. B., Turnshek, D. A., Shectman, S., Price, C., and Boroson, T. A. 1986, *Ap. J.*, **310**, 40.

Morton, D. C., York, D. G., and Jenkins, E. B. 1986, *Ap. J.*, **302**, 272.

Morton, D. C., York, D. G., and Jenkins, E. B. 1989, *Ap. J. Suppl.*, **68**, 449.

Netzer, H., and Ferland, G. J. 1984, *Pub. A.S.P.*, **96**, 593.

Pettini, M., and Boksenberg, A. 1988, in *The Epoch of Galaxy Formation*, eds. R. Ellis, C. Frenk, and J. Peacock (Dordrecht: Reidel), in press .

Pettini, M., Hunstead, R. W., Murdoch, H. S., and Blades, J. C. 1983, *Ap. J.*, **273**, 463.

Rees, M. J. 1986, *M.N.R.A.S.*, **218**, 25P.

Rees, M. J. 1988, in *QSO Absorption Lines: Probing the Universe*, proc. Space Telescope Science Institute Symposium No.2, eds. J.C. Blades, D. Turnshek, C. A. Norman, p. 107.

Sargent, W. L. W. 1987, in *I. A. U. Symposium No. 126, Observational Cosmology*, eds. A. Hewitt, G. Burbidge, and L. Fang (Dordrecht: Reidel), p. 777.

Sargent, W. L. W., Young, P. J., Boksenberg, A., Carswell, R. F., and Whelan, J. A. J. 1979, *Ap. J.*, **230**, 49.

Sargent, W. L. W., Young, P. J., Boksenberg, A., and Tytler, D. 1980, *Ap. J. Suppl.*, **42**, 41.

Sargent, W. L. W., Boksenberg, A., and Steidel, C. C. 1988, *Ap. J. Suppl.*, **68**, 539 (SBS).

Sargent, W. L. W., Steidel, C. C., and Boksenberg, A. 1989a, *Ap. J. Suppl.*, **69**, 703 (SSB).

Sargent, W. L. W., Steidel, C. C., and Boksenberg, A. 1989b, *Ap. J.*, submitted.

Saslaw, W. C. 1968, *M.N.R.A.S.*, **141**, 1.

Searle, L., and Zinn, R. 1978, *Ap. J.*, **225**, 357.

Shapiro, P. R., and Giroux, M. L. 1987, *Ap. J. (Letters)*, **321**, L107.

Shapiro, P. R., and Giroux, M. L. 1989, in *The Epoch of Galaxy Formation*, ed. C. S. Frenk (Dordrecht: Reidel), in press.

Shaver, P. A., and Robertson, J. G. 1983, in *Proc. 24th Liege Symposium, Quasars and Gravitational Lenses* (Liege: Institut d'Astrophysique), p. 598.

Silk, J. S., and Norman, C. A. 1979, *Ap. J.*, **234**, 86.

Steidel, C. C., Sargent, W. L. W., and Boksenberg, A. 1988, *Ap. J. (Letters)*, **333**, L5 .

Steidel, C. C. 1989, *Ap.J. Suppl.* (in press).

Steidel, C. C., and Sargent, W. L. W. 1989, *Ap. J. (Letters)*, **343**, L33.

Tinsley, B. M. 1978, *IAU No. 84, Large Scale Characteristics of the Galaxy*, ed. W. B. Burton (Boston: Reidel), p. 431.

Tytler, D. 1982, *Nature*, **298**, 427.

Tytler, D. 1987, *Ap. J.*, **321**, 49.

Weymann, R. J., Chaffee, F. H., Davis, M., Carleton, N. P., Walsh, D., and Carswell, R. F. 1979, *Ap. J. (Letters)*, **233**, L43.

Wolfe, A. M. 1988, in *QSO Absorption Lines: Probing the Universe*, proc. Space Telescope Science Institute Symposium No. 2, eds. J. C. Blades, D. Turnshek, and C. A. Norman, p. 297.

Wolfe, A. M., Turnshek, D. A., Smith, H. E., and Cohen, R. D. 1986, *Ap. J. Suppl.*, **61**, 249.

Yang, J., Turner, M. S., Steigman, G., Schramm, D. N., and Olive,K. A. 1984, *Ap. J.*, **281**, 493.

York, D. G. 1988, in *QSO Absorption Lines: Probing the Universe*, proc. Space Telescope Science Institute Symposium No. 2, ed. J. C. Blades, D. Turnshek, and C. A. Norman, p. 227.

York, D. G., Green, R., Bechtold, J., and Chaffee. F. H. 1984, *Ap. J. (Letters)*, **280**, L1.

York, D. G., Dopita, M., Green, R., and Bechtold, J. 1986, *Ap. J.*, **311**, 610.

Young, P. J., Sargent, W. L. W., Boksenberg, A., and Oke, J. B. 1981, *Ap. J.*, **249**, 415.

FIGURE CAPTIONS

FIG 1.—The spectra of Q0029+0722, along with the 1σ noise array: a) Region I b) Region II c) Region III d) Region IV (see text for discussion of the spectral regions).

FIG 2.—Same as Figure 1, for Q0256+0000.

FIG 3.—Same as Figure 1, for Q0301−0035.

FIG 4.—Same as Figure 1, for Q0636+6801. The spectrum of Region II (b) has a resolution of ~ 35 km s^{-1}.

FIG 5.—Same as Figure 1, except that spectra were obtained of Region II at 2 different dispersions: b) ~ 35 km s^{-1}, and c) ~ 60 km s^{-1}.

FIG 6.—Same as Figure 1, for Q1017+1055.

FIG 7.—Same as Figure 1, for Q2233+1341.

FIG 8.—Plots showing the model Lyman series and Lyman limits (dotted curve) using the parameters listed in Table 9, and the actual data (solid curve) and 1σ noise spectrum (light hatched curve) for the most complicated Lyman limit systems, a) Q0256+0000, and b) Q0636+6801. The continuum has been normalized to 1. Also shown are the corresponding Lyman α line profiles using the same parameters. The data points are represented by the square boxes, and the 1σ noise spectrum is shown with a light hatched curve.

FIG 9.—Plot illustrating several different spectral energy distributions used to represent the ionizing radiation field in the photoionization models. The solid curve is a Bruzual "young galaxy" spectral energy distribution; the short dashed line is a simple power law with $f_\nu \propto \nu^{-1.5}$; the long dashed line is a power law $\propto \nu^{-1}$; the light dotted line is the Bechtold *et al.* (1987) "Medium" spectrum (at $z = 3$); the dot-dash curve is the Bechtold *et al.* (1987) "Hard" spectrum (at $z = 3$). All of the curves have been normalized at the Lyman limit (1 Rydberg). The nature of the spectral energy distributions outside the range shown does not significantly affect the model results.

FIG 10.—A comparison of the photoionization model grids for several different ionizing radiation fields. All of the grids were run for log N(HI)=17.5: a) simple power law with $f_\nu \propto \nu^{-1.5}$, b) Bechtold *et al.* (1987) "Medium" integrated QSO radiation field, c) Bechtold *et al.* (1987) "Hard" QSO radiation field, d) Bruzual (1983) "young galaxy" stellar radiation

field.

FIG 11.—Some examples of photoionization model grids for various values of log N(HI). The radiation field used for all of these examples was one having the shape of the Bechtold *et al.* (1987) "Medium" integrated QSO field.

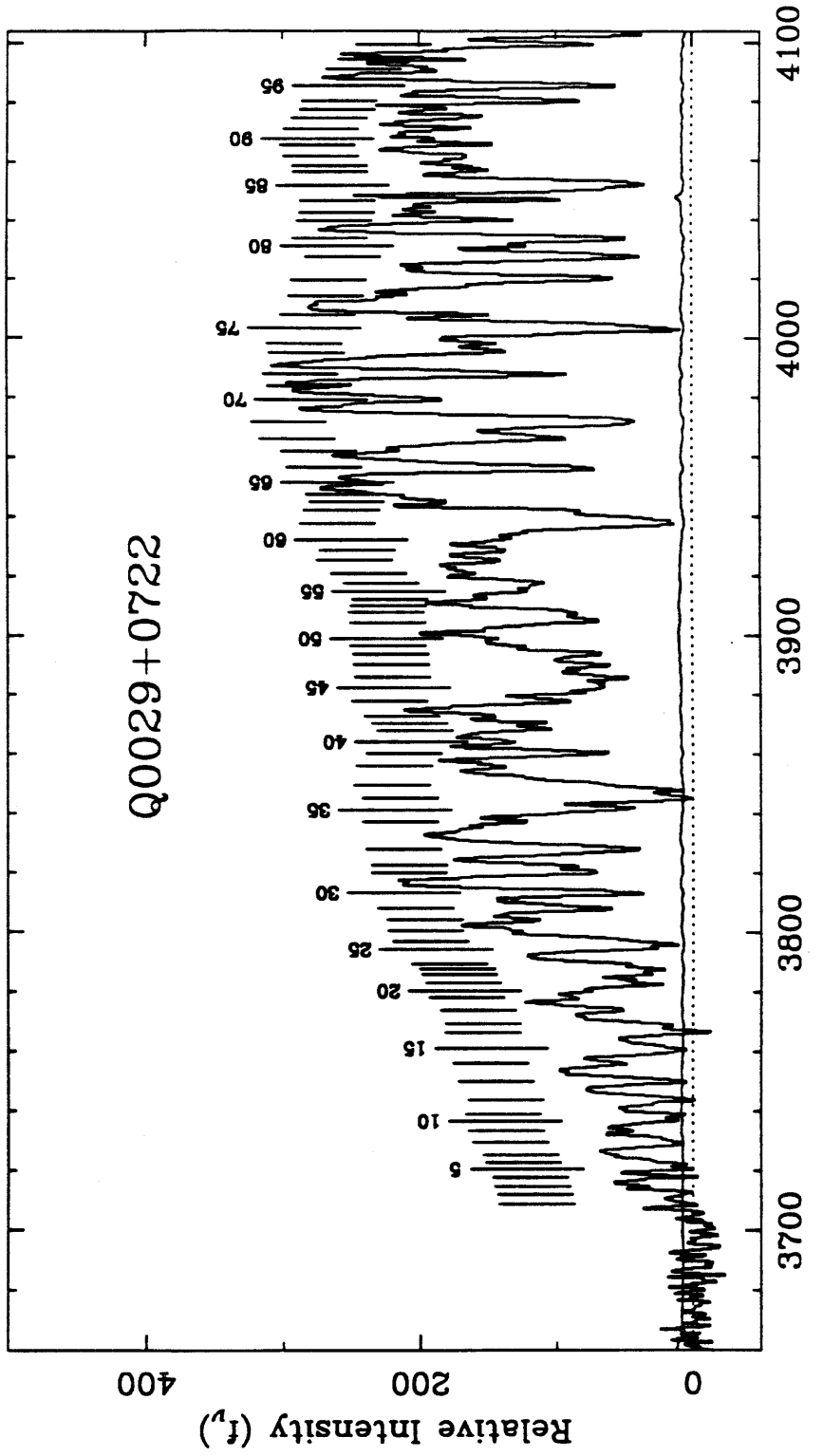
Q0029+0722
Relative Intensity (f_ν)
0
200
400
Wavelength (Å)
3700
3800
3900
4000
4100
5
10
15
20
25
30
35
40
45
50
55
60
65
70
75
80
85
90
95

Figure 1 *a.*

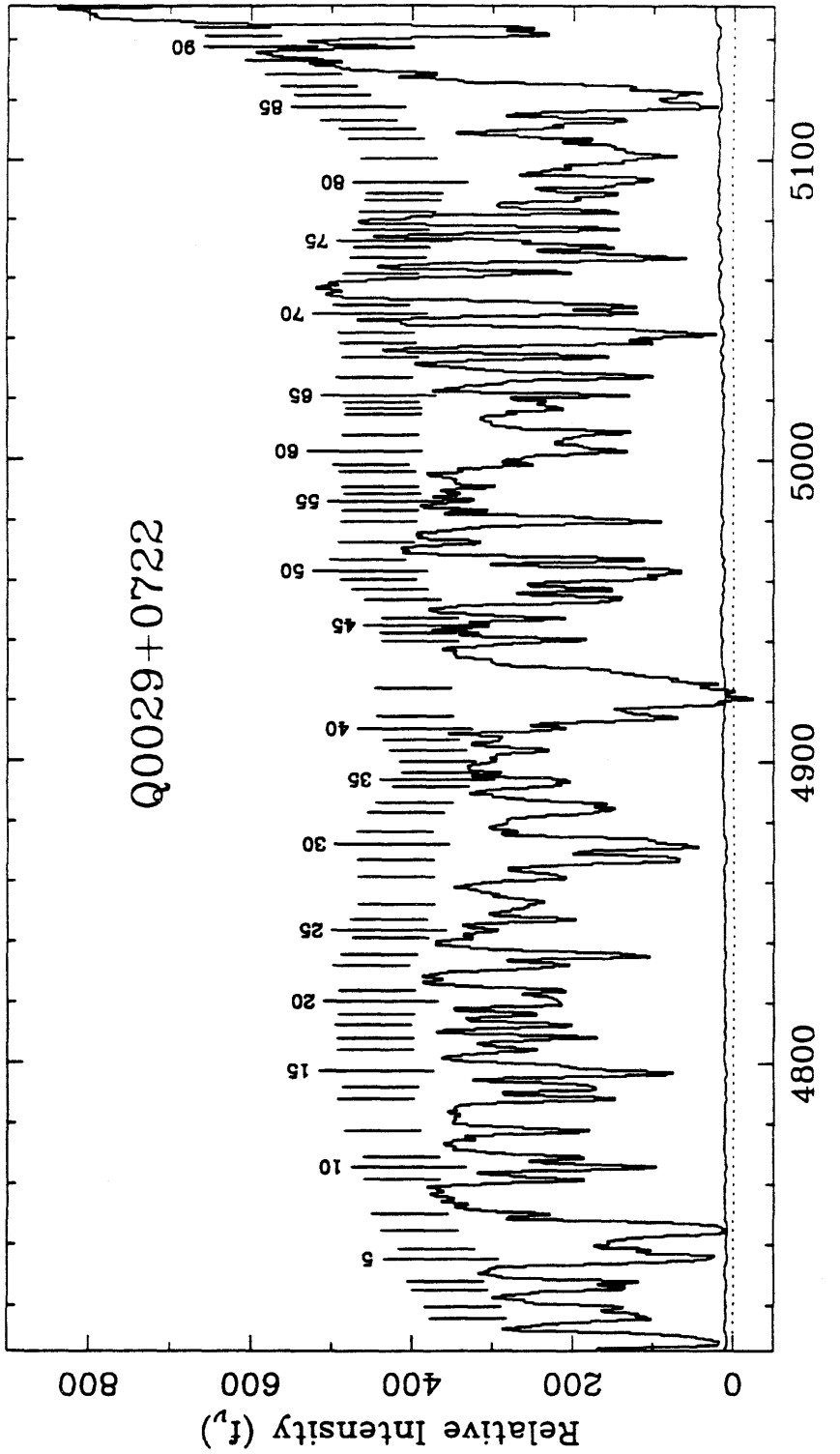
Q0029+0722
Relative Intensity (f_ν)
0
200
400
600
800
Wavelength (Å)
4800
4900
5000
5100
5
10
15
20
25
30
35
40
45
50
55
60
65
70
75
80
85
90

Figure 1 *b*.

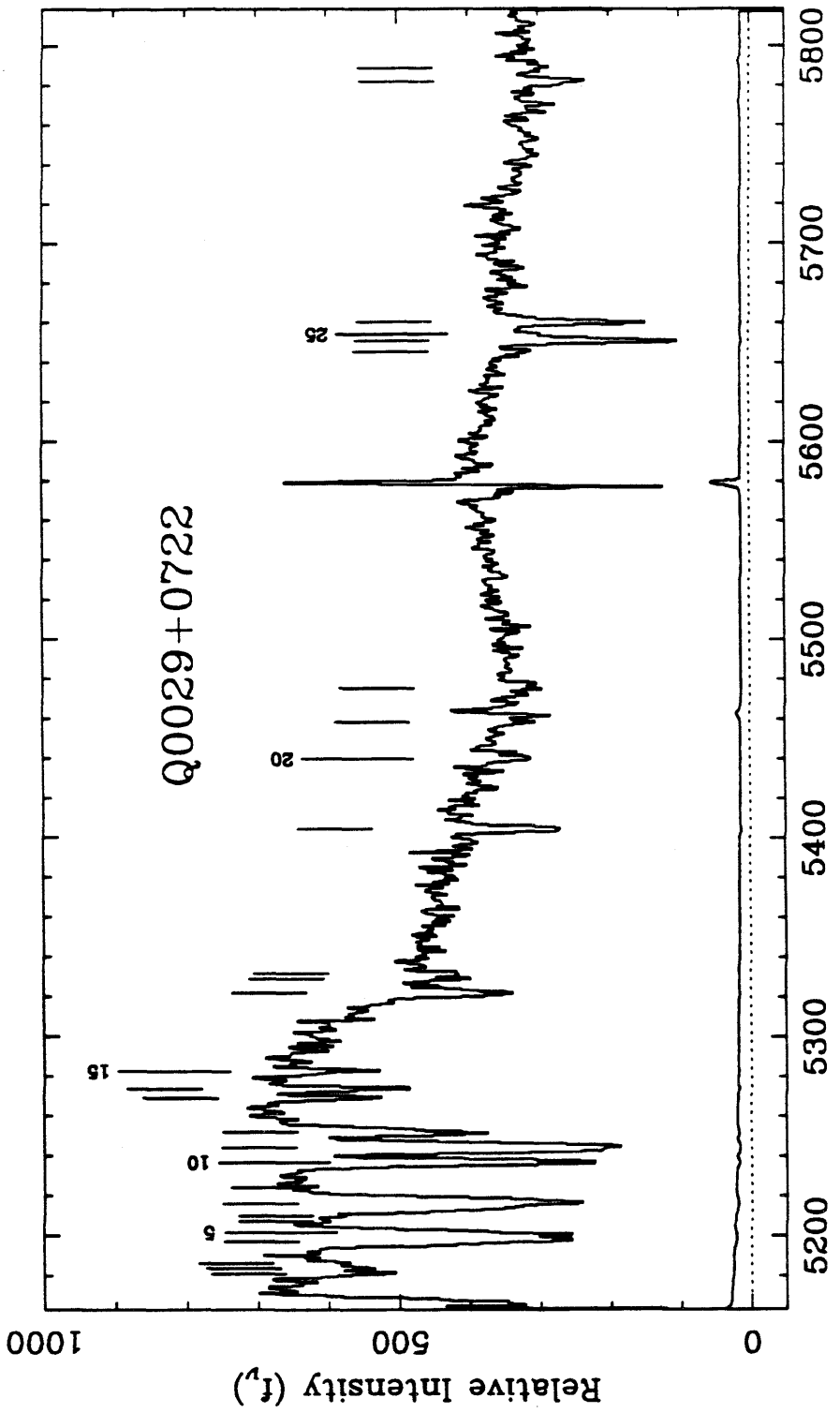
Q0029+0722
5
10
15
20
25
0
500
1000
Relative Intensity (f_ν)
5200
5300
5400
5500
5600
5700
5800
Wavelength (Å)

Figure 1 *c.*

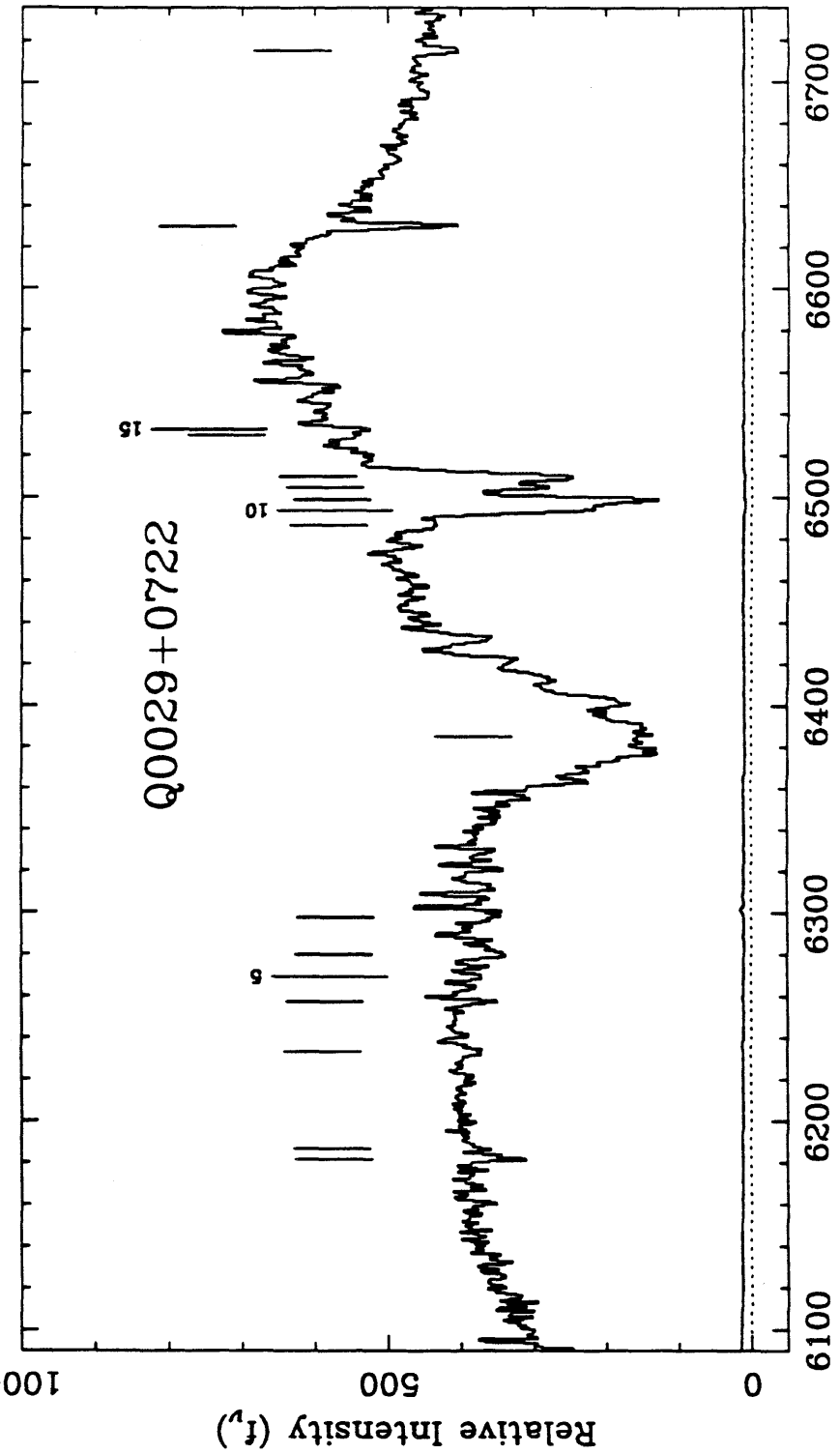
Q0029+0722
5
10
15
Relative Intensity (f_ν)
0
500
1000
Wavelength (Å)
6100
6200
6300
6400
6500
6600
6700

Figure 1 *d*.

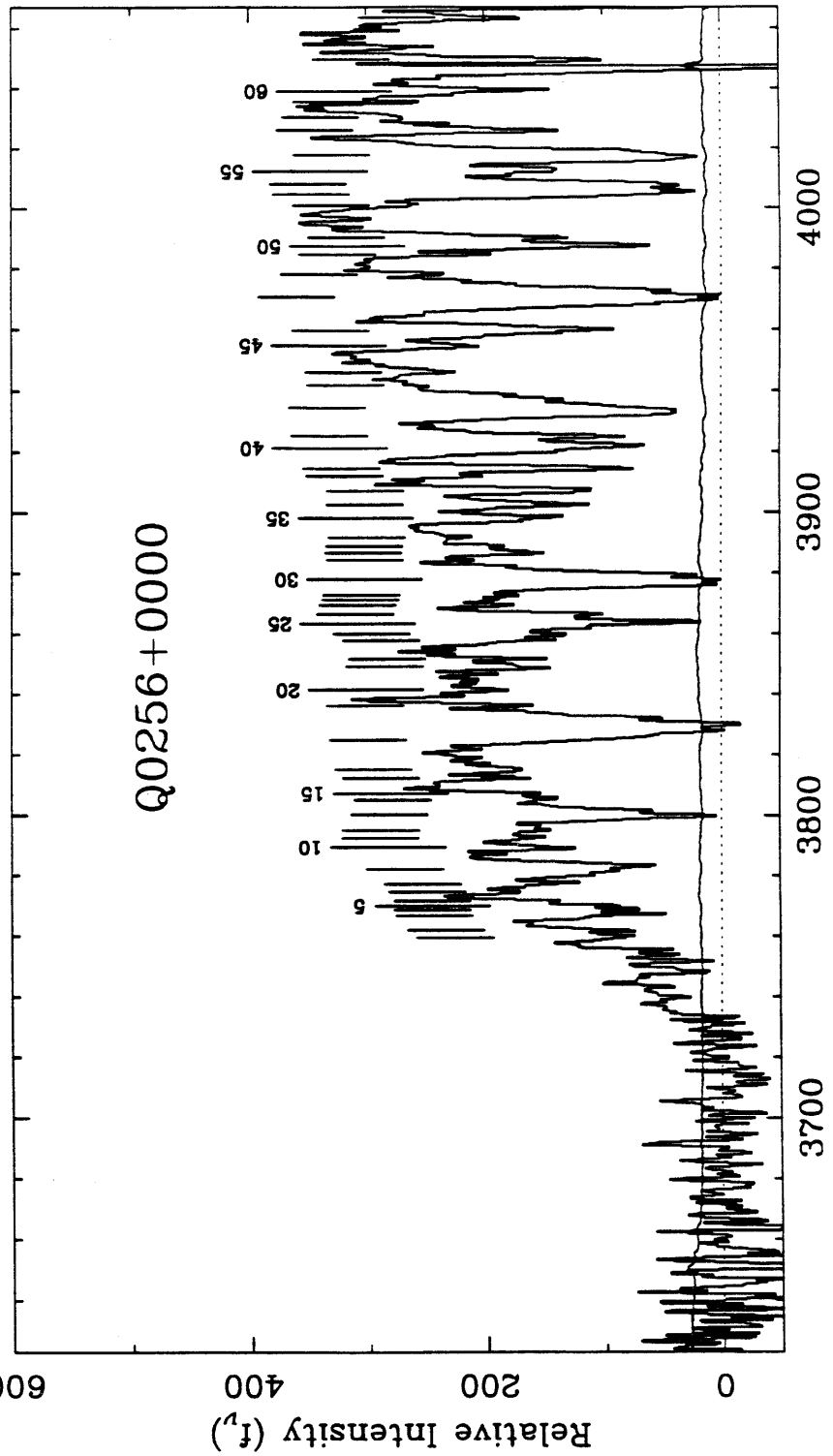
Q0256+0000
Relative Intensity (f_ν)
0
200
400
600
Wavelength (Å)
3700
3800
3900
4000
5
10
15
20
25
30
35
40
45
50
55
60

Figure 2 *a*.

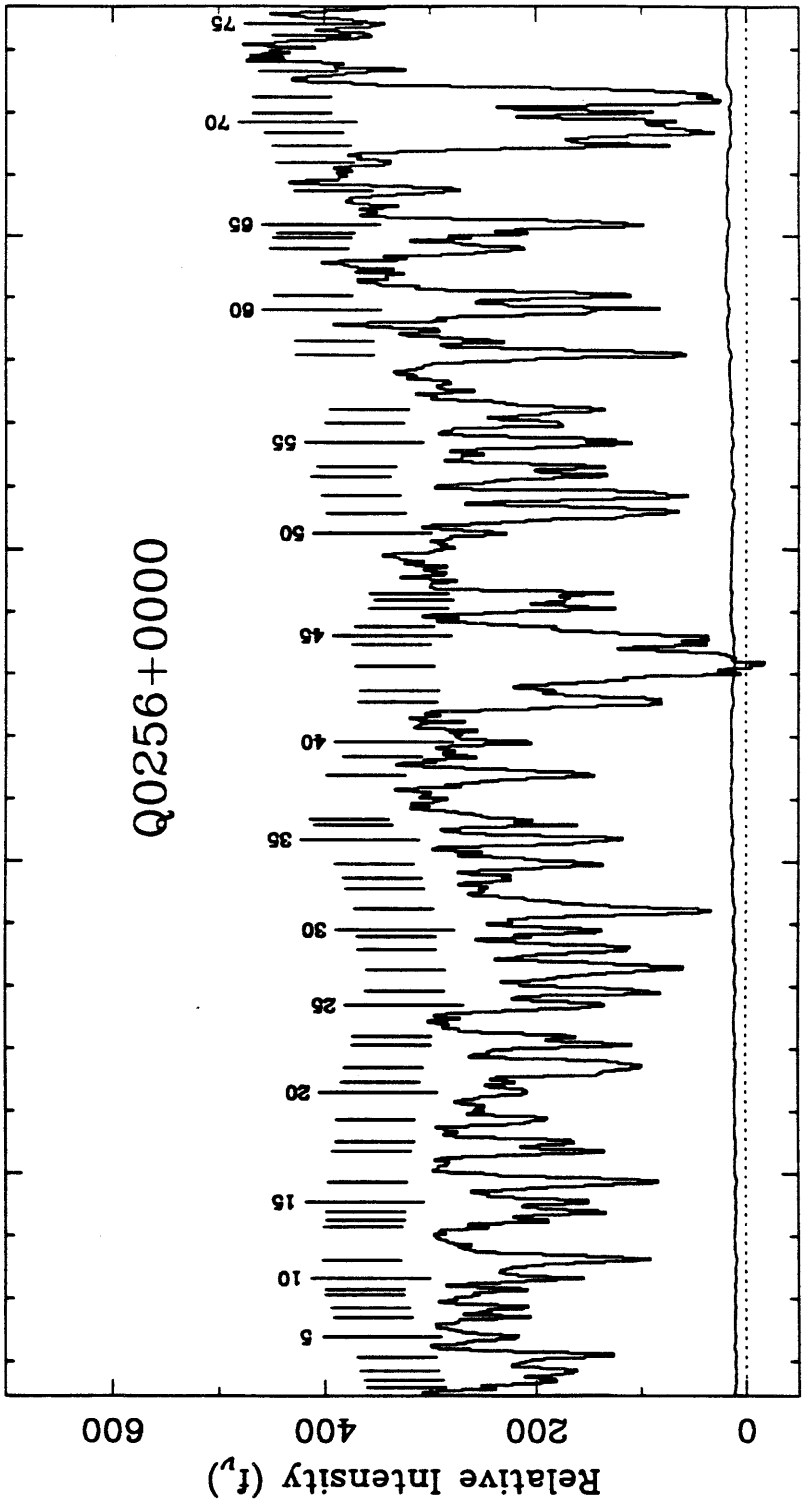
Q0256+0000
Relative Intensity (f_ν)
0
200
400
600
Wavelength (Å)
4800
4900
5000
5100
5
10
15
20
25
30
35
40
45
50
55
60
65
70
75

Figure 2 *b*.

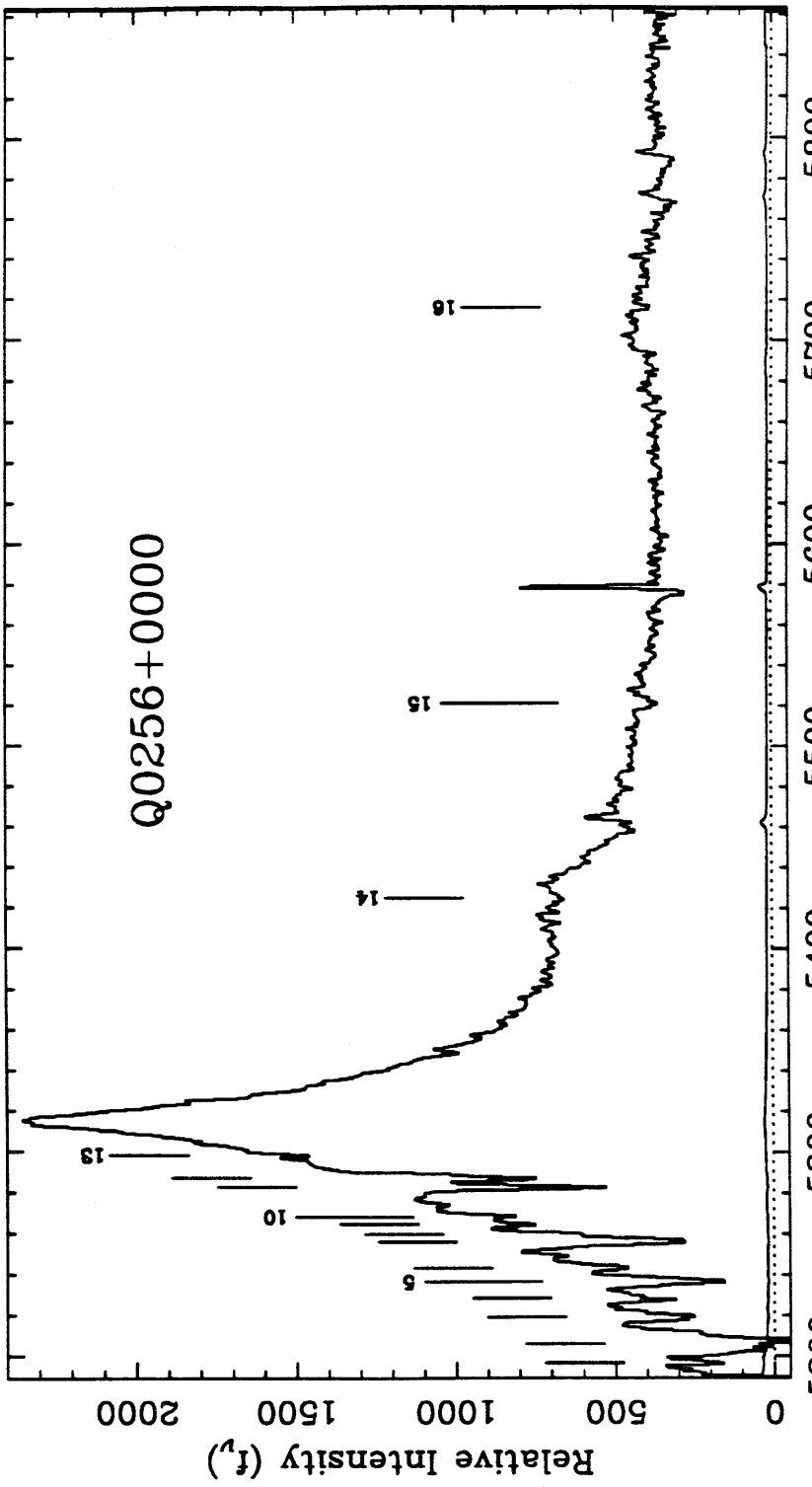
Q0256+0000
Relative Intensity (f_ν)
Wavelength (Å)
0
500
1000
1500
2000
5200
5300
5400
5500
5600
5700
5800
13
10
5
14
15
16

Figure 2 *c.*

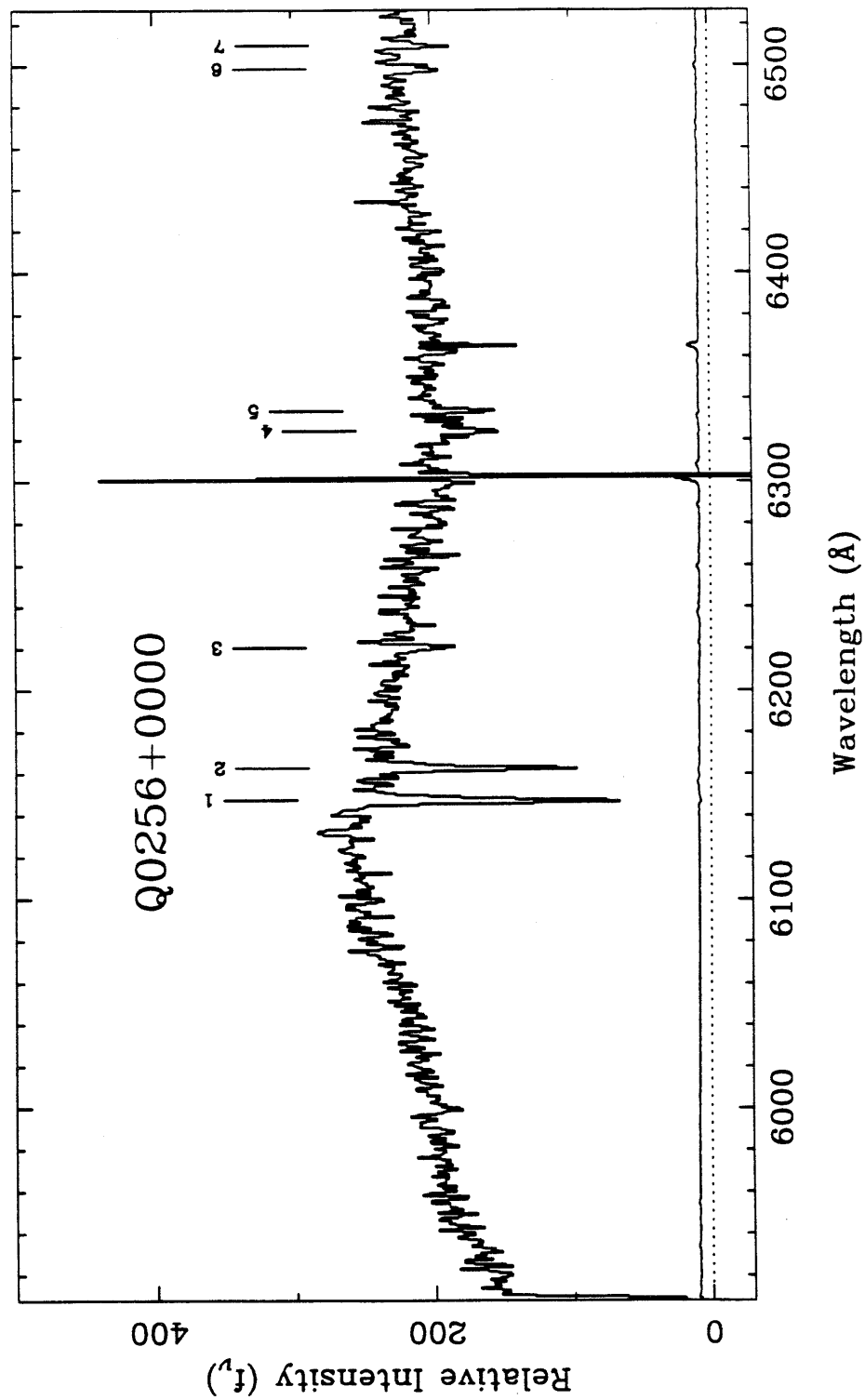
Q0256+0000
1
2
3
4
5
6
7
Relative Intensity (f_ν)
0
200
400
6000
6100
6200
6300
6400
6500
Wavelength (Å)

Figure 2 *d.*

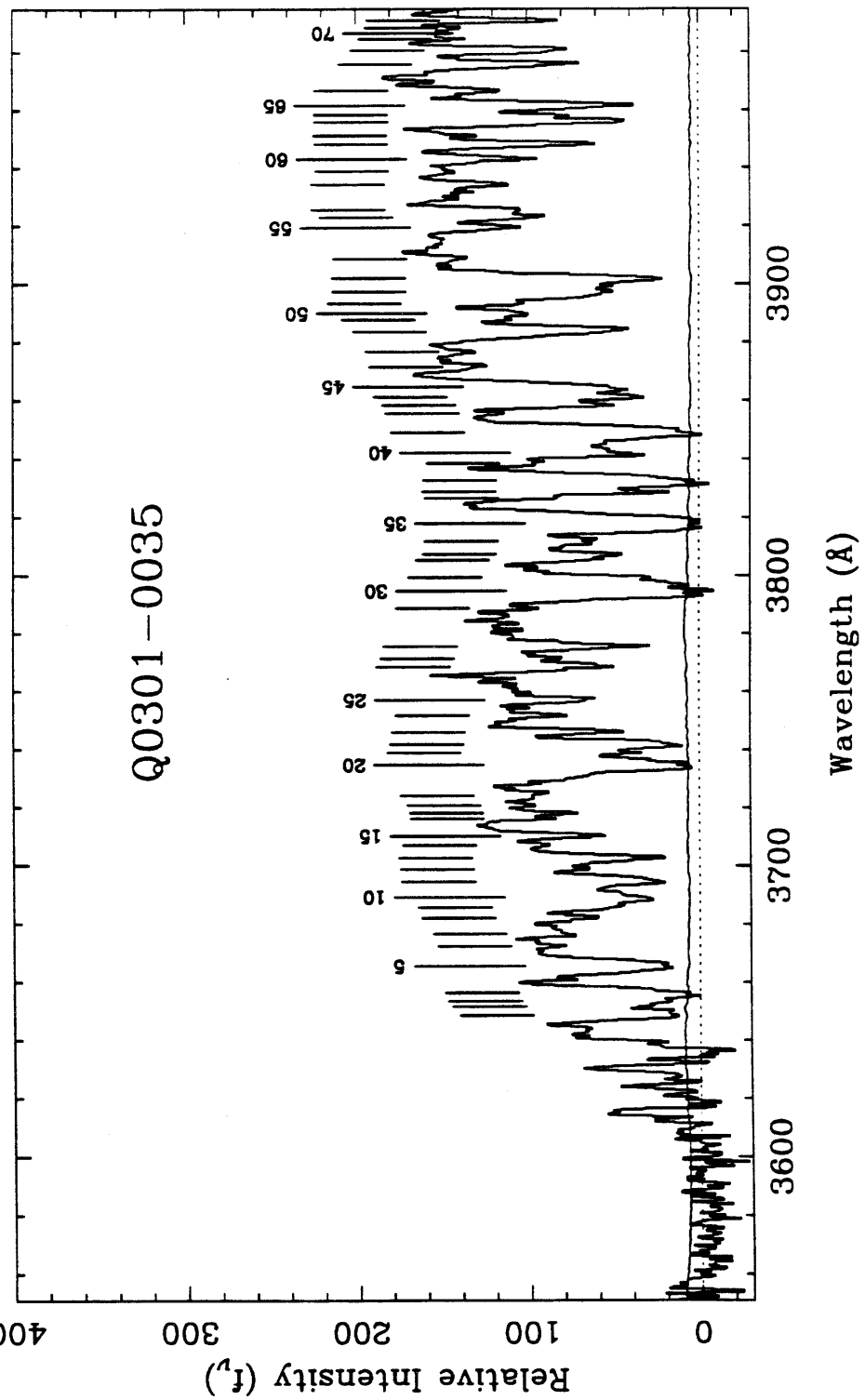
Q0301−0035
Relative Intensity (f_ν)
Wavelength (Å)
0
100
200
300
400
3600
3700
3800
3900
5
10
15
20
25
30
35
40
45
50
55
60
65
70

Figure 3 *a*.

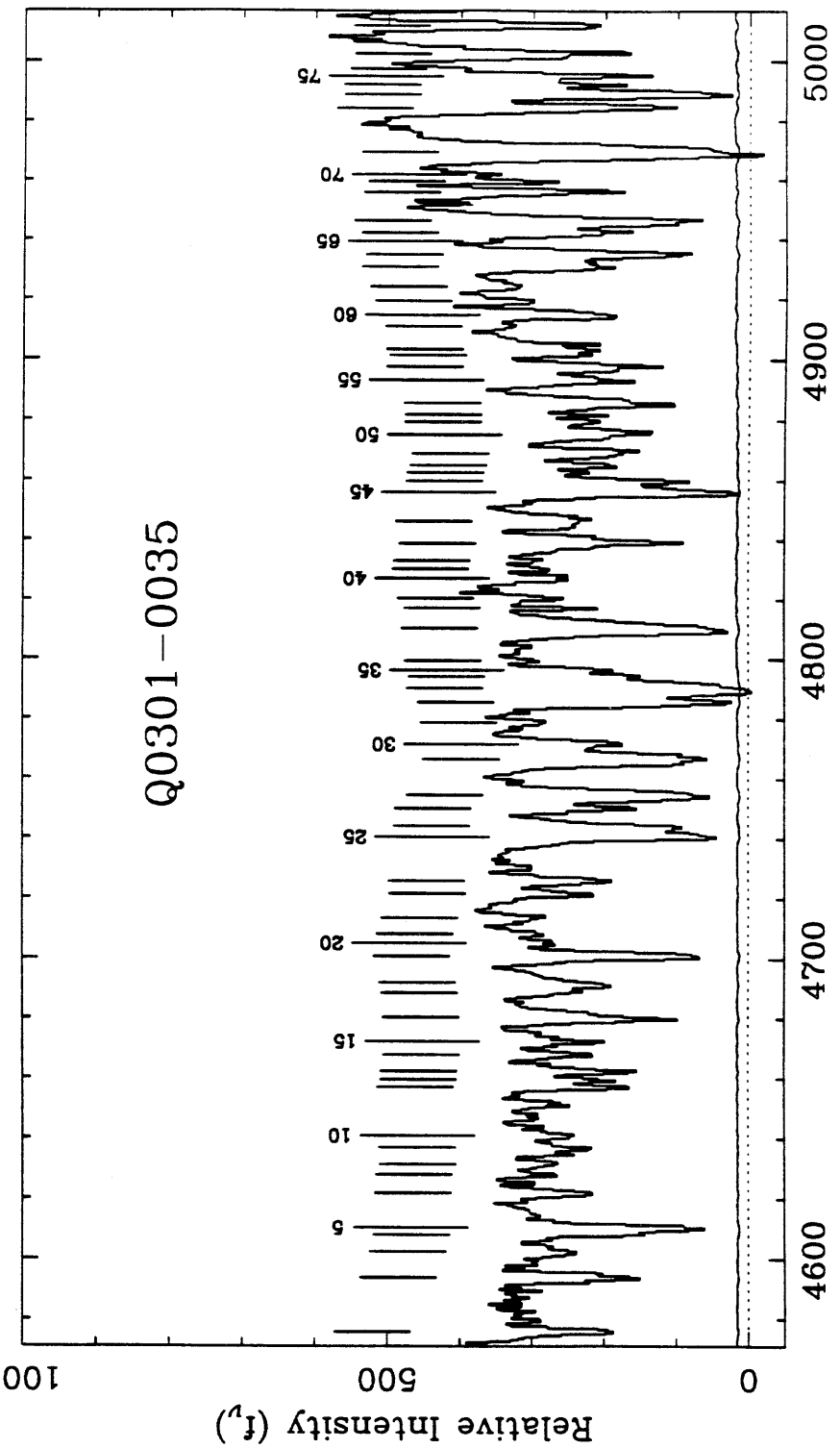
Q0301−0035
Relative Intensity (f_ν)
0
500
1000
Wavelength (Å)
4600
4700
4800
4900
5000
5
10
15
20
25
30
35
40
45
50
55
60
65
70
75

Figure 3 *b*.

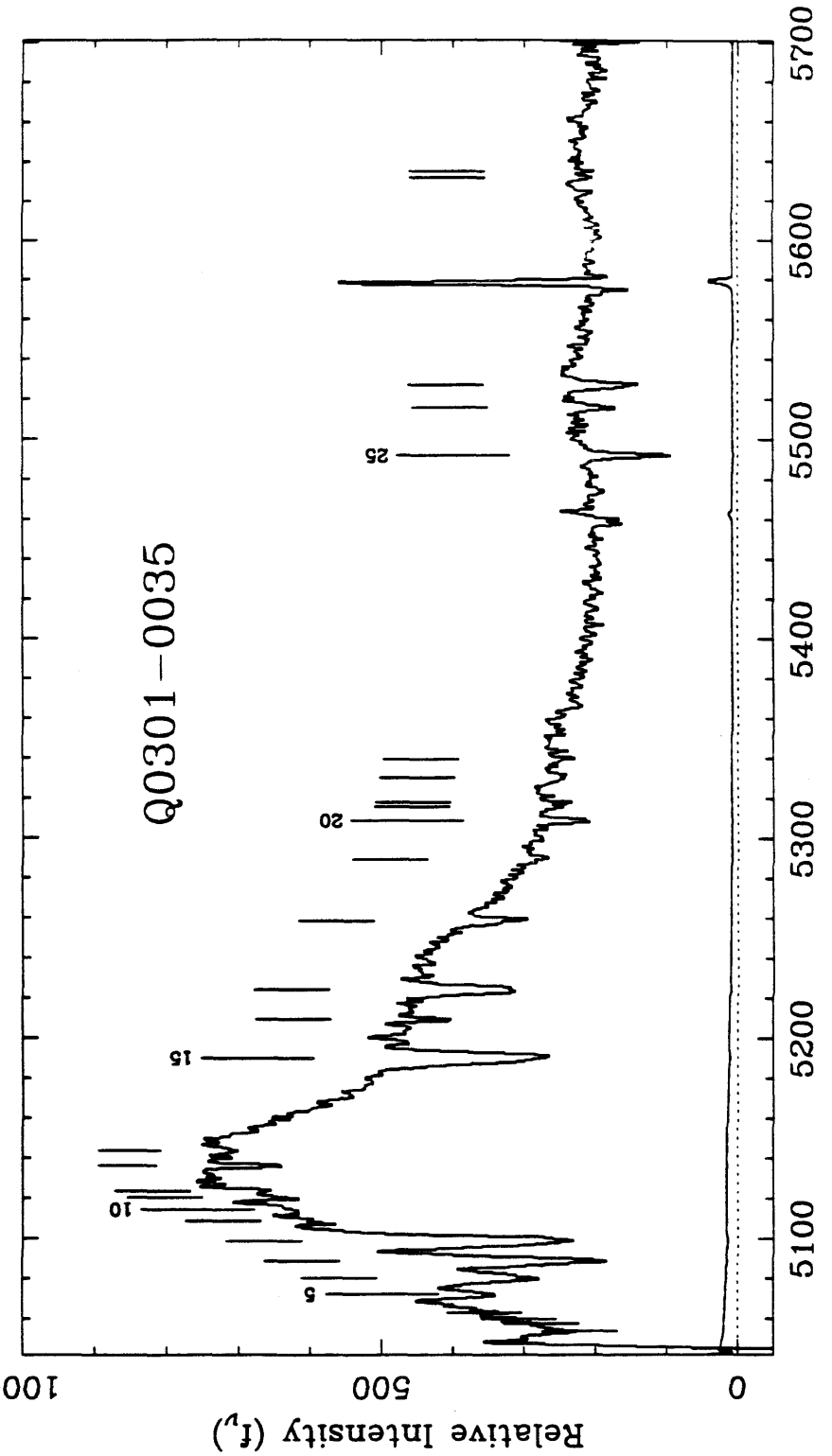
Q0301−0035
5
10
15
20
25
Relative Intensity (f_ν)
0
500
1000
Wavelength (Å)
5100
5200
5300
5400
5500
5600
5700

Figure 3 *c.*

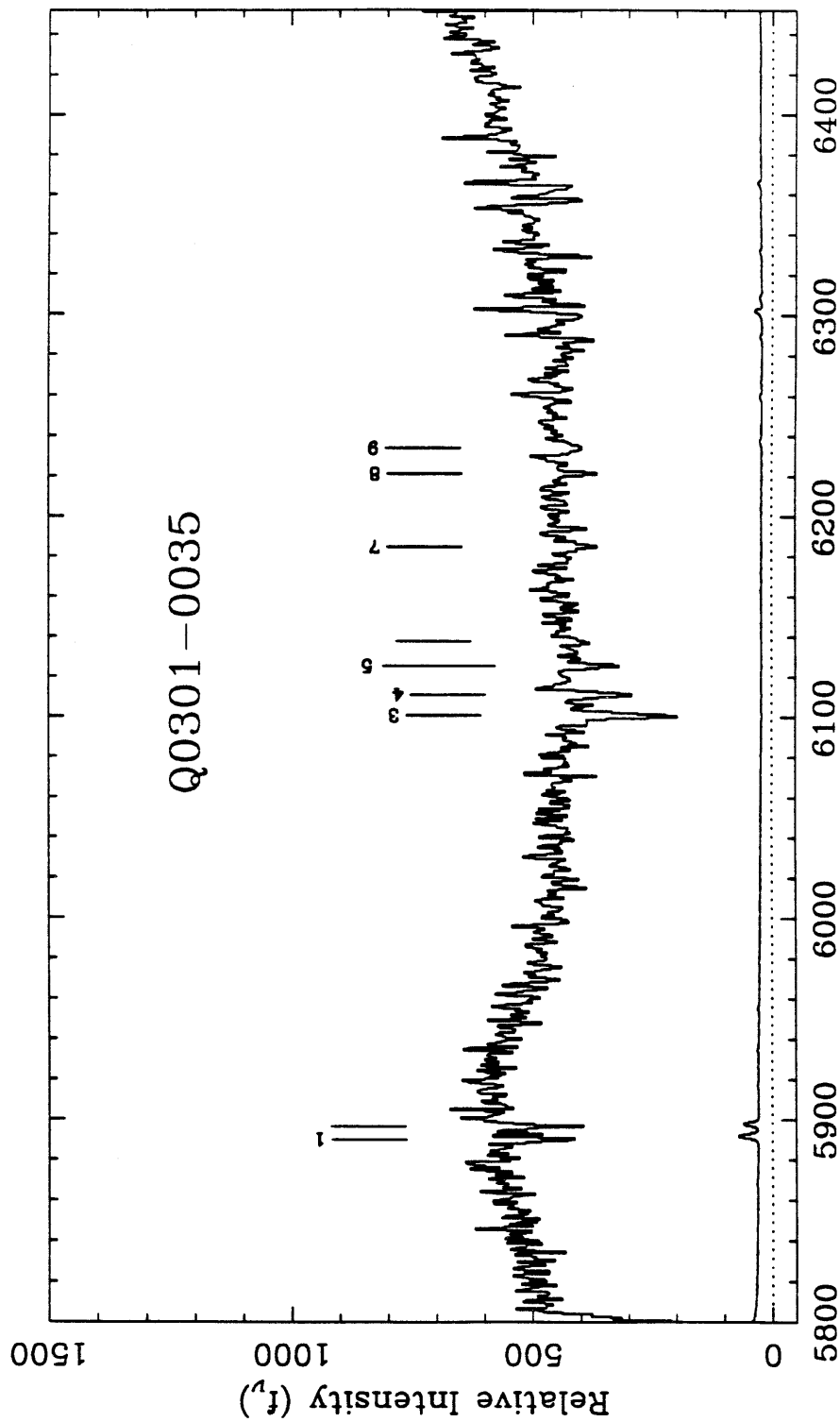
Q0301−0035
1
3
4
5
7
8
9
Relative Intensity (f_ν)
0
500
1000
1500
5800
5900
6000
6100
6200
6300
6400
Wavelength (Å)

Figure 3 *d*.

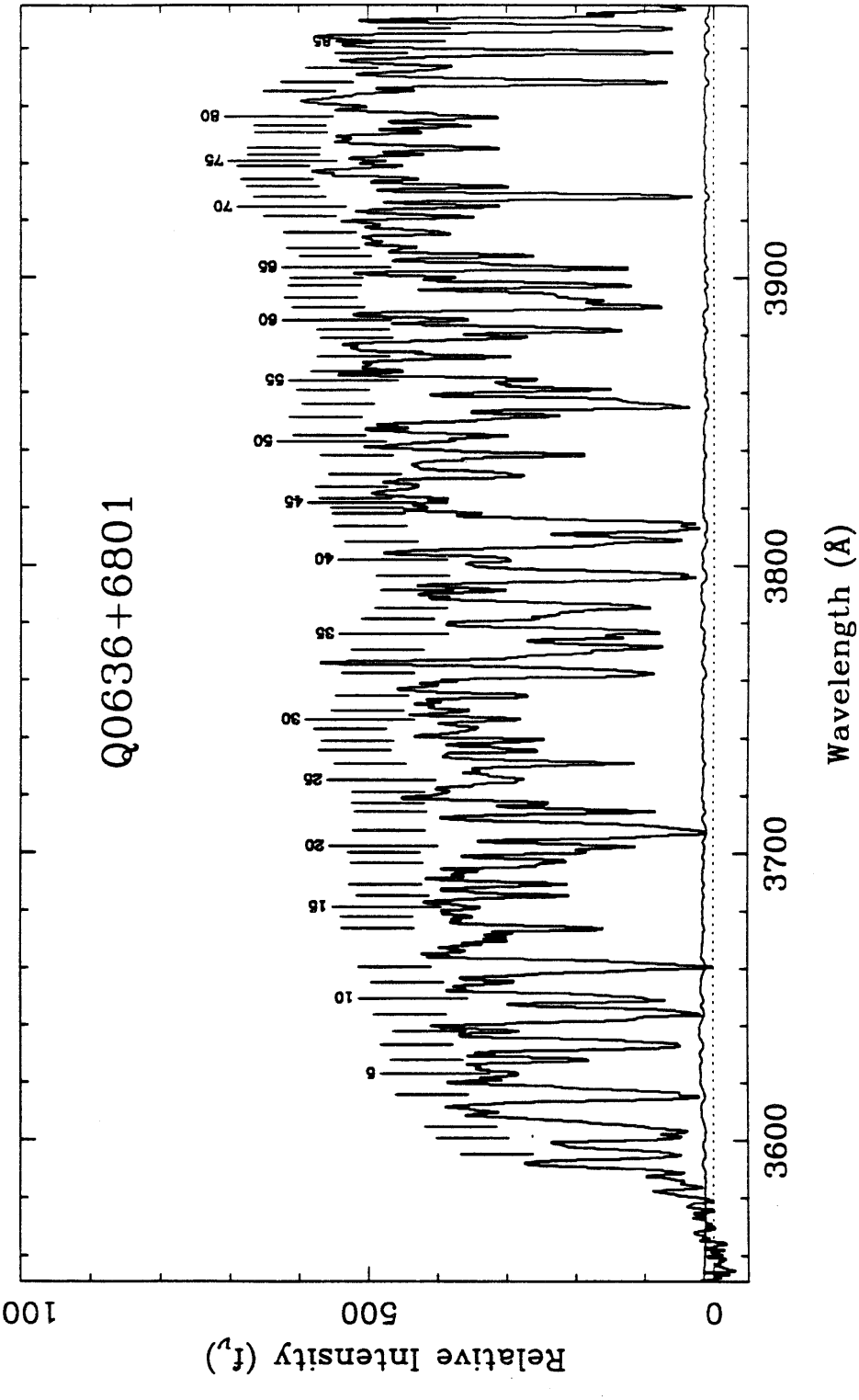
Q0636+6801
Relative Intensity (f_ν)
0
500
1000
Wavelength (Å)
3600
3700
3800
3900
5
10
15
20
25
30
35
40
45
50
55
60
65
70
75
80
85

Figure 4 *a.*

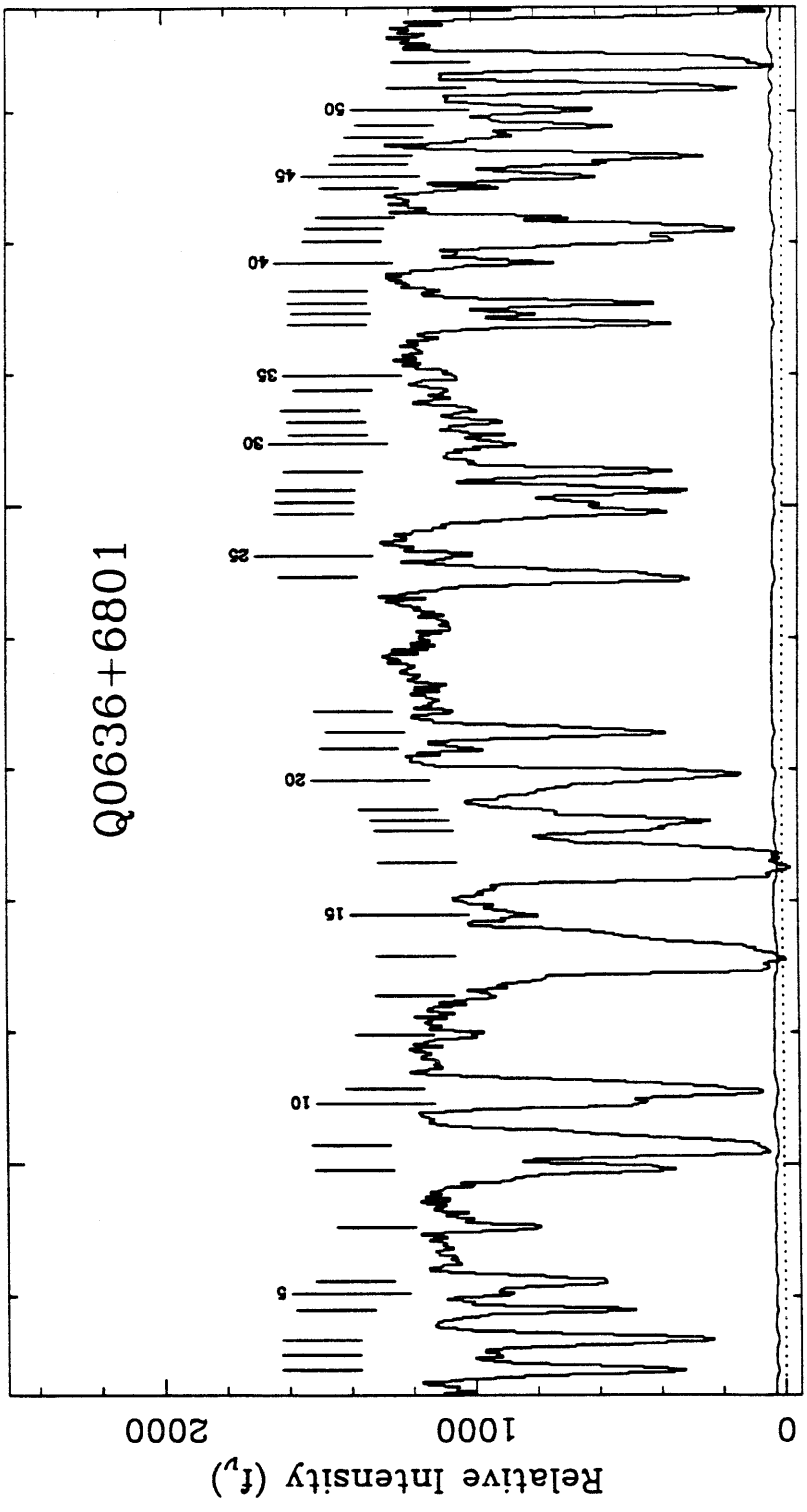
Q0636+6801
Relative Intensity (f_ν)
0
1000
2000
4700
4800
Wavelength (Å)
5
10
15
20
25
30
35
40
45
50

Figure 4 *b*.

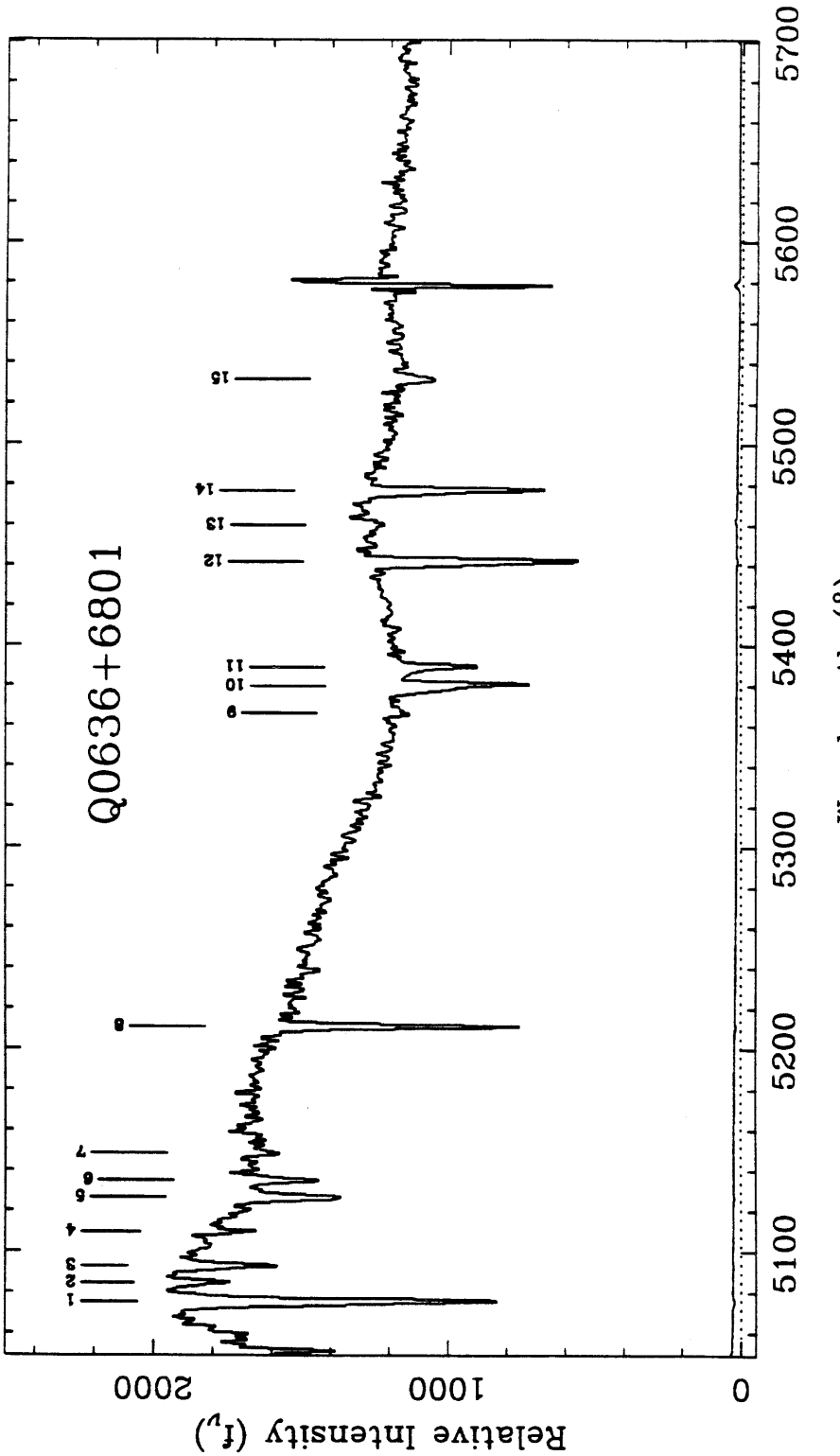
Q0636+6801
Relative Intensity (f_ν)
Wavelength (Å)
0
1000
2000
5100
5200
5300
5400
5500
5600
5700
1
2
3
4
5
6
7
8
9
10
11
12
13
14
15

Figure 4 *c*.

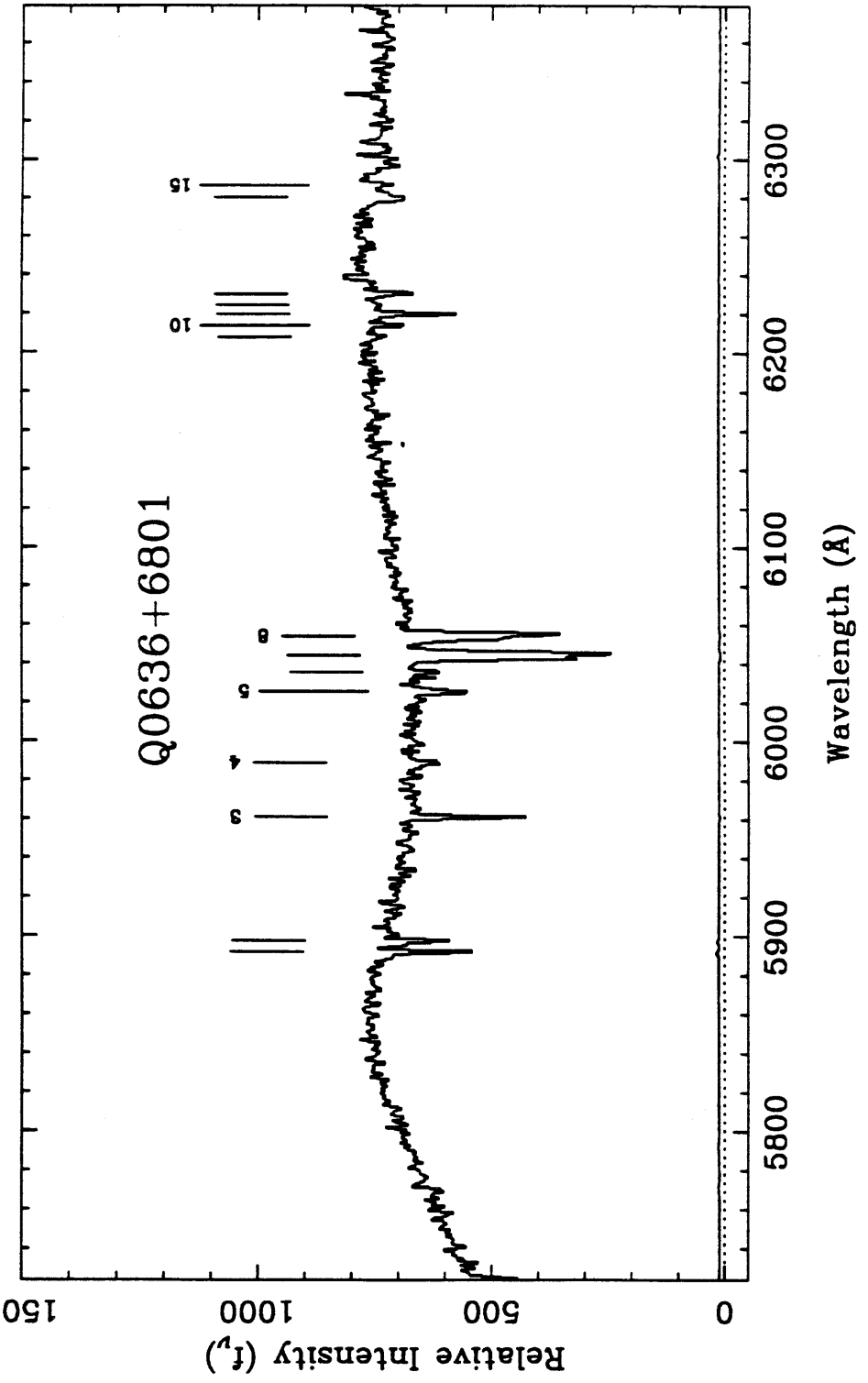
Q0636+6801
15
10
8
5
4
3
Relative Intensity (f_ν)
0
500
1000
1500
5800
5900
6000
6100
6200
6300
Wavelength (Å)

Figure 4 *d.*

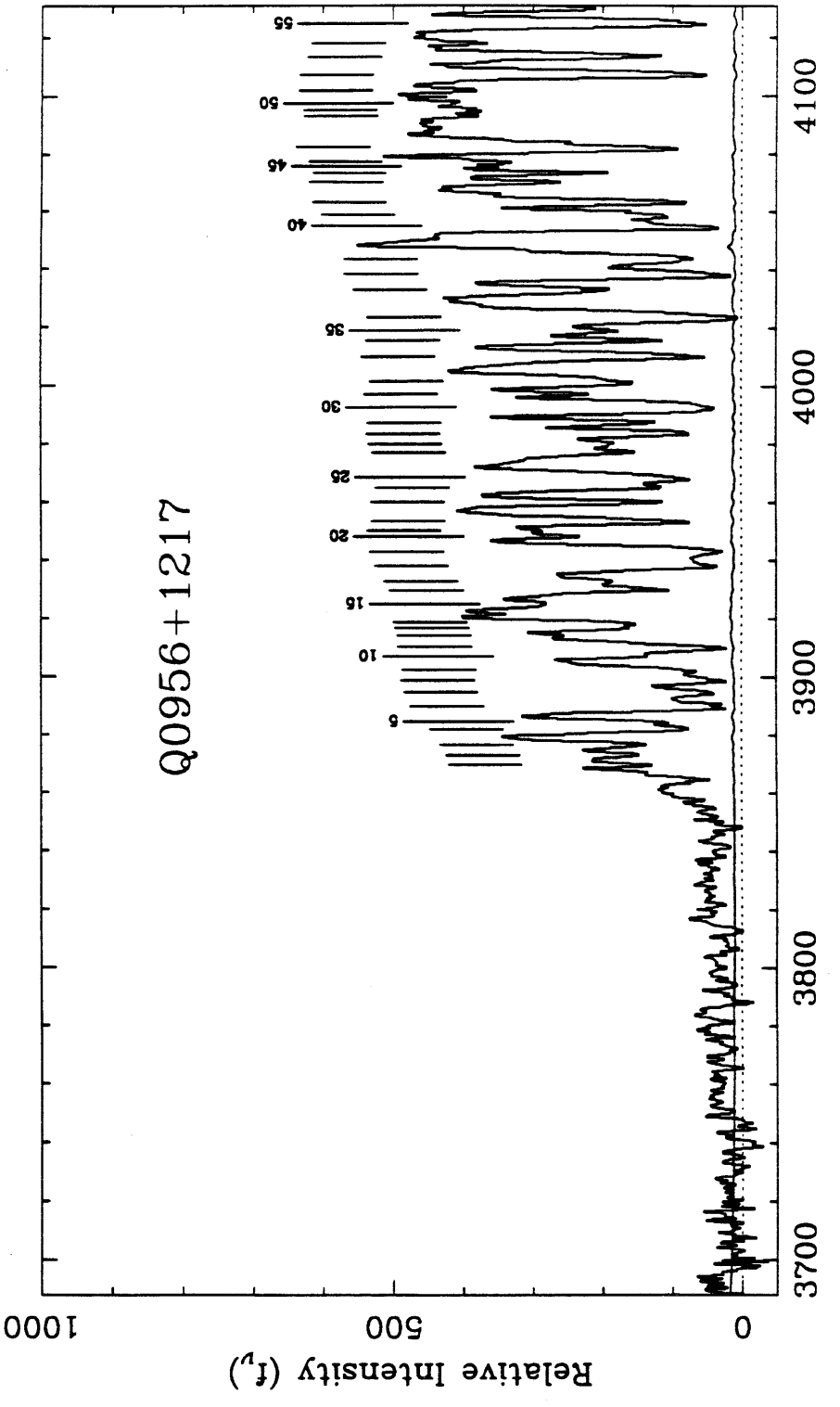
Q0956+12217
Relative Intensity (f_ν)
0
500
1000
3700
3800
3900
4000
4100
Wavelength (Å)
5
10
15
20
25
30
35
40
45
50
55

Figure 5 *a*.

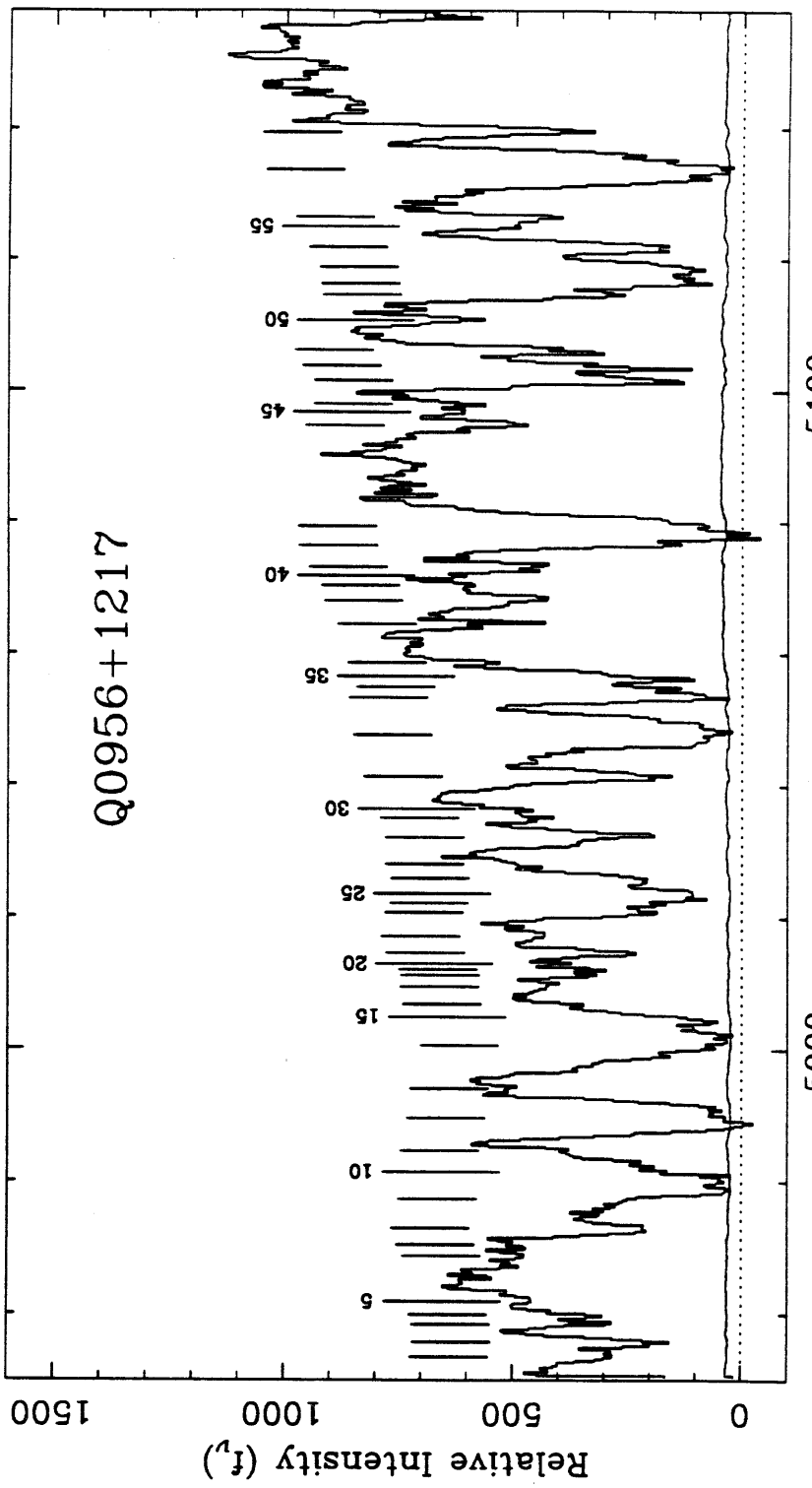
Q0956+12217
Relative Intensity (f_ν)
0
500
1000
1500
5000
5100
Wavelength (Å)
5
10
15
20
25
30
35
40
45
50
55

Figure 5 *b*.

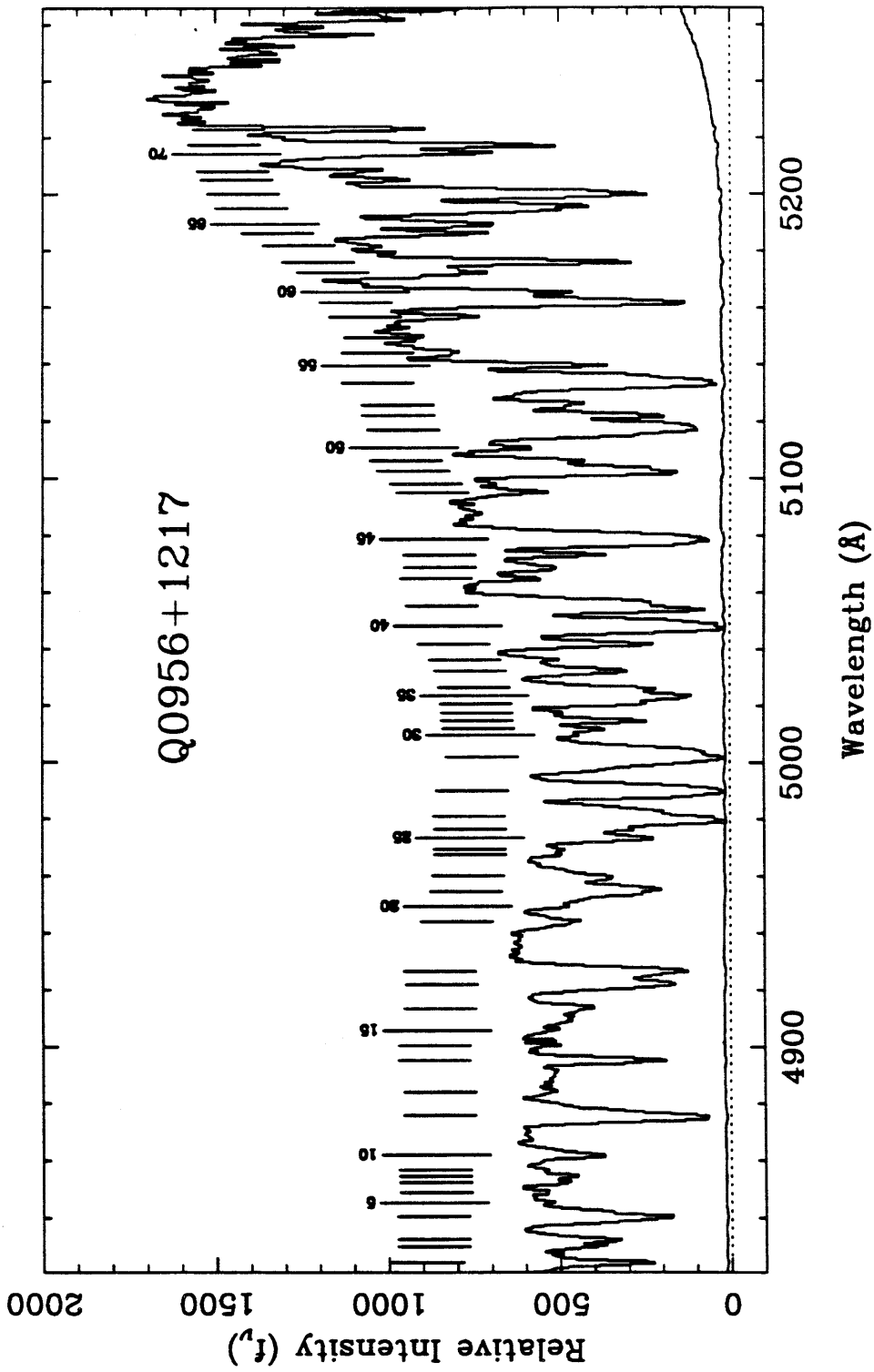
Q0956+12217
Relative Intensity (f_ν)
0
500
1000
1500
2000
Wavelength (Å)
4900
5000
5100
5200
6
10
15
30
35
35
45
45
55
55
60
60
66
73

Figure 5 *c.*

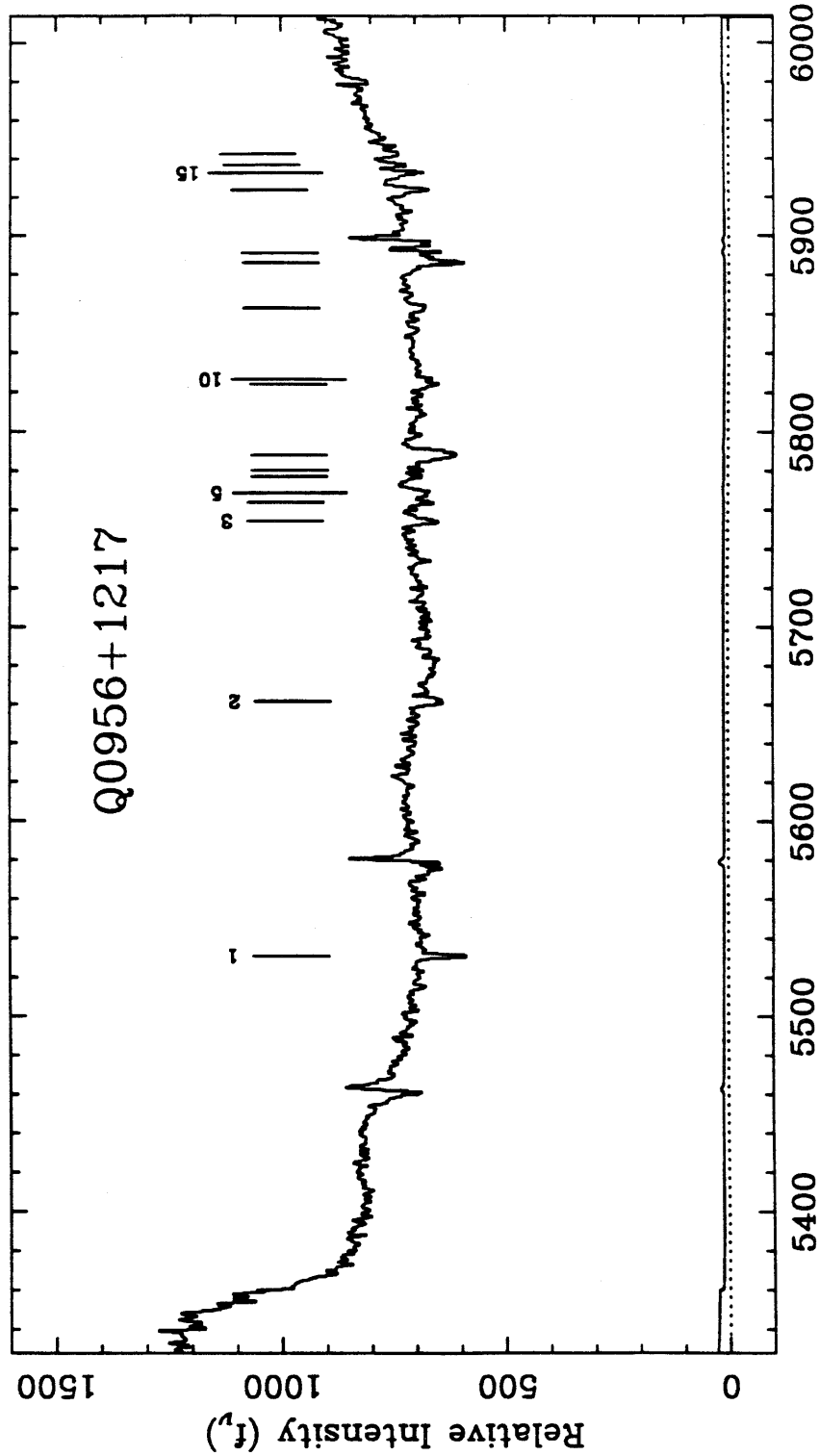
Q0956+1217
1
2
3
5
10
15
Relative Intensity (f_ν)
0
500
1000
1500
Wavelength (Å)
5400
5500
5600
5700
5800
5900
6000

Figure 5 *d*.

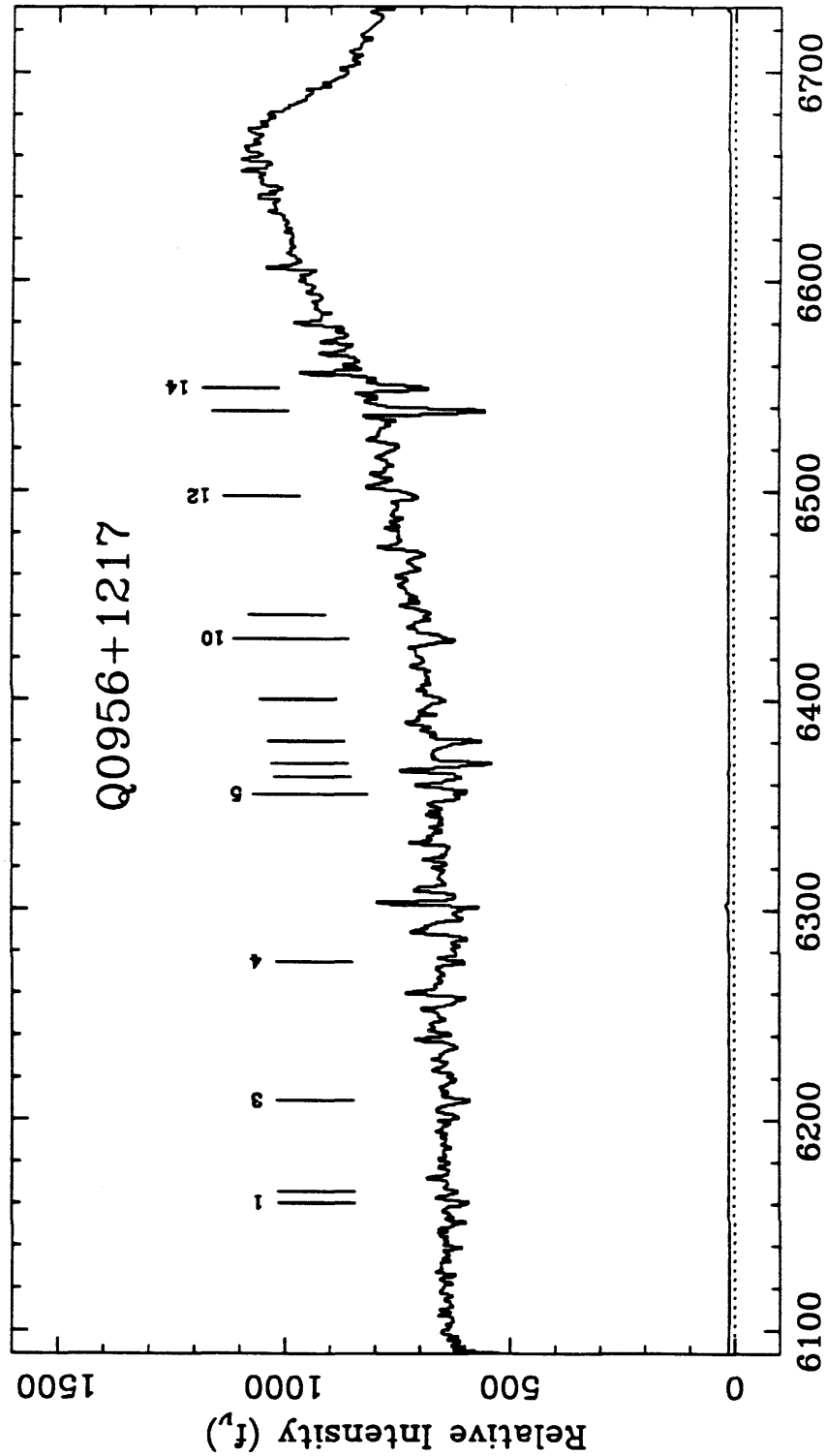
Q0956+1217
1
3
4
5
10
12
14
Relative Intensity (f_ν)
0
500
1000
1500
Wavelength (Å)
6100
6200
6300
6400
6500
6600
6700

Figure 5 *e*.

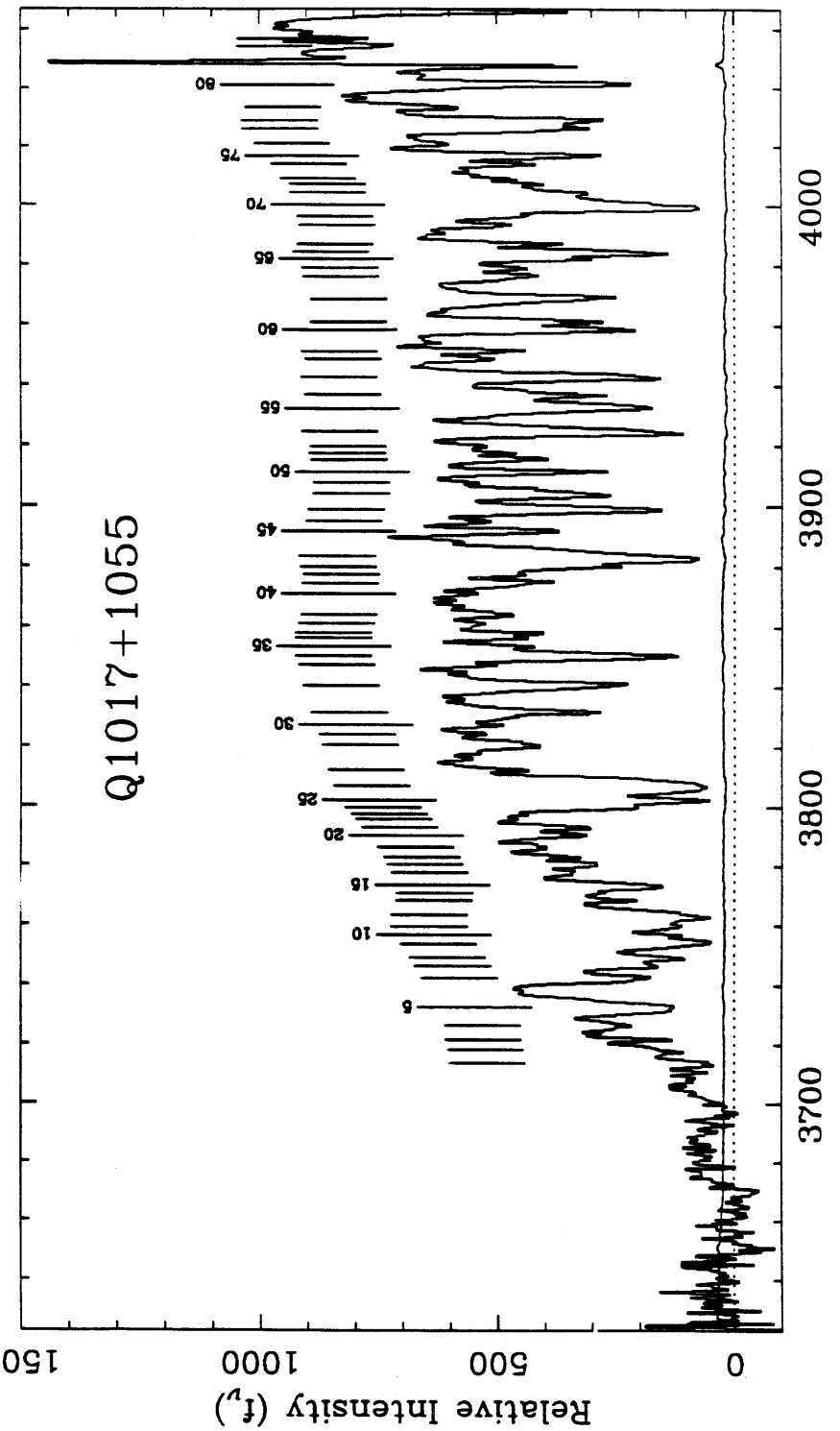
Q1017+1055
Relative Intensity (f_ν)
0
500
1000
1500
Wavelength (Å)
3700
3800
3900
4000
5
10
15
20
25
30
35
40
45
50
55
60
65
70
75
80

Figure 6 *a*.

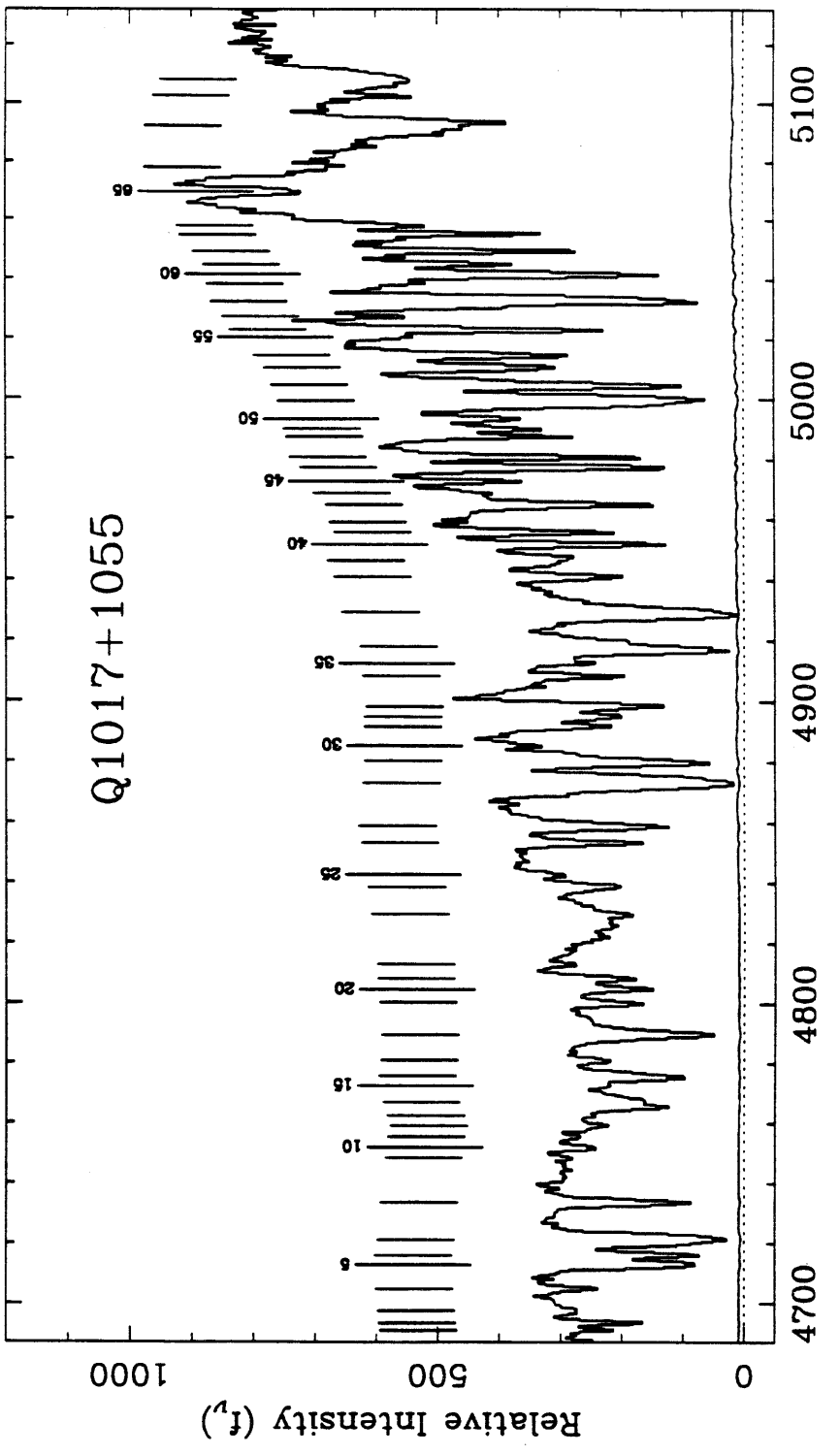
Q1017+1055
Relative Intensity (f_ν)
0
500
1000
Wavelength (Å)
4700
4800
4900
5000
5100
5
10
15
20
25
30
35
40
45
50
55
60
65

Figure 6 *b.*

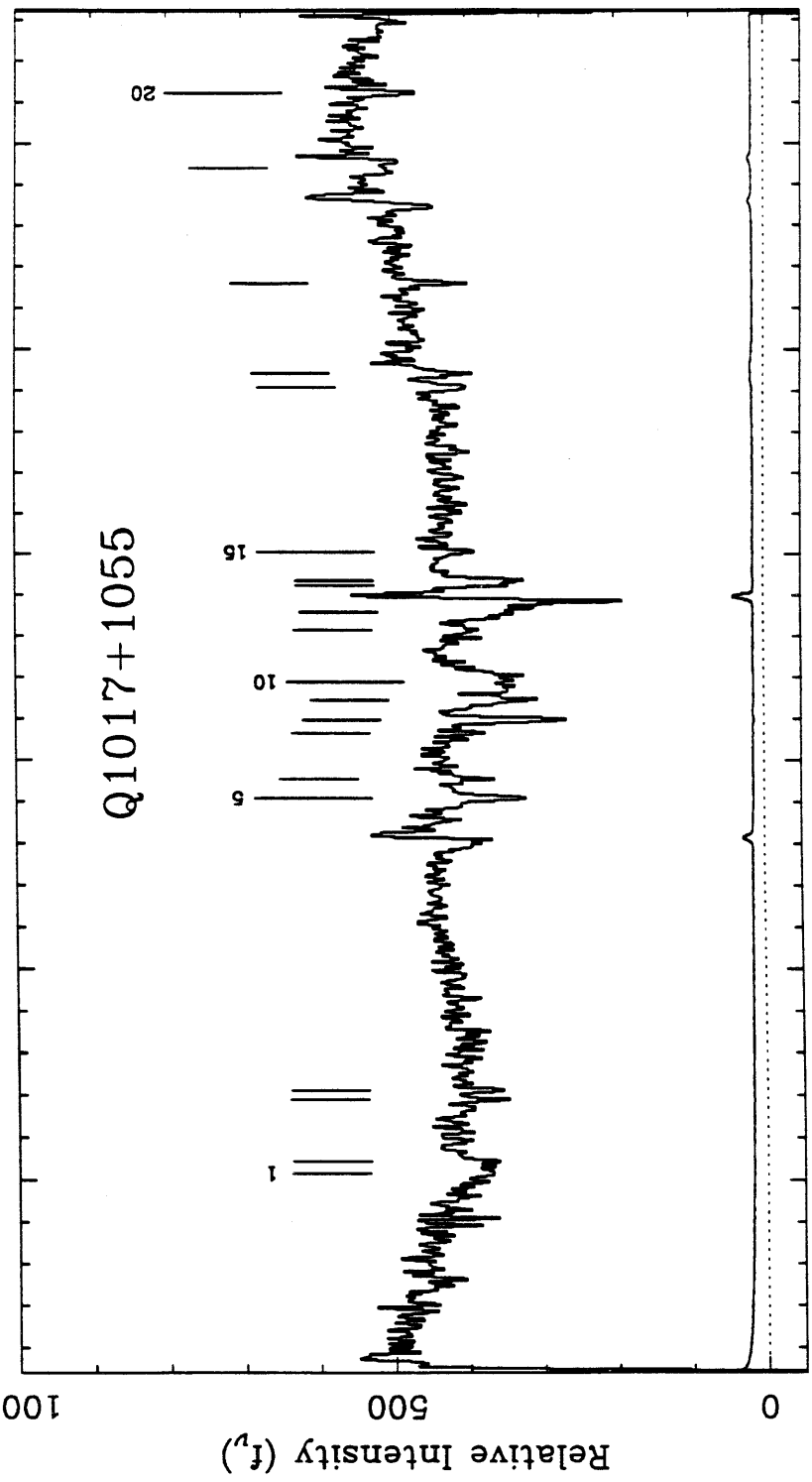
Q1017+1055
1
5
10
15
20
0
500
1000
Relative Intensity (f_ν)
5300
5400
5500
5600
5700
5800
Wavelength (Å)

Figure 6 *c*.

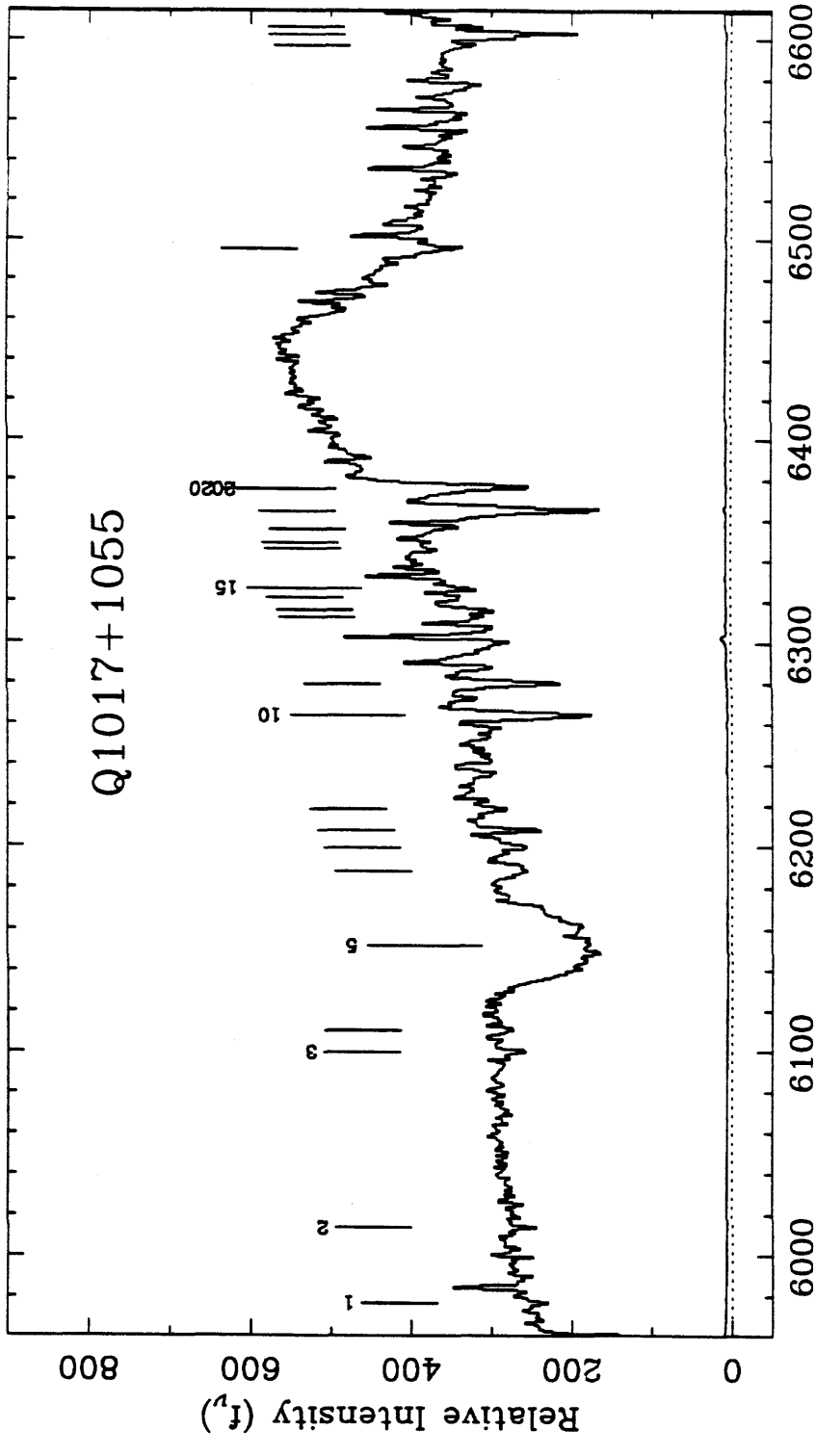
Q1017+1055
1
2
3
5
10
15
8020
Relative Intensity (f_ν)
0
200
400
600
800
6000
6100
6200
6300
6400
6500
6600
Wavelength (Å)

Figure 6 *d*.

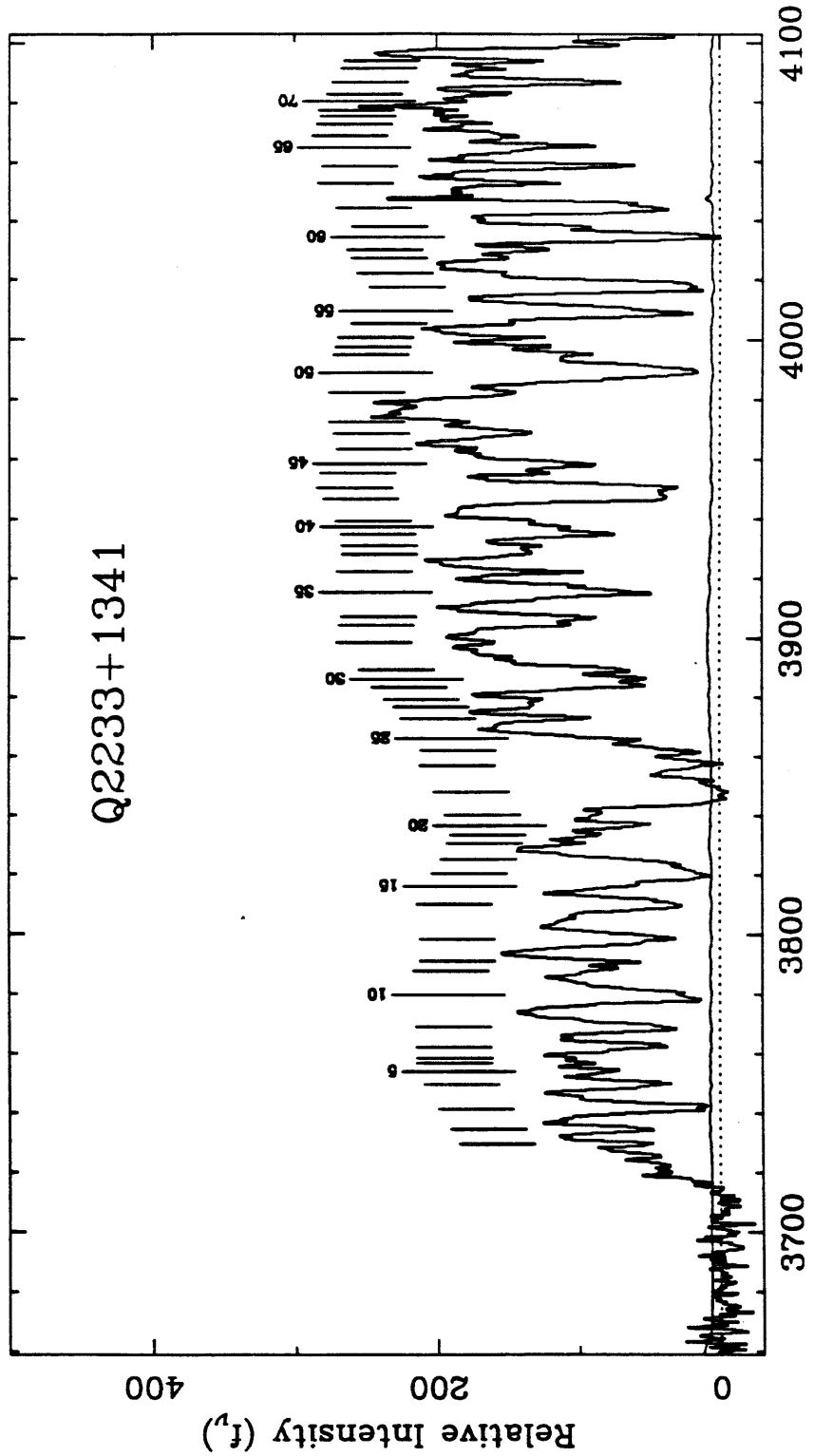
Q2233+1341
Relative Intensity (f_ν)
Wavelength (Å)
0
200
400
3700
3800
3900
4000
4100
5
10
15
20
25
30
35
40
45
50
55
60
65
70

Figure 7 *a.*

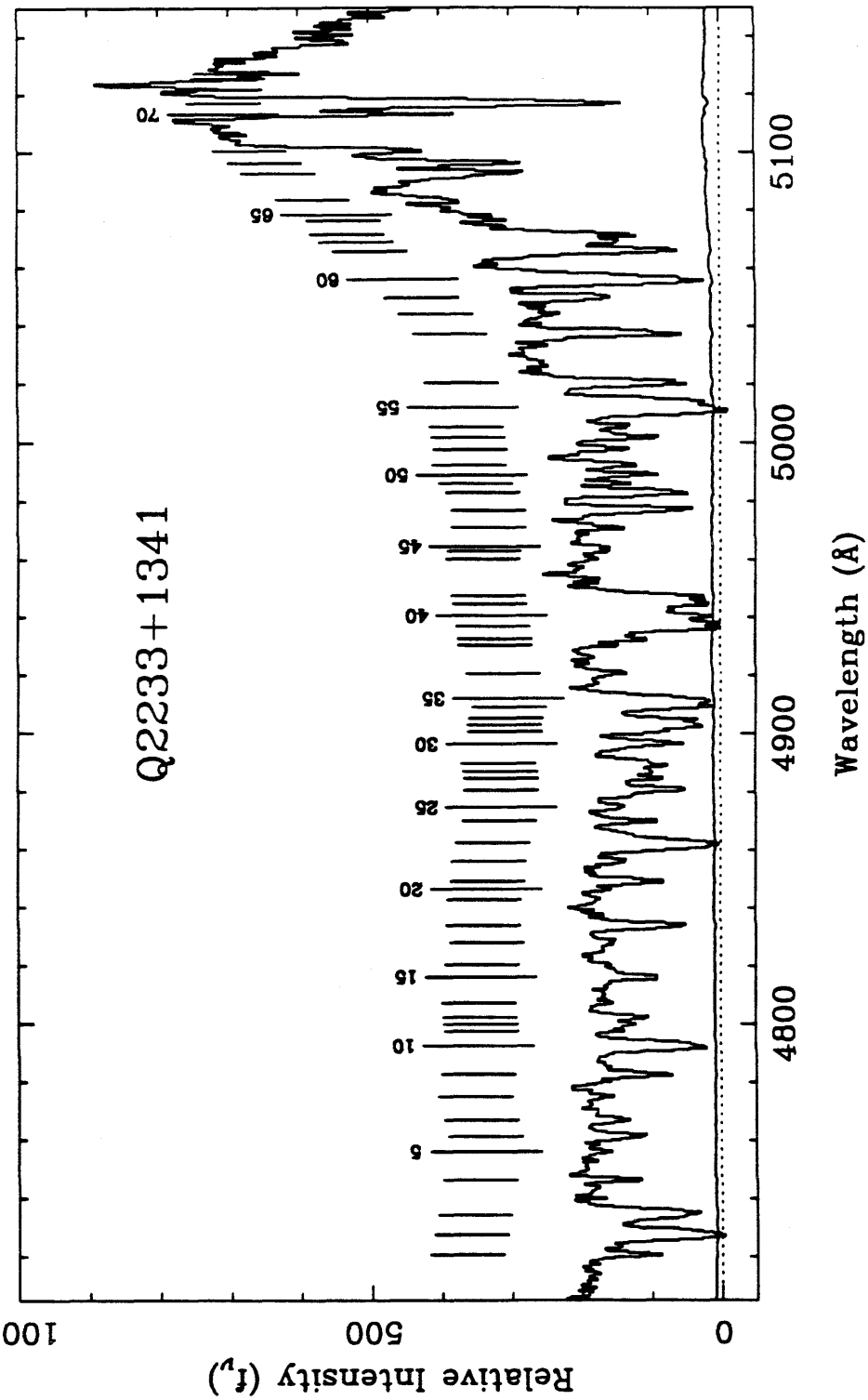
Q2233+1341
Relative Intensity (f_ν)
0
500
1000
Wavelength (Å)
4800
4900
5000
5100
5
10
15
20
25
30
35
40
45
50
55
60
65
70

Figure 7 *b*.

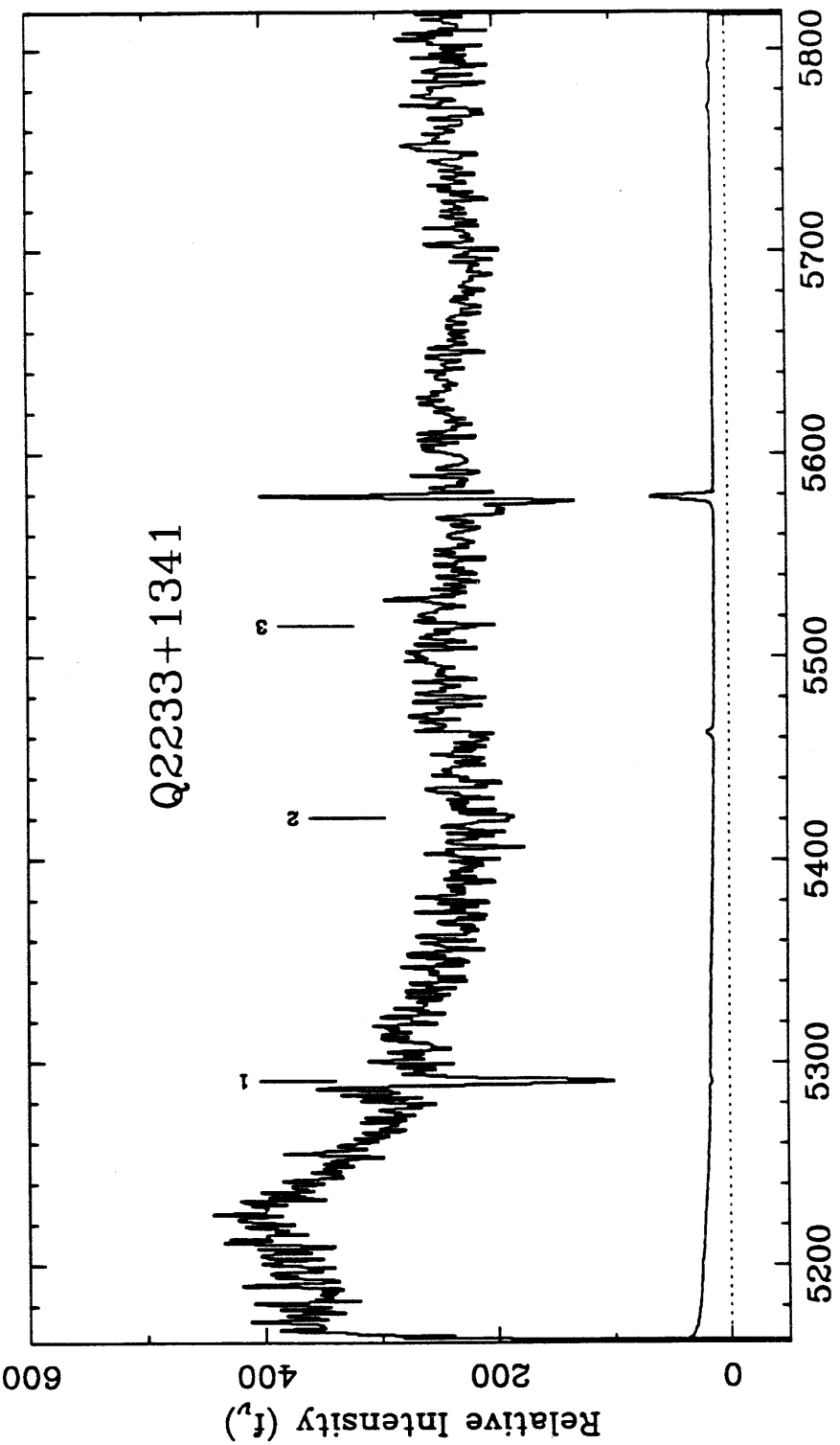
Q2233+1341
1
2
3
Relative Intensity (f_ν)
0
200
400
600
5200
5300
5400
5500
5600
5700
5800
Wavelength (Å)

Figure 7 *c.*

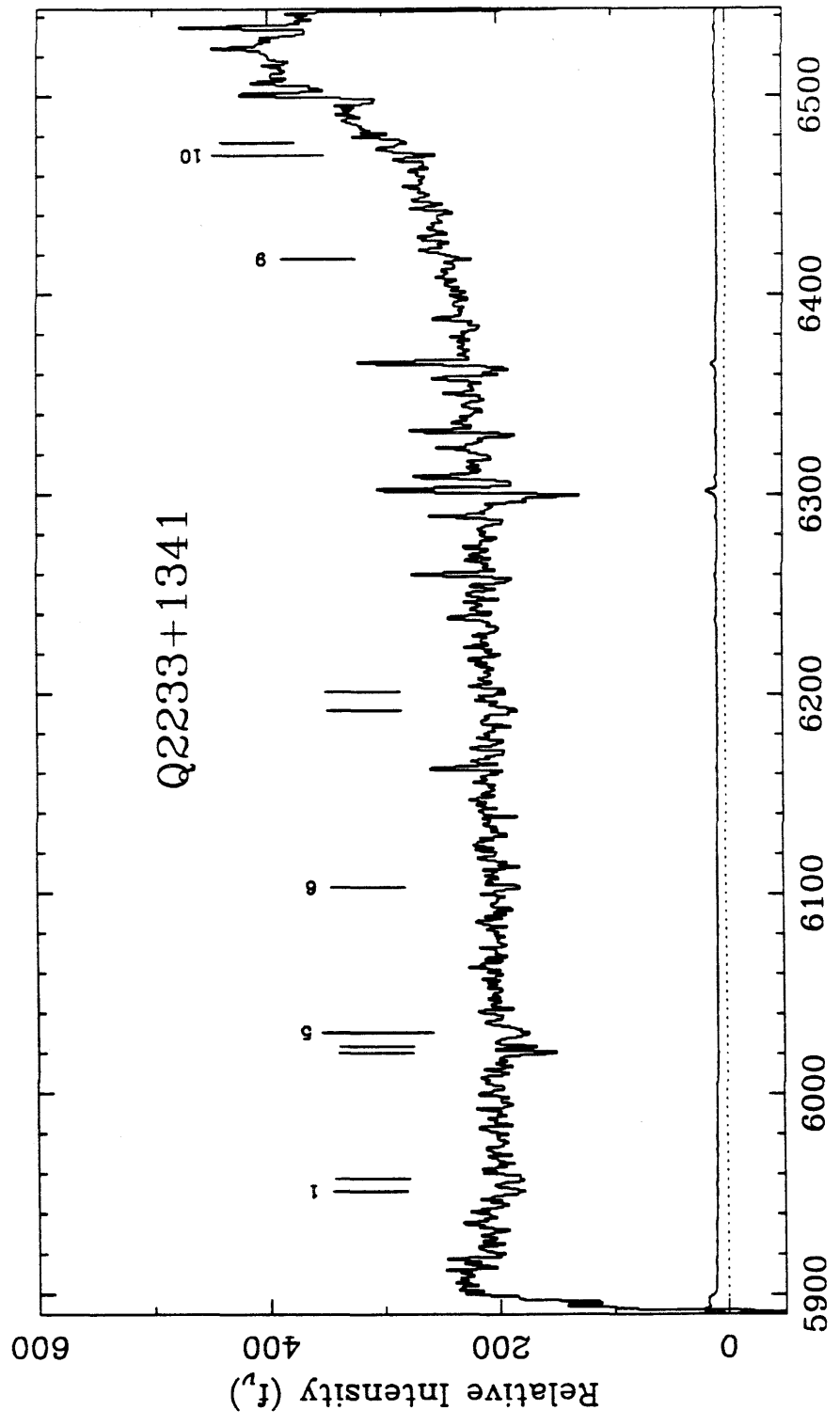
Q2233+1341
1
5
6
9
10
Relative Intensity (f_ν)
0
200
400
600
5900
6000
6100
6200
6300
6400
6500
Wavelength (Å)

Figure 7 *d.*

Figure 8 *a.*

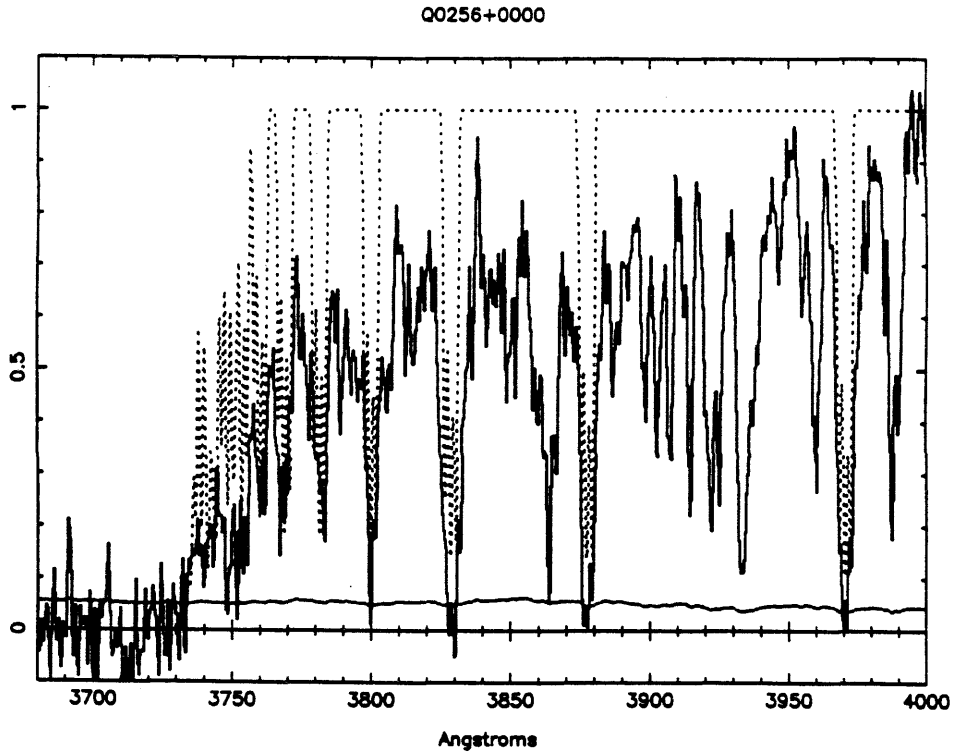
Q0256+0000
1
0.5
0
3700
3750
3800
3850
3900
3950
4000
Angstroms

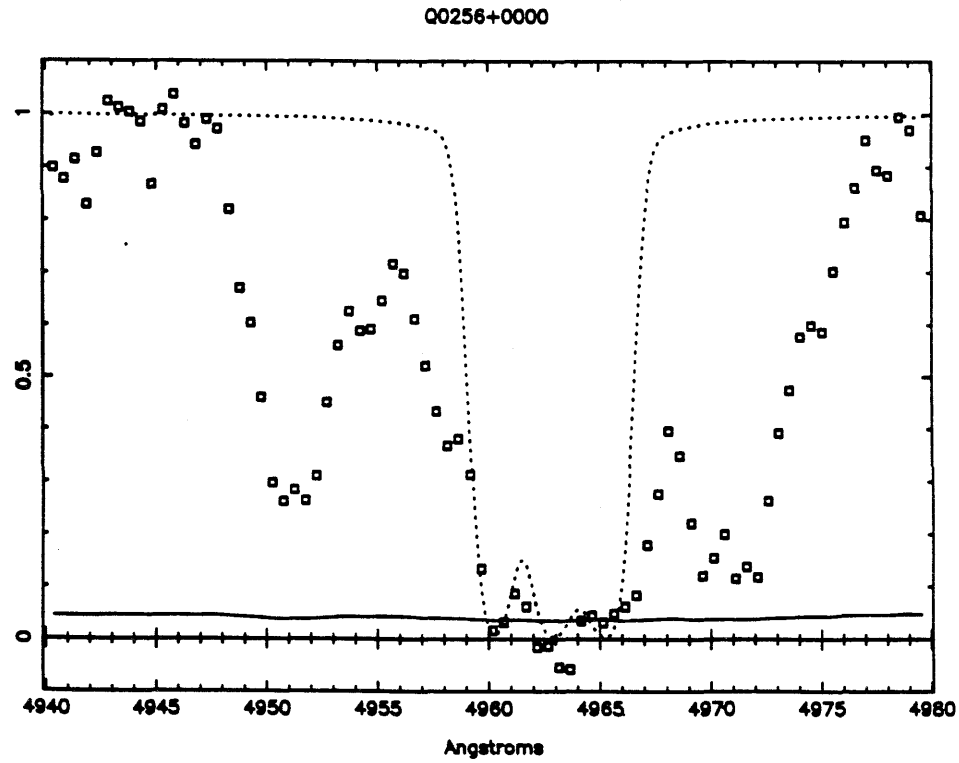
Q0256+0000
1
0.5
0
4940
4945
4950
4955
4960
4965
4970
4975
4980
Angstroms

Figure 8 *b*.

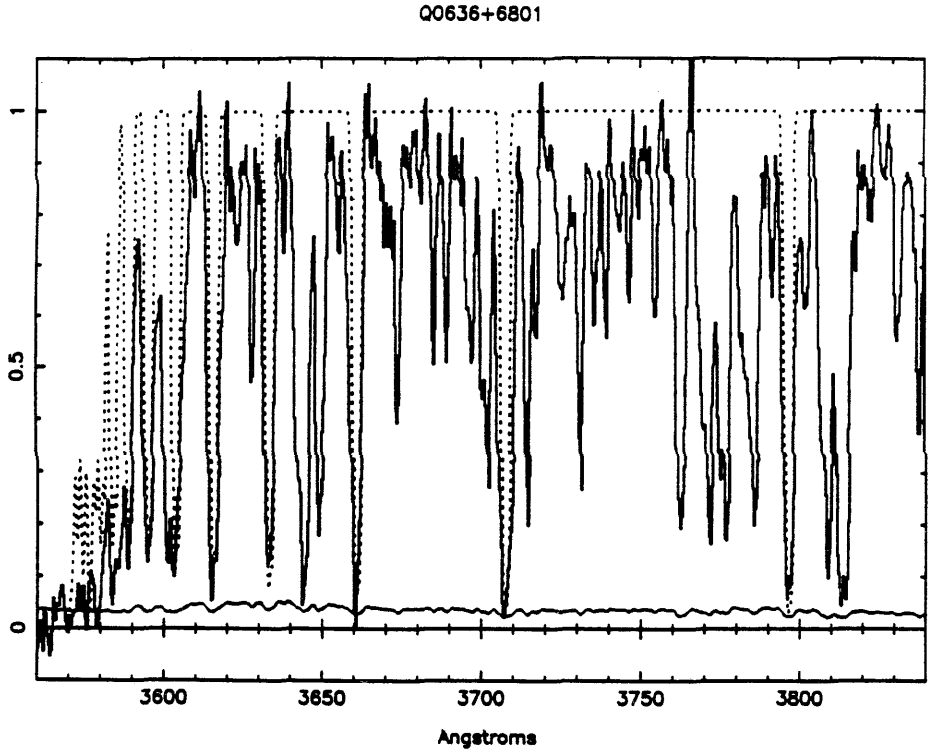
Q0636+6801
1
0.5
0
3600
3650
3700
3750
3800
Angstroms

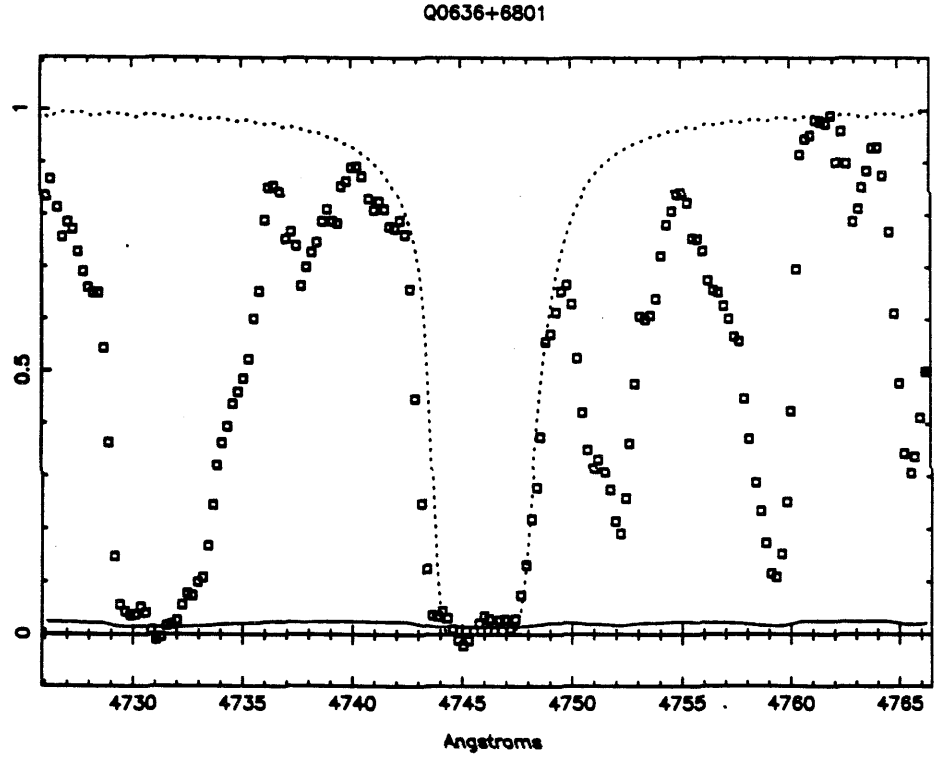
Q0636+6801
1
0.5
0
4730
4735
4740
4745
4750
4755
4760
4765
Angstroms

Figure 9

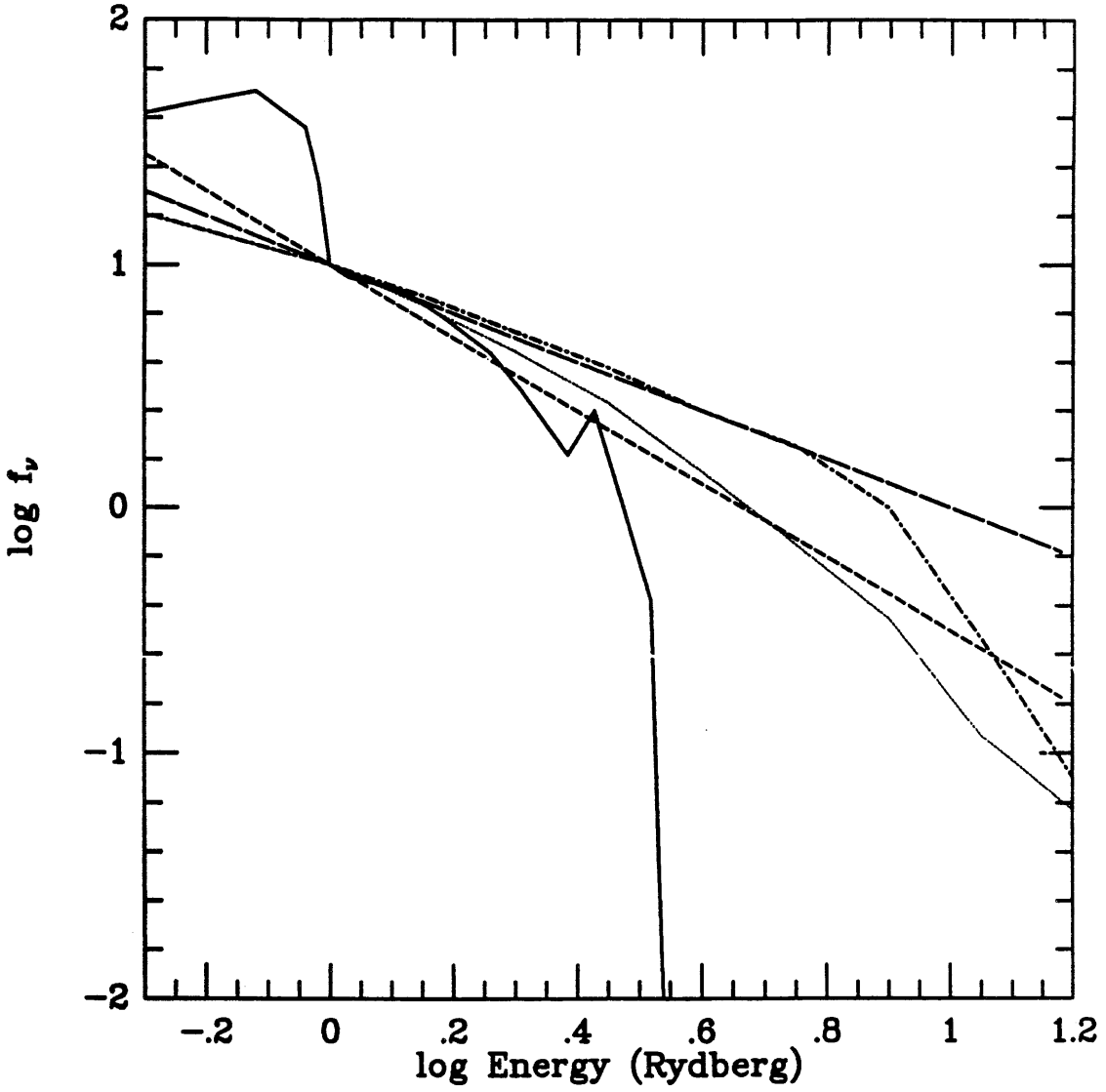

Figure 10 *a.*

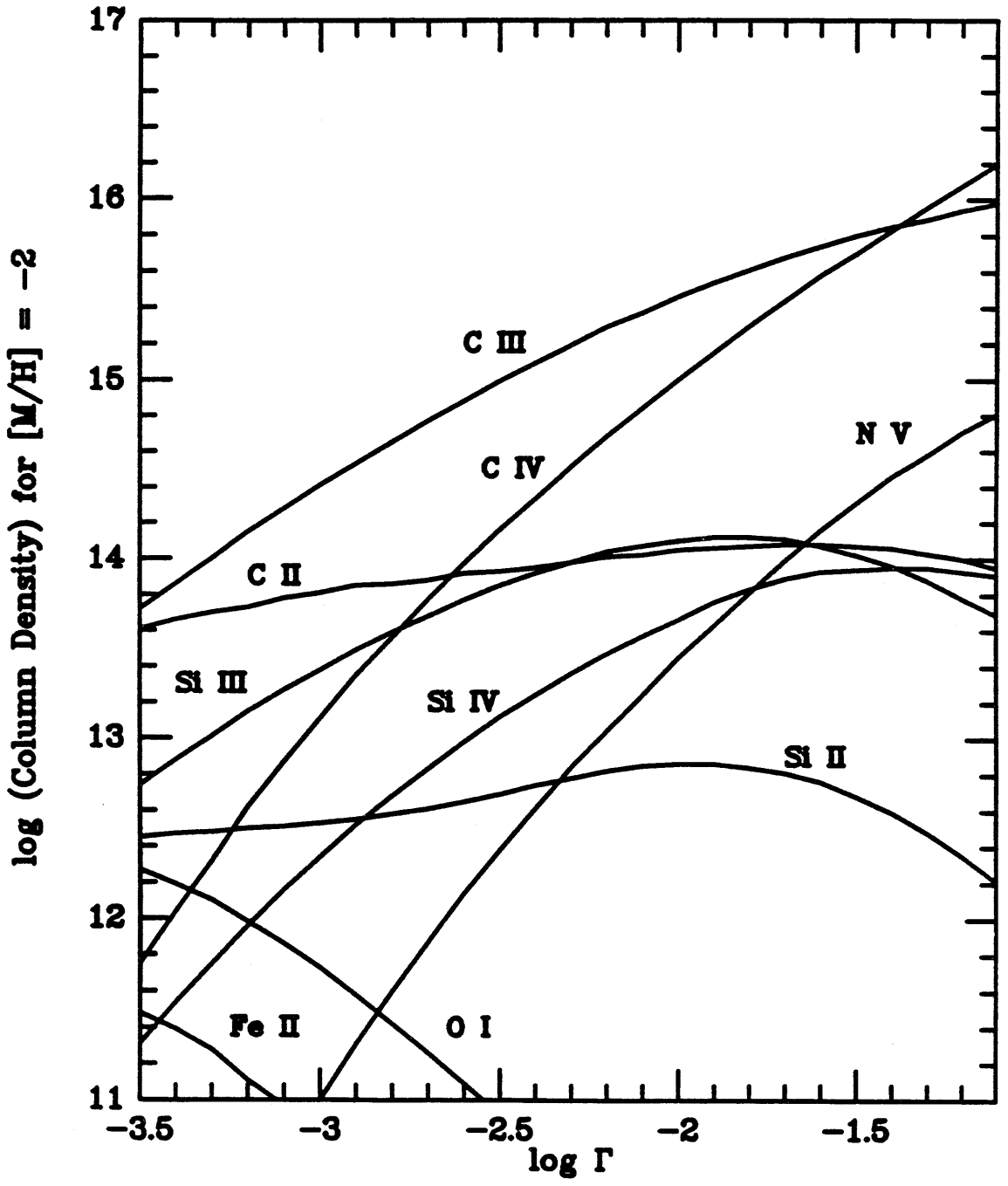
17
16
15
14
13
12
11
log (Column Density) for [M/H] = −2
C III
C IV
N V
C II
Si III
Si IV
Si II
Fe II
O I
−3.5
−3
−2.5
−2
−1.5
log Γ

Figure 10 *b*.

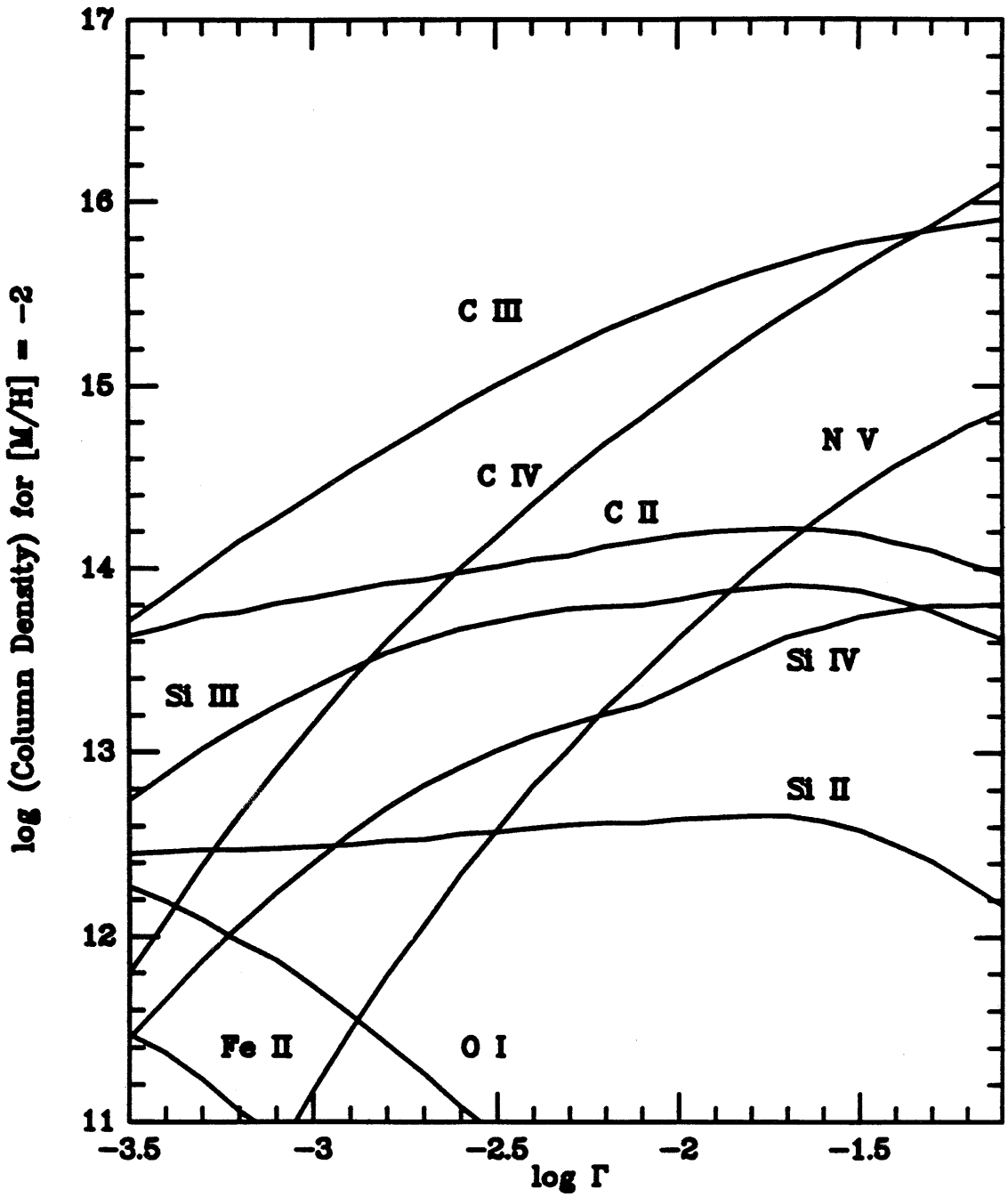
17
16
15
14
13
12
11
log (Column Density) for [M/H] = -2
C III
C IV
N V
C II
Si IV
Si III
Si II
Fe II
O I
-3.5
-3
-2.5
-2
-1.5
log Γ

Figure 10 *c*.

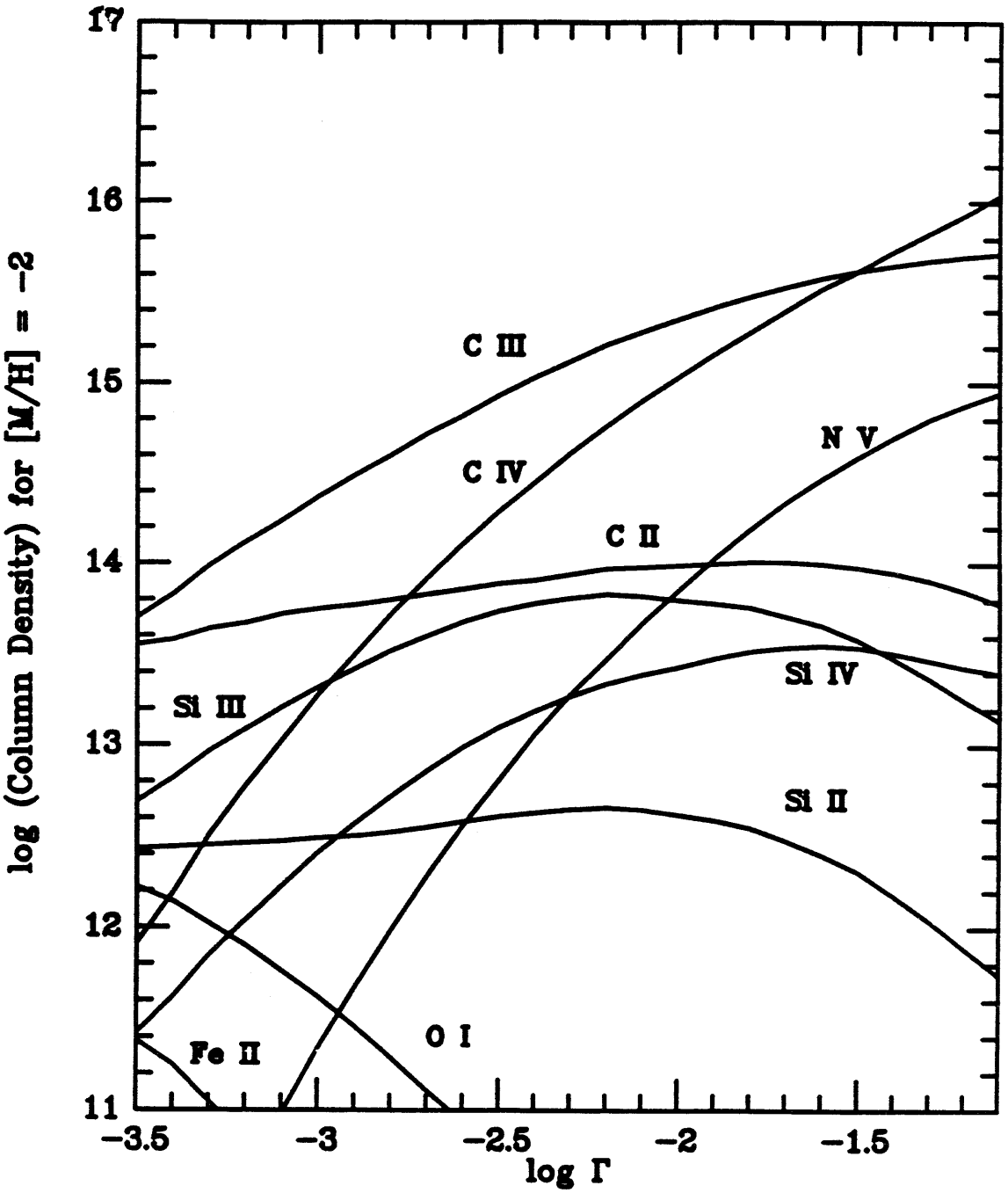
17
16
15
14
13
12
11
log (Column Density) for [M/H] = -2
C III
C IV
N V
C II
Si IV
Si III
Si II
O I
Fe II
-3.5
-3
-2.5
-2
-1.5
log Γ

Figure 10 *d*.

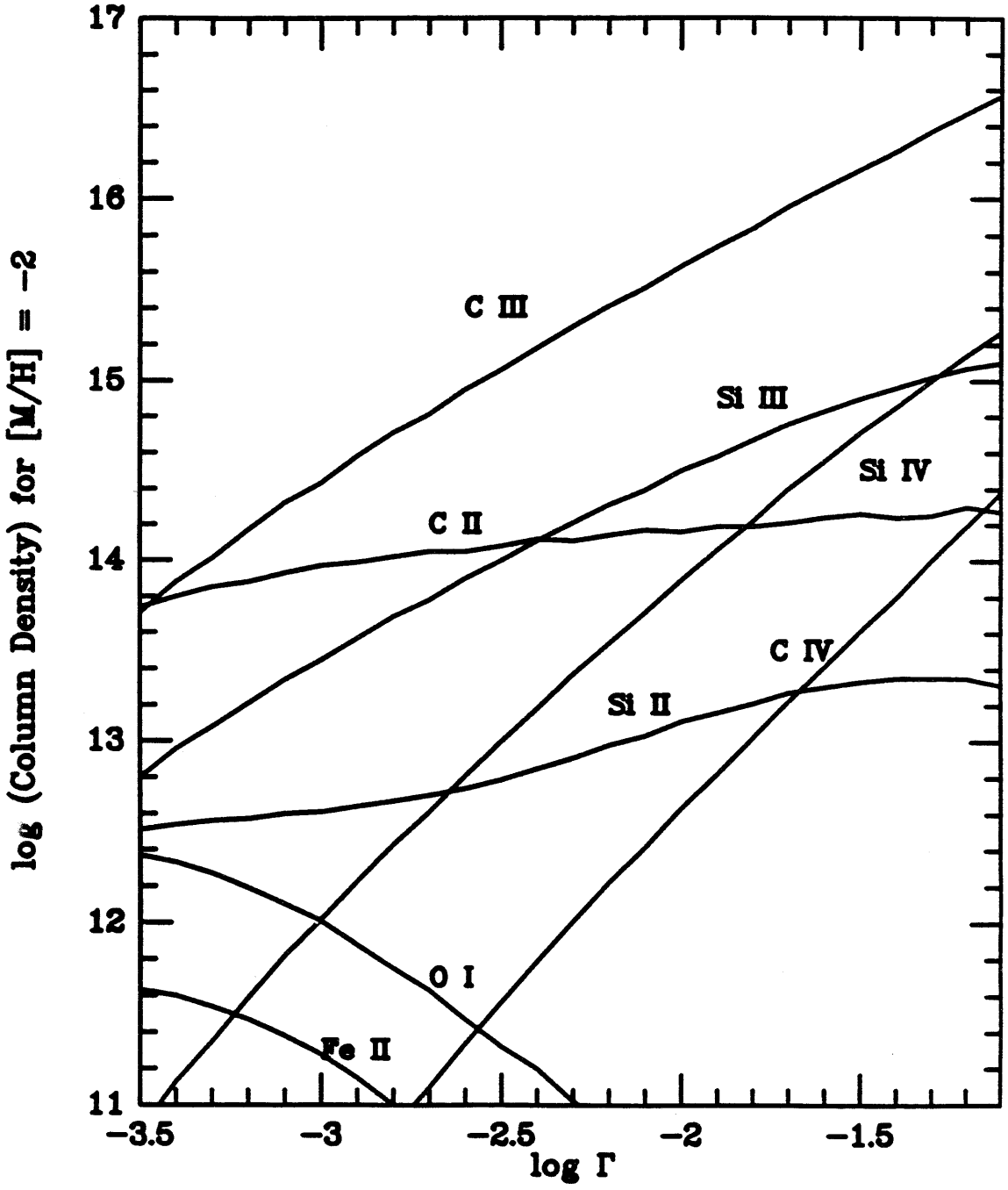
17
16
15
14
13
12
11
log (Column Density) for [M/H] = −2
C III
Si III
Si IV
C II
C IV
Si II
O I
Fe II
−3.5
−3
−2.5
−2
−1.5
log Γ

Figure 11 *a.*

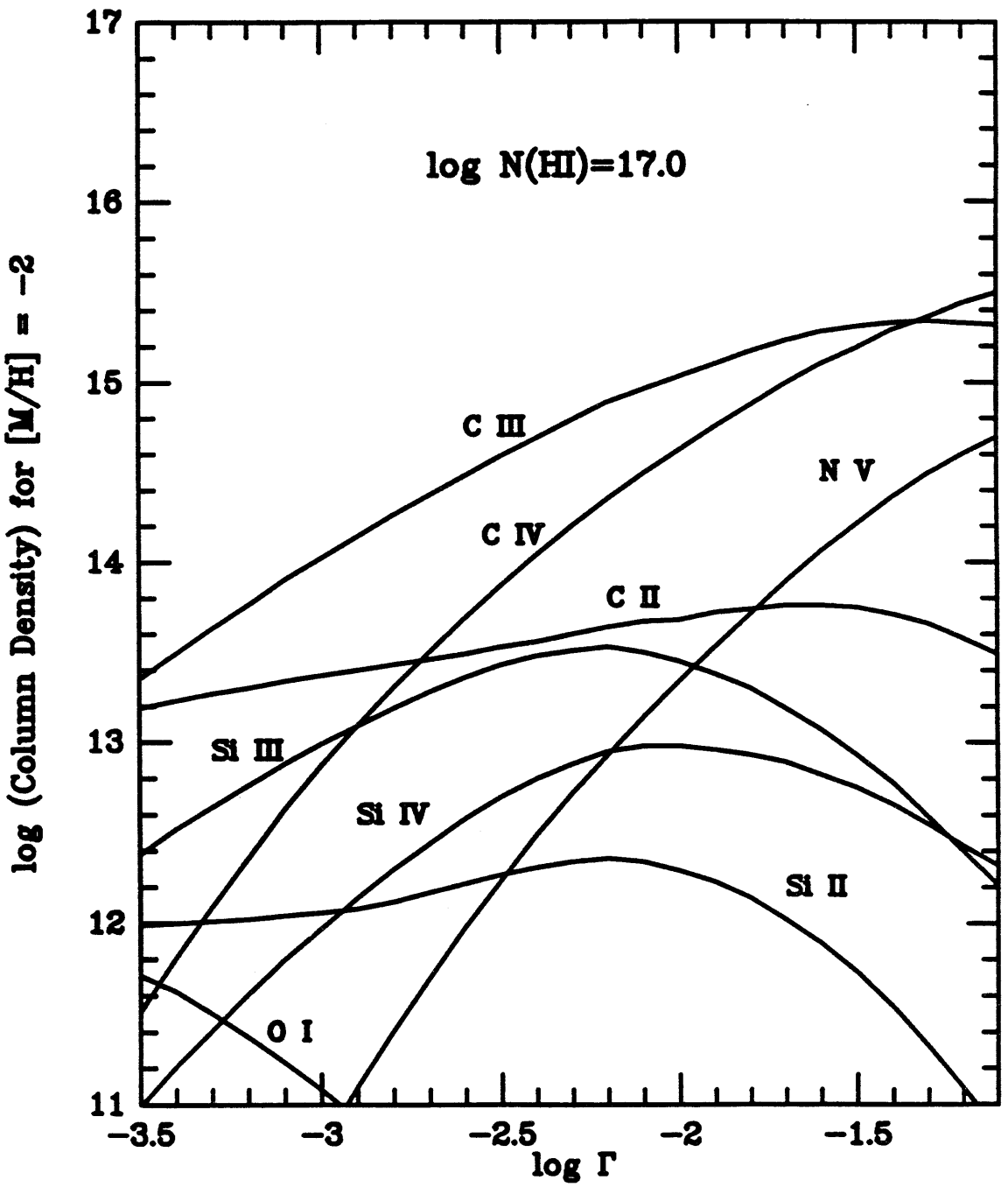
log N(HI)=17.0
C III
C IV
N V
C II
Si III
Si IV
Si II
O I
log (Column Density) for [M/H] = -2
log Γ
17
16
15
14
13
12
11
-3.5
-3
-2.5
-2
-1.5

Figure 11 *b*.

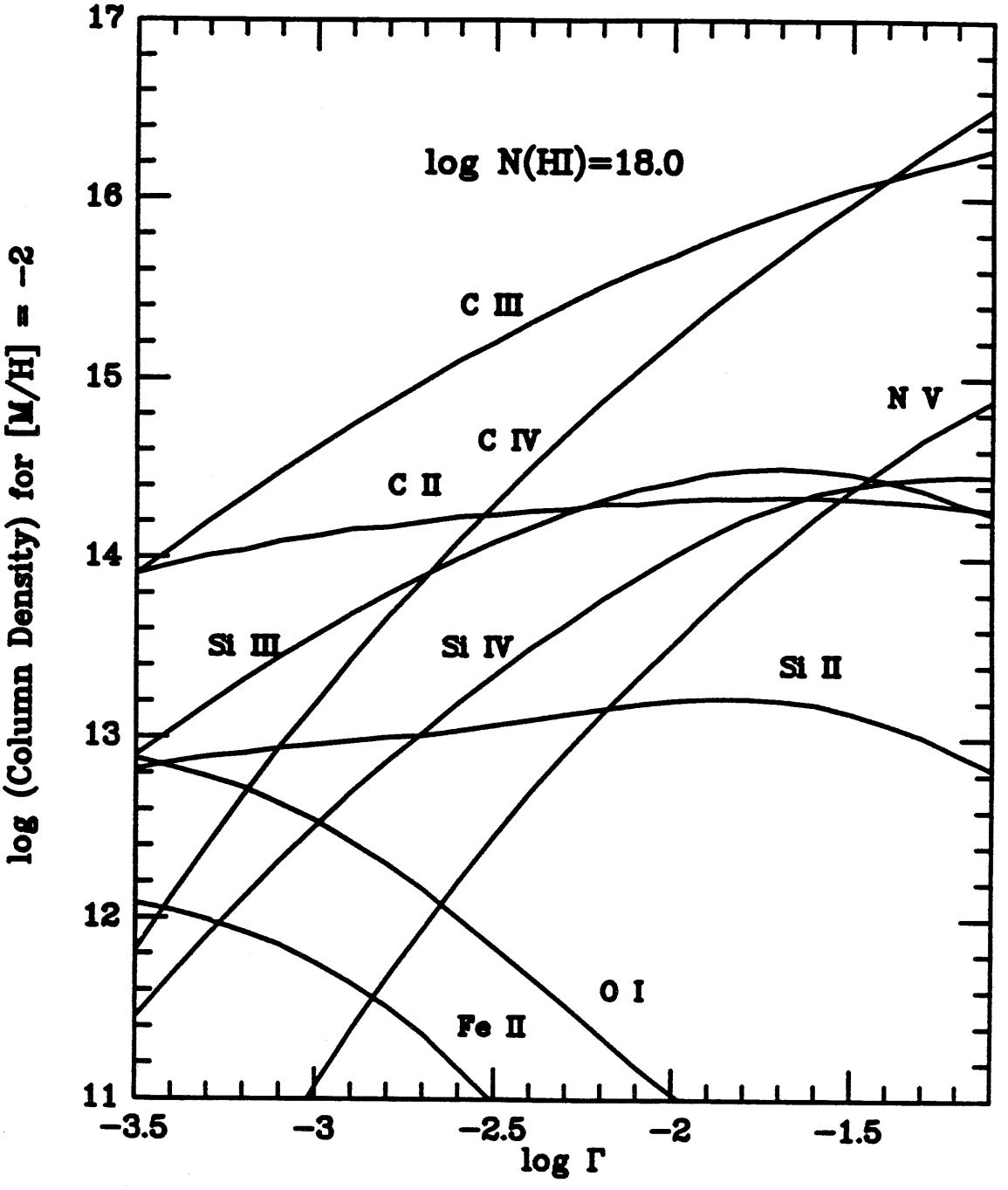
log N(HI)=18.0
C III
C IV
C II
N V
Si III
Si IV
Si II
O I
Fe II
log (Column Density) for [M/H] = -2
log Γ
17
16
15
14
13
12
11
-3.5
-3
-2.5
-2
-1.5

Figure 11 *c*.

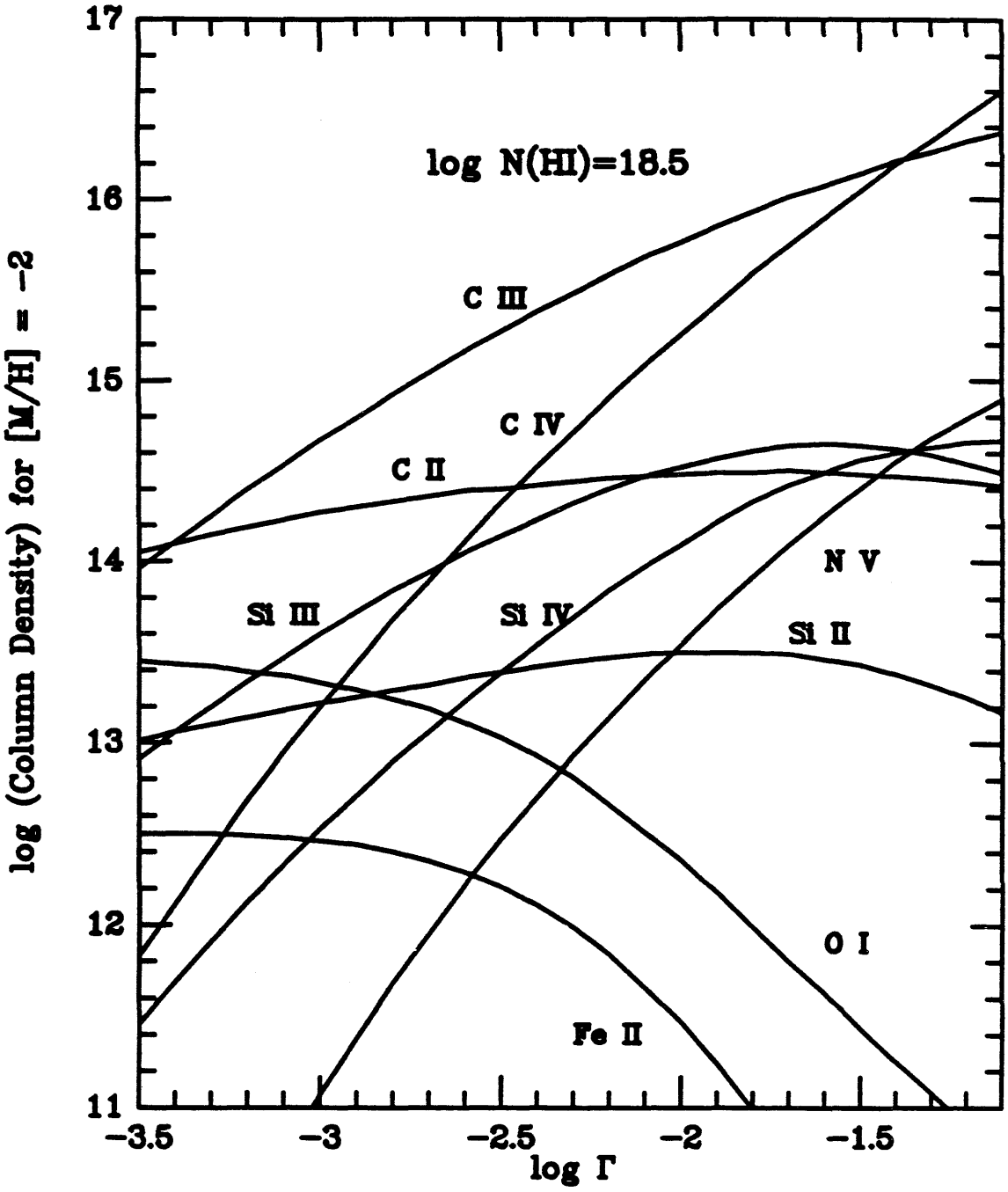
log N(HI)=18.5
C III
C IV
C II
N V
Si III
Si IV
Si II
O I
Fe II
log (Column Density) for [M/H] = -2
log Γ
17
16
15
14
13
12
11
-3.5
-3
-2.5
-2
-1.5

Figure 11 *d.*

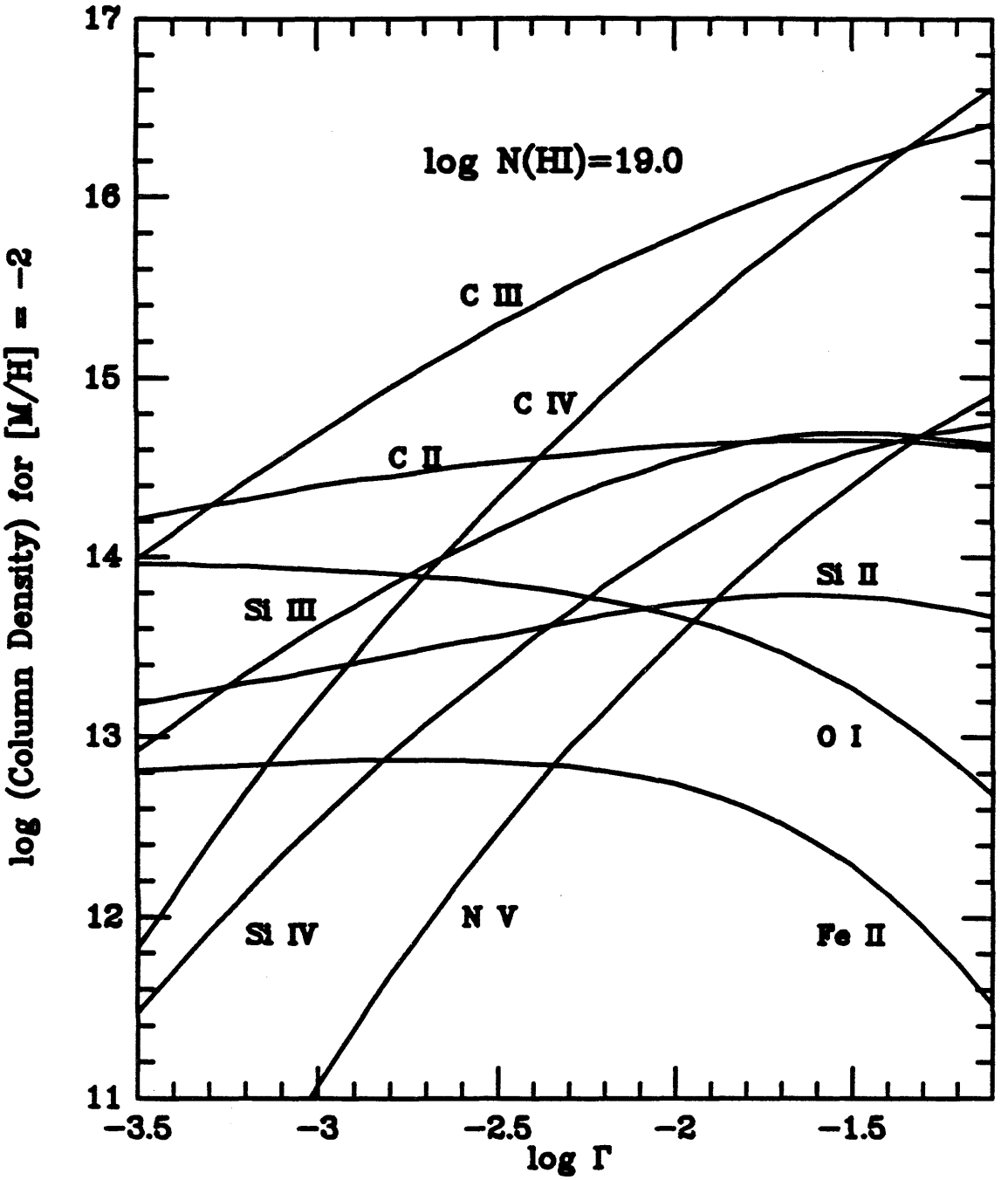
log N(HI)=19.0
C III
C IV
C II
Si II
Si III
O I
Si IV
N V
Fe II
log (Column Density) for [M/H] = -2
log Γ
17
16
15
14
13
12
11
-3.5
-3
-2.5
-2
-1.5

Appendix 1

QSO ABSORPTION LINES AND THE TIMESCALE FOR INITIAL HEAVY ELEMENT ENRICHMENT IN GALAXIES

Reprinted from *The Astrophysical Journal (Letters)* (1988, **333**, pp. L5–L8)

THE ASTROPHYSICAL JOURNAL, 333:L5–L8, 1988 October 1

QSO ABSORPTION LINES AND THE TIME SCALE FOR INITIAL HEAVY ELEMENT ENRICHMENT IN GALAXIES

CHARLES C. STEIDEL AND WALLACE L. W. SARGENT
Palomar Observatory, California Institute of Technology
AND
A. BOKSENBERG
Royal Greenwich Observatory
Received 1988 May 9; accepted 1988 July 1

ABSTRACT

Recent statistical studies of the incidence of C IV, Mg II, and Lyman limit absorption in QSO spectra reveal that the ratio of the number density of heavy element absorbers to that of H I absorbers is declining rapidly with increasing redshift beyond $z \sim 1$. We assume that this trend is due to the effects of initial heavy element enrichment in the outer parts of galaxies. We then find that the heavy element abundance increases linearly with time from $t = 1.5$ billion years to $t = 4$ billion years ($q_0 = \frac{1}{2}$, $H_0 = 50$), roughly on the dynamical time scale at these large radii. On a simple "closed box" model, the rate of gas consumption is roughly constant.

Subject headings: cosmology — galaxies: general — quasars

I. INTRODUCTION

Since the classic papers by Hoyle (1946) and Burbidge *et al.* (1957) it is believed that the heavy elements in the interstellar gas in galaxies are produced by stellar nucleosynthesis. However, so far it has only proved possible to explore the evolution of composition in time in our own Galaxy. Thus, the gradual rise, by about a factor of 3 from an initially enriched state, in the heavy element abundance of the local Galactic disk has been measured via the study of stars of different ages (Twarog 1980). The evolution of the Galactic halo population has been more controversial. Eggen, Lynden-Bell, and Sandage (1962) argued in their seminal paper that the halo was produced in a rapid initial radial collapse on a time scale of 2×10^8 yr which formed a radial gradient in the composition of the halo stars and which culminated in the formation of the disk. Some later workers argued for a large dispersion in the ages of the globular clusters and suggested that the halo was formed over a time scale of billions of years. The differences of interpretation are related to difficulties in fitting the results of stellar model evolutionary calculations for different assumed heavy element compositions to the observed color-magnitude diagrams. In any case, for a variety of reasons, our knowledge of the history of the chemical evolution of our own Galaxy is far from secure.

QSO absorption lines in principle offer a direct way of studying galactic chemical evolution by examining the composition of particular classes of absorbers as a function of redshift and hence as a function of time. Such an approach is clearly completely different to the ones used heretofore which involve the study of local stars or clusters of known age. In the course of recent work on the statistics of QSO absorption lines we have obtained the first results which are applicable to this kind of analysis. We present them in the present *Letter* as an indication of what might be possible and to encourage further observations.

II. EVOLUTION OF QSO ABSORPTION REDSHIFTS

In a Friedmann universe, the number density of absorbers is expected to vary with redshift according to the expression

$$N(z) = N_0(1 + z)(1 + 2q_0 z)^{-1/2}, \quad (1)$$

where $N_0 = \Phi_0 \pi r_0^2 c/H_0$. Here Φ_0 is the local comoving density of absorbers whose mean effective cross section is πr_0^2. This expression describes how the number of interceptions per unit redshift range should increase with increasing redshift as the absorbers get closer together. Equation (1) holds as long as the product $\Phi_0 \pi r_0^2$ remains constant; if this is not the case, we must take into account the explicit redshift dependence and substitute $N_0(z) = \Phi_0(z)\pi r_0^2(z)(c/H_0)$ for N_0. Sargent *et al.* (1980) made the first quantitative application of equation (1) to the absorption lines in the Lyα forest, and introduced the custom of representing it as a power law, $N(z) \propto (1 + z)^\gamma$, where $\gamma = 1$ for $q_0 = 0$ and $\gamma = 0.5$ for $q_0 = \frac{1}{2}$. Until recently our knowledge of the evolution of absorbers other than the Lyα forest clouds (Murdoch *et al.* 1986) was extremely uncertain. Recently, however, we have completed three large surveys which have vastly improved the situation.

Sargent, Boksenberg, and Steidel (1988; hereafter SBS) studied the absorption redshifts defined by the C IV $\lambda\lambda$1548, 1550 doublet in uniform spectra of a sample of 55 QSOs with $1.8 \leq z_{em} \leq 3.6$. A total of 229 C IV absorption redshifts with $1.2 \leq z_{abs} \leq 3.5$ were found. Several unbiased subsamples were formed, and various analyses all lead to the result that the comoving density of absorbers is decreasing with increasing redshift, and therefore that the C IV absorbers are evolving in cosmic time. This is illustrated for different subsamples in Figures 5, 6, and 7 of SBS. Quantitatively, for sample S2, $\gamma = -1.18 \pm 0.72$; the $N(z)$ curve is reproduced in Figure 1. (There is some suggestion in the data for a precipitous drop in $N(z)$ between $z \sim 2.7$ and $z \sim 3.1$, but this cannot be supported with the available data, and we shall continue the discussion

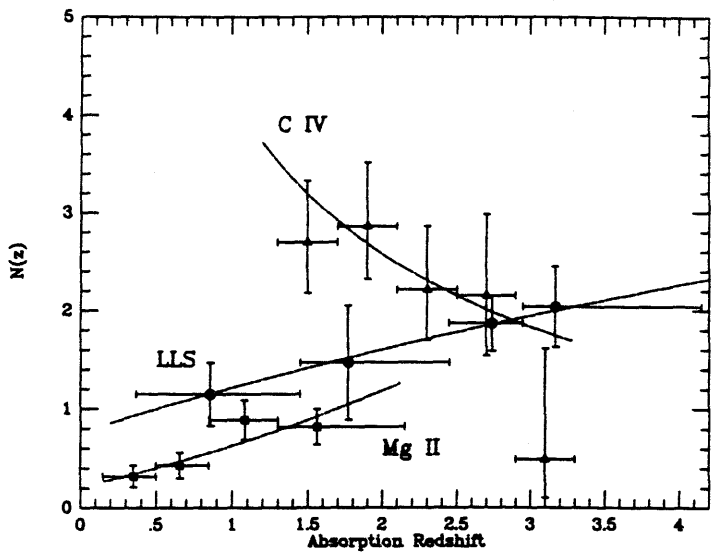

FIG. 1.—Plot showing the evolutionary curves for three types of QSO absorption systems. All of the distributions were arbitrarily binned for display purposes, but the curves represent maximum likelihood fits to the unbinned data. The error bars in the horizontal direction represent the extent of each bin. The data for C IV (*triangles; long-dashed curve*) are from SBS (their Fig. 6); the LLS curve (*circles; short-dashed curve*) is reproduced from Fig. 4 of SSB2, while the curve for Mg II (*squares; dot-dashed curve*) is reproduced from Fig. 7 of SSB2. Note that different criteria were used in compiling unbiased samples for the three types of absorbers, so that the zero point in $N(z)$ for each curve is somewhat arbitrary.

assuming that the decrease is gradual as represented by the power-law fit.) SBS also found that there is statistically significant evidence that the C IV(1548)/C IV(1550) doublet ratio increases (toward the optically thin limit) with redshift over the above range. Both trends are consistent with an actual decrease in the abundance of C IV in the absorbing gas with increasing redshift.

At the same time, there has been a considerable improvement in our knowledge of the behavior with redshift of absorption systems containing the Mg II $\lambda\lambda$2796, 2803 doublet. Sargent, Steidel, and Boksenberg (1988*a*; hereafter SSB1) found 40 Mg II redshifts in the range $0.2 \leq z_{abs} \leq 1.46$ in the spectra of the 55 QSOs observed in the C IV study by SBS. A further 62 Mg II systems in the redshift range $0.72 \leq z_{abs} \leq 1.45$ were found by Sargent, Steidel, and Boksenberg (1988*b*; hereafter SSB2) in the spectra of 58 QSOs which were observed in order to determine the incidence of Lyman limit absorption in high-redshift QSOs. Adding these new data to samples recently published by Boulade *et al.* (1988), Lanzetta, Turnshek, and Wolfe (1987), and Tytler *et al.* (1987), SSB2 assembled a complete sample of 60 Mg II redshifts with $W_0(2796) > 0.6$ Å, and covering the range $0.16 \leq z_{abs} \leq 2.12$. Qualitatively confirming the results of earlier work, the density of Mg II systems is found to increase with increasing redshift, with $\gamma = 1.55 \pm 0.52$. This is completely at variance with the behavior of C IV. However, while certainly showing a steep rise up to $z \sim 1$, there is a suggestion in Figure 7 of SSB2 (reproduced in Fig. 1 of this paper) that the Mg II evolution curve flattens off at higher redshift. One thus has an impression, which cannot be supported statistically by the available data, that the decrease in C IV number density at high redshift is a natural extension of the Mg II behavior above $z \sim 1$. It could be that there is a systematic change in the state of ionization of the absorbing gas as a function of redshift. However, the existing analyses of QSO absorption systems (e.g., using the ratio C IV/C II) give no hint of such an effect. We shall therefore assume for the remaining discussion that the evolutionary trends evidenced by the Mg II absorbers at low redshift and by the C IV absorbers at high redshift are due only to the combined effects of the expansion of the universe and systematic changes in heavy element abundance. If this hypothesis is correct, then the heavy element abundance increased in the absorbing material from high redshift down to $z \sim 1$, while for $z < 1$ the expansion of the universe became the dominant factor in determining the shape of the $N(z)$ curve.

Various lines of evidence, particularly their clustering and evolutionary properties, suggest that the Lyα forest clouds are unrelated to galaxies (see SBS, for example). The best available information on the evolution of the H I component of galaxies is afforded by the Lyman limit absorbers, which have $N(\text{H I}) > 10^{17}$ cm^{-2} and which can be observed over the whole redshift range $0.37 \leq z_{abs} \leq 4.5$ (Tytler 1982). SSB2 recently surveyed 59 QSOs with $z_{em} > 2.75$ at low resolution for Lyman limits. Combining their data on 33 LLSs with other published data, SSB2 found $N(z) \propto (1+z)^{0.68 \pm 0.54}$ over the redshift range $0.67 \leq z_{LSS} \leq 3.58$; the data are shown in Figure 1. This value for γ is consistent within the errors with both $q_0 = 0$ and $q_0 = \frac{1}{2}$ with no evolution of the absorbing objects. For these absorbers, the evolutionary curve continues to rise at the highest redshifts observed (see Fig. 1). Moreover, most of the high-redshift LLSs have accompanying heavy element lines and are therefore not associated with the Lyα forest of absorbers. The behavior of the LLSs, which we take to be representative of the H I component in galaxies, is in marked contrast to that of the C IV absorbers. Thus we infer that the decrease in C IV number density with increasing redshift is not

due to a decrease in the number of absorbers *per se*, but is due to either a systematic change in ionization state with redshift, or, as we have suggested above, to a systematic change in heavy element abundance. If this hypothesis is correct, we have a way to determine the time scale for initial heavy element enrichment in the outer parts of galaxies.

Observations of H II regions in nearby galaxies show evidence for systematic radial gradients in composition (Searle 1971). Thus, in M101, the outer H II regions have [O/H] = −0.7 at $R = 23$ kpc, while [O/H] = +0.3 at $R = 6$ kpc. The form of the oxygen gradient can be described by a power law $\mathrm{O/H} \propto R^{-1.8}$. Presumably, the effective cross section deduced from the C IV statistics refers to the radius at which the composition of the interstellar gas reaches a particular value set by the rest equivalent width cutoff used. This radius will move outward as nucleosynthesis proceeds. We shall assume that the heavy element ratio $R_{\rm HE}(z) = N_{\rm C\,IV}(z)/N_{\rm LLS}(z)$ represents the ratio of the effective cross section for C IV absorption to that for the H I component of galaxies. The behavior of $R_{\rm HE}$ with redshift then yields a time scale for heavy element enrichment. We shall assume that the above ratio is directly proportional to the chemical abundance, i.e., the absorption is on the linear part of the curve of growth. (Since it is the weak lines closest to the rest equivalent width threshold which contribute most to the observed evolution, the assumption that the lines are on the linear part of the curve of growth is reasonable. At the highest redshifts, the doublet ratio shows directly that the weakest C IV doublets in the samples used are not saturated.) For definiteness, we shall use $q_0 = \frac{1}{2}$, close to the nominal value obtained from the LLS evolution. In this case, redshift and time are related by

$$t = t_0(1 + z)^{-1.5}, \tag{2}$$

where $t_0 = 2/(3H_0) = 13.67 \times 10^9$ years for $H_0 = 50$ km s^{-1} Mpc^{-1}. For comparison, the redshift dependence of the heavy element ratio is

$$R_{\rm HE}(z) \propto (1 + z)^{-1.86 \pm 0.98}, \tag{3}$$

which translates into a time scale for changes in the typical heavy element abundance

$$t_{\rm HE}(z) \equiv \frac{R_{\rm HE}}{(dR_{\rm HE}/dt)} = \frac{t_0}{1.2}(1 + z)^{-1.54 \pm 0.81}. \tag{4}$$

Comparing equations (2) and (4), we see that, although there is a large uncertainty, the heavy element abundance as measured by $R_{\rm HE}$ increases linearly with time. This obtains roughly over the redshift interval $3.3 \geq z \geq 1.3$, which corresponds (for $q_0 = \frac{1}{2}$) to the time interval from $t = 1.5$ billion years to $t = 4$ billion years. For $t > 4$ billion years ($z < 1$) the heavy element abundance appears to have leveled off so that expansion effects dominate the $N(z)$ curve. For both the C IV and LLS absorbers, the typical line of sight passes ~50 kpc (~4 Holmberg radii) from the center of a galaxy of fiducial luminosity L^* in the Schechter (1976) luminosity function (see, e.g., SBS). For galaxies with flat rotation curves, the dynamical time scale t_D scales linearly with radius so that $t_D \sim 1$ billion years at 50 kpc. Thus, we find that the time scale for early heavy element enrichment in galaxies is of order t_D.

On the simplest "closed box" model for galactic heavy element enrichment, the heavy element abundance varies with the proportion of hydrogen consumed according to the expression

$$Z = \langle y \rangle \ln (M_T/M_G), \tag{5}$$

where $\langle y \rangle$ is the average "yield" of heavy elements from stars and $M_T = M_G + M_*$ is the total mass, gas plus stars (Searle and Sargent 1972). In a galaxy initially dominated by gas, this expression takes the form

$$Z \approx \langle y \rangle (M_*/M_G). \tag{6}$$

Thus, the result obtained above implies that gas is being transformed into stars at a constant rate with time during the initial heavy element enrichment.

These results are at first sight at variance with prevailing models of galactic evolution, which universally envisage an initial burst of star formation lasting ~1 billion years. It was by this means that the present, fairly static, composition of the local galactic disk reached its value early in the life of the galaxy. However, we must recall that the QSO absorption lines are produced predominantly in the outer parts of galaxies, where the dynamical time scales are much longer. Consequently, our results probably shed light on the evolution of Population II abundances rather than those of Population I.

III. CONCLUSIONS

The arguments presented above are necessarily crude, but, taken literally, they imply that the heavy element composition in the outer parts of galaxies reached a saturation value at a redshift of ~1, i.e., relatively recently, and that before this the enrichment proceeded roughly linearly with time for 2.5 billion years, comparable to the dynamical time scale. During this period, the rate of gas consumption was approximately constant. Beyond these results, which are still uncertain, the main point of this exercise is to show that QSO absorption lines are capable of providing information on galactic chemical evolution which is not obtainable by other means. Future work must stress the determination of actual abundances as a function of redshift for the main elements found in QSO absorption spectra.

We thank S. Phinney and R. Blandford for their comments. The observations on which this work was based were supported in part by NSF grant AST 84-16704 to WLWS. The work of AB was supported by the U.K. Science and Engineering Research Council.

REFERENCES

Boulade, O., Kunth, D., Tytler, D., and Vigroux, L. 1988, in *High Redshift and Primeval Galaxies*, ed. D. Kunth, J. Bergeron, B. Rocca-Volmerange, and J. Tran Thanh Van (Gif-sur-Yvette: Editions Frontières).
Burbidge, E. M., Burbidge, G. R., Fowler, W. A., and Hoyle, F. 1957, *Rev. Mod. Phys.*, **29**, 547.
Eggen, O., Lynden-Bell, D., and Sandage, A. 1962, *Ap. J.*, **136**, 748.
Hoyle, F. 1946, *M.N.R.A.S.*, **106**, 343.
Lanzetta, K. M., Turnshek, D. A., and Wolfe, A. M. 1987, *Ap. J.*, **322**, 739.
Murdoch, H. S., Hunstead, R. W., Pettini, M., and Blades, J. C. 1986, *Ap. J.*, **309**, 19.
Sargent, W. L. W., Boksenberg, A., and Steidel, C. C. 1988, *Ap. J. Suppl.*, **68**, in press (SBS).
Sargent, W. L. W., Steidel, C. C., and Boksenberg, A. 1988*a*, *Ap. J.*, **334**, in press (SSB1).
Sargent, W. L. W., Steidel, C. C., and Boksenberg, A. 1988*b*, *Ap. J. Suppl.*, submitted (SSB2).

Sargent, W. L. W., Young, P. J., Boksenberg, A., and Tytler, D. 1980, *Ap. J. Suppl.*, **42**, 41.
Schechter, P. 1976, *Ap. J.*, **203**, 297.
Searle, L. 1971, *Ap. J.*, **168**, 327.
Searle, L., and Sargent, W. L. W. 1972, *Ap. J.*, **173**, 25.
Shields, G. A., and Searle, L. 1978, *Ap. J.*, **222**, 821.
Twarog, B. A. 1980, *Ap. J.*, **242**, 242.
Tytler, D. 1982, *Nature*, **298**, 427.
Tytler, D., Boksenberg, A., Sargent, W. L. W., Young, P. J., and Kunth, D. 1987, *Ap. J. Suppl.*, **64**, 667.

A. BOKSENBERG: Royal Greenwich Observatory, Herstmonceux Castle, Hailsham, East Sussex BN27 1RP, England, UK

W. L. W. SARGENT and C. C. STEIDEL: Palomar Observatory, 105-24, California Institute of Technology, Pasadena, CA 91125